

AD 679135

PROGRESS REPORT NO. 33

15 September 1967 through 14 September 1968

to  
THE JOINT SERVICES TECHNICAL ADVISORY COMMITTEE

Representing: The Air Force Office of Scientific Research  
The U.S. Army Research Office  
The Office of Naval Research



Submitted by: ARTHUR A. OLINER, Director  
MICROWAVE RESEARCH INSTITUTE PROGRAMS

Coordinated by: Jerome Fox, Research Coordinator

Report  
R-452.33-68

for  
Contract AF 49(638)-1402  
Project No. 4751

Submitted  
November 1968

This document has been approved for public  
release and sale; its distribution is unlimited.

## TABLE OF CONTENTS

The Microwave Research Institute Programs .....	ix
Participating Faculty and Research Staff .....	xvii
<b>I. ELECTROMAGNETICS AND WAVEGUIDE TECHNIQUES</b>	
<b>Element-Pattern Nulls in Phased-Array Antennas: Theoretical Study</b> G.H. Knittel, A. Hessel, A.A. Oliner.....	1
<b>Element-Pattern Nulls in Phased-Array Antennas: Experimental Confirmation in a Waveguide Simulator</b> G.H. Knittel, A. Hessel, A.A. Oliner.....	5
<b>Interrelations Among Mutual Coupling, Element Efficiency and Active Impedance in Linear Arrays</b> W.K. Kahn, W. Wasylkiwskyj .....	8
<b>On the Propagation Characteristics of Periodic, Screw-Symmetric Traveling-Wave Structures</b> A. Hessel, M.H. Chen.....	13
<b>Scattering by a Multimode Corrugated Structure with Application to P Type Wood Anomalies</b> A. Hessel, A.A. Oliner, D.Y. Tseng .....	23
<b>The Field of a Line Source Embedded in a Periodically-Stratified Medium</b> T. Tamir, B. Singer .....	28
<b>Mechanism of Propagation of Electromagnetic Fields in Lossy Media</b> H.L. Bertoni, L.B. Felsen, A. Hessel.....	33
<b>Ray Method for Sound Wave Reflection in an Open-Ended Circular Pipe</b> L.B. Felsen, H.Y. Yee.....	38
<b>Boundary Layer Theory and Uniform Asymptotic Expansions in Diffraction Problems</b> E. Zauderer.....	42
<b>Effects Encountered in the Theory of Diffraction of a Focused Wave by an Opaque Obstacle</b> L.B. Felsen, L. Levy.....	44
<b>Propagation and Scattering in the Presence of Bounded Fluctuating Media</b> L.B. Felsen, S. Rosenbaum, I. Kupiec.....	47
<b>Reflection, Transmission and Scattering of Scalar Waves From a Randomly-Inhomogeneous Half-Space: One-Dimensional Case</b> S. Rosenbaum.....	50
<b>Non-Uniformity Effects in Microwave Plasma Diagnostics</b> J.W.E. Griemsmann .....	57
<b>Transients in Dispersive Media</b> L.B. Felsen.....	63

## CONTENTS

Microwave Bistatic Scattering From Capillary Waves on Water E. S. Cassedy.....	70
Effects of Microwave Radiation on the Eye S. W. Rosenthal, L. Birenbaum, I. T. Kaplan, W. Metlay, H. Schmidt, M. M. Zaret .....	73
New Millimeter-Wave Techniques: Amplifier Noise Theory B. Senitzky.....	78
New Millimeter-Wave Techniques: Amplifier Noise Experiments B. Senitzky, R. T. Kihm .....	81
II. QUANTUM ELECTRONICS AND OPTICS	
Metal Vapor Lasers W. T. Walter, R. Chimenti.....	84
Laser Frequency Stabilization J. T. LaTourrette, P. Rabinowitz.....	90
Fundamental Fluctuations in Quantum-Optical Devices S. R. Barone, M. C. Newstein, S. Harrison .....	92
Generation of High-Power Picosecond Laser Pulses G. Gould, L. Silverstein.....	93
Study of Ultra-Short Pulse Laser Systems S. R. Barone, M. C. Newstein, N. Solimene, S. Chi.....	96
Basic Studies in Optical Parametric Oscillations E. S. Cassedy, S. T. Peng.....	97
A Graphical Method of Predicting the Bandwidth of Optical Parametric Amplification E. S. Cassedy, M. Piltch.....	102
Quenching and Saturation Mechanisms in Argon Ion Lasers H. Schachter, E. Skurnick .....	105
Exact Quantization Conditions J. B. Krieger, C. Rosenzweig .....	105
Relation of Phase Shifts from Born Approximation to Fourier Transform of Potential J. B. Krieger, R. Dublin .....	108
Models of Light Beams and Photon Statistics E. Mishkin, P. Bertrand, A. Kestenbaum, K. Moy, D. Stoler.....	110
Time Dependent Phase-Space Distributions of the Stimulated Raman Effect E. Mishkin, P. Bertrand, A. Hussein, A. Kestenbaum, K. Moy, D. Rosenbaum, D. Stoler.....	112
Minimum Uncertainty States E. Mishkin, P. Bertrand, A. Hussein, A. Kestenbaum, K. Moy, D. Rosenbaum, D. Stoler.....	117

## CONTENTS

<b>Diagonal Coherent Representation</b> E. Mishkin, P. Bertrand, A. Kestenbaum, K. Moy, D. Stoler.....	120
<b>Coherence in Internally Phase-Modulated Lasers</b> E. Mishkin, P. Bertrand, A. Hussein, A. Kestenbaum, K. Moy, D. Rosen- baum, D. Stoler.....	123
<b>Optical Modes in Inhomogeneous and Moving Media</b> H. Schachner, C.H. Chi.....	126
<b>Tunable Filters for the Visible and Infrared Spectral Regions</b> L. Bergstein, R.J. Kapash.....	128
<b>Optical Measurement of Gas Flow Profiles by Perturbation of a Ring Laser</b> W.K. Kahn, P. Fenster.....	132
<b>III. PLASMA PHYSICS AND ELECTRONICS</b>	
<b>Experimental Study of Weak Plasma Turbulence Using a Hollow Cathode Discharge</b> K. Chung.....	137
<b>Steady State RF Discharge Through Efficient Electron Cyclotron Resonance</b> K. Chung, E.J. Malloy.....	141
<b>Plasma Shielding and Stability</b> E. Levi, H.W. Friedman.....	147
<b>Transient Excitation of Space Waves and Surface Waves in a Bounded, Cold Mag- netoplasma</b> L.B. Felsen, G.M. Whitman.....	151
<b>Development of a Beam Plasma Device</b> R.G.E. Hutter, H. Farber, R. Pepper, R. Eichler.....	156
<b>Internal Deflection Structures of Cathode-Ray Tubes</b> R.G.E. Hutter.....	161
<b>Study of the Radio-Frequency Mass Spectrometer</b> N.C. Peterson, P.A. Spoerri.....	167
<b>H and H<sub>2</sub> in Strong Electric Fields</b> H.J. Juretschke, A. Siatino.....	171
<b>Resonance Oscillations of Inhomogeneous Plasma Slabs</b> G. Dorman.....	179
<b>Microwave Instabilities in Semiconductor Plasmas</b> J.P. Parodi.....	183
<b>New Instabilities Due to Anisotropy in the Transverse Plane of Velocity Space</b> F.T. Stone.....	184
<b>An Investigation of VLF Hiss Emission</b> S. Gross, N. LaRocca.....	185
<b>Diffraction by Planetary Ionospheres</b> S. Gross, J. Pirraglia.....	192

## CONTENTS

### IV. SOLID STATE AND MATERIALS

Conductivity of Superconducting Tin Films at 20 GHz S. J. Freedman, R. V. D'Aiello.....	196
Fluctuation Effects in the Microwave Conductivity of Granular Superconducting Aluminum Films S. J. Freedman, R. V. D'Aiello.....	199
Thin Film Diodes M. A. Eschwei, J. Hara.....	201
Electron Shielding in Heavily Doped Semiconductors J. B. Krieger .....	206
Electrochemical Behavior of Oxide Films on Semiconductors and Metals F. C. Collins, C. Chiang, M. Schragar, L. Chen.....	207
Microwave Conductivity of Polar Semiconductors in the Presence of High Electric Field P. Das, R. H. Rifkin.....	210
Transport Properties of Compound Semiconductors at High Electric Fields R. Bharat, P. Das .....	216
Space Charge Limited Currents H. Schachter, S. Kaplan .....	219
Hot Electron Relaxation Times in Two-Valley Semiconductors and Their Effect on Bulk-Microwave Oscillators P. Das, R. Bharat .....	221
Charge-Transfer and Thermoluminescence in $CdF_2:Eu^{3+}$ E. Banks, A. Halperin, R. W. Schwartz .....	224
Magnetic Ordering in Perovskites E. Banks, N. Tashima.....	225
Dynamical Origin of Three-Dimensional Low Energy Electron Diffraction Intensities R. M. Stern, H. Taub, A. Gervais .....	226
Calculation of Activation Energies by the Half Intensity Width of Glow Curves R. Chen.....	229
Acoustoelectric Effect in Bismuth S. J. Freedman, R. C. Auger.....	234
Magnetoelastic Parametric Interactions E. S. Cassedy, C. R. Evans.....	235
The Focusing Effect induced by a D-C Driven CdS Plate W. C. Wang, P. Das.....	239
A Method for Measuring the Transducer Frequency Response of an Ultrasonic Amplifier R. Mauro.....	245

## CONTENTS

### V. CONTROL THEORY AND COMPUTER SCIENCE

Fixed Base Alignment of a Gimballess Gyroless Inertial Navigator V. Krishnan, K. Grobert .....	248
Canonical Observers in Linear Control Systems P. Dorato, M. Siswosudarmo.....	251
Optimal Bang-Bang Control of Stochastic Systems With a Small Noise Parameter P. Dorato, C. Hsieh, P.N. Robinson.....	253
Minimum Sensitivity Design of Attitude Control Systems via Lyapunov Functions P. Dorato .....	256
Modeling and Control of a Chemical Process L. Shaw, A. Kantrowitz .....	256
Variable-Length Distinguishing Sequences and Their Application to the Design of Fault Detection Experiments L. Kohavi.....	257
Design of Checking Experiments for Sequential Machines E. J. Smith, D. Farmer.....	262
Sequential Machine Identification J. Kella.....	267
The Associated Left Complete Event of a Regular Expression E. J. Smith, S. E. Gelenbe.....	269
PLAGO/360 A Load-and-Go Student Oriented PL/I Translator H. W. Lawson, Jr., S. Habib.....	272
Reliability Improvement of Digital Systems Through the Use of Majority Voters R. Bharat, B. H. Hertzendorf .....	273

### VI. COMMUNICATIONS AND INFORMATION PROCESSING

Double Error Probability in Differential FSK J. F. Oberst, D. L. Schilling.....	278
Single Channel Phase-Shift Keyed Communications J. F. Oberst, D. L. Schilling.....	281
Error Control on Real Channels J. K. Wolf, M. Muntner.....	291
High Speed Binary Data Transmission Over the Additive, Band-Limited, Gaussian Channel J. K. Wolf, L. Schiff.....	294
A Feedback Communication Scheme Based on the Kiefer-Wolfowitz Procedure R. R. Boorstyn, J. K. Wolf, R. W. Mulse.....	295
Some Results for Additive Noise Channels With Noiseless Information Feedback J. K. Wolf, T. W. Eddy.....	295

## CONTENTS

<b>Extensions of a Recursive Approach to Signal Detection</b> R. R. Boorstyn, R. L. Pickholtz.....	298
<b>Signal-Zero-Crossings as an Information Carrier</b> R. R. Boorstyn, A. L. Fawe .....	301
<b>Investigation of a Class of Nonlinear Communication Systems</b> R. R. Boorstyn, A. L. Fawe .....	308
<b>FM Noise</b> D. T. Hess, D. Yavuz.....	312
<b>An Output Signal-to-Noise Ratio Equation for the First and Second-Order Phase-Locked Loop</b> D. T. Hess, R. J. Schulman.....	316
<b>Optimizing Second-Order Phase-Locked Loop (PLL) Performance With Modulation</b> D. T. Hess, R. J. Schulman.....	323
<b>Output Signal-to-Noise Ratio of an FM Discriminator With Non-Ideal Limiting</b> D. L. Schilling, J. Refi .....	325
<b>Quantized Second Order Frequency Locked Loop</b> D. T. Hess, K. K. Clarke.....	328
<b>FM Threshold Extension Performance of the Quantized Frequency Locked Loop</b> K. K. Clarke, D. T. Hess, M. Unkauf .....	337
<b>Probability of Error Analysis for the FLL Digital Demodulator</b> K. K. Clarke, D. T. Hess, M. Unkauf .....	345
<b>Threshold Extension by Means of Spike Detection and Cancellation</b> D. L. Schilling, E. Hoffman .....	349
<b>Equivalence of FM Threshold Extension Receivers</b> D. T. Hess.....	356
<b>The Effect of a First-Order, Open Loop Holding Circuit Upon FM "Spikes" in a Video Signal</b> K. K. Clarke, F. R. Ergul.....	361
<b>Slow-Scan TV System Results</b> K. K. Clarke, F. R. Ergul.....	367
<b>Comparative TV Transmissions; Second Order Quantized Frequency Locked Loop vs. Limiter Discriminator</b> D. T. Hess, K. K. Clarke.....	372
<b>Comparison of Data Compression Schemes</b> R. R. Boorstyn, R. Stroh .....	375
<b>Optimal Adaptive Control for Data Compression Systems</b> M. Schwartz, P. Dosik .....	380
<b>Information Content of Time Series and Pictures</b> A. E. Laemmel.....	381

## CONTENTS

<b>Extremal Statistics in Computer Simulation of Digital Communication Systems</b> M. Schwartz, S. Richman.....	386
<b>Nonparametric Detection Using Extreme-Value Theory</b> D. L. Schilling, J. K. Wolf, L. B. Milstein .....	391
<b>VII. NETWORKS AND SYSTEMS</b>	
<b>Noise-Intensity Sensitivity in Optimal Stochastic Systems</b> P. Dorato .....	397
<b>System Identification</b> L. Shaw, N. N. Gupta.....	399
<b>On State Estimators for Nonlinear Systems</b> J. J. Bongiorno, Jr., Y. O. Yuksel.....	402
<b>State Estimation of a Scalar Linear System With Random Coefficients</b> R. A. Haddad, R. Fitz .....	407
<b>Minimum Sensitivity Designs</b> J. J. Bongiorno, Jr. ....	411
<b>An Application of Nonlinear Filtering to the Problem of Parameter Estimation</b> L. Shaw, B. Rubinger .....	413
<b>Computational Evaluation of Expected Performance Indices</b> L. Shaw, S. Revkin, E. Frankfort .....	415
<b>Ergodicity for Non-Stationary Processes</b> A. Papoulis.....	417
<b>Dual Optical Systems</b> A. Papoulis.....	418
<b>Interpolation With Derivatives</b> J. W. Matthews.....	422
<b>Realization of Maximum Gain RC Ladder Networks</b> H. Ruston, L. J. Degan .....	423
<b>Minimum Gyrator Synthesis</b> D. C. Youla, G. D. Ott .....	428
<b>The Maximization of Nerve Conduction Velocity</b> S. Deutsch .....	436
<b>Publications and Reports .....</b>	442
<b>New Symposium Sponsored by JSTAC .....</b>	457
<b>Distribution List .....</b>	459
<b>DD Form 1473 .....</b>	461



THE MICROWAVE RESEARCH INSTITUTE PROGRAMS  
of the  
POLYTECHNIC INSTITUTE OF BROOKLYN

Research efforts at the Polytechnic are motivated by a desire to fulfill an academic responsibility by providing a means for both faculty and graduate student body to participate in significant and fundamental research programs responsive to technological and national interests. The Microwave Research Institute Programs involve academic research activities of faculty primarily from the departments of electrical engineering, electrophysics, and physics and cover a broad spectrum ranging from basic theoretical investigations in physics, mathematics, and engineering to experimental programs involving basic measurements and the development of devices and materials. The specific structure of these programs is continually being refined; the intent here is to provide an over-all summary of some of the present activity.

It is particularly desirable to provide such a summary in annual reports to the Joint Services Technical Advisory Committee, as this permits a coherent presentation of the various phases of the Joint Services Electronics Program for the information of each of the sponsoring agencies, the Air Force Office of Scientific Research, the Army Research Office and the Office of Naval Research. The work reported is sponsored not only by the Joint Services (Contract No. AF 49(638)-1402) but also by individual contracts with various Government Agencies. The aim is to develop projects initiated under the Joint Services Electronics Program to a stature sufficient to attract individual support on their own merits, and initiate eminently deserving lines of research which cannot be accommodated within the present funding limitations. In this connection, the funding provided by the Polytechnic Institute of Brooklyn should also be mentioned, as it frequently provides for the initiation of research programs and facilities which are subsequently continued as individually-sponsored programs.

Contributions are compiled below under seven descriptive subject headings: electromagnetics and waveguide techniques; quantum electronics and optics; plasma physics and electronics; solid state and materials; control theory and computer science; communications and information processing; networks and systems.

### I. ELECTROMAGNETICS AND WAVEGUIDE TECHNIQUES

The various investigations which fall under the broad heading of electromagnetics involve the propagation, guiding, radiation and diffraction of electromagnetic waves in a large variety of environments. These include major programs in wave types near interfaces, radiation from and scattering by periodic structures, radiation from sources and scattering by obstacles in media with arbitrary properties, and a systematic exploitation of ray-optical techniques in guiding and scattering problems. Contributors to these programs have received seven prizes or awards within the past five years for the excellence of their published papers.

The program on wave types near interfaces some years ago introduced the concept of leaky waves, showed its value in the explanation of many radiation phenomena, and laid the foundations for a new class of traveling-wave antennas, the leaky-wave antenna, which permitted better agreement between theoretical and measured radiation patterns than any other type of antenna. The program led to a very general study of wave types, including several categories of complex guided waves and the lateral wave, and showed their interrelations. The lateral wave was recently shown to be the mechanism which permits most of the point-to-point communication in a jungle or forest environment. This wave in electromagnetic form has never been explicitly exhibited experimentally, however, and a project is in process which seeks to do this.

## THE MICROWAVE RESEARCH INSTITUTE PROGRAMS

The program on periodic structures has many ramifications. One phase relates to general studies of radiation from surfaces or interfaces which are modulated periodically, and in this context the Brillouin diagram for radiating periodic structures was first introduced and its usefulness clarified. This phase now includes studies of various types of log-periodic antennas and periodically-modulated slow-wave antennas. Special emphasis is placed on a new structure which is flush-mountable and can be scanned all the way from backward endfire to forward endfire. Another phase involves the study of special symmetries in periodic structures, particularly screw and glide symmetry. These symmetries permit certain mode-coupling effects to be absent; as one practical consequence, screw symmetry allows the customary pattern and impedance deterioration at exactly broadside to be avoided, thus permitting smooth scan through broadside.

Studies of scattering by periodic surfaces led to a new and physically-satisfying theory of Wood's anomalies on optical gratings, an effect which remained poorly understood for 60 years. It also is now leading to a rigorous analysis of the scattering of light by acoustically-modulated surfaces, permitting more accurate descriptions of Bragg and Raman-Nath scattering. Another study led to a new way of treating mutual coupling effects in phased arrays which takes these effects into account rigorously and automatically, and it proposed the first compensation scheme for the minimization of such effects. A current study extends this technique to the explanation of resonance effects in large phased arrays, a phenomenon that can cause the array to become unexpectedly "blind" at certain scan angles. This theoretical and experimental study seeks both a thorough explanation and methods for overcoming the problem.

The program on propagation and scattering in media with arbitrary properties was motivated by the recognition that recent technology requires a knowledge of the propagation of electromagnetic waves in physical environments of increased complexity, and of the radiation characteristics of antennas and the scattering characteristics of obstacles in these environments. Examples of such media are provided by ionized plasmas, either in the laboratory or in outer space, whose electrical properties can be described macroscopically in terms of an inhomogeneous or homogeneous isotropic dielectric, an anisotropic dielectric, or a mechanically deformable dielectric material, the choice of a particular model being dependent on the circumstances in question. In addition, turbulent processes in the medium may require the inclusion of statistical properties in its description.

When a plasma medium surrounds an antenna or a scattering object, a situation encountered when a rocket or satellite passes through the ionosphere or when a high speed vehicle re-enters the upper atmosphere, the above-mentioned processes of radiation and scattering become relevant for problems of radio communication and detection.

In order to understand the mechanism of propagation, radiation and diffraction in media having several of the complicating aspects indicated above, it is necessary to analyze first the influence of individual physical features in a particular model. Accordingly, a systematic study of selected guiding radiation and scattering problems in inhomogeneous media, in anisotropic media, in compressible plasma media, and in media with random fluctuations is being carried out within a rigorous framework. Emphasis is placed on asymptotic techniques to extract from the involved exact field expressions approximate information which permits an interpretation of, and an insight into, relevant processes in basic physical terms. In these studies, ray-optical concepts play an important role, and they also permit a generalization of the results to non-elementary structural configurations which cannot conveniently be analyzed by alternative techniques.

Recently, ray optics has also been found useful for the analysis of scattering by discontinuities in waveguides, for the description of radiating structures, and for the calculation of interaction between adjacent radiating elements. While ray optics is a discipline best suited to the determination of high-frequency effects (in a regime where the wavelength is small compared to critical structural dimensions), it has provided accurate results even at low frequencies. The careful exploration of the range of applicability of ray-optical procedures in propagation, guiding, radiation and scattering problems in a general environment provides the motivation for much of the quasi-optic

## THE MICROWAVE RESEARCH INSTITUTE PROGRAMS

phase of the electromagnetics program.

The programs in microwave technology involve studies relating to microwave components, equipment and techniques, for requirements beyond those encountered in the present microwave art. Such requirements arise in connection with a super-high-power capability, millimeter operating wavelengths, extremely short switching times, and other special response and performance characteristics. The approach is partially experimental, based on previous experience with microwave component development, and partially analytical, based on known solutions of field problems, known network-theoretic considerations or applications of new solid-state effects.

In a study on a new class of millimeter and submillimeter wavelength devices the use of neutral gases as active media is being investigated. An appreciable interaction exists between molecular electric dipole moments and electromagnetic radiation so that one-millimeter wavelength radiation will be attenuated by 15 db/inch in  $10^{-4}$  atmosphere up to several thousand GHz and it is the basis for three devices, a low noise amplifier, a calorimeter and a modulator, which at present cannot be made with either solid or fluid media.

In the multimode waveguide program, present areas of interest include selective mode-coupling control through the synthesis of transverse impedance sheets with a prescribed variation of parameters, development of new measuring techniques in a multimode environment, and application of multimode techniques to components using oversized waveguides.

Current topics of interest in the high-power area include the investigation of the interaction of high power microwaves with various media, including breakdown in gases, liquids and solids, the investigation of nonlinear phenomena such as the measurement of the electro-optic coefficient, studies of the spatial propagation of breakdown in gases, and techniques for the development of high-power waveguide components.

It has long been known that there are various biological hazards attendant on the use of high microwave power. The human is particularly sensitive in this respect. There exists, therefore, strong motivation for the establishment of tolerance limits and, ultimately, safety standards. A study of the effects of microwave radiation on the eye, employing rabbits as subjects, is being undertaken as a joint effort of the Institute and the Zaret Foundation.

## II. QUANTUM ELECTRONICS AND OPTICS

The general area of quantum electronics, which comprises that part of electronics in which quantum-mechanical effects become important, has recently received major stimulation within the Institute's electronics program by recent additions to the staff. The new program in quantum electronics and lasers consists of a number of different projects. In two of these projects, new lasers are under development whose characteristics will advance the state of the art. In various other projects, phenomena induced by lasers are being studied.

Visible and near-visible lasers with an efficiency and power comparable to the far infrared  $\text{CO}_2$  laser are still lacking. An apparatus for investigating the promising metal-vapor lasers in this connection is under construction. An eventual goal is to demonstrate the usefulness of the pulsed copper-vapor laser to gated viewing systems and holography. Under a second project, the  $\text{CO}_2$  laser will be frequency stabilized using a passive  $\text{CO}_2$  absorption cell as a reference. Factors which limit the stability of this and other stabilized lasers are being studied. Eventually, this system will be used to make fundamental and useful frequency and length measurements.

A study is underway of the feasibility of generation of very-high-temperature ( $10^8$  K) high-density plasmas by short powerful laser pulses. The goal is to make spectroscopic observations of highly-ionized heavy atoms. Specifically, if substantial numbers of one-electron ions can be produced it may be possible for the first time to measure and compare with fundamental theory hyperfine splittings and the Lamb shift in the visible part of the spectrum.

## THE MICROWAVE RESEARCH INSTITUTE PROGRAMS

The high intensities achievable in laser beams can perturb atomic energy levels and radically alter the shape and polarization of spectral lines. The theory of these phenomena has recently been worked out. Eventually, it is hoped that this interesting Stark effect at optical frequencies will be observed and compared with the theory. Another theoretical study in progress aims at understanding the irreducible quantum fluctuations always present in the output of lasers and other quantum electronic devices, from the point of view of first principles. The study will also clarify the ranges of validity of various phenomenological theories.

The program on nonlinear optics has several theoretical and experimental phases, dealing primarily with parametric processes. Recent projects have stressed the interaction of light with elastic waves, including the study of stimulated Brillouin scattering and an elastic-wave parametric amplifier using an optical idler. Theoretical studies have employed a Floquet expansion which takes all the harmonics into account, and is rigorous to within the small-signal regime. The familiar Brillouin diagram for purely spatial periodic structures has been generalized to include the time domain, and it is being used to map all possible competing interactions. The rigorous boundary-value problem for a light beam incident on an acoustically-modulated or laser-modulated medium is being solved and will be applied to a variety of cases.

New insight regarding the characteristics of optical resonators, such as those commonly employed in optical masers, has been gained from recent studies. Whereas previous work generally assumes that the medium within the resonator is homogeneous and isotropic, here the medium is treated as inhomogeneous and dispersive.

In one investigation, the effect of inhomogeneity and anisotropy in both the host and active medium of a laser cavity upon its normal (or stationary) modes was studied. A parallel development of some interest is that a refinement of simple ray optics predicted features of the electromagnetic field within optical resonators and beam waveguides previously derived from solutions of an integral equation. It may be pointed to remark that this development of ray theory benefited from the recognition of a formal analogy with microwave network theory.

The program on quantum optics has centered on free coherent radiation fields. The invariance properties of the double integral and diagonal representations of operators, in terms of the coherent states were studied. It was shown that a unique diagonal representation always exists for bounded operators, hence for every density operator, and unbounded operators which are polynomials in the boson creation and annihilation operators.

The statistical properties of the electromagnetic field are suitably studied with the aid of the quantum-mechanical correlation functions. These have been now conveniently expressed in terms of the Stokes operators.

Previous studies of the anti-correlation effect extended to the multimode fields. This repulsion effect arises in the theory because the quasi-probability functional  $P(\alpha)$  in the diagonal representation of the density measure may assume negative values over certain parts of the complex  $\alpha$  plane. Studies of interacting radiation fields are concerned with the formulation and solution of the quantum equations of motion in a multimode laser amplifier model.

### III. PLASMA PHYSICS AND ELECTRONICS

Plasmas are being studied in terms of fundamental processes and as media for the propagation of various types of waves.

Among the fundamental problems there are investigations into the initial development of gaseous discharges by time-resolved spectroscopy, and into the natures of instabilities in plasma formation, as well as into the underlying structure of the trans-

## THE MICROWAVE RESEARCH INSTITUTE PROGRAMS

port theory usually applied in plasma problems.

Other topics under investigation are the interaction of plasmas, and supersonic plasma shock waves, with microwave fields of high power, and the coupling of acoustic, electromagnetic and optical waves in various configurations. In particular, interactions between laser light and plasmas are under investigation, as well as the inverse possibility of high-temperature plasma generation by lasers.

The characteristics of dynamical processes in plasmas are being studied both theoretically and experimentally. Particular attention focuses on the investigation of equilibrium configurations and their stability, by taking the effects of nonlinearities fully into account.

The approach followed concepts of first choosing a physical model, which, while retaining the salient features of the process under consideration, is sufficiently simple that exact solutions of the nonlinear equations can be found. Then, the model is refined and approximate solutions are obtained by using a specially-developed perturbation technique. This procedure has already yielded some interesting results, such as the conditions under which the two-stream instability saturates, and its saturation level, the maximum amount of energy which can be stored at the upper hybrid frequency, the exact density profiles in plasmas confined by material walls, and the stringent compatibility conditions which govern the diffusion process and the fact that those conditions preclude the attainment of a laminar flow in the presence of appreciable magnetic fields.

The same method of attack is now being applied to more complex situations involving inhomogeneities in the statistics and in the medium, drift waves, wave-wave interactions and nonlinear Landau damping.

In the laboratory, agreement between theory and experiment has been established in the case of resistive and Rayleigh-Taylor instabilities.

A new experimental program in gaseous plasmas has been initiated which will study plasma turbulence. To meet the stringent theoretical requirements for this study, a sophisticated hollow-cathode-discharge arc system and an electrodeless plasma device using a novel rf power-coupling scheme are being built. The hollow-cathode arc is capable of producing a quiescent, marginally-collisional plasma of high density and moderate temperature. The rf-produced plasma will be a quiescent, warm, collisionless, currentless plasma of moderate density.

The fluctuation spectra will be obtained and will be related to studies of the physical mechanisms and nonlinear behavior of the plasma fluctuations. These results will be correlated with nonlinear and quasi-linear theories of plasma turbulence, with particular attention paid to the effective growth rate and possible nonlinear stabilization effects. Further, these plasmas will be used for the measurement of plasma diffusion and for studies of plasma waves.

The radiophysics of natural terrestrial and extraterrestrial phenomena is another new program area. Emphasis is on upper atmospheric and ionospheric research, solar physics and radio astronomy. Initial efforts are in ionospheric physics and solar radio physics incorporating both experimental and theoretical endeavors. In particular, current programs are concerned with the nature and physics of ionospheric irregularities and with the temporal variations of the ionosphere. An ionospheric laboratory for observational research has been started. The facility enables soundings of the ionosphere, and the data will be utilized in theoretical efforts aimed at the interpretation of irregularities and diurnal variations.

## IV. SOLID STATE AND MATERIALS

The solid state research ranges over a wide area of experimental activities encompassing the creation of new or better materials, the investigation of many specific properties of solids, and the application of these materials and effects to practical situations. In addition, there are active programs in various aspects of solid state theory.

In the area of materials development, an important sector is concerned with new

## THE MICROWAVE RESEARCH INSTITUTE PROGRAMS

magnetic compounds involving rare earth ions, and with the production of high quality ferrites in both bulk and thin film form. Programs involving thin films include the development of high mobility semiconducting layers, and the preparation of highest quality single crystal films of the noble and the ferromagnetic metals. In addition, there are systematic efforts to produce good insulating barriers on semiconductor and metal single crystal surfaces, for application in tunneling and other devices.

Among the properties of interest, those related to electromagnetic interactions play a central role. Electron transport in semiconductors is studied for hot-electron nonlinear effects, and for surface interactions. Size and surface effects in carrier transport in magnetic fields, especially as related to the band structure and to surface relaxation mechanisms, are investigated in thin films and high purity single crystals at low temperatures. One group of studies centers on the spin dependence of electrical conduction in magnetic materials, while another is concerned with the characteristics of thin tunneling junctions, either vacuum or insulating, between normal or superconducting materials. New research includes the interaction of microwaves with superconductors of granular structure and specially shaped boundaries.

Studies in magnetism include a program of ferromagnetic and spin-wave resonance in metals and ferrites aiming at clarifying the boundary conditions on the magnetization, as well as at applying the nonlinear characteristics in the resonant domain. A fundamental investigation concerns the nature of the magnetic coupling between rare-earth ions as revealed by the pressure dependence of the Curie temperature. Another study is looking at the origins of the frequency dependence of magnetic anisotropy in ferrites. A very active program in magnetic resonance of ESR and NMR is elucidating details of electronic structure in many of the materials used in other investigations.

Optical investigations include the determination of the Stark effect of excitons in alkali halides, and the systematic study of the dynamic properties of rare-earth activated phosphors, with emphasis on the mechanism of energy transfer between luminescent centers. A broad investigation of the Faraday effect in ferromagnetic metals aims at clarifying details of their band structure, especially as a function of temperature. Photoelectric emission is being carried out on pure clean single crystal surfaces, in order to analyze in detail the energy and momentum distribution of the emerging electrons. At very short wavelengths, in the X-ray region, studies are pursued on quantitative aspects of the resonant Borrmann transmission in perfect single crystals under conditions where three or more distinct beams are in strong interaction.

X-ray investigations are concerned with crystal structures, perfection, thermal effects and charge distributions in a wide range of materials. Structural surface effects and the nature of surface interactions are being studied by low-energy electron diffraction, including adsorption phenomena and epitaxial growth. The LEED program is also concerned with a series of studies, with the fundamental interactions giving rise to diffraction intensities, and with the possible effect of polarizing scattering cross sections on observed intensities.

Examples of multiple-wave interactions are being studied with the acousto-electric effect in bismuth, electron-phonon interactions in piezoelectric semiconductors, and spin-wave phonon couplings in insulators.

Theoretical studies include a fundamental program in electron-phonon interactions in magnetic fields, the investigation of transport phenomena in very anisotropic semiconductors, the theory of slow-electron scattering in solid surfaces, and the interpretation of photoelectron excitation in terms of band structure. In addition, there are calculations of the energy band structure of solids such as aluminum, at energies considerably above the Fermi level.

## V. CONTROL THEORY AND COMPUTER SCIENCE

Control systems are systems which automatically regulate anything from space vehicle guidance to traffic flow along highways. Typical of current applications under consideration are satellite attitude control and temperature control for buildings and chemical reactors.

## THE MICROWAVE RESEARCH INSTITUTE PROGRAMS

The theory of control systems can be studied apart from particular applications. Means for arriving at stable optimal performance can be studied using mathematical models. Models of current interest are defined by differential equations, especially those with stochastic parameters. Useful solutions often require research and experimentation with computational techniques.

Computational methods are also being studied for identifying and characterizing the component systems and stochastic signals which are used in the design of communication and control systems. Lack of perfect identification leads naturally to the study of means for reducing the sensitivity of system performance to unknown variations in system parameters. Component imperfections also require careful study of system reliability, and means for improving this reliability.

In addition to standard computational applications, digital computers are being used for studies of learning controllers, pattern recognition, and automatic optimization. A newly-obtained on-line experimental computer (PDP-8) is being used to process signals, i.e., perform averaging, calculate probability density, etc., obtained from laboratory experiments dealing with communications and control systems. An extended on-line computer facility is being developed for the purpose of processing data representing English text and selecting a best compression code, based upon the redundancy properties of the text.

In the area of Computer Science, several diverse activities are pursued: switching and automata theory, computer generation of sound and music, and computer languages.

Work in switching and automata has focused upon two areas: the machine decomposition problem, which explores ways of finding uniform (i.e., iterative) arrays which realize sequential machines with prescribed classes of modules or cells, and the diagnostics problem which seeks ways of designing efficient input/output testing experiments for sequential machines.

Work in computer languages presently deals with the development of microprogramming techniques; its object is to find ways of designing computers with variable instruction sets such that each set is best for some class of computational problems. A new translator for the PL/I language, called PLAGO/360, is currently under development. This project was initiated in order to provide an alternative to utilizing the IBM PL/I compiler which has an average job time of two and one-half minutes using the IBM System/360 Model 50 at the PIB Computer Center. Version I of PLAGO/360 is expected to reduce this time to approximately five seconds.

Medical Electronics, an area comprising signal analysis techniques applied to biologically-derived signals, feedback theory and analog simulation of biological systems, and specialized instrumentation for evaluation of medically-significant quantities, is being developed extensively. Particular problems include signal-flow representation of the cardiovascular system with emphasis on the study of dye dilution simulation and development of a patient-weighting device for continuous monitoring in connection with the use of an artificial kidney.

## VI. COMMUNICATIONS AND INFORMATION PROCESSING

The research program in communications and information processing covers the areas of analog and digital transmission, and the reception of signals transmitted through fading and nonfading media. The use of coding for error correction, phase-locked loops and frequency demodulators using feedback for threshold improvement, and the development of new and improved circuitry for use in all aspects of these problems are under study.

With the advent of satellite communications and deep space probes, the use of low-threshold receivers such as the phase-locked loop and frequency demodulators using feedback has become imperative. Commercial receivers commonly have thresholds of 7db. Receivers built under this program have achieved thresholds as low as 0 db. Studies concerning the effect of loop delay on threshold and the use of a phase-locked loop to detect a frequency-shift-keyed signal and for phase-shift keying are currently in progress.

## THE MICROWAVE RESEARCH INSTITUTE PROGRAMS

The response of an fm discriminator and phase-locked loop to analog and digital fm signals transmitted through fading channels is under investigation. Experimental facilities available include wideband fm generators, low-frequency white noise sources, a wideband fm discriminator, fading channel simulators and a probability density analyzer, all developed under this program. The channel simulators are capable of simulating the ionosphere or troposphere and most other frequency and time dispersive channels.

A study of traveling-wave tubes to determine distortion and multiple-access capability is also in progress.

The development of new and improved circuits for the production and detection of both analog and digital modulations is under study. Emphasis in these investigations is upon new conceptual approaches and upon circuit approaches that lend themselves to construction using integrated circuit techniques. Specific projects currently underway include three different types of wideband fm generators, a class of new wideband fm generators, a wideband PDM system, various diversity systems, as well as investigations of transistor oscillators, mixers and envelope detectors.

Modern statistical theory and its application to communication systems, signal detection and other fields is under study. Some specific projects which have been worked on include: general study of information theory; narrow-bandwidth transmission of television pictures; high-speed transmission of facsimile pictures; design of digital coding apparatus; problems involved in pulse transmission; reduction of multi-path echo distortion; application of recent statistical methods to basic communication theorems; study of abstract and practical properties of digital codes; and the optimum detection of weak signals in noise and other random interferences. One of the features of modern communication theory is the ability to define quantitatively an amount of information and a loss of information due to errors. Another feature is the consideration that a communication system must be designed to handle not one but an ensemble of signals and, therefore, a statistical approach is almost necessary.

### VII. NETWORKS AND SYSTEMS

The advent of integrated circuitry has brought the network designer face to face with problems involving the synthesis of structures containing both lumped and distributed elements. Recent studies have revealed that such (passive) networks are described by rational multi-variable positive-real functions. Conversely, this program has also succeeded in showing that such functions are realizable as driving point impedances of networks containing a finite number of the usual lumped, passive components and a finite number of ideal commensurate transmission lines operating in the TEM mode. Many of the configurations resulting from the synthesis procedure are impractical for microwave implementation. Consequently, attention is now being concentrated on filter structures of special type. One such type, involving shunt, capacitively-loaded cascaded lines, appears very promising.

The numerical difficulties involved in synthesizing complex filters are considerable. To alleviate this situation a computer-oriented algorithm has been devised for partitioning a filter into a cascade of two simpler ones. The method reduces the process to the solution of a homogeneous system of equations with constant coefficients and is easily programmed.

Also being continued is the earlier work dealing with the analysis and synthesis of large-scale systems via the state-variable approach. It appears that a minimal-gyrator synthesis for nonreciprocal, lumped, passive n-ports will soon be available.

Studies in classical network theory continue with emphasis on approximation techniques, sensitivity analysis, realistic synthesis schemes, and computer-aided design.

In another program, network and system concepts are being extended to space coordinates and applied to optics. Problems in optical filtering, image restoration, holography and apodization are being investigated. Optical processing is being used in pattern recognition.

New areas of stochastic modeling are being explored. In particular, the applications to earthquake engineering and the design of high-speed rail vehicles are being dealt with.

The theory of characteristic processes is being applied to propagation phenomena, with applications to coherence and interference.



POLYTECHNIC INSTITUTE OF BROOKLYN

E. Weber, President

F. M. Beringer, Dean of Science  
M. H. Bloom, Dean of Engineering

F. R. Eirich, Dean of Research  
A. B. Giordano, Dean of Graduate Studies

MICROWAVE RESEARCH INSTITUTE STEERING COMMITTEE

A. A. Oliner, Director

H. J. Juretschke

E. J. Smith

J. Fox

FACULTY AND RESEARCH STAFF PARTICIPATING IN  
MICROWAVE RESEARCH INSTITUTE PROGRAMS

DEPARTMENT OF CHEMISTRY

Faculty

E. Banks  
(Acting Head)

F. C. Collins

S. L. Holt

B. R. McGarvey

N. C. Peterson

Fellows and Research Associates

L. Chen

J. DeLuca

R. Poignant

N. Tashima

C. Chiang

M. Mizushima

P. A. Spoerri

DEPARTMENT OF ELECTRICAL ENGINEERING

Faculty

E. J. Smith (Acting Head)

P. Dorato

S. Maurer

A. G. Schillinger

E. J. Angelo, Jr.

R. F. Drenick

A. McKellar

H. Schlosser

P. Balaban

A. B. Giordano

E. Mishkin

J. Schwartz (visiting)

C. Belove

C. Hachemeister

M. Nalecz (visiting)

M. Schwartz

L. Bergstein

R. A. Haddad

J. F. Oberst

P. Serafim

R. Bharat

D. T. Hess

M. Panzer

S. Shapiro

J. J. Bongiorno, Jr.

D. Hunt

A. Papoulis

L. Shaw

R. R. Boorstyn

R. Karp

R. Pickholtz

M. L. Shooman

L. Braun, Jr.

J. Kella (visiting)

J. E. Rijnsdorf  
(visiting)

L. Strauss

K. K. Clarke

F. Kozin

D. Rosenbaum

J. G. Truxal

E. Coffman

V. Krishnan

A. L. Rosenberg

F. Wahlers

P. Crepeau

H. W. Lawson

H. Ruston

W. C. Wang

J. Crump

A. Levis

H. Schachter

G. Weiss

P. Das

W. A. Lynch

D. L. Schilling

J. K. Wolf

S. Deutsch

L. Magid

DEPARTMENT OF ELECTRICAL ENGINEERING

Research Associates and Instructors

B. Berenstein	S. M. Finkelstein	M. Messinger	G. Schuster
P. Bertrand	S. Habib	M. Miller	F. T. Stone
C. H. Chi	E. Hoffman	J. P. Parekh	D. A. Weigel
D. Doucette	R. Kapash	R. Rifkin	A. Weis
D. Farmer	J. W. Matthews	G. Sarma	R. Yager

Research Assistants, Trainees, Fellows and Graduate Assistants

M. E. Arkun	S. Gelenbe	D. Mayer	C. L. Song
A. R. Basilico	J. Gilchrist	W. R. McShane	R. Stroh
J. M. Bauza	S. Goldstein	S. Mehra	P. W. Staecker
P. Berman	N. N. Gupta	L. B. Milstein	T. S. Sundresh
S. Billis	J. Hadjiligiou	M. Muntner	R. Teich
H. Blum	B. R. Horowitz	L. M. Orloff	N. Tepedelenlioglu
R. F. Botta	A. Hussein	P. W. Osborne	P. Trentacoste
R. Breschi	C. Kaman	S. F. Rashba	M. Unkauf
B. J. Bunin	A. Kantrowitz	S. B. Revkin	S. Wainberg
F. Cassara	S. Kaplan	S. Richman	E. Walvick
C. M. Charles	R. C. Kavee	B. Rubinger	W. E. Weiler
C. Y. Chiang	A. Kestenbaum	V. Sahni	J. Wilkes
R. R. Clarke	I. Kohavi	R. A. Schlueter	L. P. Winkler
E. DeLoatch	O. S. Kosovych	E. Schroepel	O. M. Wu
C. Devieux	G. Krishnamurti	R. J. Schulman	E. A. Yanchak
J. Disabato	J. M. L. Lam	R. Schultz	D. Yavuz
K. Dougherty	A. Levy	Z. A. Simic	M. Yogev
H. A. Edels	E. J. Lancevich	I. M. Singh	Y. Yuksel
C. R. Falchetti	H. D. MacMillian	M. Somin	F. Zak
A. Fawe	R. Mauro	A. J. Snyder	I. Zaslou
R. Fitz			

DEPARTMENT OF ELECTROPHYSICS

Faculty

A. A. Oliner (Head)	J. W. E. Griemsmann	A. E. Laemmel	S. W. Rosenthal
H. L. Bertoni	S. H. Gross	J. T. LaTourrette	B. Senitzky
E. S. Cassedy, Jr.	A. Hessel	L. Levey	J. Shmoya
K. Chung	R. G. E. Hutter	E. Levi	L. M. Silber
H. Farber	W. K. Kahn	R. C. M. Li	M. Sucher
L. B. Felsen	G. H. Knittel	S. Rosenbaum	T. Tamir
G. Gould			D. C. Youla

**DEPARTMENT OF ELECTROPHYSICS**

Research Scientists

M. C. Newstein                      N. Solimene                      W. T. Walter

Research Associates and Instructors

L. Birenbaum                      D. Jacenko                      P. Rabinowitz                      P. Tissi  
M. A. Eschwei                      R. Pepper                      B. Rudner

Research Assistants

C. Clarke                      E. J. Malloy                      K. Stuart

Postdoctoral Fellows

J. Bach Andersen                      S. Iiguchi                      K. Mikoshiba                      S. T. Peng  
A. Csurgay                      S. Przedziecki

Fellows, Trainees and Graduate Assistants

L. Assadourian	E. Fitzgerald	I. Kupiec	G. Quigley
G. Bein	H. Friedman	R. Lang	J. W. Ra
M. H. Chen	S. Gaglione	N. LaRocca	C. V. R. Rao
S. Chew	L. Geller	G. Louie	C. H. Shih
S. Chi	J. Gladstone	M. Lubelski	L. Silverstein
T. M. Chien	I. Haber	T. McNamary	H. Stalzer
R. Chimenti	S. Harrison	M. Mazzocchi	E. Torrero
C. H. Chiou	H. C. Huang	M. Narcowich	G. M. Whitman
S. Choudhary	H. Jo	G. D. Ott	N. Wright
R. S. Chu	C. Jung	B. Perry	A. Yanez
R. Eichler	R. Keller	M. Piltch	H. Y. Yee
H. J. Eun	R. T. Kihm	J. Pirraglia	K. Yen
C. R. Evans	W. C. Ko	G. Pisano	Y. B. Yu
P. Fenster	T. Y. Kou		

**DEPARTMENT OF MATHEMATICS**

Faculty

H. Hochstadt (Head)                      L. Zauderer

**DEPARTMENT OF PHYSICS**

Faculty

H. J. Juretschke (Head)	S. J. Freedman	M. Menes	H. W. Schieuning
D. S. Boudreaux	J. B. Krieger	B. Post	R. M. Stern
R. Chen	L. B. Mendelsohn	D. B. Scarl	D. Stoler
G. Dorrman			N. Wainfan

DEPARTMENT OF PHYSICS

Research Scientist

S. R. Barone

Research Associates

A. Gervais

K. Kanematsu

Graduate Assistants, Fellows and Trainees

F. Allario

G. Haber

L. Indyk

M. Stevens

G. T. Alfieri

J. Hara

W. Moller

H. Taub

R. C. Augeri

V. Hoffstein

J. S. Punturieri

## I. ELECTROMAGNETICS AND WAVEGUIDE TECHNIQUES

Bertoni, H. L.	Hessel, A.	Louie, G.	Sentizky, B.
Birenbaum, L.	Jacenko, D.	Maurer, S.	Serafim, P.
Cassedy, E. S.	Kahn, W. K.	Mazzocchi, M.	Shmoys, J.
Chen, M. H.	Kaplan, I. T.	Metlay, W.	Singer, B.
Choudhary, S.	Kihm, R. T.	Oliner, A. A.	Sucher, M.
Chu, R. S.	Knittel, G. H.	Przedziecki, S.	Tamir, T.
Clarke, C.	Kupiec, I.	Ra, J. W.	Tseng, D. Y.
Crepeau, P.	Lang, R.	Rosenbaum, S.	Wasyliwskyj, W.
Felsen, L. B.	Levey, L.	Rosenthal, S. W.	Yee, H. Y.
Griemsmann, J. W. E.	Li, R. C. M.	Schmidt, H.	Zaret, M. M.
			Zauderer, E.

### ELEMENT-PATTERN NULLS IN PHASED-ARRAY ANTENNAS: THEORETICAL STUDY G. H. Knittel, A. Hessel and A. A. Oliner

A considerable amount of progress in understanding the "unusual" element-pattern null effect in phased-array antennas has been made in the past year. An example of a measured element pattern (the radiation pattern of one element in the array with all others terminated) exhibiting this unusual null is shown in Fig. 1. This figure plots the element pattern gain in dB versus angle from broadside,  $\theta$ . It was published by Diamond<sup>1</sup> and was measured with an array of rectangular waveguide in a triangular grid ("brick" array). Notice that the pattern has a null at an angle substantially closer to broadside

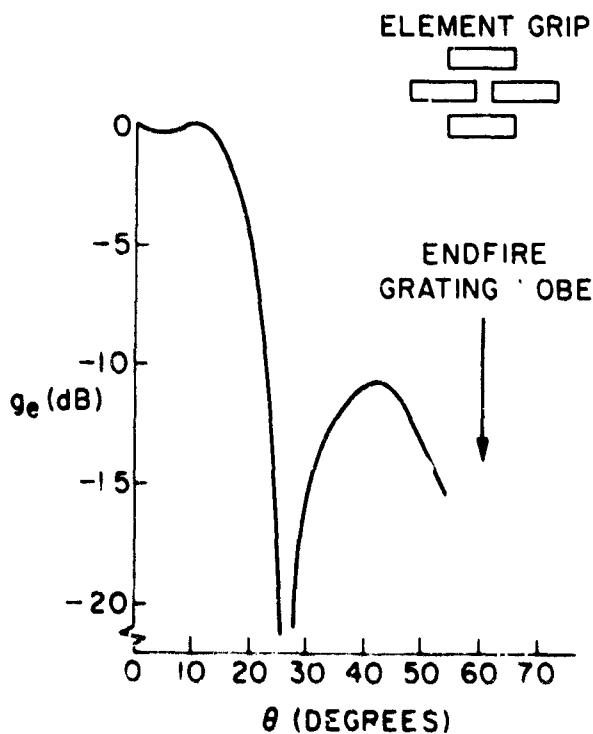


Fig. 1 Measured Element Pattern, H Plane, "Brick" Array (from Diamond)

than that for which an endfire grating lobe can exist (when all elements are excited)<sup>2, 3, 4</sup>. Although the possibility of such a null was expected at the latter angle, it was not expected at angles closer to broadside and is in this sense "unusual".

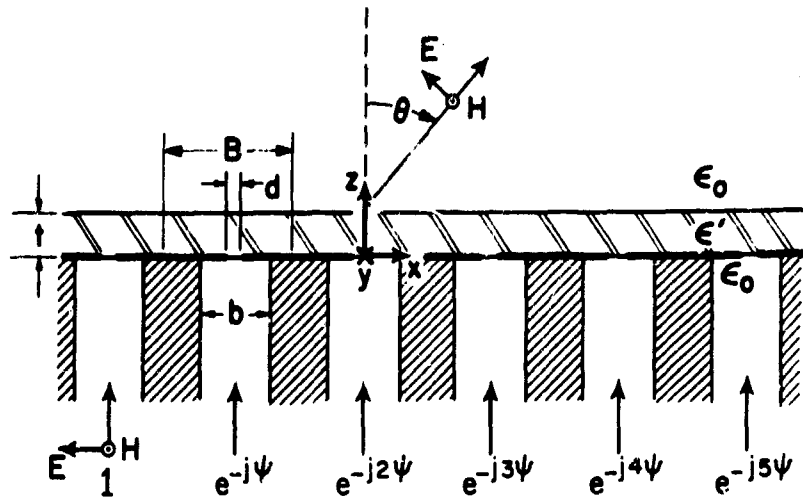
It is well known that the element-pattern null is directly related to a complete-reflection condition which exists in the array when all the elements are excited. At this precise complete-reflection condition, one finds that the fields on the surface of the array have a surface-wave-like character.

A null in the element pattern of an array is extremely serious since the gain of the array at a particular scan angle is proportional to the element pattern gain at that angle, and the array is blind at those angles for which the element pattern has a null. This blindness manifests itself by a complete reflection of the incident power in the array. It is of great importance to a phased-array radar that this phenomenon be avoided within the design scan volume. The present study is intended to accomplish this by attaining an understanding of the phenomenon, conditions under which it may exist, and means by which it may be avoided.

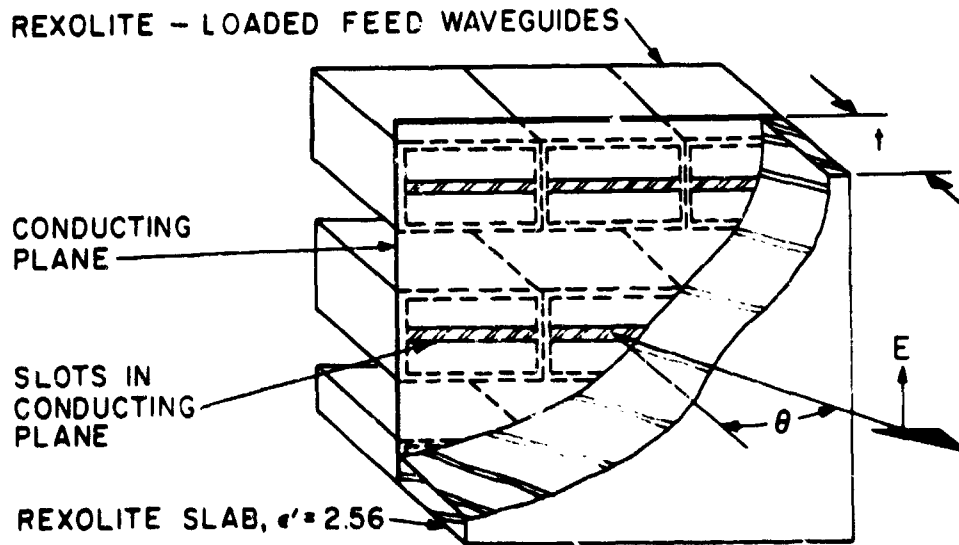
In a comprehensive theoretical study of the phenomenon, three different infinite phased-array structures have been examined. One of these is the brick array scanned in the H plane, for which a measured element pattern is shown in Fig. 1. This array is designed to work with the dominant ( $TE_{10}$ ) mode in the waveguides; it has no dielectric loading either inside or outside the waveguides.

The other two structures studied theoretically are shown in Fig. 2. The two-dimensional array of slots in a conducting plane (Fig. 2(a)) is fed by TEM modes in parallel-plate waveguides and is scanned in the E plane. The array is covered by a dielectric slab. The initial study of this structure was done for the case in which the aperture widths,  $d$ , are small. This permits the representation of the aperture electric field by the dominant mode of the aperture and enables one to derive a simple equivalent network for the array. This network has been used to determine much of the behavior of the null phenomenon by inspection<sup>5</sup>, and to show the relation between the phenomenon and the forced resonance of a higher mode in the dielectric. A further study of the structure for wider apertures utilized a more sophisticated technique in which the aperture electric field was represented by the first two or three lowest-order modes of the aperture. In this case the detailed behavior of the null was found to be somewhat different from that in the narrow-aperture case, but many of the essential features were the same.

The array of slots in a rectangular grid (Fig. 2(b)) is fed by  $TE_{10}$  modes in rectangular waveguide and is scanned in the H plane. The height of the slots may be varied from very small to a height equal to that of the feeding waveguides. A dielectric slab covers the array; the feed guides are also loaded with dielectric so that the  $TE_{10}$  modes are not too close to cutoff.



(a) Two-Dimensional Array of Slots Covered by a Dielectric Slab



(b) Array of Slots in a Rectangular Grid Covered by a Dielectric Slab

Fig. 2 Two Structures which Exhibit the Element-Pattern Null Phenomenon

The theoretical study of the aforementioned structures was usually done by approximating the aperture electric field with the two lowest-order modes of the aperture. The ratio of the two modal voltages is then determined from the Galerkin method (of solution

of integral equations) thus specifying the shape of the aperture field at all scan angles. The aperture field shape is then used in a positive-real expression for array admittance  $Y$ , derived by requiring conservation of the complex power across the aperture plane. The array reflection coefficient and element pattern are then computed from  $Y$  by standard relationships.

From the above study of various array structures it has been concluded that the unusual element-pattern null is caused by the presence of a leaky wave in the structure<sup>6</sup>.

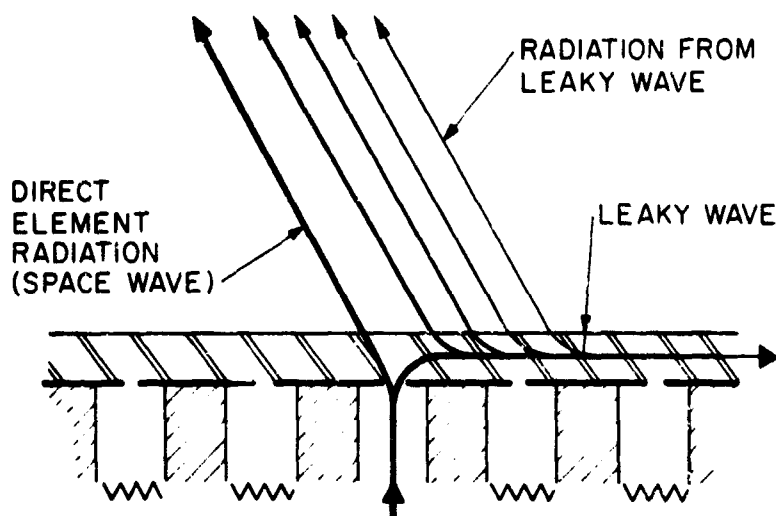


Fig. 3 Sketch showing Interference between Direct Element Radiation and that from Leaky Wave to Produce Element-Pattern Null on Left Side of Pattern

The way in which this leaky wave causes the null is illustrated in Fig. 3. The direct radiation from the element is exactly cancelled by that from the leaky wave which is supportable by the array. The attenuation constant of the leaky wave determines the width of the null.

As mentioned earlier, when all the elements of the array are excited, as in radar operation, the element-pattern null manifests itself as a complete reflection of the incident power. This is brought about by a cancellation of coupling from the dominant mode of the aperture field to the radiating mode in space by coupling from the higher modes of the aperture field. Thus the radiating mode in space is not excited and therefore the conductance of the array admittance becomes zero at the resonant or complete-reflection condition.

The above characteristics of the phenomenon identify it as a relative of the famous Wood's anomaly on optical reflection gratings<sup>7</sup>. This phenomenon has been long known (since 1902) on optical gratings but has apparently been only recently observed on



microwave transmission gratings, with the much increased use of phased-array antennas.

Joint Services Technical Advisory Committee  
AF 49(638)-1402

G. H. Knittel

#### REFERENCES

1. B. L. Diamond, "Resonance Phenomena in Waveguide Arrays," IEEE G-AP International Symposium Digest, Oct. 1967, pp. 110-115.
2. C. P. Wu and V. Galindo, "Surface Wave Effects on Dielectric Sheathed Phased Arrays of Rectangular Waveguide," The Bell System Technical Journal, Vol. 47, Jan. 1968, pp. 117-142.
3. G. F. Farrell, Jr. and D. H. Kuhn, "Mutual Coupling in Infinite Planar Arrays of Rectangular Waveguide Horns," IEEE Trans. Antennas and Propagation, Vol. AP-16, No. 4, (July 1968), pp. 405-414.
4. C. P. Wu and V. Galindo, "Surface Wave Effects on Phased Arrays of Rectangular Waveguides Loaded With Dielectric Plugs," IEEE Trans. Antennas and Propagation, Vol. AP-16, No. 3, (May 1968), pp. 358-360.
5. G. H. Knittel, A. Hessel and A. A. Oliner, "Element-Pattern Nulls in Phased Arrays and Their Relation to Guided Waves," to be published in Proc. IEEE, (special issue on Electronic Scanning) scheduled for Nov. 1968.
6. A. Hessel, G. H. Knittel and A. A. Oliner, "On the Theory of Resonances in Phased-Array Antennas," URSI Fall Meeting Digest, p. 62, Oct. 1967.
7. A. Hessel and A. A. Oliner, "A New Theory of Wood's Anomalies on Optical Gratings," Applied Optics, Vol. 4, No. 10, Oct. 1965.

#### ELEMENT-PATTERN NULLS IN PHASED-ARRAY ANTENNAS: EXPERIMENTAL CONFIRMATION IN A WAVEGUIDE SIMULATOR

G. H. Knittel, A. Hessel and A. A. Oliner

In order to experimentally confirm some of the preceding theoretical study, the measured performance of the array in Fig. 2(b) of the preceding section was obtained by simulating the array in a waveguide simulator<sup>1</sup>. This device precisely simulates an infinite array with an array of only a few elements by imaging in the walls of a waveguide: the simulation is valid at a particular set of frequencies and scan angles determined by the mode which is used in the simulator waveguide.

In the present case, only 1-1/2 elements of the array were constructed in order to simulate the array at a scan angle of about  $38^\circ$  in the H plane, with element spacing of about 0.52 wavelengths<sup>2</sup>. An exploded view of the simulator is shown in the photograph in Fig. 1. Standard L-band waveguide connects to a dielectric-loaded transformer (shown in the figure) which connects to a half-height feed waveguide. (The



Fig. 1 Exploded view of Waveguide Simulator for Array in Fig. 2(b) of the preceding section showing Rexolite-Loaded Feed Waveguides, Slot Plate, Rexolite Slab, and Simulator Waveguide

adjacent half-height, half-width feed guide is truncated a short distance behind the aperture since it has no propagating modes.) A separate slot plate covers the feed guides so as to permit control of the height of the radiating slot. The rexolite slab adjoins the slot plate and is enclosed by the simulator waveguide. An air-filled waveguide taper (not shown) connects the simulator waveguide to standard L-band guide. Measurements of the reflection and transmission coefficients of the structure were made by exciting the L-band guide behind the aperture in the  $TE_{10}$  mode and then varying frequency. At each frequency, the simulator exactly represents the infinite array at a different scan angle.

A comparison of the theoretical and experimental performance of the array of Fig. 2(b) of the previous section is given in Fig. 2 for the case in which the height of the slots is equal to that of the feed waveguides. Notice the agreement between the measured and computed performance, especially at the complete-reflection (or resonance) condition  $f = 1.370$  GHz. The measurements thus confirm the adequacy of the

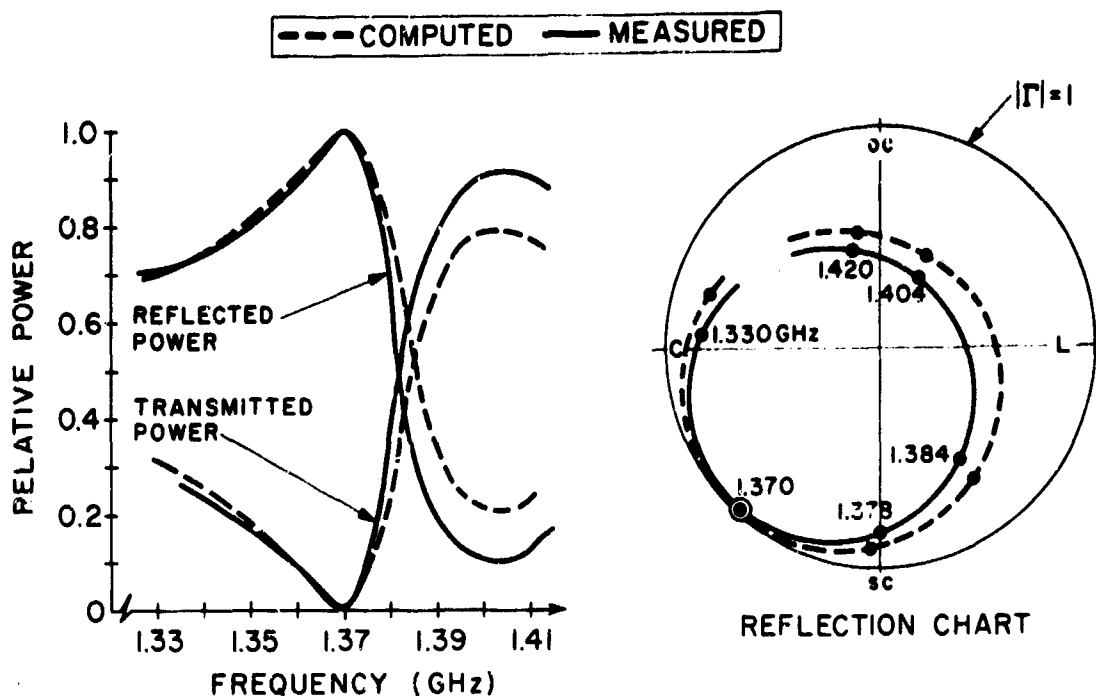


Fig. 2 Performance of Array in Fig. 2(b) of the preceding section with Open-Ended Feed Waveguides

two-mode field approximation used in the computations and also show, for the first time, that the phenomenon is indeed characterized by a complete reflection (magnitude of reflection coefficient greater than  $0.99$ )<sup>2</sup> of the incident power in an infinite array.

Additional measurements were made in the simulator for the case of narrow height slots. In these cases, the frequency for resonance and the value of reflection coefficient at resonance agreed well with theoretical predictions but the reflection curve off resonance was different than the theoretical curve. This difference is probably due to a loss observed in the measurements which becomes greater as the slots are made narrower. For very narrow slots, this loss amounts to as much as 30% of the incident power. Special precautions were taken in the measurements to ensure that the loss was not caused by poor contact between the various waveguide components. It appears, rather, that the loss is caused primarily by dissipation in the slot plate and is therefore present in an actual array as well as in the simulator. The presence of this loss is important, and should probably be taken account of in future theoretical studies and in computations of the element-pattern null phenomenon.

## REFERENCES

1. P. W. Hannan and M. A. Balfour, "Simulation of a Phased-Array Antenna in Waveguide", IEEE Trans. Antennas and Propagation, Vol. AP-13, May 1965, pp. 342-353.
2. W. S. Gregorwich, A. Hessel, G. H. Knittel and A. A. Oliner, "A Waveguide Simulator for the Determination of a Phased-Array Resonance", IEEE G-AP International Symposium Digest, September 1968, pp. 134 - 141.

## INTERRELATIONS AMONG MUTUAL COUPLING, ELEMENT EFFICIENCY AND ACTIVE IMPEDANCE IN LINEAR ARRAYS

W. K. Kahn and W. Wasylkiwskyj

We present a systematic formulation of the interrelationships among mutual coupling, element efficiency and active impedance for infinite (uniformly spaced) linear arrays. These relations are formally deduced from an (infinite order) difference equation.

Of this list of important array parameters only the element efficiency requires special introduction. In his analysis of mutual coupling effects in infinite arrays, Hannan<sup>1</sup> introduced this element efficiency, which may be defined as the ratio of power radiated by an element in the terminated array environment and the power available at an element. This quantity is a gross measure of mutual coupling effects and mismatch in the active array. There exists an upper bound on this efficiency (necessary mutual coupling effects), which is a function of array geometry only. Calculations of this bound for linear and various planar arrays were published recently<sup>2</sup>.

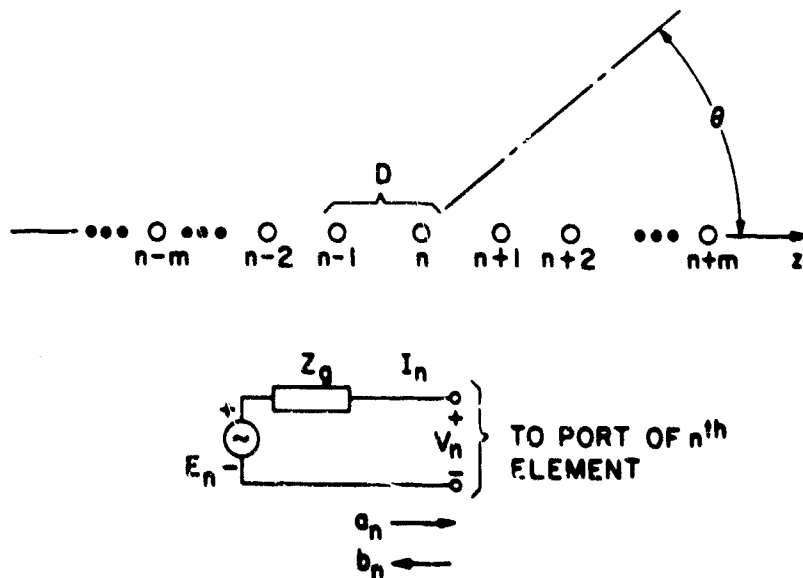


Fig. 1 Infinite Linear Array

An infinite linear array is composed of identical equally spaced reciprocal elements as shown in Fig. 1. Each element is driven by a voltage generator  $E_n$  with internal impedance  $Z_g$ . The elements of the (infinite dimensional) open-circuit impedance matrix

$$z_{\nu} = z_{-\nu} = \frac{V_{n+\nu}}{I_n} \Big|_{I_{n+\nu} = 0, \nu \neq 0} \quad (1)$$

are independent of  $n$  in view of the symmetry of the array. The port voltages of the array are therefore related to the port currents  $I_n$  by the infinite order difference equation

$$\lim_{N \rightarrow \infty} \sum_{\nu=-N}^{\nu=N} z_{\nu} I_{n+\nu} = V_n \quad (2)$$

It is convenient to employ a scattering description in terms of incident and reflected wave amplitudes normalized to the complex impedance  $Z_g = R_g + jX_g$ ,

$$2\sqrt{R_g} a_n = V_n + Z_g I_n \quad (3a)$$

$$2\sqrt{R_g} b_n = V_n - Z_g^* I_n \quad (3b)$$

The elements of the scattering matrix relating these wave quantities  $S = [S_{mn}]$  then have the usual physical interpretation of transducer power gain.

Let the  $m^{\text{th}}$  array element be excited by a unit amplitude incident wave. Then the currents satisfy

$$\lim_{N \rightarrow \infty} \sum_{\nu=-N}^{\nu=N} z_{\nu} \hat{I}_{n+\nu m} + Z_g \hat{I}_{nm} = 2\sqrt{R_g} \delta_{mn} \quad (4)$$

The solution of this equation can be written as

$$\hat{I}_{nm} = \frac{1}{2\pi} \int_{-\pi}^{\pi} \frac{2\sqrt{R_g} e^{-j(n-m)\xi}}{Z_g + Q(\xi)} d\xi \quad (5)$$

where

$$Q(\xi) = \lim_{N \rightarrow \infty} \sum_{\nu=-N}^{\nu=N} z_{\nu} e^{-j\nu\xi} \quad (6)$$

By superposition, the current due to arbitrary incident waves  $a_m$  are then

$$\begin{aligned}
 I_n &= \sum_{m=-\infty}^{\infty} \hat{I}_{nm} a_m \\
 &= \frac{1}{2\pi} \int_{-\pi}^{\pi} d\xi e^{-jn\xi} \left( \frac{2\sqrt{R_g} \sum_{m=-\infty}^{\infty} a_m e^{jm\xi}}{Z_g + Q(\xi)} \right) .
 \end{aligned} \tag{7}$$

When the excitation

$$a_m = e^{-jma} \tag{8}$$

is prescribed at each element the sum in the numerator of Eq. (7) can be replaced by the delta function  $2\pi \delta(\xi - \alpha)$ , and integration yields the currents

$$I_n(\alpha) = \frac{2\sqrt{R_g} e^{-jn\alpha}}{Z_g + Q(\alpha)} . \tag{9}$$

Direct calculations based on the equivalent circuit given in Fig. 1 with  $E_n = 2\sqrt{R_g} e^{-jn\alpha}$  identifies  $Q(\alpha)$  as the input impedance to an element in the array excited with uniform amplitude and phase progression, Eq. (8). The (open circuit) mutual impedances are coefficients in the complex Fourier expansion of the active impedance obtained with this excitation. The active reflective coefficient is

$$\rho(\alpha) = \frac{Q(\alpha) - Z_g^*}{Q(\alpha) + Z_g} . \tag{10}$$

The active reflection coefficient seen at any one antenna port (say, the  $m^{\text{th}}$ ) is the sum of the ordinary reflection coefficient at the  $m^{\text{th}}$  port plus the contributions from all the remaining elements

$$\rho(\alpha) = \sum_{n=-\infty}^{\infty} S_{mn} e^{-jn\alpha} . \tag{11}$$

Thus, the normalized mutual scattering parameters are also the Fourier expansion coefficients of the active reflection coefficient Eq. (10).

On comparing excitation  $E_n$  and response  $I_n$ , Eq. (9), in respect of their dependence on the index  $n$ , uniform amplitude and linear phase variation is identified as the eigen-excitation of the array. This characteristic form results from the symmetry of the array, and is independent of the particular values of  $\alpha$ , which of course derive from a

particular form of element. As previously pointed out in connection with finite arrays<sup>3</sup>, for eigen-excitations the radiation pattern obtained from an array is undisturbed by mutual coupling, i. e., the normalized pattern is precisely the same as would be calculated from a zero order calculation in which mutual coupling is neglected. The point just made is crucial. It extends the correspondence in scan space of visible and invisible regions for a particular phase progression of impressed antenna currents to a rigorous correspondence for a particular phase progression of antenna excitations by generators with finite internal impedance in which normally mutual coupling would be expected to play a role.

The overall effect of mutual coupling on array performance is measured by the element efficiency  $\eta$ , defined as the ratio of the realized gain to the directive gain of an element in the terminated array environment. This is equivalent to the ratio of the power actually radiated by an element in the terminated array environment to the power available at an element. For an array of lossless antennae,

$$\eta = \frac{P(\text{radiated})}{P(\text{available})}; \quad (12a)$$

$$= 1 - \sum_{m=-\infty}^{\infty} |S_{nm}|^2; \quad (12b)$$

$$= 1 - \frac{1}{2\pi} \int_{-\pi}^{\pi} |r(\alpha)|^2 d\alpha; \quad (12c)$$

$$= \frac{2R_g}{\pi} \int_{-\pi}^{\pi} \frac{R_e Q(\alpha)}{|Z_g + Q(\alpha)|^2} d\alpha. \quad (12d)$$

As is evident from Eq. (12b) the element efficiency is a definite measure of the strength of mutual coupling. The stronger the mutual coupling among the elements of the array, the smaller is the value of the element efficiency. The formula (12c) for  $\eta$  follows directly from Eq. (12b) and the expression Eq. (11) for  $r(\alpha)$ ; (1) is simply multiplied by its conjugate and the resulting series integrated over a fundamental interval in  $\alpha$ . It is evident from (12c) that the element efficiency is a measure of the active reflection coefficient magnitude, excitation Eq. (8), averaged over a fundamental interval in  $\alpha$ . It may be objected that, since  $|r(\alpha)|$  is necessarily unity over portions of the interval  $-\pi < \alpha < \pi$  for which all radiation lobes are in the invisible region, the element efficiency does not represent an appropriate measure of  $|r(\alpha)|$  over the scan range of interest, i. e., the values of  $\alpha$  for which a real radiated beam exists. This objection is removed by normalizing the element efficiency to the ideal or maximum element efficiency  $\eta_0$  which accounts

for just this feature. For  $0 < kD < \pi$  the quantity

$$1 - \frac{\eta}{\eta_i} = \frac{1}{2kD} \int_{-kD}^{kD} |\rho(\alpha)|^2 d\alpha \quad (13)$$

is the active reflection coefficient squared averaged over the visible region alone.

The formula Eq. (12d) follows from Eqs. (12c) and (10). Provided no grating lobes enter, i. e., provided  $0 < kD < \pi$ , the limits  $-\pi$  to  $+\pi$  in Eq. (12d) may be replaced by  $-kD$  to  $+kD$ . When the radiated power in Eq. (12a) is written as an integral over the element pattern in the terminated array environment, comparison with Eq. (12d) leads directly to the  $\text{Re}Q(\alpha)$  as a function of  $\alpha$ .

The significant interpretation of the element efficiency in terms of the active reflection coefficient of arrays excited by generators with uniform amplitude and linear phase may be broadened somewhat. Formulas (12c) and (12d) still follow even if the relative phases of the generators are modified by arbitrary increments  $\delta_n$ , dependent on the element but independent of scan angle  $E_n = 2\sqrt{R_g} e^{-jn\alpha + j\delta_n}$ . Under these circumstances the active reflection coefficient should take on new values  $\rho'_n(\alpha)$  as a function of scan, but still have the same mean-square value over a fundamental interval  $-\pi < \alpha < +\pi$ . A case of practical interest consisting of alternate elements fed through polarity reversal transformers, corresponds to

$$\begin{aligned} \delta_n &= 0, \quad n \text{ even;} \\ &= \pi, \quad n \text{ odd.} \end{aligned}$$

Of course, this special case can alternatively be viewed in more conventional terms as shift in origin  $\alpha = \alpha' + \pi$ , and the same conclusion drawn. Further details and extensions of this work are contained in Refs. 4-7.

Joint Services Technical Advisory Committee  
AF 49(638)-1402

W. K. Kahn

#### REFERENCES

1. P. W. Hannan, "The Element-Gain Paradox for a Phased Array Antenna," IEEE Transactions on Antennas and Propagation, AP-12, 4, pp. 423-433 (July 1964).
2. W. K. Kahn, "Ideal Efficiency of a Radiating Element in an Infinite Array," IEEE Transactions on Antennas and Propagation, AP-15, 4, pp. 534-538 (July 1967).
3. W. K. Kahn and W. Wasylkiwskyj, "Coupling, Radiation and Scattering by Antennas," Proceedings Symposium on Generalized Networks, Vol. XVI, Polytechnic Institute of Brooklyn, April 1966.
4. W. K. Kahn and H. Kurs, "Minimum Scattering Antennas," IEEE Transactions on Antennas and Propagation, AP-13, 5, pp. 671-675 (September 1965).



5. W. Wasykiwskyj and W. K. Kahn, "A Formulation of the Interrelation Among Mutual Coupling, Element Efficiency, Active Impedance and Patterns in Linear Arrays," (to be published in *Alta Frequenza*).
6. W. Wasykiwskyj and W. K. Kahn, "Mutual Coupling and Element Efficiency for Infinite Linear Arrays," (to be published in *Proceedings IEEE*).
7. W. Wasykiwskyj, "A Network Theory of Coupling, Radiation and Scattering by Antennas," Dissertation for the Degree, Ph. D., (E. E.) Polytechnic Institute of Brooklyn, June 1968.

#### ON THE PROPAGATION CHARACTERISTICS OF PERIODIC, SCREW-SYMMETRIC TRAVELING-WAVE STRUCTURES

A. Hessel and M. H. Chen

The Brillouin ( $kd - \hat{\beta}d$ ) diagrams of periodically-loaded waveguides normally exhibit stop bands at values of the phase delay per period,  $\hat{\beta}d$ , equal to an integral multiple of  $\pi$ . When, in addition to periodicity, other symmetries are present, some of the stop bands may be eliminated<sup>1, 2, 3</sup>. This becomes important in applications to radiating structures such as traveling-wave arrays or log-periodic antennas. In the former case, the appearance of a stop band may delimit the scan range; in the latter the wide-band operation may be impaired. Examples of such symmetries are, in crystal terminology, the glide-reflection-symmetry and the screw-symmetry. A glide-reflection-symmetric structure remains invariant with respect to an operation consisting of a translation by half its geometric period  $d$ , followed by a reflection with respect to a glide plane. A periodic structure is said to possess an  $N$ -fold screw axis when it remains invariant with respect to the screw-symmetry operation  $S_N$  consisting of a translation by  $\frac{d}{N}$ , followed by a rotation of  $\frac{2\pi}{N}$  radians. Figure 1 shows a circular waveguide, periodically loaded with irises and possessing a 3-fold screw axis. An important step towards understanding the role of symmetry in the formation of  $kd - \hat{\beta}d$  diagrams of periodic guiding structures was made in Ref. 1. However, due to limitations in the method of analysis employed, these results are incomplete in the case of screw-symmetry and do not apply to cases for which two degenerate, cross-polarized modes are present in an empty guide. Such a situation always arises in a circular or coaxial geometry, when the empty waveguide mode is not of the angularly symmetric variety.

The following is a description of an approach that permits a systematic prediction of the qualitative form of the Brillouin diagram of screw-symmetric closed-waveguide structures. The approach is based on Pierce's mode-coupling principle, applied to a suitable set of empty waveguide modes. The open-structure cases will not be considered now, although the basic method is still applicable.

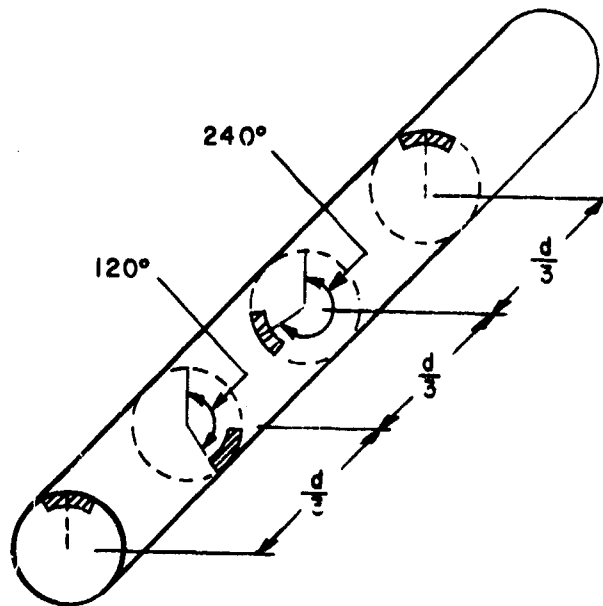


Fig. 1 Periodically Iris-Loaded Circular Waveguide with a 3-Fold Screw Axis

**The Generalized Floquet Theorem:**

In the case of a periodic structure with an  $N$ -fold screw axis, the Brillouin diagram is most clearly exhibited in terms of the screw-symmetry operator  $S_N$  wavenumber spectrum arising from the solution of an eigenvalue problem for the electromagnetic field  $\underline{\psi}$

$$S_N \underline{\psi} = s_N \underline{\psi} = e^{-j\hat{n} \frac{d}{N}} \underline{\psi} . \quad (1)$$

The eigenvalue problem Eq. (1) is referred to as the Generalized Floquet's Theorem and replaces the usual Floquet's Theorem as expressed in the eigenvalue problem for the translation operator  $T_d$ , i. e.,

$$T_d \underline{\psi} = e^{-j\hat{n} d} \underline{\psi} . \quad (2)$$

The interpretation of Eq. (1) is that, in going from one observation point to another, spaced by  $\frac{d}{N}$  and rotated by  $\frac{2\pi}{N}$  radians, the modal field  $\underline{\psi}$  on a structure with an  $N$ -fold screw axis multiplies itself by a complex constant  $e^{-j\hat{n} d}$ .

Consider the analysis of the propagation characteristics of a traveling-wave, periodic structure possessing an  $N$ -fold screw axis. A full utilization of symmetry at the onset of the analysis brings about a considerable simplification and, more importantly, permits

a simple deduction of a scheme for the determination of the qualitative form of the Brillouin diagram of the structure. To take advantage of the symmetry, one introduces at periodic intervals,  $\frac{d}{N}$  apart along the waveguide axis  $z$ , different coordinate systems in the  $xy$  plane, each frame rotated by an angle  $\frac{2\pi}{N}$  radians with respect to its predecessor. This set of coordinate systems has the identical symmetry as that of the traveling-wave structure. Along with each coordinate system one introduces a suitable modal vector basis of a form which is invariant under rotation. The transformation between the neighboring modal basis is expressed in terms of a rotation matrix ( $R$ ). The virtue of this transformation of the modal basis is that in terms of its own modal basis the description of every section of length  $\frac{d}{N}$  of the structure is the same. Hence, the modal voltage-current relation sampled at periodic intervals,  $\frac{d}{N}$  on the traveling wave periodic structure with an  $N$ -fold screw axis, may symbolically be represented in terms of an iterative

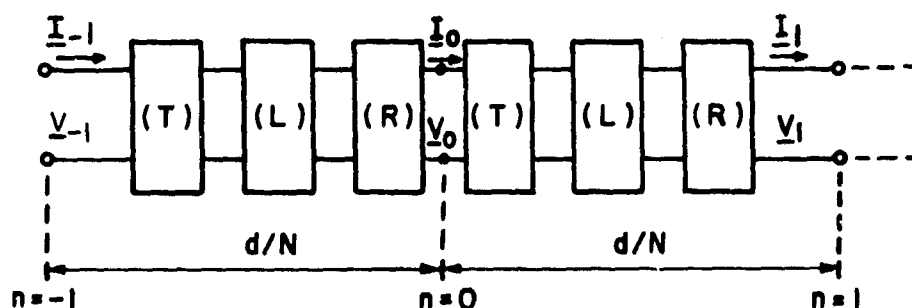


Fig. 2 An Iterative Network Representation of Periodic Traveling Wave Structure with an  $N$ -Fold Screw Axis

network shown in Fig. 2, where  $\underline{V}_n = \{V_{ni}\}$ ,  $\underline{I}_n = \{I_{ni}\}$  denote the various modal voltages and currents at the reference plane of the  $n$ -th coordinate system. Here (T) and (L) denote, respectively, the transfer matrices representing the loading and the portion of the empty waveguide that are present in the cell of length  $\frac{d}{N}$ . One observes that the network of Fig. 2 has the period  $\frac{d}{N}$ , the so-called effective period which is different from the geometrical period of the structure. The dispersion relation which is obtained via application to the network of Fig. 2 of the standard Floquet's Theorem expresses the Generalized Floquet Theorem for the screw-symmetric structure and yields the representation of the  $N$ -fold screw operator ( $S_N$ ), i. e.

$$(S_N) = (T)(L)(R) \quad (3)$$

**Determination of the Qualitative Brillouin Diagram:**

The network representation of Fig. 2, which leads to the Generalized Floquet's Theorem Eq. (2) with  $(S_N)$  given by Eq. (3), has interesting implications and yields directly a scheme for the determination of a suitable set of empty waveguide dispersion curves. As a follow-up, the qualitative form of the Brillouin diagram for a structure with screw-symmetry is obtained as a consequence of the mode-coupling principle.

Consider, in the limit of vanishing loading, relations Eqs. (2) and (3). In this case,  $(T) \rightarrow (1)$ , while  $(L)$  and  $(R)$  remain unchanged. Thus, the dispersion relation for the empty waveguide modes becomes

$$\left| (L)(R) - e^{-j\hat{\kappa} \frac{d}{N}} \right| = 0 \quad (4)$$

It is important to realize that in the network of Fig. 2, save for periodicity, no other symmetries are present. Therefore, according to Pierce's mode-coupling theory, all intersections of the various dispersion curves resulting from Eq. (4), i. e., arising in the limit of vanishing loading, will couple and produce stop bands in the contradirectional case.

**Examples:**

The above general considerations have been applied to two specific structures with a 3-fold screw axis:

- a) a periodic stack of parallel strip gratings;
- b) a circular waveguide, periodically loaded with small conducting discs.

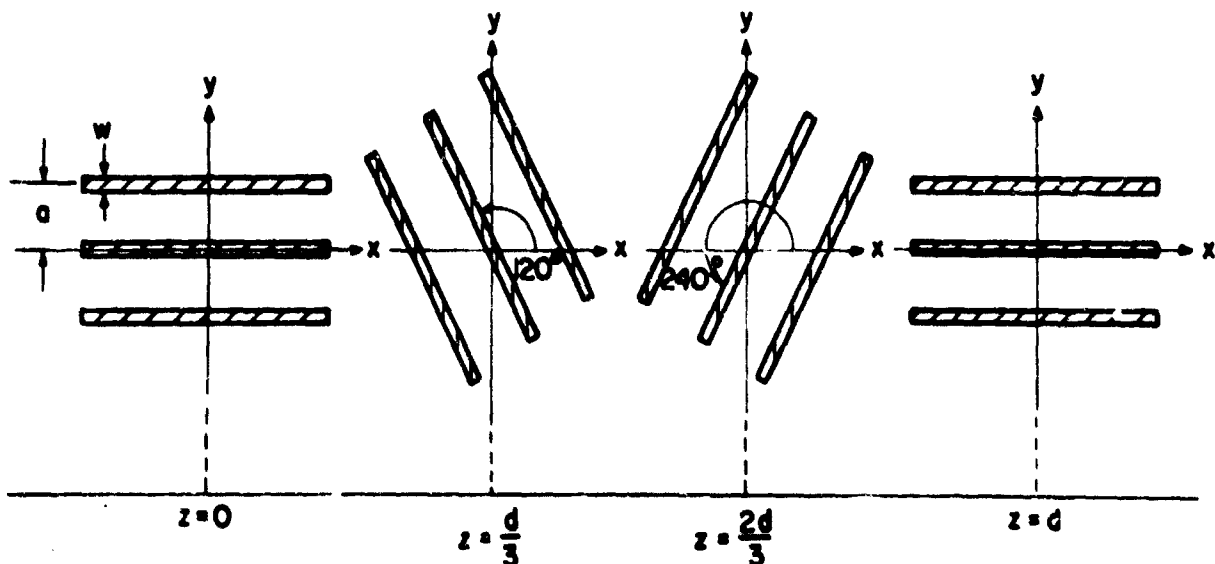


Fig. 3 Schematic Diagram of a Parallel Stack of Gratings with a 3-Fold Screw Axis

Example (a): The structure, shown schematically in Fig. 3, consists of an infinite stack of zero-thickness, perfectly-conducting strip gratings, spaced  $\frac{d}{3}$  apart and sequentially rotated clockwise by  $120^\circ$ . The strip spacing "a" is chosen less than  $\lambda/2$  so that no diffracted spectral orders appear. No spatial variation in the xy plane is assumed. In the absence of higher-mode interaction, the electromagnetic field may be represented in terms of two spatially orthogonal TEM plane waves. A cell of the equivalent network of Fig. 2 is shown in Fig. 4. The loading inductance and capacitance  $jX$  and  $jB$  have been obtained from Ref. 4. The matrices (T), (L) and (R) have the form

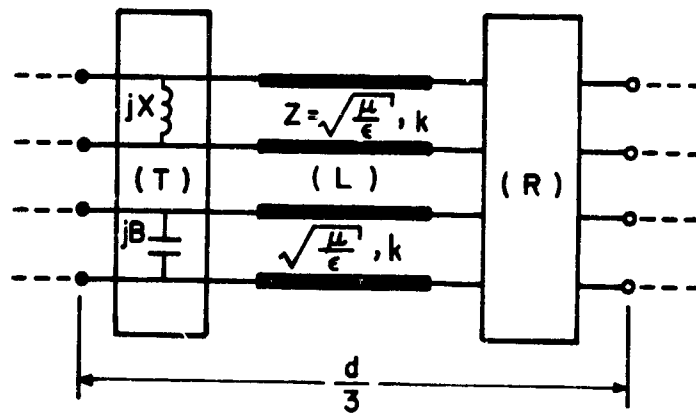


Fig. 4 A Unit Cell of the Equivalent Network of the Structure Corresponding to Fig. 3

$$\begin{aligned}
 (T) &= \begin{pmatrix} 1 & 0 & 0 & 0 \\ \frac{1}{jX} & 1 & 0 & 0 \\ 0 & 0 & 1 & 0 \\ 0 & 0 & jB & 1 \end{pmatrix} & (L) &= \begin{pmatrix} \cos \frac{kd}{3} & jZ \sin \frac{kd}{3} & 0 & 0 \\ \frac{j}{Z} \sin \frac{kd}{3} & \cos \frac{kd}{3} & 0 & 0 \\ 0 & 0 & \cos \frac{kd}{3} & jZ \sin \frac{kd}{3} \\ 0 & 0 & \frac{j}{Z} \sin \frac{kd}{3} & \cos \frac{kd}{3} \end{pmatrix} \\
 R &= \begin{pmatrix} -\frac{1}{2} & 0 & \frac{\sqrt{3}}{2} & 0 \\ 0 & -\frac{1}{2} & 0 & \frac{\sqrt{3}}{2} \\ -\frac{\sqrt{3}}{2} & 0 & -\frac{1}{2} & 0 \\ 0 & -\frac{\sqrt{3}}{2} & 0 & -\frac{1}{2} \end{pmatrix} & & (5)
 \end{aligned}$$

With Eqs. (4) and (5), the free space modal propagation constants become

$$\hat{\kappa}d = \pm (kd + 2\pi + 6\pi n) \quad (6a)$$

and  $(n = 0, \pm 1, \dots)$

$$\hat{\kappa}d = \pm (kd - 2\pi + 6\pi n) \quad (6b)$$

The modes corresponding to Eqs. (6a) and (6b) are, respectively, right and left circularly-polarized.

In the limit of vanishing loading, i. e., for  $X \rightarrow \infty$ ,  $B \rightarrow 0$ , of the structure of Fig. 4, the dispersion curves given by Eqs. (6a) and (6b) are shown in Fig. 5.

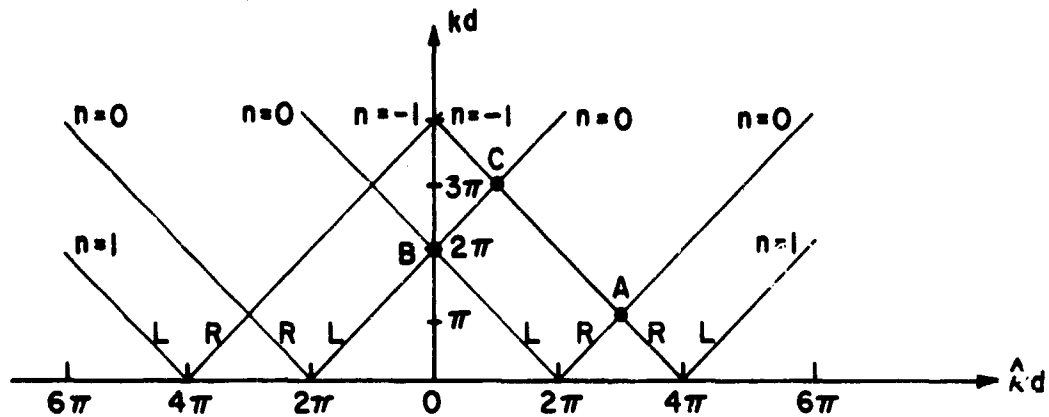


Fig. 5 The  $kd-\hat{\kappa}d$  Diagram for  $S_3$  for the Grating Structure of Fig. 3, in the Limit of Vanishing Loading. R and L denote Right and Left Circularly-Polarized Modes.

Upon introduction of finite loading, the modes of Fig. 5 will couple at every point of synchronism, i. e. at each intersection. One observes the following characteristic features of the Brillouin diagram: whereas, at A ( $kd = \pi$ ) the two right circularly-polarized modes couple in a symmetric fashion, and at B ( $kd = 2\pi$ ) the two L modes couple symmetrically, the coupling of an R to an L mode is asymmetrical due to a different relative location with respect to C of the stop bands which will appear at A and B. In contrast to the standard Brillouin diagram for  $T_d$  (in the limit of vanishing loading), which does not distinguish between the two degenerate cross-polarized modes, the Brillouin diagram for ( $S_N$ ) removes this degeneracy via the two oppositely-circularly-polarized modes, which correspond to different eigenvalues of  $S_N$ . Thus, instead of the usual  $n = 0$  pair of straight 45° lines through the origin of the  $kd-\hat{\kappa}d$  plane, representing the two forward and two backward traveling cross-polarized waves, the diagram

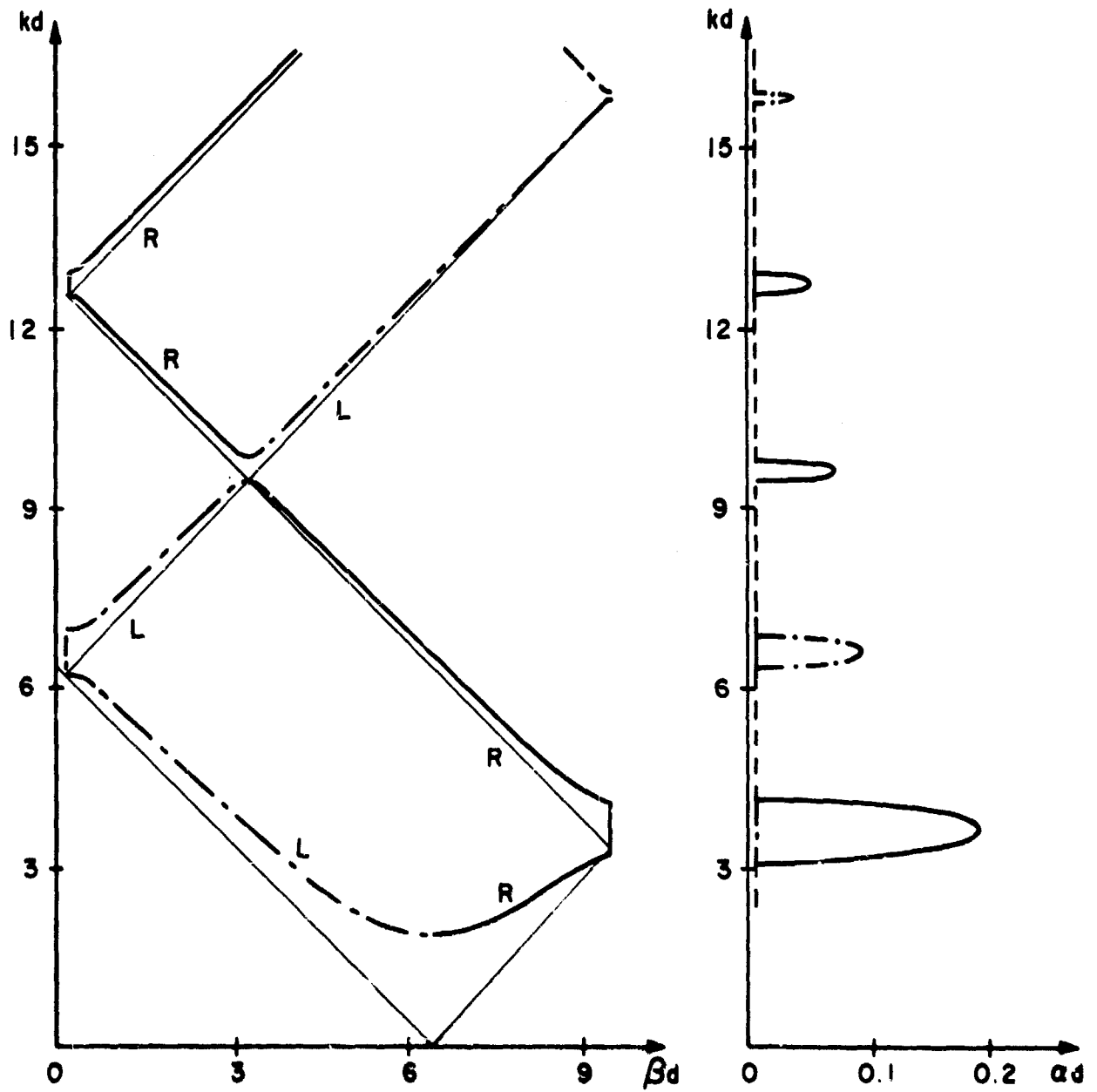


Fig. 6 Calculated Wavenumber Spectrum of  $S_3$  for the Iterative Grating Structure of Fig. 3 with  $a/d = 0.05$ ,  $w/d = 10^{-2}$

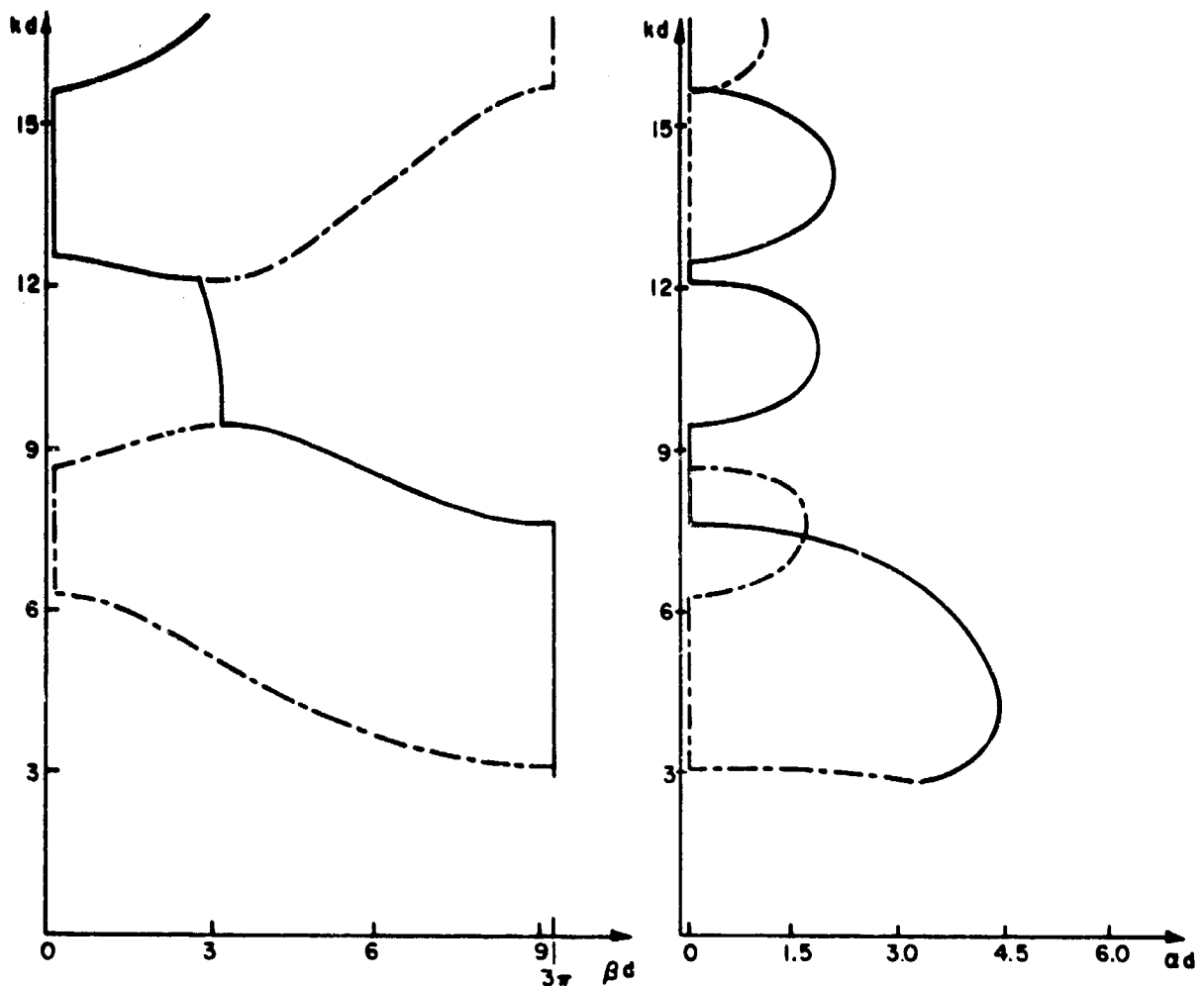


Fig. 7 Calculated Wavenumber Spectrum of  $S_3$  for the Structure of Fig. 3,  $a/d = 0.05$ ,  $w/d = 0.001$

of Fig. 5 displays, for  $n=0$ , two pairs of  $45^\circ$  straight lines, originating on the  $\hat{\beta}d$  axis at  $\pm 2\pi$ , and representing the right and left circularly-polarized TEM modes. Two calculated Brillouin diagrams are shown in Figs. 6 and 7. In Fig. 6, which corresponds to extremely narrow strips, the dispersion curves of the two circularly-polarized modes of the unloaded structure are also shown. As expected, in view of the contra-directional coupling, a stop band appears at each intersection of the various straight lines and their space harmonics. The stop band at  $kd \approx 3\pi$  is asymmetrical. This is clearly visible in Fig. 7 where the variation of the phase constant in the stop band is conspicuous.

Example (b): The propagation characteristics of a circular waveguide with  $S_{11}$ , periodically loaded with transverse small circular perfectly-conducting discs have been



considered. The empty waveguide propagation constants are  $\kappa_{m\ell}$ ,  $m$  denotes the angular variation  $e^{-jm\varphi}$  ( $m=0, \pm 1, \dots$ ) and  $\ell$  the radial mode index. In a traveling mode basis, one has the diagonal forms

$$(L) = \begin{pmatrix} \dots & -j\kappa_{m\ell} \frac{d}{3} & & \\ & e & & \\ & & 0 & \\ & & & j\kappa_{m\ell} \frac{d}{3} \\ 0 & & & e & \dots \end{pmatrix}, \quad R = \begin{pmatrix} \dots & -j\frac{2\pi}{3}m & & \\ & e & & \\ & & 0 & \\ & & & -j\frac{2\pi}{3}m \\ 0 & & & e & \dots \end{pmatrix} \quad (7)$$

Substitution of Eq. (7) into Eq. (4) yields directly

$$\hat{\kappa}_{m\ell n} d = \pm (\kappa_{m\ell} d + 2\pi n + 6\pi m) \quad (n=0, \pm 1, \dots) \quad (7a)$$

for the propagation constant of the right and left elliptically-polarized modes.

The Brillouin diagram corresponding to (7a) is constructed with the help of the standard form of  $\kappa_{m\ell} = \sqrt{k^2 - k_{cm\ell}^2}$ . It is noted that for modes with no angular variation ( $m=0$ ) where no degeneracy is possible

$$\kappa_{m\ell} = \pm (\kappa_{m\ell} + 6\pi n) \quad , \quad (8)$$

i. e., for the  $n=0$  curve  $\hat{\kappa}_{m\ell} = \kappa_{m\ell}$ . For  $m \neq 0$ , the  $n=0$  dispersion curves are displaced by  $2\pi m$  in a fashion similar to that in Example (a). Fig. 8 presents an illustration of the Brillouin diagram for  $S_3$  in the limit of vanishingly small loading, based on the  $H_{11}$  mode of circular guide. The features of this diagram resemble those of Fig. 5.

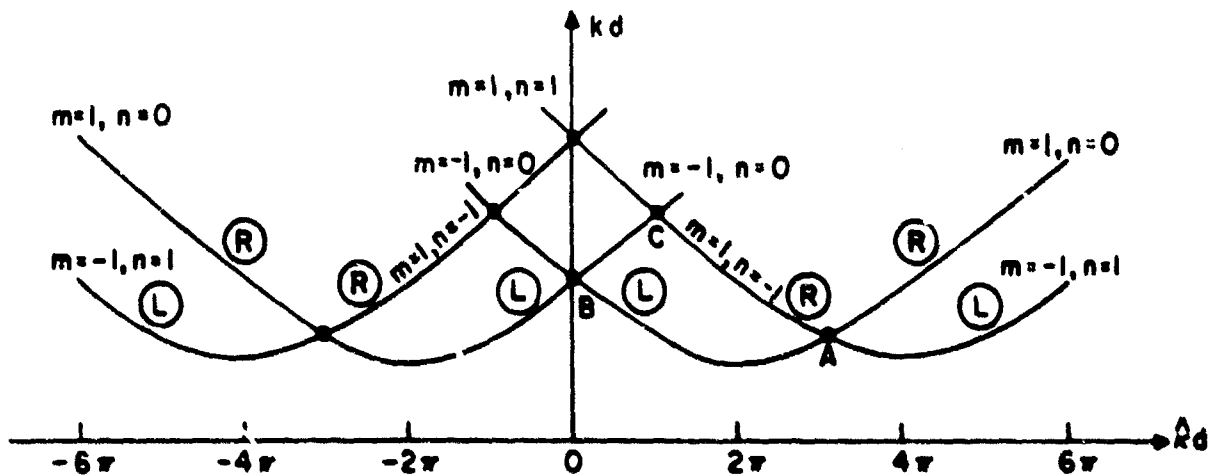


Fig. 8 The Wavenumber Spectrum of  $S_3$  of a Periodically-Loaded Circular Waveguide, Propagating the  $H_{11}$  Mode Only, with a 3-Fold Screw-Axis, in the Limit of Vanishing Loading

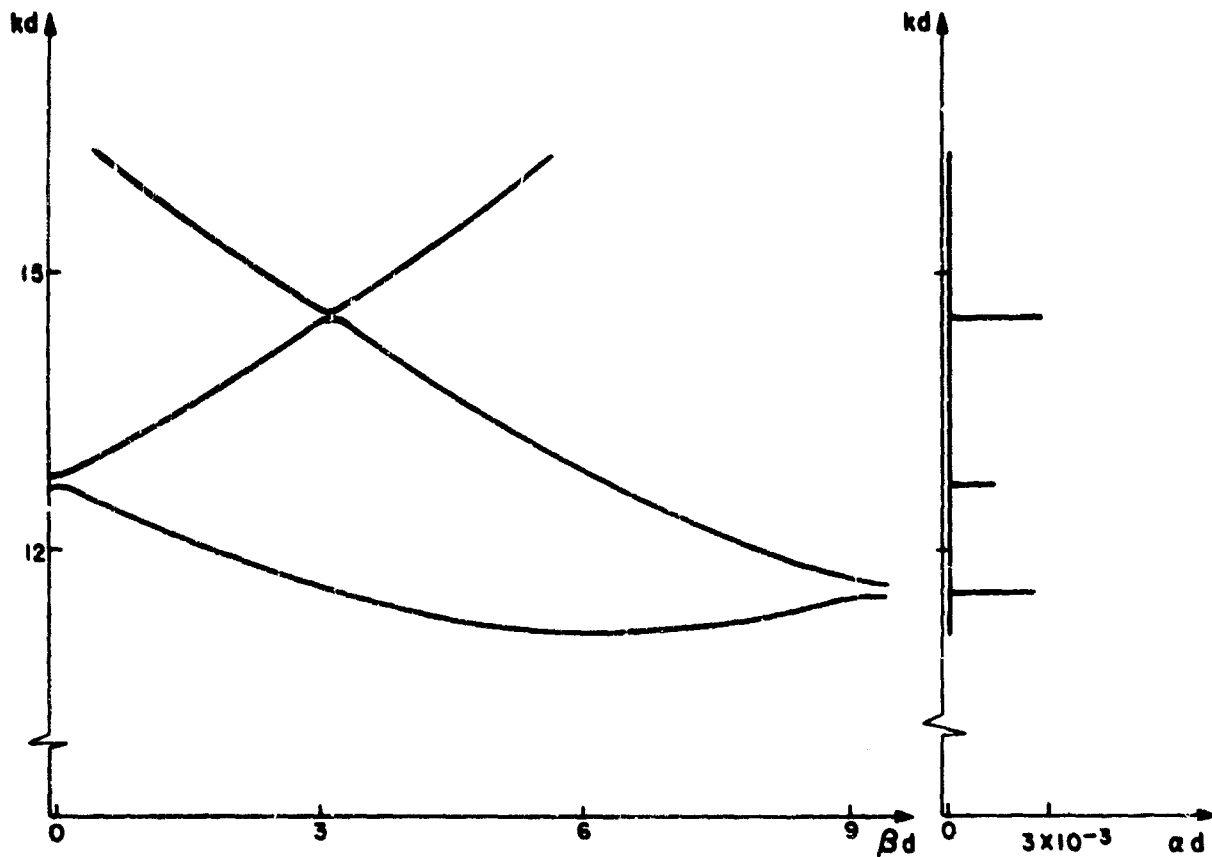


Fig. 9 The Wavenumber Spectrum of  $S_3$  for a Periodically-Disc-Loaded Circular Waveguide for  $a = 1$ ,  $R_0 = 0.3$ ,  $r_0 = 0.1$

When the loading is finite, the wavenumber spectrum of  $S_3$  for this type of structure calculated via the small obstacle procedure, is shown in Fig. 9, which applies for  $d/a > 7$ . Here " $a$ " is the radius of the waveguide,  $r_0$  the radius of the disc, and  $R_0$  the radial distance of the disc center from the origin. Only the stop band at  $kd \approx 14.4$  is due to the coupling of  $LadR$  modes; other stop bands correspond to coupling between like modes. It is seen that the stop bands at the value of  $kd$  corresponding to that of  $A$  but at  $\hat{\beta}d = \pi$ , as well as that corresponding to the value of  $kd$  at  $B$  but for  $\hat{\beta}d = 2\pi$ , have been eliminated.

As a final comment, one may predict that the largest "wavenumber bandwidth" will appear in coaxial structures operating in the TEM mode with  $m = 0$ . In this case, for  $N = 3$ , in the limit of vanishing loading the wavenumber spectrum of  $S_3$  is shown in Fig. 10. One observes that the two stop bands at  $\hat{\beta}d = \pi$  and at  $\hat{\beta}d = 2\pi$  have been eliminated.

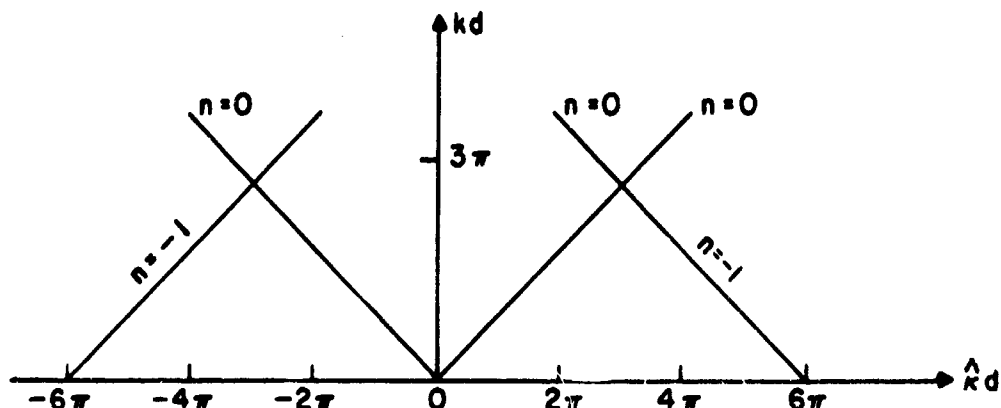


Fig. 10 Wavenumber Spectrum for  $S_3$  in the Limit of Vanishing Loading of a Coaxial Structure

Joint Services Technical Advisory Committee  
AF 49(638)-1402

A. Hessel

#### REFERENCES

1. P.J. Crepeau and P.R. McIsaac, "Consequences of Symmetry in Periodic Structures." Proc. IEEE, Vol. 52, pp. 33-43. Jan 1964.
2. A. Hessel and A.A. Oliner, "Basic Properties of Periodic Waveguides with Glide-Reflection Symmetry." Electromagnetic Theory Proceedings of a Symposium held at Delft, The Netherlands. Ed. J. Brown (New York: Pergamon Press, 1967).
3. R.C.M. Li and A. Hessel, "Experimental and Theoretical  $k$ - $\beta$  Diagram of a Glide-Symmetrically Loaded Rectangular Waveguide." Abstract of the 1966 URSI Spring Meeting, pp. 128-129.
4. N. Marcuvitz, "Waveguide Handbook," pp.280 and 284. (New York: McGraw-Hill, 1951).

#### SCATTERING BY A MULTIMODE CORRUGATED STRUCTURE WITH APPLICATION TO P TYPE WOOD ANOMALIES

A. Hessel, A. A. Oliner and D. Y. Tseng

Although Wood anomalies of the S type (E or TM polarization) have been studied extensively by many investigators,<sup>1,2</sup> those of the P type (H or TE polarization) are far less well understood. These anomalies refer to rapid, and originally unexpected, variations in the amplitudes of the diffracted orders with change in frequency or incidence angle of a plane wave which illuminates a diffraction grating of the reflection type. Experimentally, the presence of these P type anomalies, under appropriate conditions, has been well established by the work of Palmer<sup>3,4</sup> their appearance was shown to be related to the use of deeply-grooved gratings. Most of the theories of Wood anomalies

are based on a multiple-scattering approach which is applied to structures with shallow grooves or arrays of reflecting elements with dimensions small relative to wavelength. Under those conditions, these theories were able to confirm only the S type anomaly, but not the P type.

Recently, Hessel and Oliner<sup>2</sup> treated the subject of Wood anomalies from a new point of view. They showed that these anomalies need not occur near the Rayleigh wavelength, and that they can be related to the guided waves supportable by the reflection grating. In their theory, the S type Wood anomaly was examined and explained in terms of an idealized surface reactance model of a planar periodic structure. Also, an explanation for the existence of the P type anomalies was offered on the basis of this model. However, in explaining the possible presence of the P type anomalies, their model required the existence of proper TE surface waves in the limit of small modulation of the structure. Moreover, the idealized surface reactance structure considered in that theory need not always be a physically realizable one.

In order to investigate the possible presence of P type anomalies theoretically, on a more realistic model, the planar corrugated structure was chosen. This structure offers the advantages of being physically realizable, possessing the required groove depth parameter (i. e., the corrugation depth) for the study of P type anomalies, and, it is amenable to a rigorous analysis. Since the planar corrugated structure does not support a proper TE surface wave in the limit of small modulation (i. e., when the corrugation depth approaches zero), the theory of Hessel and Oliner is not valid for this excitation. However, their theory is applicable to corrugated structures for TM polarization.

The corrugated structure for which the scattering analysis was undertaken is shown in Fig. 1. The incident plane wave possesses TE polarization (electric field parallel to the grooves) with no variation, and the spacing of the grooves is such that propagating diffracted orders may be present, in addition to the reflected wave. The analysis is

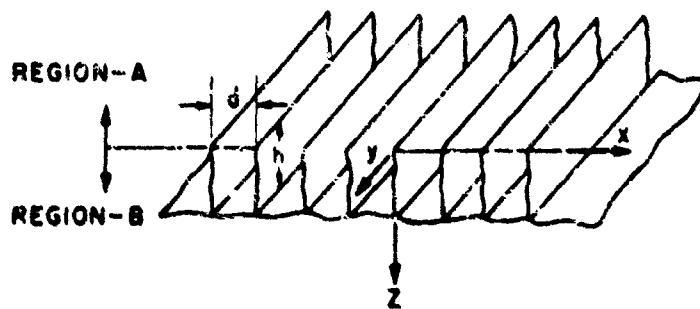


Fig. 1 Planar Corrugated Structure

phrased generally so as to account for multimode conditions of operation.

The present analysis shows that a form of P type anomaly does indeed exist. To our knowledge, these results constitute the first theoretical confirmation of such anomalies for a physically-realizable structure. Unlike the characteristic behavior of the usual (S type) Wood anomalies, these P type anomalies appear to be broad, and they exhibit some unusual features. Under certain conditions, a total (100%) power conversion takes place between the incident plane wave and the  $n = -1$  diffracted spectral order, with the amplitude of the specularly-reflected wave becoming zero at this point. In the neighborhood of such points, large power exchanges take place. The appearance of such P type anomalies is shown to be directly associated with the solution of the dispersion relation for the structure. As formulated, the analysis is valid for any number of propagating modes in both the air and corrugation regions of the structure.

For the analysis of the planar corrugated structure, the electromagnetic problem is formulated on the basis of a scattering matrix which represents the junction discontinuity between the air and the corrugation regions of the structure. The scattered and incident modal components of the field are related at the junction by the elements of the scattering matrix. As for the matrix elements themselves, they are determined explicitly from the solution of the field problem for a modified structure, which consists of an infinite array of parallel, conducting half-planes. Function-theoretic techniques involving a complex Fourier transform are utilized for the construction of the integral representation of the field. By an appropriate deformation of the contour in the inversion integral, the effects of the higher mode contributions to the problem are explicitly accounted for. It is this feature which allows the higher mode contributions to be handled in a systematic manner.

Numerical computations made from the analytic expressions for the plane wave reflection coefficients for the planar corrugated structure show that P type anomalies do exist, and the locations of these anomalies can be predicted theoretically on general grounds. These anomalies are shown to be of a type not previously recognized. They differ from the classical (Rayleigh) type and the resonance (Hessel-Oliner) type in that they are broad and, under appropriate conditions, may be characterized by a zero amplitude in the specularly-reflected wave. Under these circumstances, total (100%) power conversion to the higher spectral order takes place; an example is shown in Fig. 2. The conditions under which this anomaly will take place are given in terms of the angle of incidence (or, alternatively, in terms of the frequency) of the incident wave and the corrugation depth. By imposing these conditions on the expression for the specular reflection coefficient, it is shown analytically that a zero amplitude is indeed obtained in that coefficient.

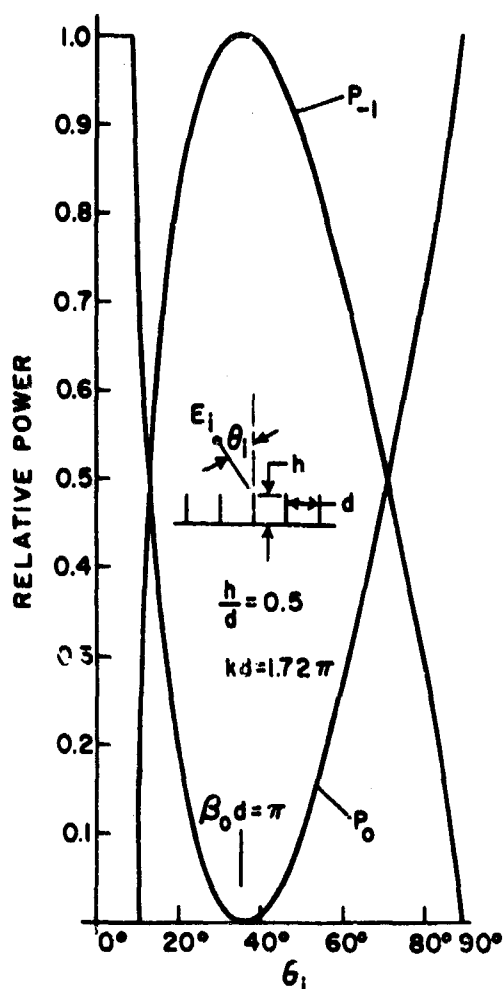


Fig. 2 P Anomalies for Plane Waves with TE Polarization Incident on a Corrugated Structure for which  $h/d = 0.5$ . The Bragg-angle Anomaly Corresponds to  $\beta_0 d = \pi$ .

The theory of Hessel and Oliner<sup>2</sup> shows that the occurrence of anomalies is related to the presence of guided (leaky) waves supportable by the scattering structure. The properties of these guided waves are, of course, obtained from the solution to the dispersion relation for the structure. In the case of the corrugated structure, there are no H mode guided waves in the usual sense, and the solution to the dispersion relation yields mostly improper waves which conform to a vertical line at  $\beta_0 d = \pi$ , in a  $kd$  vs.  $\beta_0 d$  diagram. It is of considerable interest that nevertheless the occurrence of the broad P type anomalies described above can be directly related to this solution to the dispersion relation; in fact, the above-mentioned curve in the  $kd$  vs.  $\beta_0 d$  diagram permits the location of these anomalies in frequency and angle to be determined graphically in rather accurate fashion.

As the plot in Fig. 2 indicates, the peak of the anomaly occurs at  $\beta_0 d = \pi$ , in agreement with the comment above regarding the dispersion diagram. In addition, this peak is seen to correspond to 100% power conversion into the  $n = -1$  spectral order; at this point, the amplitude of the specularly reflected ( $n = 0$ ) wave goes to zero and the  $n = -1$  spectral order is scattered precisely in the direction opposite to that of the incoming plane wave. Since  $\beta_0 d = \pi$  corresponds to the Bragg condition in a periodic structure, these resonance effects may be referred to as Bragg angle anomalies. When 100% conversion occurs, the peak of the anomaly corresponds to the presence of an improper root, with zero attenuation, of the dispersion relation. This condition is thus analogous to the Brewster angle condition (although for the opposite polarization), where the vanishing of the plane-wave reflection coefficient is associated with an improper root of the dispersion relation with zero attenuation.

A three-port network representation of the interface discontinuity between the air region and the corrugation region has been derived for the case for which the reflected and the  $n = -1$  diffracted waves are present in the air region and only the dominant mode is above cut-off in the corrugations. This representation, which is simple in form, has been incorporated into an overall transverse network for the corrugated structure. This latter network has been found useful in offering a simple explanation as to when and why the anomalies occur. They occur when the incident plane wave mode is impedance matched to the  $n = -1$  spectral order mode by means of a transformer which couples these modes to the  $H_{10}$  mode propagating in the corrugations.

Air Force Cambridge Research Laboratories  
Office of Aerospace Research  
AF 19(628)-4324

A. Hessel

Joint Services Technical Advisory Committee  
AF 49(638)-1402

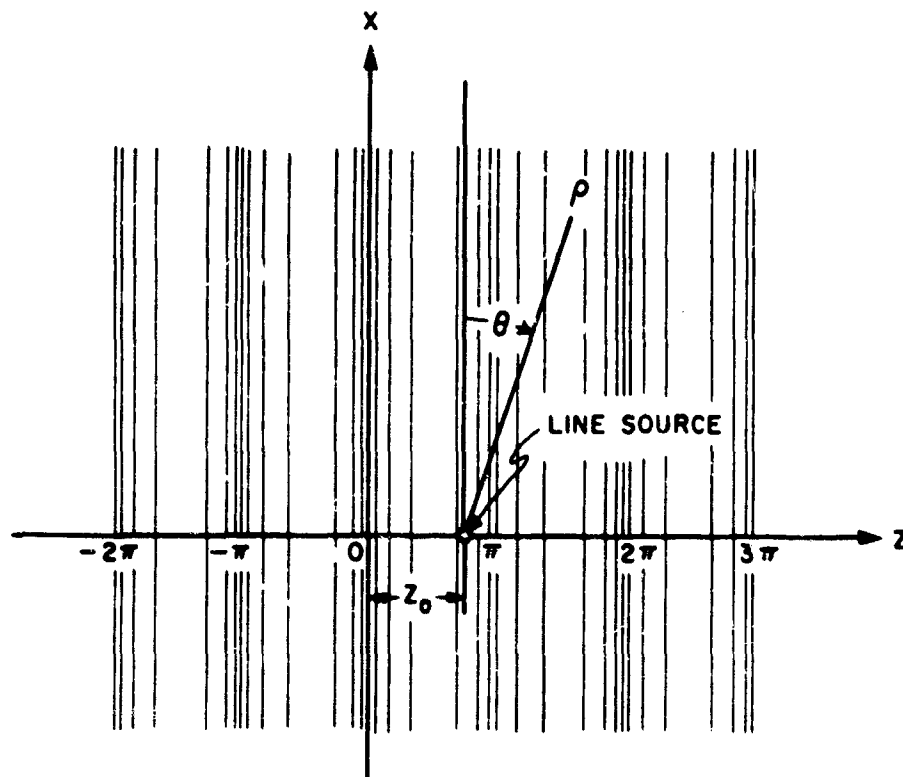
#### REFERENCES

1. V. Twersky, "On Multiple Scattering of Waves," J. Res. Natl. Bur. Std., 64D, 715 (1960).
2. A. Hessel and A. A. Oliner, "A New Theory of Wood's Anomalies on Optical Gratings," Appl. Opt., 4, 1275 (1965).
3. C. H. Palmer, "Parallel Diffraction Grating Anomalies," J. Opt. Soc. Am., 42, 269 (1952).
4. C. H. Palmer, "Diffraction Grating Anomalies. II - Coarse Gratings," J. Opt. Soc. Am., 4b, 50 (1956).
5. C. H. Palmer, "Comment on the article by Yakovlev and Gerasimov on the Intensity Distribution in the Spectrum of Diffraction Gratings," J. Opt. Soc. Am., 51, 1438 (1961).

### THE FIELD OF A LINE SOURCE EMBEDDED IN A PERIODICALLY-STRATIFIED MEDIUM

T. Tamir and B. Singer

The present work is concerned with the rigorous derivation of the far field produced by a finite electromagnetic source in a periodically-stratified configuration which is representative of a large class of periodic structures. The solution obtained may therefore be regarded as the canonic form of a field pertinent to a number of applications which include diffraction of light by ultrasonic waves, Brillouin scattering processes and other wave interactions. These phenomena usually involve a strong wave that produces a modulation of the electromagnetic properties of a medium which in turn causes a diffraction of a weaker wave. Although results are available for the simpler case of plane wave incidence, no rigorous treatments seem to exist for realistic situations corresponding to localized finite sources. In the absence of such solutions, a clear understanding of the power flow mechanism is difficult and a geometric optical interpretation (or an extension thereof) is not evident.



$$\epsilon(z) = \epsilon_0 (1 - M \cos 2z)$$

Fig. 1 Geometry of the Sinusoidally-Stratified Medium:  
 $\epsilon(z) = \epsilon_0 (1 - M \cos 2z)$



The configuration describing the wave interaction process is shown in Fig. 1 where, as usual, it is assumed that the stronger wave produces a modulation of the permittivity while the permeability  $\mu_0$  of the medium remains unaffected. The permittivity therefore exhibits a variation about an average value  $\epsilon_0$ ; this variation is confined, for simplicity, to the  $z$  coordinate and is assumed to be sinusoidal in form, such that

$$\epsilon(z) = \epsilon_0 (1 - M \cos 2z) \quad (1)$$

where, for convenience, the periodicity (cell) length was normalized to  $\pi$ . The modulation coefficient  $M$  is usually very small in practice, being of the order of  $10^{-4}$  or less.

In general, the modulated medium behaves both as a phase and as an amplitude grating with respect to an incident electromagnetic wave whose energy is therefore scattered in a rather complicated pattern. To allow for a large variety of possible incident fields, the present work examines the case of a basic source in the form of a filamentary, uniform, electric current located at  $z = z_0$ . This is evidently the Green's function statement for the present two-dimensional problem whose solution yields the possibility of examining the fields of other source distributions by simple superposition techniques. The rigorous formal solution is obtained for the present canonic problem and its asymptotic result is evaluated to a first order of the modulating (perturbing) parameter  $M$ . Although this is sufficient for most realistic cases, the accuracy may be improved by extending the method described herein to any desirable order.

Due to the present choice for the source, the electric field  $E$  occurs along the  $y$  coordinate only and the magnetic field is derived from it via Maxwell's equations. A complete solution of the problem is thus given directly by the scalar electric field  $E$  whose rigorous formal expression is:

$$E = \frac{1}{2\pi} \sum_{m,n} \int_{-\infty}^{\infty} e^{2i(mz_0 + nz)} \frac{a_m(\cdot) a_n(\cdot)}{W(k_x; z_0)} e^{-i[k_x x + \nu |z - z_0|]} dk_x \quad (2)$$

where a time dependence  $\exp(-i\omega t)$  is assumed and suppressed. The quantity  $\nu = \nu(k_x)$  is the Floquet exponent pertinent to a Mathieu differential equation which represents the wave equation for the present problem and possesses a Wronskian denoted by  $W(k_x; z_0)$ . The functions  $a_m(\cdot)$  and  $a_n(\cdot)$  indicate the appropriate Fourier coefficient for the Mathieu functions and they correspond to the space harmonics of the respective Floquet-type characteristic solutions.

The discussion is henceforth restricted to frequencies such that  $0 < k = \frac{\omega}{c} z_0 < 2$ , where all lengths are normalized with respect to  $z_0$  units. This restriction means that there is not more than one angular direction  $\theta$  that satisfies the Bragg condition  $k \sin \theta = N$  ( $N = \text{integer}$ ). One may then derive solutions of Eq. (2) accurate to a first order

in M. For that purpose one uses expansions appropriate to the Mathieu functions which show that

$$\nu = \pm \sqrt{1 \pm \sqrt{(1 - k^2 + k_x^2)^2 - (\frac{1}{2} M k^2)^2}} \quad (3)$$

It may furthermore be shown that, to the same approximations, it is sufficient to retain  $m, n = 0, \pm 1$  in Eq. (2) and disregard the higher space harmonics of the Floquet expansions.

The integrals in Eq. (2) are evaluated by carrying out a saddle-point integration in the complex  $k_x$  plane which, due to relation (3), is a six-sheeted Riemann surface. The saddle-point equation is a cubic whose three solutions are intimately related to the observation point  $(\rho, \theta)$  and the Bragg angle  $\theta_B$ . The latter satisfies the condition that, at  $\theta = \theta_B$ :

$$k \sin \theta_B = 1 \quad (4)$$

A ray which initially starts from the sources at  $\theta = \theta_B$  would, if geometrical optics were valid, be interpreted as a local plane wave whose phase-shift across a periodicity (cell) distance is equal to  $\pi$ . In that case, regions separated by integral numbers of cells produce reflections which add in phase. This phenomenon may be phrased in terms of a stop-band for propagation with respect to a wave initially incident at  $\theta = \theta_B$ . Such a situation corresponds to total reflection and ordinary geometric optical techniques are then no longer valid. This total reflection effect is instrumental in distinguishing between the following three differently-behaving regions:

Region 1:  $\theta_B < |\theta| < \pi$

In this region, the cubic saddle point equation yields two complex and one real solutions. Only the latter is significant and it yields the asymptotic result:

$$E^{(1)} \sim \sqrt{\frac{2\pi}{k^2}} e^{i(k\rho - \frac{\pi}{4})} \left[ 1 - \left(\frac{Mk^2}{4}\right)^2 \left( \frac{e^{-2iz} + e^{2iz_0}}{1 - k \sin \theta} + \frac{e^{2iz} + e^{-2iz_0}}{1 + k \sin \theta} \right) \right] \quad (5)$$

This is essentially a cylindrical wave perturbed by the terms of order M and represents a result that may be obtained also by a WKB analysis. Hence the field  $E^{(1)}$  corresponds to a ray emitted by the source at an angle very close to  $\theta$ .

The wedge regions  $\theta_B < |\theta| < \pi/2$  are indicated in Fig. 2 where the critical angle  $\theta_B$  is also shown. The energy emitted at  $\theta = \theta_B$  would travel along the various possible paths shown in the figure if simple reflections were considered. It is then clear that these paths cannot penetrate into region 1 (below  $\theta_B$ ) and the stop-band effect discussed above does not therefore occur therein. The identity of result (5) with that obtainable

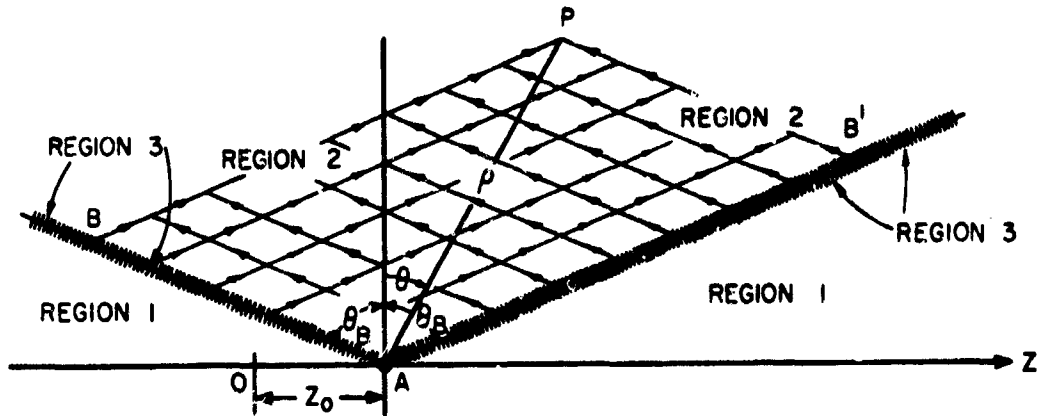


Fig. 2 The Different Diffraction Regions  
 The trajectories shown describe possible paths taken by "Bragg rays" which connect the source with an observation point P in Region 2 via numerous successive reflections. Note that such a ray complex cannot extend beyond  $|\theta| = \theta_B$ .

from a WKB analysis is consequently expected since geometric optical arguments are applicable in this domain.

Region 2: ( $|\theta| < \theta_B$ )

This region is characterized by the fact that all of the energy flow initially emitted at  $\theta \approx \theta_B$  or  $\theta \approx -\theta_B$  must leak, after one or several reflections, into the interior of the wedge  $|\theta| < \theta_B$ ; hence a portion of the energy reaches any observation point P, as shown by the various paths in Fig. 2. This phenomenon is reflected in that all of the three saddle points in (2) are now real. The first one of these yields a field  $E_1^{(2)}$  identical to  $E^{(1)}$  in Eq. (5), to which one must add two more fields  $E_2^{(2)}$  and  $E_3^{(2)}$  contributed by the two saddle points which now are real rather than complex. The two additional fields are given by

$$E_{2,3}^{(2)} \sim \frac{\sqrt{M}}{k_0} f_{2,3}(\theta) \left[ 1 \pm \frac{e^{2iz_0}}{a(\theta)} \right] \left[ 1 \pm \frac{e^{-2iz}}{a(\theta)} \right] e^{i[\sqrt{k^2-1} x + z - z_0]} \quad (6)$$

where  $f_{2,3}(\theta)$  and  $a(\theta)$  are functions of the polar angle  $\theta$ . It is noted that  $E_{2,3}^{(2)}$  are of order  $M^{1/2}$  and therefore these fields are larger than the second term of  $E_1^{(2)} = E^{(1)}$  given by Eq. (5). It can be shown that, whereas  $E_1^{(2)}$  is interpreted as a power flow in the direction  $\theta$ , the additional components  $E_{2,3}^{(2)}$  represent power flow which is emitted by the source at angles just below and just above  $\theta_B$ , respectively. Hence  $E_{2,3}^{(2)}$  is termed a "Bragg" field.

If terms with the same phase dependence are grouped together in Eq. (6), the Bragg field may be written as:

$$E_2^{(2)} + E_3^{(2)} \sim \sqrt{\frac{M}{k\rho}} g(\theta) \left\{ \left(\frac{AB'}{AB}\right)^{1/4} e^{i[k\rho \cos(\theta - \theta_B) + \phi(\theta)]} + \left(\frac{AB}{AB'}\right)^{1/4} e^{-i[k\rho \cos(\theta + \theta_B) + \phi(\theta)]} \right\} \quad (7)$$

where  $AB$  and  $AB'$  are the sides of the parallelogram shown in Fig. 2, and  $g(\theta)$  and  $\phi(\theta)$  are functions of the polar angle.

The last expression justifies an interpretation of the Bragg field in terms of plane waves progressing at the Bragg angles  $\pm \theta_B$ . These waves are successively reflected and the total Bragg field may therefore be said to reach the observation point via a multitude of parallel paths, as shown in Fig. 2. The greatest utility of expression (7) is, however, in that it points the way towards a geometric optical extension of the diffracted Bragg field to a larger class of problems involving additional boundaries and/or scattering objects placed in the periodically-stratified medium.

### Region 3: $|\theta| \approx \theta_B$

This region corresponds to the range where one of the two additional ("Bragg") saddle points is arbitrarily close to the first saddle point. The field in this case contains a component  $E_1^{(3)} = E^{(1)}$  given by Eq. (5); in addition, a term  $E_2^{(3)}$  appears to produce a transition between the fields in regions 1 and 2. This transition component is in the form:

$$E_2^{(3)} \sim \frac{M^{2/3}}{(k\rho)^{1/3}} h(\rho, \theta) \quad (8)$$

where  $h(\rho, \theta)$  includes an Airy function. Hence, although  $E_2^{(3)} \rightarrow 0$  with  $M \rightarrow 0$  or  $\rho \rightarrow \infty$ , as expected, it decreases less rapidly than all of the other field components with respect to both  $M$  and  $\rho$ . Consequently,  $E_2^{(3)}$  accounts for a radiation peak at an angle very close to  $\theta_B$ .

A good understanding of the nature of the three distinct regions described above enables a straightforward extension of the result for the case when the Bragg condition is satisfied for several angles  $\theta = \theta_{BN}$  ( $N=1, 2, 3, \dots$ ). It may be then shown by a simple geometric construction that, except at  $|\theta| \approx \theta_{BN}$ , the Bragg field anywhere is given by contributions which are analogous to those discussed for region 2 above. However, more than two such contributions may appear for  $N > 1$ , but their number, as well as their initial power flow direction, can easily be ascertained.

In conclusion, the two-dimensional field produced by line sources in an unbounded periodic medium was found to exhibit three varieties of characteristic regions: (1) a domain wherein simple geometric optical techniques are valid and the field consists of a cylindrical wave with additional diffraction terms of order  $M$ , where  $M$  denotes a perturbing quantity which produces the periodicity; (2) regions wherein the dominant additional diffraction waves are of order  $M^{1/2}$  and these correspond to a Bragg-type

propagation mechanism; (3) narrow transition regions centered around the Bragg directions of the medium wherein radiation peaks occur due to a term proportional to  $M^{2/9}/\rho^{1/3}$  in the field expressions. The Bragg-type waves may be cast in a mathematical form which indicates the possibility of a geometric optical extension in regions wherein ordinary geometric optical arguments are otherwise invalid. The radiation peak effects in the Bragg angle regions are particularly strong at large distances and at periodicity (cell) lengths which are of the order of a wavelength. However, the diffraction effects are important even at shorter distances in applications, such as optical imaging, where the question of optical aberrations is of considerable interest.

Air Force Cambridge Research Laboratories  
Office of Aerospace Research  
AF 19(628)-4324

T. Tamir

#### MECHANISM OF PROPAGATION OF ELECTROMAGNETIC FIELDS IN LOSSY MEDIA

H. L. Bertoni, L. B. Felsen and A. Hessel

While considerable attention has been given to electromagnetic radiation problems involving lossy media, study of such problems has primarily been limited to identification of the wave types occurring in, and to the evaluation of the radiated fields for, configurations amenable to rigorous analysis<sup>1,2,3</sup>. Little attempt has been made to understand the physical mechanism by which the fields radiated by a source reach an observation point, e. g., the path and local region of propagation. The object of this investigation is to determine the path and local region of propagation of the fields in a lossy medium. It is hoped that such knowledge will lead to a systematic method for calculating approximately the fields radiated in lossy configurations not amenable to rigorous analysis.

To clarify what is meant by the path and region of propagation, the propagation of the field from the source to the observation point is viewed as occurring in two steps. First, the source illuminates a (real or mathematical) plane located between it and the observation point. The fields in this plane are viewed as an equivalent source distribution, and one seeks that area in the plane whose illumination is principally responsible for establishing the fields at the observation point. The "center" of this area may be regarded as locating the intersection of the path of propagation with the plane, and the area itself is taken as the projected cross-section of the three-dimensional region through which the main portion of the fields propagates. It is well known that for lossless media, the paths of propagation are the rays of geometrical optics and the area in the plane then corresponds to the first few Fresnel zones.

For configurations containing lossy media two cases occur. First, those fields that do not traverse regions having different loss tangents (e. g., the fields radiated in an infinite, homogeneous, lossy medium) propagate along the rays of geometrical optics.

In this case, the area in the plane whose illumination is principally responsible for the field at the observation point again corresponds to the first few suitably-defined Fresnel zones. However, for fields traversing regions having different loss tangents (e.g., the fields penetrating a lossy medium from free space), the paths of propagation are not the conventional rays since in the extension of ray optics to this case, the rays connecting real source and observation points travel through complex space<sup>4,5,6</sup> (formed by allowing the space coordinates to take on complex values). In the present investigation, these aspects are considered for a simple example and they clarify certain basic features of propagation in inhomogeneous lossy media.

#### The Region of Propagation:

For simplicity, a two-dimensional problem is considered in which a plane wave (source at infinity) is incident obliquely from free space on the planar interface between free space and a lossy medium located in the region  $z > 0$  (see Fig. 1). The incident electric field  $\underline{E}_i$  is taken as

$$\underline{E}_i = \frac{1}{T} \underline{x}_0 e^{-j(\eta_0 y + \kappa_0 z)} \quad (1)$$

where  $\eta_0$  is the real transverse wave number,  $\kappa_0 = \sqrt{k_0^2 - \eta_0^2}$ , and  $k_0 = \omega \sqrt{\epsilon_0 \mu_0}$  is the free space wave number. The amplitude  $1/T$ , where  $T$  is the transmission

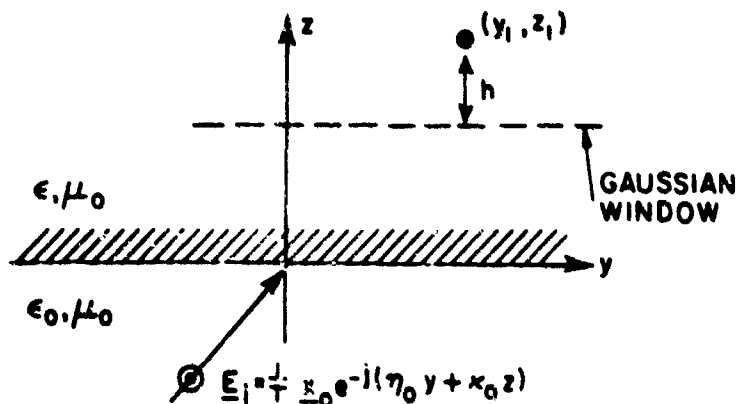


Fig. 1 Planar Interface Configuration

coefficient at the interface, is chosen so that the electric field  $\underline{x}_0 E_t$  transmitted into the lossy medium is given by

$$\underline{E}_t = e^{-j(\eta_0 y + \kappa_0 z)} \quad (2)$$

In Eq. (2),  $\kappa_0 = \sqrt{k^2 - \eta_0^2}$  where the complex wave number  $k$  for the lossy medium is given by  $k = \omega \sqrt{\epsilon \mu}$ .

In order to find the region through which the dominant portion of the fields propagate in reaching an observation point  $(y_1, z_1)$  in the lossy medium, an idealized "window" is inserted in the lossy medium parallel to the  $y$  axis at a variable distance  $h$  below the observation point (see Fig. 1). This sampling window is assumed to be of zero thickness and to transmit the fields essentially over a limited range of  $y$ . The  $y$  coordinate of the center of the window is then adjusted so that, for a minimum window width, the field at the observation point approximates  $\underline{E}_t$  to some fixed accuracy. By this process the area in the  $z = z_1 - h$  plane whose illumination is principally responsible for the field at  $(y_1, z_1)$  is determined. The location and width of this region in the  $z = z_1 - h$  plane, when considered as a function of  $h$ , traces out the entire principal region of propagation.

In order to avoid diffraction effects, which in the case of lossy media can be exponentially stronger than the transmitted fields, the function describing the transmittance of the window should be entire. The Gaussian function  $e^{-\alpha(y-y_c)^2}$ , which possesses the necessary properties and is mathematically simple to treat, is used here. The window is centered at  $y = y_c$  and has a  $1/e$  half-width  $W_g = 1/\sqrt{\alpha}$ . Using the Gaussian window function, the electric field at  $z = (z_1 - h)^+$  is given by

$$\underline{E}_g = e^{-j[\eta_0 y + \gamma_0(z_1 - h)]} e^{-\alpha(y - y_c)^2} \quad (3)$$

Taking the Fourier transform of Eq. (3) and multiplying by  $e^{-j\alpha h}$ , where  $\alpha = \sqrt{k^2 - \eta^2}$  and  $\eta$  is the transform variable, the field at  $(y_1, z_1)$  can be written in terms of an inverse transform as

$$\underline{E}_g(y_1, z_1) = \frac{e^{-j[\eta_0 y_c + \gamma_0(z_1 - h)]}}{2\sqrt{\alpha}} \int_{-\infty}^{\infty} e^{-j[\eta(y_1 - y_c) + \alpha h]} e^{-\frac{1}{4\alpha}(\eta - \eta_0)^2} d\eta \quad (4)$$

The integral in Eq. (4) can be evaluated approximately by the method of steepest descent.

As a function of  $y_c$ , the steepest descent approximation of Eq. (4) is found to have a maximum magnitude at some value of  $y_c$ . For  $y_c$  in the vicinity of this value and for  $\alpha$  small, the steepest descent evaluation of Eq. (4) is found to give

$$E_g(y_1, z_1) \approx E_t(y_1, z_1) \left\{ \frac{e^{-\alpha \left[ (y_c - y_{cm})^2 + 2jd(y_c - y_{cm}) \cdot d \right] / (1 - 2ja h \frac{k^2}{s_0^3})}}{\sqrt{1 - 2ja h \frac{k^2}{s_0^3}}} \right\} \quad (5)$$

where

$$y_{cm} = y_1 - h \operatorname{Re} \frac{\eta_0}{s_0}; \quad d = -h \operatorname{Im} \frac{\eta_0}{s_0}. \quad (6)$$

For  $\alpha$  small and under the approximation  $e^x = 1 + x$ , the magnitude of the deviation of the exponential term in the brackets of Eq. (5) from unity will be minimum for  $y_c = y_{cm}$ , independent of  $\alpha$ . Thus, it is seen from Eq. (5) that if the magnitude of the difference of the exponential from unity is some fixed value,  $\alpha$  will be greatest, i. e.,  $W_g$  least, when  $y_c = y_{cm}$ . Because of the above described behavior of Eq. (5), this expression is interpreted as implying that the fields at  $(y_1, z_1)$  are established principally by the illumination in some region of the plane  $z = z_1 - h$  centered about the point  $y_{cm}$ .

Requiring the bracket term of Eq. (5) to be approximately unity at  $y_c = y_{cm}$ , so that  $E_g$  will be approximately equal to the field  $E_t$  in the absence of the window, determines an upper limit on  $\alpha$ , i. e., a lower limit on the half-width  $W_g$ . The half-width in turn gives the region centered about  $y_{cm}$  in the  $z = z_1 - h$  plane whose illumination is principally responsible for the fields at  $(y_1, z_1)$ . With the upper limit for  $\alpha$ , it can be argued that the relative error made in using Eq. (5) for  $E_g$  at  $y_c = y_{cm}$  is less than the deviation from unity of the bracketed term in Eq. (5) if  $|s_0| h > 1$ .

The bracketed term in Eq. (5) at  $y_c = y_{cm}$  will differ from unity by an amount whose magnitude is less than some fixed quantity if the denominator and the exponential individually differ from unity by an amount whose magnitude is less than half that quantity. Choosing, for the sake of argument, an error of  $2/\pi^4$  ( $\approx .02$ ), the denominator will differ from unity by an amount whose magnitude is less than  $1/\pi^4$  if

$$\alpha h \left| \frac{k^2}{s_0^3} \right| < \frac{1}{\pi^4}; \quad W_g > \pi^2 \sqrt{h \left| \frac{k^2}{s_0^3} \right|}. \quad (7)$$

In view of Eq. (7), the exponential at  $y_c = y_{cm}$  will differ from unity by an amount



whose magnitude is less than  $1/\pi^4$  if

$$\alpha d^2 < \frac{1}{\pi^4} ; \quad W_g > \pi^2 |d| \quad (8)$$

Taking  $W_g$  so as to satisfy both Eqs. (7) and (8) insures that  $E_g = E_t(1+\alpha)$  with  $|\alpha| < 2/\pi^4$ , which implies that it is principally the illumination over this region of half-width  $W_g$  centered at  $y_{cm}$  in the plane  $z = z_1 - h$  that gives rise to the fields at  $(y_1, z_1)$ . For lossless media ( $\epsilon$  real,  $d = 0$ ) Eq. (7) reduces to the form of the well-known Fresnel criterion and  $y_{cm}$  represents the intersection of the geometric-optical ray passing through  $(y_1, z_1)$  with the plane  $z = z_1 - h$ . The primary effect of loss on the width of the region of propagation is to impose a condition, linear in  $h$ , that must be satisfied in addition to the Fresnel criterion. For  $h < \left| \frac{k^2}{\epsilon_0^3} \right| / \left( \text{Im} \frac{\eta_0}{\epsilon_0} \right)^2$ , condition (7) determines  $W_g$  while for  $h$  greater than this value, Eq. (8) determines  $W_g$ . Note that the value of  $h$  for which Eqs. (7) and (8) are the same is independent of the error limit.

It has been found that the location  $y_{cm}$  of the region giving the principal contribution to the fields at  $(y_1, z_1)$ , and the condition (8) on its width, have simple interpretations in terms of the complex ray passing through the point  $(y_1, z_1)$ . This interpretation is expected to hold in more complicated problems, which will be examined in the future.

National Science Foundation  
GU-1557

H. Bertoni

#### REFERENCES

1. "Special Issue on Electromagnetic Waves in the Earth", IEEE Trans. Ant. Prop., AP-11 (1963), pp. 206-387.
2. A. Banos, "Dipole Radiation in the Presence of a Conducting Half-Space," (New York: Pergamon Press, 1966).
3. D. Staiman and T. Tamir, "Nature and Optimization of the Ground (Lateral) Wave Excited by Submerged Antennas", Proc. IEEE, 113 (1966) pp. 129-1310.
4. B. D. Seckler and J. B. Keller, "Geometrical Theory of Diffraction in Inhomogeneous Media", J. Acoust. Soc. Am., 31 (1959), pp. 192-205.
5. K. G. Budden and G. W. Jull, "Reciprocity and Nonreciprocity with Mangetoionic Rays", Can. J. of Physics, 42 (1964), pp. 113-130.
6. Yu. A. Kravtsov, "Complex Rays and Complex Caustics", Radiophysics, 9-10 (1967), pp. 1283-1304 (in Russian).

**RAY METHOD FOR SOUND WAVE REFLECTION IN AN OPEN-ENDED CIRCULAR PIPE**

L. B. Felsen and H. Y. Yee

In previous reports<sup>1</sup>, it has been shown how a ray-optical technique can be employed for the study of radiation and reflection from the open end of a parallel plane waveguide, both in the dominant mode and in the multimode regimes. The purpose of the present investigation is to demonstrate that the technique remains applicable also for the open-ended circular waveguide configuration. While the previous studies were carried out for the electromagnetic wave problem, we now consider acoustic wave propagation in a hard-walled circular tube.

In the analysis, the discontinuity at the mouth of the circular tube is regarded as an equivalent non-isotropic ring source whose radiation back into the tube establishes the reflected waves. The characteristics of this induced source are known in terms of its far zone radiation pattern which is established by viewing the rim locally as a straight edge excited by a plane wave descriptive of the incident mode. The rays originating at the ring source and reflected repeatedly from the tube wall must be converted into modal form if the modal reflection and coupling coefficients are to be extracted. Finally, by taking into account multiple diffraction between relevant points on the rim, one can refine the above-sketched primary diffraction computation.

While the basic approach to the calculation of the reflected modes in the circular geometry is the same as in the parallel plane configuration, there are important differences which place further strain on the ray method. The ray interpretation is effective for those propagation and diffraction phenomena which behave locally like plane waves. A mode in a parallel plane region can be decomposed exactly into two plane waves, and the scattering of these plane waves by a straight edge discontinuity is known rigorously from classical diffraction theory. The conversion of the multiply reflected ray field into modal form can also be performed within a rigorous framework. These features are not present in the circular geometry where the modes, expressed in terms of Bessel functions, behave like local plane waves only sufficiently far from the waveguide axis. The replacement of the curved rim by a local straight edge constitutes a further approximation, as does the manner of summing the multiply reflected rays emanating from the rim into modal form. Thus, various ray constructs which apply in the parallel plane geometry without approximation do so only asymptotically in the circular configuration.

Basic to the analysis of the scattering problem is the evaluation of modes excited in a circular pipe by a non-isotropic ring source. To assess the validity and quality of this ray-acoustical calculation, the rigorously solvable isotropic ring source problem has been considered in some detail. It is found that the ray solution, when converted into modal form, yields the high-frequency asymptotic approximation of the exact result

for the higher order modes, in regard to the coordinate dependence of the modes as well as the radial amplitudes. This asymptotic correspondence does not extend to the lowest mode when the ring source is uniform, and it holds only with poor accuracy for the lowest mode when the ring source has a one-cycle ( $\cos \theta$ ) variation. To extend the range of validity of the ray-acoustical calculation, we replace various asymptotic approximations for the higher order modes by their exact generating functions, and we extrapolate the resulting forms even to the lowest mode, thereby forcing the asymptotic ray-acoustical mode series into its exact equivalent. When the ring source is non-isotropic, the ray-acoustical calculation provides the same asymptotic mode series but with modal amplitudes modified by the source pattern function. Use of the substitutions mentioned above transforms this series into an exact solution of the wave equation, with approximate modal amplitude coefficients which, however, reduce to the exact ones in the isotropic case where the pattern function equals unity. This being done, the remaining calculation of the modal reflection and coupling coefficients for the open-ended tube is analogous to that for the parallel plane configuration.

Since exact results are available for reflection from the open end of a thin-walled tube, these may serve to check the accuracy of the reflection coefficients calculated by the ray method. Curves computed from exact formulas for some of the lower ( $ka$ ) values ( $k$  = free-space wavenumber,  $a$  = tube radius) are given in Ref. 2 and are shown solid in Fig. 1; part (a) of the figure presents the reflection coefficient amplitude while part (b)

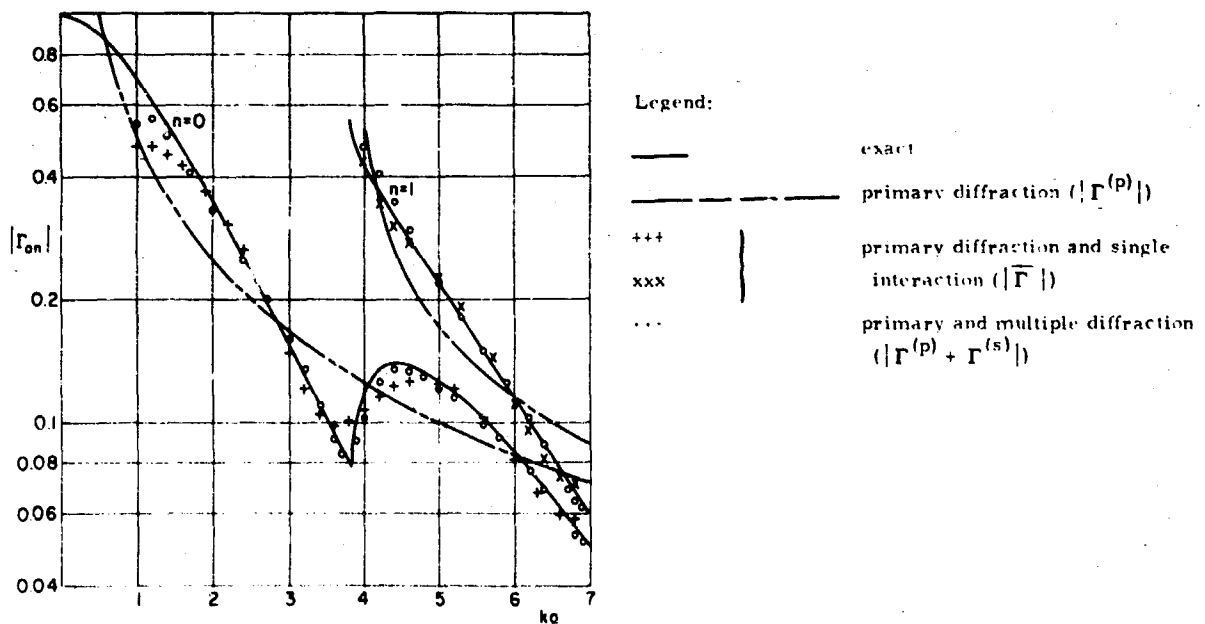


Fig. 1(a) Reflection Coefficient Amplitudes for  $n = 0$  and  $n = 1$  Mode, with  $q = 0$  Mode Incident

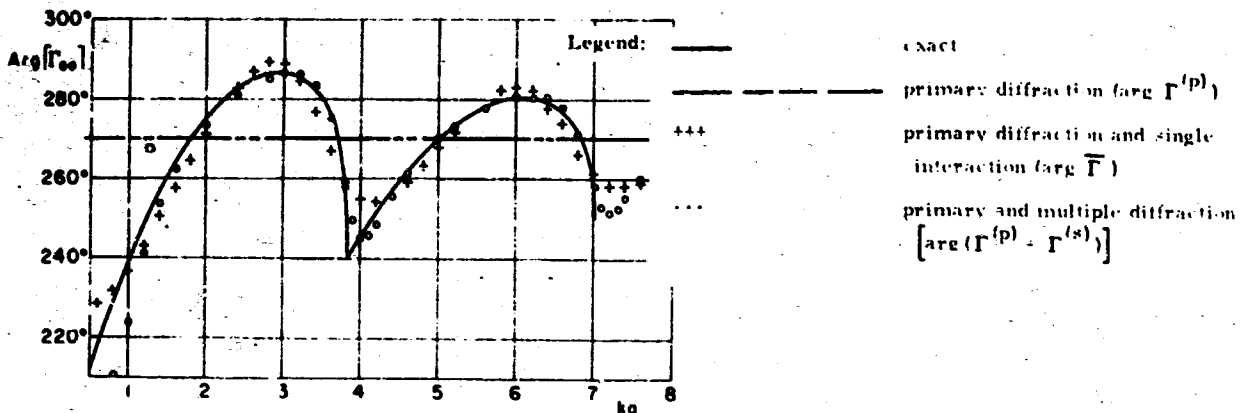


Fig. 1(b) Reflection Coefficient Phase for  $n = 0$  Mode, with  $q = 0$  Mode Incident

shows the phase.  $\Gamma_{qn}$  refers to the reflected wave observed in the  $n$ -th mode due to an incident  $q$ -th mode, with the mode indices  $n$  or  $q$  relating to the radial periodicity (the curves refer to the azimuthally symmetric case). The dashed curves, obtained from very simple primary diffraction formulas, are seen to predict the average behavior of the relevant quantities. They do not account for undulations which are particularly pronounced near the cutoff point of any of the propagating modes. Inclusion of single interaction of the primary diffraction fields across the mouth of the tube gives rise to the results indicated by crosses in Fig. 1 and produces much of the fine structure. Even these formulas are quite elementary. Inclusion of multiple interaction, indicated by black dots, provides further refinement and remarkable accuracy even at  $(ka)$  values close to unity for the lowest symmetric mode and also near the cutoff point of higher order modes.

The accuracy of results computed by the ray method thus having been established even at low frequencies, the method can be used with confidence for calculations for which exact data are not known or not readily available. An illustration is the reflection coefficient chart for the unflanged guide excited in the lowest symmetric mode as shown in Fig. 2, carried out to large  $(ka)$  values. These curves are obtained by using the multiple interaction formulation. Since the ray technique is expected to be better at high frequencies, there is no reason to suspect the accuracy of these computations except in the vicinity of the cutoff point of any given mode. Therefore, the curves have been terminated before the cutoff point is reached. The ray method also accounts without difficulty for flanged terminations for which no exact solutions are known. For the special case of a right-angle flange, one finds the solid curves in Fig. 3, against which the previously obtained results for the unflanged case are shown for comparison. Evidently, the presence of the flange reduces the reflection coefficient magnitude from its value for the unflanged case, a not unexpected result since the flange softens the edge singularity associated with a thin-walled tube. The quality of these results should be

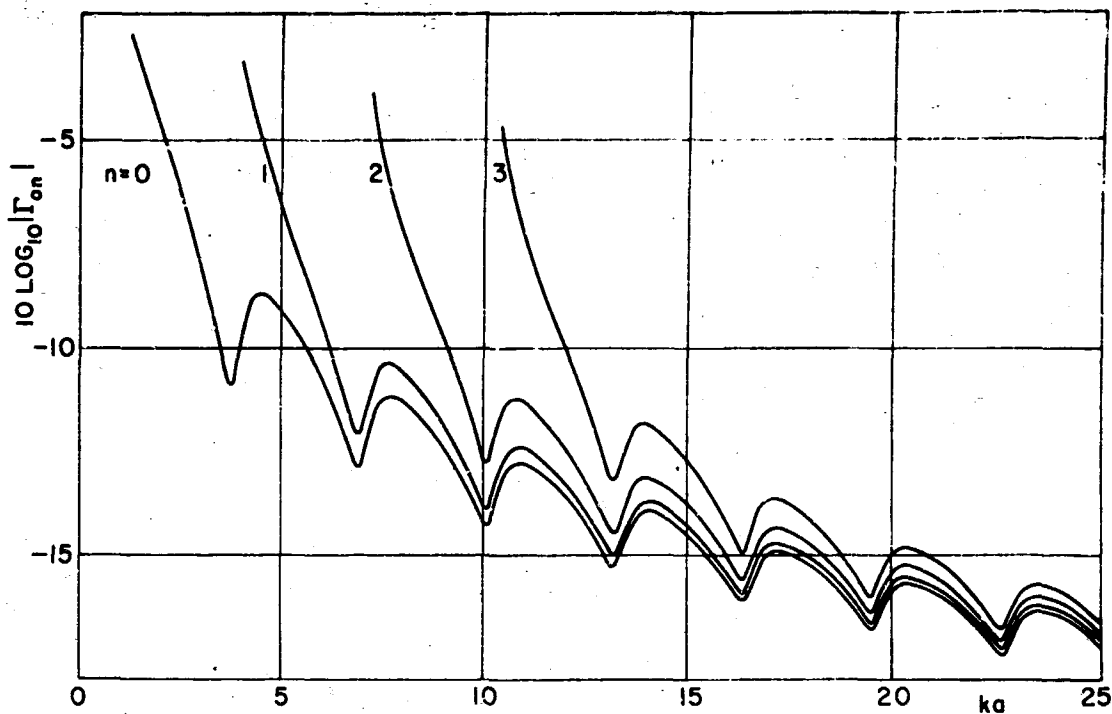
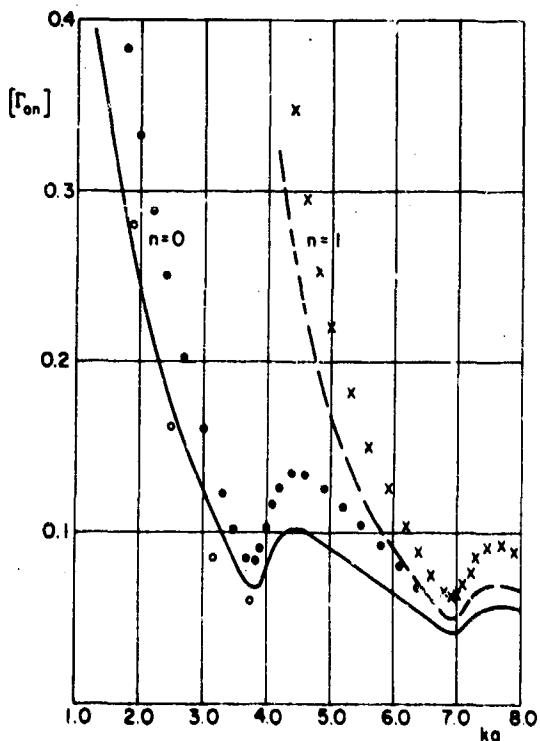


Fig. 2 Reflection Coefficient Amplitudes for Higher Order Modes, with  $q = 0$  Mode Incident



Legend: — flanged, ... unflanged.  
 ooo variation: (flanged pipe)

Fig. 3 Reflection Coefficient Amplitude: Comparison of Flanged and Unflanged Pipes, with  $q = 0$  Mode Incident

comparable to that achieved for the unflanged pipe. Also shown are low-frequency data obtained by the variational method<sup>2</sup> which are seen to agree reasonably well with our calculations.

Joint Services Technical Advisory Committee  
AF 49(638)-1402

L. B. Felsen

#### REFERENCES

1. Progress Report No. 31 to JSTAC, Polytech. Inst. of Brooklyn Report No. R-452. 31-67, pp. 1-9; Progress Report No. 32 to JSTAC, Report No. R-452. 32-67, pp. 21-29.
2. L. A. Wainstain, "The Theory of Sound Waves in Open Tubes," Zh. Tekh. Fiz. (Russian), 19(1949), p. 911-930.
3. J. W. Miles, "The Coupling of a Circular Cylindrical Tube to a Half-Infinite Space," J. Acoust. Soc. Am. 20(1948), p. 652-664.

#### BOUNDARY LAYER THEORY AND UNIFORM ASYMPTOTIC EXPANSIONS IN DIFFRACTION PROBLEMS

E. Zauderer

In a previous report<sup>1</sup> a method was presented for obtaining uniform asymptotic expansions in and near transition regions that occur in the asymptotic solution of various electromagnetic diffraction problems. The method was based on the use of the boundary layer theory to determine the special functions which must enter into the uniform expansion. We refer to Ref. 1 for a full discussion and references.

It was emphasized<sup>1</sup> that the choice of boundary layer variables plays an important role in determining the form of the boundary layer expansion and, subsequently, the assumed form of the uniform expansion. To determine the field asymptotically in the transition regions using either the boundary layer method or the uniform method, the ray expansions outside the transition regions must be known. It is the confluence of a set of rays or, equivalently, the wavefronts which invalidate the ray expansions.

An example in the vicinity of a smooth two-dimensional caustic with two sets of boundary layer coordinates was considered as in Ref. 1. One coordinate was a length along the caustic curve. The other was either the normal distance from the curve or a distance along the positive or negative tangent line (which correspond to the ray directions). We next introduce another possible set of coordinates. Let  $\psi = \text{const.}$  be the wavefronts of the incoming field and  $\tau = \text{const.}$  be the wavefronts of the outgoing field (i. e. the field after it has passed the caustic). Using the  $(\tau, \psi)$ -coordinate system we can immediately obtain ray expansions away from the caustic in the form,

$$u = \begin{cases} e^{ik\phi(x,y)} \sum_{n=0}^{\infty} v_n(x,y) k^{-n} \\ e^{ik\psi(x,y)} \sum_{n=0}^{\infty} w_n(x,y) k^{-n} \end{cases}$$

At the caustic these expansions fail, for  $\phi = \text{const.}$  and  $\psi = \text{const.}$  are tangent to each other along it. Accordingly we seek a new system of boundary layer coordinates. One appropriate set is

$$\alpha = \begin{cases} \phi, & \beta = \phi - \psi \\ \psi \end{cases}$$

and another is

$$\alpha = \frac{\phi + \psi}{2}, \quad \beta = \frac{\phi - \psi}{2}$$

since  $\phi$  and  $\psi$  are symmetric near the caustic. In any case, the coordinate  $\beta$  undergoes the stretching, since it essentially gives the distance from the caustic curve which is located at  $\beta = 0$ . That the appropriate stretching is of order  $k^{-1}$  is not difficult to motivate. While the argument of the exponential and Airy functions that arise from this boundary layer approach are exactly those that occur in the uniform expansion, the boundary layer expansion obtained by standard perturbation methods would still not yield the correct uniform expansion. To achieve it we must proceed as in Ref. 1.

In the neighborhood of a shadow boundary, e. g. that arising in diffraction by a half-plane, or in the transition region for the lateral waves in the interface problem, the above approach involving wavefront coordinates and their differences leads directly to the Weber functions that are known to occur in these problems. Then, it is easy to generate a uniform asymptotic expansion.

In cases where three or more wavefronts coalesce to form a transition region, the situation is more complicated since that generally means that two or more boundary layers intersect. Thus, more than one boundary layer variable must be stretched and the "uniform" boundary layer coordinates must reflect this fact. Such cases occur near the cusp of a caustic or near a finite caustic.

Joint Services Technical Advisory Committee  
AF 49(638)-1402

E. Zauderer

#### REFERENCES

1. E. Zauderer, "A Technique for Obtaining Uniform Asymptotic Expansions from Boundary Layer Theory as Applied to Diffraction Problems," Progress Report No. 32 to the Joint Services Technical Advisory Committee, PIBMRI Report No. R-452, 32-67 (Sept. 1967).

### EFFECTS ENCOUNTERED IN THE THEORY OF DIFFRACTION OF A FOCUSED WAVE BY AN OPAQUE OBSTACLE

L. B. Felsen and L. Levey

A converging wave may form a region of geometric optical shadow whose boundary is the caustic of the rays characterizing the wave. As is well known, Airy integrals are appropriate canonical functions for the description of the high frequency fields in the neighborhood of the caustic. Geometric optical shadow regions also occur when a non-convergent wave is incident upon an opaque obstacle. The shadow boundaries consist in this case of those rays which just graze the obstacle. Expressions for the high frequency fields near the grazing rays involve Fresnel integrals as canonical functions.

When an opaque object is illuminated by a convergent wave, new phenomena are encountered since both types of shadow boundary curves (i. e., caustic and grazing ray) are present. This is illustrated in Fig. 1 in which are shown some of the rays (numbered

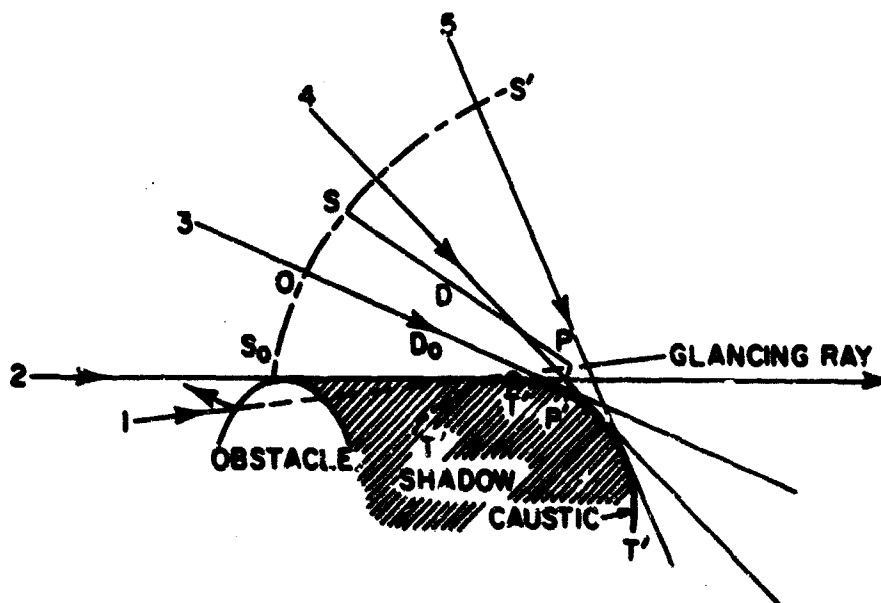


Fig. 1 Terminated Caustic

1 through 5) of a two-dimensional converging wave that, in the absence of an obstacle, possesses the caustic  $T'TT''$ . The shadow region in the presence of the obstacle is bounded by the curve  $S_0 TT'$  composed in part of the grazing ray (2) and in part of the caustic  $TT'$  of the undisturbed rays of the wave. Neither an Airy integral nor a Fresnel integral can serve as a canonical function in expressions for the high frequency fields in the vicinity of the point of contact  $T$  of the two distinct curves delimiting the shadow region. A transition function applicable to this region is considered here.

A composite shadow boundary having features similar to those of Fig. 1 can also occur for certain problems involving layered inhomogeneous media. An integral formulation



and analysis of such problems is given in Ref. 2. Aspects of the transition function to be discussed are also relevant to scattering problems involving certain curved strips and non-uniformly illuminated apertures.

One procedure yielding the desired transition function consists in part of determining an equation for this field that is simpler than the reduced wave equation and is applicable as an approximation in a layer about the composite shadow boundary. This approach has been applied in Ref. 1 to a smooth caustic for which only one of two spatial variables needed to be "stretched". For the composite shadow boundary considered here, the "stretching" of two spatial variables is required.

It is convenient to employ caustic components  $(\xi, \eta)$ , defined in terms of the caustic of the incident wave, as spatial variables. From a point in the illuminated region a tangent is drawn to the caustic, as shown in Fig. 2 for P and P'.  $\eta$  is equal to the arc-

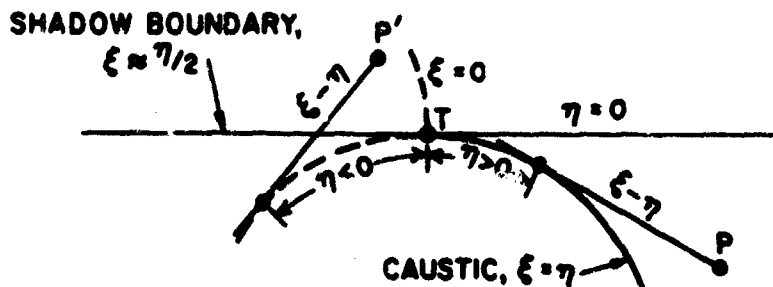


Fig. 2 Caustic Coordination

length along the caustic from the contact point T to the corresponding point of tangency and  $\xi$  is equal to the sum of  $\eta$  and the length along the tangent. If the total field  $u(\xi, \eta)$  is expressed in the form

$$u(\xi, \eta) = e^{ik\xi} e^{-i2/3k\xi^3/2a^2} w_1(\xi, \eta), \quad (1)$$

where  $t = \xi - \eta$  and "a" is the radius of curvature of the caustic at T, and the caustic coordinates are "stretched" by the substitution

$$x = \left(\frac{ka}{2}\right)^{1/3} \frac{\xi}{a}, \quad y = \left(\frac{ka}{2}\right)^{2/3} \left(\frac{\xi - \eta}{a}\right)^2, \quad (2)$$

then the approximate boundary layer equation derived from the reduced wave equation is given by

$$i \frac{\partial w}{\partial y} + \gamma w_1 + \frac{\partial^2 w_1}{\partial x^2} = 0. \quad (3)$$

(Relevant details leading to Eq. (3) may be found in Refs. 3 and 4 in connection with problems of a different character but similar geometry.)

Equation 3 is a parabolic differential equation of the form applied by Fock<sup>3</sup> and others in analyses of the high frequency fields near the surfaces of convex diffracting bodies. Whereas in these analyses, solutions to Eq. (3) are obtained by separation of variables, in the present case appropriate solutions are in the form of "incomplete Airy functions". These functions are defined by integrals of the form

$$\mathcal{J}(\alpha, \beta) = \int_{\beta}^{\infty} e^{i(1/3 s^3 + \alpha s)} ds \quad (4)$$

where the upper limit lies within one of the three sectors of the  $s$ -plane for which the integral converges. If we let  $\alpha = -y$  and  $\beta = -x$ , it is simple to show that Eq. (4) satisfies Eq. (3).

The transition function for the region about the point of contact is given by Eq. (1) with

$$\begin{aligned} w_1 &= \frac{k^{1/6} A[\theta(\tau)]}{\sqrt{\pi} 2^{1/6} a^{1/3}} e^{-i\pi/4} \mathcal{J}_1(-y, -x) \\ &= \frac{k^{1/2} A[\theta(\tau)]}{\sqrt{\pi} 2^{1/6} a^{1/3}} e^{-i\pi/4} I_1(-t'^2, -\xi'; k) \end{aligned} \quad (5)$$

$A(\theta)$  is a prescribed (and assumed slowly varying) function which determines the amplitude of the incident geometric optical field along the rays arriving from the direction  $\theta$ .  $\theta(\tau)$  designates the direction of the ray tangent to the caustic at  $\tau$ . The integral  $I_1$  is defined by

$$I(\alpha, \beta; k) = \int_{\beta}^{\infty} e^{ik[1/3 s^3 + \alpha s]} ds$$

and

$$\xi' = \frac{\xi}{(2a^2)^{1/3}}, \quad t' = \frac{t}{(2a^2)^{1/3}}.$$

Subscripts on  $I$  and  $\mathcal{J}$  denote that the upper limits are taken in the sector  $0 \leq \arg s < \frac{\pi}{3}$ . It is noted that  $I_1$  has saddle points at  $s = \pm t'$ .

To demonstrate that an appropriate transition function for the region about  $T$  is given by Eqs. (1) and (5), it should be shown that the resulting expression connects in a continuous manner with other high frequency descriptions of the field known to be valid in the various geometric optical domains in the neighborhood of  $T$ . This has been done and requires a detailed examination of the asymptotic properties of the relevant incomplete Airy functions which will not be carried through here. We will, as an example,

consider only the case when the field point departs from T but remains near the caustic.

The caustic is described by the curve  $\xi - \eta = t = 0$  so that in the lit region near the caustic  $\xi > t \approx 0$ . The integral  $I_1$  has two neighboring real saddle points. Its endpoint is to the left of the negative saddle point and recedes from it as the field point moves away from T. It may be shown that in this case

$$I_1 \sim \frac{2\pi}{k^{1/3}} \text{Ai}(k^{2/3} \alpha) - \frac{1}{ik} \frac{1}{\alpha + \beta^2} e^{ik(1/3 \beta^3 + \alpha \beta)} + O\left(\frac{1}{k^2}\right) \quad (6)$$

When Eq. (6) is substituted in Eqs. (1) and (3), the first term reproduces the high frequency field associated with the region about a smooth caustic of a converging wave. The second term may be shown to be descriptive of the field diffracted by the obstacle at the grazing point of the incident wave.

Air Force Cambridge Research Laboratories  
Office of Aerospace Research  
F 19628-68-C-0072

L. Levey

#### REFERENCES

1. R. N. Buchal and J. B. Keller, "Boundary Layer Problems in Diffraction Theory," *Comm. Pure Appl. Math.* **XIII** (1960), 85-114.
2. L. Levey and L. B. Felsen, "On Transition Functions Occurring in the Theory of Diffraction in Inhomogeneous Media," *J. Inst. Maths. Applics.*, **3** (1967), 76-97.
3. V. Fock and L. Wainstein, "On the Transverse Diffusion of Short Waves Diffracted by a Convex Cylinder," in *Electromagnetic Theory and Antennas*, ed. by E. C. Jordan, (Oxford: Pergamon Press, 1963), 11-25.
4. G. D. Malyuzhinets and L. A. Vaynshteyn, "Transverse Diffusion in Diffraction by an Impedance Cylinder of Large Radius, Part I, Parabolic Equation in Ray Coordinates," *Radio Engineering and Electronic Physics*, **6**, (1961), 1106-1117.

#### PROPAGATION AND SCATTERING IN THE PRESENCE OF BOUNDED FLUCTUATING MEDIA

L.B. Felsen, I. Kupiec and S. Rosenbaum

The major portion of the technical literature on propagation in fluctuating media is concerned with regions of unbounded extent, and scattering due to finite regions has usually been taken into account by the Born approximation. Use of the Born approximation involves the assumption that the average field in the fluctuating medium differs little from that in the exterior, thereby limiting the applicability to tenuous media and to weak fluctuations. To this order of approximation, the boundary conditions on the surface between the exterior and the fluctuating medium play no role in the formulation of the scattering problem.

When the average properties of the scattering medium differ markedly from those of the exterior region, or when the scattering medium fluctuates strongly, the above-

mentioned boundary conditions can no longer be ignored. If the medium boundary itself undergoes fluctuations, as is indeed the case for applications such as scattering from turbulent plasmas, even the proper formulation of the boundary conditions becomes a major undertaking. For this reason, it is advisable to explore first the effect of deterministic boundary conditions. In this connection, it is of special interest to ascertain under what circumstances certain average propagation and scattering characteristics in the presence of bounded media can be determined from those in unbounded media merely by assigning to the finite scattering volume the refractive index properties descriptive of propagation of the average field in the infinite volume. If this can be done, calculation of the average field in the presence of a bounded fluctuating medium is carried out in the same manner as for a deterministic medium. Evidently, such a procedure ignores the possibility of coupling from the fluctuating field to the average field via the boundary surface.

We are presently involved in a program aimed at the clarification of the questions raised above. A convenient starting point is the "bilocal" approximation<sup>1</sup> which, in an unbounded randomly-fluctuating medium with sufficiently long correlation time, leads to a modified refractive index  $n'$  for the average (coherent) wave that accounts for continuous scattering into the fluctuating (incoherent) wave. The incoherent field, however, is singly scattered in the sense that, once generated by the average wave, it propagates through a medium described by the average refractive index  $\langle n \rangle$  without further scattering (the fluctuating refractive index is written as  $n(\underline{r}) = \langle n \rangle + n_1(\underline{r})$ ). In performing a calculation, one first finds the average field  $\langle u \rangle$  and uses it as the driving term for the determination of the incoherent field  $u_1 = u - \langle u \rangle$ . It may now be appreciated why the above-mentioned procedure for bounded media, if applicable, simplifies substantially the evaluation of the coherent as well as the incoherent fields. In one of the very few papers attempting to deal with bounded fluctuating media by a method superior to the Born approximation, validity of this procedure has in fact been assumed without justification<sup>2</sup>.

Our efforts at clarifying the influence of a boundary on the dispersive properties of a fluctuating medium have proceeded along two different lines, both utilizing the bilocal approximation. The first, and more rigorous, seeks a self-consistent solution of the bilocal equations subject to the correct (though idealized) boundary conditions on the total field, thereby allowing for coupling between the average and incoherent fields at the interface. Due to complexity encountered in this approach, results have been obtained so far only for a one-dimensional problem wherein a plane wave impinges normally from vacuum onto a fluctuating half space, with the fluctuations in the medium constrained to the coordinate along the propagation direction. Two different methods, valid for different parameter ranges, have been employed in the one-dimensional case. The first, by S. Rosenbaum, provides in the limit of small-scale fluctuations (correlation length  $a \rightarrow 0$ )

but for arbitrary  $\langle n \rangle$  an approximate differential equation for the average field which can be solved in terms of Bessel functions<sup>3</sup>. The second, used by I. Kupiec, reduces the problem to an integral equation of the Wiener-Hopf type which can be solved by standard techniques; the value of the average refractive index  $\langle n \rangle$  is now required to be approximately the same as in vacuum, but finite correlation lengths "a" are allowed if the medium fluctuations are sufficiently weak. Both approaches exhibit coupling effects due to the interface which affect the propagation properties of the coherent wave, especially when the refractive index fluctuations are large or when  $\langle n \rangle$  differs substantially from unity. Implications of the results obtained by the different methods are now under study. The calculations are also being compared with available exact numerical data for scattering by a one-dimensional random slab<sup>4</sup>, and with the simple but semi-heuristic method in Ref. 2.

The second line of approach alluded to above is motivated phenomenologically. In this investigation, carried out primarily by I. Kupiec, it is assumed that a plane wave incident from vacuum on a fluctuating half space (fluctuations are now permitted in two dimensions) generates in the medium an average plane wave with a modified and as yet unspecified amplitude  $A$  and wavenumber  $\bar{k} = k_0 \bar{n}$ , where  $k_0$  is the wavenumber in vacuum.  $\bar{n}$  is assumed to be complex to account for scattering into the incoherent field. To determine properties of  $\bar{n}$ , the energy scattered out of a cylindrical volume excited by the average wave is computed in the bilocal approximation, due account being taken of the presence of the interface, and this scattered energy is equated to the energy loss experienced in the same volume by the postulated plane wave. The resulting energy balance equation provides a relation between the real and imaginary parts of  $\bar{n}$  (it does not specify  $\bar{n}$  completely), and this relation turns out to be the same as in an unbounded medium (i. e., it does not depend on the presence of the interface). This result suggests that description of the transmitted field in terms of a single modified plane wave may be possible provided that the plane wave amplitude,  $(\text{Re } \bar{n})$  and  $(\text{Im } \bar{n})$  are selected so as to incorporate in some sense the properties of the interface. The validity of this conjecture is under investigation.

Air Force Cambridge Research Laboratories  
Office of Aerospace Research  
F 19628-68-C-0072

L. Felsen

Advanced Research Projects Agency  
Nonr 839(38)

#### REFERENCES

1. V. I. Tatarskii and M. E. Gertsenshtein, "Propagation of Waves in a Medium with Strong Fluctuations of the Refractive Index," *Soviet Phys. JETP* 17 (1963), p. 458.
2. P. Bassanini, et al., "Scattering of Waves by a Medium with Strong Fluctuations of Refractive Index," *Radio Science (New Series)* 2 (1967), p. 1.
3. S. Rosenbaum, "Reflection, Transmission and Scattering of Scalar Waves from a Randomly Inhomogeneous Half-Space. One-Dimensional Case," this report.

4. A. R. Hochstim and C. P. Martens, "Radar Scattering from a Plane Parallel Turbulent Plasma Slab with Step Function Fluctuations in Electron Density," Report IDA/HQ 67-6376, Institute for Defense Analyses, Washington, D. C., Sept. 1967.

REFLECTION, TRANSMISSION AND SCATTERING OF SCALAR WAVES FROM A RANDOMLY-INHOMOGENEOUS HALF-SPACE: ONE-DIMENSIONAL CASE

S. Rosenbaum

The propagation and scattering characteristics of scalar waves in randomly fluctuating, statistically homogeneous and unbounded media have been the subject matter of several intensive investigations in recent years<sup>1-9</sup>. It is well understood at least within the range of validity of the so called "bilocal" approximation to the Dyson equation<sup>3, 4</sup>, which possesses the merit of simplicity and which has broadened the range of validity of the Born approximation to a considerable extent particularly in the limit of small scale fluctuations. More recent work has been carried out which provides a more refined approximation to the Dyson equation, by accounting for multiple scattering to a still higher order (when compared with the "bilocal" approximation) and which is energetically self-consistent to a given order in some suitably selected small parameter<sup>7-9</sup>.

The simplicity of the analytical investigations in the statistically homogeneous unbounded domain stems from the fact that exact formal solutions to the Dyson equation are readily obtainable since the resulting integral (or integrand-differential) equation involve integral operators of the convolution type. Consequently, the Dyson equation is diagonal in the Fourier representation and is readily solvable. This simplifying feature is lost whenever the transmission media under study are statistically inhomogeneous or of finite extent. The "mass" operator no longer depends exclusively on the difference  $\underline{r} - \underline{r}'$  and the domain of integration is generally finite. As a result, plane waves no longer constitute eigensolutions of the Dyson equation. A recent work by Bassanini et al.<sup>10</sup> which attempted the study of scattering characteristics of a scalar wave from a randomly fluctuating half-space (in the "bilocal" approximation) suffers from an inherent inconsistency which will become evident later, and which is rectified for the simpler one-dimensional case formulated below.

The one-dimensional case, although of relatively little importance, has recently attracted the attention and interest of several investigators, due to its relative simplicity which provides additional physical insight into the scattering processes, and the recent availability of exact Monte Carlo type computations pertaining to the one-dimensional random slab<sup>11</sup>, which highlight the failure of the conventional Born approximation.

Formulation and Description of the Problem:

A monochromatic plane wave with suppressed time dependence  $\exp(j\omega t)$ ,

$$u_0(z) = e^{-jk_0 z}, \quad k_0^2 \equiv \omega^2 \mu_0 \epsilon_0 \quad (1)$$

is incident upon the half-space  $z > 0$  filled with a randomly fluctuating medium, characterized by a random permittivity function

$$\hat{\epsilon}(z) = \langle \hat{\epsilon} \rangle (1 + \epsilon(z)) \quad (2)$$

where the temporal fluctuations are presumed slow and thus regarded as changes in the realizations of the random function  $\epsilon(z)$  (quasi-monochromatic approximation).

The statistical characteristics of a scalar wavefunction  $u(z)$  are sought, which obey the one-dimensional reduced wave equations (note:  $k^2 = k_0^2 \langle \hat{\epsilon} \rangle$ ,  $\langle \epsilon(z) \rangle = 0$ )

$$\left( \frac{d^2}{dz^2} + k^2 \right) u_2(z) = -k^2 \epsilon(z) u_2(z), \quad z > 0 \quad (3)$$

$$\left( \frac{d^2}{dz^2} + k_0^2 \right) u_1(z) = 0, \quad z < 0 \quad (4)$$

together with the radiation condition at  $z \rightarrow \pm \infty$  and the continuity conditions

$$u_1(0) = u_2(0), \quad \frac{\partial u_1(0)}{\partial z} = \frac{\partial u_2(0)}{\partial z} \quad (5)$$

where the subscripts 1 and 2 denote the regions  $z < 0$  and  $z > 0$ , respectively.

In the region  $z < 0$ , one obtains

$$u_1(z) = e^{-jk_0 z} + \Gamma e^{jk_0 z}, \quad z < 0 \quad (6)$$

where  $\Gamma$ , the reflection coefficient, is a random variable whose characteristics are determined below. It is convenient to separate the coherent wave ( $\psi(z) \equiv \langle u(z) \rangle$ ) from the fluctuating (incoherent) part (to be denoted by  $\varphi(z) = u(z) - \psi(z)$ ) which results in

$$\psi_1(z) = e^{-jk_0 z} + \langle \Gamma \rangle e^{jk_0 z} \quad (7)$$

$$\varphi_1(z) = \tilde{\Gamma} e^{jk_0 z}, \quad \tilde{\Gamma} \equiv \Gamma - \langle \Gamma \rangle \quad (8)$$

The field in the random half-space, to be determined to the "bilocal" order, obeys the following pair of coupled equations:

$$\left( \frac{d^2}{dz^2} + k^2 \right) \varphi_2(z) = -k^2 \langle \epsilon(z) \varphi_2(z) \rangle \quad (9)$$

$$\left(\frac{d^2}{dz^2} + k^2\right) \varphi_2(z) = -k^2 \epsilon(z) \psi_2(z) \quad (10)$$

The incoherent wave, evaluated consistently with the required continuity conditions at  $z=0$ , results in

$$\varphi_1(z) = k^2 \int_0^{\infty} dz' G_1(z, z') \epsilon(z') \psi_2(z'), \quad z < 0 \quad (11)$$

where  $G_{1,2}(z, z')$  denotes the zeroth order Green's function appropriate to the configuration of Fig. 1. The expression Eq. (11) is in accord with the continuity conditions.

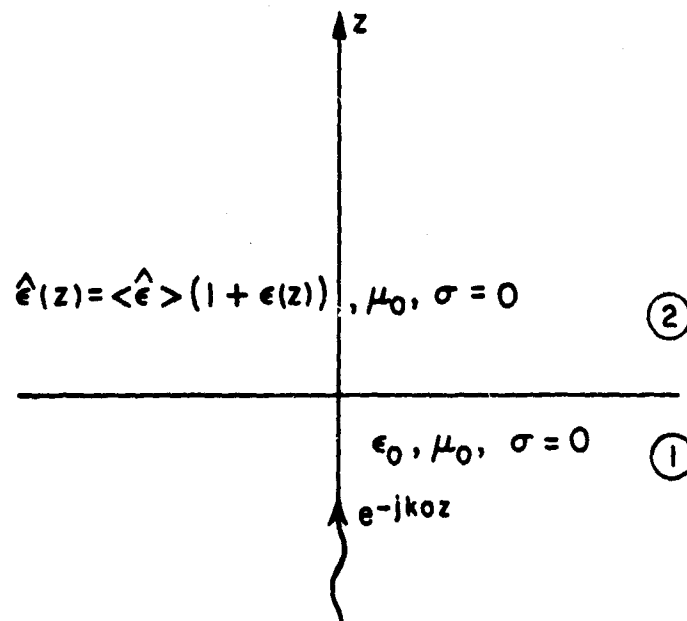


Fig. 1 Physical Configuration

$$\varphi_1(0) = \varphi_2(0), \quad \frac{\partial \varphi_1(0)}{\partial z} = \frac{\partial \varphi_2(0)}{\partial z} \quad (12)$$

as well as the radiation conditions at  $z \rightarrow \pm \infty$ . From Eq. (11) one obtains

$$\langle \epsilon(z) \varphi_2(z) \rangle = k^2 \int_0^{\infty} dz' G_2(z, z') B_{\epsilon}(z, z') \psi_2(z') \quad (13)$$

where  $B_{\epsilon}(z, z') = \langle \epsilon(z) \epsilon(z') \rangle = B_{\epsilon}(z-z')$  denotes the correlation function of the presumably wide sense homogeneous process  $\epsilon(z)$ . The substitution of Eq. (13) into Eq. (9) results in the following integrodifferential equation for  $\psi_2(z)$ :



$$\left(\frac{d^2}{dz^2} + k^2\right) \psi_2(z) = -k^4 \int_0^{\infty} dz' K(\hat{z}) \psi_2(z') - k^4 \Gamma_0 \int_0^{\infty} dz' \hat{K}(\hat{z}) e^{-j2kz'} \psi_2(z'), \quad z > 0$$

$$\left(\frac{d^2}{dz^2} + k_0^2\right) \psi_1(z) = 0, \quad z < 0$$
(14)

where  $G_2(z, z')$  has been written in the form,

$$G_2(z, z') = G_0(\hat{z}) + \Gamma_0 \hat{G}_0(\hat{z}) e^{-2jkz'}, \quad \hat{z} \equiv z - z'$$

$$G_0(\hat{z}) = \frac{1}{2jk} e^{-jk|\hat{z}|}, \quad \hat{G}_0(\hat{z}) = \frac{1}{2jk} e^{-jk\hat{z}}, \quad \Gamma_0 = \frac{k - k_0}{k + k_0}$$
(15)

and the quantities

$$K(\hat{z}) \equiv B_c(\hat{z}) G_0(\hat{z}) \quad \text{and} \quad \hat{K}(\hat{z}) \equiv B_c(\hat{z}) \hat{G}_0(\hat{z})$$

have been defined. The inconsistency in Ref. 10, which roughly follows the same analytical sequences, stems from the fact that the expression for  $\psi_2$  substituted into the equivalent of Eq. (9) is inconsistent with the continuity conditions of Eq. (12). Although expressions for  $\psi_1$  and  $\psi_2$  satisfying Eq. (12) are eventually obtained, they do not coincide with those initially used for the substitution into Eq. (9); consequently the second term of the right-hand side of Eq. (14) is missing.

In the limit of small scale fluctuations  $B_c(\hat{z})$  (and thus  $K(\hat{z})$  and  $\hat{K}(\hat{z})$ ) is sharply peaked at  $\hat{z} = 0$ . Therefore, subject to the exclusion of observation points near the interface to within several correlation lengths, the limits of integration in Eq. (14) may be extended over the infinite domain  $-\infty < z' < \infty$ . In the limit  $\langle \xi \rangle \rightarrow 1$ , the last term on the right-hand side of Eq. (14) may be omitted. The resultant equation is of the Wiener-Hopf type and is readily solvable without extending the range of integration.

The solution to Eq. (14) which satisfies the radiation condition at  $z \rightarrow \infty$  is of the form

$$\psi_2(z) = e^{-j\pi z} \sum_{n=0}^{\infty} a_n(\pi) e^{-j2knz}$$
(16)

It follows upon the substitution of Eq. (16) into Eq. (14), and from the orthogonality of the exponential that

$$-\pi^2 + k^2 + 2\pi k^4 K(\pi) = 0, \quad a_0 \neq 0$$
(17)

and

$$\frac{a_n}{a_{n-1}} = - \frac{2\pi k^4 \Gamma_0 \hat{K}(\eta + 2kn)}{-(\eta + 2kn)^2 + k^2 + 2\pi k^4 K(\eta + 2kn)} \quad (18)$$

where  $K(\eta)$  and  $\hat{K}(\eta)$  denote the Fourier transforms of  $K(\hat{z})$  and  $\hat{K}(\hat{z})$ , respectively.

As could be anticipated, the dispersion relation (17) (from which  $\eta$  is determined) is identical with that obtained for the unbounded domain, and entirely independent of the boundary conditions.

In the limit of small scale fluctuations, the infinite series defined by Eqs. (16-18) may be summed up in closed form; however, this limit may be treated directly by the analytical sequence illustrated below.

In this limit Eq. (14) may readily be shown to reduce to

$$\left[ \frac{d^2}{dz^2} + k^2 (1 - j\alpha - j\alpha \Gamma_0 e^{-j2kz}) \right] \psi_2(z) = 0 \quad (19)$$

where  $\alpha \equiv \sigma^2 ka$  is a conveniently defined, dimensionless parameter, in which  $\sigma^2 \equiv B_e(0)$  and  $a$ , the correlation length, is conventionally defined via,  $a = \sigma^{-2} \int_0^\infty B_e(\hat{z}) d\hat{z}$ .

It follows from Eq. (17) (in the limit  $ka \rightarrow 0$ ) that

$$\left( \frac{\eta}{k} \right)^2 \equiv \nu^2 = 1 - j\alpha \quad (20)$$

The introduction of a new independent variable

$$y = \sqrt{j\alpha \Gamma_0} e^{-jkz}, \quad \frac{d^2}{dz^2} \rightarrow -k^2 y \frac{d}{dy} y \frac{d}{dy}$$

results in the equation

$$\left[ -y \frac{d}{dy} y \frac{d}{dy} + \nu^2 - y^2 \right] \psi_2(y) = 0 \quad (21)$$

which is readily recognized to be of the Bessel type. We select for  $\psi_2(z)$  that independent solution which satisfies the radiation condition at  $z \rightarrow \infty$ , i. e.,

$$\psi_2(z) = A J_\nu \left( \sqrt{j\alpha \Gamma_0} e^{-jkz} \right), \quad z > 0 \quad (22)$$

This choice is indeed in accord with the radiation condition as may be observed from the power series expansion of Eq. (22), in which each term separately satisfies the desired condition.

It should be noted that if sources exist within the half-space  $z > 0$  the complementary solution will be needed as well.

The mean reflection and transmission coefficients follow readily from the continuity conditions at  $z=0$ , which lead to the expression,

$$A = 4 \left\{ \sqrt{j\alpha\Gamma_0} \left[ \left( \frac{1}{\nu} + \frac{k}{k_0} \right) J_{\nu-1}(\sqrt{j\alpha\Gamma_0}) + \left( \frac{1}{\nu} - \frac{k}{k_0} \right) J_{\nu+1}(\sqrt{j\alpha\Gamma_0}) \right] \right\}^{-1} \quad (23)$$

and

$$\langle \Gamma \rangle = \frac{\left( \frac{1}{\nu} - \frac{k}{k_0} \right) J_{\nu-1}(\sqrt{j\alpha\Gamma_0}) + \left( \frac{1}{\nu} + \frac{k}{k_0} \right) J_{\nu+1}(\sqrt{j\alpha\Gamma_0})}{\left( \frac{1}{\nu} + \frac{k}{k_0} \right) J_{\nu-1}(\sqrt{j\alpha\Gamma_0}) + \left( \frac{1}{\nu} - \frac{k}{k_0} \right) J_{\nu+1}(\sqrt{j\alpha\Gamma_0})} \quad (24)$$

Under the condition  $|\alpha\Gamma_0| \ll 1$  which often prevails in actual physical situations, Eq. (24) reduces to

$$\langle \Gamma \rangle = \frac{k_0 - \eta + \frac{1}{4}jk\alpha\Gamma_0}{k_0 + \eta - \frac{1}{4}jk\alpha\Gamma_0} \quad (25)$$

In the limit  $\Gamma_0 \rightarrow 0$  the reflection coefficient  $(k_0 - \eta)(k_0 + \eta)^{-1}$  is that derived by simply replacing the fluctuating medium by an effective medium obtained from the analysis of the corresponding unbounded problem. This procedure is clearly unjustified in the general case.

The incoherent wave intensity in free half-space ( $z < 0$ ) follows directly from Eq. (11):

$$\langle |v_1(z)|^2 \rangle = \frac{k^2 T_0}{4} \int_0^\infty dz_1 \int_0^\infty dz_2 B_c(z_1 - z_2) e^{-jk(z_1 - z_2)} v_2(z_1) v_2^*(z_2) \quad (26)$$

which in the small scale limit reduces to:

$$\langle |v_1(z)|^2 \rangle = \frac{k^2 |T_0|^2}{4} \cdot 2_a |A|^2 \int_0^\infty dz_1 \left| J_\nu(\sqrt{j\alpha\Gamma_0}) e^{-jkz_1} \right|^2 \quad (27)$$

where  $T_0 = 2k(k+k_0)^{-1}$ . The expression for  $\langle |v_2(z)|^2 \rangle$  follows from Eq. (11) in an analogous manner.

Before terminating the discussion, the following comments should be made. Although the physical interpretation of the wavefunctions represented by Eqs. (16-18) or Eq. (22) is not completely transparent, it is clear that the appearance of the high order terms ( $\sim \exp[-jx(\eta + 2kn), n \geq 1]$ ) represents the interaction between the coherent field and the incoherent wave reflected from the interface. This effect which is considerable in one-dimensional configurations may play a secondary role when a three-dimensional problem is considered. This anticipation stems from the following rather vague physical observation. In the one-dimensional case the waves (both coherent and incoherent) are confined to the postulated one-dimensional space. Both waves propagate along the same direction at almost equal speeds providing suitable conditions for mutual interaction. In the multidimensional scattering configuration, on the other hand, the incoherently scattered wave is virtually radial (in the limit  $ka \ll 1$ ) and only a small part of the energy carried by the incoherent wave can be found within the spectral range suitable for effective interaction. Consequently, any attempt to extend one-dimensional results or interpretations to the multidimensional case should be approached with caution. The work reported here is incomplete in several respects (even within the framework of the one-dimensional problem): a) The starting point of the analysis has been the "bilocally" approximated Dyson equation which is particularly useful in the limit of small scale fluctuations. The scattering from a randomly fluctuating half-space in the limit of large scale fluctuations is currently under investigation. b) Also under study is the more significant (but considerably more complicated) slab problem. In the small scale limit, the coherent wavefunctions no longer satisfy Bessel's equation but the more complicated Mathieu equation.

Air Force Cambridge Research Laboratories  
Office of Aerospace Research  
F 19628-68-C-0072

S. Rosenbaum

Advanced Research Projects Agency  
Nonr 839(38)

#### REFERENCES

1. R. C. Bourret, "Stochastically Perturbed Fields, with Applications to Wave Propagation in Random Media," *Nuovo Cimento*, Vol. 26, 1, (1962).
2. R. C. Bourret, "Propagation of Randomly Perturbed Fields," *Can. J. Phys.*, Vol. 40, 782, (1962).
3. V. I. Tatarskii and M. E. Gertsenshtein, "Propagation of Waves in a Medium with Strong Fluctuations of the Refractive Index," *Soviet Phys. JETP*, Vol. 17, 2, 458, (1963).
4. V. I. Tatarskii, "Propagation of Electromagnetic Waves in a Medium with Strong Dielectric-Constant Fluctuations," *Soviet Phys.* Vol. 19, 4, 946, (1964).
5. W. P. Brown, "Propagation in Random Media - Cumulative Effect of Weak Inhomogeneities," *Trans. on Ant. & Prop.*, AP-15, 1, 81, (1967).
6. U. Frisch, "Wave Propagation in Random Media II - Multiple Scattering by N-Bodies (Provisional version), *Inst. d'Astrophysique*, Paris, (1965).
7. K. Furutsu, "On the Statistical Theory of Electromagnetic Waves in a Fluctuating Medium I," *J. Res., N. D. S.*, 67D, 303, (1963).

8. W. P. Brown, "Coherent Field in a Random Medium - Effective Refractive Index," Proceedings of the Symposium on Modern Optics, PIB, 1967.
9. S. Rosenbaum, "On Energy-Conserving Formulations in a Randomly Fluctuating Medium," Proceedings of the Symposium on Turbulence of Fluids and Plasmas, PIB, 1968.
10. P. Bassanini, C. Cercignani, F. Sernogiotto and G. Tironi, "Scattering of Waves by a Medium with Strong Fluctuations of Refractive Index," Radio Science, Vol. 2, No. 1, p. 1, (1967).
11. A. K. Hochstim, C. P. Martens, "Radar Scattering from a Plane Parallel Turbulent Plasma Slab with Step Function Fluctuations in Electron Density," Report IDA/HA 67-6376, Inst. for Def. Analyses, Wash., D. C., Sept., 1967.

#### NON-UNIFORMITY EFFECTS IN MICROWAVE PLASMA DIAGNOSTICS

J. W. E. Griemsmann

Possible electromagnetic errors are analyzed for a particular  $TM_{010}$  mode cavity diagnostic measurement used in wake studies in ballistic ranges. The wake is modeled by a cylindrical plasma column having a radial distribution of electron density specified by  $N = N_p e^{-\alpha r^2}$  where  $r$  is the radius and  $N_p$  is the peak electron density. Wide ranges of average and peak electron density along with several pertinent collision frequencies are considered, including values extending beyond those for which the cavity measurement is intended. One source of error investigated is the effect of the usual measurement assumption that the cavity measures the total count of electrons within its field regardless of the distribution of electrons. The other source of error investigated is the possibility for power leakage through the open pipes of the cavity via higher modes which are conceivably capable of propagating under non-uniform conditions. The influence of non-uniform electron distribution on the error have been determined for a wide range of electron density and formulas derived for hybrid lossy leakage modes.

Shown in Fig. 1 is a schematic depicting cavity diagnostics of a ballistic range wake as used at Lincoln Laboratories.<sup>1</sup> The phase measuring circuit scheme indicated there is used to measure a wide range of electron densities. The arrangement may be shown, in any case, to measure the radial input admittance  $Y_{in}$  to the plasma column corrected for appropriate evanescent fringe field effects of the open pipes as illustrated in Fig. 2. Not taken into account in this measurement are the possibilities of power leakage out the open pipes via spurious modes and the possibilities for spurious Tonks-Dattner electro-acoustic resonances.<sup>2</sup>

Several examples of the radial electron density distribution for the cylindrical plasma models are shown in Fig. 3 normalized to uniform density. The maximum ratio of peak

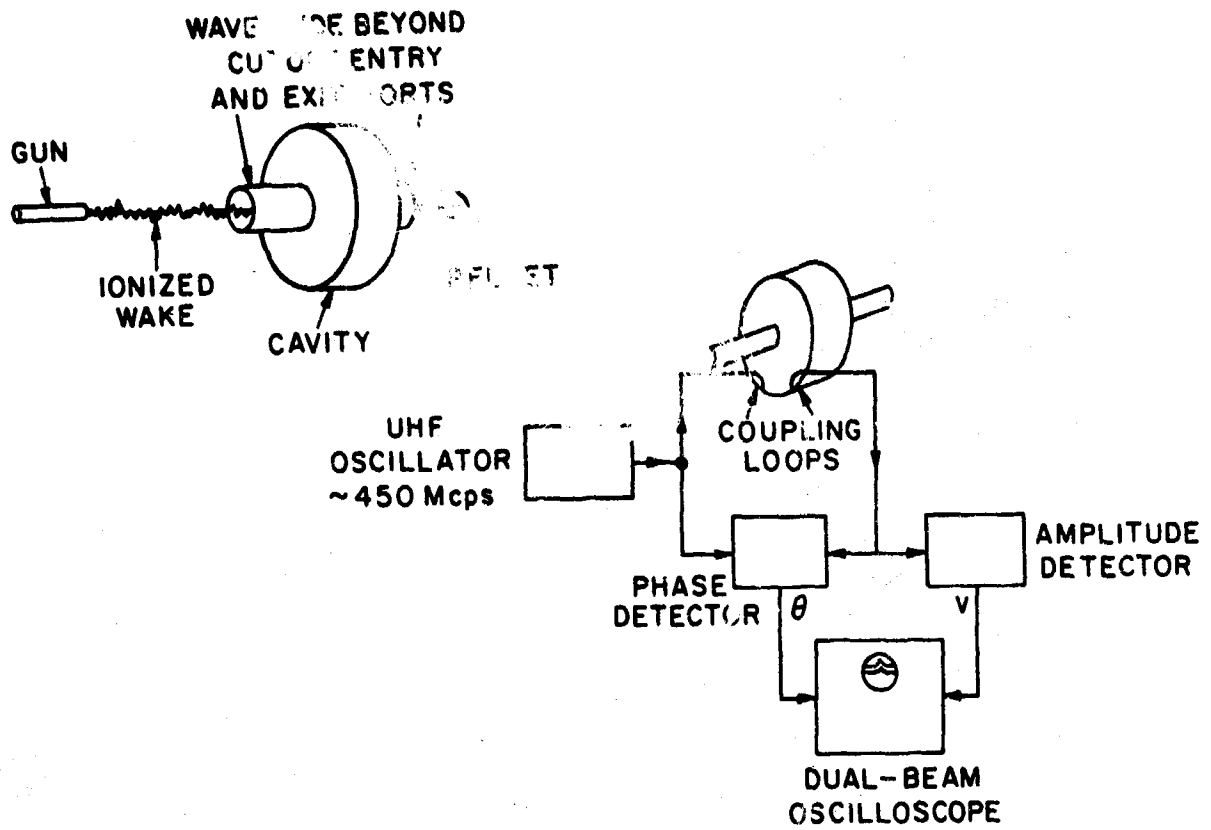


Fig. 1 Schematic of Wake Diagnostics  
(Lincoln Laboratory)

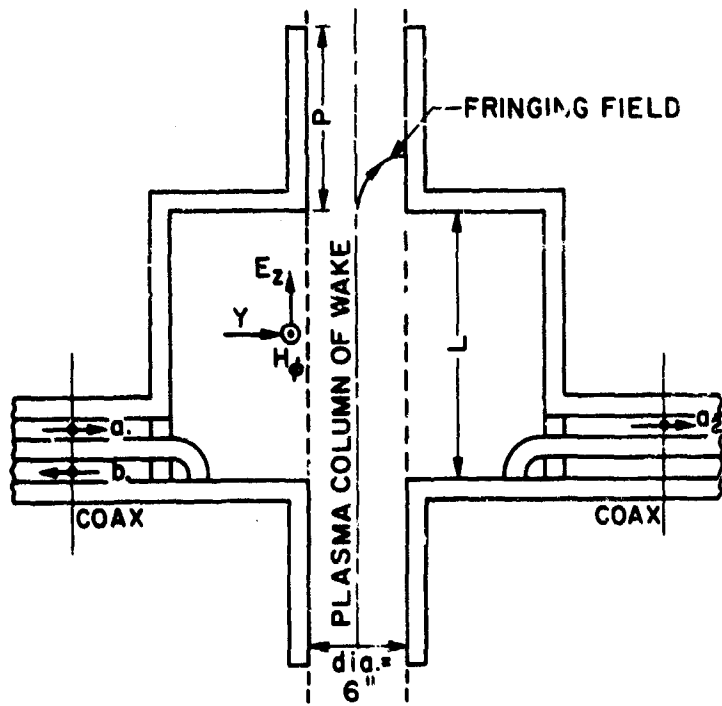


Fig. 2 Schematic of Cavity

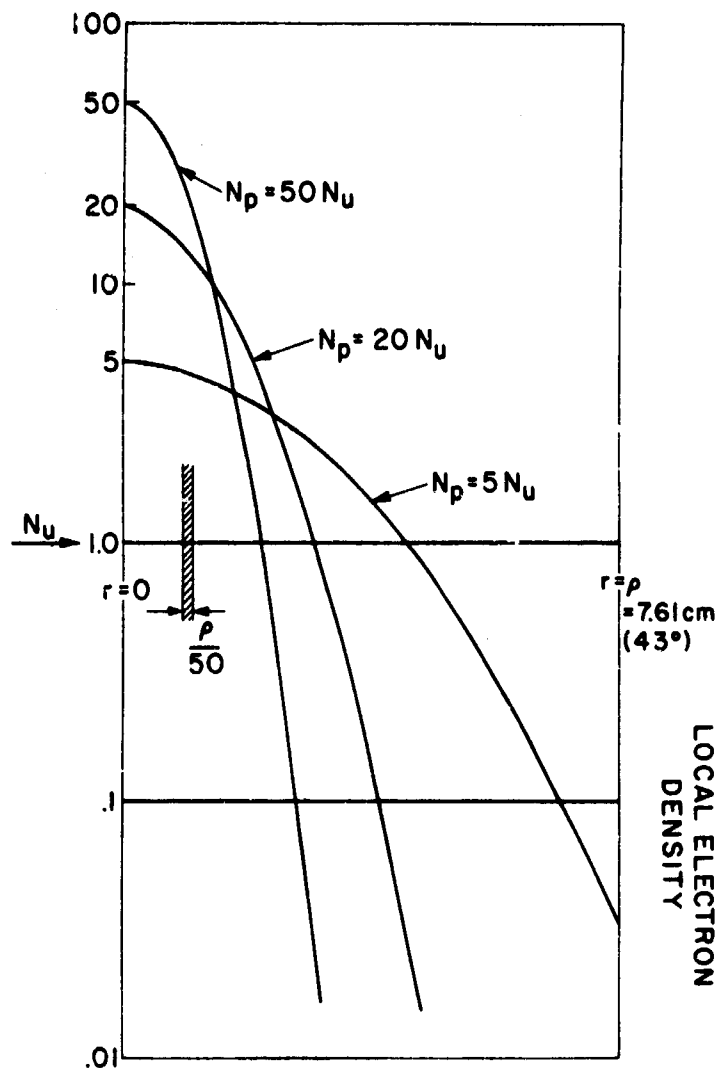


Fig. 3 Typical Electron Density Distributions

value of electron density occurring at the axis ( $r = 0$ ), was about 50 times the average density. The range of average density,  $N_u$ , was from  $10^7$  electrons per cc to  $2.5 \times 10^9$  electrons per cc. The critical density at 450 megacycles per second was thus exceeded locally in many cases. Collision frequency values,  $\nu$ , chosen were  $10^7$ ,  $10^8$ , and  $2.5 \times 10^9$  (1/sec). For the purpose of analysis, this distribution was further assumed to be represented by 50 cylindrical shells, in each of which the electron density was assumed to be uniform and equal in value to the average electron density for that shell. Radial transmission line relationships<sup>3</sup> were used to perform the analysis on a computer.

To determine measurement errors caused only by the electron density distribution, fringe field effects were neglected, and the  $TM_{010}$  mode field assumed uniform in the axial direction (infinite length plasma column). Shown in Fig. 4, for this case, is the

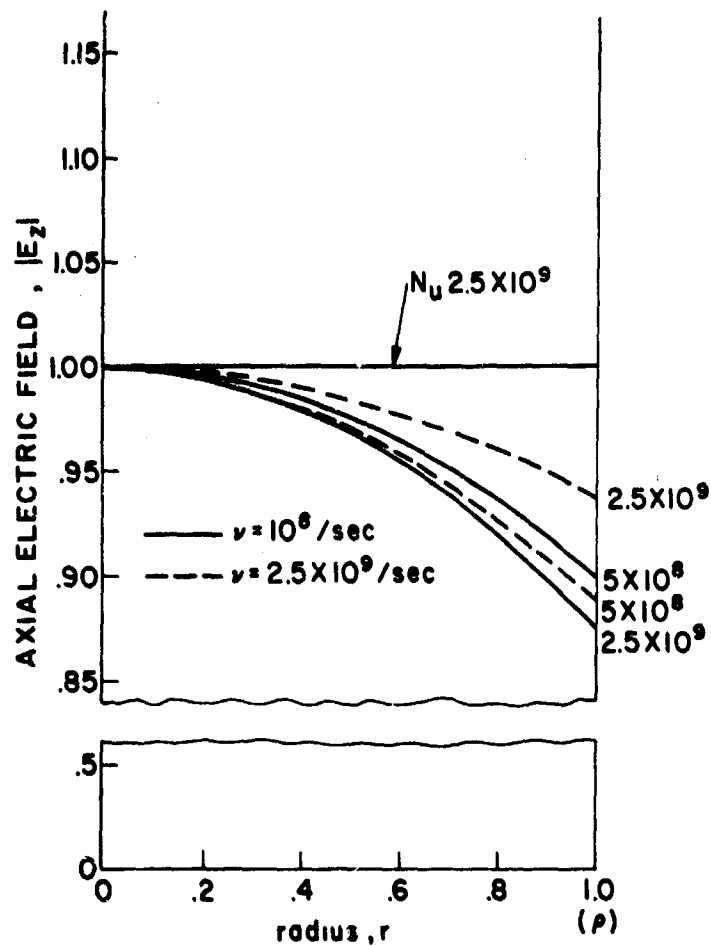


Fig. 4 Uniform Plasma Distribution

influence of the presence of uniform electron density on the axial electric field distribution. The fields are normalized to that at the axis and plotted on a suppressed scale. When the electron density is as low as  $2.5 \times 10^7$  electrons per cc, the distribution of the axial electric field is essentially equivalent to that of free space, namely, a  $J_0$  Bessel function distribution. For higher densities the electric field at the axis,  $r=0$ , is seen to be weaker with respect to the field at the input surface of the column,  $r=a$ . An interesting effect observable in the figure is that a higher collision frequency dampens the degree of magnitude change with increasing electron density.

In the computation used to obtain Fig. 4, the admittance at the input surface  $r=a$  of the plasma column is also calculated. Under the basic diagnostic measurement assumption that the input admittance is reasonably independent of electron density distribution, this value (designated as  $Y_{pu}$ ) is the value that is expected to be measured.



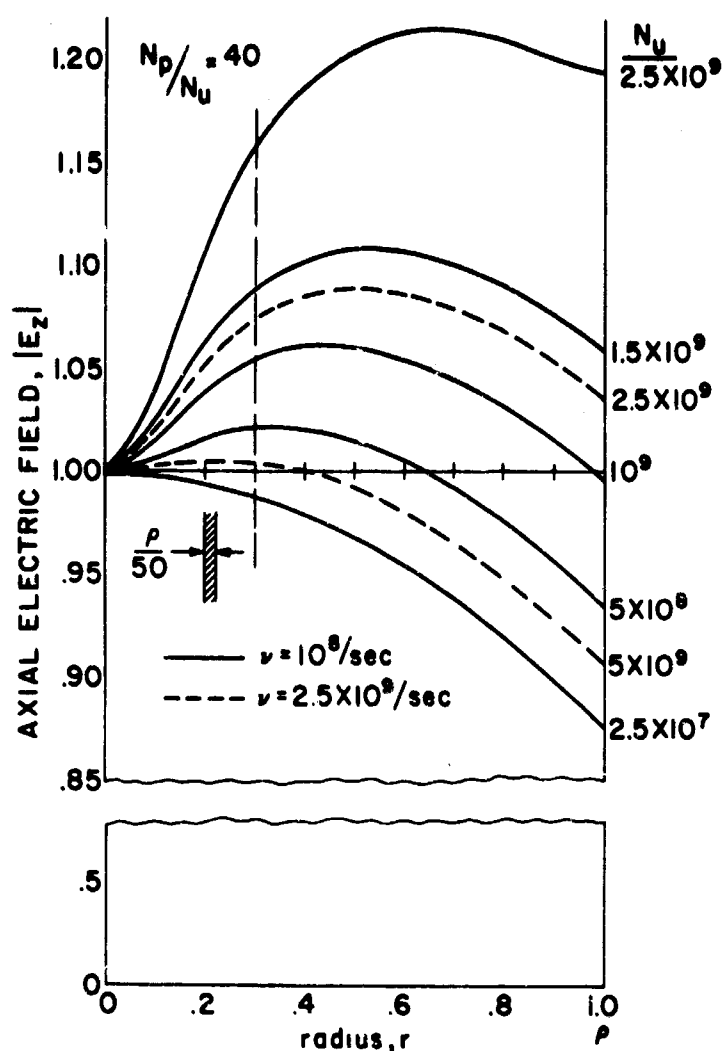


Fig. 5 Influence of Non-Uniform Distribution

The plot of Fig. 5 displays on a suppressed scale typical variations of axial electric field with radial position for an extreme peak to uniform density ratio of 40, again for the case of no axial field variation. The radius at which the local electron density equals the uniform electron density is shown as the vertical dotted line in the graph. The shielding effect of the extremes of electron density toward the center can be observed. The admittance values at the input surface to the column are also calculated for this case and designated as  $Y_{pn}$ .

Typical values of measurement error are caused by non-uniformity effects and tabulated in Fig. 6 along with the expression used for computation of error. The admittance  $Y_0$  is that measured at the input radius of the plasma column with the plasma and

$N_u$	$\nu$	$Y_u$	ERROR	
			$\frac{N_p}{N_u} = 5$	$\frac{N_p}{N_u} = 50$
$1.25 \times 10^8$	$10^8$	$.0007205 + j.3626640$	.077	.107
(1/20)	$2.82 \times 10^9$	$.0102260 + j.3728273$	.079	.119
$2.5 \times 10^8$	$10^8$	$.0014306 + j.3423846$	.068	.083
(1/10)	$2.82 \times 10^9$	$.0203775 + j.3625645$	.076	.108
$1.5 \times 10^9$	$10^8$	$.008055 + j.1472723$	(-).003	(-).100
(3/5)	$2.82 \times 10^9$	$.1179084 + j.2600734$	.056	.112

$$\text{ERROR} = \left| \frac{\Delta}{\Lambda_0} \right| = \left| \frac{Y_{pn} - Y_{pu}}{Y_{pu} - Y_0} \right|$$

$$\underline{f = 450 \times 10^6} \quad \underline{N_c = 2.5 \times 10^9} \quad \underline{Y_0 = j.3830910}$$

Fig. 6 Table of Errors

air removed (vacuo). For the values of electron density chosen (namely, 1/20, 1/10, and 3/5 of critical), and for the typical collision frequencies indicated, the measured values with non-uniformity present would be too high by at most 12%. The one negative value is beyond practical cavity measurement range. Another conclusion evident in the table is that the non-uniformity error is not diminished by going to lower electron densities at least in the range indicated. Also illustrated in part is that non-uniformity errors can occur for relatively modest non-uniformities such as  $N_p/N_u = 5$  with further error increasing only slowly with further density peaking. This latter effect may be caused by the further effective reduction of electrical radius in which most of the plasma lies. The electrical radius of the plasma column  $\frac{2\pi}{\lambda} a$  (where  $\lambda$  is the free space wavelength) is  $43^\circ$ . The above conclusion should be applied only to plasma of commensurate electrical dimensions.

Development of a specialized computer optimization program has been required to evaluate the leakage characteristics of the most detrimental leakage modes. To date

no quantitative bases for serious leakage problems have been determined.

Advanced Research Projects Agency  
Nonr 839(38)

J. W. E. Griemsmann

#### REFERENCES

1. M. Labitt, M. A. Herlin, "Application of the Resonant Cavity Method to the Measurement of Electron Densities and Collision Frequencies in the Waves of Hypervelocity Pellets," Tech. Rept. 248, Lincoln Lab., M. I. T.
2. Personal Communication and Preliminary Report from Dr. Karl-Birger Persson, N. B. S., Boulder, Colo.
3. C. G. Montgomery, R. H. Dicke, E. M. Purcell, "Principles of Microwave Circuits, published in Rad. Lab. Series (New York: Dover Press), Chapter 8, p. 240.

#### TRANSIENTS IN DISPERSIVE MEDIA

L. B. Felsen

##### 1. Introduction

The propagation of transient signals in dispersive media, a subject of long-standing interest in electromagnetics<sup>1,2</sup>, has received increased attention more recently because of its relevance to pulsed excitation of waveguides<sup>3</sup>, whistler propagation in magnetospheric ducts<sup>4</sup>, ionospheric<sup>5</sup> and VLF<sup>6</sup> propagation problems, plasma diagnostics<sup>7</sup>, etc. While certain special situations admit of a closed form solution for the transient field in terms of known functions, it is generally necessary to resort to an integral representation, usually involving a (real or complex) frequency integration of the time-harmonic result. Often, the latter is itself given only in the form of series or integrals, thereby adding to the overall complexity in the formulation of the space-time dependent field. Therefore, it has been necessary to resort to approximation procedures in order to gain explicit information about the nature of the transient response. If the field is excited by a localized source, its time-harmonic behavior in the far zone can usually be deduced by asymptotic (saddle point) techniques based on the largeness of the distance (in wavelengths) from the source region to the observation point. Since the same large parameter appears also in the resulting integral over frequency, a similar asymptotic procedure permits - often without the need for additional assumptions - the extraction of the transient response in relatively simple form. The result can be interpreted in terms of one or more "packets" of plane waves, each having a central frequency  $\omega$ , a wavenumber  $k$ , and an amplitude  $A$ , all depending on the observation point  $\underline{r}$  and on the observation time  $t$ . This simple description fails, and must be

modified, in transition regions corresponding to specific values of  $\underline{r}$  and  $t$  for which individual wave packets either are not yet fully developed or are modified by mutual interaction.

While these general aspects are well known<sup>8</sup> and some of them have also recently been summarized<sup>9</sup>, there are certain gaps in the discussion of the transient field observed at a distant observation point  $\underline{r}$  at arbitrary observation times  $t$ , especially when the dispersive properties of the medium are such as to admit of cutoffs and resonances (as in a magnetoplasma). For this reason, a more complete asymptotic treatment of the frequency integral is appropriate. It is also worthwhile to emphasize simple graphical procedures which provide quick and often quantitative insight into the propagation mechanism without the need for elaborate numerical computation.

An interesting interpretation of transient signal propagation stems from the introduction of space-time rays<sup>10-15</sup> which are only beginning to be exploited systematically by the electromagnetic propagation specialist. These concepts have been reviewed and extended for specific excitation problems by utilization of the dispersion surfaces characteristic of the medium, especially in the presence of interfaces or boundaries.

## 2. Asymptotic Evaluation of the Complex Frequency Integral

After the far-zone solution of a time-harmonic radiation or diffraction problem has been accomplished and analytic continuation into the complex frequency plane performed, determination of the transient response for a particular wave constituent requires evaluation of the typical integral

$$I = \int_{-\infty + i\alpha}^{\infty + i\alpha} f(\nu) e^{iq(\nu)} d\nu, \quad q(\nu) = \nu(\nu)r - \omega t, \quad \alpha > 0, \quad (1)$$

where  $\nu(\nu)$  denotes the frequency dependent wavenumber of the local plane wave contributing to the far zone field (in an anisotropic medium,  $\nu(\nu)$  is in general related to the ray refractive index),  $r$  is a typical (large) distance parameter, and  $f(\nu)$  is the local plane wave amplitude (which may actually depend algebraically on  $r$  although this dependence has not been indicated). The generic form, Eq. (1), accommodates many propagation phenomena in homogeneous isotropic and anisotropic media. The above-mentioned far zone approximation, if it has been utilized,

usually involves the more precise restriction  $|\xi(\omega)|r \gg 1$ , i. e.,  $\xi(\omega) \neq 0$ , which must be kept in mind in subsequent manipulations of the integral in Eq. (1). It will be assumed that  $\xi(\omega) \sim \omega/c$  as  $\omega \rightarrow \infty$  in the upper half plane,  $c$  being the speed of light in vacuum, and that the system is quiescent for time  $t < 0$ . The latter requirement can be met by taking the integration path above all of the singularities in the integrand and implies furthermore, on assumption that  $f(\omega)$  does not behave exponentially for large  $\omega$ , that  $I = 0$  for  $t < r/c$ .  $\xi(\omega)$  is generally a multivalued function of  $\omega$  which must be defined so that  $\text{Im} \xi > 0$  on the integration contour.

a. Result for most observation times

Since the exponent in Eq. (1) contains the large parameter  $r$ , one may employ the conventional saddle point approximation which states that the major contributions to  $I$  arise from the vicinity of the saddle points  $\omega_s$  determined by

$$q'(\omega_s) = 0, \quad \text{or} \quad \xi'(\omega_s) = \frac{t}{r} = \frac{1}{v_g(\omega_s)}, \quad t > \frac{r}{c}, \quad (2)$$

where the prime denotes the derivative with respect to the argument, and  $v_g(\omega) = \left[ d\xi/d\omega \right]^{-1}$  is the group velocity of a wave packet centered at the frequency  $\omega$ . For dominant effects, only real saddle points are of interest, and only those which render  $q(\omega)$  real. Then from the standard approximation for an isolated saddle point at  $\omega = \omega_s > 0$  (i. e.,  $q''(\omega_s) \neq 0$ ,  $f(\omega_s)$  finite):

$$I_{\omega_s} \sim \sqrt{\frac{2\pi}{r|\xi''(\omega_s)|}} f(\omega_s) e^{i[\xi(\omega_s)r - v_s t \pm \omega/4]}, \quad \xi''(\omega_s) > 0. \quad (3)$$

Since  $I$  in Eq. (1) must be a real function of  $r$  and  $t$ , saddle points occur in pairs at  $\pm \omega_s$  and  $I_{-\omega_s} = I_{\omega_s}^*$ . Thus, the contribution from the saddle point pair at  $\pm \omega_s$  is given by the familiar formula:

$$I \sim 2 \sqrt{\frac{2\pi}{r|\xi''(\omega_s)|}} |f(\omega_s)| \cos \left[ \xi(\omega_s)r - v_s t \pm \omega/4 \right], \quad \xi''(\omega_s) > 0, \quad (4)$$

where  $\theta = \arg f$ . The direction of the steepest descent path leading away from the saddle points at  $\pm \omega_s$  is  $+45^\circ$  when  $\xi''(\omega_s) > 0$  and  $-45^\circ$  when  $\xi''(\omega_s) < 0$ . One deforms the original path into the steepest descent paths only near the saddle points and uses elsewhere path segments lying in "valleys" near the real  $\omega$ -axis, thereby avoiding the complication of finding the complete steepest descent paths. Any

singularities crossed during the path deformations carried out in connection with the saddle point procedure must be added to the result in Eq. (4), as are contributions from other relevant saddle point pairs.

Since a constant value of  $(r/t)$  in Eq. (2) implies a constant value of  $\omega_s$ , the wave packet in Eq. (4) moving at the group velocity maintains its center frequency  $\omega_s$  and wavenumber  $k_s(\omega_s)$ . On the other hand, if  $r$  is fixed and  $t$  is allowed to vary, or vice versa, the saddle point frequency changes with  $t$  or  $r$ . A difficulty in applying Eq. (3) stems from the fact that  $\omega_s(r, t)$  is known only implicitly since  $\xi'(t)$  in Eq. (2) is generally a complicated function. However, as is evident from Eq. (2), the existence, multiplicity and general behavior of the saddle point(s) can be ascertained from a plot of  $v_g(\omega)/c$  or, equivalently, of  $c(d^2/d\omega^2)$  vs.  $\omega$  by locating the intersection points on these plots with a horizontal line at a height  $(r/ct)$  and  $(ct/r)$ , respectively. If the  $\xi'$  and  $\omega$  axes are labelled  $\tau$  and  $\omega_s$ , respectively, these plots provide directly the behavior of each  $\omega_s$  with  $\tau = ct/r$ . One may also use a plot of the amplitude factor in Eq. (4) vs.  $\omega$  together with the curve of  $\omega_s(\tau)$  to construct the envelope of the oscillations corresponding to each distinct saddle point. These aspects are illustrated in Figs. 1 and 2 for a dispersion curve and amplitude function  $N$  appropriate to extraordinary mode propagation across the d.c. magnetic field in a cold magnetoplasma.

#### b. Transition regions

The simple saddle point result descriptive of well-developed, isolated wave packets fails in transition regions where individual wave packets are not yet fully developed or where strong interaction with other wave packets occurs. For fixed observation points  $r$ , the transition phenomena occur at and near selected observation times  $t$ . For transients caused by a suddenly switched-on time-harmonic signal,  $f(\omega)$  in Eq. (1) has simple pole singularities at the signal frequency  $\omega_0$ , and transition phenomena occur near: a) time of arrival of the first response ( $t_s \rightarrow \tau$ ); b) very long observation times ( $t_s \rightarrow t_{1,2,3}$ ); c) time of arrival of transient at a group velocity maximum ( $t_s \rightarrow t_{ss}$ ); d) time of arrival of main signal ( $t_s \rightarrow t_0$ ); e) time of arrival of main signal when this corresponds also to the time of arrival of a group velocity maximum ( $t_s \rightarrow t_0 = t_{ss}$ ). Uniform asymptotic approximations have been obtained in all of these transition regions, thereby making results available for arbitrary observation times.

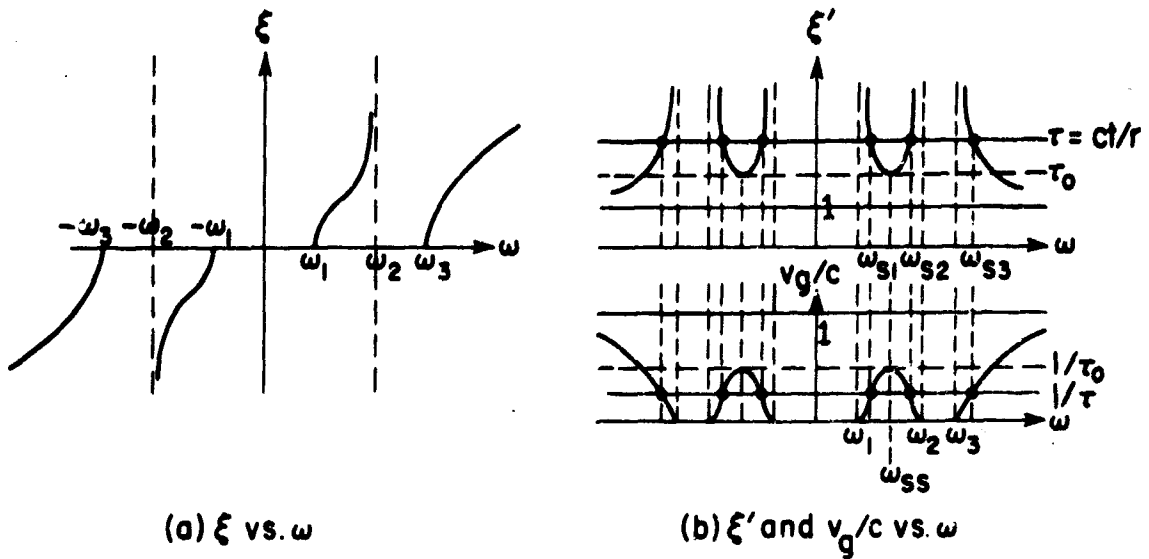


Fig. 1 Dispersion Curve (Propagating Branches Only) and Related Plots

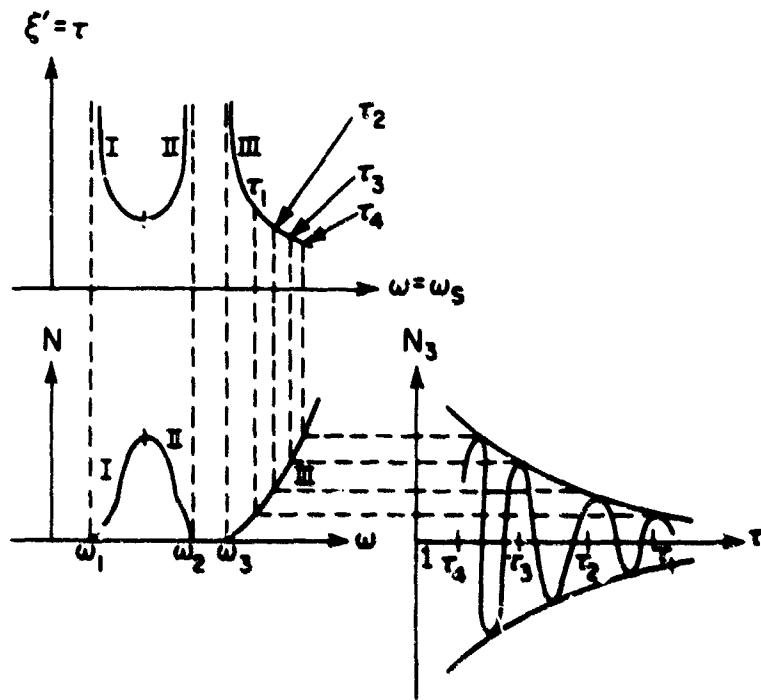


Fig. 2 Graphical Construction of Time Response from Frequency Plots for Branch III of Dispersion Curve. Similar Plots are used for Branches I and II.

1. Space-Time Rays

While the utility of ray concepts for the interpretation and even the construction of asymptotic time-harmonic fields is well established, much less customary is

a corresponding development for non-harmonic space-time dependent fields (see however Refs. 10-15). In the time-harmonic regime, rays define the space trajectories of the energy emitted continuously by the source. Under transient conditions, rays describe the location in space and time of a wave packet centered around a given frequency. Just as the  $\underline{k}$ -surfaces for constant  $\omega$  have proved useful in the treatment of propagation, radiation and scattering problems in the sinusoidal steady state, so can the full  $(\omega, \underline{k})$  dispersion surfaces be employed for transient processes. Some observations to this effect for propagation in infinite media have been made in the literature<sup>10,15</sup>, and we have extended these considerations to bounded media.

The saddle point condition expressed by Eq. (2) can be used to define a set of trajectories or rays in  $(r, ct)$  space. Each ray is given in the present case of a homogeneous medium by a straight line whose slope is determined by a particular frequency  $\omega_g$  and corresponding wavenumber  $k_g$ , as a result of which the group velocity is also a constant. Since only the times  $t > r/c$  are relevant and  $v_g < c$  for normally dispersive media, the rays in the  $(r, ct)$  plane lie in a region confined to an angular extent of  $\pm 45^\circ$  about the  $ct$ -axis (the smaller the group velocity, the more nearly is a ray parallel to the  $ct$ -axis). By moving along a ray, one finds the space-time location of a particular wave packet characterized by a constant frequency  $\omega_g$ ; by moving parallel to the  $ct$ -axis, one finds the frequency variation in the wave packets reaching a fixed observation point  $r$  at times  $t > r/c$ ; and by moving parallel to the  $r$ -axis, one finds the frequency distribution of wave packets in space at any instant of time  $t$ .

It can be shown that the space-time rays in  $(r, ct)$  space correspond to the properly oriented normals to the  $(-)$  branch of the  $(kc, \omega)$  dispersion surface, and that in the presence of an interface between two media, the frequency  $\omega_g$  of the incident ray is preserved in the reflected and refracted rays. This condition can be used to chart the progress of the space-time reflected and refracted rays. A simple example pertaining to reflection and transmission of a pulsed plane wave incident normally on a plane boundary between vacuum and an isotropic plasma is shown in Fig. 3, where the excitation function  $\delta(x) \delta(t)$  corresponds to a point source in  $(x, ct)$  space. The dispersion curve for the plasma is (with  $\omega = kc$  and  $\omega_p$  representing the plasma frequency):  $(kc)^2 - \omega^2 + \omega_p^2 = 0$ , while that for the vacuum is:  $(kc)^2 - \omega^2 = 0$ . The preceding considerations permit the complete tracking of the incident, reflected and refracted ray trajectories as indicated in Fig. 3.



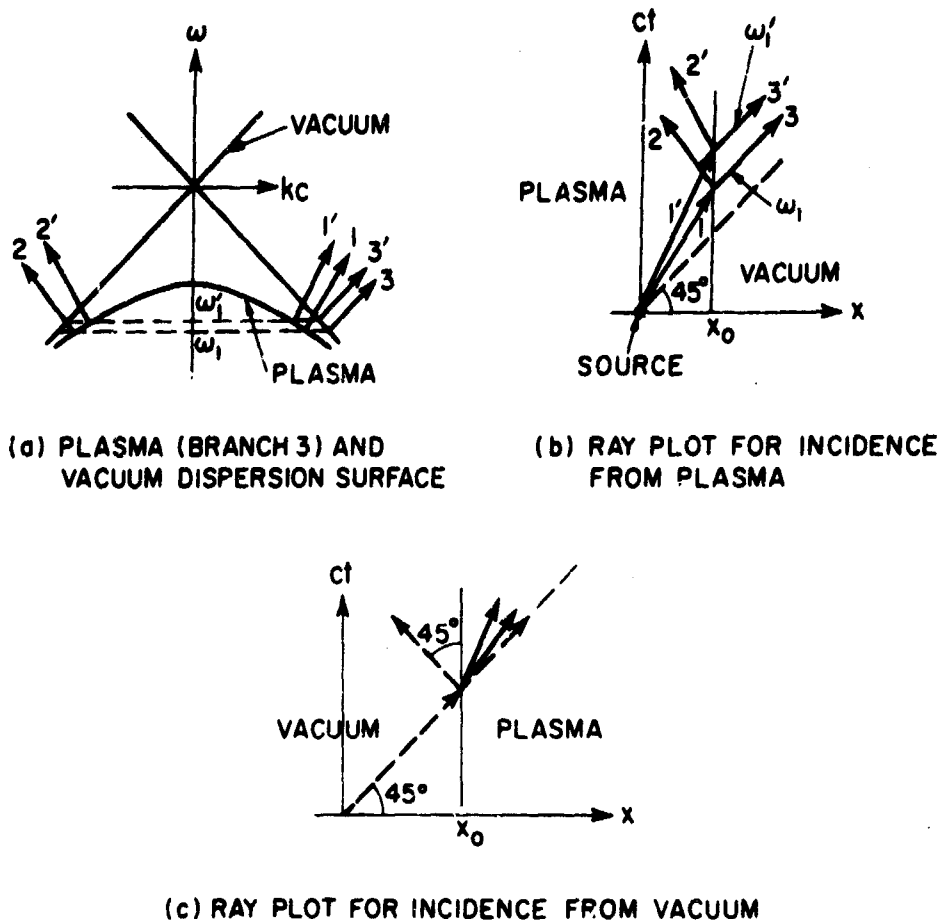


Fig. 3 Plane Wave Reflection and Refraction at Plasma Interface

The procedure is being utilized to construct quantitative expressions for the transient field and is to be further extended to accommodate anisotropic dispersive media and also media with temporally varying properties.

Air Force Cambridge Research Laboratories  
Office of Aerospace Research  
F 19628-68-C-0072

L. B. Felsen

#### REFERENCES

1. A. Sommerfeld, "On the Propagation of Light in Dispersive Media", *Am. Physik* 44 (1914), p. 177-202.
2. L. Brillouin, "Wave Propagation and Group Velocity", (New York: Academic Press, 1960).
3. C. M. Knop and G. I. Cohn, "Comments on Pulse Waveform Degradation due to Dispersion in Waveguides", *IEEE Trans. on Microwave Theory and Techniques (Correspondence)*, MTT-11 (1963), p. 445-447.

4. R. A. Helliwell, "Whistlers and Related Ionospheric Phenomena", (Stanford: Stanford University Press, 1965).
5. V. L. Ginzburg, "The Propagation of Electromagnetic Waves in Plasmas", (New York: Pergamon Press, 1964), Sec. 21.
6. J. R. Wait, "Pulse Propagation in Terrestrial Waveguides", IEEE Transactions AP-13 (1965), p. 904-918.
7. H. J. Schmitt, "Pulse Distortion in a Gyrotropic Plasma", IEEE Transactions on Antennas and Propagation, AP-13 (1965).
8. D. S. Jones, "The Theory of Electromagnetism", (New York: Pergamon Press, 1964), pp. 681-695.
9. J. R. Wait, "Propagation of Pulses in Dispersive Media", Radio Science 69D (1965), p. 1387-1401.
10. M. J. Lighthill, "Group Velocity", J. Inst. Maths. Applics. 1 (1965), p. 1-28. Also contains other references.
11. R. M. Lewis, "Asymptotic Theory of Transients", Electromagnetic Wave Theory (Proceedings of the Delft Symposium), ed. J. Brown, (New York: Pergamon Press, 1967), pp. 845-869.
12. N. Bleistein and R. M. Lewis, "Asymptotic Expansions of Solutions of Initial-Boundary Value Problems for a Dispersive Hyperbolic Equation", *ibid.*, p. 871-890.
13. R. M. Lewis and N. Bleistein, "Asymptotic Solutions of a Dispersive Hyperbolic Equation with Variable Coefficients", Courant Institute of Mathematical Sciences, New York University, Report No. Emp-206, June 1965.
14. M. J. Lighthill, "Studies on Magneto-Hydrodynamic Waves and Other Anisotropic Wave Motions", Phil. Trans. Ray. Soc. London, Sec. A, 252 (1960), p. 397-430, Appendix B.
15. H. Pöeverlein, "Sommerfeld-Runge Law in Three and Four Dimensions", Phys. Rev. 128 (1962), p. 956-964.

#### MICROWAVE BISTATIC SCATTERING FROM CAPILLARY WAVES ON WATER

E. S. Cassedy

In a previous report<sup>1</sup>, measurements of microwave backscattering from capillary waves on water were reported. The purposes of these measurements were: 1) to confirm the Bragg scattering nature of this phenomenon and 2) to obtain experimental data on polarization dependence of the back-scattering from capillary waves on water. The 22 GHz microwave setup has now been reconstructed in order to make bistatic scattering measurements as indicated schematically on Fig. 1. That is, the scattered microwave fields may now be received over a range of observation angles ( $\theta_r$ ) for a given angle of incidence ( $\theta_t$ ) and not limited as in the previous setup to the backscattering angle.

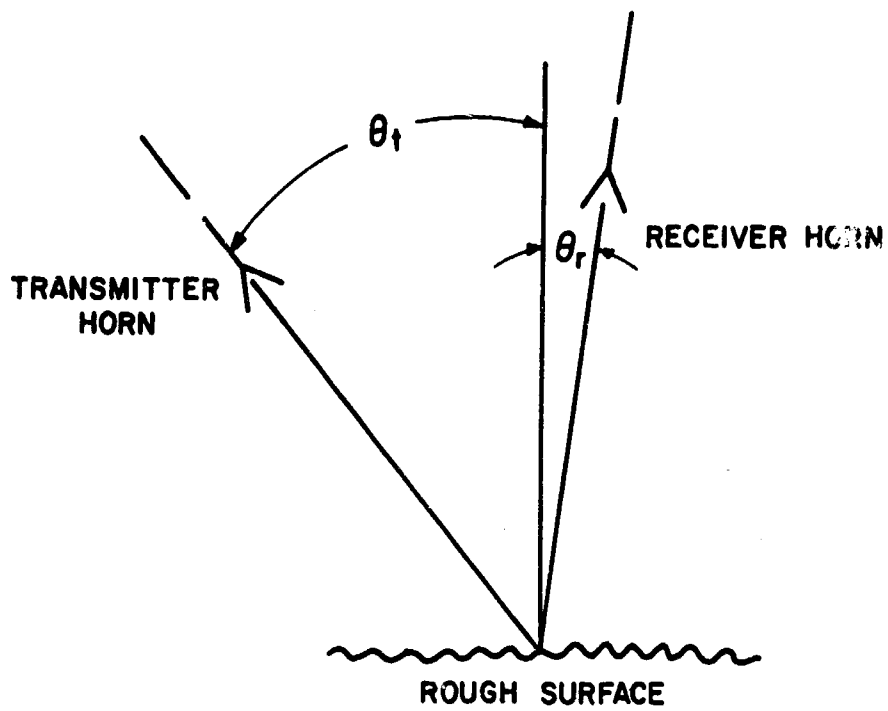


Fig. 1 Bistatic Scattering Range - Schematic View

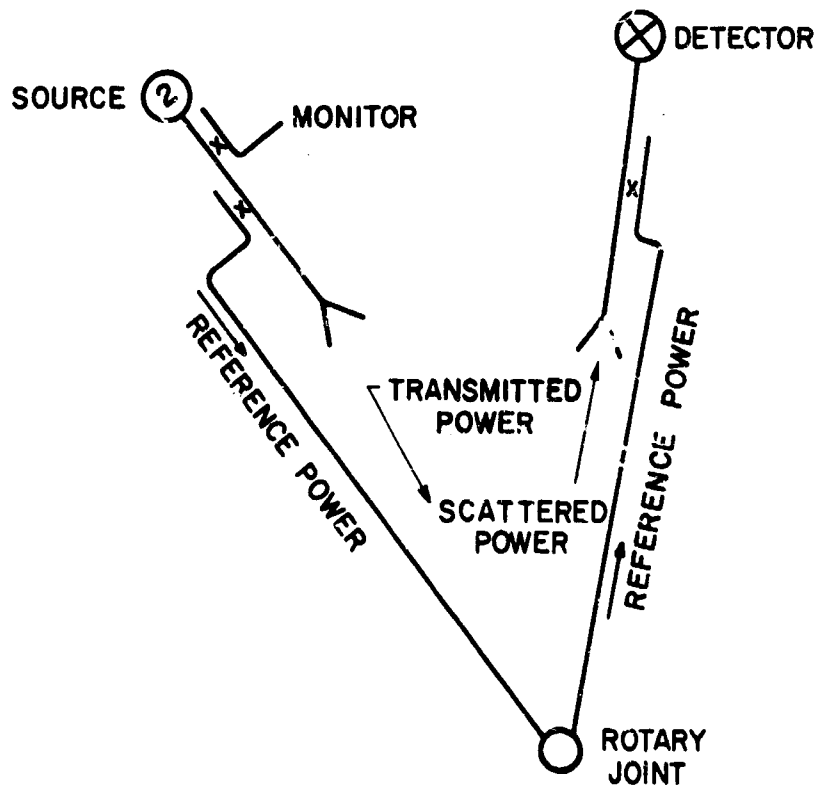


Fig. 2 Microwave Homodyne Set-Up

The receiving system for the bistatic setup, shown schematically on Fig. 2, is a homodyne (or synchronous mixing<sup>2</sup>) receiver. The homodyne receiver provides<sup>2</sup> linear detection and attains a sensitivity improvement over a simple video detection. In the homodyne operation used here, the received scattered power is mixed with reference power coupled from the transmitter. Since the microwave fields are scattered from a moving rough surface, they have doppler-shifted frequencies. The doppler frequency shift for scattering from sinusoidal traveling-wave ripples is just that of the water ripple itself (or a harmonic thereof)<sup>3</sup>. The detected homodyne signal is the doppler frequency (i.e., the water-wave frequency or one of its harmonics).

Reference power for homodyne detection is provided in the bistatic setup by means of the microwave circuit indicated in Fig. 2. The microwave circuit consists of directional couplers and two waveguide arms. The waveguide arms are connected through a rotary joint in order to provide reference power of constant power and phase as the receiver is rotated. The reference arm is also provided with a variable attenuator (not shown) in order to adjust the reference power for optimum signal to noise ratio<sup>2</sup>. Finally, the transmitter is monitored as indicated for constant power output and the detector is provided with a stub tuner (not shown) for optimum match.

The bistatic scattering range just described can be used to continue the measurements of polarization dependence of scattering described in the previous report<sup>1</sup>. That is, the ratio of vertical to horizontal scattering may be compared for several Bragg scattering orders, without being restricted to the incidence angles<sup>1</sup> defined by the Bragg (back scattering) condition. Even more important, however, the cross-polarization ratio on scattering may now be measured conveniently with the present receiver in contrast to the previous setup where it could not.

The forementioned scattering measurements all relate to a sinusoidally modulated surface. This surface is created<sup>1</sup> by means of capillary waves driven by a polystyrene wedge attached to a loud speaker cone. The speaker cone is, in turn, fed by a (sinusoidal) signal generator and audio amplifier. The same transducer system may, however, be driven by a random signal and thereby create a randomly rough surface on the water. For this purpose a noise generator has been constructed and is being used to drive the speaker-wedge transducer assembly. This system is intended to permit the experimental study scattering from randomly rough surfaces of the form treated earlier<sup>3</sup> in theory.

Joint Services Technical Advisory Committee  
AF 49(638)-1402

E. S. Cassedy

#### REFERENCES

1. J. W. Ra and E. S. Cassedy, "The Polarization Dependence of Microwave Back-scattering from Sinusoidal, Capillary Waves on Water," Progress Report No. 32 to JSTAC, Polytech, Inst. of Brooklyn Report No. 452.32-67, pp. 45-49.

2. M.E. Brodwin, et al., "Low Level Synchronous Mixing," 1953 IRE Convention Record, Part 10, pp. 55-57.
3. J.D. DeLorenzo and E.S. Cassedy, "A Study of the Mechanism of Sea Surface Scattering," IEEE Trans. on Antennas and Propagation, AP-14 (1966), pp. 611-620.

### EFFECTS OF MICROWAVE RADIATION ON THE EYE

L. Birenbaum, I. T. Kaplan, W. Metlay, S. W. Rosenthal, H. Schmidt, M. M. Zaret

For some time, we have been engaged in work of a bio-engineering nature: a measurement, at microwave frequencies, of the power levels just sufficient to cause injury to the eye. The method uses one eye of an anesthetized rabbit to terminate a length of waveguide. This permits direct measurement of the power entering (or dissipated in) the eye. Details of the procedure and the results of earlier work at 5.5, 5.4 and 70 GHz have been described in previous reports of this series<sup>1,2,3</sup>. Here, we wish to present some new data for 5.2 and 4.2 GHz; to evaluate our results to date with a view toward finding how the threshold levels depend on frequency; and finally to discuss some new work we have just started at 0.8 GHz.

A summary of our C-band work is shown below in Fig. 1, illustrating the cataractogenic thresholds so far observed. The 5.5 and 5.4 GHz curves, reported earlier, are composites of the pulsed and CW exposures listed in Table 1, and were obtained by

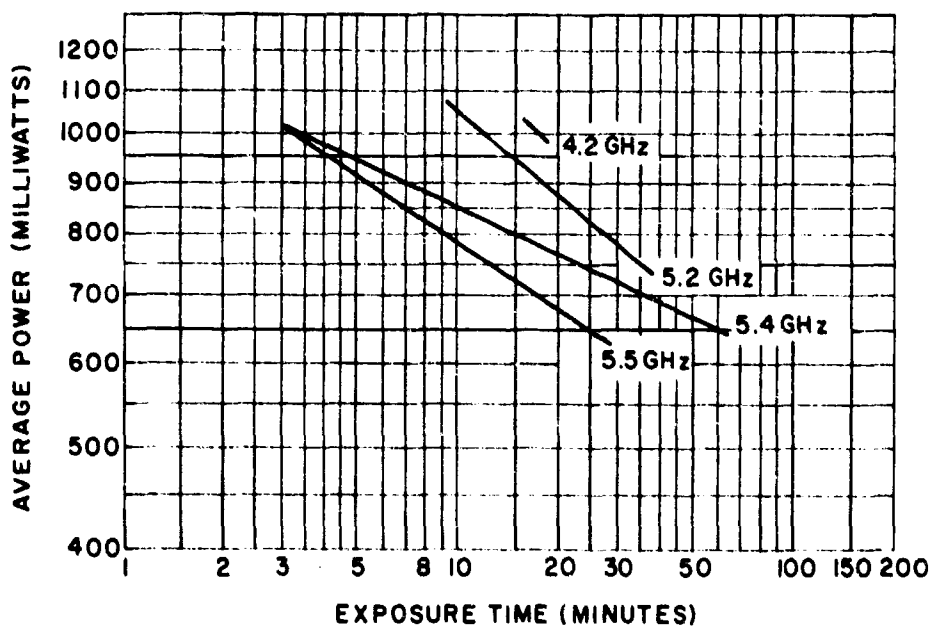


Fig. 1 Single-Exposure Cataractogenic Thresholds

**TABLE 1**  
**TABULATION OF C-BAND EXPOSURES**

<u>Frequency (GHz)</u>	<u>Number of Exposures</u>	<u>Type</u>
5.5	100	pulsed
	62	CW
5.4	28	pulsed
	36	CW
5.2	58	pulsed
4.2	22	pulsed

making use of the adapter of Fig. 2. The same device was used to obtain the data from which the 5.2 and 4.2 GHz curves were drawn, representing pulsed data only. All of the pulsed work was done with .001 duty cycle power. Before it was possible to work at

STANDARD C-BAND FLANGE,  
3 5/8" DIAMETER

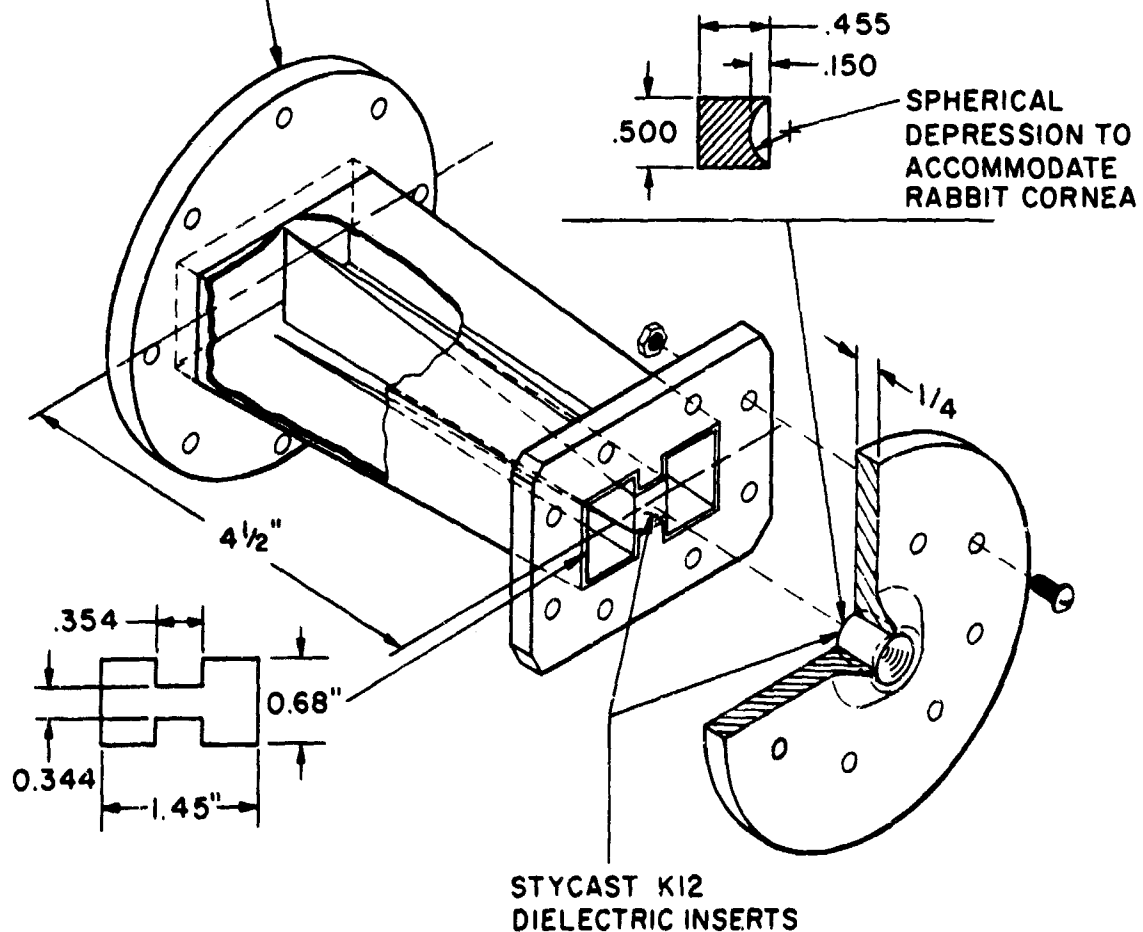


Fig. 2 Two-Section Transition from Standard C-band Waveguide to Rabbit Eye

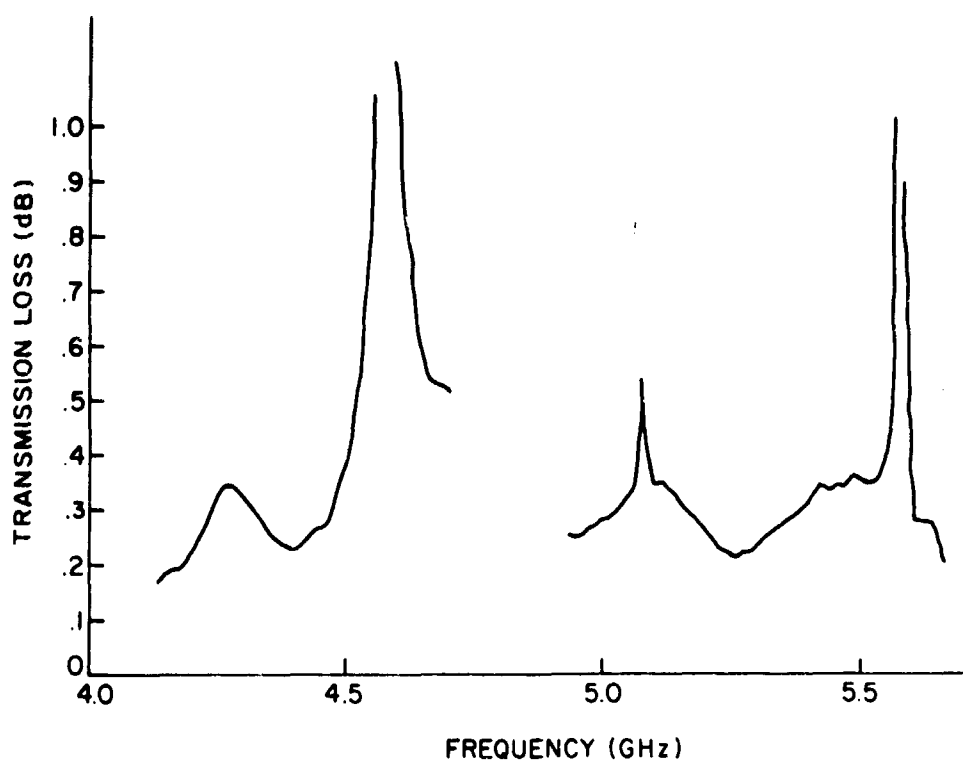


Fig. 3 Estimated Transmission Loss of Adapter

4.2 GHz, it was necessary to extend the adapter loss measurements shown in the right half of Fig. 3 much lower in frequency to find out whether the adapter was usable; that is, to make sure that there existed no internal resonances within the structure. The left half of Fig. 3 illustrates a very pronounced resonance at 4.6 GHz, but a useful region near 4.2 GHz. This data was obtained as follows: the circular waveguide end of the adapter was short-circuit terminated, and the standing wave ratio "r" in the input rectangular waveguide was measured. The quantity  $10 \log \left( \frac{r+1}{r-1} \right)$  was then computed, and used as an estimate of the transmission loss. A sharp rise in the loss was assumed to indicate the existence of a spurious mode resonance in the ridged section of the adapter.

Inspection of Fig. 1 suggests that the cataractogenic effectiveness of C-band microwave power decreases as the frequency decreases. Verification of this conclusion by measurement over a much wider frequency band would be of considerable interest. With this objective in mind, a simpler, less problematical, irradiating device was conceived and built (see Fig. 4). By virtue of its coaxial construction, it holds forth the possibility of a truly broadband measurement. The initial model, also shown in Fig. 4, had two serious deficiencies. One of these became apparent after irradiations conducted with the equipment shown in Fig. 5. Central circumscribed corneal opacities were observed, obviously resulting from the high field concentration near the center

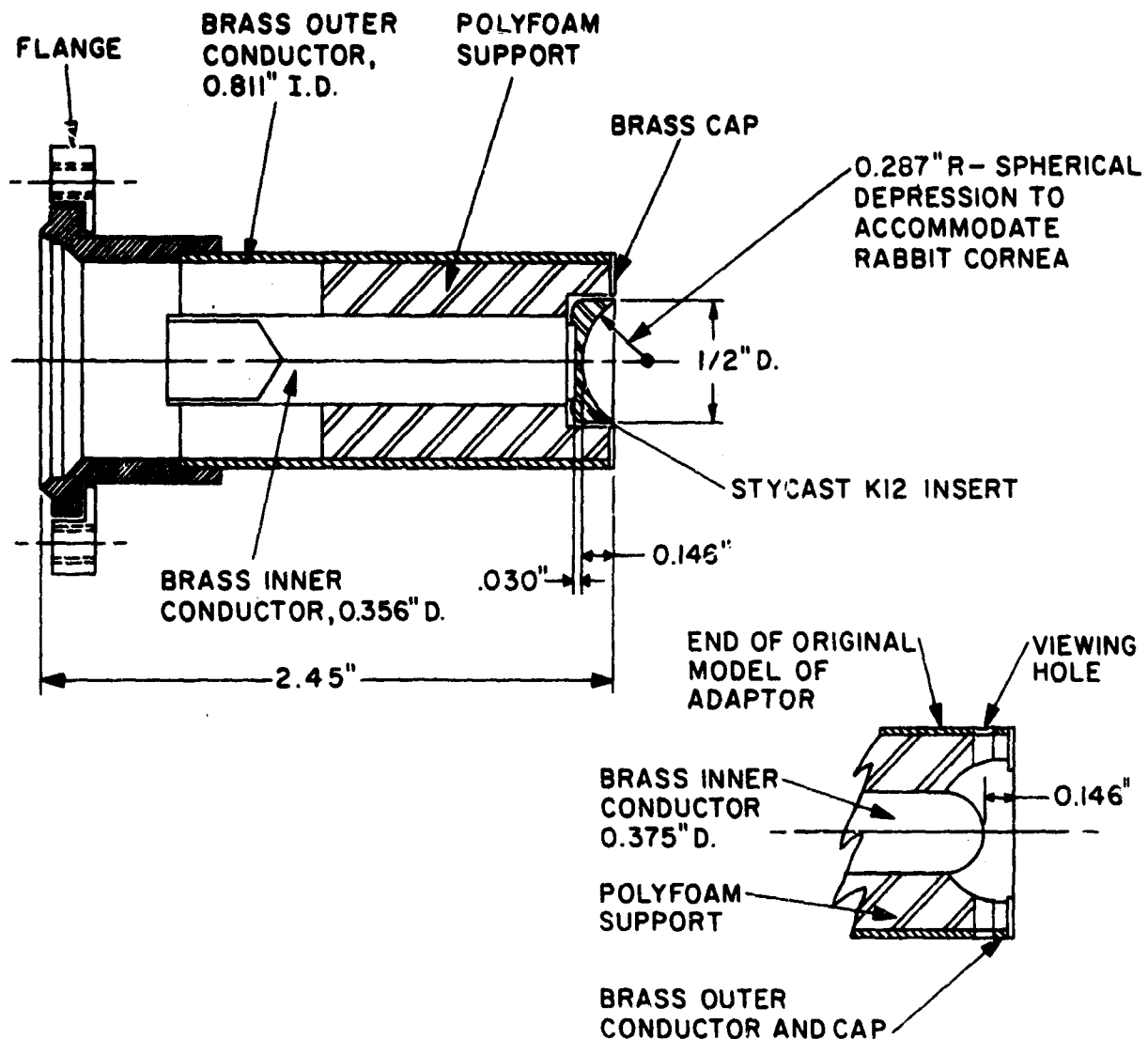


Fig. 4 Coaxial Adapter for 800 MHz Irradiation

conductor. In addition, comparison with the C-band results was not too meaningful because of the different physical location of the cornea: in one case, it was in contact with the Styrcast, and in the other mainly exposed to air. For these reasons, the observed cataractogenic threshold, near the 1 watt level, at 0.8 GHz, of about 15-20 minutes, is not regarded as valid. Future observations are planned with the improved model. Of special interest here is that this frequency lies at the upper limit of the UHF television band, and there seems no reason why these measurements cannot be extended lower in frequency. Significant also is the proximity to 915 MHz, one of the two ISM frequencies currently being utilized for domestic microwave ovens.

To gain insight into the physical processes involved, one approach to use is the one suggested by Clark<sup>4</sup> in an early paper using data provided subsequently by Schwan<sup>5</sup>. The



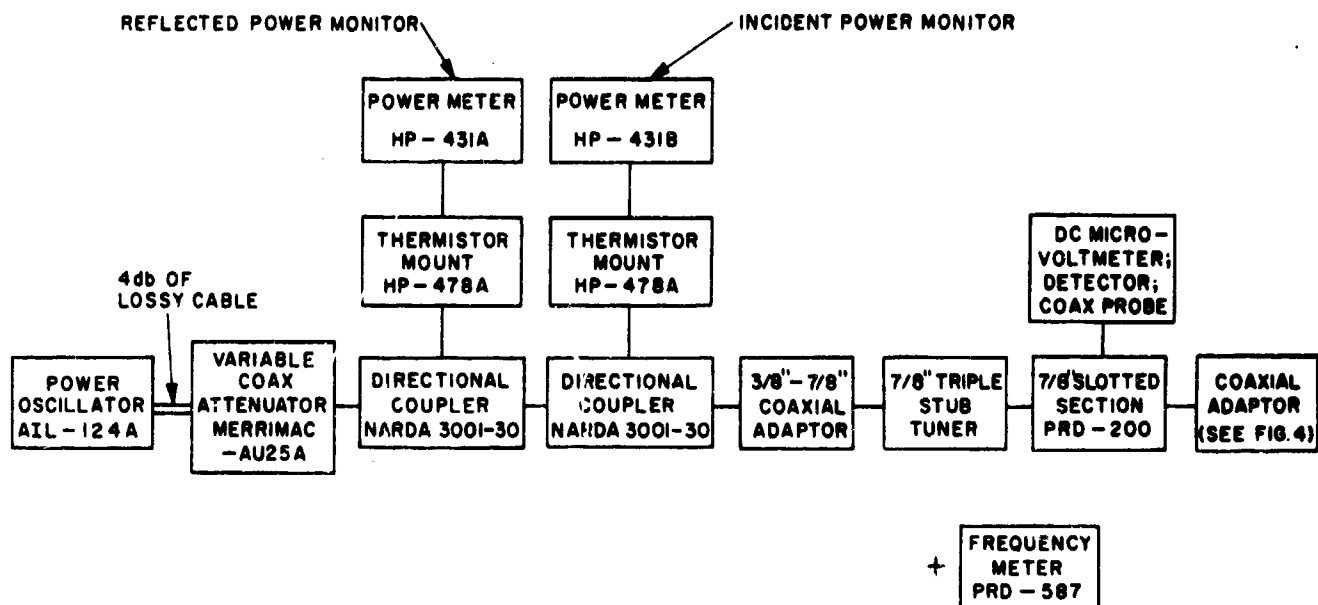


Fig. 5 Equipment Arrangement used for 800 MHz Irradiation

eye here is viewed as a layered medium upon which is normally incident a plane wave. By virtue of the losses in the cornea, in the aqueous fluid in the anterior chamber, in the lens, and in the vitreous medium, there is associated with the incident wave a limited depth of penetration. The decay of the field amplitude within the eye-model defines the rate at which microwave energy, converted into heat, is deposited within the eye as a function of depth. The temperature rise is determined by the specific heats of the several regions, the rate at which heat is lost, principally through the front layer, and the length of time during which the process takes place. A careful analysis of the simplest possible one-dimensional layered model that can be considered should give some interesting results, especially since Schwan<sup>5</sup> has presented electrical data for both the lens and the vitreous medium over a wide frequency range.

The results of the 5.5 GHz work have been incorporated into a paper to be published in IEEE Transactions on Bio-Medical Engineering in the January, 1969 issue.

Microwave aspects of the work described above were the responsibility of Mr. L. Birenbaum and Prof. S. W. Rosenthal of the Electrophysics Department.

The biological work was done by Dr. I. T. Kaplan, Chief Psychologist, Zaret Foundation; Dr. W. Metlay, Asst. Prof. of Psychology, Hofstra; Dr. H. Schmidt, Ophthalmologist; and Dr. M. M. Zaret, Ophthalmologist and Director of Research for the Zaret Foundation. Zaret Foundation, Subcontract No. 100-4 to PIB  
U. S. Army Medical Research-Development Command  
DADA-17-68-G9249

L. Birenbaum

## REFERENCES

1. L. Birenbaum, et al., Progress Report No. 32 to JSTAC, Polytech. Inst. of Brooklyn, Report No. R-452. 32-67, pp. 50-53.
2. L. Birenbaum, et al., Progress Report No. 29 to JSTAC, Polytech. Inst. of Brooklyn, Report No. R-452. 29-66, pp. 123-126.
3. L. Birenbaum, et al., Progress Report No. 28 to JSTAC, Polytech. Inst. of Brooklyn, Report No. R-452. 28-65, pp. 144-150.
4. J. W. Clark, "Effects of Intense Microwave Radiation on Living Organisms," IRE Proc., Vol. 39, No. 9, (1950), pp. 1028-1032.
5. H. P. Schwan, "Survey of Microwave Absorption Characteristics of Body Tissues," Proc. of the 2nd Tri-Service Conference on Biological Effects of Microwave Energy, Report ARDC-TR-58-54, AD-131477, (1958), pp. 126-145.

## NEW MILLIMETER-WAVE TECHNIQUES: AMPLIFIER NOISE THEORY

B. Senitzky

An amplifier which uses a gas as the active medium and is suitable for operation in the millimeter wave region has been described in a previous report<sup>1</sup>. The device consists of a small cylindrical cavity filled with gas which exhibits a rotational resonance at the frequency  $\omega_0$ . When the cavity and molecular resonances coincide, a monochromatic pump of frequency  $\omega_0$  can saturate the gas resonance and cause weak signals in the vicinity of the pump frequency to be reflected with gain.

The noise of the amplifier arises from the spontaneous emission of the gas molecules within the cavity. An expression was derived in the previous report<sup>1</sup> for the average power emitted per molecule per mode which is valid only for a single molecule and does not account for the absorbing (or amplifying) properties of the medium and electromagnetic structure. The analysis of these effects will be outlined here. A more complete discussion is given in the literature<sup>2, 3</sup>.

The basic problem is this. We have a strong monochromatic signal incident on a gas-filled resonant cavity which is coupled to a waveguide. (The signal is "strong" because it affects the properties of the gas medium.) What is the resulting noise spectrum which will be measured in the dominant mode of the waveguide? To solve this problem we will: 1) find the power radiated by a typical molecule into a lossless cavity mode, 2) find the classical current source that radiates the same power into the lossless cavity mode, and 3) use this classical source to find the noise power emitted by all molecules to the waveguide in the presence of losses.

The power radiated by a typical molecule into a lossless cavity mode of frequency  $\omega_0$  is found to be

$$P = 4\pi \operatorname{Re} \int_{-\infty}^t e^{i\omega_0(t-t')} \langle j(t) j(t') \rangle dt' \quad (1)$$

where  $j(t)$  is the projection of the molecular current operator  $\underline{j}(t)$  on the normal mode field  $\underline{A}_0(\underline{r})$  and  $\underline{r}$  is the position vector in the cavity. Thus  $j(t) = \underline{j}(t) \cdot \underline{A}_0(\underline{r})$ , where we are not explicitly writing out the spatial dependence of  $j(t)$ . The molecular current operator  $\underline{j}(t)$  is equal to the rate of change of the electric dipole moment operator  $\underline{p}(t)$ . The bracketed quantity,  $\langle j(t) j(t') \rangle$  is the molecular current correlation function averaged over the appropriate quantum mechanical ensemble. This quantity can be explicitly evaluated in terms of the mean time between collisions and the dipole matrix elements between the molecular energy eigenfunctions.

Let us now represent a molecule by a classical stochastic current source,  $\underline{j}(t)$ , and compute the power,  $P$ , radiated by a typical source into the lossless cavity mode of frequency  $\omega_0$ . We find that

$$P = 4\pi \int_{-\infty}^t \cos \omega_0(t-t') \overline{j(t) j(t')} dt' \quad (2)$$

where  $j(t)$  is defined as before and the bar indicates an average over the classical ensemble. If  $\langle j(t) j(t') \rangle$  is real and

$$\overline{j(t) j(t')} = \langle j(t) j(t') \rangle, \quad (3)$$

the noise power radiated by a typical molecule will be the same whether it is found from the classical ensemble in Eq. (2) or the quantum mechanical ensemble in Eq. (1). We can use Eq. (3) to find the properties of the classical ensemble and then use this ensemble in our further calculations.

The classical stochastic source current can be written as

$$j(t) = j_a(t) \cos \omega_0 t + j_f(t) \sin \omega_0 t,$$

where  $j_a(t)$  and  $j_f(t)$  are slowly varying with respect to  $\omega_0$ . These quantities represent the amplitudes of noise currents which are phased for AM and FM with respect to the coherent pump field. From Eq. (3) we find the following properties for the ensemble representing the classical stochastic noise sources:

$$\begin{aligned} \overline{j_f(t) j_f(t')} &= \omega_0^2 |p_{12}|^2 A_0^2(\underline{r}) (2n_1 n) e^{-(t-t')/\tau}, \\ \overline{j_a(t) j_a(t')} &= \overline{j_f(t) j_f(t')} \cos \omega' (t-t') / \tau, \\ \overline{j_a(t) j_f(t')} &= \overline{j_a(t)} = \overline{j_f(t)} = 0, \end{aligned} \quad (4)$$

where  $\tau$  is the mean time between collisions,  $n$  is the molecular density,  $n_1$  is the molecular density in either the lower or upper state of the transition (these being essentially equal for the conditions considered),  $|p_{12}|$  is the magnitude of the electric dipole moment operator component parallel to the normal mode field direction and

$\omega' = |P_{12}| F_c(\underline{r})/K$ , where  $F_c(\underline{r})$  is the amplitude of the pump field in the cavity.

The properties of the lossy cavity at the frequency  $\omega = \omega_0 + \delta$  can be characterized by the cavity quality factor  $Q$ , where

$$Q^{-1} = Q_{\text{ext}}^{-1} + Q_{\text{wall}}^{-1},$$

and the electrical properties of the gas by the complex susceptibilities ( $\chi(\delta) = \chi'(\delta) + i\chi''(\delta)$ ) to fields which amplitude and phase modulate the pump. These susceptibilities are designated respectively as  $\chi_a(\delta)$  and  $\chi_f(\delta)$ . The description of the medium in these terms and expressions for the susceptibilities have been previously given<sup>4,5</sup>. Over a limited range of frequency,  $\delta$ , and for a sufficiently strong pump ( $\omega' \gg 1$ ), the imaginary part of  $\chi_a(\delta)$  can change sign and the gas amplifies AM components.  $\chi_f(\delta)$  does not change sign so the gas always attenuates FM components. An expression for the noise power per frequency interval radiated by the gas into the waveguide is

$$P(\delta) = \frac{2}{\omega_0 Q_{\text{ext}}} \left[ \frac{\int n d\underline{r} \int_{-\infty}^t \overline{j_a(t) j_a(t')} \cos \delta(t-t') dt'}{\left(2\delta \omega_0^{-1} + 4\pi \overline{\chi'_a(\delta)}\right)^2 + \left(Q^{-1} + 4\pi \overline{\chi''_a(\delta)}\right)^2} + \frac{\int n d\underline{r} \int_{-\infty}^t \overline{j_f(t) j_f(t')} \cos \delta(t-t') dt'}{\left(2\delta \omega_0^{-1} + 4\pi \overline{\chi'_f(\delta)}\right)^2 + \left(Q^{-1} + 4\pi \overline{\chi''_f(\delta)}\right)^2} \right] \quad (5)$$

where the bar over the susceptibilities indicates that these quantities are averaged over the cavity field intensity.

When the pump signal is removed ( $\omega' = 0$ ) and the cavity is in equilibrium of a temperature  $T$ , the above expression reduces to

$$P(\delta) = \left(1 - |\Gamma(\delta)|^2\right) kT/2\pi$$

where  $\Gamma(\delta)$  is the reflection coefficient of the gas-filled cavity. This familiar result can be readily obtained by applying the principle of detailed balance to a cavity in equilibrium with a waveguide at a temperature  $T$ .

If the pump power is increased we can distinguish two cases: "optically thin" and "optically thick". In the "optically thin" case we assume that the medium absorption is negligible so we can neglect the susceptibilities in the denominator of Eq. (5). If, in addition, the cavity bandwidth is greater than the molecular linewidth ( $\omega_0 Q_{\text{ext}}^{-1} \gg \omega_0', \tau^{-1}$ ), the output spectrum will be as shown in Fig. 1 on p. 73 of Ref. 2 ( $K$  in that figure is equal to our  $\omega'$ ). That figure shows three Lorentzian curves:

a single FM noise curve with a peak at  $\delta = 0$  and two AM noise curves with peaks at  $\delta = \pm \omega'$ . If the medium is "optically thick" and in the amplifying condition ( $\chi_a'' < 0$ ), the denominator of the first term on the right-hand side of Eq. (5) approaches zero and the FM noise components at the output will be negligible compared to the AM components.

In summary, the computation outlined above shows how the noise spectrum of the amplifier is affected by the strong coherent pump and indicates the degree of correlation of the output noise with the pump strength.

U. S. Army Electronics Command  
DAAB07-68-C-0344

B. Senitzky

National Science Foundation  
GU-1557

#### REFERENCES

1. B. Senitzky, "New Millimeter-Wave Techniques: Amplifier Noise Theory," Progress Report No. 32, R-452.32-67, 15 March 1967-14 Sept. 1967, Contract AF 49(638)-1402, pp. 54-57.  
  
T. Kihm and B. Senitzky, "New Millimeter-Wave Techniques: Amplifier Noise Experiment," Progress Report No. 32, R-452.32-67, 15 Mar. 1967-14 Sept. 1967, Contract AF 49(638)-1402, pp. 58-61.  
  
M. Newstein, "Spontaneous Emission in the Presence of a Prescribed Classical Field," Progress Report No. 32, R-452.32-67, 15 Mar. 1967-14 Sept. 1967, Contract AF 49(638)-1402, pp. 72-75.
2. B. Senitzky, "Noise in the Presence of Strong Coherent Signals," IEEE Trans. on M. T. T., Vol. 16, No. 9, (Sept. 1968) (Special Issue on Noise).
3. M. Newstein, "Spontaneous Emission in the Presence of a Prescribed Classical Field," Phys. Rev. 167, 89, (1968).
4. B. Senitzky and H. Liebe, "Amplification of 1.2 mm Radiation by a Two-Level Quantum System," Applied Physics Letters, 8, 252 (1966).
5. B. Senitzky, G. Gould and S. Cutler, "Millimeter-Wave Amplification by Resonance Saturation," Phys. Rev. 130, 1460, (1963).

#### NEW MILLIMETER-WAVE TECHNIQUES: AMPLIFIER NOISE EXPERIMENTS

B. Senitzky and R. T. Kihm

The experimental verification of the theory described in the previous section is the primary goal of the work described here.

To build a gas amplifier for operation at 140 GHz requires the completion of the

following tasks: 1) the construction of a cavity with a sufficiently high quality factor; 2) the fabrication of a circulator which is not available commercially; and 3) the synthesis of deuterium cyanide ( $\text{DC}^{12}\text{N}^{15}$ ).

1) A cylindrical cavity, 0.2 in. diameter and 0.5 in. length, was designed and constructed to operate in the  $\text{TE}_{09}$  mode. The measured unloaded cavity Q was 12,500. This value was high enough for our purpose.

2) A Y-junction ferrite circulator, to be used with the cavity, was designed and fabricated. Its forward loss was 1.5 dB and the isolation was 23 dB. We feel that the latter value can be increased with further effort; nevertheless it is adequate for our purpose.

3)  $\text{DC}^{12}\text{N}^{15}$  was synthesized by first making "heavy" sulfuric acid and then using the salt-acid reaction:

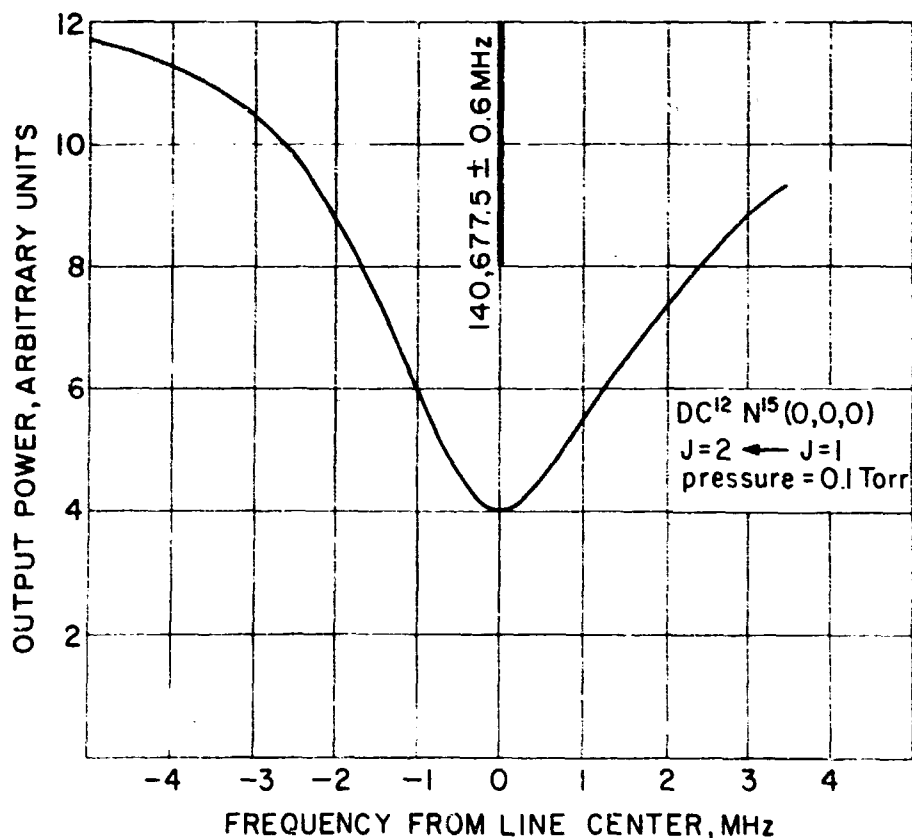
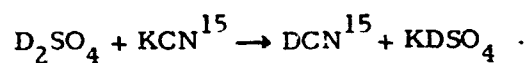
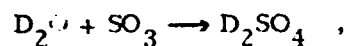


Fig. 1 Absorption Line, 0, 0, 0 Vibrational State,  $J = 2 \leftarrow J = 1$  Rotational Transition

In order to measure the gas purity we built a microwave spectrometer using a 20 cm absorption cell. The measured absorption spectrum of the  $J = 2 \leftarrow J = 1$  transition of the ground vibrational state is shown in Fig. 1. This line has not been previously measured but its location is in good agreement with the rotational constant obtained from the  $J = 1 \leftarrow J = 0$  transition<sup>1</sup>. The absorption coefficient of this line decreased in time without a concurrent pressure decrease. A measurement of the absorption line of  $\text{HC}^{12}\text{N}^{15}$  indicated that as the  $\text{DC}^{12}\text{N}^{15}$  line was weakening, the  $\text{HC}^{12}\text{N}^{15}$  line became stronger, thus proving that the  $\text{DC}^{12}\text{N}^{15}$  was converting to  $\text{HC}^{12}\text{N}^{15}$ . From a study of rates as a function of pressure it appeared that the isotopic conversion was taking place at the wall.

The absorbed constituent on the wall causing this conversion was not identified. Furthermore, the conversion could not be eliminated by a low temperature bake-out. We are presently constructing a system which can be baked-out at a temperature of 400°C.

U. S. Army Electronics Command  
DAAB07-68-C-0344

B. Senitzky

Joint Services Technical Advisory Committee  
AF 49(638)-1402

#### REFERENCE

1. B. Senitzky, "Rotational Spectrum of  $\text{HC}^{12}\text{N}^{15}$  and  $\text{DC}^{12}\text{N}^{15}$ ," Jour. of Chem. Physics, Vol. 45, 409 (1966).

## II. QUANTUM ELECTRONICS AND OPTICS

Barone, S.R.	Gould, G.	Moy, K.	Schlosser, H.
Bergstein, L.	Harrison, S.	Newstein, M.C.	Senitzky, B.
Bertrand, P.	Hussein, A.	Oliner, A.A.	Silverstein, L.
Cassedy, E.S.	Kahn, W.K.	Peng, S.T.	Skurnick, E.
Chi, C.H.	Kapash, R.J.	Piltch, M.	Solimene, N.
Chi, S.	Kestenbaum, A.	Rabinowitz, P.	Stern, R.
Chimenti, R.	Krieger, J.B.	Rosenbaum, D.	Stoler, D.
Chiou, C.H.	LaTourrette, J.T.	Rosenzweig, C.	Tamir, T.
Dublin, R.	Maurer, S.	Scarl, D.	Walter, W.T.
Fenster, P.	Mishkin, E.	Schachter, H.	Wang, W.C.

### METAL VAPOR LASERS

W. T. Walter and R. Chimenti

The development of the carbon dioxide laser has opened up new horizons in high power lasers. Many kilowatts of average power output at 10.6 microns have already been demonstrated. It is the high efficiency of the CO<sub>2</sub> laser that has made it feasible to construct such high average power systems. Electrical conversion efficiencies of 10-25 percent have been achieved. The output of the CO<sub>2</sub> laser, however, is in the far infrared. A question has been raised whether similar laser systems are possible with visible outputs. Can a system be developed that utilizes an electronic energy level structure similar to the vibrational-rotational structure of the carbon dioxide molecule?

Visible gas lasers have usually employed one or two of the rare gases as the active medium. The difference in energy level structure between the rare gas lasers and the CO<sub>2</sub> laser is striking because of the large gap between the ground and the first excited energy level in the rare gases. The vapor of a metal, such as copper, can provide an energy level structure where laser levels much closer to the ground level can be utilized. A comparison between the energy levels involved in the CO<sub>2</sub> laser, the copper laser, and the argon ion laser is given in Fig. 1. In all three cases, the upper laser level has been set at 100 and the other energy levels scaled appropriately. Thus the ordinate scale indicates relative energy. The fraction of the ground-to-upper-laser-level energy of excitation returned by the laser photon may now be directly compared. It is 41 percent in CO<sub>2</sub>, 64 percent in copper and 7 percent in ionized argon.

Operation of the three metal vapor lasers previously reported is illustrated in Fig. 2. It is appropriate to emphasize that these are not ion lasers. The excitation and laser action take place in the neutral atom. The excitation mechanism is provided



by electron collisions. Those energy levels in the neutral atom that are both close to and optically connected with the ground level can be efficiently and selectively excited by electron collisions. This is particularly evident in the manganese laser where the  $y^6P^0$  level is populated in preference to  $z^8P^0$  and  $z^4P^0$  which lie closer to, but are not as strongly coupled to the  $^6S$  ground level.

These metal vapor lasers have operated only in a pulsed mode thus far. If they are to operate continuously the lower laser level must be efficiently and selectively depopulated; for example, by inelastic collisions of the second kind with other atoms or molecules. A program to investigate a possible lengthening of the laser pulse upon the addition of certain quenching molecules is planned later this year.

The basic requirement of a pulsed metal vapor laser is in the presence of a metastable atomic energy level between the ground level and a resonance level. At the start of a current pulse, a transient population inversion is produced which lasts until the laser transition equalizes the upper resonance and lower metastable level populations.

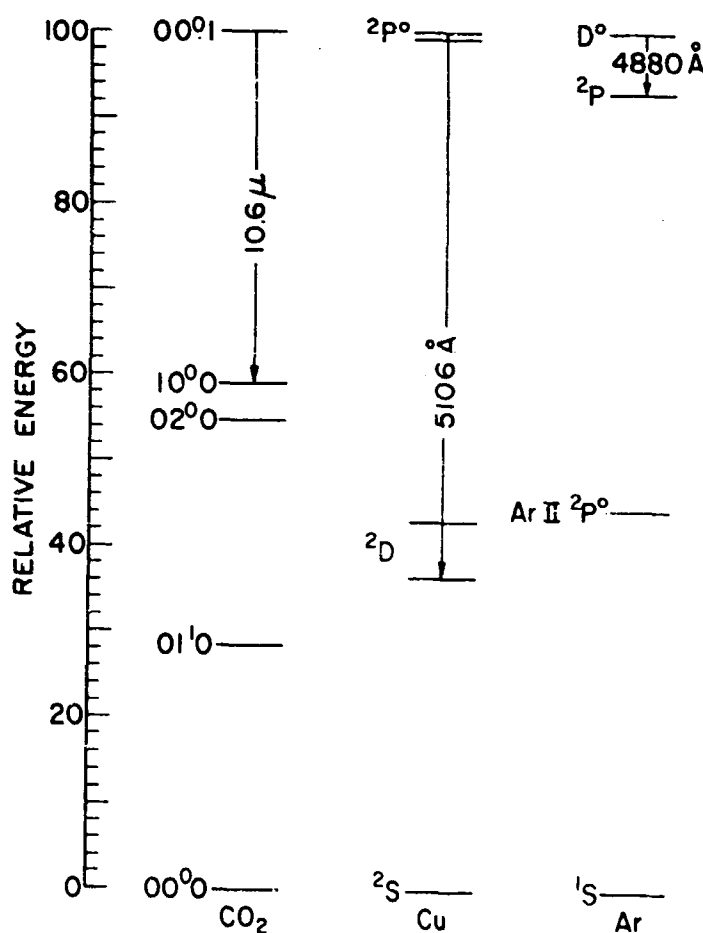


Fig. 1 Comparison of the Relative Energy Levels Involved in the Carbon Dioxide, Copper, and Argon Lasers

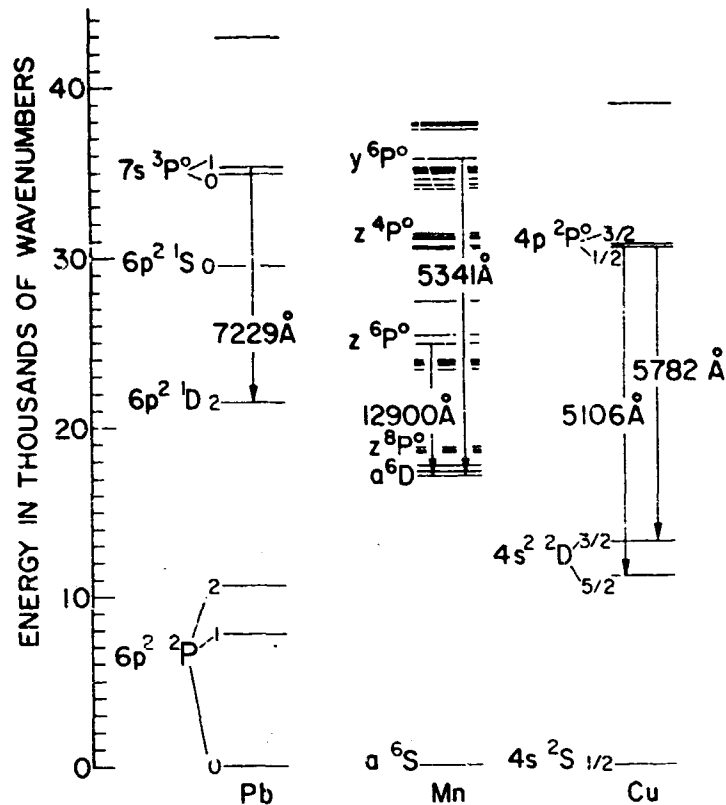


Fig. 2 Comparison of the Pulsed Lead, Manganese, and Copper Lasers

The metastable atoms are then relaxed back to the ground level by inelastic atom-atom and atom-wall collisions in preparation for the next pulse. The inter-pulse period necessary to relax the lower laser level and deionize the plasma will determine the maximum laser pulse repetition rate and hence the average power. Additional criteria necessary for the most efficient operation of this class of pulsed gas discharge lasers have been treated previously.<sup>1</sup>

All of these pulsed metal vapor lasers are very high gain transitions, in fact so high that it has been difficult to measure an unsaturated small signal gain. Recently Silfvast and Deech<sup>2</sup> have measured a 6 dB/cm gain for the 7229 Å line in lead.

Of all the pulsed metal vapor lasers, the most promising possibility of a high-efficiency, visible laser is the copper laser.<sup>1, 3</sup> A research program is underway to systematically investigate the copper laser.<sup>4</sup> The lead laser suffers from competition with strong uv and blue lines to the  $^3P_1$  and  $^3P_2$  levels of the ground configuration. Because of the multiplicity of the levels in manganese, five or six green and an equal number of infrared transitions can oscillate at the same time. The energy level structure

of copper, on the other hand, is remarkably free of other levels and their possible parasitic absorption of energy. The theoretical limit on the pulsed copper laser's efficiency is 38 percent, and an ultimate overall efficiency of 5 to 10 percent is expected.

Thus far the best results from a copper laser have been:

- 40 kW peak power
- 0.5 W average power
- 16 nsec pulse width
- 1,000 pps pulse repetition frequency
- 1.2% electrical conversion efficiency

These results were obtained from a 5 cm diam. tube with an active region ~ 80 cm long at a temperature of  $\sim 1520^{\circ}\text{C}$  which corresponds to a copper density of  $\sim 2 \times 10^{15}$  atoms/cm<sup>3</sup>.

Two new furnaces are nearly complete. The first furnace utilizes a platinum-rhodium heating element and a hot zone which can be as large as 4.4 cm diam. x ~ 80 cm long. This furnace is shown in Fig. 3. The second furnace has a graphite heating element and a hot zone 4.4 cm diam. x ~ 20 cm long. This furnace has a maximum temperature capability of  $2700^{\circ}\text{C}$  and can attain that temperature in 30 minutes. These two furnaces will be used for laser-probing-laser experiments and time resolved studies of energy level populations of a pulsed copper discharge.

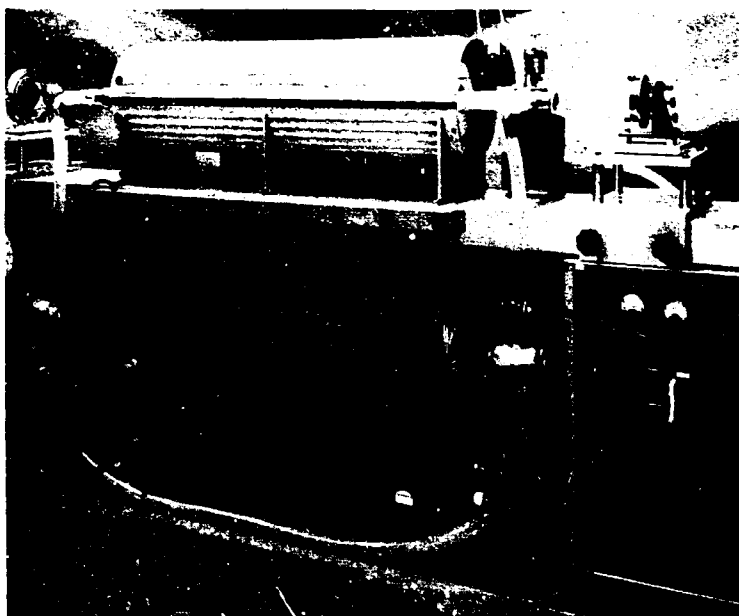


Fig. 3 New Platinum-Rhodium Furnace for Metal Vapor Laser Research

During construction of the furnaces a mercury vapor discharge in the form of a commercial fluorescent tube was used as a substitute load for the electrical excitation system. The air spark gap previously employed as a fast switch to apply a charged capacitor across the metal vapor load was replaced by a 5C22 hydrogen thyatron. In this form we were able to increase the pulse repetition frequency from kHz to 10 kHz and also shorten the current pulse risetime. We are hopeful that these and other improvements being made will enable us to increase the average power output of the copper laser by at least one order of magnitude and also enable us to try other elements which because of larger transition probabilities require faster current risetimes.

In addition to the copper, lead, and manganese lasers previously reported, other pulsed metal vapor lasers are possible. Some of the most likely possibilities have been tabulated in Table IV of Ref. 1. For example, the elements silver and gold are included with copper in column Ib of the periodic table. A comparison of the energy level diagrams of these three elements is given in Fig. 4. In silver the metastable  $^2D$  levels are displaced upward to overlap the  $^2P^o$  resonance levels. Therefore, no visible pulsed laser transitions were expected in the neutral atomic vapor of silver.

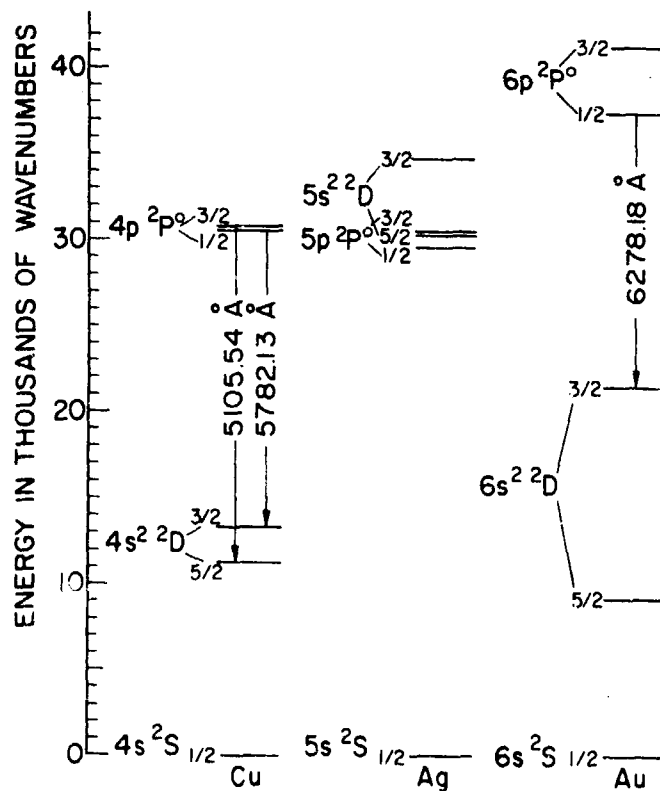


Fig. 4 Comparison of Copper, Silver, and Gold Energy Levels Indicating the Gold Laser Transition at  $6278\text{\AA}$

In gold the relative position of the  $^2P^{\circ}$  and  $^2D$  levels is the same as in copper; however, the fine structure splitting of each level has greatly increased. The yellow  $5782 \text{ \AA}$  line in copper corresponds to the red  $6278 \text{ \AA}$  line in gold with almost identical transition probabilities ( $2 \times 10^6 \text{ sec}^{-1}$ ). Therefore, laser action was expected on this transition. The green  $5106 \text{ \AA}$  line in copper, however, corresponds to the  $3123 \text{ \AA}$  ultra-violet line in gold which has a transition probability 40 times larger than the copper transition. The lifetime of the  $^2P^{\circ}_{3/2}$  level when the resonance radiation is trapped is only  $\sim 10$  nanoseconds. Therefore, laser action was not expected on this transition because the upper level lifetime is much shorter than the risetime of the current pulse using the present excitation configuration.

When silver and gold were tried experimentally, these expectations were confirmed. No visible laser transitions were found in silver, and a single transition at  $6278.6 \text{ \AA} \pm 0.6 \text{ \AA}$  was observed in gold as predicted in Table IV of Ref. 1. This is a high-gain transition similar to copper. Superradiance was observed from a hot zone 1 cm diam. x 80 cm long at  $\sim 1500^{\circ}\text{C}$  without any mirrors. The results with silver and gold add to our understanding of the pulsed metal vapor lasers and support the proposed excitation processes.

A paper<sup>5</sup> presenting the foregoing results was presented at the International Quantum Electronics Conference in Miami on May 16, 1968. Recently four new laser lines were reported by Deech and Sanders<sup>6</sup> in the atomic vapors of calcium and strontium. These four lines had been previously predicted<sup>1</sup>. Of the twenty-four laser lines predicted in Table IV of Ref. 1, five have now been experimentally demonstrated.

National Science Foundation  
GU-1557

W. T. Walter

Joint Services Technical Advisory Committee  
AF 49(638)-1402

#### REFERENCES

1. W. T. Walter, N. Solimene, M. Piltch, and G. Gould, "Efficient Pulsed Gas Discharge Lasers," *IEEE J. Quantum Electronics* QE-2, 474 (1966).
2. W. T. Silfvast and J. S. Deech, "Six dB/CM Single-Pass Gain at  $7229 \text{ \AA}$  in Lead Vapor," *Appl. Phys. Letters* 11, 97 (1967).
3. W. T. Walter, "40 - kW Pulsed Copper Laser," *Bull. Am. Phys. Soc.* 12, 90(1967).
4. W. T. Walter, "Pulsed Metal Vapor Lasers," Progress Report No. 32 to the Joint Services Technical Advisory Committee, Polytechnic Institute of Brooklyn, Report No. R-452.32-67, p. 65-68.
5. W. T. Walter, "Metal Vapor Lasers," *IEEE J. Quantum Electronics* QE-4, 355(1968).
6. J. S. Deech and J. H. Sanders, "New Self-Terminating Laser Transitions in Calcium and Strontium," *IEEE J. Quantum Electronics* QE-4, 474(1968).

## LASER FREQUENCY STABILIZATION

J. T. LaTourrette and P. Rabinowitz

In the previous report<sup>1</sup>, we outlined our proposed technique for stabilizing the frequency of a  $10.6\ \mu\text{CO}_2$  laser and indicated the advantages of our approach. The major distinction between this and previous laser frequency stabilization methods is the use of a passive, thermally excited absorption cell as the reference. This provides a significant improvement in the control of the parameters that influence the frequency of line center in the reference cell.

During the interim period we have made considerable progress in the design and construction of the experimental apparatus. In addition, a significant alteration in the technique for generating the error signal has been incorporated into the apparatus and should improve the ultimate performance.

The new technique for sensing line center, recently demonstrated with a neon laser<sup>2</sup>, depends on the saturation properties of an inhomogeneously broadened line in the presence of a strong standing wave field. The phenomenon which is referred to as the "Lamb Dip" was described phenomenologically by Gould and Bennett in terms of "hole burning."<sup>3</sup> In essence, their description is: if a standing wave field is set up in an inhomogeneously broadened medium at a frequency removed from line center, two groups of molecules will interact strongly with the field (namely, those molecules which as a result of the Doppler shift associated with their motion are in resonance with the field). The result on the medium is to "burn" two holes in the absorption profile symmetrically with respect to line center, the hole widths being determined by the degree of saturation. For a saturation parameter of the order of unity (weakly saturated), this width is characteristic of the homogeneous line width. If the frequency of the saturating field is tuned towards line center, the absorption may initially increase as the two holes approach one another. However, as the holes overlap the absorption decreases because components of the standing wave field are now competing for the same group of molecules. The net result is a peak in the transmission at line center for an absorbing medium but with a width characteristic of the hole width rather than the Doppler width. As a result, it becomes possible to utilize a reference which is much narrower than the Doppler line width. In  $\text{CO}_2$  this narrowing may be as much as a factor of 100. The performance of the stabilized system depends on our ability to sense the line center as well as the fundamental stability of the center. The new technique promises to improve matters on both counts. The expression for the signal to noise in sensing line center is proportional to the quantity  $(\frac{\alpha}{\Delta\nu})^2$  where  $\alpha$  is the absorption coefficient and  $\Delta\nu$  is the width of the reference, so that a reduction in absorption along with an equal reduction in reference line width will not change the ability to sense line center. That is the situation with  $\text{CO}_2$ . Because the homogeneous line width is determined by collisions, we can reduce the width by reducing

the density of gas, but with an equal reduction of the absorption coefficient. An optimum pressure appears to be about .050 torr which is a reduction of a factor of 20 in density from what had originally been planned. The reference linewidth will be about  $5 \times 10^5$  Hz as compared with a Doppler width of  $5 \times 10^7$  Hz or a narrowing of 2 orders of magnitude. Since the dominant cause of shifts in the line center are produced by collision, the reduction of the collision rate by more than an order of magnitude is in itself a major improvement. Furthermore, because the optimum modulation frequency in generating the error signal is lowered to a few hundred kilocycles, the detection response is improved, the electronics are simplified, and a deleterious relativistic effect associated with the phase modulation is reduced in magnitude.

One obvious difficulty with the reduced reference line width is the narrowing of the discriminant range to about  $5 \times 10^5$  Hz. This puts a greater requirement on the passive stability necessary from the lasers.

Two sealed-off  $\text{CO}_2$  lasers have been designed and constructed for optimum passive stability. The lasers incorporate Brewster's angle NaCl windows with the resonator reflectors external to the plasma tube. The fundamental resonator spacers are three 30 mm diameter invar rods which are rigidly held transversely by a series of stainless steel clamps. Reentrant mirror supports are used to give temperature compensation for reduction of long term thermal drifts of resonator length. Short term stability is primarily maintained by the massive construction. The resonator is of the folded confocal type, with an adjustable iris over the spherical reflector for transverse mode control. The tuning is achieved by stacked piezo-electric elements.

In initial tests single mode operation at 0.7 watts was obtained with a measured passive stability of about a part in  $10^8$  per minute as judged from the shift of the scanned power tuning curve. Although the salt windows have been enclosed with a desiccant, several tube failures have occurred due to water vapor attacking the windows. As a result, we are attempting to replace the windows with Irtran IV which is non-hygroscopic but which has slightly poorer transmission than NaCl. Although testing of the lasers has not been completed because of the window difficulties, we believe the preliminary results indicate an adequate passive stability.

National Science Foundation  
GU-1557

P. Rabinowitz

#### REFERENCES

1. J. T. LaTourrette and P. Rabinowitz, "High Frequency Stabilization," Progress Report No. 32 to JSTAC, Polytech. Inst. of Brooklyn, Report No. R-452. 32-67, pp. 69-72.
2. J. Hall, "Stabilized Lasers," 1968 International Quantum Electronics Conference, 16P-1.
3. W. R. Bennett, Jr., "Gas Lasers," Applied Optics, Supplement on Optical Masers (1962).

## FUNDAMENTAL FLUCTUATIONS IN QUANTUM-OPTICAL DEVICES

S. R. Barone, S. Harrison and M. C. Newstein

The objective of this research is to develop theoretical understanding of the fundamental quantum fluctuations responsible for the limiting noise properties of quantum optical devices (such as lasers and parametric amplifiers). Two complimentary efforts are being pursued. In one, we are attempting to isolate the significant parametric effects which occur in both driven and self-oscillating systems. The analysis of these effects promises to lead to useful generalizations of the "Fluctuation-Dissipation" theorem and an improved phenomenological noise theory. In the second effort we are attempting to develop a dynamical laser theory from first principles, with emphasis on the consequences of the quantum fluctuations at the macroscopic level.

A previously described calculation of spontaneous emission from driven systems<sup>1</sup> has been extended in order to relate it more closely to physical systems which have been proposed to provide experimental verification at optical frequencies<sup>2</sup>. Instead of a non-degenerate two level system, we have allowed for orientation degeneracy in a  $J=1$  electric dipole transition radiating into free space. The angular dependence of the radiated field, as well as the spectrum, becomes a function of the driving signal. The results could, perhaps, have been anticipated. If the polar angle  $\theta$ , is measured from the polarization axis of the applied field, the power spectrum consists of the sum of two terms, one proportional to  $(1+\cos^2\theta)$  and one to  $(\sin^2\theta)$ . The first term is multiplied by the ordinary Lorentzian spectrum characteristic of spontaneous emission from the un-driven atom. The second term is modified in the same way as was previously discussed for the non-degenerate two level system. This analysis indicates the feasibility of a simple experiment to observe these effects at optical frequencies using the output from a c. w. laser as the driving signal.

A promising approach to the development of useful generalizations of the "Fluctuation-Dissipation" Theorem is based on relations derived by S. R. Barone<sup>3</sup> in connection with his dynamical laser theory. When one considers a linear system (field) coupled to two other systems, one of which will represent a thermal bath, the other a driven two level system. Barone's relations express the fluctuations of the linear system in terms of those of the coupled system and the various response functions. Other relations, corresponding to Dyson's Equations in field theory, express the connections between the response functions. These relations are general and intuitive; they are not, however, closed and the evaluation of the fluctuations still involves solving dynamical equations. Their usefulness for phenomenological theories is: 1) they are general relations for the quantities specifically of physical interest, (fluctuations and response functions), and 2) their form suggests useful approximation methods. As an example of the latter point, we have treated the interaction with the driven system (the driving field is taken to be



prescribed) in the non-correlation approximation<sup>4</sup> and recovered the results of our previous calculation<sup>1</sup>, since the dynamical information is present in the response functions. This being verified, we will extend the investigation to the question of the mutual effects of the radiating two level systems on the field fluctuations. In this connection we are interested in the effect on the angular distribution as well as the spectral distribution of the spontaneous emission, in particular, in the conditions under which atom-atom correlations (such as occur with the correlated states described by Dicke<sup>5</sup>) become important.

A previously developed dynamical laser theory<sup>3</sup> has been extended to allow for the investigation of the build-up of atom-atom correlations from the near threshold to the above threshold range.

Air Force Cambridge Research Laboratories  
Office of Aerospace Research  
F 19628-68-C-0177

M. C. Newstein

#### REFERENCES

1. M. Newstein, "Spontaneous Emission in the Presence of a Prescribed Classical Field," *Phys. Rev.* 167, 1, (1968).
2. The effect on the noise properties of an amplifier operating at millimeter-wave frequencies is discussed in a forthcoming article "Noise in the Presence of Strong Coherent Signals" by B. Senitzky.
3. S. R. Barone, "Dynamical Theory of Laser Oscillators," to be published.
4. J. Schwinger, "Brownian Motion of Quantum Oscillator," *J. Math. Phys.* 2, 3, (1961).
5. R. H. Dicke, "Coherence in Spontaneous Radiation Processes," *Phys. Rev.* 93, 99 (1954).

#### GENERATION OF HIGH-POWER PICOSECOND LASER PULSES

G. Gould and L. Silverstein

As described in a previous report<sup>1</sup>, the possibilities of generating high-temperature plasmas by means of very high power solid-state lasers are being investigated. The goal is 10 KEV or  $10^8$  °K, which is 10 times the figure mentioned in the previous report. Preliminary feasibility studies show that optimum results will be attained if the laser pulse duration is reduced to the minimum attainable value, while the peak power is simultaneously maximized. In this way, plasma heating can occur in the most efficient regime, in which the plasma density is such that the plasma is not transparent to the laser radiation.

This optimum heating regime occurs early in the plasma generation process, before the plasma expands appreciably and before an appreciable fraction of the radiation can escape via bremsstrahlung. Calculations of various plasma parameters during the

heating and expanding phase of its existence, using typically expected initial values, indicate that it would be desirable to obtain laser pulses as short as 1 to 10 picoseconds (1 picosecond =  $10^{-12}$  sec) in duration, with peak power levels of the order of 10 to 100 gigawatts. Primarily as a result of the investigations of A. J. DeMaria and others at United Aircraft Corporation, it is now possible to generate single (or multiple) high power (~10 GW), short duration (~10 picoseconds) pulses of coherent laser light, and to manipulate and detect such pulses with relative ease.<sup>2, 3</sup> The theoretical minimum pulse length of 0.2 picosecond has not yet been achieved. A goal of this project is to experimentally investigate the limitations on pulse shortness and spatial coherence.

Techniques have been developed for detecting the presence and detailed structure of ultra-short pulses by means of two-photon absorption and subsequent fluorescence in certain materials.<sup>4</sup> Not surprisingly, such techniques must be physical rather than electronic in nature, since even the fastest traveling wave devices have bandwidths of no more than 10 GHz, and are therefore not suitable for timing phenomena in the picosecond range. These picosecond laser pulses have extremely high electric field strengths. This opens the possibility of observing various kinds of nonlinear optical phenomena in materials.<sup>5</sup> Thus, the ultra-short pulse laser may be put to a variety of uses in the exploration of fundamental physical phenomena in materials.

Under an AFOSR Contract, M. Newstein, N. Solimene and S. Barone are developing a theory of mode locked laser operation (described elsewhere in this report) which can be applied to nonlinear phenomena. One of our objectives is to perform experiments to which the theory would apply. In particular, a joint goal is to shed light on what limits the shortness and coherence of the pulses.

In view of the above considerations, it is planned to build a flexible apparatus for generating and studying the effects of ultra-short pulses. This equipment is now being designed and parts are being obtained.

This project, as well as others at the Graduate Center, has benefited from the transfer of laser research equipment from Control Data Corporation to the Institute. So far, the value of this equipment is approximately \$250,000. These transfers were expedited by the cognizant agencies (ARPA, AFOSR, RADC, AFAVIONICS, ONR, AFCL) who favored continuation at the Institute of the laser research program which had been terminated at the Control Data Corp. (formerly TRG Inc.). This, in turn, was possible because the integrity of the former TRG laser research group has been maintained at PIB, with partial support by the Joint Services contract and by the NSF Science Development Program.

Among the items transferred from Control Data were an estimated \$50,000 worth of ruby rods. The pulse generator is being designed to utilize these rubies. Since

most picosecond pulses have been generated in glass in the past, new knowledge will be added to the state of the art. In order to use the rubies and to investigate various cavity configurations, the high power laser is being assembled from components rather than by purchase of a complete manufactured system.

One feature of the cavity design is the use of a ring laser configuration together with mode selection. This will test the possibility that the spatial coherence of the output pulses can be improved without loss of energy if the radiation is in the form of traveling waves, rather than standing waves. Standing wave patterns with modes tend to encourage multimode operation. A side benefit would be the improvement in the spatial coherence of ordinary Q-switched pulses, as well as of picosecond pulses.

Simultaneous with the design and construction of the high power laser system, a suitable laboratory facility is being fitted out. Construction of the laboratory, including installation of adequate electrical power, a water supply for cooling the laser rod and the pumping flash lamps, is presently nearing completion. The work area devoted to the high-power solid-state laser investigations is centered about a 4' x 16' cast-iron surface plate weighing 17,000 lbs., which was obtained from the Naval Depot in Mechanicsburg, Pennsylvania. This unit, which provides a massive and stable work surface, has been installed on a base so designed that it may be floated off the floor by means of inflated airplane tire innertubes. It is thus decoupled from floor-borne vibrations, and so will also be useful in laser stability studies. Additional equipment is in the process of either design or purchase.

National Science Foundation  
GU-1557

G. Gould and L. Silverstein

Joint Services Technical Advisory Committee  
AF 49(638)-1402

#### REFERENCES

1. G. Gould and L. Silverstein, "Pulsed Laser Generation of High-Temperature Plasmas," TAC Progress Report No. 32, PIBMRI, pp. 109-112.
2. A. J. DeMaria, et al., "Ultra-Short Light Pulses," Science, 23 June 1967, pp. 1557-1568.
3. A. J. DeMaria and H. A. Heynu, "Investigation of Means for Generating High-Energy and Extremely Narrow Laser Pulses," United Aircraft Research Laboratories, Report No. F-920475-5, March 1967.
4. J. A. Giordmaine, et al., "Two-Photon Excitation of Fluorescence by Picosecond Light Pulses," Appl. Phys. Lett., 1 Oct. 1967, pp. 216-218.
5. M. J. Brienza, et al., "Optical Rectification of Mode-Locked Laser Pulses," UAC Research Labs., Report No. UAR-F229.

## STUDY OF ULTRA-SHORT PULSE LASER SYSTEMS

S. R. Barone, S. Chi, M. C. Newstein, N. Solimene

By exploiting certain non-linear interactions within the laser oscillator, optical pulses of duration as short as  $10^{-12}$  seconds have been produced<sup>1</sup>. The development of such short pulses requires the excitation of many longitudinal modes encompassing the frequency range corresponding to the inverse of the time duration. Many previous analytic studies have started with a modal expansion of the field and then a determination of conditions under which the expansion coefficients corresponded to the short-pulse or "mode-locked" situation<sup>2, 3, 4, 5</sup>. Because of the large number of modes involved in the interesting situations of very short pulses, limited information can be obtained from this approach. Serious calculational difficulties are also associated with the essential non-linearity of the dynamical equations. Some useful information has been obtained by numerical methods<sup>6, 7</sup>. These suffer from the usual limitations that one does not get general expressions, but rather each set of parameters requires another numerical evaluation. In addition to this, one often cannot tell whether the finite numerical procedure has converged to the true solution. Both of these difficulties are particularly exaggerated for the systems under consideration.

We have been investigating these phenomena using an analytic approach which avoids the modal expansion. The pertinent resonator characteristics are accounted for by a temporal periodicity requirement on the field. We have ignored transverse spatial effects. The resonance condition is used to eliminate the field from the dynamical equations for the material-field systems. The resulting non-linear equations have been investigated for various configurations of active medium and saturable absorber.

Certain interesting limiting cases have been solved exactly. One such case is a one-way circulating cavity filled with active medium not subjected to pumping excitation ( $T_1 = \infty$ ). Here one obtains periodic circulating pulses, related to the non-periodic pulses discussed in connection with "self-induced" transparency<sup>8</sup>. The physical situation which is being modeled is quite different from that ordinarily occurring in pulse-forming lasers. However, one does see how it is possible to find circulating solutions which can match the cavity period even though the controllable material parameters are prescribed.

In more realistic situations, even though the non-linear equations have not been solved, it has proved possible to obtain many qualitative features of behavior. In particular, it has been determined that some apparently stable pulsing solutions<sup>6</sup> obtained after a limited number of numerical iterations, are really unstable and would eventually settle down to constant, non-pulsing solutions. Interest still attaches to these transient pulsing solutions, since small modifications of the physical system could keep them from decaying. Their study has been facilitated by the use of transformations which

convert the form of the differential equations to those which describe easy-to-visualize mechanical systems (particle in potential well with friction).

We have extended the approach to include the effect of saturable absorbers in the cavity. Qualitative arguments can be given to show that this increases the likelihood of excitation of ultra-short pulses. Some quantitative insight has come from the modal expansion type of argument. We are presently investigating these phenomena from the point of view previously described.

Air Force Cambridge Research Laboratories  
Office of Aerospace Research  
F 19628-68-C-0177

M. C. Newstein

#### REFERENCES

1. A. J. DeMaria, D. A. Stetser, and W. H. Glenn, Jr., "Ultrashort Light Pulses," *Science* 156, 1557 (1967).
2. M. J. DiDomenico, Jr., "Small Signal Analysis of Internal Modulation of Lasers," *J. Appl. Phys.* 35, 2870 (1964)
3. S. E. Harris and C. P. McDuff, "Theory of FM Laser Oscillation," *IEEE J. Quantum Electronics* QE-1245 (1965).
4. C. L. Tang, H. Statz, "Maximum Emission Principle and Phase Locking in Multimode Lasers," *J. Appl. Phys.* 38, 2963 (1967).
5. C. A. Sacchi, G. Soncini and O. Svelto, "Self-Locking of Modes in a Passive Q-Switched Laser," *Nuovo-Cimento* 48, 58 (1967).
6. C. L. Tang, H. Statz, "Large-Signal Effects in Self-Locked Lasers," *J. Appl. Phys.* 39, 1(1968).
7. J. A. Fleck, Jr., "Origin of Short-Pulse Emission by Passively Switched Lasers," *J. Appl. Phys.* 39, 7(1968).
8. S. L. McCall and E. L. Hahn, "Self-Induced Transparency by Pulsed Coherent Light," *Phys. Rev. Lett.* 18, 908 (1967).

#### BASIC STUDIES IN OPTICAL PARAMETRIC OSCILLATIONS

E. S. Cassedy and S. T. Peng

A general formulation of the scattering of light by a parametrically-modulated slab and numerical calculations relating thereto have been reported previously<sup>1,2</sup>. It was shown that the problem could be treated in a compact manner which includes the effects of all frequencies of the small-signal model and includes all significant coupling of normal (Floquet) modes at the boundaries. Calculations following from this theory include the effects of discontinuities in refractive index which are not present in other theories. In addition, a novel "surface wave" effect has been predicted from this theory to exist under certain specified conditions.<sup>2</sup>

The boundary effects discussed previously all relate to stable<sup>3</sup> interactions. In the present report, by contrast, we wish to discuss potentially-unstable interactions<sup>3</sup> in a parametrically-modulated slab. The use of the Brillouin diagram for the prediction of such interactions is treated in an accompanying study. The geometry of this slab and its excitation are shown in Fig. 1.

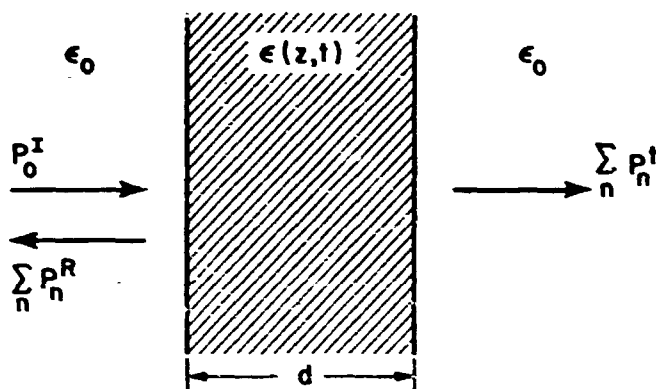


Fig. 1 Scattering of a Monochromatic Wave by a Parametric Slab

The case of potentially-unstable interaction<sup>3</sup> has been found to be particularly interesting since it may result in optical parametric oscillation in bounded regions such as resonators.

In order to achieve the co-flow, potentially-unstable interaction so that the signal wave may be amplified, we assume a medium with the following basic dispersion<sup>3</sup>:

$$\epsilon(\omega) = \epsilon \left[ 1 + \frac{p}{1 + j\omega} \right],$$

where  $\epsilon$ ,  $p$ , and  $q$  are constants and  $\omega$  is the signal frequency. The dispersion curves for such a medium were computed and plotted in Fig. 2 on the Brillouin diagram. For a monochromatic plane wave incident, the scattered field was also computed and the transmitted power plotted in Fig. 3. From this curve we observe the exponentially growing gain of the signal wave versus slab thickness.

Since the signal wave can gain energy from the pump wave, and if we can confine the signal wave to stay in the parametric slab, the signal wave will start to build up continuously with time and, thus, parametric oscillation can follow. To confine the signal wave in the parametric slab, we may introduce larger discontinuities at the interface boundaries. For example, we may increase the discontinuities by increasing the dielectric constant of the slab. The scattered field for various values of dielectric constant was calculated and the transmitted power (at  $\omega_0$ , the input signal frequency) vs.

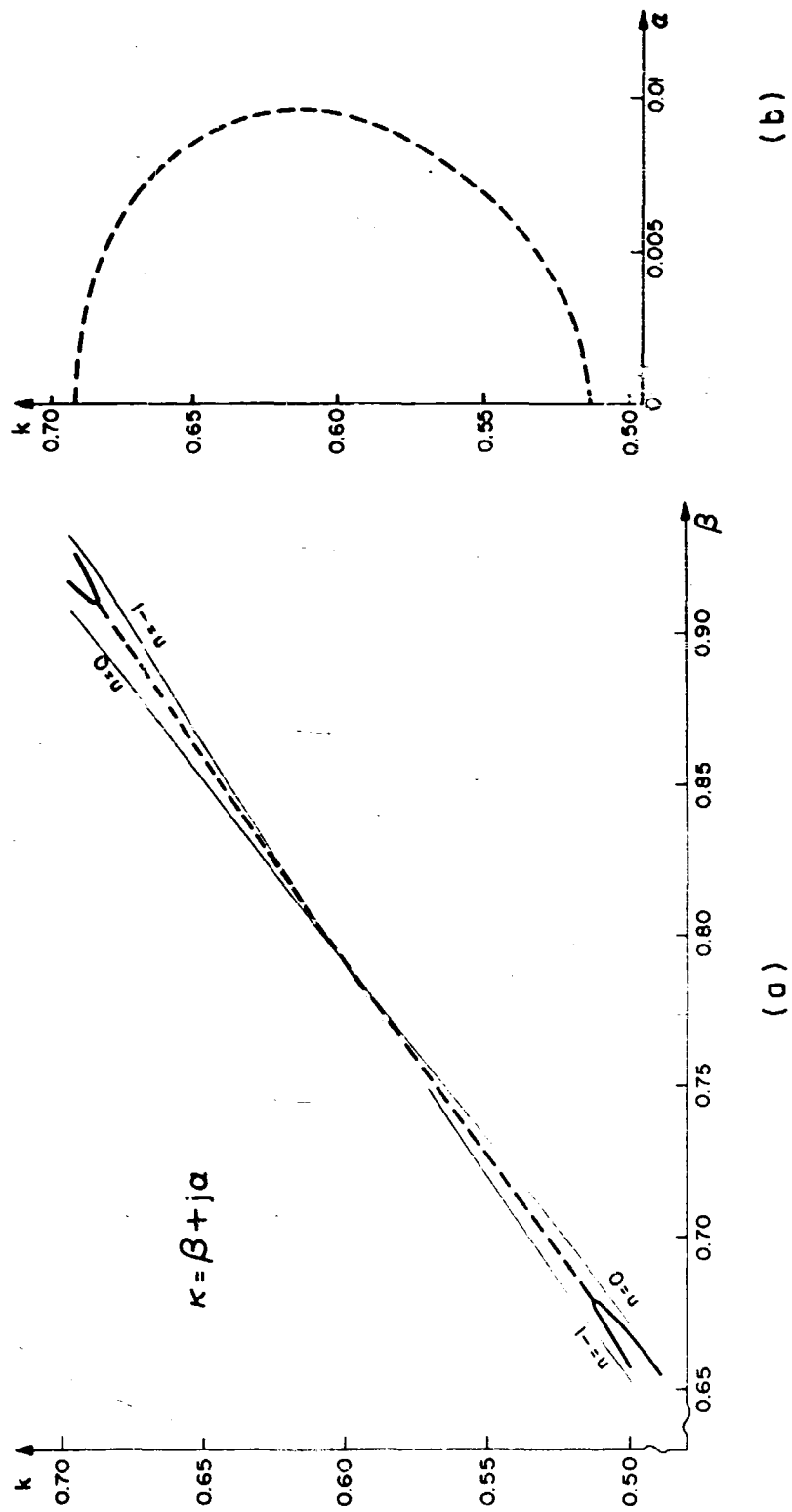


Fig. 2 Brillouin Diagram - Co-Flow Potentially-Unstable Parametric Interaction

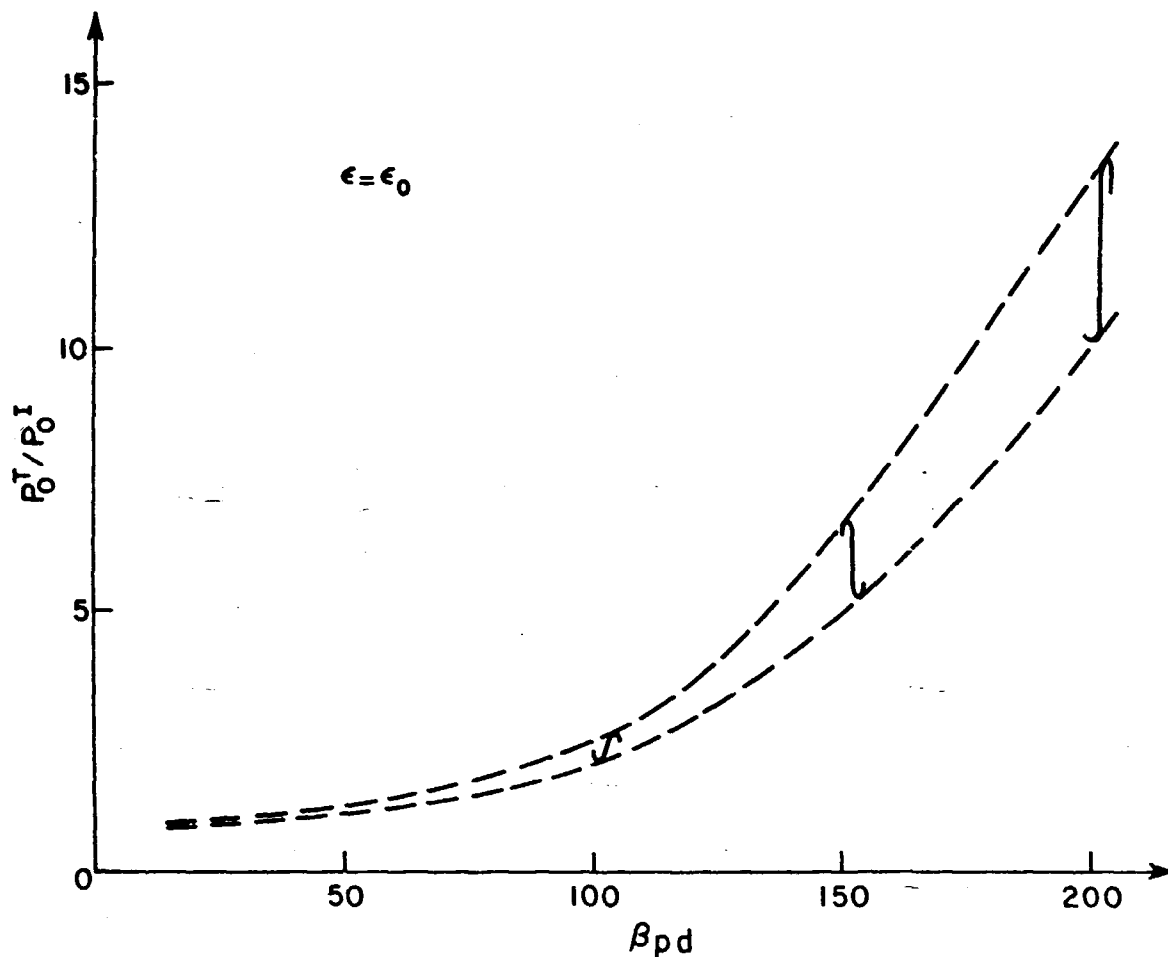


Fig. 3 Transmitted Power vs. Slab Thickness

( $P_0^T$  = Power transmitted at incident frequency)

the slab thickness  $d$  is plotted in Fig. 4, for three cases. From these curves, we observe that the peak gain of the transmitted wave (at frequency  $\omega_0$ ) increases with increasing dielectric constant or, equivalently, with increasing discontinuities at the interface boundaries. If the discontinuities increase indefinitely, the gain will increase indefinitely, indicating oscillation. That is, in the extreme case of infinite gain we may obtain the scattered field in the absence of incident field and this is what is known as oscillation.

There is good evidence that the resonances indicated here may be related analytically to the time-growing solutions in the case of absolute instabilities<sup>3,4</sup>. This question will be pursued, since it seems to lead to a rigorous treatment of oscillations in bounded parametric media, from which important aspects such as oscillator thresholds and frequency-pulling effects may be approached with rigor.



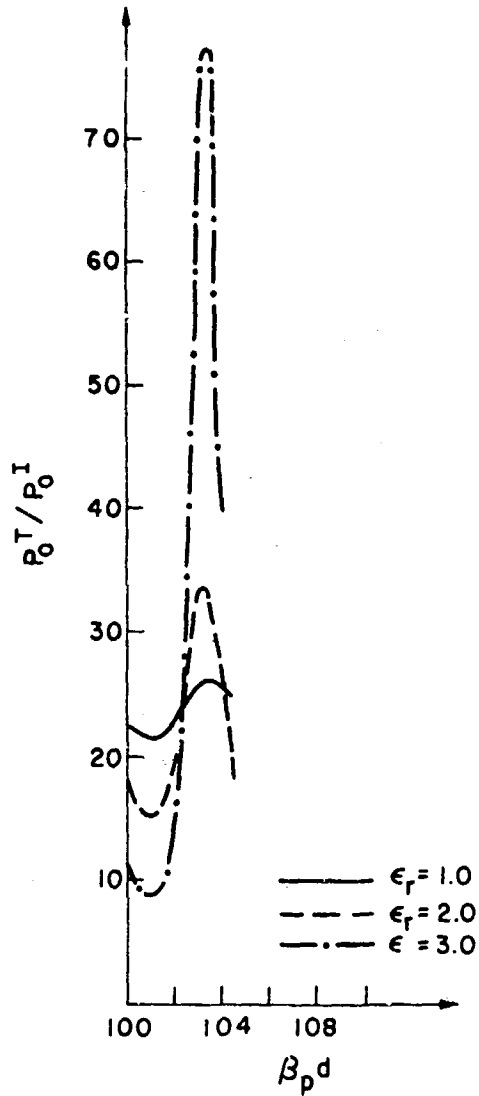


Fig. 4 Transmitted Power vs. Slab Thickness (expanded scale)

Air Force Cambridge Research Laboratories  
Office of Aerospace Research  
F19628-68-C-0075

S. T. Peng

Joint Services Technical Advisory Committee  
AF 49(638)-1402

REFERENCES

1. E. S. Cassedy and S. T. Peng, Progress Report No. 29 to JSTAC, Polytech. Inst. of Brooklyn, Report No. R-452.29-66, pp. 40-44.
2. E. S. Cassedy and S. T. Peng, Progress Report No. 31 to JSTAC, Polytech. Inst. of Brooklyn, Report No. R-452.31-67, pp. 13-18.

3. S. T. Peng and E. S. Cassedy, "Scattering of Light Waves at Boundaries to Parametrically Modulated Media," Proc. of Symposium on Modern Optics, P.I.B., N. Y., March, 1967.
4. E. S. Cassedy, "Dispersion Relations in Time-Space Periodic Media: Part II - Unstable Interactions," Proc. IEEE, Vol. 55, 1154-1168 (1967).

### A GRAPHICAL METHOD OF PREDICTING THE BANDWIDTH OF OPTICAL PARAMETRIC AMPLIFICATION

E. S. Cassedy and M. Piltch

The Floquet approach to the analysis of traveling-wave parametric processes has been developed at this Institute<sup>1,2,3</sup>. In this approach, a slab of dielectric with time-space  $(\omega_p, \beta_p)$  periodically-modulated permittivity may be represented by a simple transmission line model. The line incorporates the time-space periodicity (due to the pump wave) by means of a shunt capacitance with a prescribed time-space variation. Wave propagation on this structure is described by the telegrapher's equation with time-space periodic coefficients. The transmission line is assumed thereby to behave linearly to small signals propagating in the presence of the pump.

It has been shown<sup>1</sup> that Floquet's theorem is applicable for generating solutions to this equation for any set of parameters except those defining the "sonic" region<sup>1</sup>. If we know the basic circuit parameters (related to the basic material parameters) and the pump modulation parameters, we can obtain (eigenvalue) dispersion relations  $\omega(\kappa)$  or  $\kappa(\omega)$ . Here,  $\omega$  and  $\kappa$  are the temporal and spatial frequencies of the Floquet modes (infinite in number) which are the allowed waves in the modulated medium. If we plot the dispersion relations of these Floquet modes on a Brillouin diagram, each mode has its own dispersion curve. The intersection of any two of these curves represents a region in  $\omega$ - $\kappa$  space where the parametric coupling of modes can occur<sup>1</sup>. If either  $\omega$  or  $\kappa$  is complex, the interaction can be of an active nature with the signal waves continuously extracting energy from the pump wave<sup>1,2,3</sup>.

The Brillouin diagram for the medium has a cell (or zone) structure determined by the pump wave parameters<sup>1</sup>. That is, the diagram is periodic in  $\omega_p$  and  $\beta_p$ . This is the graphical representation of the Floquet solutions and is the basis for the graphical construction prescribed in what follows.

The graphical construction will be employed here to display the bandwidth of the parametric amplification<sup>3</sup> (leading to oscillation) achieved experimentally in single-crystalline uniaxial lithium niobate. The basic dispersion relation is plotted in Fig. 1

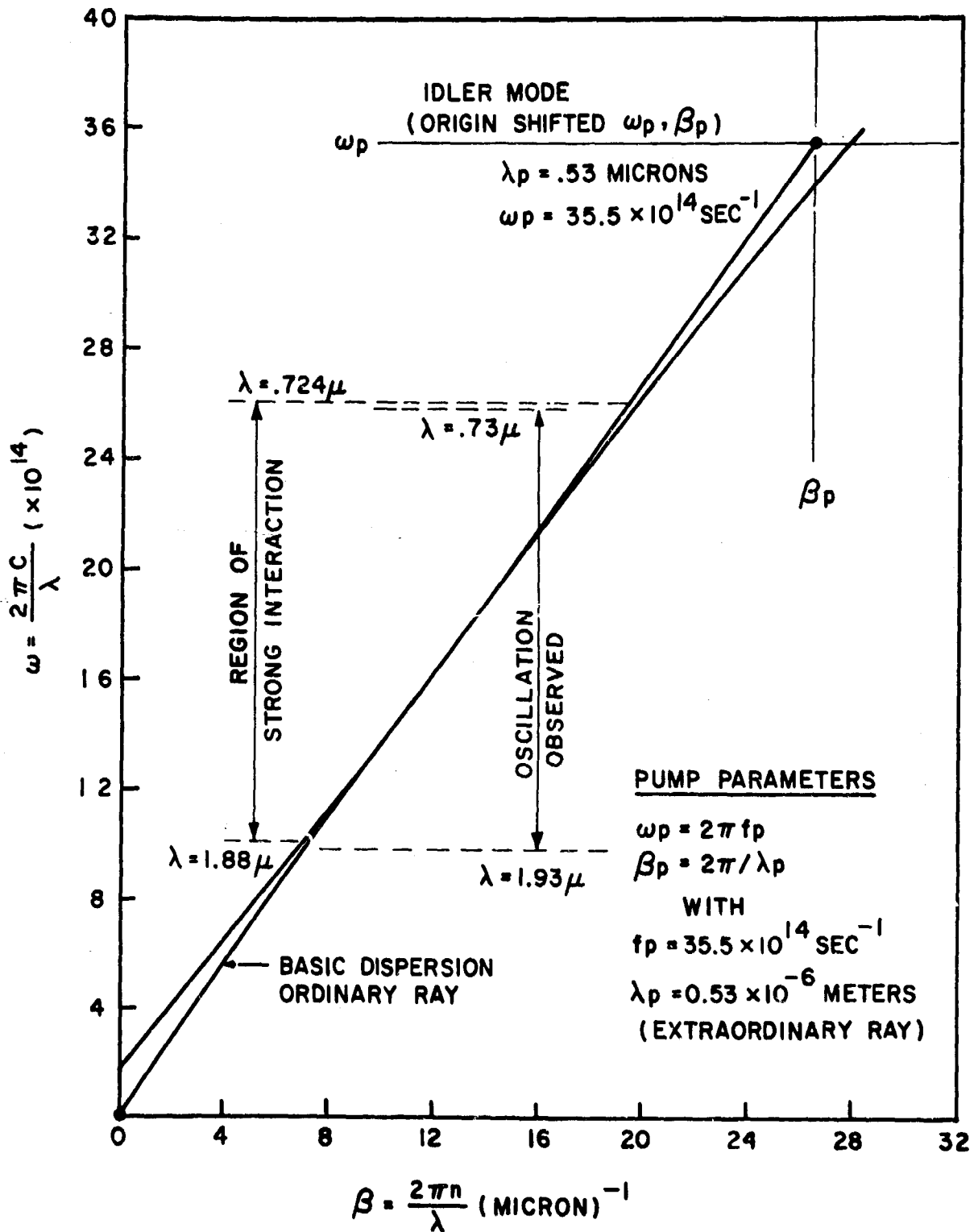


Fig. 1 Brillouin Diagram for Optical Parametric Amplification

from experimental refractive index data for the signal waves which propagate in the lithium niobate as ordinary rays. The idler mode of the medium is then exhibited by the zone displacement of the diagram with the pump parameters  $\omega_p$  and  $\beta_p$ <sup>1,3</sup> corresponding to a pump wavelength of 5300 Angstroms. The pump wave propagates as an extraordinary ray and thus travels faster than the signal in lithium niobate (a negative uniaxial crystal). The idler mode, however, has an ordinary ray dispersion curve and is plotted accordingly with the appropriate slope. Wherever there is an intersection of the two dispersion curves representing the two modes, there will be parametric coupling<sup>1</sup>. The interesting region of the diagram in this case shows an interaction identified as that utilized in the parametric oscillator reported by Giordmaine<sup>4</sup>. The signal ( $\omega, \beta$ ) and idler ( $\omega - \omega_p, \beta - \beta_p$ ) modes have dispersion curves which are approximately tangent over a wide range of wavelengths symmetric about the "degenerate point"  $\lambda_{\text{signal}} = 2 \lambda_{\text{pump}}$  at 1.06 microns wavelength. This condition on the diagram indicates a "coflow" interaction<sup>1,3</sup>, since both the signal and first time-space harmonics are forward waves.

The probable interaction region is read from the diagram in Fig. 1 to extend from  $\omega = 10 \times 10^{14} \text{ sec}^{-1}$  to  $26 \times 10^{14} \text{ sec}^{-1}$ , corresponding to wavelengths of  $\lambda = 1.88 \mu$  to  $\lambda = .724 \mu$ , respectively. This prediction is in close agreement with the experimental results of Giordmaine<sup>4</sup>, who observed parametric oscillation in the wavelength region .73 to 1.93 microns. A quantitative determination of the bandwidth of the interaction can be made from the approximate quadratic dispersion relation<sup>5,6</sup> for any specified modulation index. The bandwidth will turn out in all cases to be wider than the range of exact tangency, making the graphical estimate shown quite reasonable.

This graphical method for predicting parametric interactions has also been used for other optical interactions and was found to be in close agreement with experiment. Stimulated Brillouin scattering has been identified in this manner, including a novel form reported by Hsu and Kavage<sup>6</sup>. A comprehensive report showing the wide applicability of the method will be completed soon.

Air Force Cambridge Research Laboratories  
Office of Aerospace Research  
F19628-68-C-0075

M. Piltch

Joint Services Technical Advisory Committee  
AF 49(638)-1402

#### REFERENCES

1. E. S. Cassedy and A. A. Oliner, "Dispersion Relations in Time-Space Periodic Media: Part I - Stable Interactions," Proc IEEE, 51, 1342 (1963).
2. E. S. Cassedy, "Dispersion Relations in Time-Space Periodic Media: Part II - Unstable Interactions," Proc. IEEE 55, 1154 (1967).
3. S. T. Peng and E. S. Cassedy, "Scattering of Light Waves at Boundaries to Parametrically Modulated Media," Proc. of Symp. on Modern Optics, Polytech. Inst. of Brooklyn, N. Y., March 1967.

4. J. A. Giordmaine and R. C. Miller, "Optical Parametric Oscillation in the Visible Spectrum, " Applied Physics Letters 8, 298 (1966).
5. S. T. Peng, "Scattering and Propagation of Electromagnetic Waves in Bounded Parametrically Modulated Media," Ph. D. Thesis, Technical Report PIBMRI-1374-67, Polytech. Inst. of Brooklyn, June 1968.
6. H. Hsu and W. Kavage, "Stimulated Brillouin Scattering in Anisotropic and Observation of Phonons," Physics Letters 15, 207 (1965).

#### QUENCHING AND SATURATION MECHANISMS IN ARGON ION LASERS

E. Skarnick and H. Schachter

Since the discovery of ion lasers, as high power (1-10 watts) visible (blue, green, yellow, red), light sources, the question of their excitation mechanisms has been a subject of much controversy.

The question of the quenching and saturation mechanisms, especially has been one which has received much attention. It has been suggested by numerous authors that radiation trapping (re-absorption of photons) in the lower laser level transition is responsible for quenching and also responsible for the observance of "ring modes" which occur concurrently.

It has been determined that radiation trapping cannot quench the laser and that a better model to explain the experimental results is one which suggests A II ion depletion by further ionization to A III and A IV ions. After an application of the theory of radiation trapping in a Doppler broadened argon discharge, it was calculated that quenching should occur below the known threshold current of argon lasers ( $10 \text{ A/cm}^2$ ), thereby refuting the trapping theory of quenching. The ion depletion model was found to yield more reasonable quenching currents of about  $100 \text{ amp/cm}^2$ .

Further work is being done to explain and predict the "ring modes" by analyzing the possible modes in a resonator containing an active medium with a spatially perturbed gain profile. Also an analysis of why radiation trapping does not appear is being undertaken.

Joint Services Technical Advisory Committee  
AF 49(638)-1402

H. Schachter

#### EXACT QUANTIZATION CONDITIONS

C. Rosenzweig and J. B. Krieger

It has been known for many years that in the special case of the one-dimensional harmonic oscillator the standard WKB quantization condition gives rise to the exact

values for the energy. Proofs of varying degrees of rigor have been advanced which demonstrate the exactness of the quantization condition. One method simply compares the WKB result to the eigenvalues obtained from an exact solution of the Schrodinger equation. Although this constitutes a completely rigorous demonstration it is obviously not useful in determining the correctness of the quantization rule in precisely those cases where it is of the most interest, i. e., when the Schrodinger equation cannot be solved in closed form, nor does it offer any deep insight into the WKB method.

A second method proceeds by showing that all additional higher-order correction terms to the WKB integral vanish for a given potential.<sup>1</sup> These proofs, however, are not entirely rigorous since they fail to take cognizance of the fact that these correction terms are only asymptotically valid, as  $\hbar \rightarrow 0$ . Thus, when we prove that all higher-order terms are zero, we can only state that the correction to our quantization condition is asymptotically zero. It is still possible to have correction terms of order  $e^{-|a|/\hbar}$ , which are nonzero but which have an asymptotic series representation consisting entirely of zeros, i. e., if we add to the harmonic oscillator potential a term which is small and negative in a region outside the classical turning points and zero elsewhere, then all the higher-order correction terms will be zero because they only involve the behavior of the potential between the turning points. However, if we calculate the expectation value of the Hamiltonian using the unperturbed ground state wave function we find immediately that the perturbed ground state energy must be lower than the unperturbed ground state by terms of  $O(e^{-|a|/\hbar})$ .

Furthermore, there are known cases for which the WKB integral does not give rise to the exact eigenvalues, but a modified WKB integral does. In these cases it is not even clear what "correction" terms we must show are actually zero. Thus a different approach is necessary if we are to prove the exactness of the WKB or modified WKB quantizations.

Recently Froman and Froman<sup>2</sup> have devised a new method to handle this problem. They have developed an encompassing, rigorous approach to the entire theory of the WKB approximation. Part of their work deals with the WKB quantization condition and by use of their formalism they are able to prove rigorously the exact nature of the quantization condition for the special case of the one-dimensional harmonic oscillator. They also show that for radial problems, the modified quantization rule including the Langer correction is exact for both the three-dimensional isotropic harmonic oscillator and the coulomb potential.

Until several years ago these three cases were the only known examples of potentials for which simple exact quantization rules existed. Bailey<sup>3</sup> then discovered several other potentials which give rise to exact quantization conditions by use of either the

WKB or modified WKB quantization condition. However, he could give no justification as to why these results should hold, other than that they provided the same results as obtained by an exact analytical solution of the Schrodinger equation.

We have been able to show that all of Bailey's quantization rules can be obtained by applying the formalism of Froman and Froman to the potentials under consideration. We thus avoid the direct recourse of comparing our results to the results of solving Schrodinger's equation in order to verify the exactness of the conditions.

Furthermore, we have been able to prove that if

$$V(r) = \frac{-\lambda e^{-\alpha r}}{(1-e^{-\alpha r})} + \frac{be^{-\alpha r}}{(1-e^{-\alpha r})^2} \quad 0 < r < \infty$$

then there exists an exact quantization rule. When this quantization rule was integrated and the resulting eigenvalues obtained they were indeed the same as those previously found by a complete solution of the Schrodinger equation.

Of even greater interest is the possibility of proving exact quantization conditions even in the case where no analytic solution has yet been obtained. Using the method of Froman and Froman we have been able to prove that the eigenvalues of

$$V(x) = Ae^{2ax} + Be^{-2ax} \quad -\infty < x < \infty \quad (1)$$

are the solutions of the unmodified WKB quantization condition, i. e.,

$$\int_{x_1}^{x_2} \sqrt{\frac{2m}{\hbar^2} [E_n - V(x)]} dx = (n + \frac{1}{2})\pi \quad (2)$$

where  $x_1$  and  $x_2$  are the zeros (classical turning points) of  $E - V(x)$ .

There are no known analytic solutions of the Schrodinger equation for either the energy eigenvalues or the eigenfunctions for the case of the potential given by Eq. (1). Nor can Eq. (2) be integrated in terms of elementary functions.

In order to provide an independent check on the validity of this last quantization condition a numerical integration was performed of the quantization integral. The problem was made dimensionless by choosing  $\frac{\hbar a}{\sqrt{2mA}} = 1$ . The special case  $A = B$  was chosen and the energy value which satisfied the quantization equation for the ground state ( $n=0$ ) was found to be 2.32 to 3 significant figures. This value was checked by numerically integrating the Schrodinger equation and was found to be correct.

Thus a new, and potentially very powerful, technique has been developed for obtaining the energy eigenvalues even for those cases in which no analytic solutions are available.

The details of the derivations indicated above have recently been published.<sup>4</sup>

National Science Foundation  
Grant GY 752

J. B. Krieger

#### REFERENCES

1. P. N. Argyres, *Physics* 2, 131 (1965).
2. N. Froman and P. O. Froman, "JWKB Approximation; Contributions to the Theory" (North-Holland, Amsterdam 1965).
3. P. B. Bailey, *J. Math. Phys.* 5, 1293 (1964).
4. C. Rosenzweig and J. B. Krieger, *J. Math. Phys.* 9, 849 (1968).

#### RELATION OF PHASE SHIFTS FROM BORN APPROXIMATION TO FOURIER TRANSFORM OF POTENTIAL

J. B. Krieger and R. Dublin

The Born approximation<sup>1</sup> plays an important role in the quantum theory of scattering since it provides a simple way of approximately calculating the scattering amplitude directly from the potential instead of requiring the intermediate, and usually numerical, step of calculating the phase shifts. The main difficulty concerning the use of the Born approximation in any scattering problem is the determination of its range of validity. Thus there are the well known conditions<sup>2</sup> that if either

$$|V(r)| \ll \hbar^2 / \mu r^2$$

or

$$|V(r)| \ll \hbar v / r$$

where  $V(r)$  is the potential at the point  $r$  and  $v$  is the velocity of the incoming particle, then the first Born approximation (F. B. A.) is valid. The calculation of the second and higher Born approximations gives a systematic, although often involved, means of improving the approximation while at the same time studying its rate of convergence.

A second means of determining the validity of the F. B. A. and of improving its accuracy, is through an investigation of the Born approximation to the phase shifts, which is the subject of this note.

It is well known<sup>3</sup> that

$$\delta_{lB} = - \frac{2\mu k}{\hbar^2} \int_0^{\infty} j_l^2(kr) V(r) r^2 dr \quad (1)$$

where  $\delta_{lB}$  is the F. B. A. for the  $l^{\text{th}}$  phase shift for a particle of mass  $\mu$  and wave number  $k$  scattering from a spherically symmetric potential  $V(r)$  and  $j_l$  is a spherical Bessel



function of order  $\ell$ . A necessary condition for the validity of the F. B. A. is that<sup>3</sup>

$$\delta_{\ell B} \ll 1$$

for all  $\ell$ . A knowledge of the  $\delta_{\ell B}$  is of practical interest since it has been found in some cases that substitution of the approximate phase shifts into the exact expression for the scattering amplitude results in an improvement on the F. B. A. amplitude when the  $\delta_{\ell B}$  are not all small compared to one.<sup>4</sup> Furthermore, even if the phase shifts for the low  $\ell$  states are not correctly given by the F. B. A., they are useful in constructing the correct scattering amplitude<sup>5, 6</sup> i. e.,

$$\begin{aligned} f(\theta) &= \frac{1}{2ik} \sum_{\ell} (2\ell + 1) (e^{2i\delta_{\ell}} - 1) P_{\ell}(\cos \theta) \\ &= \frac{1}{2ik} \sum_{\ell=0}^n (2\ell + 1) (e^{2i\delta_{\ell}} - 1) P_{\ell}(\cos \theta) \\ &\quad + \frac{1}{2ik} \sum_{\ell=n+1}^{\infty} (2\ell + 1) 2i\delta_{\ell B} P_{\ell}(\cos \theta) \end{aligned}$$

where we have used  $\delta_{\ell} \approx \delta_{\ell B} \ll 1$  for  $\ell > n$ . Then using<sup>7</sup>

$$f_B(\theta) = \frac{1}{2ik} \sum_{\ell=0}^{\infty} (2\ell + 1) 2i\delta_{\ell B} P_{\ell}(\cos \theta)$$

we have

$$f(\theta) = \frac{1}{2ik} \sum_{\ell=0}^n (2\ell + 1) (e^{2i\delta_{\ell}} - 1 - 2i\delta_{\ell B}) P_{\ell}(\cos \theta) + f_B(\theta).$$

Thus we can calculate  $f$  with high accuracy knowing only  $f_B$ ,  $\delta_{\ell}$  and  $\delta_{\ell B}$  for only those  $\ell$  for which the F. B. A. is not valid. The knowledge of the  $\delta_{\ell B}$  is also useful for determining whether a given potential satisfies the Friedel sum rule<sup>6, 8</sup> for scattering in solids having free carriers capable of screening out the potential at large distances.

Finally, we note that it is often the case that we know the Fourier transform of the potential, but are not able to analytically perform the inversion to obtain  $V(r)$ , as in the case of dielectric screening in solids,<sup>9</sup> so that it is useful to derive an equation that relates  $\delta_{\ell B}$  directly to the Fourier transform of  $V(r)$  to replace Eq. (1). We have derived such a relationship and find that  $\delta_{\ell B}$  can be simply written in terms of integrals in  $K$  space over domain  $0 < K < 2k$  of the Fourier transform of the potential multiplied by simple polynomials in  $K$  of highest degree  $2\ell$ . As an application, we discuss the validity of the Born approximation for the field of a dielectrically screened ionized impurity in a solid.

## REFERENCES

1. M. Born, Zeits f. Physik, 38, 803 (1926).
2. L. Landau and E. Lifshitz, "Quantum Mechanics," (Addison-Wesley Publishing Co., Inc., Reading, Massachusetts, 1958) p. 409.
3. N. F. Mott and H. S. W. Massey, "The Theory of Atomic Collisions," (Oxford University Press, Oxford, 1949) 2nd Edition, p. 191.
4. L. I. Schiff, "Quantum Mechanics," (McGraw-Hill Book Company, Inc., New York, 1955) 2nd Edition, p. 166.
5. See Reference 3, p. 194.
6. J. B. Krieger and S. Strauss, Phys. Rev. 169, 674 (1968).
7. See Reference 3, p. 119.
8. J. Friedel, Phil. Mag. 43, 153 (1952).
9. J. Lindhard, Kgl. Danske Videnskat. Selskat Mat.-Fys. Medd. 28, No. 8 (1954).

## MODELS OF LIGHT BEAMS AND PHOTON STATISTICS

P. Bertrand, A. Kestenbaum, E. Mishkin, K. Moy, D. Stoler

Our previous discussion<sup>1</sup> of anticorrelation effects in stationary fields have been carried out by considering a photon counting experiment and its photon counting distribution. However, since the factorial moments are directly related to the correlation functions by the integral<sup>2</sup>

$$\left\langle \frac{m!}{(m-n)!} \right\rangle = \int \dots \int G^{(n)}(x'_1 \dots x'_n, x''_1 \dots x''_n) \prod_{j=1}^n (x'_j, x''_j) d^4 x'_j d^4 x''_j$$

it may be shown that the observation of a correlation or an anticorrelation effect will depend on the sign of the expression:  $G^{(2)}(x_1 x_2, x_2 x_1) - \{G^{(1)}(x_1, x_1)\}^2$ , which is a measure of the non-random tendency of the photons to be received by the detector.

Expressions for the correlation functions can then be found for a given field, since

$$G^{(n)}(x_1 \dots x_n, x_n \dots x_1) = \text{Tr} \{ \rho E^-(x_1) \dots F^-(x_n) E^+(x_n) \dots E^+(x_1) \}$$

If we expand the electric field operator  $E^+(\underline{x}, t)$  in terms of plane wave mode functions,

$$E^+(\underline{x}, t) = \sum_k i \sqrt{\frac{\hbar \omega_k}{2}} u_k(\underline{x}) e^{-i\omega_k t} a_k$$

we get for single mode fields,

$$G^{(1)}(\underline{x} t_1, \underline{x} t_1) = A \text{tr} \{ \rho a^\dagger a \}$$

$$G^{(2)}(\underline{x} t_\rho, \underline{x} t_2, \underline{x} t_2, \underline{x} t_\rho) = A^2 \text{tr} \{ \rho a^\dagger a^\dagger a a \}$$

where  $A = \frac{1}{2} \hbar \omega u^*(\underline{r}) u(\underline{r})$  is a constant independent of space and time.

Thus the second order correlation function is independent of the time delay  $\tau = t_2 - t_1$ , and therefore will be constant.

We consider now some examples:

a. Laser Field: The density operator  $\rho$  is described by the diagonal representation  $P(\alpha) = \delta^{(2)}(\alpha - \gamma)$  so that

$$G^{(2)}(x_1 x_2, x_2 x_1) = \{G^{(1)}(x_1, x_1)\}^2$$

b. Chaotic Field: We have  $P(\alpha) = \frac{1}{\pi \langle n \rangle} e^{-|\alpha|^2 / \langle n \rangle}$ , where  $\langle n \rangle$  is the average number of photons, and

$$G^{(2)}(x_1 x_2, x_2 x_1) = 2 \{G^{(1)}(x_1, x_1)\}^2$$

c. Field with N photons: With:

$$P(\alpha) = \frac{N!}{(2N)!} \frac{1}{2\pi |\alpha|} e^{-|\alpha|^2} \left\{ \frac{\partial}{\partial |\alpha|} \right\}^{2N} \delta(|\alpha|)$$

we find

$$G^{(2)}(x_1 x_2, x_2 x_1) = \frac{\{G^{(1)}(x_1, x_1)\}^2}{N}$$

d. Laser with noise: The superposition of a laser field with a chaotic field give rise to a field described by

$$P(\alpha) = \frac{1}{\pi \langle n \rangle} e^{-\frac{|\alpha - \gamma|}{\langle n \rangle}}$$

and

$$G^{(1)}(x_1, x_1) = A(\langle n \rangle + |\gamma|^2)$$

$$G^{(2)}(x_1 x_2, x_2 x_1) = 2A^2 \langle n \rangle^2 L_2\left(-\frac{|\gamma|^2}{\langle n \rangle}\right)$$

where  $L_2$  is a Laguerre polynomial.

These results are compared in Fig. 1.

We see then that, although  $G^{(2)}(x_1 x_2, x_2 x_1)$  is constant, its value gives us information on the nature of the field.

For fields such that:  $G^{(2)}(x_1 x_2, x_2 x_1) = \{G^{(1)}(x_1, x_1)\}^2$  we will observe a correlation effect in a counting experiment.

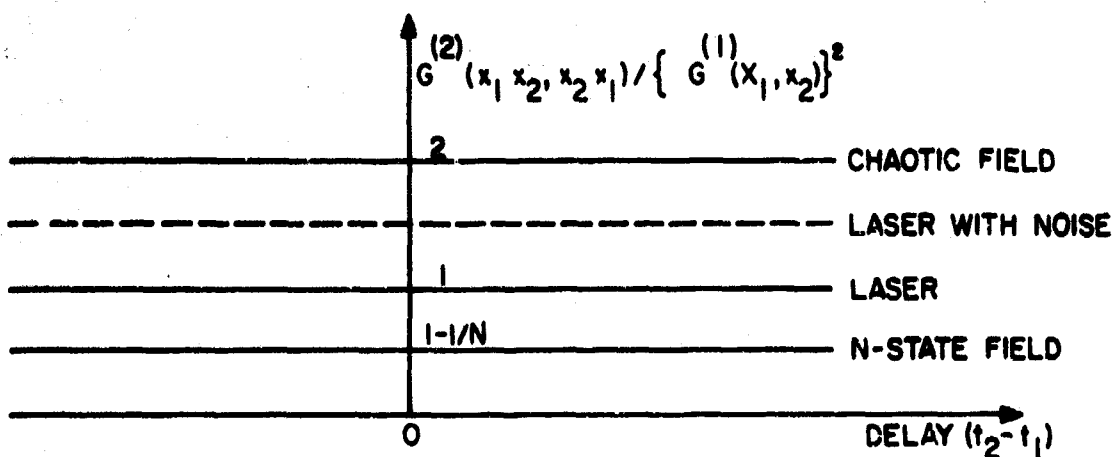


Figure 1

Where:  $G^{(2)}(x_1, x_2, x_2, x_1) < \{G^{(1)}(x_1, x_1)\}^2$ , we will observe an anticorrelation effect.

Office of Naval Research  
N00014-67-A-0438-0001

P. Bertrand and E. Mishkin.

## REFERENCES

1. P. P. Bertrand and E. A. Mishkin, "Anti-Correlation Effects in Single Mode Fields," *Physics Letters*, Vol. 24A, No. 3, p. 188.
2. R. J. Glauber, "Quantum Optics and Electronics," Les Houches (New York: Gordon and Breach, 1964).

## TIME DEPENDENT PHASE-SPACE DISTRIBUTIONS OF THE STIMULATED RAMAN EFFECT

P. Bertrand, A. Hussein, A. Kestenbaum, E. Mishkin, K. Moy, D. Rosenbaum, D. Stoler

A full statistical description of the three coupled fields system is provided by the time dependent density operator  $\rho(t)$ , the characteristic function  $\mathcal{X}(\eta, \zeta, \xi, t)$  which uniquely specifies  $\rho(t)$ , or some other species of the phase-space unambiguously related to  $\rho(t)$  such as for example the weighting function  $P(\alpha, \beta, \gamma, t)$  and Wigner function  $W(\alpha, \beta, \gamma, t)$ .<sup>1-3</sup> We consider for this purpose the set of unitary 3-mode displacement operators<sup>2, 4-11</sup>

$$D(\alpha, \beta, \gamma) = \exp(\alpha a^\dagger + \beta b^\dagger + \gamma c^\dagger - \text{h.c.}); D^\dagger(\alpha, \beta, \gamma) = D(-\alpha, -\beta, -\gamma); \quad (1)$$

$$D(\alpha, \beta, \gamma)|0\rangle = |\alpha, \beta, \gamma\rangle.$$

and the set of their Hermitian Fourier transforms

$$\begin{aligned}
 T(\alpha, \beta, \gamma) &= \pi^{-6} \int d^2\eta d^2\zeta d^2\xi D(\eta, \zeta, \xi) \exp(\alpha\eta^* + \beta\zeta^* + \gamma\xi^* - \text{c. c.}); \\
 D(\alpha, \beta, \gamma) &= \int d^2\eta d^2\zeta d^2\xi T(\eta, \zeta, \xi) \exp(\alpha\eta^* + \beta\zeta^* + \gamma\xi^* - \text{c. c.})
 \end{aligned}
 \tag{2}$$

The displacement operators  $D$  and Hermitian operators  $T$  from orthogonal sets

$$\text{Tr} \{D(\alpha, \beta, \gamma) D^\dagger(\alpha', \beta', \gamma')\} = \pi^3 \delta^2(\alpha - \alpha') \delta^2(\beta - \beta') \delta^2(\gamma - \gamma');$$

$$\text{Tr} \{T(\alpha, \beta, \gamma) T(\alpha', \beta', \gamma')\} = \pi^{-3} \delta^2(\alpha - \alpha') \delta^2(\beta - \beta') \delta^2(\gamma - \gamma');$$

$$\text{Tr} \{T(\eta, \zeta, \xi) D^\dagger(\alpha, \beta, \gamma)\} = \pi^{-3} \exp(\alpha^*\eta + \beta^*\zeta + \gamma^*\xi - \text{c. c.}).$$

Both of these sets are complete and Fourier integral expansions of arbitrary operators  $F$  can be found in terms of either operators  $D(\alpha, \beta, \gamma)$  or  $T(\alpha, \beta, \gamma)$

$$F = \pi^{-3} \int d^2\eta d^2\zeta d^2\xi \mathcal{F}_D(\eta, \zeta, \xi) D(\eta, \zeta, \xi);$$

There inverse Fourier transforms

$$\begin{aligned}
 \text{Tr} \{F D^\dagger(\eta, \zeta, \xi)\} &= \mathcal{F}_D(\eta, \zeta, \xi); \\
 \text{Tr} \{F T(\eta, \zeta, \xi)\} &= \mathcal{F}_T(\eta, \zeta, \xi),
 \end{aligned}
 \tag{6}$$

are obtained by multiplying both sides of Eq. (5) by  $D^\dagger(\eta, \zeta, \xi)$  and  $T(\eta, \zeta, \xi)$ , respectively, and taking subsequently their traces while considering the orthogonality conditions, Eqs. (3).

The Fourier transforms Eqs. (2) are particular integral expansions Eq. (5) of the operators  $T$  and  $D$ , see Eq. (4).

The characteristic function  $\mathcal{X}(\alpha, \beta, \gamma, t)$  and the Wigner function  $W(\alpha, \beta, \gamma, t)$  are expected values, at time  $t$ , of the unitary operator  $D(\alpha, \beta, \gamma)$  and the Hermitian operator  $T(\eta, \zeta, \xi)$ , respectively.

$$\begin{aligned}
 \langle D(\alpha, \beta, \gamma) \rangle &= \text{Tr} \{\rho(t) D(\alpha, \beta, \gamma)\} = \mathcal{X}(\alpha, \beta, \gamma, t); \quad \mathcal{X}(0, 0, 0) = W(0, 0, 0) = 1. \\
 \langle T(\alpha, \beta, \gamma) \rangle &= \text{Tr} \{\rho(t) T(\alpha, \beta, \gamma)\} = W(\alpha, \beta, \gamma, t);
 \end{aligned}
 \tag{7}$$

The Wigner function  $W$  is the Fourier transform of the characteristic function  $\mathcal{X}$  for the operator  $T$  is the Fourier transform of  $D$

$$W(\alpha, \beta, \gamma, t) = \pi^{-6} \int d^2\eta d^2\zeta d^2\xi \mathcal{X}(\eta, \zeta, \xi, t) \exp(\alpha\eta^* + \beta\zeta^* + \gamma\xi^* - \text{c. c.})$$

Equations (7) having the same form as Eqs. (6), their inverse transforms Eq. (5) are the expansions of the density matrix  $\rho(t)$  in terms of the operators  $D$  and  $T$

$$\begin{aligned}
 \rho(t) &= \pi^{-3} \int d^2\eta d^2\zeta d^2\xi \mathcal{X}(\eta, \zeta, \xi, t) D^\dagger(\eta, \zeta, \xi); \\
 \rho(t) &= \pi^3 \int d^2\eta d^2\zeta d^2\xi W(\eta, \zeta, \xi) T(\eta, \zeta, \xi).
 \end{aligned}
 \tag{9}$$

Equation (7) specifies the characteristic function  $\chi(\alpha, \beta, \gamma, t)$  and the Wigner function  $W(\alpha, \beta, \gamma, t)$  in the Schrodinger picture. Written in the Heisenberg representation, which is often more suited for our computations, they read

$$\begin{aligned}\chi(\alpha, \beta, \gamma, t) &= \text{Tr} \{ \rho D(\alpha, \beta, \gamma, t) \}; \\ W(\alpha, \beta, \gamma, t) &= \text{Tr} \{ \rho T(\alpha, \beta, \gamma, t) \} \\ D(\alpha, \beta, \gamma, t) &= \exp \{ \alpha a^\dagger(t) + \beta b^\dagger(t) + \gamma c^\dagger(t) - \text{h. c.} \} \end{aligned} \quad (10)$$

The two representations coincide at time,  $t = 0$ .

In the computations we often make use of the normally and antinormally ordered forms of the displacement operator  $D$

$$\begin{aligned}D_N(\alpha, \beta, \gamma) &= \exp(\alpha a^\dagger + \beta b^\dagger + \gamma c^\dagger) \exp(-\alpha^* a - \beta^* b - \gamma^* c) \\ &= \exp \frac{1}{2} (|\alpha|^2 + |\beta|^2 + |\gamma|^2) D(\alpha, \beta, \gamma) \\ D_A(\alpha, \beta, \gamma) &= \exp(-\alpha^* a - \beta^* b - \gamma^* c) \exp(\alpha a^\dagger + \beta b^\dagger + \gamma c^\dagger) \\ &= \exp \frac{1}{2} (-|\alpha|^2 - |\beta|^2 - |\gamma|^2) D(\alpha, \beta, \gamma). \end{aligned} \quad (11)$$

Their expected values define the normally and antinormally ordered characteristic functions, respectively,

$$\begin{aligned}\langle D_N(\alpha, \beta, \gamma, t) \rangle &= \text{Tr} \{ \rho(t) D_N(\alpha, \beta, \gamma) \} = \exp \frac{1}{2} (|\alpha|^2 + |\beta|^2 + |\gamma|^2) \chi(\alpha, \beta, \gamma, t); \\ \langle D_A(\alpha, \beta, \gamma, t) \rangle &= \text{Tr} \{ \rho(t) D_A(\alpha, \beta, \gamma) \} = \exp \frac{1}{2} (-|\alpha|^2 - |\beta|^2 - |\gamma|^2) \chi(\alpha, \beta, \gamma, t). \end{aligned} \quad (12)$$

The density matrix  $\rho(t)$  of many important fields has a well behaved diagonal representation in form of a statistical mixture of projection operators along the coherent states

$$\rho(t) = \int d^2\alpha d^2\beta d^2\gamma P(\alpha, \beta, \gamma, t) |\alpha \beta \gamma\rangle \langle \gamma \beta \alpha| \quad (13)$$

Another phase space distribution is the positive definite matrix element<sup>\*</sup>

$$R(\alpha, \beta, \gamma, t) = \text{Tr} \{ \rho(t) |\alpha \beta \gamma\rangle \langle \gamma \beta \alpha| \} \quad (14)$$

Using now the first of Eqs. (9) and Eqs. (12) it is easily shown that the  $P$  and  $R$  functions are Fourier transforms of the normally and antinormally ordered characteristic

\* This definition of  $R$ -function differs from the one given by R. J. Glauber by the exponential factor  $\exp(|\alpha|^2 + |\beta|^2 + |\gamma|^2)$ , see R. J. Glauber, Phys. Rev., **131**, 276 (1963) Eq. 6-11; it leads to a simple sequence of Fourier transforms of the characteristic functions  $\chi_N, \chi, \chi_A$ , see Eqs. (8) and (15).

functions  $X_N$  and  $X_A$ , respectively.

$$\begin{aligned}
 P(\alpha, \beta, \gamma, t) &= \pi^{-6} \int d^2\eta d^2\zeta d^2\xi X_N(\eta, \zeta, \xi, t) \exp(\alpha\eta^* + \beta\zeta^* + \gamma\xi^* - \text{c. c.}) \\
 R(\alpha, \beta, \gamma, t) &= \pi^{-6} \int d^2\eta d^2\zeta d^2\xi X_A(\eta, \zeta, \xi, t) \exp(\alpha\eta^* + \beta\zeta^* + \gamma\xi^* - \text{c. c.})
 \end{aligned}
 \tag{15}$$

The P representation<sup>4,12-18</sup> is particularly suited for the computation of expected values of normally ordered operators leading to classical-like integrals.  $P(\alpha, \beta, \gamma, t)$  is not a probability distribution, it may attain negative values over certain regions of the  $\alpha, \beta$  and  $\gamma$  planes. When the fields are coherent,  $P(\alpha, \beta, \gamma)$  is a product of  $\delta$ -functions. For other nonclassical fields it may be more singular and outside the class of tempered distributions.

The Wigner function  $W(\alpha, \beta, \gamma)$ , a species of a quantum mechanical phase space distribution, exists for all states of the field as a well behaved function. It is also a quasiprobability distribution and is not necessarily positive over the whole  $\alpha, \beta, \gamma$  planes.

The exponential factor in  $X_A(\alpha, \beta, \gamma, t) = \exp(-|\alpha|^2 - |\beta|^2 - |\gamma|^2) X_N(\alpha, \beta, \gamma, t)$  insures the existence of the positive definite distribution  $R(\alpha, \beta, \gamma, t)$ , see Eqs. (15).

We turn now to the central problem in the statistical analysis of the three mode system, the specification of the density matrix  $\rho(t)$ , when the initial statistics or  $\rho(0)$  are known. The Fourier integral expansions (4.9) of  $\rho(t)$  and the following interrelations of the various phase space distributions permit a variety of approaches. In all of these use is to be made of the solutions of the equations of motion which specify the mode operators in terms of their initial values. Insertion of the explicit solutions of  $a(t)$ ,  $b(t)$ ,  $c(t)$  and of their adjoints in the Heisenberg form Eq. (10) of  $X(\alpha, \beta, \gamma, t)$  and  $W(\alpha, \beta, \gamma, t)$ , using a proper transformation of their coefficients,

$$\alpha_0, \beta_0, \gamma_0 \rightarrow \alpha_t, \beta_t, \gamma_t \tag{16}$$

$\alpha_t, \beta_t, \gamma_t$  are functions of  $\alpha_0, \beta_0, \gamma_0$  and time  $t$ , leads, as shown below, to identical functional values of  $X$  and  $W$  throughout the time evolution of the system.

$$X(\alpha_t, \beta_t, \gamma_t, t) = X(\alpha_0, \beta_0, \gamma_0, 0); W(\alpha_t, \beta_t, \gamma_t, t) = W(\alpha_0, \beta_0, \gamma_0, 0) \tag{17}$$

When the parameters of the  $X$  and  $W$  distributions follow classical equations of motion analogous to those of the mode parameters  $a(t)$ ,  $b(t)$ ,  $c(t)$ ,

$$\begin{bmatrix} \alpha_0 \\ \beta_0 \\ \gamma_0 \end{bmatrix} \rightarrow \begin{bmatrix} \alpha_t e^{-i\omega_a t} \\ \beta_t e^{i\omega_b t} \\ \gamma_t e^{i\omega_c t} \end{bmatrix} = M(t) \begin{bmatrix} \alpha_0 \\ \beta_0 \\ \gamma_0 \end{bmatrix} \tag{18}$$

where  $M(t)$  is the matrix solution of the equations of motion. The unitary operators  $D$  and the Hermitian operators  $T$  are invariant under the transformations Eq. (16)

$$\begin{aligned} D(\alpha_t, \beta_t, \gamma_t, t) &= D(\alpha_0, \beta_0, \gamma_0, 0); \\ T(\alpha_t, \beta_t, \gamma_t, t) &= T(\alpha_0, \beta_0, \gamma_0, 0) \end{aligned} \quad (19)$$

The detailed proof is given in Appendix A of Ref. 19. In view of the Heisenberg form Eqs. (10) of the characteristic and Wigner functions, this proves the above asserted invariance Eq. (17) of their functional forms and values.

The exponential  $\exp(-|\alpha|^2 + |\beta|^2 + |\gamma|^2)$  is shown in Appendix A of Ref. 19 Eq. (A.7), to be constant when the parameters  $\alpha, \beta, \gamma$  evolve in time in accordance with Eqs. (18). It follows hence, considering the definitions of the normally and anti-normally ordered operators  $D_N$  and  $D_A$ , that the products

$$\exp(\mp |\alpha_t|^2) D_{N/A}(\alpha_t, \beta_t, \gamma_t, t) = \exp(\mp |\alpha_0|^2) D_{N/A}(\alpha_0, \beta_0, \gamma_0) \quad (20)$$

also retain their functional forms and values when the mode operators follow their equations of motions and the coefficients  $\alpha, \beta, \gamma$  evolve in time along analogous trajectories.

The normally and anti-normally ordered characteristic functions  $\mathcal{X}_N, \mathcal{X}_A$  and their Fourier transforms  $P(\alpha, \beta, \gamma, t), R(\alpha, \beta, \gamma, t)$  do not follow the invariance rules of the  $\mathcal{X}$  and  $W$  functions, since the operators  $D_N, D_A$  are not constant under the transformations Eq. (2.9) of Ref. 19 and (18), however the equalities

$$\exp(\mp |\alpha_t|^2) \mathcal{X}_{N/A}(\alpha_t, \beta_t, \gamma_t, t) = \exp(\mp |\alpha_0|^2) \mathcal{X}_{N/A}(\alpha_0, \beta_0, \gamma_0, 0) \quad (21)$$

are valid under the same transformations.

Office of Naval Research  
N00014-67-A-0438-0001

E. Mishkin

#### REFERENCES

1. F. Wigner, "On Quantum Correction for Thermodynamic Equilibrium," *Phys. Rev.* **40**, 749 (1932).
2. J. F. Moyal, "Quantum Mechanics as a Statistical Theory," *Proc. Camb. Phil. Soc.* **45**, 99 (1948).
3. Ref. 12, Lecture XIII.
4. R. J. Glauber, "Photon Correlations," *Phys. Rev. Letters* **10**, 84 (1963); "Quantum Theory of Optical Coherence," *Phys. Rev.* **130**, 2529 (1963); "Coherent and Incoherent States of the Radiation Field," *Phys. Rev.* **131**, 2766 (1963).
5. H. Weyl, "The Theory of Groups and Quantum Mechanics," (Dover, New York), pp. 272-6.



6. M. S. Bartlett and J. E. Moyal, "Transition Probabilities of Quantum-Mechanical Oscillators," *Proc. Camb. Phil. Soc.* 45, 545 (1949).
7. U. Fano, "Description of States in Quantum Mechanics," *Rev. Mod. Phys.* 29, 74 (1957).
8. J. Schwinger, "Unitary Transformations and the Action Principle," *Proc. Nat. Acad. Sci. (U. S. A.)*, 46, 883 (1960).
9. A. E. Glassgold and D. Holiday, "Quantum Statistical Dynamics of Laser Amplifiers," *Phys. Rev.* 139, A1717 (1965).
10. J. R. Klauder, J. McKenna and D. G. Currie, "On Diagonal Coherent-State Representation for Quantum-Mechanical Density Matrices," *J. Math Phys.* 6, 743 (1965).
11. J. C. T. Pool, "Mathematical Aspects of the Weyl Correspondence," *J. Math Phys.* 7, 66 (1966).
12. R. J. Glauber, "Quantum Optics and Electronics," *Les Houches* edited by C. deWitt et. al., (Gordon and Breach, New York, 1965), pp. 65-185.
13. E. C. G. Sudarshan, "Equivalence of Semi-Classical and Quantum Mechanical Description of Statistical Light Beams," *Phys. Rev. Letters* 10, No. 7, 277 (1963).
14. K. E. Cahill, "Coherent-State Representation for the Density Operator," *Phys. Rev.* 138, B1566 (1965).
15. C. L. Mehta and E. C. G. Sudarshan, "Relation Between Quantum and Semiclassical Description of Optical Coherence," *Phys. Rev.* 138, B274 (1965).
16. J. R. Klauder, "Improved Version of the Optical Equivalence Theorem," *Phys. Rev. Letters* 16, 534 (1966).
17. R. Bonifacio, L. M. Narducci and E. Montaldi, "Conditions for Existence of a Diagonal Representation for General Quantum Mechanical Operators," *Phys. Rev. Letters* 16, 1125 (1966); "On Glauber's Representation for General Quantum Mechanical Operators," *Nuovo Cimento XLVII*, 890 (1967).
18. M. M. Miller and E. A. Mishkin, "Representation of Operators in Quantum Optics," *Phys. Rev.* 164, 1610 (1967).
19. F. A. Mishkin, "Photon Statistics of the Stimulated Raman Effect," *Research Report PFB EE 68 0009*.

MINIMUM UNCERTAINTY STATES

P. Bertrand, A. Hussein, A. Kostenbaum, E. Mishkin, K. Moy, D. Rosenbaum, D. Stoler

The coherent Glauber states  $|\alpha\rangle$  of quantum are known to be minimum uncertainty states for which the Hermitian observables  $\hat{q}$ ,  $\hat{p}$  satisfy the relation

$$\Delta q \Delta p = \frac{\hbar}{2} \tag{1}$$

The inverse of this statement is not necessarily true. The nonstationary  $|\alpha\rangle$  states, and the stationary Fock states  $|n\rangle$ , form two distinct bases of the Hilbert space spanned by the vector states of the single mode field, the first being continuous, nonorthogonal

and overcomplete and the second discrete, orthogonal and complete. The physical importance of these characteristic states of the photon annihilation operator  $\hat{a}$  and Hamiltonian  $\hat{H} = \hbar\omega (a^\dagger a + \frac{1}{2})$  is well known and there arises the question of existence of other complete sets of vectors spanning the same Hilbert space unobtained from the  $|a\rangle$  and  $|n\rangle$  sets by any physically trivial unitary transformation.<sup>2</sup> The characteristic states  $|\gamma\rangle$  of the non-Hermitian operator

$$\hat{\gamma} = a + \epsilon a^\dagger; \quad -1 < \epsilon < 1; \quad (2)$$

$$\hat{\gamma}|\gamma\rangle = \gamma|\gamma\rangle \quad (3)$$

$\gamma$  is a continuous complex variable, satisfy the condition (Eq. 1) with<sup>3</sup>

$$(\Delta q)^2 = \frac{\hbar}{2\omega} \frac{1-\epsilon}{1+\epsilon}; \quad (\Delta p)^2 = \frac{\hbar\omega}{2} \frac{1+\epsilon}{1-\epsilon}; \quad (4)$$

The characteristic states  $|\gamma\rangle$  can be obtained from the ground state  $|\gamma = 0\rangle = |0\rangle_\gamma$ , which coincides with the vacuum state  $|0\rangle$  for  $\epsilon = 0$ , following the operation

$$|\gamma\rangle = D(\zeta)|0\rangle_\gamma \quad (5)$$

of the unitary displacement operator

$$D(\zeta) = D^{-1}(-\zeta) = \exp\left(\frac{\zeta\hat{\gamma}^\dagger - \zeta^*\hat{\gamma}}{1-\epsilon^2}\right); \quad D^\dagger(\zeta) = D^{-1}(\zeta) \quad (6)$$

These operators form an Abelian group but for a phase factor

$$D(\zeta)D(\zeta') = D(\zeta + \zeta') \exp\left(\frac{\zeta\zeta'^* - \zeta^*\zeta'}{2(1-\epsilon^2)}\right) \quad (7)$$

The unitary operators  $D(\zeta)$  displace the  $\gamma$  operators in the following manner

$$\begin{aligned} D(\zeta)\hat{\gamma}D^{-1}(\zeta) &= \hat{\gamma} + \zeta \\ D(\zeta)\hat{\gamma}^\dagger D^{-1}(\zeta) &= \hat{\gamma}^\dagger + \zeta^* \end{aligned} \quad (8)$$

Considering the normally ordered expansion of the  $D(\zeta)$  operator, the minimum uncertainty state  $|\gamma\rangle$  has the series expansions

$$\begin{aligned} |\gamma\rangle &= \exp\left\{-\frac{|\gamma|^2}{2(1-\epsilon^2)}\right\} \sum_{n=0}^{\infty} \frac{(\gamma/\sqrt{1-\epsilon^2})^n}{\sqrt{n!}} |n\rangle_\gamma \\ &= \exp\left\{-\frac{|\gamma|^2}{2(1-\epsilon^2)}\right\} \sum_{n=0}^{\infty} \frac{(\gamma^\dagger)^n}{n!(1-\epsilon^2)^{n/2}} |n\rangle_\gamma \end{aligned} \quad (9)$$

where the characteristic states

$$|n\rangle_Y = \frac{(\hat{Y}^\dagger)^n}{\sqrt{(1-\epsilon^2)^n n!}} |0\rangle_Y \quad (10)$$

of the Hermitian operator  $\hat{Y}^\dagger \hat{Y}$

$$\hat{Y}^\dagger \hat{Y} |n\rangle_Y = (1-\epsilon^2) n |n\rangle_Y \quad (11)$$

$$\hat{Y} |n\rangle_Y = \sqrt{(1-\epsilon^2)n} |n-1\rangle_Y; \quad \hat{Y}^\dagger |n\rangle_Y = \sqrt{(1-\epsilon^2)(n+1)} |n+1\rangle_Y$$

form a complete orthonormal set

$$\langle n | n' \rangle_Y = \delta_{nn'}; \quad (12)$$

$$\sum_{n=0}^{\infty} |n\rangle_Y \langle n|_Y = 1$$

The minimum uncertainty states  $|Y\rangle$  form an overcomplete family of states

$$\frac{1}{\pi(1-\epsilon^2)} \int |Y\rangle \langle Y| d^2 Y = 1 \quad (13)$$

This allows a representation of arbitrary field vectors  $|f\rangle$  and operators  $\hat{A}$  in terms of the  $|Y\rangle$  states.

$$|f\rangle = \frac{1}{\pi(1-\epsilon^2)} \int |Y\rangle \langle Y| f \rangle d^2 Y; \quad (14)$$

$$\hat{A} = \frac{1}{\pi^2(1-\epsilon^2)^2} \int |Y_1\rangle \langle Y_1| \hat{A} |Y_2\rangle \langle Y_2| d^2 Y_1 d^2 Y_2; \quad A(Y_1, Y_2) = \langle Y_1 | \hat{A} | Y_2 \rangle$$

representations which are invariant under the transformations

$$\langle Y | f \rangle \rightarrow \langle Y | f \rangle' = \langle Y | f \rangle + g(Y) \exp \left\{ -\frac{|Y|^2}{2(1-\epsilon^2)} \right\}, \quad (15)$$

$$R |Y_1, Y_2^*\rangle \rightarrow R' |Y_1, Y_2^*\rangle = R |Y_1, Y_2^*\rangle + g(Y_1) \exp \left\{ -\frac{|Y_1|^2}{2(1-\epsilon^2)} \right\} h(Y_2, Y_2^*)$$

$g(Y)$ ,  $h(Y, Y^*)$  are arbitrary functions of  $Y$  and  $Y^*$ .

To be useful, the representation of state vectors and operators must be unique; therefore to insure uniqueness we will choose the weight functions  $\langle Y | f \rangle$  and  $\langle Y_1 | \hat{A} | Y_2 \rangle$  to be entire functions of  $Y$  and  $Y_1, Y_2$ .

$$\langle Y | f \rangle = f(Y) \quad (16)$$

$$\langle Y_1 | \hat{A} | Y_2 \rangle = A(Y_1, Y_2)$$

Existence of the P-representation. The characteristic function  $\mathcal{X}(\eta)$  is defined by the average

$$\mathcal{X}(\eta) = \langle e^{\eta a^\dagger - \eta^* a} \rangle = \text{Tr} \{ \rho e^{\eta a^\dagger - \eta^* a} \}$$

so that for the minimum uncertainty states we have

$$\mathcal{X}(\eta) = e^{-\frac{|\eta + \epsilon \eta^*|^2}{2(1 - \epsilon^2)}} e^{\frac{(\eta + \epsilon \eta^*)\gamma^* - (\eta^* + \epsilon \eta)\gamma}{1 - \epsilon^2}}$$

The Wigner function is then defined as the Fourier transform of the characteristic function  $W(\alpha)$

$$W(\alpha) = \frac{1}{\pi} \int \exp(\eta \alpha^* - \eta^* \alpha) \mathcal{X}(\eta, \eta^*) d^2 \eta$$

and the P-representation for the density operator  $\rho$

$$\rho = \int P(\alpha) |\alpha\rangle \langle \alpha| d^2 \alpha$$

if it exists, is given by the Fourier transform of

$$X_N(\eta) = e^{+\frac{|\eta|^2}{2}} \mathcal{X}(\eta)$$

However since  $X_N(\eta)$  is not a square integrable function the Fourier transform is not defined in the usual sense and  $P(\alpha)$  is a very singular function which belongs to the space of tempered distributions.

Office of Naval Research  
N00014-67-A-0438-0001

P. P. Bertrand and E. A. Mishkin

#### REFERENCES

1. R. J. Glauber, "Coherent and Incoherent States of the Radiation Field," *Phys. Rev.* **131**, No. 6, 2766, (1963).
2. M. M. Miller and E. A. Mishkin, "Representation of Operators in Quantum Optics," *Phys. Rev.* **164**, 1610 (1967).
3. P. Bertrand and E. A. Mishkin, "Minimum Uncertainty States" (to be published).

#### DIAGONAL COHERENT REPRESENTATION

P. Bertrand, A. Kestenbaum, E. Mishkin, K. Moy, D. Stoler

We consider a single mode electromagnetic field interacting with two energy level pumping molecules. The diagonal representation of the density operator in terms of the coherent states provides a convenient quantum mechanical description analogous

in form to the classical one for the purpose of computing the statistical properties of the light beams. The total Hamiltonian reads

$$H_T = H_f + H_a + V = \hbar\omega_0 (a^\dagger a + \frac{1}{2}) + \hbar\omega_0 \sum_{n=1}^{\infty} c_n^\dagger c_n + \hbar \sum_{n=1}^{\infty} (\kappa c_n a^\dagger + \kappa^* c_n^* a)$$

where  $H_f$  represents the free electromagnetic energy,  $H_a$  the energy of the atomic system and  $V$  an interaction term with the non-resonant terms omitted. The density operator for the entire system in the interaction picture follows the differential equation

$$i \hbar \partial_t \rho = [V(t), \rho] \tag{1}$$

where

$$V(t) = e^{-\frac{i}{\hbar} (H_f + H_a)t} V e^{\frac{i}{\hbar} (H_f + H_a)t} \tag{2}$$

To obtain a solution of the differential equation, we assume that there are initially more atoms in the ground state than in the excited state. The atomic system acts then as a damping mechanism.<sup>1</sup>

An integration of Eq. (1) leads to power series expansion of  $\rho$  in terms of  $V(t)$ . Differentiating it and taking the trace with respect to the atomic system under the assumption that  $V(t)$  contains only non-diagonal elements in a representation in which  $\rho(0)$  is diagonal leads to

$$\frac{\partial \rho_f}{\partial t} = \frac{1}{(i\hbar)^2} \int_0^t \text{Tr}_u [V(t), V(t'), \rho(t')] dt' \tag{3}$$

The approximation

$$\rho(t) \approx \rho_f(t) \times \rho_u(0) + \Delta\rho(t) \tag{4}$$

holds true when the atomic system is large and interaction with the field does not appreciably alter its density operator. When the two systems are weakly coupled  $\Delta\rho$  is much smaller than the first term and can be ignored. We make the additional assumption that the effects of interaction are dissipated away very fast. This is essentially a Markoffian assumption which permits to replace  $\rho_f(t')$  in the integral by its present value  $\rho_f(t)$ . Under these assumptions we obtain

$$\frac{\partial \rho_f}{\partial t} = -\frac{1}{\hbar^2} \int_0^t \text{Tr}_u [V(t), V(t') \rho_f(t) \times \rho_u(0) - \rho_f(t) \times \rho_u(0) V(t')] dt' \tag{5}$$

and hence,

$$\begin{aligned} \frac{\partial \rho_f}{\partial t} = & -|\kappa|^2 t(a^\dagger a \rho_f(t) N_- + a a^\dagger \rho_f(t) N_+ - 2a^\dagger \rho_f(t) a N_+ - 2a \rho_f(t) a^\dagger N_- \\ & + \rho_f(t) a^\dagger a N_- + \rho_f(t) a a^\dagger N_+) \end{aligned} \quad (6)$$

$N_+$  and  $N_-$  are the initial number of atoms in the excited and ground states respectively. Assuming a diagonal  $P$  representation

$$\rho_f(t) = \int P(\alpha, t) |\alpha\rangle \langle \alpha| d^2\alpha = \int P(\alpha, t) \wedge d^2\alpha \quad (7)$$

Substituting this expression into Eq. (6) and integrating by parts leads to the differential equation for  $P(\alpha, t)$

$$\frac{1}{t} \frac{\partial P}{\partial t} = |\kappa|^2 \langle S(0) \rangle \left[ \alpha \frac{\partial P}{\partial \alpha} + \alpha^* \frac{\partial P}{\partial \alpha^*} + 2P(\alpha) + \frac{2N_+}{\langle S(0) \rangle} \frac{\partial^2 P}{\partial \alpha \partial \alpha^*} \right]$$

where

$$\langle S(0) \rangle = N_+ - N_- < 0 \quad (8)$$

This equation can be solved by means of the Green's function which corresponds to a solution for an initial coherent representation for the field. We obtain the result

$$\begin{aligned} P_G(x, y, t) = & \frac{|\langle S(0) \rangle|}{\pi N_+} \sum_{n_x, n_y=0}^{\infty} \frac{e^{-(n_x + n_y)|\kappa|^2 \langle S(0) \rangle t^2}}{2^{n_x + n_y} n_x! n_y!} \\ & e^{-(x^2 + y^2)} H_{n_x}(x) H_{n_y}(y) H_{n_x}(x') H_{n_y}(y') \end{aligned} \quad (9)$$

where  $H_{n_x}$  is the Hermite polynomial of order  $n_x$ .

The solution for an arbitrary initial diagonal representation of the field can be written in the form

$$P(\alpha, t) = \int P_G(\alpha, t) P(\alpha', 0) d^2\alpha'$$

Office of Naval Research  
N 00014-67-A-04, 38-0001

A. Kestenbaum and E. Mishkin

#### REFERENCES

1. R. K. Yangness and F. Block, "Dynamical Theory of Nuclear Induction," Phys. Rev., Vol. 89, pp. 728-739
2. M. Lax, "Quantum Relaxation, the Shape of Lattice Absorption and Inelastic Neutron Scattering line," J. Phys. Chem. Solids, Vol. 25, pp. 487-503 (1964)
3. A. Kestenbaum and E. A. Mishkin, "Diagonal Coherent Representation," Bull. Am. Phys., April, 1968.

COHERENCE IN INTERNALLY PHASE-MODULATED LASERS

P. Bertrand, A. Hussein, A. Kestenbaum, E. Mishkin, K. Møy, D. Rosenbaum, D. Stoler

Internal modulation in lasers may be accomplished by a variation of a parameter affecting either the loss in the cavity or the phase of the oscillating field. Since an investigation of the coherent properties of a field requires its quantization, we limit ourselves to the second method, thereby avoiding the complexities of a quantum mechanical treatment of losses.

Phase modulation may be accomplished by the insertion of a crystal responding to the linear electro-optic effect<sup>1,2</sup> into the cavity, and the application of an electric field across it thereby achieving variations in the dielectric constant of the medium. Coupling between various modes is obtained when the modulation is harmonically varied at a frequency precisely or nearly equal to a multiple of the intermode spacing  $C/2L$ .

Assuming variations in the dielectric constant in the form

$$\epsilon = \epsilon_0 + \epsilon_1(\underline{r}) \cos(\omega t + \varphi) \tag{1}$$

and treating the atomic medium classically and linearly, we may write the Hamiltonian of our system as

$$H(t) = \sum_{\ell} \hbar \omega_{\ell} (a_{\ell}^{\dagger}(t)a_{\ell}(t) + \frac{1}{2}) - \hbar \cos(\omega t + \varphi) \sum_{\ell, k} \kappa_{\ell k} (a_{\ell}^{\dagger}(t) - a_{\ell}(t))(a_k^{\dagger}(t) - a_k(t)) \tag{2}$$

where it was further assumed that the single pass gain was exactly equal to the single pass loss for each mode. In Eq. (2)  $a_{\ell}^{\dagger}(t)$  and  $a_k(t)$  are the creation and annihilation operators for the  $\ell$ 'th and  $k$ 'th mode respectively, and obey the equal time commutation rule

$$[a_{\ell}(t), a_k^{\dagger}(t)] = \delta_{\ell k} \tag{3}$$

and  $\kappa_{\ell k}$  is the coupling constant between the two modes given by

$$\kappa_{\ell k} = \frac{\sqrt{\omega_{\ell} \omega_k}}{4} \int_V \frac{\epsilon_1(\underline{r})}{\epsilon_0} E_{\ell}(\underline{r}) \cdot E_k(\underline{r}) d\underline{r} \tag{4}$$

where  $E_{\ell}(\underline{r})$  and  $E_k(\underline{r})$  are the spatial eigenfunctions used in the expansion of the electric field, and where the integration extends over the volume of the modulator.

For resonant modulation,  $\omega = \omega_{k+1} - \omega_k \ll \omega_k$ , and the Heisenberg equation of motion may be expressed as

$$i\hbar \frac{da_n}{dt} = \hbar \omega_n a_n(t) + \hbar \kappa [e^{i(\omega t + \varphi)} a_{n+1}(t) + e^{-i(\omega t + \varphi)} a_{n-1}(t)] \tag{5}$$

where it is assumed that  $\kappa$  is constant over the range of frequencies of interest,

If the light beam traverses the modulator  $m$  times while in the cavity, the field as represented by the various operators is given by

$$a_{\ell}(t) = \sum_n a_{\ell+n}(0) J_n(2\kappa\tau m) e^{in(\tau + \frac{\pi}{2})} e^{-i\omega_{\ell} t} \quad (6)$$

where  $a_{\ell+n}(0)$  is the value of the operators in the Schroedinger representation,  $J_n(x)$  are the  $n^{\text{th}}$  order Bessel functions of the first kind, and  $\tau$  is the time spent by the beam inside the modulator in a single pass through it.

The result of Eq. (6) may be employed to examine the effects of the modulation process on the coherent properties of the field. This is most readily accomplished by means of the diagonal or P-representation.<sup>3</sup> If we focus our attention on the single mode representation of the central mode (usually the mode closest to the center of the atomic line), we obtain for the case of initially coherent modes the expression

$$P(\beta, t) = \delta^2(\beta - \bar{a}(t)) \quad (7)$$

where

$$\bar{a}(t) = e^{-i\omega_0 t} \sum_n a_n J_n(2\kappa\tau m) e^{in(\tau + \frac{\pi}{2})} \quad (8)$$

where  $a_n$  is the degree of coherent excitation of the  $n^{\text{th}}$  mode. A representation such as that of Eq. (7) implies the preservation of the coherent character of the excitation in the mode and suggests that the modulation process transfers energy between the coupled modes in a coherent (definite phase) fashion. If initially the central mode is in an  $|n\rangle$  state, and all other modes in their vacuum states, the P-representation for the central mode is given by

$$P(z, w, t) = L_n \left[ -J_0^2(2\kappa\tau m) \left( \frac{\partial^2}{\partial w^2} + \frac{\partial^2}{\partial z^2} \right) \right] \{ (\delta) \delta(z) \} \quad (9)$$

where  $L_n$  is the  $n^{\text{th}}$  order Laguerre polynomial. This expression is of limited use especially when the initial number of photons in the mode is large. In cases where P-representation is highly singular, it is convenient to use two other phase-space distributions<sup>4</sup> in computing statistical averages of the field. For the present case we obtain

$$W(\alpha, t) = 2\pi e^{-|\alpha|^2} (-1)^n (2J_0^2(2\kappa\tau m) - 1)^n L_n \left[ \frac{4J_0^2(2\kappa\tau m) |\alpha|^2}{2J_0^2(2\kappa\tau m) - 1} \right] \quad (10)$$



and

$$\langle a | \rho(t) | a \rangle = e^{-|a|^2} (-1)^n (2J_0^2(2\kappa\tau m) - 1)^n L_n \left[ \frac{J_0^2(2\kappa\tau m) |a|^2}{J_0^2(2\kappa\tau m) - 1} \right] \quad (11)$$

where  $W(a, t)$  is the Wigner function and  $\langle a | \rho(t) | a \rangle$  is the diagonal matrix element of the density operator in the coherent states  $|a\rangle$ . In contrast to the highly singular  $P(z, w, t)$ ,  $W(a, t)$  and  $\langle a | \rho(t) | a \rangle$  are both square integrables, and the latter is additionally a positive definite function.

Description of the total field requires a multimode representation, which for initially coherent modes has the form

$$P(\{\beta_j\}, t) = \prod_{j=1}^N P_j(\beta_j, t) \quad (12)$$

where

$$P_j(\beta_j, t) = \delta^2(\beta_j - \bar{a}_j(t)) \quad (13)$$

with

$$\bar{a}_j(t) = \sum_n a_n J_{n-j}(2\kappa\tau m) e^{i(n-j)(t + \frac{\pi}{2})} e^{-i\omega_j t} \quad (14)$$

which indicates a lack of correlation between the modes coupled by the modulator.

For a non-resonant modulation  $\omega_{k+1} - \omega_k = \omega - \Delta\omega$  where  $\Delta\omega$  is obviously the deviation from the intermode spacing, the Heisenberg equation of motion has the solution

$$a_\ell(t) = \sum_n a_{\ell+n}(0) J_n(mT(\tau)) e^{in\theta(t)} e^{-i\omega_\ell t} \quad (15)$$

where  $m$  is once more the number of passes the light beam makes through the modulator and

$$T(\tau) = \frac{4\kappa \sin \frac{\Delta\omega\tau}{2}}{\Delta\omega} \quad (16)$$

and

$$\theta(\tau) = \tau + \frac{\pi}{2} + \frac{\Delta\omega\tau}{2} \quad (17)$$

with  $\tau$  being the time necessary for a single transit through the modulating crystal.

A solution of the form of Eq. (15) is identical in structure to that of Eq. (6) so that the modulation would once more transfer energy coherently from one mode to another.

For initially coherent modes the multimode field may once more be represented by a  $P$ -representation of the form

$$P(\{a_j\}, t) = \prod_{j=1}^N \delta^2(\beta_j - \bar{a}_j(t)) \quad (18)$$

where

$$\bar{a}_j(t) = \sum_n a_n J_{n-j}(mT(\tau)) e^{i(n-j)\theta(\tau)} e^{-i\omega_j t} \quad (19)$$

We may deduce the form of the field corresponding to a single FM oscillation from this last expression. If the central mode is made to become the carrier of the FM oscillation, all  $a_n = 0$  except  $a_0$  of the central mode, so that

$$\bar{a}_j(t) = a_0 J_{-j}(mT(\tau)) e^{-ij\theta(\tau)} e^{-i\omega_j t} \quad (20)$$

so that the positive frequency part of the total electric field in the cavity has Bessel function amplitudes for its average value.

Office of Naval Research  
N 00014-67-A-0438-0001

A. Kestenbaum and E. Mishkin

#### REFERENCES

1. S. E. Harris and O. P. McDuff, "Theory of FM Laser Oscillation," IEEE J. of Quantum Electronics 1, 245 (1965).
2. A. Yariv, "Internal modulation in multimode laser oscillators," J. of Applied Phys. 36, 388 (1965).
3. R. J. Glauber, "Coherent and incoherent states of the radiation field," Phys. Rev. 131, 2766 (1963).
4. R. J. Glauber, "Quantum Optics and Electronics," 1964, Les Houches, C. DeWitt, A. Blandin, and C. Cohen-Tannoudji, Eds. (New York: Gordon and Breach, 1965).

#### OPTICAL MODES IN INHOMOGENEOUS AND MOVING MEDIA

C. H. Chi and H. Schachter

Optical cavity modes in inhomogeneous moving media are being studied. The Green's function in such a medium is described by Maxwell's equations:

$$\nabla \times \mathbf{E} = -j \omega \mathbf{H}$$

$$\nabla \times \mathbf{H} = j \omega \mathbf{D} + \mathbf{J}$$

$$\mathbf{B} = \mu(\mathbf{r}) \mathbf{H} + \bar{\mathbf{n}}(\mathbf{r}) \times \mathbf{E}$$

$$\mathbf{D} = \epsilon(\mathbf{r}) \mathbf{E} + \bar{\mathbf{n}}(\mathbf{r}) \times \mathbf{H}$$

where

$$\bar{a}(\underline{r}) = \begin{vmatrix} a(\underline{r}) & 0 & 0 \\ 0 & a(\underline{r}) & 0 \\ 0 & 0 & 0 \end{vmatrix}$$

$a(\underline{r})$ ,  $\epsilon(\underline{r})$ ,  $v(\underline{r})$  are functions of space coordinates, speed and refractive index of the medium.

In terms of vector and scalar potentials the Maxwell's equations become

$$\begin{aligned} \nabla \times (\bar{\mu}_1 \nabla \times \bar{A}) - j\omega \nabla \times [\bar{\mu}_1 \cdot (\bar{\Omega} \times \bar{A})] - \nabla \times [\bar{\mu}_1 (\bar{\Omega} \times \nabla \phi)] - j\omega \bar{\Omega} \times \{\bar{\mu}_1 \nabla \times \bar{A} - j\omega \bar{\mu}_1 \bar{\Omega} \times \bar{A} - \bar{\mu}_1 \bar{\Omega} \times \nabla \phi\} \\ = \omega^2 \epsilon \bar{a} \bar{A} - j\omega \epsilon \bar{a} \nabla \phi + \bar{J} \end{aligned}$$

$$\bar{\mu}_1 \nabla \times \bar{A} \quad E = -j\omega \bar{A} - \nabla \phi$$

where  $\bar{\mu}_1 = (\mu \epsilon)^{-1}$

For the case where the velocity of the medium is constant and the medium is homogeneous, one can obtain a closed form solution for all possible orientations of the electric dipole by letting

$$\Omega \frac{\partial \hat{\phi}}{\partial x} + j\omega \mu \epsilon a^2 \hat{\phi} + a \nabla' \cdot \hat{A} = 0$$

where

$$\nabla' = x_0 \frac{\partial}{\partial x} + y_0 \frac{\partial}{\partial y} + z_0 \frac{\partial}{\partial z'}$$

$$z' = \sqrt{a} z \quad \hat{\phi} = \hat{\phi}_e^{j\omega \Omega z} \quad \hat{A} = \hat{A}_e^{j\omega \Omega z}$$

The results show that the optical cavity power loss and field distribution is the same as that of a homogeneous stationary medium but the frequency of the resonant modes are shifted from that of the stationary medium by the relations:

$$f_m = \left[ \begin{array}{c} i - \frac{n^2 v^2}{c^2} \\ \frac{v^2}{c^2} \\ 1 - \frac{v^2}{c^2} \end{array} \right] f_s$$

m: moving medium

s: stationary medium

v: speed of medium

c: speed of light in vacuum

n: refractive index of the medium

For the case where the velocity is constant and inhomogeneity is quadratic in one

direction, two-dimensional solutions are being sought. The Green's function due to a transverse dipole source in such an inhomogeneous moving medium shows that when the E-M wave and the medium are travelling in the same direction the effect of inhomogeneity (such as focusing) is reduced, and when the medium and the E-M wave travel in opposite directions the effect of inhomogeneity is increased. Additional studies involve calculations of power loss, frequency shift and field distributions in optical cavities.

Joint Services Technical Advisory Committee  
AF 49(638)-1402

C.H. Chi  
H. Schachter

#### TUNABLE FILTERS FOR THE VISIBLE AND INFRARED SPECTRAL REGIONS

R. J. Kapash and L. Bergstein

Theoretical and experimental investigations have been carried out on the two-cavity frustrated total reflection filter (FTR filter) to determine its applicability as a tunable band pass filter for the visible and infrared spectral regions. The physical configuration of the filter is shown in Figs. 1 and 2. Not shown is the piezoelectric transducer which is used to vary the degree of coupling of the two resonant layers.

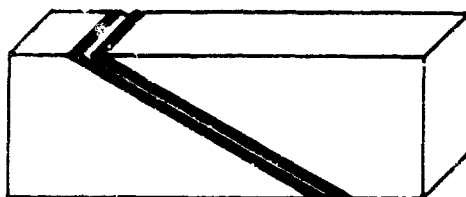


Fig. 1 Physical Orientation of the Prisms and Coatings

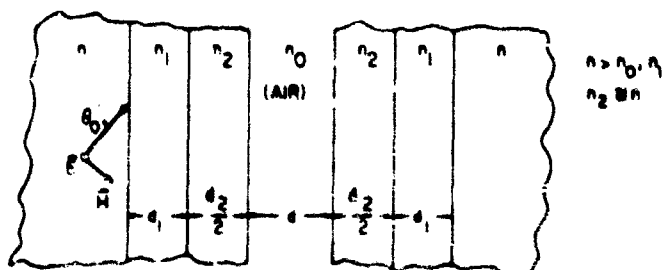


Fig. 2 Schematic of the Five Layers of the Tunable Frustrated Total Reflection Filter Showing a TE Wave Incident at  $\theta_0$ .

The basis of the technique for tuning the pass band of the FTR filter is the well-known effect that occurs when two identical resonant systems are coupled together. The coupling removes the degeneracy; the resonances of the coupled system split and move further apart with increasing coupling.

The filter is oriented in such a position that the incident light strikes the first low refractive index layer at an angle greater than the critical angle for total reflection. Since the first layer is of finite thickness, some of the incident energy can tunnel through into the second layer. The same phenomenon occurs in the third and fifth layers; the energy being resonant in the second and fourth layers is coupled by the evanescent field in the third or middle layer.

If we make the simplifying assumptions about the indices of refraction

$$n_0 = n_1 \text{ and } n = n_2, \tag{1}$$

the transmission coefficient of the filter in the case of an incident transverse electric wave arriving at angle  $\theta_0$ , becomes\*

$$|T|^2 = \frac{1}{1 + (\cos z a_z \sinh 2\gamma \cosh \epsilon + \cosh z \gamma \sinh \epsilon)^2} \tag{2}$$

$$\theta_0 = \sin^{-1} \sqrt{\frac{1}{2} \left[ 1 + \left( \frac{n_0}{n} \right)^2 \right]} \tag{3a}$$

$$a_z = n\pi d_z \sqrt{\frac{1}{2} \left[ 1 - \left( \frac{n_0}{n} \right)^2 \right]} / \lambda \tag{3b}$$

$$\gamma = 2n\pi d_1 \sqrt{\frac{1}{2} \left[ 1 - \left( \frac{n_0}{n} \right)^2 \right]} / \lambda \tag{3c}$$

$$\epsilon = 2\pi n d \sqrt{\frac{1}{2} \left[ 1 - \left( \frac{n_0}{n} \right)^2 \right]} / \lambda \tag{3d}$$

The wavelength for unity transmission is given implicitly as a function of the separation  $d$  by  $\tanh \epsilon = -\cos z a_z \tanh z \gamma$  (4)

In Fig. 3 we show the variation of the center wavelength and the variation of the Q of the filter for unity transmission as a function of the relative separation  $d/d_2$  for various values of  $d_1/d_2$ . The resonant frequency of each of the uncoupled filters is taken to be  $\lambda_0/2$ .

---

\*The assumptions about the refractive indices, while greatly simplifying the equations, do not alter the essential properties of the filter. The result of the different indices of refraction is an overall reduction in the transmission by a constant factor. The choice of a TM wave would have resulted in a different  $\lambda_0$  and  $\theta_0$ , but the essential properties of the filter would be the same.

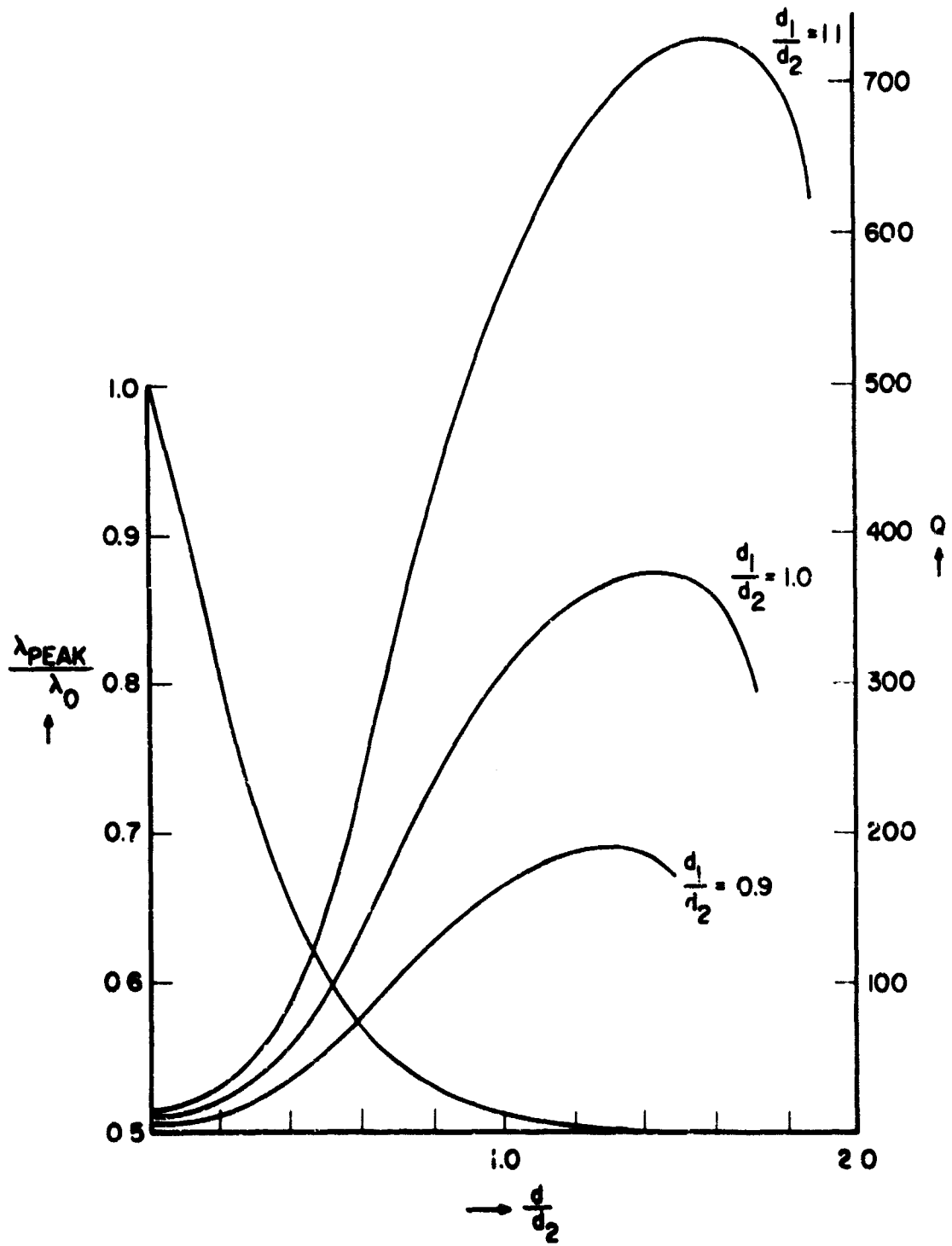


Fig. 3 The Dependence of the Wavelength of Peak Transmission and the Q on the Relative Spacing  $d/d_2$

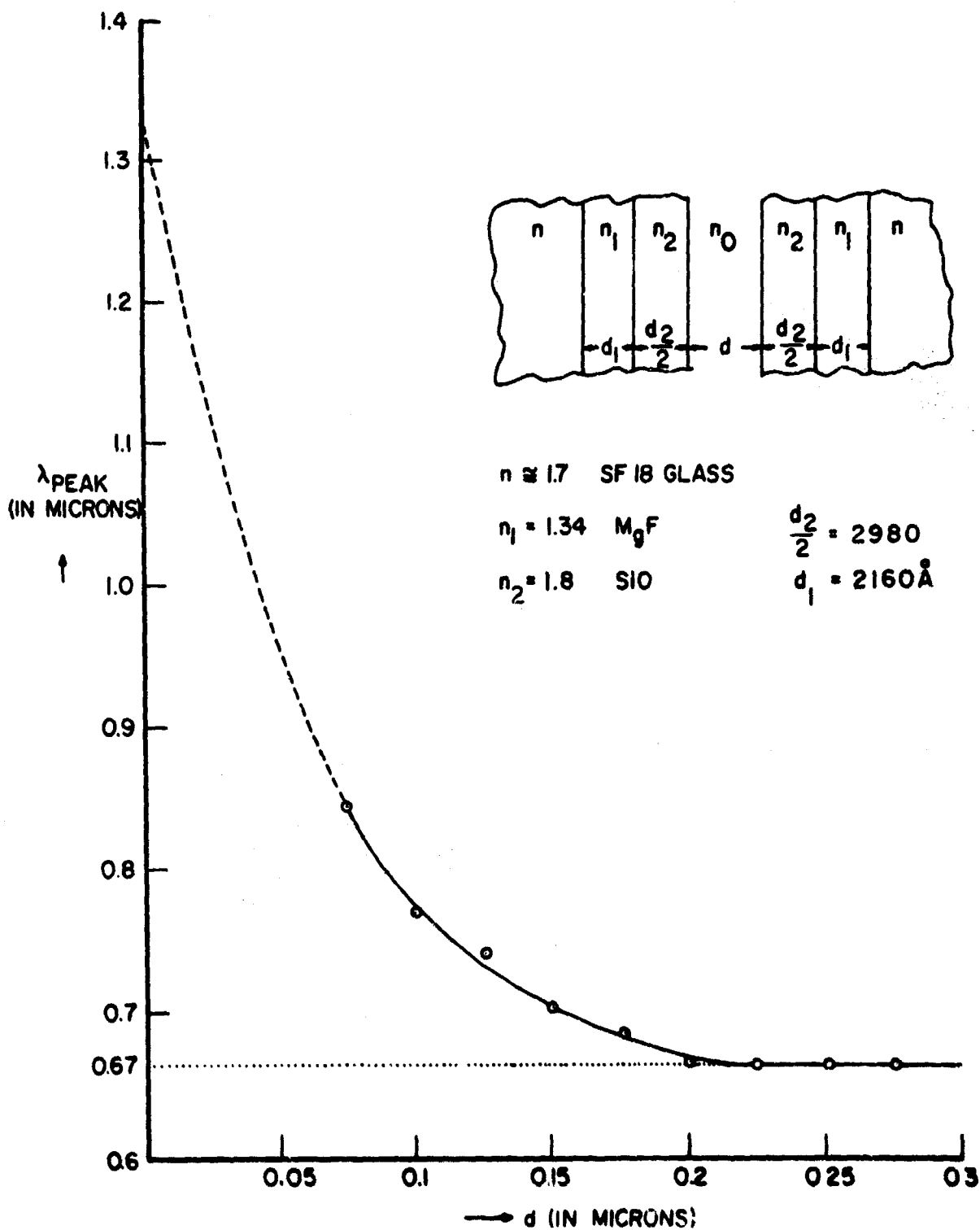


Fig. 4 Measured Dependence of the Wavelength of Peak Transmission on the Spacing  $d$

The useful region of the characteristics is for practical reasons from  $d/d_2 = 0.5$  to  $d/d_2 = 1.0$ . For a filter with  $d_2 = 1500 \text{ \AA}$  ( $\lambda_0/2 \cong 6000 \text{ \AA}$ ) it is not possible to separate the two surfaces by less than  $750 \text{ \AA}$ . Beyond  $d/d_2 = 1.0$  the change in the resonant frequency for a given change in spacing is too small to be useful.

We show in Fig. 4 experimental results for a filter designed for  $\lambda_0/2 = 6300 \text{ \AA}$ . The high refractive index layers were of silicon monoxide ( $n_2 = 1.9$ ), and the low refractive index layers were of magnesium fluoride ( $n_1 = 1.3$ ). The prisms were made of SF-18 glass ( $n = 1.7$ ).

The results have shown that the technique discussed for tuning the pass band of the FTR filter is indeed sound. There are a number of problems in designing the filter for the visible spectrum. The most obvious is the need for the surfaces of the filter to be flat to a fiftieth of a wavelength or better for separations of the order of several hundred angstroms to be meaningful. Also, when dealing with such small separations, it is necessary to compensate very carefully for thermal expansion. These problems do not exist when the filter is designed to operate in the infrared spectral regions above 5 microns, and the filter seems ideally suited to act as a tunable band pass filter in this region.

Joint Services Technical Advisory Committee  
AF 49(638)-1402

R. J. Kapash  
L. Bergstein

## OPTICAL MEASUREMENT OF GAS FLOW PROFILES BY PERTURBATION OF A RING LASER

W. K. Kahn and P. Fenster

In 1851 Fizeau<sup>1</sup> reported fringe shift measurements indicating that the velocity of light in a moving medium differed from that in the same medium at rest. In 1964 Macek<sup>2</sup> and his co-workers succeeded in utilizing this effect in the measurement of the velocity of gas, liquid and solid media with a ring laser. The present work represents an experimental and theoretical assessment of the capabilities of the ring laser for measuring gas flow profiles. Measurements are reported for a range of Reynolds numbers including both laminar and turbulent flows and for a variety of tube diameters. Special emphasis is on the conditions preceding the establishment of the equilibrium flow profiles in round tubes.

For a moving medium of length  $b$  and velocity  $V_0$ , as in Fig. 1, for the two counter-circulating waves the frequency difference is

$$\Delta f = \frac{2bV_0}{\lambda L} (1 - 1/n^2),$$



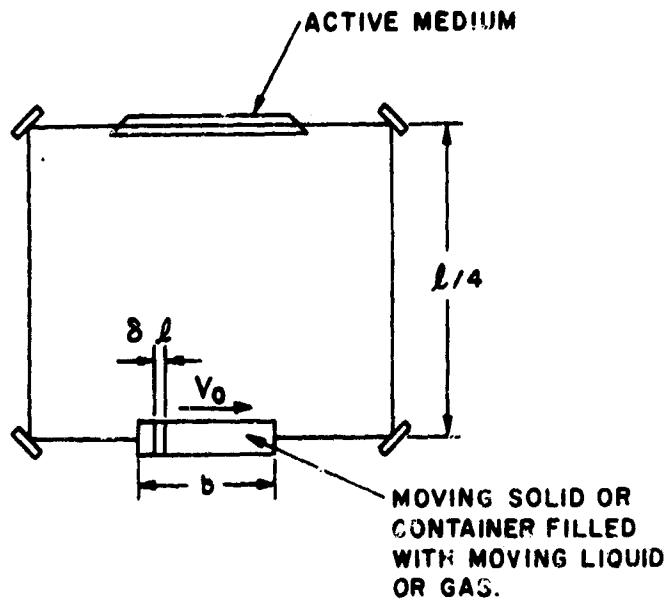


Fig. 1 Schematic of Ring Laser Gas Flow Measurement Apparatus

where  $n$  is the refractive index of the medium,  $\lambda$  is the free space wavelength of the light and  $c$  is the velocity of light in vacuum.

The order of magnitude of this effect is strongly dependent on  $n$ . The results can be separated into two ranges:  $n \approx 1$  and  $n \gg 1$ . For  $n$  near unity

$$\Delta f \approx 4bV_0(n-1)/\lambda l.$$

Gases, which generally meet this requirement, have the additional property that  $(n-1)$  is proportional to  $\rho$ , the mass density.<sup>2</sup> Thus  $\Delta f$  is a measure of the mass flow of gas. For air at standard conditions:<sup>3</sup>

$$(n-1) \approx 2.9 \times 10^{-4}.$$

and for the one meter ( $= l/4$ ) square ring (with moving gas also of length one meter)

$$\Delta f \approx 460 \text{ Hz per meter/second}$$

for  $\lambda_0 = 6328 \text{ \AA}$ . For liquids, the effect would be two or three orders of magnitude greater.

If the velocity of the gas varies over the cross section of the tube, then by changing the cross-sectional position of an axial laser beam an average profile can be constructed from the variation of frequency with position of the beam. If the flow velocity profile varies with axial position in the tube, then in order to obtain an actual velocity profile at a particular cross-sectional plane, the measured average mass flow profile must be analyzed considering this variation.

The results of some of the flow experiments<sup>4,5</sup> are given graphically in Figs. 2-4.

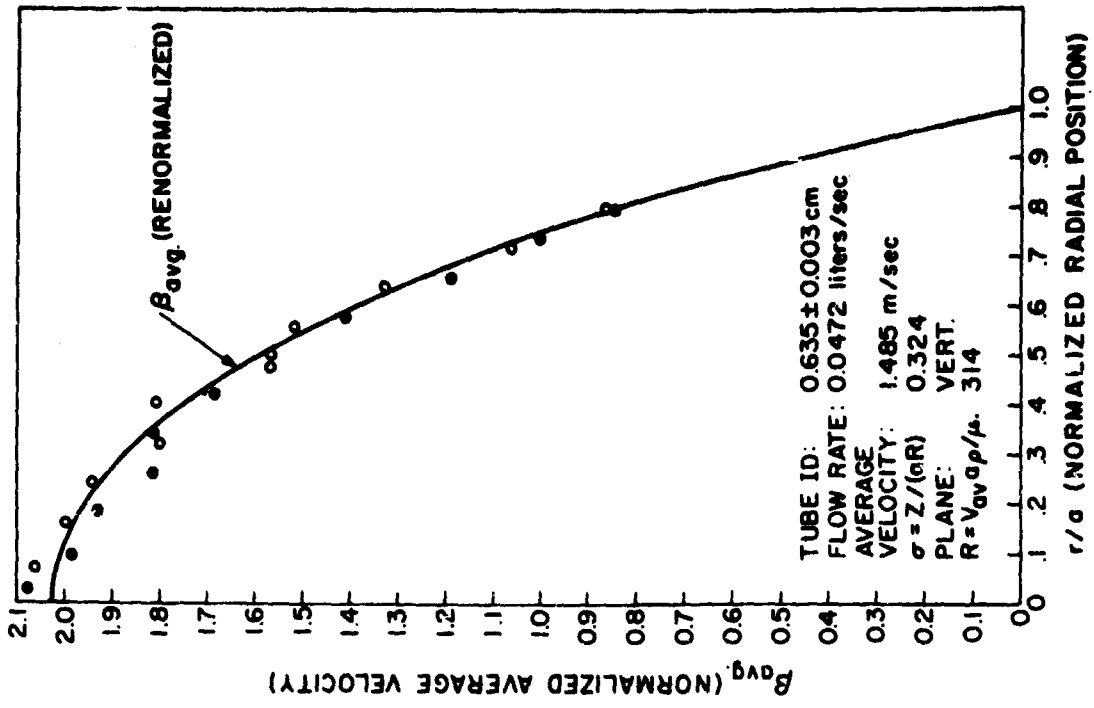


Fig. 3 Normalized Average Velocity for Laminar Flow Development (Vertical Plane)

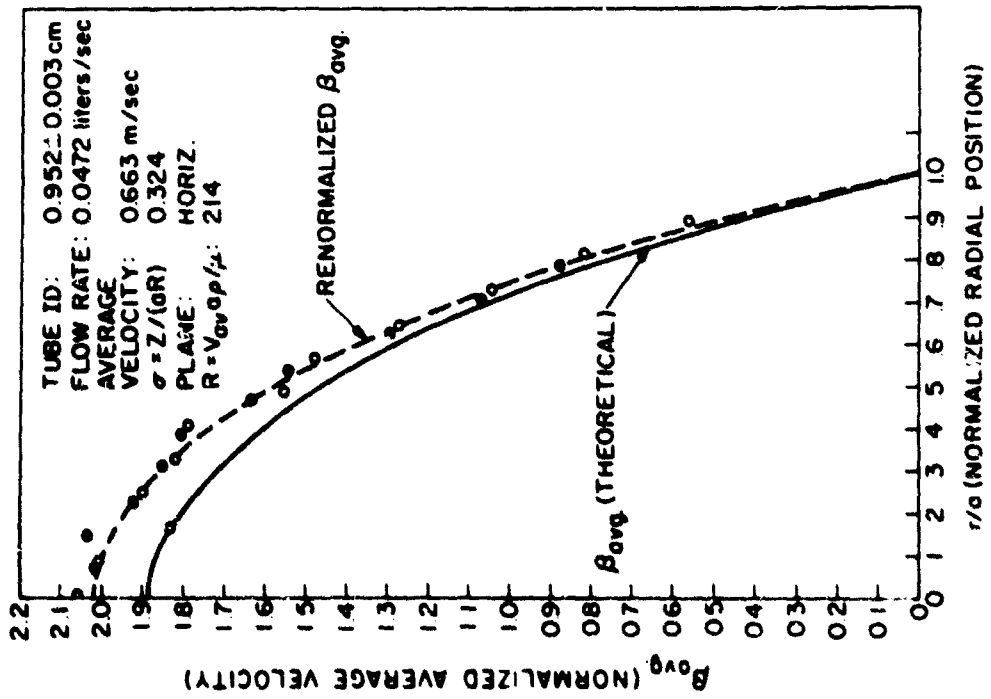


Fig. 2 Normalized Average Velocity for Laminar Flow Development (Horizontal Plane)

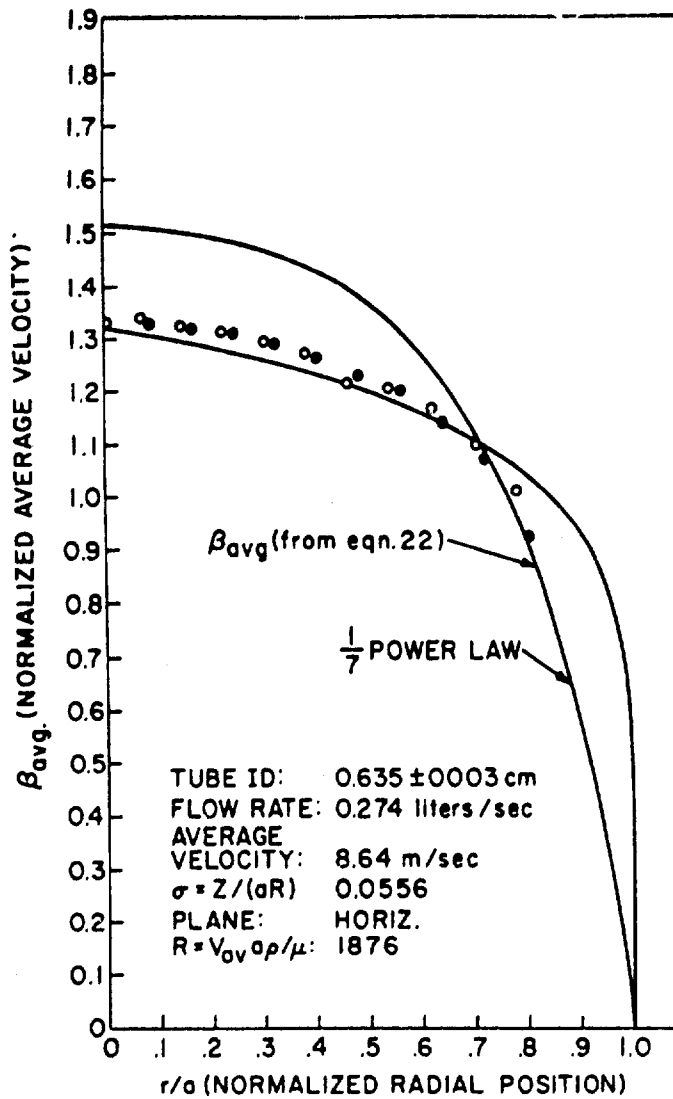


Fig. 4 Normalized Average Velocity for Turbulent Flow

The average velocity of gas flow in the axial direction has been found experimentally for several radii. This has been done for both horizontal and vertical tube cross sections through the axis of the tube. The figures themselves give the average values of gas flow (normalized to the average gas flow over the cross section of the tube) plotted as a function of normalized radial position. The theoretical curves based on measured flow and tube length for each case are also given, as are curves with the same shape renormalized to a value of average velocity which yields the best fit to the experimental data. In the case of the vertical profiles these renormalized curves, designed to best fit the horizontal data (and in theory the same as the vertical profile), are given with the experimental results. In each case, data from either side of the

center line is indicated by different symbols. In the horizontal cases, the experimental points marked with a filled circle represent points on the outside portion of the tube referring to the center of the TWLO; the empty circles represent inside points. For vertical profiles, filled circles represent the upper portion; empty ones, the lower.

Joint Services Technical Advisory Committee  
AF 49(638)-1402

W.K. Kahn

National Aeronautics and Space Administration  
NsG(T)-71

#### REFERENCES

1. H. Fizeau, *Compt. Rend.* 33, 349 (1851) and *Ann. I. Phys. U. Chem. Eng.* 3, 457 (1853).
2. W. M. Macek, J. R. Schneider, and R. M. Salamon, "Measurement of Fresnel Drag with the Ring Laser," *J. Appl. Phys.* 35, 2556 (1964).
3. J.C. Owens, "Optical Refractive Index of Air: Dependence on Pressure, Temperature and Composition," *Appl. Opt.* 6, 51 (1967).
4. P. Fenster, Dissertation for the Degree Ph.D. (Electrophysics), Polytechnic Institute of Brooklyn, June 1968.
5. P. Fenster and W.K. Kahn, "An Optical Technique for Measurement of Gas Flow Profiles Utilizing a Ring Laser," to be published in *Applied Optics*, Dec. 1968.

### III. PLASMA PHYSICS AND ELECTRONICS

Bein, G.	Griemsmann, J. W. E.	Mauro, R.	Shmoys, J.
Bertoni, H. L.	Gross, S.	Mendelsohn, L.	Silverstein, L.
Chung, K.	Haber, I.	Parekh, J. P.	Sistino, A.
Das, P.	Hessel, A.	Pepper, R.	Spoerri, P. A.
Dorman, G.	Hutter, R. G. E.	Peterson, N. C.	Stalzer, H.
Eichler, R.	Jacenko, D.	Pirraglia, J.	Stone, F. T.
Farber, H.	Juretschke, H. J.	Pisane, G.	Stuart, K.
Felsen, L. B.	LaRocca, N.	Rifkin, R.	Torrero, E.
Friedman, H. W.	Levi, E.	Rosenbaum, S.	Wainfan, W.
Gaglione, S.	Malloy, E. J.	Seraphim, P.	Wang, W. C.
Gould, G.			Whitman, G. M.

#### EXPERIMENTAL STUDY OF WEAK PLASMA TURBULENCE USING A HOLLOW CATHODE DISCHARGE

K. Chung

A real plasma is rarely 'quiescent' and possesses many forms of random noise and partially coherent oscillations. These fluctuations of plasma are intimately related to the instabilities and the transport processes of the plasma. If we describe the plasma fluctuation by a spectral function  $I_{kT}^{\vec{r}}(\vec{r}, t)$ , of the fluctuating physical quantity, the 'weak plasma turbulence' is characterized by sharply peaked spectral lines. In the weak turbulence regime the growth rates of the unstable waves are much smaller than the characteristic frequencies, and the interactions between separate wave packets are weak. In a steady state plasma, one observes the quasi-steady state equilibrium spectra of plasma fluctuation.

Previously we observed the density and potential fluctuations of highly ionized Argon plasma produced by a hollow cathode discharge<sup>1</sup>. We have further examined the experimental data.

The hollow cathode discharge could be operated either in a quiescent state or in weakly turbulent states. By varying plasma parameters slightly, it was possible to make transitions from one state to the other. Single electrostatic probes were used primarily to detect the fluctuations, and the signals were processed through an electronic correlator and a spectrum analyzer.

The data showed two distinctive weak turbulence lines. Following the current prevailing theory, which predicts initially excited unstable waves by the linear instability theory and explains the saturation spectra by quasi-linear or non-linear effects, the two distinctive modes found in the hollow cathode discharge were identified with (1) an electrostatic ion cyclotron wave and (2) a drift wave instability.

Identification of these modes was accomplished by checking the frequency dependence on plasma parameters, the amplitude distributions across the plasma column, the propagation directions and damping effects. The electrostatic ion cyclotron instability is an electrostatic mode which propagates at an angle to the confining magnetic field.

Its characteristic frequency is approximately 1.2 times that of the ion cyclotron frequency and carries strong harmonics. The free energy responsible for this mode is associated with the axially-streaming high-energy electrons from the cathode. This particular mode can be stabilized by increasing ion temperature through ion cyclotron damping. This mode was found to be very effective in enhancing the plasma loss across the magnetic field. The drift wave observed in another weakly turbulent state was a pure  $m=1$  mode propagating along the electron drift direction. This observation is believed to be the first one using a hollow cathode discharge plasma. The dominating term in the growth rate is due to the collisional effect. It is found that the ratio of the electron temperature gradient to the density gradient,  $d \ln T_e / d \ln n_e$ , is critical in the marginal stability condition. If the ratio is bigger than unity, this mode becomes unstable. The detailed experimental data and discussion on the observation of these unstable modes are given in Ref. 2.

Although the weak turbulence lines were observed, their definitive roles in the plasma transport processes were not yet quantitatively established. Realizing that recent theoretical and experimental efforts are focused on finding the controlling physical mechanisms in plasma particle transport processes, we decided to further this study by obtaining more experimental data to define the role of plasma weak turbulence in the plasma loss mechanism. We designed a new hollow cathode discharge system and constructed the device. Figure 1 describes this new hollow cathode discharge system at Polytechnic Institute of Brooklyn. It is composed of (1) a high vacuum system using three NRC VHS 6 diffusion pumps and a Kinney mechanical pump, (2) a strong magnet system of 15 PEM 10" air core magnets and 300KW regulated power supplies and (3) sectionized 6 in. I.D. 6 ft. long discharge chamber. The expected plasma parameters are:

plasma density ( $n_e \approx n_i$ )	$\sim 10^{13}$ /cc
operating neutral pressure	$\sim 10^{-4}$ Torr
electron temperature	$\leq 10$ e. V.
ion temperature	$\leq 1$ e. V.
plasma radius	$\sim 2$ cm
Debye length	$\sim 10^{-4}$ cm

The initial experimental study on this device is (1) establishing 'quiescent' and 'weakly turbulent' modes of operation and (2) measuring the direct particle loss rates across the

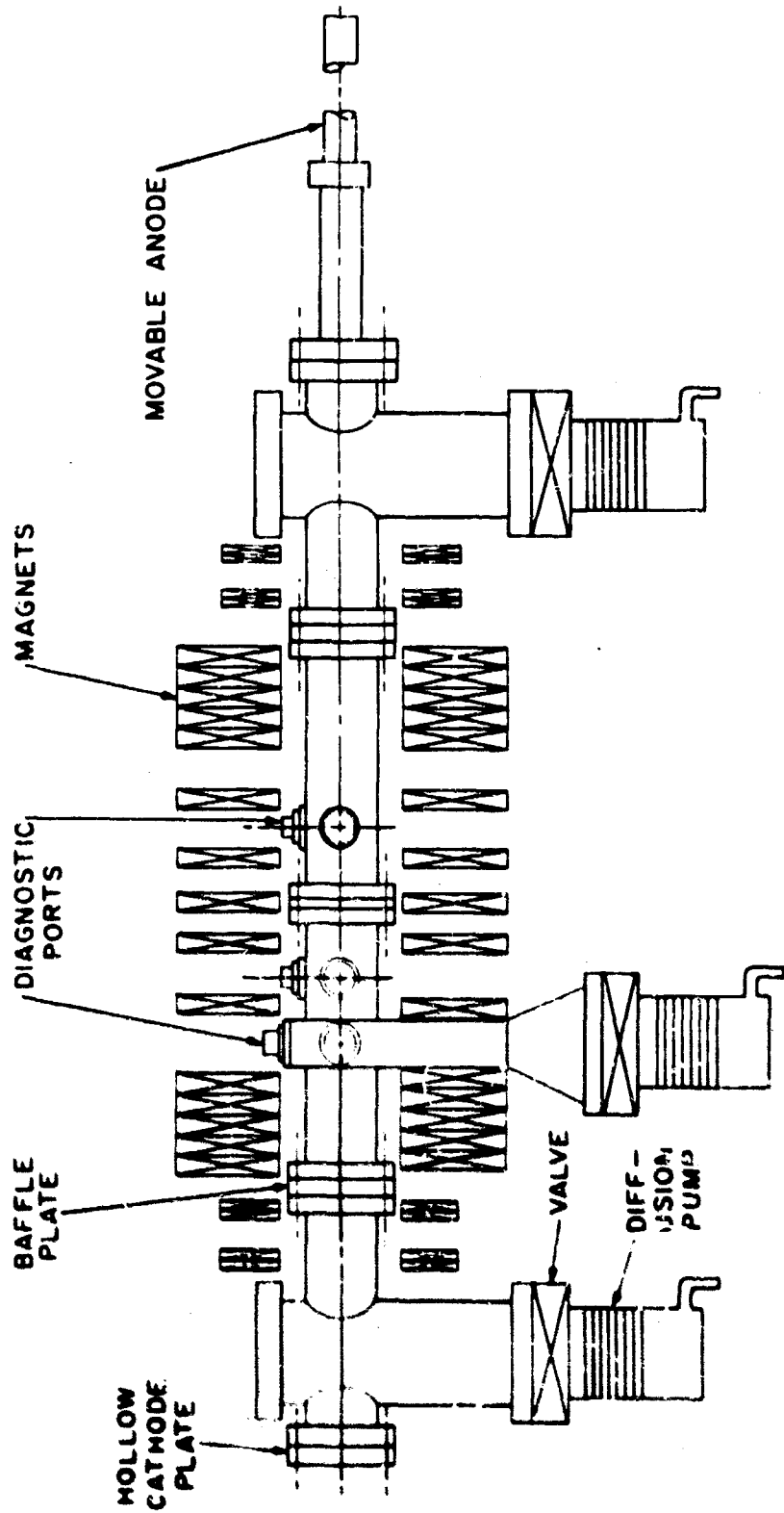


Fig. 1(a) Schematic Diagram of the Hollow Cathode Arc System

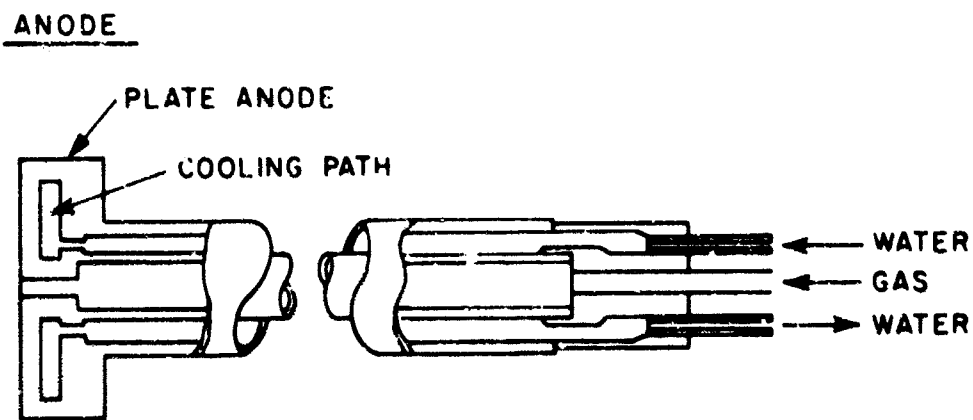
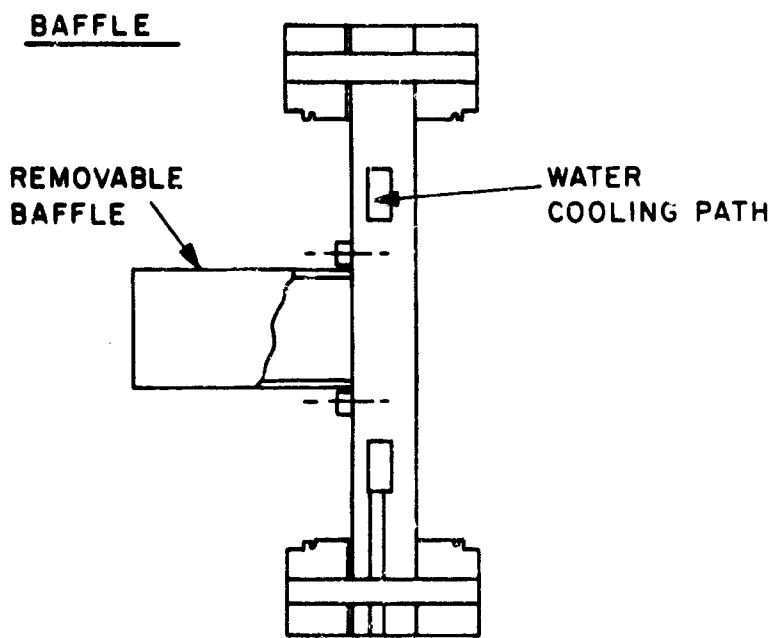
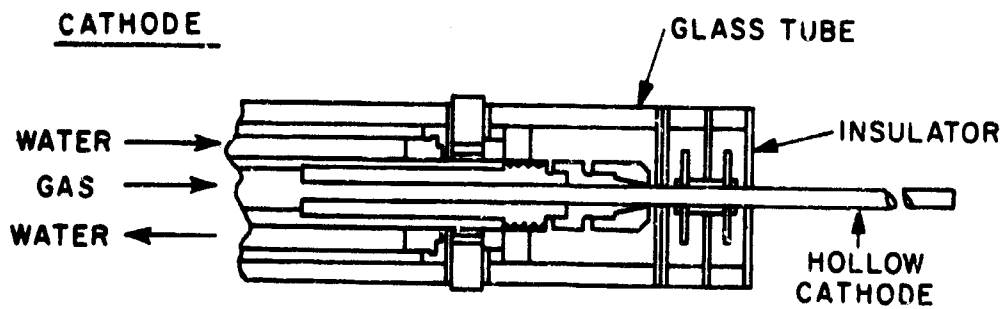


Fig. 1(b) Cathode, Anode and Baffle of the Hollow Cathode Arc



magnetic field and comparing this with the indirect particle loss rate obtained from the cross correlations between density and potential fluctuations.

National Science Foundation  
GU-1557

K. Chung

#### REFERENCES

1. K. Chung and J. Small, "Oscillations in the Hollow Cathode Arc Column," *Bull. Amer. Phys. Soc.*, Vol. 12, 496 (1967).
2. K. Chung and D. J. Rose, "Low Frequency Fluctuations in a Weakly Turbulent Hollow Cathode Discharge Plasma," *PIBMRI Symposium on Turbulence of Fluids and Plasmas* (1968).

#### STEADY STATE RF DISCHARGE THROUGH EFFICIENT ELECTRON CYCLOTRON RESONANCE

K. Chung and E. J. Malloy

When a high frequency electromagnetic field is imposed on a magnetoplasma, there is an appreciable energy transfer from the field to the plasma through the electrons. The field causes an ordered oscillatory motion of randomly moving thermal electrons, which in turn lose or randomize the energy associated with the orderly motion through collisions. This transfer of the field energy into the plasma becomes very effective if the applied frequency is equal to the electron cyclotron frequency. The average energy transfer per unit volume can be written approximately as

$$\frac{1}{2} \frac{v_p^2 c^2 \omega}{v} \left[ \frac{\frac{v}{v} \left( \frac{v^2}{v^2} + \frac{v_c^2}{v^2} - 1 \right) + 2 \frac{v}{v}}{\left( \frac{v^2}{v^2} + \frac{v_c^2}{v^2} - 1 \right)^2 + 4 \frac{v^2}{v^2}} \right] |E_y|^2,$$

where  $v_p$ ,  $v$ ,  $v_c$  and  $v$  are respectively the plasma frequency, the electron collision frequency, the electron cyclotron frequency and the applied frequency. The above expression is derived from the simplified Langevin equation and Maxwell's equations neglecting the ion motion and assuming only an azimuthal electric field. At the cyclotron resonance, the energy transfer is roughly  $10^3$  times more efficient than the non-resonant transfer if the collision frequency is one-hundredth the applied frequency. Thus, it is attractive to produce a collision-rare electrodeless plasma by the electron cyclotron resonance mechanism. In principle, highly ionized plasmas can be obtained using available conventional rf sources.

Figure 1 is the schematic diagram of the electron cyclotron plasma device which is in operation. A magnetron which can deliver power up to 200 W is used as the rf source. A Helmholtz pair of water-cooled magnet coils provide the axial magnetic

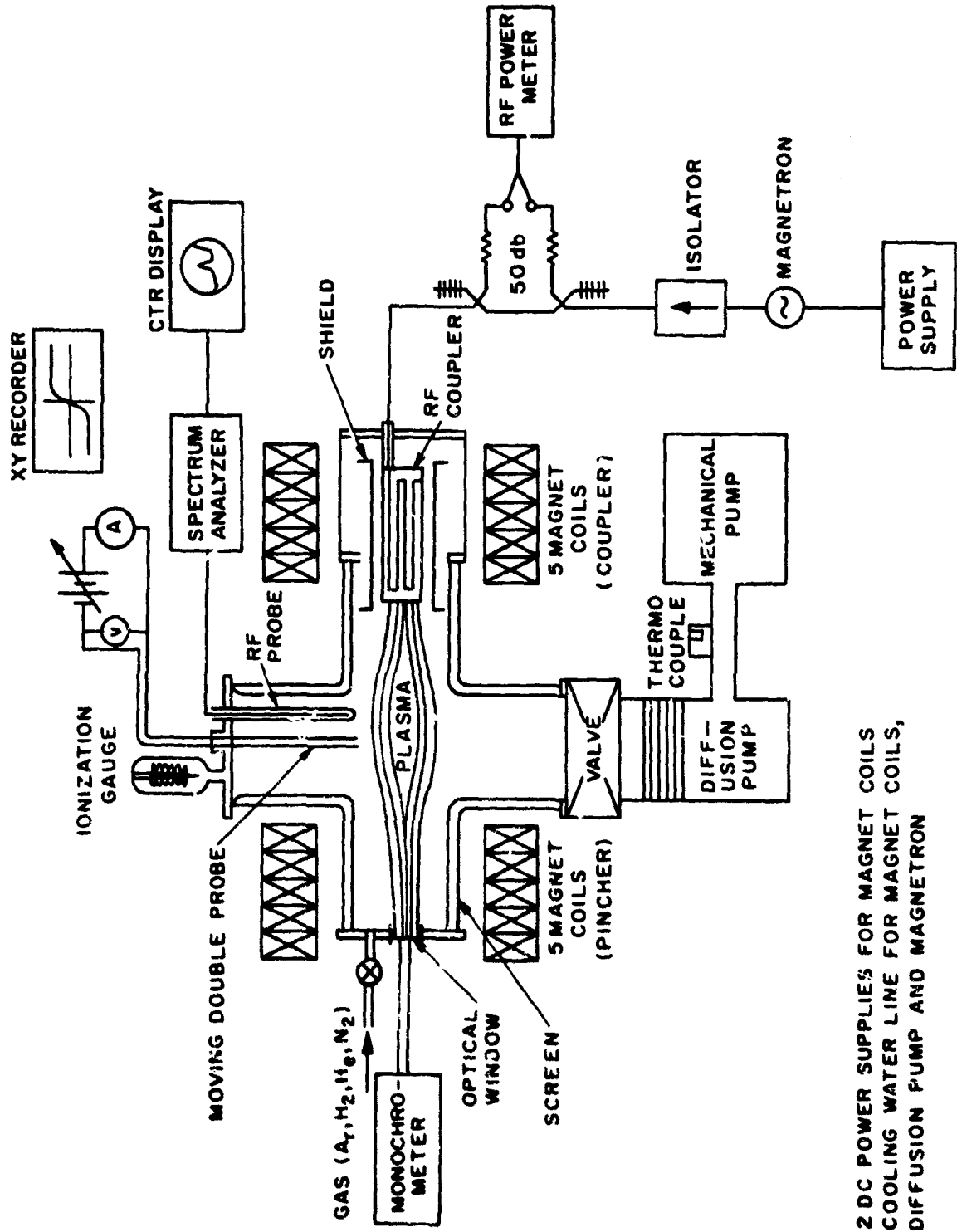


Fig. 1(a) Schematic View of the Electron Cyclotron Plasma Device

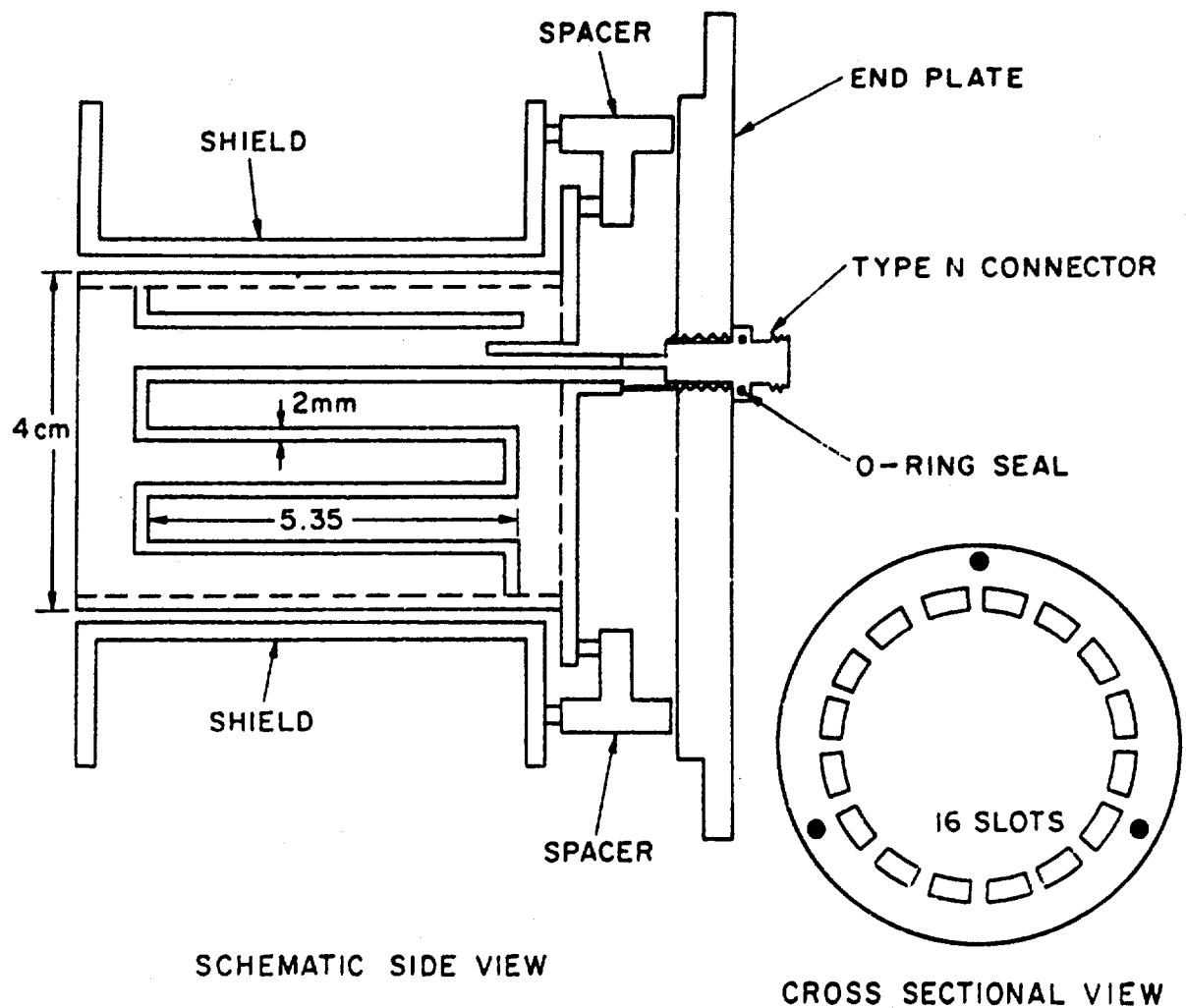


Fig. 1(b) RF Coupler Used for the Electron Cyclotron Plasma Device

field up to 1.2k Gauss. The applied frequency is set at 2.8 GHz and the rf power is applied to the plasma through a slotted cylindrical coupler<sup>1</sup>. This coupler is more efficient and convenient than either open-ended waveguides or cavities, which can be used to produce plasma. The advantage of this coupler is that rf energy can be transferred into the plasma effectively over a broad band of the applied frequency. The perturbation caused by the plasma on the matching condition is not important for this coupler. The total input power is the sum of (1) radiative loss from the coupler, (2) dissipative loss into the structure, (3) direct transfer into the plasma and (4) generation of plasma waves. The relative portion of energy loss through each mechanism changes as the operating condition is changed. In Fig. 2 the plasma density measured by a double probe is plotted against the average magnetic field over the coupler. The secondary peak of the density at a lower field is caused by the non-uniformity of the

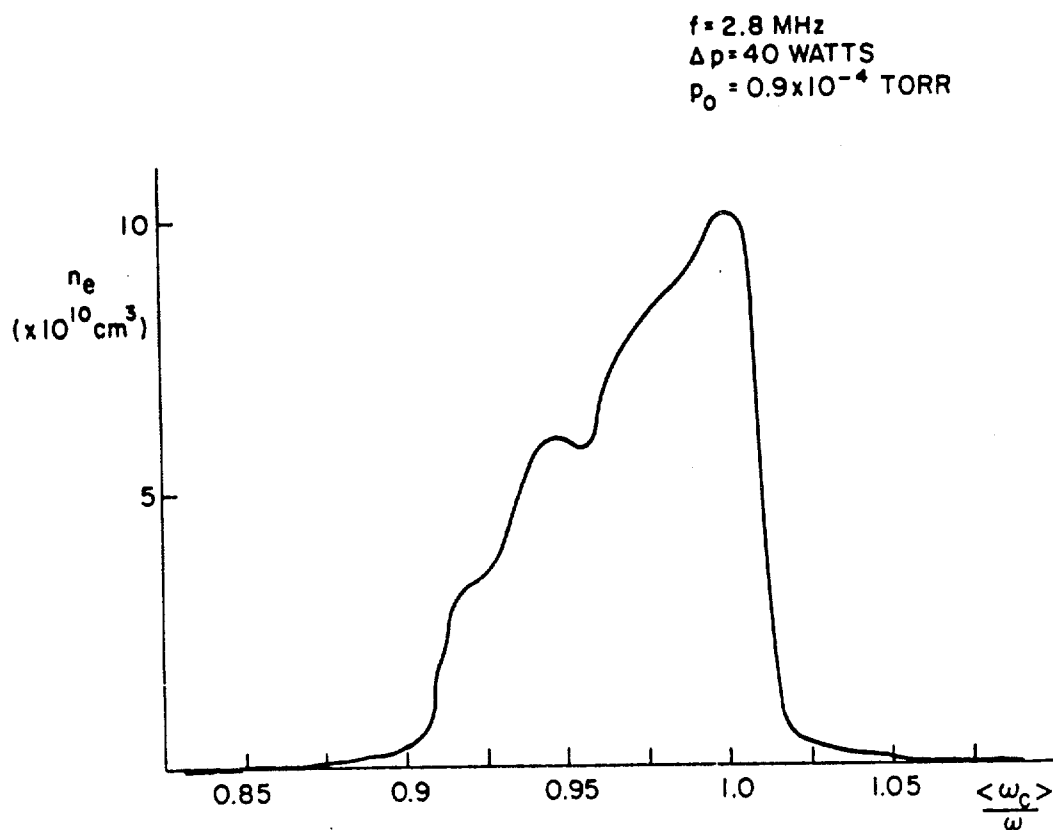


Fig. 2 Plasma Density on the Axis as the Magnetic Field Varied

magnetic field over the coupler. The probe was located on the axis and 5 inches off the coupler.

Plasma produced in the coupler region diffuses and is pushed out into the 'external' region. The acceleration of the plasma from the coupler is due to the constancy of the magnetic moment and the axial gradient of the magnetic field. The external plasma is thus formed along the confining magnetic field lines. Typically, the external plasma has an electron density of  $10^9 - 10^{11} \text{ cm}^{-3}$  and a temperature of 5-20 eV, depending on the applied power level and the neutral pressure. Almost any gas can be used and air, argon, helium, nitrogen and hydrogen have been tested. In general, at a fixed power level the density increased while the electron temperature decreased as the neutral pressure was increased. However, in the practical operating ranges, the collision frequencies are smaller than the electron cyclotron frequencies and the mean free paths are bigger than the characteristic length of the device. Because of these properties, the plasma produced by this device is a close realization of the collisionless plasma. Another important characteristic of the plasma is that the noise level

can be suppressed very low. This is a very desirable property for the performance of experiments in weak plasma turbulence and diffusion studies.

At present, we are looking for unstable modes which can be generated by this coupling structure. We have observed a couple of very interesting phenomena: (1) formation of plasma striations along the magnetic field and (2) electrostatic oscillation at the ion cyclotron frequency and its coupling with a low frequency mode. Plasma striations were observed in the Barium plasma clouds at high altitudes recently and drew considerable interest because of the possible role of these striations in plasma transport processes. In laboratory plasmas, some filamentary structures were reported only in current carrying plasmas and explained by the possible non-uniform electrode mechanism<sup>2</sup>. Our observation of plasma striations is done in a currentless (thus electrodeless) steady-state plasma. In Fig. 3 we show the picture of plasma



Fig. 3 Plasma Striations Observed in the Electron Cyclotron Plasma  
(Neutral Pressure =  $2 \times 10^{-4}$  torr; Input Power = 10 Watts)

striations in the electron cyclotron plasma. The number of striations is not equal to the number of slots in the coupling structure and, in fact, can be varied by changing only the external magnetic field at a fixed neutral pressure and rf power level. Since the change of the external magnetic field causes a change in the power transfer of the rf energy into the plasma, the change of plasma striations may be due to the generation of different modes in the plasma. This point will be cleared as more data become available. One of the unstable modes detected by floating Langmuir probes corresponds to electrostatic oscillations near the ion cyclotron frequency and its harmonics. The power spectra shown in Fig. 4 are the ion cyclotron oscillations observed in argon plasma. The successive pictures show the development of the unstable mode as the rf



↑      ↑  
 0      40kHz  
 POWER LEVEL    TOP : 20 W  
                   MIDDLE : 40 W  
                   BOTTOM : 60 W

Fig. 4 Oscillations at Ion Cyclotron Frequency in Argon Plasma

power level is increased. The broadening of the spectral line can be explained by the mode-mode coupling between the ion cyclotron oscillation and another low frequency mode which, in this case, may be the ion acoustic mode. As the power level is increased the low frequency mode gets unstable, and the coupling broadens the ion cyclotron oscillation.

National Science Foundation  
GU-1557

K. Chung

#### REFERENCES

1. G. Lisitano, Proceedings of the Seventh International Conference on Ionization Phenomena in Gases, Vol. 1, pp. 464-467, Greldevinska Knjiga Publishing House (1966).
2. H. S. Robertson and W. B. Pardo, "Plasma Instabilities and Anomalous Transport", pp. 250-252, University of Miami Press (1966).

## PLASMA SHIELDING AND STABILITY

E. Levi and H. W. Friedman

Instabilities in the plasma sheaths seriously impair the performance of gaseous plasma instruments and devices, such as Langmuir probes, fluorescent lamps, lasers, and magnetoplasma dynamic power converters. Langmuir probes are currently being used as a diagnostic tool in fluid dynamic studies. A recent investigation at PIB has examined the basis for this technique, and has shown that the conditions under which such measurements have been obtained may, however, lead to instabilities in the probe performance that invalidate the experimental results. The effect of magnetic fields as well as the effect of emission of particles from electrodes has also been investigated. It was found that a stable sheath can form only in front of the cathode or insulated walls, and for small values of the magnetic field component parallel to the wall surface. Emission of particles by the wall has, in general, a destabilizing effect.

The space-charge-sheath which shrouds a plasma confined by material walls plays a role in plasma physics similar to that of a boundary layer in fluid dynamics; the stability of the sheath determines the character of the diffusion and wave propagation processes deep inside the body of the plasma<sup>1</sup>. Yet, in the many studies of the sheath very little attention has been paid to the problem of stability. The well-known Bohm criterion for stability<sup>2</sup> applies only to the special case in which no electric current flows through the plasma. Moreover, in his derivation Bohm did not really prove stability, but merely established the conditions under which a plasma can shield itself from an electric field by forming a space charge sheath. Since in the sheath the densities of the electrons and ions are not equal, there occurs a relative streaming of the ions past the electrons, even in the case when the fluxes of the two species to the confining walls are equal and the plasma carries no electric current. Such a situation is known to be potentially unstable<sup>3</sup>, especially when the drift velocities are high, and the Bohm criterion requires the ions to be supersonic.

A connection between shielding and the microstability of a collisionless plasma was made by Engelmann<sup>4</sup>. Engelmann, however, did not address himself to the problem of the sheath, and his criterion requires knowledge of the distribution functions which are not directly observable. We therefore examined the behavior of the plasma using both the Vlasov equations and an equivalent macroscopic representation<sup>5,6</sup>. This procedure provides a prescription for handling the singularities occurring at the sound of speed<sup>7,8</sup> and sheds light on their physical significance. Engelmann's stability criterion can then be recast in terms of macroscopic observables, a form which can be displayed graphically and readily applied to physical situations.

In most practical situations the mean free-path exceeds the thickness of the sheath, so that the sheath can be considered as collisionless, even though the plasma structure

as a whole may be collision dominated. Under these circumstances it is possible to apply the macroscopic criterion to examine the space charge sheath and derive necessary and sufficient conditions for shielding and stability. Since the derivation of the stability criterion does not pose any restriction with regard to particle fluxes and electric currents, current-carrying plasmas are within the scope of the investigation.

It is found that

1. In the particular case of zero current, Bohm's condition ensures stability as well as shielding, so that Bohm's stability criterion is not only recovered but also rigorously proved.
2. In the case of arbitrary current, the necessary and sufficient conditions for shielding derived by us are consistent with measurements obtained by means of Langmuir probes and their recent interpretation<sup>9</sup>. In particular, the knee in the current-voltage characteristic near electron saturation is predicted and can be evaluated quantitatively. Also the dependence of ion saturation current on the electron, rather than ion, temperature is confirmed.
3. A one-to-one correspondence between shielding, i. e., the formation of a space charge sheath, and stability of the plasma exists over the range of impressed voltages for which both electron and ion currents can flow.
4. When either the ion or the electron currents are driven far into saturation and one of the species is repelled, the plasma may be shielded but unstable. Careful experiments conducted by Belenov et al.<sup>10</sup> indeed confirm that when the current is driven into saturation, a shielded plasma exhibits an instability. This is associated with oscillations of the plasma-sheath interface.

These recent findings of ours justify the acceptance of Bohm's stability criterion in the case of zero current and prove that the dynamics of the sheath govern the rate of collection of charged particles by conducting walls biased with respect to the plasma potential. The results obtained, on the one hand, confirm that Langmuir probes provide a reliable diagnostic tool when used within the original scope of application, namely, in steady state situations and when the current drawn does not reach saturation. On the other hand, these results warn against indiscriminate usage of Langmuir probes in new applications such as the study of turbulent fluctuations<sup>11</sup>, ionized wakes<sup>12, 13</sup> and hypersonic flow fields<sup>14</sup>. In fact, when the probe is driven into saturation to detect turbulent fluctuations, the observed fluctuations may well originate in the probe itself. Some doubts are also cast on the current interpretation of data taken under transient conditions in hypersonic flows and on the use of flush probes in the study of boundary layers<sup>15</sup> and sheaths. The possibility of inducing instability should also discourage the proposed D-C biasing of radio frequency probes<sup>16</sup>.

Disclosure of these results is particularly timely since many of the projected



on-board measurements will be made with the help of such probes. In addition, similar diagnostic techniques might be applied to the study of ionospheric exospheric and nuclear environments.

The macroscopic stability criterion is not restricted in its scope to perfectly-absorbing, nonemitting walls, as in the case with Langmuir probes. The stability of the sheaths which form near the surface of positively and negatively biased emitting electrodes has also been investigated<sup>17</sup> and it was found that emission of particles has, in general, a destabilizing effect. In particular the anode sheath is always unstable.

Finally, the effect of magnetic fields restraining the motion of particles has been considered<sup>17</sup>. Depending on the intensity of the magnetic field component parallel to the wall one can distinguish 3 cases: (1) weak field, where the Larmor radii of both the electrons and ions are much larger than the thickness of the sheath assumed to be in the order of the Debye length, (2) moderate field, where the sheath thickness is smaller than the ion Larmor radius, but larger than the electron Larmor radius, (3) strong field, where the sheath thickness is the dominant length.

In the first regime, the magnetic field has no effect on the sheath and the attracted species must be supersonic in order to satisfy the stability criterion. However, when the magnetic field intensity exceeds a certain critical value, the compatibility condition which allows transonic transition cannot be fulfilled<sup>18</sup>. There exists, indeed, abundant experimental evidence<sup>19</sup> that, under such circumstances, the rate of particle transport is anomalously high.

In the second regime, the problem ceases to be one-dimensional since the electrons are prevented from reaching the wall by crossing the collisionless sheath. They can only escape along the magnetic lines of forces giving rise to what has become known as Simon diffusion<sup>20</sup>.

A fully developed turbulent regime can be expected when, with an even higher magnetic field component parallel to the wall, the ion Larmor radius becomes smaller than the Debye length and both electrons and ions are prevented from crossing a collisionless sheath.

Matters are further complicated when sustenance of the electric current hinges on the release of particles from the electrodes. In this case, in addition to the question of stability of the space charge sheath, there arises the problem that the magnetic field may prevent the electrons from acquiring sufficient energy to produce ionizing collisions. In this case, a one-dimensional space-charge-sheath cannot perform its double function of shielding the plasma and of providing the energy required to maintain the supply of particles.

In conclusion, a stable space-charge-sheath seems to represent more the excep-

tion than the rule, since it can form only at the cathode or on insulated walls, and for relatively small values of magnetic field component parallel to the wall surface.

Advanced Research Projects Agency  
Nonr 839(38)

E. Levi

#### REFERENCES

1. A. Cavaliere, F. Engelmann, and A. Sestero, "Propagation of Ion Waves In a Plasma Flow Towards a Transonic Point," *Phys. Fluids* 11, 158 (1968).
2. D. Bohm, "The Characteristics of Electrical Discharges in Magnetic Fields," A. Guthrie and R. K. Wakerling, Eds. (New York: McGraw-Hill Book Co., Inc., 1949) Chap. 3.
3. O. Penrose, "Electrostatic Instabilities of a Uniform Non-Maxwellian Plasma," *Phys. Fluids*, 3, 258 (1960).
4. F. Engelmann, M. Feix and E. Minardi, "Connection Between Shielding and Stability in a Collisionless Plasma," *Il Nuovo Cimento*, 30, 830 (1963).
5. H. W. Friedman and E. Levi, "Plasma Shielding and Stability, Part I", (paper submitted to the *Physics of Fluids*).
6. H. W. Friedman and E. Levi, "Plasma Shielding and Stability, Part II", (paper submitted to the *Physics of Fluids*).
7. H. W. Friedman, "Nonlinear Asymptotic Analysis of the Positive Column," *Phys. Fluids* 10, 2053 (1967).
8. H. W. Friedman and E. Levi, "Singularities of the Two-Fluid Plasma Equations and Their Relation to Boundary Conditions," *Phys. Fluids* 10, 1499 (1967) - Comments by K. J. Tourian and G. A. S. Elton, Jr. 11, 697 (1968). Reply by the authors 11, 698 (1968).
9. F. F. Chen, "Plasma Diagnostic Techniques," R. H. Huddlestone and S. L. Leonard, Eds. (New York, London: Academic Press, 1965).
10. P. E. Belenkov, A. T. Kapin, A. A. Plyutto and V. N. Ryzhkov, "Current Instability in the Selection of Charged Particles from Plasma," *Zhur. Tekn. Fiz.*, Vol. 34, No. 12, Dec. 1964 (English Transl. *Soviet Phys. - Tech. Phys.* Vol. 9, No. 12, June 1965).
11. A. Demetriades, and E. L. Doughman, "Langmuir Probe Diagnostics of Turbulent Plasmas," *AIAA J.*, 4, 451 (1966).
12. R. F. Richardson and J. Herman, "Hypersonic Wake Structure Observed with Electrostatic Probes," Lincoln Laboratory Project Press Report PPP-59 (November 1966).
13. A. Kirkpatrick, A. Cantin, and D. Heckman, "Electrostatic Probe Measurements in the Turbulent Wakes of Hypersonic Spheres Fired in a Ballistic Range," AGARD Meeting on Fluid Physics of Hypersonic Wakes, Colorado (May 1967).
14. A. A. Sonin, "Free Molecule Langmuir Probe and Its Use on Flowfield Studies," *AIAA J.*, 4, 1588 (1966).
15. H. R. Bredfeldt, W. E. Sharfman, H. Guthart and T. Morita, "Boundary-Layer Ion Density Profiles as Measured by Electrostatic Probes," *AIAA J.*, 5, 91 (1967).
16. K. C. Balmain, "Plasma Probe Studies," Aeronomy Report No. 11, University of Illinois, Urbana, Ill., May 1, 1966.
17. H. W. Friedman and E. Levi, "The Stability of Space-Charge-Sheath in MMD Devices," (Paper prepared for the 6th Symposium on MMD Riga U.S.S.R., Sept. 1968).
18. H. W. Friedman and E. Levi, "Singularities of the Fluid Equations and Their Relation to Anomalous Diffusion," *Phys. Fluids* 11, 678 (1968).

19. "Plasma Instabilities and Anomalous Transport," W. B. Pardo and H. S. Robertson, Eds. (Coral Gables, Florida: University of Miami Press, 1966).
20. A. Simon, "Diffusion of Arc Plasmas Across a Magnetic Field," Proc. United Nations International Conference on the Peaceful Uses of Atomic Energy, Geneva (1958) Vol. 32, p. 343.

## TRANSIENT EXCITATION OF SPACE WAVES AND SURFACE WAVES IN A BOUNDED, COLD MAGNETOPLASMA.

L. B. Felsen and G. M. Whitman

### 1. Introduction

Studies of wave propagation in dispersive plasma media performed in the literature have dealt with plane wave or source-excited fields in unbounded homogeneous regions, or with plane wave propagation and reflection from plane boundaries. The present study has been undertaken to explore wave phenomena attributable to the simultaneous presence of boundaries and of a localized source, with special emphasis on the excitation and behavior of surface waves. It was also desired that the medium exhibit both the cutoff and resonance phenomena characteristic of a general dispersive environment. A simple structure incorporating the necessary features involves a magnetic line current located above a perfectly conducting plane, the entire configuration being embedded in a homogeneous, cold, lossless magnetoplasma with gyrotropic axis parallel to the source direction. In the time-harmonic steady state, this arrangement can support a unidirectional surface wave.

Since the time-harmonic solution for this configuration and its far zone asymptotic approximation are available in the technical literature<sup>1</sup>, the major task in providing the transient solution in integral form involves the analytic continuation of the time-harmonic result from positive real to complex frequencies. This is straightforward for the incident and reflected wave constituents but not quite so for the unidirectional surface wave with its restricted spatial and frequency domains of existence. These and other function-theoretic aspects of the problem have been considered in detail and involve use of uniform asymptotic representations in the time-harmonic solution. After the result is put into the desired form, the theory formulated in a related study<sup>2</sup> becomes applicable and has been used to derive the transient fields for impulsive excitation, as contributed by the incident and reflected (space wave) and the surface wave constituents. Numerical calculations for typical parameter ranges exhibit the field variation in regular and in transition regions. Salient features of these fields

reveal a strong dependence on the observation angle for the reflected constituent, as well as peculiarities associated with the surface wave. Owing to the unidirectional character of the latter in the time-harmonic regime, waves in certain frequency intervals are propagated only to one side or the other of the source region. A comparison has also been made between the solutions for line source and plane wave excitation in an unbounded medium in order to assess differences in the transient behavior.

Since the preceding discussion is based on asymptotic approximations of the frequency integrals and thereby on the existence of a large parameter (proportional to the observation distance) in the integrand, it is of interest to know how large the parameter must be in order to furnish an acceptable result. This type of assessment has been carried out by comparing various asymptotic approximations with the exact value of a certain special integral. It is found that even moderately large parameter ranges are accommodated by the asymptotic formulas, thereby making these approximations useful over a broad range of physical variables.

## 2. Asymptotic Evaluation of the Transient Response

The calculations described in the Introduction have been performed for impulsive excitation in Ref. 3. For the incident and reflected waves, the relevant dispersion curve is shown in Fig. 1 of Ref. 2 and admits, for sufficiently long observation times,

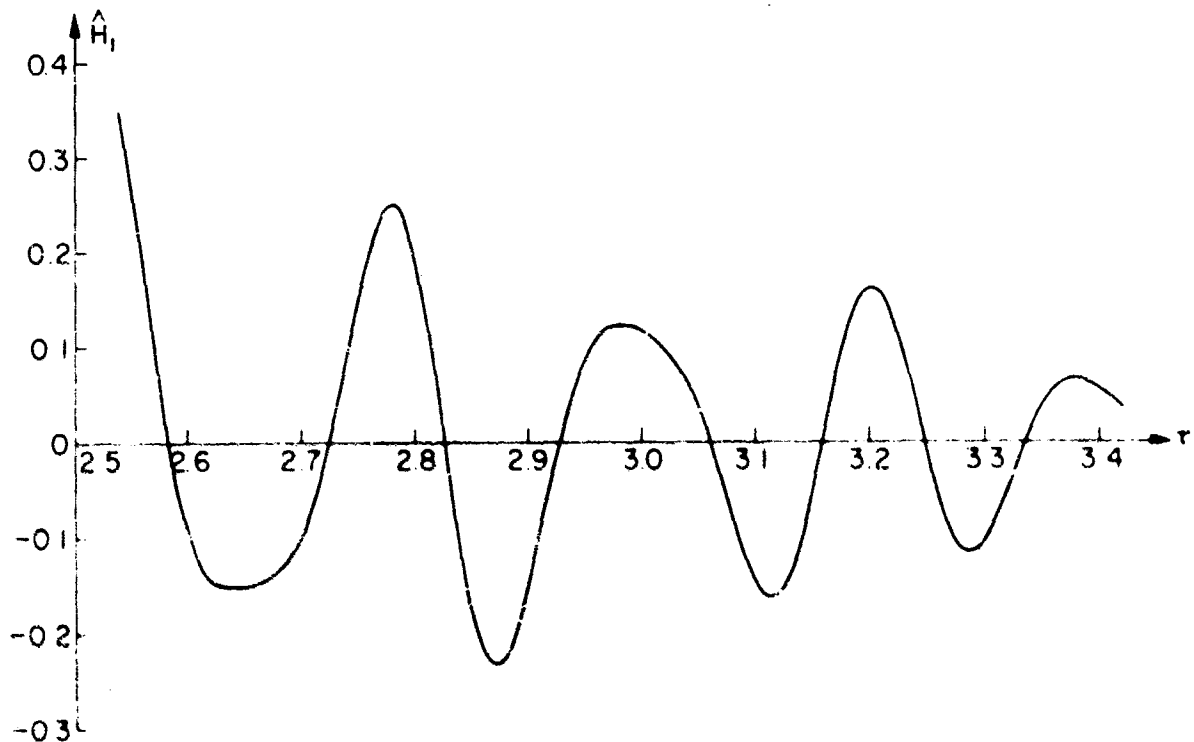


Fig. 1 (a) Behavior at Longer Observation Times  $\tau \gg \tau_0$  ( $\epsilon_0 = 2.52$ )

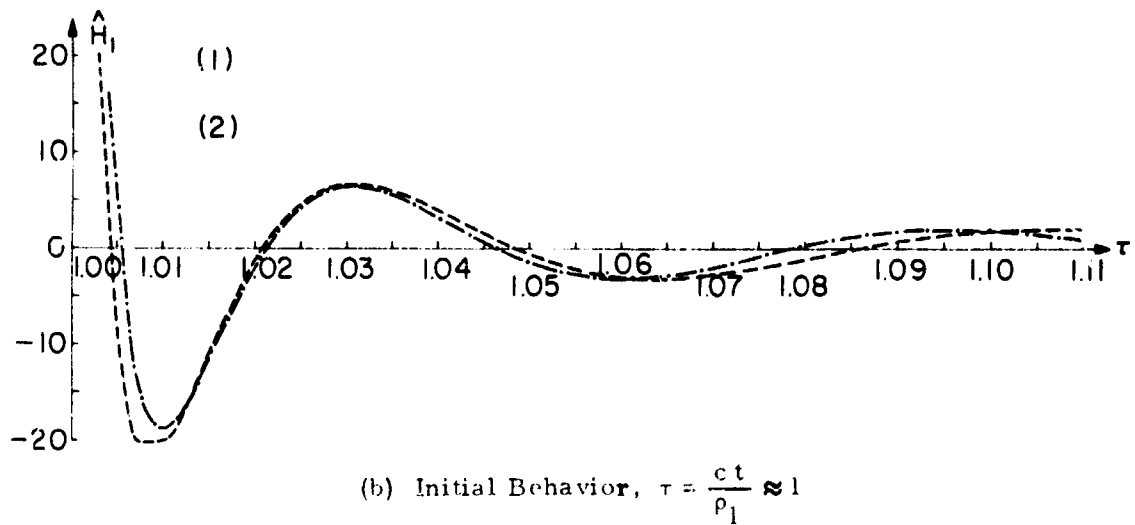


Fig. 1 Transient Behavior of Incident Magnetic Field for  $R^2 = 0.5$ .

$$\omega_p = 3 \times 10^6 \text{ cps}, \quad \zeta \equiv \omega_p \rho_1 / c = 30$$

three wave constituents which propagate at the same group velocity but are characterized by different frequencies  $\omega_p$ . The latter aspect introduces beat phenomena into the composite transient response, shown for the incident magnetic field in Fig. 1(a) ( $R = \omega_c / \omega_p$ , where  $\omega_c$  = cyclotron frequency,  $\omega_p$  = plasma frequency;  $\rho_1$  = distance from source to observation point). For very short observation times, only a single wave propagates, and Fig. 1(a) shows the discrepancy between the correct initial behavior (curve 1) for  $\tau = 1.03$  and the simple saddle point approximation noted in Ref. 2 (curve 2); for  $\tau = 1.01$ , curve 2 is appropriate. Evidently, for the chosen set of parameters, the simple saddle point formula predicts the response correctly for almost all arrival times (no field is present for  $\tau = 1$ ). Other transition phenomena discussed in Ref. 2 have also been analyzed.

When the source and observation points are both located on the boundary, (and are separated by a distance  $y$ ), the surface wave is excited with maximum amplitude. Under these circumstances, the relevant plot of  $\gamma_p'(t) = (d/dt) (\gamma_p(t))$ , where  $\gamma_p(t)$  is the propagation constant for the surface wave, is shown in Fig. 2. Saddle points may be

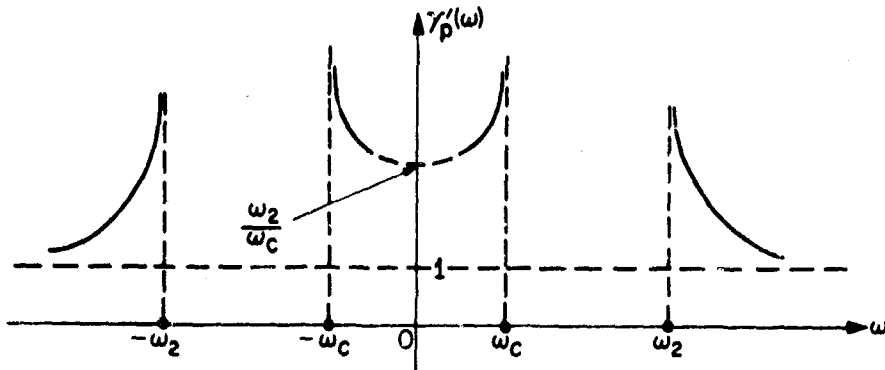


Fig. 2 Typical Plot of  $\gamma'_p$  vs.  $\omega$  for Surface Wave

found from Fig. 2 by drawing the horizontal line  $\gamma'_p = (ct/y)$  and recording the intersections with the  $\gamma'_p$  vs.  $\omega$  curve. For  $y > 0$ , i.e., on one side of the source, one may show that real saddle points in the frequency integral occur only on the branch  $|\omega| > \omega_2$  in Fig. 2. Asymptotic evaluation of the integral for large  $y$  then yields via the simple saddle point formula<sup>2</sup> for excitation by a temporal impulse:

$$H_s(\underline{r}, t) \sim A_s(\omega_s) \cos \left[ q(\omega_s) - \frac{\pi}{4} \right], \quad |\omega_s| > \omega_2, \quad y > 0, \quad (1)$$

where  $q(\omega) = (y/c) [\gamma'_p - \omega\tau]$ ,  $\tau = ct/y$ ,  $\omega_s$  is the solution of  $q'(\omega_s) = 0$  and  $A_s(\omega_s)$  is

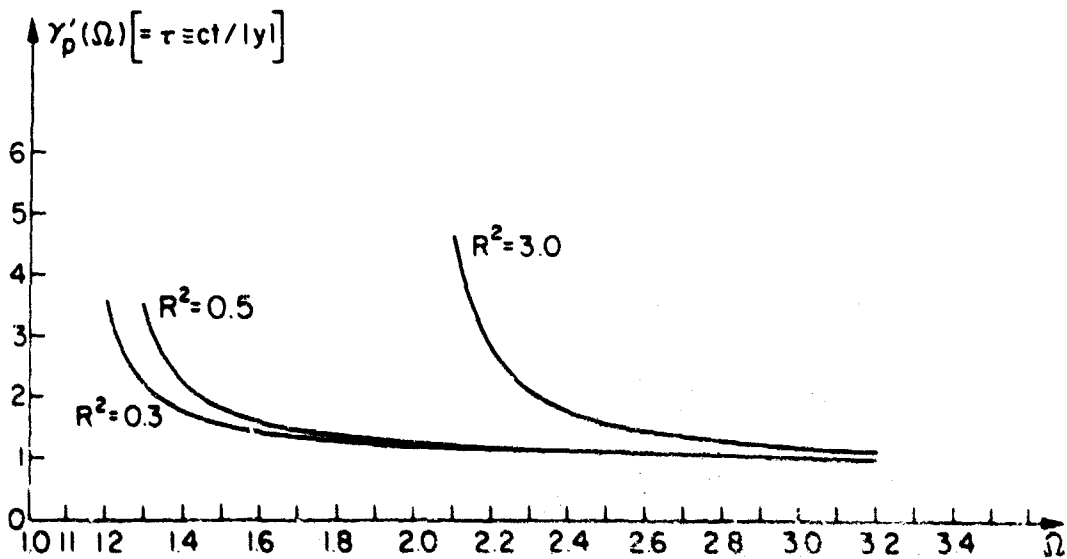


Fig. 3 (a)  $\gamma'_p$  vs.  $\Omega (\gamma'_p = \gamma'_p/\omega_p)$

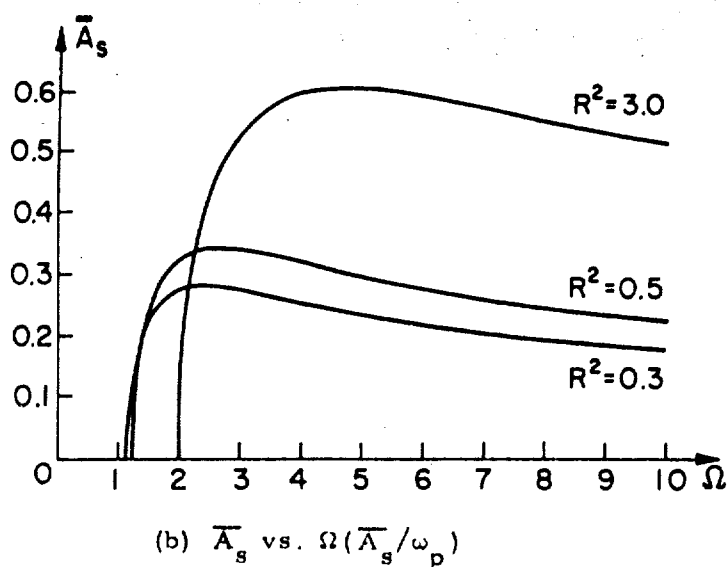


Fig. 3 Plots of Relevant Quantities for the Surface Wave when  $\gamma > 0$

an amplitude depending on  $\gamma''_p$  and on the plasma parameters. Typical plots of  $A_s(\omega)$  and  $\gamma'_p(\omega)$  vs.  $\omega$  are shown in Fig. 3 ( $\Omega = \omega/\omega_p$ ).

For  $\gamma < 0$  ( $\theta = -\pi/2$ ), one may show<sup>3</sup> that surface wave contributions to the complex frequency integral arise only from the range  $|\omega| < \omega_c$  (i.e., saddle points are determined from the low frequency branch of the curve in Fig. 2) and that Eq. (1) remains valid for the asymptotic approximation of the transient field providing  $\gamma$  is replaced by  $|\gamma|$  everywhere except in the expression for  $q(\omega_s)$ , and the saddle points are confined to the interval  $|\omega_s| < \omega_c$ .

A striking feature of the transient response is the occurrence of wave packets with frequencies in the range  $|\omega_s| > \omega_2$  only for positive  $\gamma$  while those with frequencies  $|\omega_s| < \omega_c$  are found only for negative  $\gamma$ . This contrasts the direct and reflected field behavior where a given pass band frequency response may be detected in both directions. These anomalous characteristics of the surface wave are the transient counterpart of its unidirectional feature in the time-harmonic regime; in the latter, propagation for  $\omega > \omega_2$  occurs only along the (+y) but not along the (-y) direction, whereas the converse is true for  $\omega < \omega_c$ , with no propagation at all occurring in the stop band  $\omega_c < \omega < \omega_2$ . Since the delta function source excites all frequencies, the unidirectional nature of the surface wave at any given frequency serves to direct appropriate frequencies either to one side or the other of the source region.

Study of the curves in Fig. 3 reveals other interesting features. For  $y > 0$ , the amplitude  $A_s(\omega) \rightarrow 0$  as  $\omega \rightarrow \infty$ . While the saddle point result Eq. (1) does not apply in this range, it can be shown nevertheless that  $A_s(\omega)$  tends to zero at high frequencies (corresponding to  $t = y/c$ ), in contrast to the direct and reflected field amplitudes which tend to infinity (for impulse excitation). This behavior is ascribed to the fact that the existence of the surface wave on a perfect conductor is contingent on the presence of the plasma medium; a perfect conductor in vacuum does not support a surface wave. For  $\omega \rightarrow \infty$ , the plasma refractive index approaches that of vacuum so that the surface wave is not excited in this range. The surface wave amplitude builds up only for those later observation times corresponding to  $\omega_s$  low enough to sense the plasma.

Air Force Cambridge Research Laboratories  
Office of Aerospace Research  
F 19628-68-C-0072

G. M. Whitman and L. B. Felsen

#### REFERENCES

1. S. R. Seshadri, "Excitation of Surface Waves on a Perfectly Conducting Screen Covered with Anisotropic Plasma", IRE Trans. on Microwave Theory and Techniques, MTT-10 (1962), pp. 573-578.
2. L. B. Felsen, "Transients in Dispersive Media", in this Report.
3. G. M. Whitman, "Transient Excitation of a Bounded Cold Magnetoplasma", Electrophysics Dept., Polytech. Inst. of Brooklyn, Report No. PIBEP-68-001 (1968).

#### DEVELOPMENT OF A BEAM PLASMA DEVICE

R. G. E. Hutter, H. Farber, R. Pepper, R. Eichler

It is the objective of this project to investigate the feasibility of low noise amplification of microwave signals as well as the feasibility of high microwave noise generation and/or amplification in beam-plasma configurations.

Initially, the studies are devoted to basic investigations of the noise properties of the plasma medium and the resulting effects in various beam-plasma interaction configurations.

The theoretical approach is patterned after the analogous noise theory for traveling wave tubes; the significant difference is due to the "noisiness" of the "waveguide" represented here by the plasma. The plasma medium surrounding the electron beam acts as a distributed noise source, which impresses noise signals onto the electron beam. The noise properties of the plasma are described by the fluctuation dissipation theorem, a generalization of Nyquist's theorem. A generalization of the expressions



for the "noise figure" for the case of distributed noise sources has been obtained.

An experimental device has been designed to determine the noise level on an electron beam before it enters the plasma interaction region and after it leaves, thereby making it possible to determine the influence of the noisy plasma medium. The experimental results will be used to check the theoretical investigations that are currently being carried on. Currently the device is being assembled, and the final checking of the design parameters will be carried out shortly.

A modular approach has been used in the design of the beam plasma device. The device consists of four basic structures. These are: (a) an electron gun, (b) a hot-cathode mercury discharge, (c) a pair of tunable, moveable, microwave cavities, and

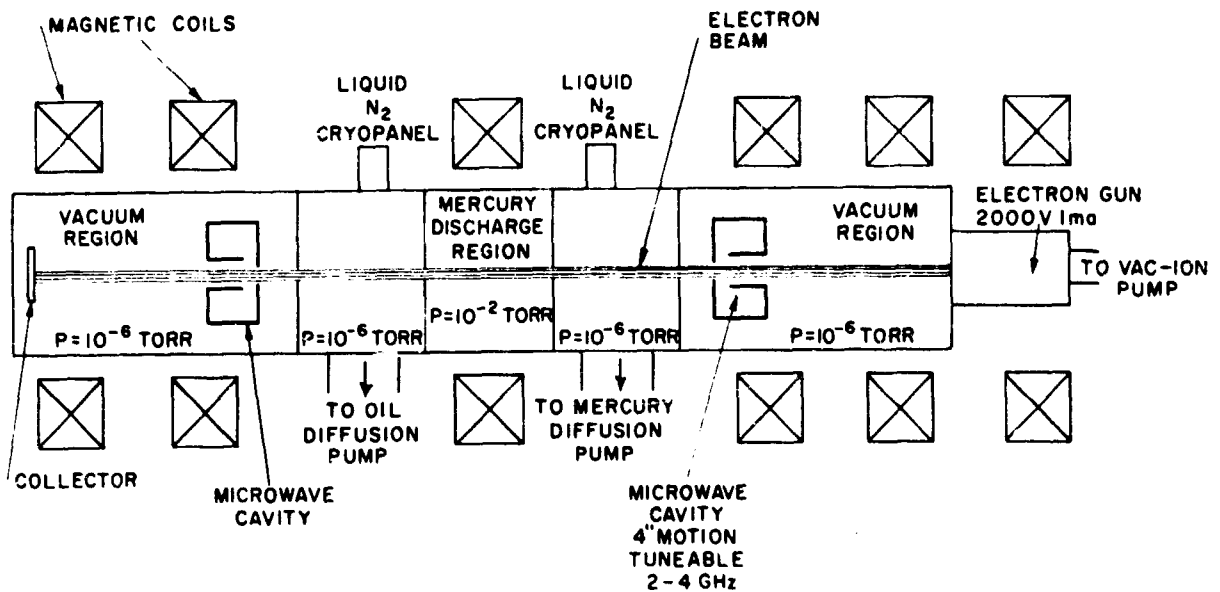


Fig. 1 Schematic of Beam Plasma Device

(d) a set of magnet coils. The device is shown schematically in Fig. 1. In addition to the basic structures mentioned above, there are three functional units for maintaining a high vacuum in the system.

The device may be divided into the following sub-assemblies: a) the electron gun; b) the plasma, c) the microwave coupling circuits, d) the vacuum chambers and pumping systems, and e) the magnet system.

a) The electron gun is designed to produce a one ma beam at 2,000 volts with a beam diameter of 0.10 inches. The cathode is a tungsten impregnated type since it may receive more ion bombardment than in the usual high vacuum tube.

b) Several different types of discharges were studied for the production of a plasma. A hot cathode mercury discharge was chosen since electron densities of the

order of  $10^8$  per c. c. could be attained with low fields. These in turn would not disturb the beam.

The cathode is a one inch diameter tungsten impregnated element. The cathode to anode spacing is four inches. The overall dimensions of the discharge chamber are two inches in diameter by five inches long. These dimensions may be changed by the use of suitable spacers.

The mercury vapor may be readily replaced by other gases, such as argon or xenon. Additional reasons for choosing mercury as our initial gas are discussed in the paragraph on the vacuum system.

c) The signal on the electron beam is sampled by two reentrant type (klystron) cavities which are mounted on a universal carriage. Problems of precise movement in a vacuum system have been solved by using recently developed filled polyimide bearings. Each of these cavities may be tuned from 2 to 4 GHz and can move four inches along the beam. These cavities may be replaced by similar cavities to cover other frequency bands; and broadband probes may be used in conjunction with the cavity, or by themselves.

The unloaded  $Q$  of these cavities ranges from 200 to 400 depending on the resonant frequency. The coupling gap of these cavities is .020" long with a diameter of 0.125 inch.

d) The vacuum pumping system has three separate functional groups. The electron gun region and the main vacuum chamber are joined by the small hole in the anode; this permits the two chambers to be differentially pumped. In addition, this region can be closed by a butterfly valve and removed as a unit from the major vacuum chamber. The discharge chamber has only two small openings into the main chamber which should permit a very large pressure differential between the two chambers.

The major pumping system, during normal operating conditions, will be using a mercury diffusion pump, and two liquid-nitrogen-cooled cryopanel. The combination of the cryopanel and a liquid nitrogen trap may result in pressures below  $10^{-6}$  torr even with relatively high mercury vapor pressures in the discharge chamber. Measurements on a mock-up version of this portion of the tube have demonstrated its feasibility. It is hoped that, by the differential pumping of the gun region, pressures in that region will be in the  $10^{-8}$  torr range.

During standby periods, a fast oil diffusion pump will be used instead of the mercury pump to maintain the system at  $10^{-7}$  torr. Each pump may be isolated from the system by separate butterfly valves.

The mercury vapor pressure in the discharge will be controlled by controlling the temperature of a mercury liquid reservoir which is behind the discharge anode. If we

use another gas such as argon or xenon which does not solidify at liquid nitrogen temperatures, both pumps will have to be used to obtain good vacuum conditions since the cryopanel will be ineffective.

e) An axial magnetic field will be produced by a set of six coils with i. d of eight inches and an o. d. of 15". Fields in excess of 1200 gauss can readily be attained.

The major components and concepts in the design of the device have already been checked out. The evaluation of how well these components work as a unit will be carried out shortly.

The complete assembly (without magnets), the microwave cavity carriage

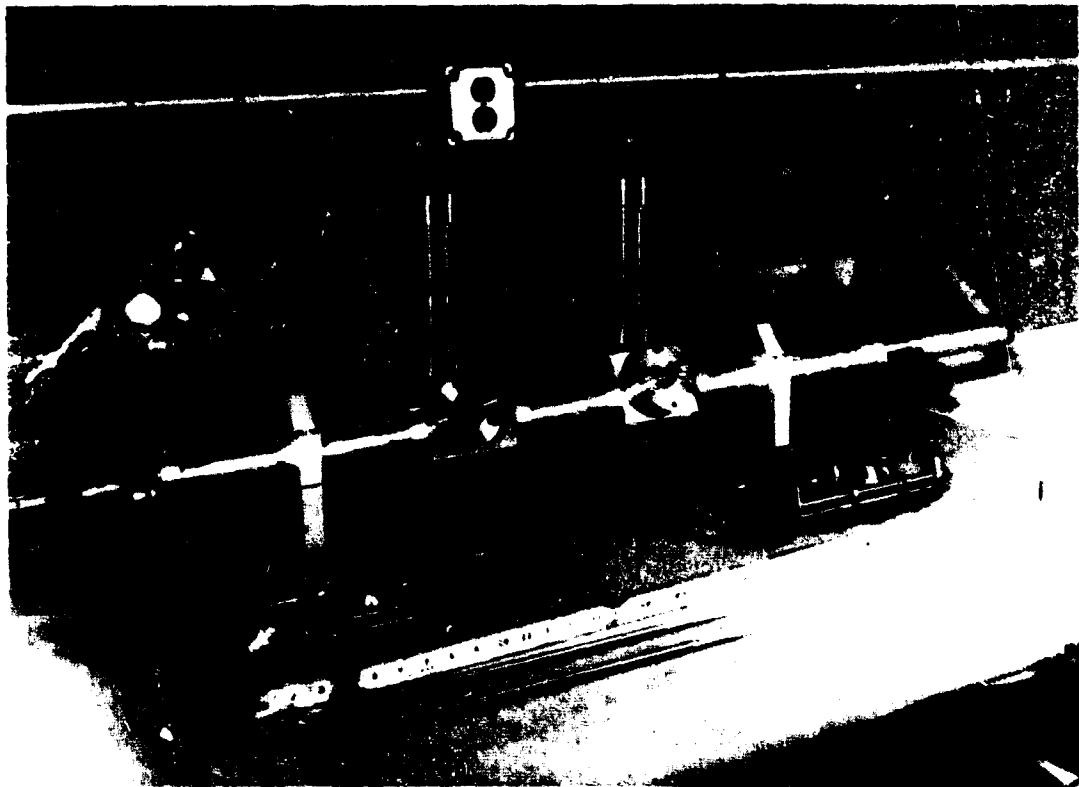


Fig. 2 Complete Assembly

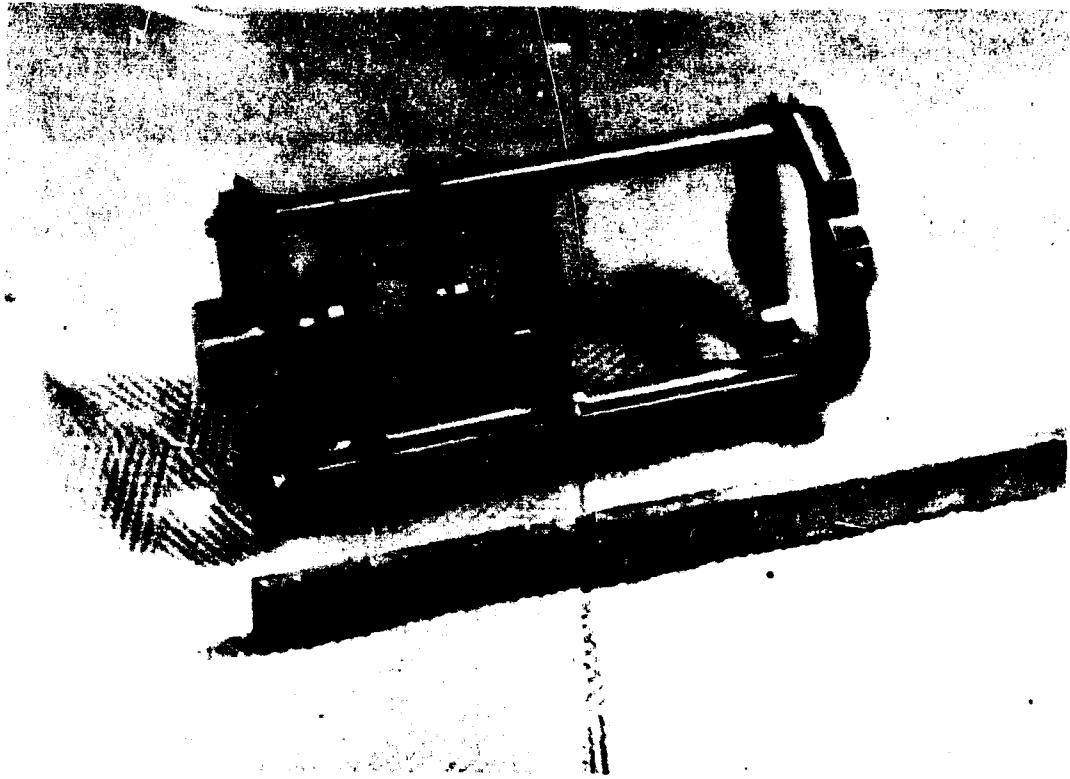


Fig. 3 Microwave Cage

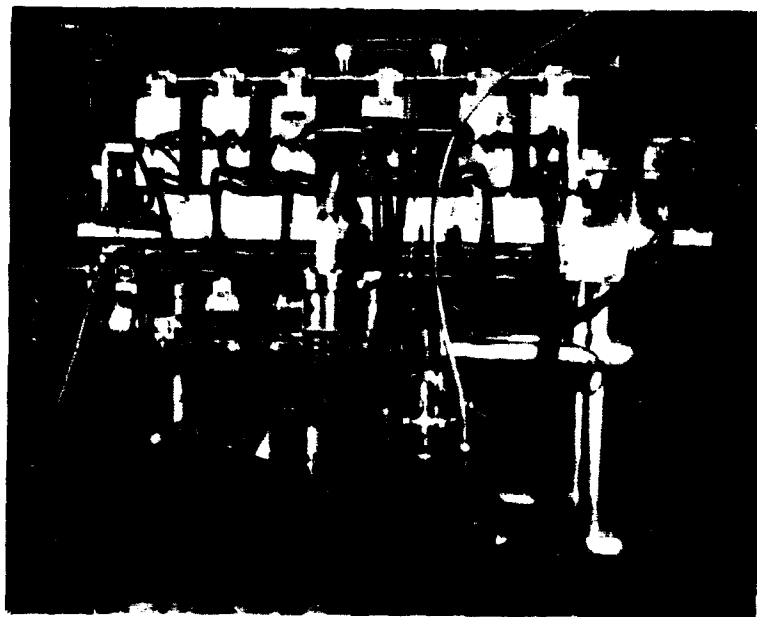


Fig. 4 Assembly with Magnet System

and the assembly with the magnets are shown in Figs. 2, 3 and 4, respectively.

In summary, an electron-beam-plasma device is being assembled to study the coupling of plasma noise energy to an electron beam. The device uses a modular design to permit carrying out a wide variety of experiments; e. g., in addition to the experiments that have been implied, two sections of the unit may be coupled together to study the noise characteristics of electron guns. Further, the modular design permits major changes in any one section without a major change in the overall device.

Advanced Research Projects Agency  
Nonr 839(38)

H. Farber

#### INTERNAL DEFLECTION STRUCTURES OF CATHODE-RAY TUBES

R. G. E. Hutter

The purpose of the investigation was to carry out research and development leading to the design of practical electron guns for cathode-ray tubes that will permit wide-angle electrostatic deflection of the electron beam with a minimum of deflection-distortion and defocusing, and which yield electron spots that are as small as possible.

Work on this project began on July 1, 1966 and terminated on June 30, 1968. The experimental part of the program was carried out at the General Telephone and Electronics Research Laboratories, N. Y., under subcontract to the Polytechnic Institute of Brooklyn.

##### Summary of Accomplishments of the Program:

At the outset of the program it was known that the incorporation of the so-called "two-dimensional" lens element into the conventional electron gun of a cathode-ray tube could solve the problem of reduction of deflection defocusing.

It was not known that correction up to  $25^{\circ}$  half-angle deflection could be obtained.

During the course of the work we have shown that electron guns incorporating two-dimensional lens elements can correct defocusing effects up to at least 25 degrees.

Three versions were tried:

1. Guns, making use of elliptical apertures. The electron lenses in these guns consist of Einzel-lenses formed by apertured discs; the apertures are elliptical and the major axis of the ellipse of the center electrode is rotated ninety degrees with respect to the elliptical apertures of the two outer electrodes. Such guns produce round and elliptical electron spots and hence are suitable for predistorting the electron beam before it enters the deflection system (see Ref. 1: Report No. 1, p. 4, Fig. 1; Report No. 2, p. 3, Fig. 1).

2. Guns, making use of slit electrode lenses. The electron lenses in these guns consist of Einzel-lenses formed by discs with slit apertures; the slit of the center electrode is oriented ninety degrees with respect to the slits in the outer electrodes.

The performance is similar to that of guns described above (see Ref. 1: Report No. 2, p. 11, Fig. 9).

3. Guns, making use of a single slit electrode. These guns are shown in Figs. 1 and 2. (See Ref. 1: Report No. 6, pp. 3 and 7, Figs. 1 and 5, respectively).

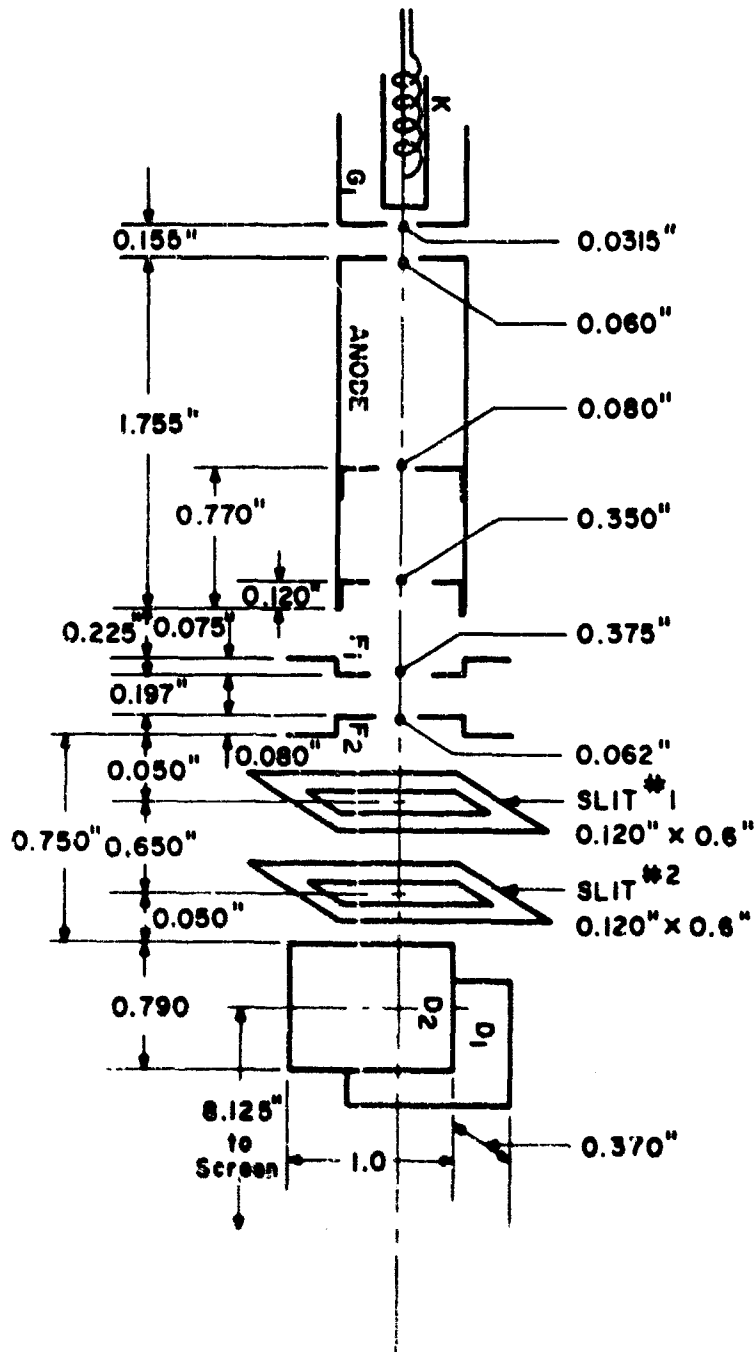


Fig. 1 FT-1 Electron Gun and Deflection Plate System

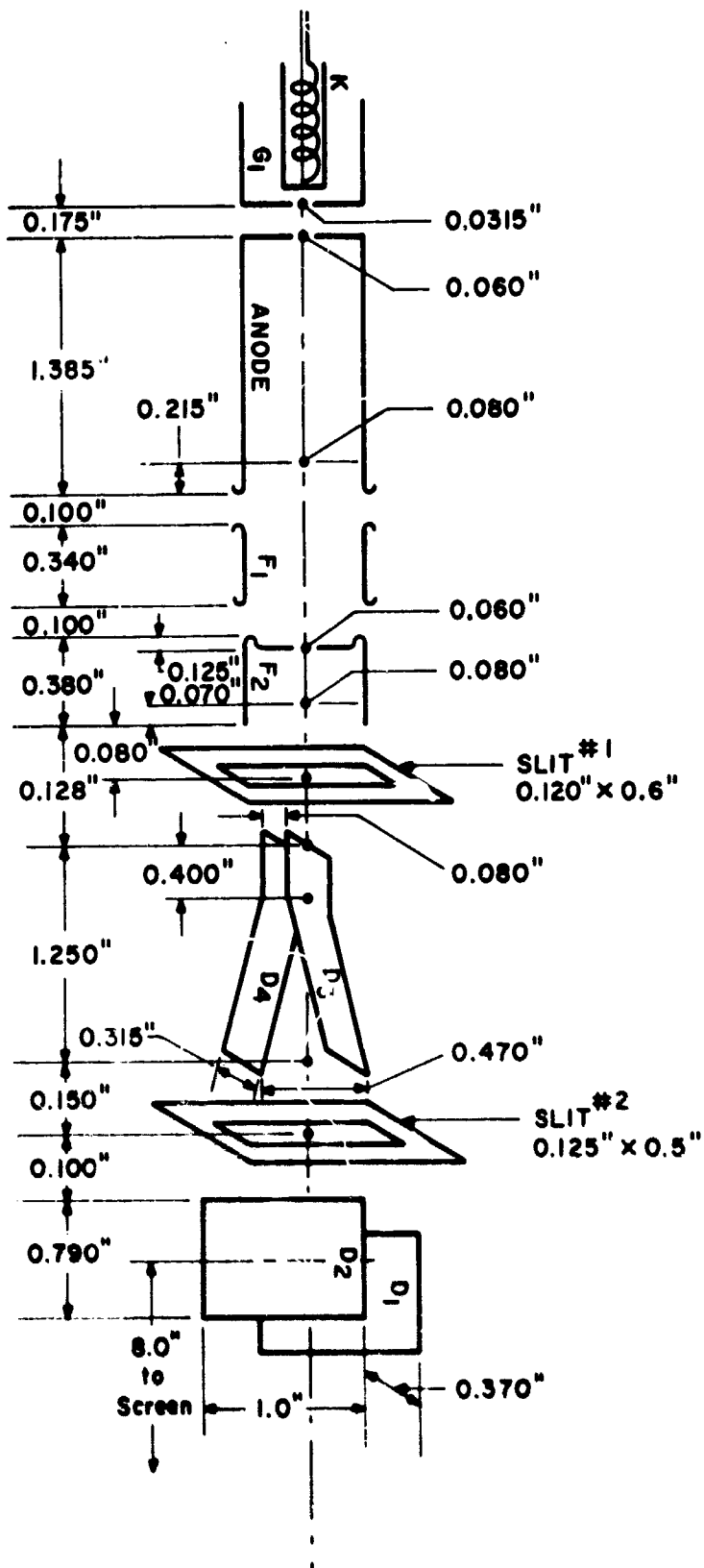


Fig. 2 FT-2 Electron Gun and Deflection Plate System

The final gun design made use of the third of these versions. This choice was determined by expediency considerations. A gun of the type of the second version is judged to be better. Unfortunately, a fair amount of effort was devoted to a study of the cylinder-electrodes (Report 2<sup>1</sup>, p. 15 ff., Fig. 14) which did not prove to be very useful and were finally discarded. Shortage of time did not permit us to return to a study of version 2 above.

One other factor contributed to the discontinuation of the effort on gun version two. Experimentation with such guns seems to indicate that the voltage range of slit electrode lenses (as well as elliptical lenses) was not sufficient to correct for defocusing effects. It was at that time not appreciated how strong the defocusing effects of electrostatic deflection fields really are. Hence the voltage range of a slit-Einzel-lens is normally not sufficient to predistort the electron beam. The dynamic beam pre-distortion schemes, mentioned above, can only correct up to deflection angles at which a completely unfocused beam becomes line-focused at the screen. (If, however, an intermediate beam focus is introduced the above statement need not be true. This method has not received sufficient attention during the program.) The use of the pre-distortion schemes requires first the determination of the distance between deflection system and screen such that at 25 degrees an unfocused beam is just focused into a line by deflection defocusing.

Taking all these factors into account it is possible to correct for deflection defocusing effects up to angles of 25 degrees, however, only at the expense of reduction of deflection sensitivity (see Report 5<sup>1</sup>, p. 3, Sec. IV). In order to maintain deflection sensitivity, post acceleration must be used. This is relatively simple for one-gun tubes; it is difficult for multi-gun tubes. Multi-gun, inline tubes most likely would require a cylindrical post acceleration field. No effort was made to design such a field.

#### Final Design:

The electron guns, shown schematically in Figs. 1 and 2, were designed for the purpose of demonstrating undistorted deflection at a half-angle of 25 degrees. Sealed-off tubes incorporating these electron guns were turned over to the U. S. Army Electronics Laboratories. The two-gun structures, FT-1 and FT-2, demonstrate the application of the predistortion system used with differing gun geometries.

In this design the last round aperture of a conventional gun is followed by a slit-electrode, slit no. 1 (slit no. 2 is a deflection shield to reduce fringing-field spot degradation), which precedes the crossed-deflection electrodes. These deflection plates are designed to permit 25° half-angle deflection and the distance from these electrodes to the screen is determined so that an unfocused spot becomes line-focused at the screen at 25°, or greater deflection angle. No attention has been given to optimizing deflection



sensitivity in these designs.

If the predistortion slit is parallel to the vertical-deflection electrodes, and hence at right angles to the horizontal-deflection electrodes, spot correction for vertical deflection is achieved by lowering the potential of the last round aperture electrode. Spot correction for horizontal deflection is achieved by raising this potential. In each situation the focusing potential of the center electrode of the Einzel lens must also be revised. The correction voltages required as a function of the deflection voltage (or angle) have, of course, been determined.

The principle of operation of this design has been known for some time and is fully described in Ref. 2 of Report No. 1<sup>1</sup>.

Figures 3 and 4 illustrate the results, in terms of spot growth, obtained with each structure at wide angle deflection along the major deflection axis. Although the

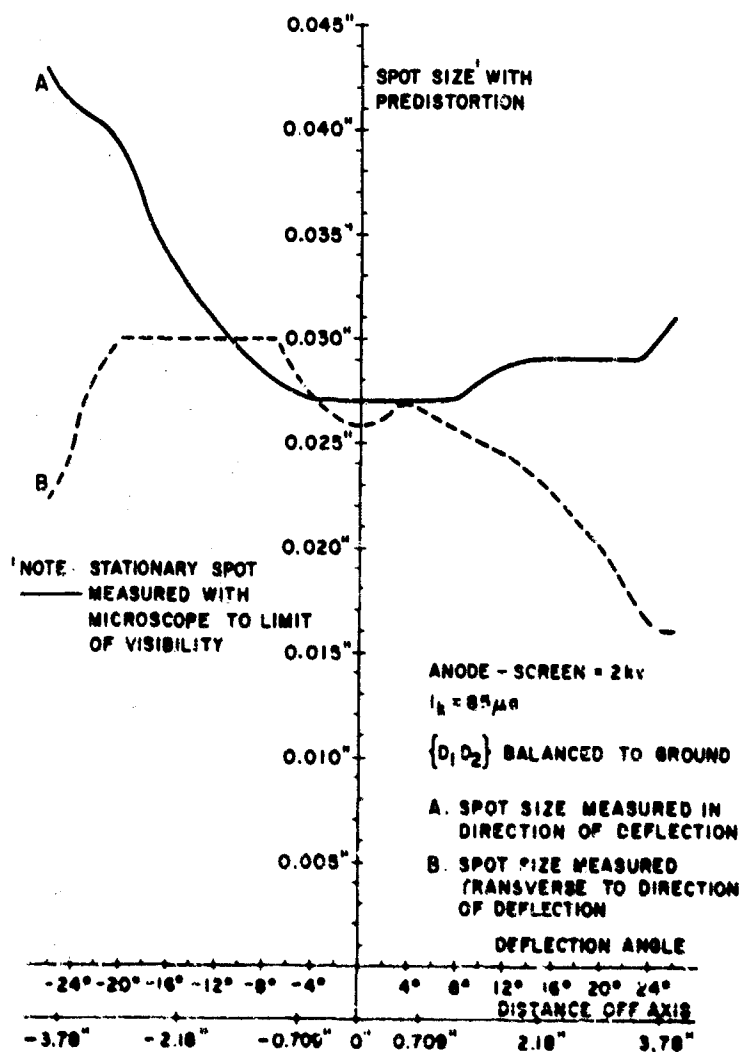


Fig. 3 Spot Size with Predistortion vs. Deflection Angle, FT-1

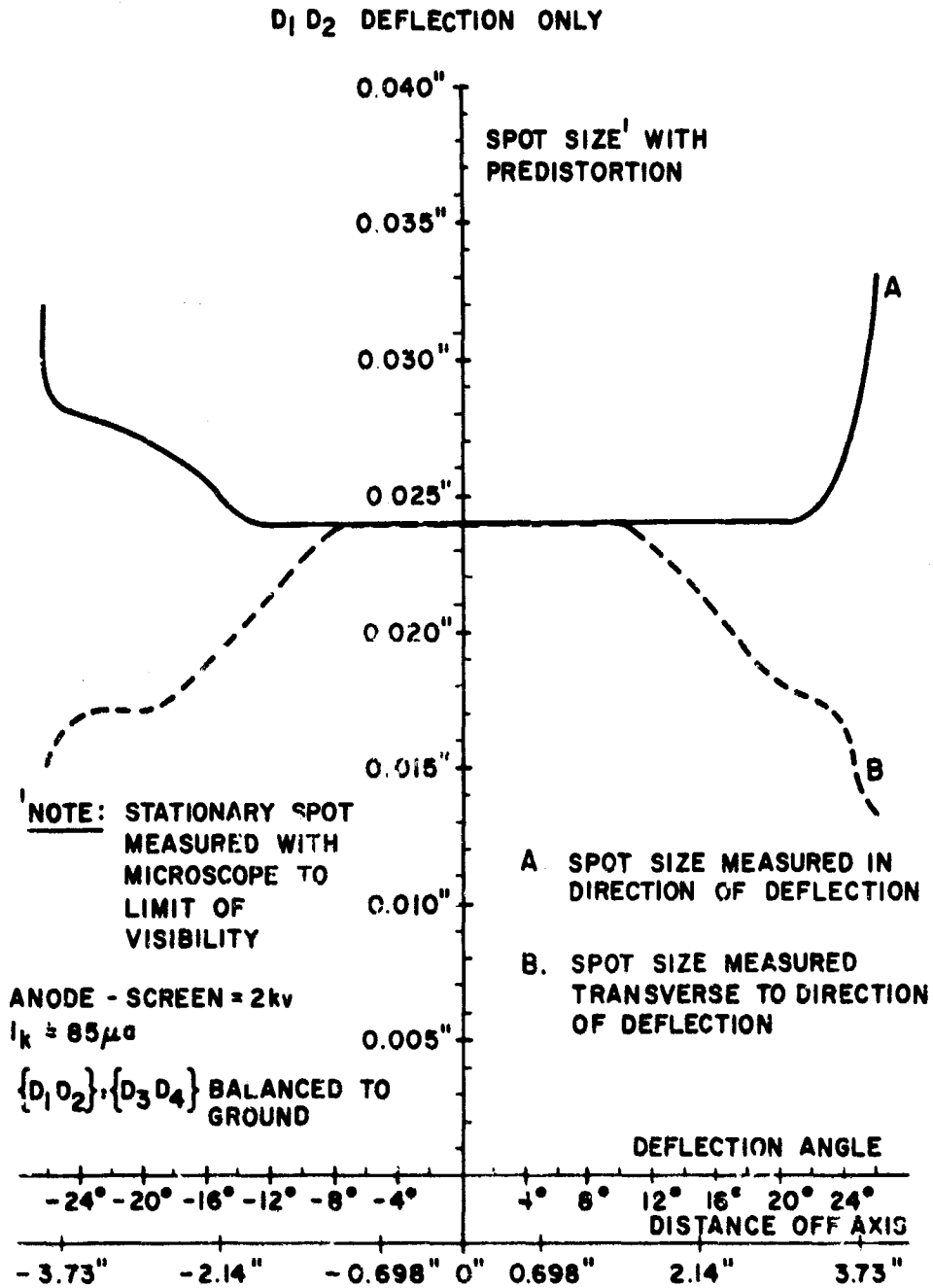


Fig. 1 Spot Size with Predistortion vs. Deflection Angle, FT-2

method of spot correction used is capable of acting in conjunction with orthogonal deflection fields, only correction in the direction of wide angle scan was evaluated. Structure FT-2, incorporating an orthogonal plate system, is available for this type of further evaluation.

Final Conclusion:

If one disregards questions of deflection sensitivity, a slit-electrode electron gun

can be designed to correct for defocusing effect of an electrostatic deflection system up to half-angle of deflection of 25 degrees. Post acceleration should be studied further to improve deflection sensitivity.

U. S. Army Electronics Command  
DA 28-043-AMC-02449E

R. G. E. Hutter

#### REFERENCES

1. R. G. E. Hutter, "Wide-Angle Internal Deflection Structures of Cathode-Ray Tubes," Research and Development Technical Reports ECOM-02449-1 to 6, U. S. Army Electronics Command, Ft. Monmouth, N. J. for period 1 July 1966 through 30 June 1968.

#### STUDY OF THE RADIO-FREQUENCY MASS SPECTROMETER

N. C. Peterson and P. A. Spærri

A radio-frequency mass spectrometer achieves mass discrimination by means of a radio-frequency voltage applied to a series of grids through which an ion is accelerated or decelerated depending on the relationship between its  $m/e$  value and the phase and frequency of the rf signal. The ions of a resonant mass which have been accelerated are then able to overcome a retarding potential at the end of the sorting structure and are collected. The resolving power of this type of spectrometer has been found to depend on the spacing and number of successive grids, or stages in the sorting structure, and on the relative amplitudes of the applied rf and retarding potentials.

The theoretical basis for the operation of the analyzing structure is being investigated using a one dimensional model. The equations of motion of an ion in the rf field are solved numerically using a digital computer. Figure 1 is a graph of energy vs. initial phase near resonance under "small signal" conditions, when the rf amplitude is small (1 volt peak) relative to the initial ion energy (150 v). Under these conditions the position of the energy maximum depends only on the  $m/e$  value and the initial energy, but the resolution is very poor, reaching a maximum of about 25 after 10 stages. As the rf amplitude is increased, the frequency of the energy maximum shifts and the curves become more asymmetric as shown in Fig. 2. A typical mass peak is shown in Fig. 3. It is apparent that ions of resonant mass are accelerated and thus arrive at successive stages out of phase with the rf signal. One possible solution to this problem would be to include a retarding stage after each two or three stages to return the ions to their initial energy. Another possibility which would not involve any changes in the analyzing structure would be to frequently modulate the rf signal to compensate for the increasing velocity and shorter transit time between successive grids of the resonant ions.

Experiments are in progress to test the results of the theoretical calculations; particularly as regards the ion collection efficiency and resolution.

National Science Foundation  
GU-1557

N. C. Peterson and P. A. Spærri

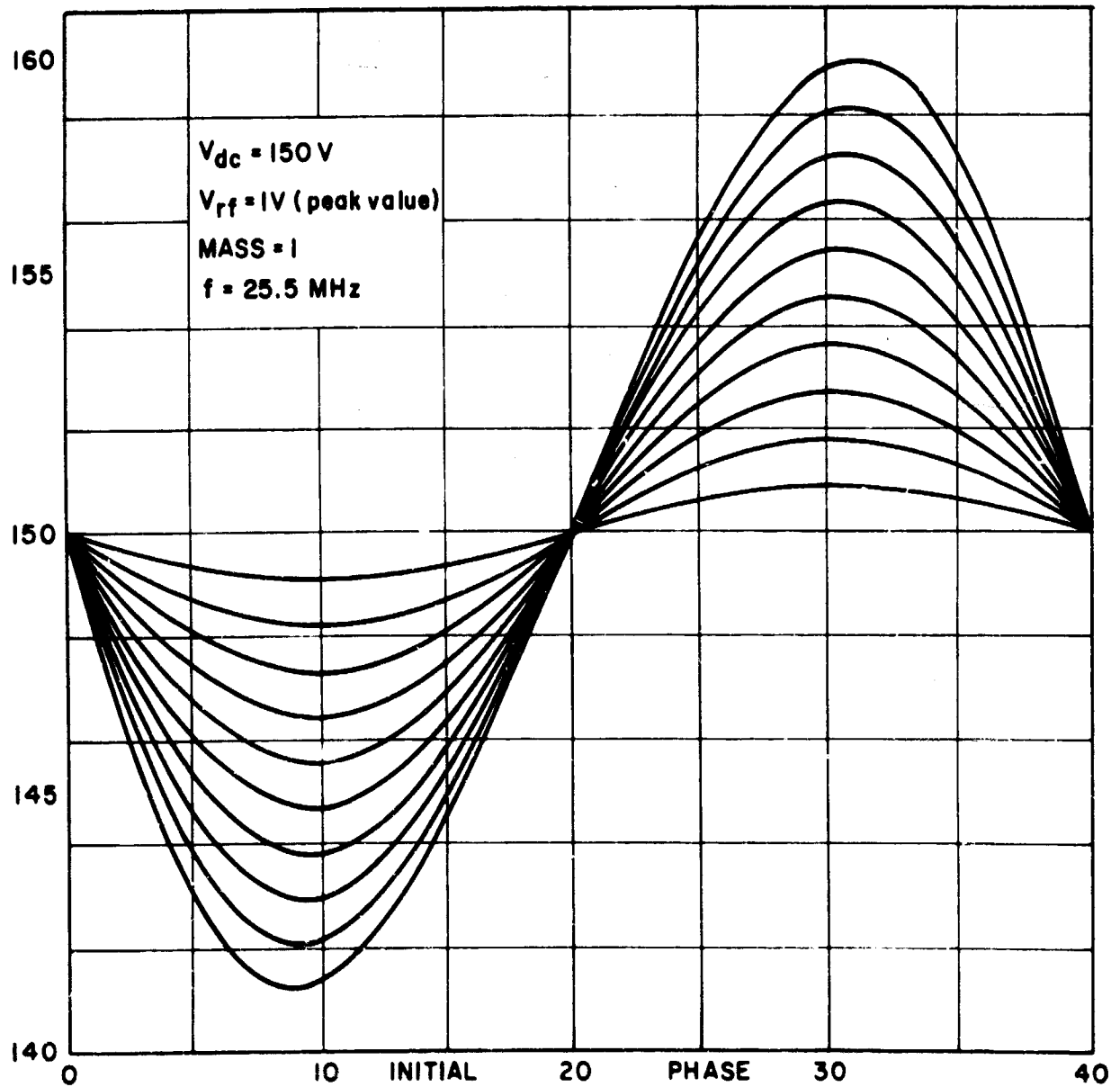


Fig. 1. Energy vs Initial Phase (Small-signal conditions)

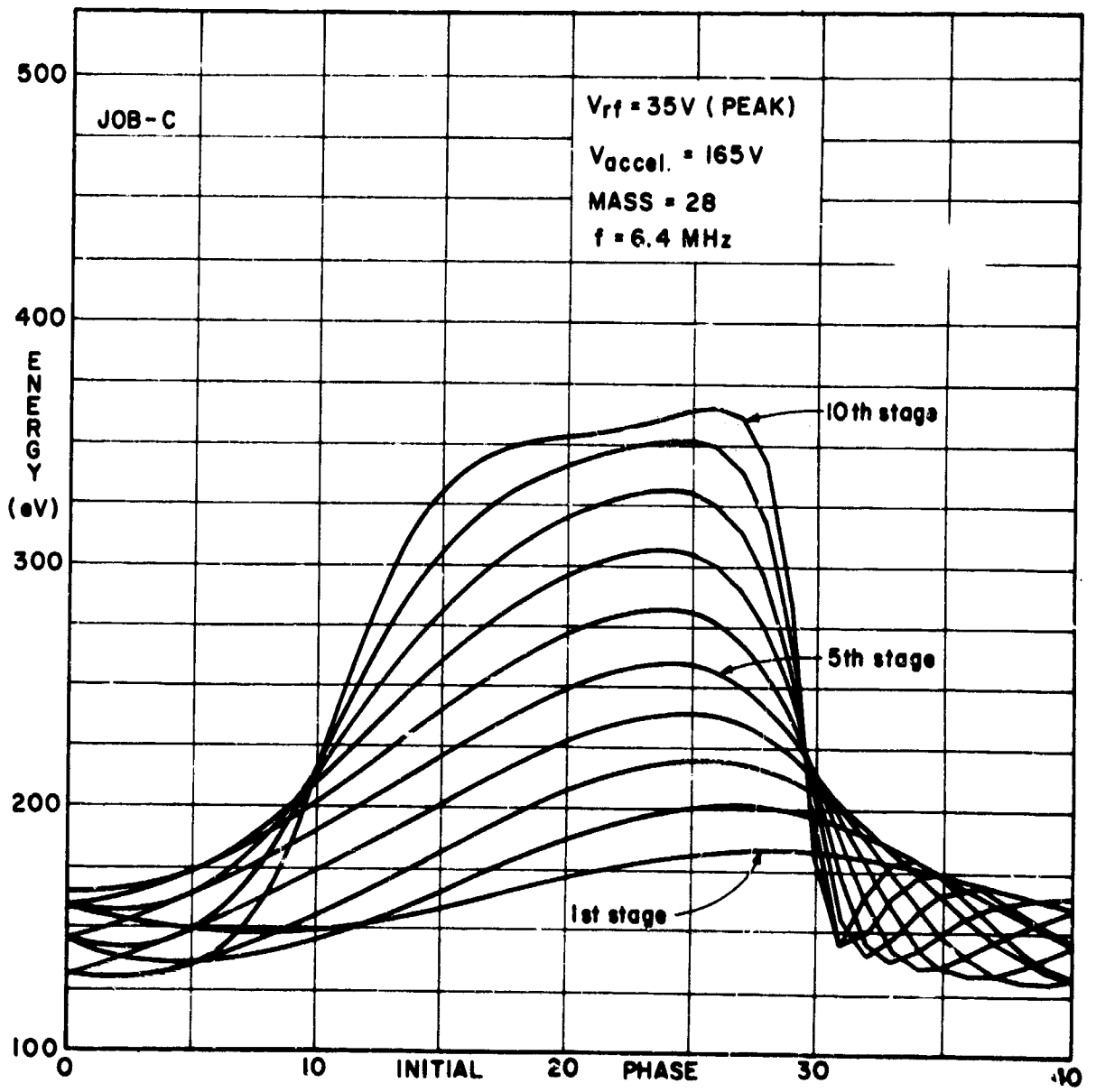


Fig. 2. Energy vs Initial Phase at Resonance

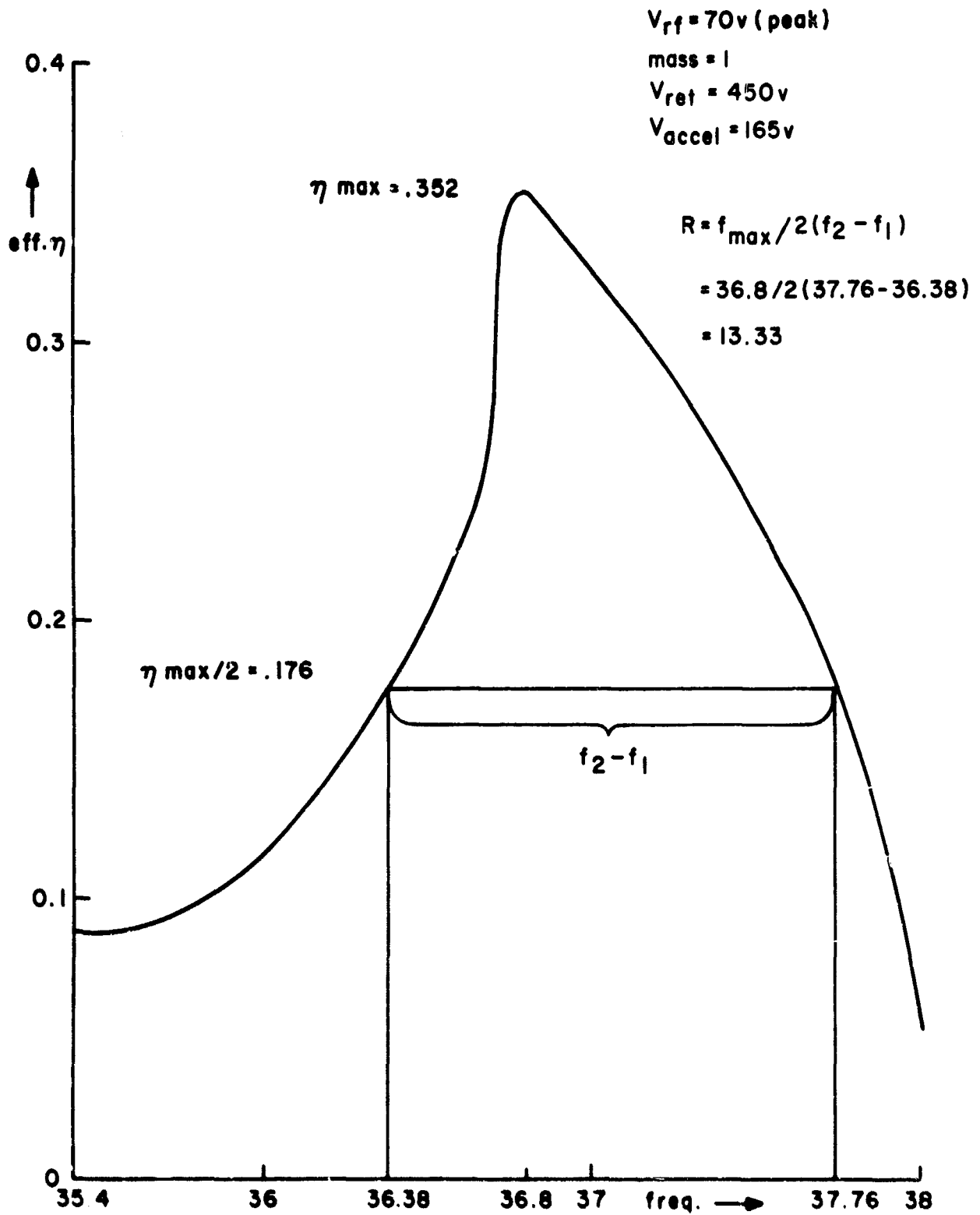


Fig. 3. Theoretical Mass Peak

H AND H<sub>2</sub> IN STRONG ELECTRIC FIELDS

A. Sistino and H. J. Juretschke

We have studied simple variational models of the ground state wave functions of H and H<sub>2</sub> in uniform electric fields, for use in the study of the behavior of molecules in the strong fields of the field emission and field ionization microscope. The wave functions have been constructed in terms of a small set of parameters chosen by physical arguments to reproduce properly the polarization distortion expected in the electric field, and also to lead to limiting forms at the highest fields which can be identified as field-ionized states.

Figure 1 presents the model for the hydrogen atom. The electric field gives rise to the potential  $V$ , and we assume a wave function consisting of a spherically symmetric exponential plus an angle-dependent term in the exponent, to describe the polarization distortion. This is a simple generalization of the textbook wavefunction employed for variation calculations at low fields, where only the first term of the expansion of the  $\delta_1$  exponential is retained. If  $\delta_1$  approaches  $\delta_0$  in magnitude,  $\psi$  will not decay with increasing  $r$ , along  $\theta = \pi$ , and in that sense this limit corresponds to ionization. Considering both  $\delta_0$  and  $\delta_1$  as variational parameters, the ground state energy  $E_0$  and the electric field can be conveniently related by the common  $\delta_0$ , which has the range between 8/9 and unity. At the same time  $\delta_1$  goes from 1/3  $\delta_0$  to zero. At  $\delta_0 = 8/9$  the electric field reaches a maximum value and the energy a minimum value. For higher electric fields the problem has no stationary solution, and thus this model gives a maximum field before absolute field ionization, of about 0.1 a. u. The life time of the localized states in very high field has not yet been computed, but inspection of the potential in relation to the energy suggests that above 0.06 a. u. field ionization becomes very likely. This agrees well with data from the field ion microscope. Between zero and maximum field the polarization energy varies as shown by the solid curve. For comparison, the crosses show the result of second order perturbation theory, probably good at all fields in this range, and the best WKB result of Rice and Good.<sup>1</sup> The reasonable overall behavior of this model suggests that it ought to be useful in computing other effects involving H-atoms in strong electric fields.

Figure 2 shows the Hamiltonian and the trial wave function for H<sub>2</sub>. The field is along the axis AB. The wave function can be constructed systematically following the arguments used in the case of the H-atom to describe polarization distortion. It consists of products of exponentials, one each centered on a proton, and another expressing the distortion due to both the other charges and the applied field, in some average fashion.

If  $\epsilon = 0$ , symmetry demands that the  $\delta'_g$  are equal in pairs, and this case has

actually been worked out a number of times in the references shown. As expected, the best wave function describes electrons localized on each proton, but attracted towards the center of the molecule. The energy of the field-free case is  $-4.06$  eV, only a little bit better than that obtained by Rosen<sup>2</sup> (using a wave function in which essentially the polarization exponential was replaced by the first term in the expansion), but probably the best two parameter value.

If the electric field is not zero, all four  $\delta$ 's are different, to reflect the bias of the applied electric field. Figure 3 shows the ground state energy as a function of internuclear spacing at various field strengths. As expected, the energy decreases with field, and generally shows a minimum at some finite  $R$ . For sufficiently high field, no stable solutions exist at large  $R$ , and the dashed line indicates the transition boundary for the existence region. At  $\epsilon = 0.14$  a.u. the minimum has been replaced by a point of inflection, indicating that while a state exists, it has a lifetime of only one molecular vibration period, with the nuclei moving apart and then being separately ionized. At  $\epsilon = 0.12$  a.u. only the vibrational ground state can barely exist, at  $\epsilon = 0.10$  a.u. both the lowest and the first vibrational states can be accommodated in the energy minimum.

The lifetime of these states against various ionization processes has not yet been computed, but it is estimated that at  $\epsilon = 0.03$  a.u. electron tunneling becomes likely.

A striking feature of these curves is that the equilibrium spacing increases with field, and that the energy minimum becomes shallower. Both effects indicate that even though electron transfer charges one nucleus negative, the two ends of the dipole are successively more attracted by the external electric field than by the field of each other.

Figure 4 shows the polarization energy, at equilibrium, as a function of  $\epsilon^2$ . The low-field slope gives a polarizability of  $5.52$  a.u., lower than the exact value of  $6.38$  of Kolos and Wolniewicz (using many parameters) but considerably better than obtained by other simple wave functions. At high fields a contribution proportional to  $\epsilon^4$  becomes noticeable.

Figure 5 shows in detail the field dependence of the internuclear spacing  $R$ , and of the vibrational force constant  $k$ . The changes are pronounced only in very high field ( $0.05$  a.u.  $\rightarrow 2.5$  volt/ $\text{\AA}$ ), but should be detectable in precision experiments at lower fields. As the field increases,  $k$  actually goes to zero, and although in the range of fields where  $k$  becomes very small the isolated molecule is not sufficiently stable for long time observations, the lower energies of vibrational states may become noticeable in steady-state field emission experiments.

Finally, Fig. 6 shows the one-electron factors  $\phi_a$  and  $\phi_b$  making up the molecular wavefunction, both in the absence of  $\epsilon$ , and at high  $\epsilon$ . The wave function amplitude is plotted along the internuclear axis. As already mentioned, the zero-field symmetric



curves show the accumulation of charge near the molecular center. The high field wave functions shift the electrons predominantly to nucleus A, and this charge is, in fact, polarized to the right, away from the molecule. The second localized contribution, while still peaked at B, is so polarized in the same direction that it is spread out nearly uniformly throughout the interior of the molecule. Such a distorted wave function must be used to discuss field ionization, and it is clear that life times, electron energy distributions, and angular distributions of field emission will depend sensitively on this distortion. As an example, the simultaneous emission of two electrons can be expected

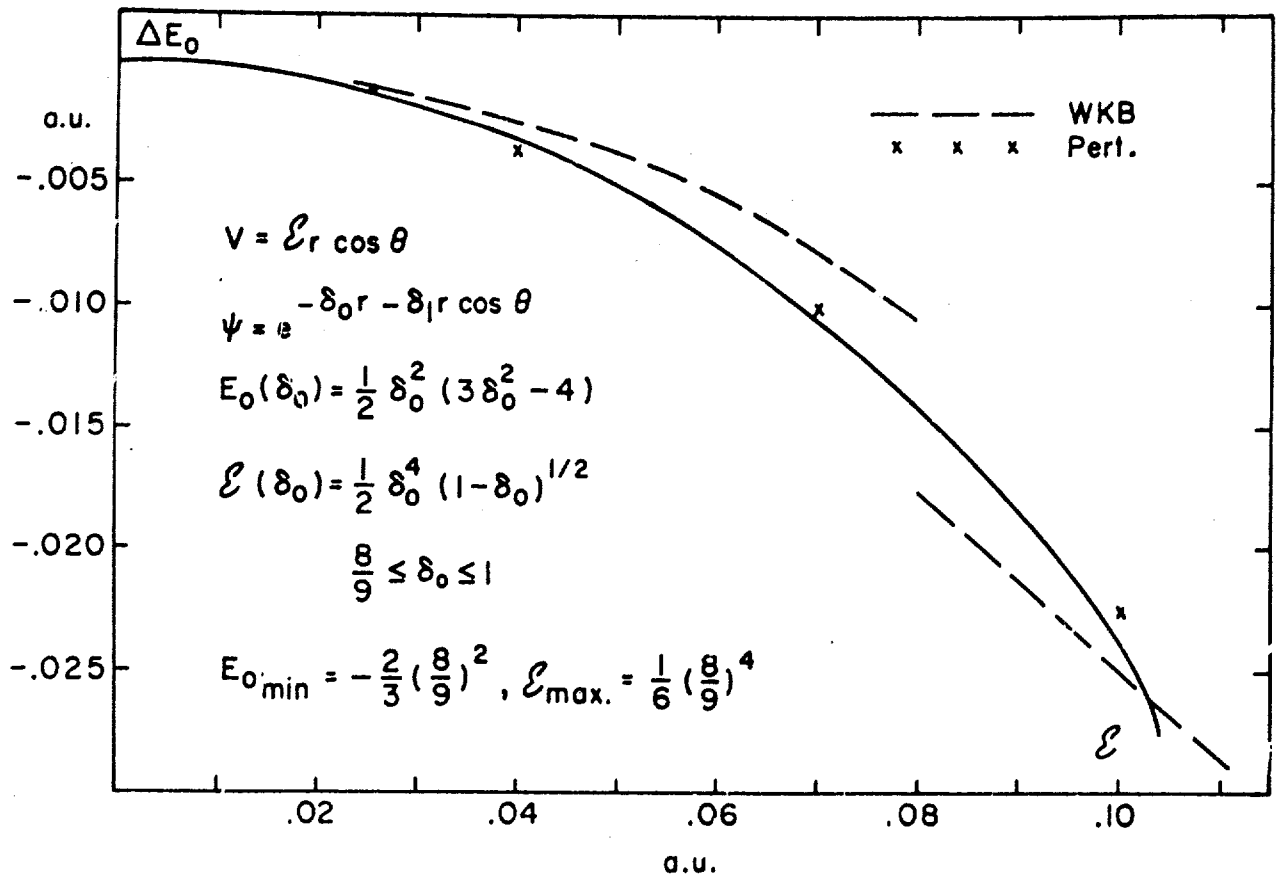
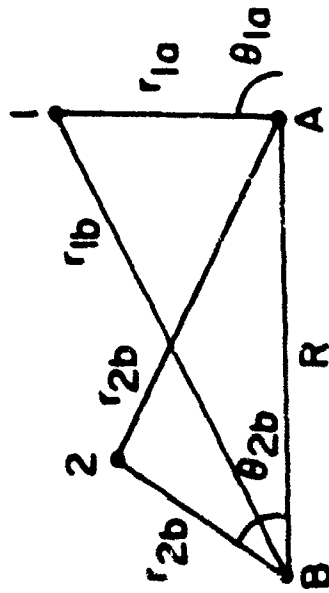


Fig. 1 Variational wave function for H in an electric field  $c$ . Formulas give the results for the energy  $E_0$  and  $\mathcal{E}$  as a function of the parameter  $\delta_0$ . Graph shows  $E_0$  vs  $c$ .

H<sub>2</sub> IN ELECTRIC FIELD

$$H = \frac{1}{2}P_1^2 + \frac{1}{2}P_2^2 - \frac{1}{r_{1a}} - \frac{1}{r_{1b}} - \frac{1}{r_{2a}} - \frac{1}{r_{2b}} + \frac{1}{R} + \frac{1}{r_{12}} + \frac{1}{R} - \mathcal{E}(r_{1a} \cos \theta_{1a} + r_{2b} \cos \theta_{2b})$$



$$\psi_A(1,2) e^{-\delta_1 r_{1a} - \delta_2 r_{1b} - \delta_3 r_{2b} - \delta_4 r_{2a}}$$

$$\bar{\Psi} = \psi_A(1,2) + \psi_A(2,1)$$

$$\mathcal{E} = 0: \delta_1 = \delta_3 = 1.089$$

$$\delta_2 = \delta_4 = 0.129$$

Fig. 2. Variational wave function and Hamiltonian in an electric field  $\epsilon$  for  $H_2^+$ . References refer to earlier use of this function with  $\delta_1 = \delta_3, \delta_2 = \delta_4$ .

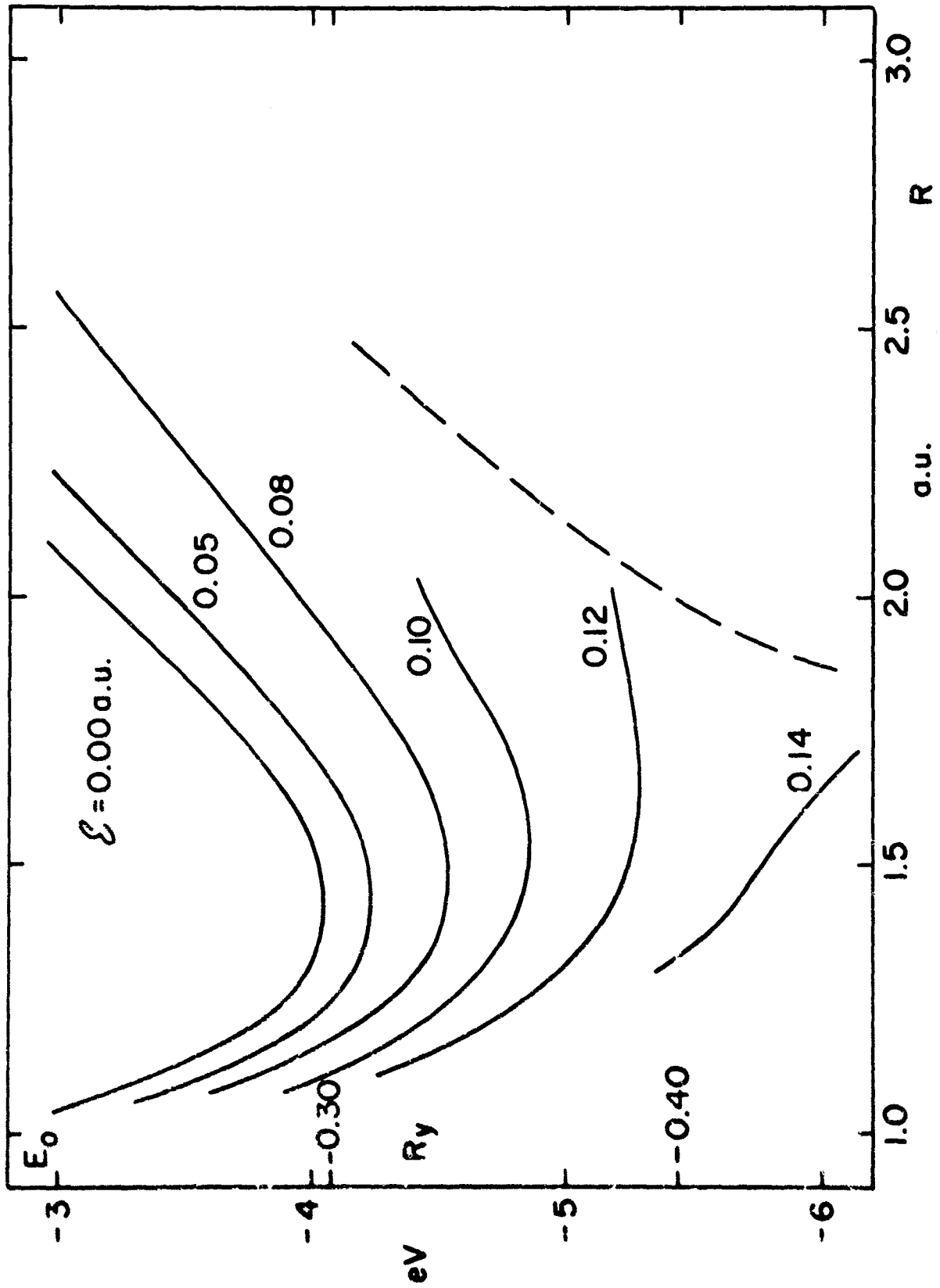


FIG. 3 Ground state energy of  $H_2$  vs internuclear spacing  $R$ , at different values of electric field  $\epsilon$ .

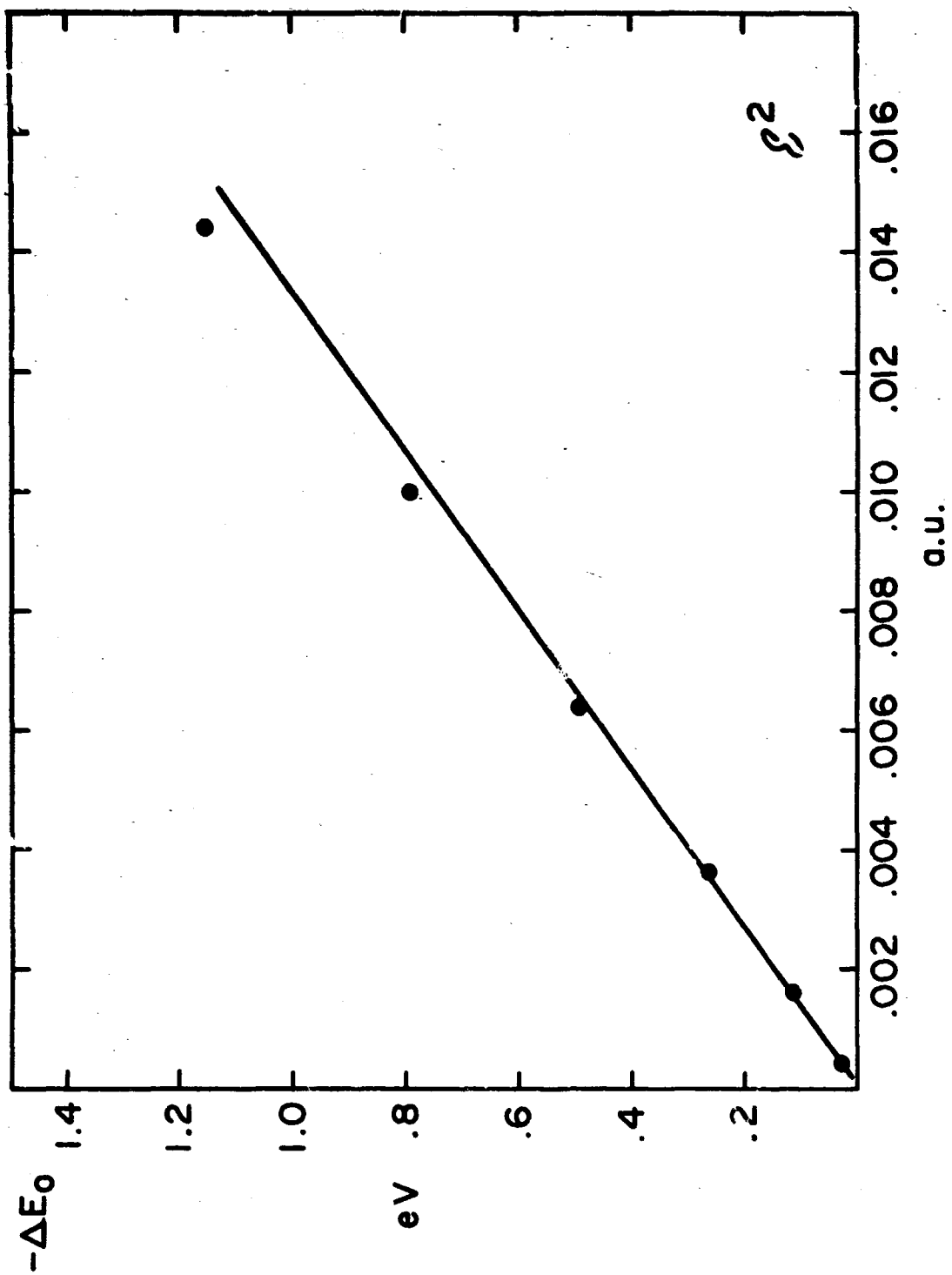


Fig. 4 Polarization energy of  $H_2$  vs  $\epsilon^2$ .

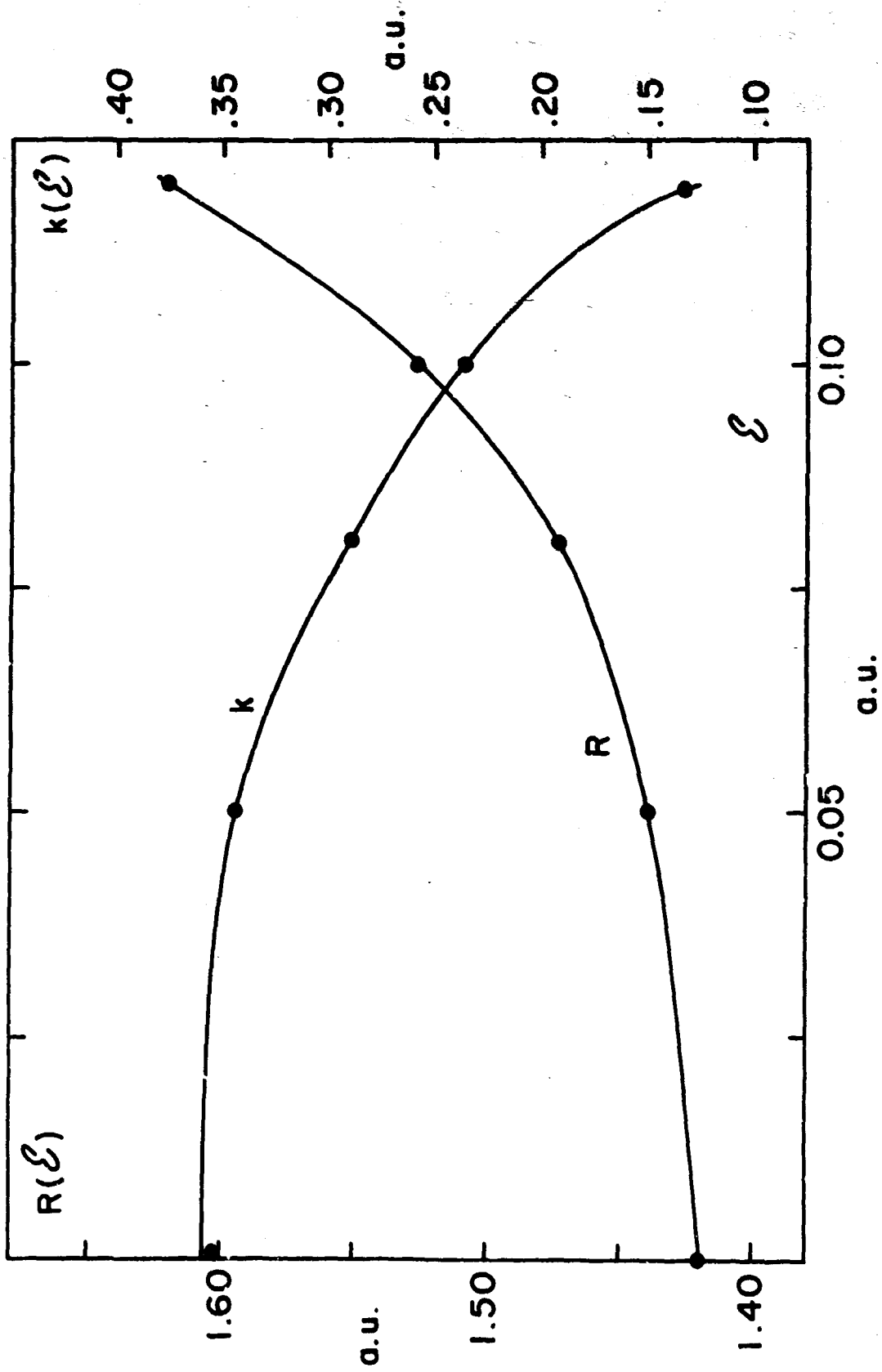


Fig. 5 Equilibrium spacing  $R$ , and molecular force constant  $k$ , vs.  $\epsilon$ .

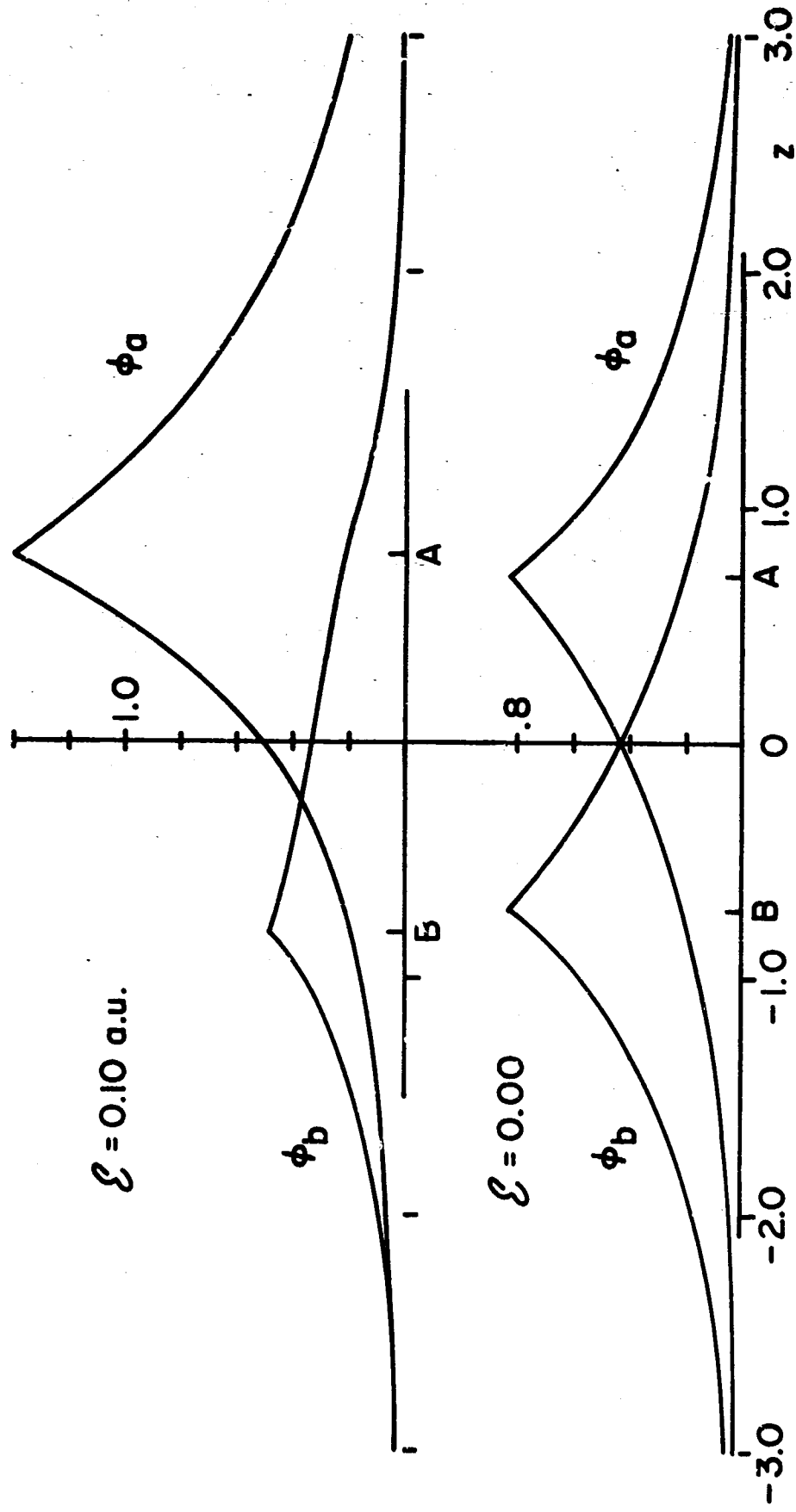


Fig. 6 One electron wave function factors in  $H_2$ , for  $\epsilon = 0$ , and  $\epsilon = .10$

to contain two energy peaks of unequal intensity, based on the asymmetry of  $\phi_a$  and  $\phi_b$ .

National Aeronautics and Space Administration  
NsG-589

H. J. Juretschke

#### REFERENCES

1. M. H. Rice and R. H. Good, Jr., J. Opt. Soc. Am. 52, 239 (1962).
2. N. Rosen, Phys. Rev. 38, 2099 (1931).

#### RESONANCE OSCILLATIONS OF INHOMOGENEOUS PLASMA SLABS

G. Dorman

##### I. Introduction

The collective oscillations of low-temperature, highly inhomogeneous laboratory plasma columns (Tonks-Dattner resonances) have recently come under intensive theoretical and experimental investigation.<sup>1-7</sup> These resonance properties of plasmas have important applications (diagnostic tools, amplification devices, radiation and scattering from satellite and meteor trails) as well as being a precise quantitative check between plasma theory and experiment.

Previous theoretical investigations have either been based on a fluid model or on severely truncated versions of the Vlasov equation. Though agreement between theory and experiment have been good in most instances, the unjustified nature of these models places great uncertainty on their range of applicability. The research reported here applies the full linearized Vlasov equation to the investigation of the properties of inhomogeneous plasmas.

##### II. Eigenvalue and Boundary Value Problems

The basic equations are the linearized Vlasov equation

$$\frac{\partial f}{\partial t} + v \frac{\partial f}{\partial x} - \frac{e}{m} E_0 \frac{\partial f}{\partial v} - \frac{e}{m} E \frac{\partial f_0}{\partial v} = 0 \quad (1)$$

and Poisson's equation

$$\frac{\partial E}{\partial x} = -4\pi e \int_{-\infty}^{\infty} f dv \quad (2)$$

These equations can be combined self-consistently. Assuming  $e^{-i\omega t}$  dependence for all perturbed quantities,

$$\frac{dE}{dx} = \frac{4\pi e^2}{m} \int_{-\infty}^{\infty} dv' \int_{-\infty}^t dt' E(x') e^{-i\omega(t'-t)} \frac{\partial f_0(x', v')}{\partial v'} \quad (3)$$

The integrals are to be evaluated along the equilibrium orbits of the particle. If the

equilibrium electron distribution function is Maxwellian,

$$f_0(x, v) = n_0(x) \sqrt{\frac{m}{2\pi KT}} e^{-\frac{mv^2}{2KT}} \quad (4)$$

such that

$$E_0(x) = -\frac{KT}{e} \frac{n_0'(x)}{n_0(x)} \quad (5)$$

then an expansion in powers of the temperature gives, in a straightforward way, the low-temperature expansion<sup>8</sup> (LTE) differential equation:

$$E''(u) + \psi'(u) E'(u) + \frac{1}{3} \left[ \psi'(u) + AB(A e^{-\psi} - 1) \right] E(u) = \frac{1}{3} A^2 B e^{-\psi} E_1 \quad (6)$$

where

$$A = \frac{\omega^2}{\omega_{P_0}^2}, \quad B = \frac{L^2}{\lambda_{D_0}^2}, \quad u = \frac{1}{L} x$$

and

$$\psi(u) = \ln \left| \frac{n_0(u)}{n_0(0)} \right|$$

and  $E_1$  is an externally incident electric field (and  $\omega_{P_0}^2$  is the maximum value of the plasma frequency,  $\lambda_{D_0}^2 = \frac{KT}{m\omega_{P_0}^2}$ , and  $L$  is the width of the plasma slab).

In a master's thesis by R. Guidone<sup>9</sup> results using Eq. (6) for eigenvalue and boundary-value problems have been compared with results obtained using the analogous equation given by the fluid theory,<sup>5</sup>

$$E''(u) - \frac{1}{3} \psi'(u) E'(u) + \frac{1}{3} B [A - e^{-\psi}] E(u) = \frac{1}{3} ABE_1. \quad (7)$$

(Modifications of these equations having some theoretical or approximative interest have also been considered in Guidone's thesis.)

The eigenvalue problems (i. e.,  $E_1 \neq 0$  and  $E(0) = 0 = E(1)$ ) investigated were the cases of constant density and of small variation from constant density:

$$n_0(u) = n_0 [1 - \alpha u^2] \quad (8)$$

where  $|\alpha| \ll 1$ . The eigenvalues obtained from Eqs. (6) and (7) agree to first order in  $\alpha$  and  $1/B$ :



$$A_n = 1 + \frac{3\pi^2(2n-1)^2}{4B} + \alpha \left[ \frac{2}{(2n-1)^2\pi^2} - \frac{1}{3} \right] \quad (9)$$

where  $n = 1, 2, 3, \dots$

The boundary-value problem investigated consisted of an externally incident wave,  $E_1 e^{-i\omega t}$ , incident at  $u = -1$  on a plasma of density

$$n_0(u) = \begin{cases} n_0 \cos^2(\alpha \frac{\pi}{2} u) & , \quad -1 < u < 0 \\ n_0 & , \quad 0 < u < \infty \end{cases}$$

where  $0 \leq \alpha \leq 1$ . The calculations were done numerically for various values of A and B. The primary results of this investigation can be summarized as showing that Eqs. (6) and (7) give qualitatively similar results but quantitatively differ considerably. For  $\omega > \omega_P$ , the calculated fields differ considerably both in the sheath and in the constant density region. For  $\omega < \omega_P$ , the fields in the constant density region were almost identical even though the fields in the sheath were markedly different.<sup>10</sup>

### III: Landau Damping

The broadening of the resonance peaks due to dissipative effects in the plasma has also been precisely measured.<sup>11</sup> Raether and Jackson<sup>12</sup> have reported calculations based upon a severely modified version of the Vlasov equation, (i. e., the important  $E_0 \frac{\partial f}{\partial v}$  term has been neglected) and only applicable for a very specific density profile,  $n_0(u) = n_0 [1 + \nu \cos(2\pi u)]$ ,  $0 < |\nu| < 1$ . We have retained the full effect of the plasma inhomogeneity by combining the low-temperature expansion result with a further perturbative expansion of the full Vlasov equation in powers of  $\gamma_n/\omega_n$ , where  $\gamma_n$  is the collisionless (Landau) damping rate and  $\omega_n$  is the frequency of the  $n^{\text{th}}$  resonance peak. The result is

$$\frac{\gamma_n}{\omega_n} = \frac{\sum_{k, k'=1}^{\infty} E_k^{(n)} n_{kk'} E_{k'}^{(n)} J_{k'}^{(n)}}{\sum_{k, k'=1}^{\infty} E_k^{(n)} n_{kk'} E_{k'}^{(n)}} \quad (10)$$

where

$$J_k^{(n)} = \begin{cases} \frac{\sqrt{\pi}}{\sqrt{8}} \frac{A_n B(A_n B + C_k)^{\frac{1}{2}}}{(\pi^2 k^2 + D_k)^{3/2}} \exp \left[ -\frac{1}{2} \left( \frac{A_n B + C_k}{\pi^2 k^2 + D_k} \right) \right], & z_k \text{ real} \\ 0 & , z_k \text{ imaginary} \end{cases}$$

and  $z_k = [(A_n B + C_k)/(\pi^2 k^2 + D_k)]^{1/2}$ . Here  $E_k^{(n)}$  is the  $k^{\text{th}}$  Fourier coefficient of the (normalized, dimensionless) electric field for the  $n^{\text{th}}$  resonance peak and, defining  $n_0(u) = n_0(0) \exp[\psi(u)]$ , then

$$n_{kk'} = \int_0^1 du \sin(\pi ku) e^{\psi(u)} \sin(\pi k'u)$$

$$C_k = - \int_0^1 du \sin(\pi ku) (\psi'' + 6(\psi')^2) \sin(\pi ku)$$

and

$$D_k = -2 \int_0^1 du \sin(\pi ku) (\psi')^2 \sin(\pi ku)$$

Setting  $\psi(u) = 0$  in Eq. (10) reproduces the familiar constant density result. The quantities,  $C_k$  and  $D_k$ , represent the displacement, due to the plasma inhomogeneity, of the poles in the plasma dispersion function.

Equation (10) is completely applicable for any density and to obtain numerical results only requires the solution of the eigenvalue problem of Eq. (6) in order to obtain  $A_n$  and  $E_k^{(n)}$ . Calculations have been carried out for a density profile given by  $e^{\psi} = \cos^2[\alpha(u - \frac{1}{2})]$ , where the plasma is confined between  $u = 0$  and  $u = +1$ , and  $\alpha$  is the inhomogeneity parameter, varying between zero and 1. The eigenvalues and eigenfields are calculated using a variational principle due to Barston.<sup>13</sup> Results have been obtained for  $50 \leq B \leq 50,000$ . The most interesting results can be summarized as follows:

1. for low enough temperatures ( $B > 10^3$ ) the damping rate increases greatly with increasing inhomogeneity (for example, for  $B = 5000$ , the damping rate of the lowest mode increases from  $\sim 10^{-10}$  for  $\alpha = 0$  to 0.38 for  $\alpha = 0.95$ ). For higher temperatures the rate of increase is much smaller and for  $B \approx 50$  the damping decreases with increasing  $\alpha$ ;
2. for large enough  $\alpha$  and high enough temperature the damping is zero because  $z_k$  is imaginary. The cutoff temperature (i. e., the lowest temperature for which the damping is zero) depends critically on  $\alpha$ . Thus  $\gamma_n = 0$  for  $\alpha = 0.9$  and  $B \lesssim 50$ , for  $\alpha = 0.95$  and  $B \lesssim 200$ , and for  $\alpha = 0.99$  and  $B \lesssim 1000$ .

Further calculations are under way using different density profiles.

Joint Services Technical Advisory Committee  
AF 49(638)-1402

G. Dorman

#### REFERENCES

1. D. Romell, *Nature* **167**, 243 (1951).
2. A. Dattner, *Ericsson Tech.* **13**, 309 and 350 (1957); *Phys. Rev. Letters* **10**, 205 (1963).

3. P. E. Vandenplas and R. W. Gould, *Physica* 28, 357 (1961).
4. A. M. Messiaen and P. E. Vandenplas, *Physica* 28, 537 (1962); *Plasma Physics* 4, 267 (1962); *Plasma Physics* 6, 459 (1964); *Nuclear Fusion* 5, 47 (1965).
5. J. V. Parker, J. C. Nickel, and R. W. Gould, *Phys. Fluids* 7, 1489 (1964).
6. F. C. Hoh, *Phys. Rev.* 133, A1016 (1964).
7. E. M. Barston, *Phys. Rev.* 139, A394 (1965).
8. G. Dorman, *J. Appl. Phys.* 37, 2321 (1966).
9. R. Guidone (Master's Thesis, PIB, 1968); unpublished.
10. Compare with J. Pavkovich, Stanford University Microwave Lab. Report No. 1093 (1963); K. Harker, *Phys. Fluids* 8, 1946 (1965); and W. Leavens, *J. Res. Natl. Bur. Std. (Radio Sci.)* 69D, 1321 (1965).
11. R. W. Huggins and M. Raether, *Phys. Rev. Letters* 17, 745 (1966).
12. E. A. Jackson and M. Raether, *Phys. Fluids* 9, 1257 (1966).
13. E. M. Barston; to be published.

#### MICROWAVE INSTABILITIES IN SEMICONDUCTOR PLASMAS

J. P. Parekh

A study of instabilities (convective or absolute) in semiconductor structures (infinite and bounded) involving drifted carriers and subjected to a magnetostatic field is being continued. The emphasis is being changed from ferromagnetic semiconductors to nonmagnetic semiconductors. Ferromagnetic semiconductors are interesting because of the fact that, unlike the nonmagnetic semiconductors, only a one-carrier plasma is necessary for making an instability possible. However, the currently available materials have been theoretically found to be unamenable to practical observation of useful growth rates because of the magnetic losses which are involved.

A topic which is being currently studied is a growing quasi-static surface-wave propagating parallel to the interface between an electron-hole plasma half-space and a dielectric half-space. The semiconductor is subjected to a magnetostatic field which lies in the plane of the interface and is aligned normal to the common direction of propagation and drift. A simplified investigation on this subject has been reported by Kino<sup>1</sup> which ignores the important effects of surface recombination and diffusion. A detailed study involving these effects is being made and it is anticipated that a new low-frequency mode of instability exists besides the one found by Kino.

Joint Services Technical Advisory Committee  
AF 49(638)-1402

J. P. Parekh

#### REFERENCES

1. Kino, G. S., "Growing Surface Waves in a Semiconductor in the Presence of a Transverse Magnetic Field," *App. Phys. Lett.*, 12, 312 (1968).

## NEW INSTABILITIES DUE TO ANISOTROPY IN THE TRANSVERSE PLANE OF VELOCITY SPACE

F. T. Stone

A general multistream approach for analyzing infinite beam-magnetoplasma systems was outlined in the last report<sup>1</sup>. In that report, the special case of waves propagating along an applied D. C. magnetic field was discussed. It was found that the Fourier Transform of the Electric Field,  $\underline{E}_\omega$ , had to satisfy:

$$\frac{k_c^2}{\omega^2} \underline{E}_{T\omega} = \underline{K} \cdot \underline{E}_\omega + \underline{K}_1 \cdot \underline{E}_{\omega + \Omega} + \underline{K}_2 \cdot \underline{E}_{\omega + 2\Omega} + \underline{K}_3 \cdot \underline{E}_{\omega - \Omega} + \underline{K}_4 \cdot \underline{E}_{\omega - 2\Omega} \quad (1)$$

where  $\Omega = qB_0/m$  is the cyclotron frequency of the species of charged particles considered. Note that  $\Omega$  carries the sign of charge. For more than one species we must let  $\underline{K}_1 \cdot \underline{E}_{\omega + \Omega}$  go over into  $\sum_s \underline{K}_{1s} \cdot \underline{E}_{\omega + \Omega_s}$ , etc. The elements of the various tensors are functions of  $\omega$  and  $k$  as well as the plasma parameters.

Equation (1) implies that an Electric Field at  $\omega_0$  produces currents at  $\omega_0 \pm \Omega$  and  $\omega_0 \pm 2\Omega$  which in turn act as sources for  $\underline{B}$  and  $\underline{E}$ . If azimuthal symmetry in velocity space is present, i. e., if the system is composed of  $m$  streams with  $\underline{V}_{0m} = \hat{i}_x V_{Tm} \cos(\Omega t - \phi_m) - \hat{i}_y V_{Tm} \sin(\Omega t - \phi_m) + \hat{i}_z V_m$  and beams with all  $\phi$  between 0 and  $2\pi$  are present with equal strength for each  $V_T$ , these currents sum to zero and  $\underline{K}_1$  through  $\underline{K}_4$  are zero tensors. Actually, complete symmetry is a more restrictive condition than is necessary.  $\underline{K}_1$  and  $\underline{K}_3$  become zero tensors if there is  $180^\circ$  rotational symmetry in the transverse plane of velocity space, i. e., if for each beam with a certain  $V_T$  and  $\phi_0$  there exists an equal strength beam with  $V_T$  and  $\phi_0 + \pi$ , while  $\underline{K}_2$  and  $\underline{K}_4$  become zero terms if there is  $90^\circ$  rotational symmetry in the transverse plane, i. e., for each beam with  $V_T$  and  $\phi_0$  there exists equal strength beams with  $V_T$  and  $\phi_0 + \pi/2$ ,  $\phi_0 + \pi$ , and  $\phi_0 + 3\pi/2$ . The resulting dispersion equation for  $\underline{K}_1$  through  $\underline{K}_4$  zero can be factored into the form:

$$\left(\frac{k_c^2}{\omega^2} - K_L\right) \left(\frac{k_c^2}{\omega^2} - K_R\right) K_{11} = 0 \quad (2)$$

where  $K_L$  and  $K_R$  are the usual dielectric tensor diagonal terms in rotating coordinates.

If arbitrary anisotropy in the transverse plane of velocity space is allowed, the solution to Eq. (1) is:

$$\underline{E}(z, t) = \left[ \hat{i}_x E_{11} + (\hat{i}_x + j\hat{i}_y) e^{j\Omega t} E_L + (\hat{i}_x - j\hat{i}_y) e^{-j\Omega t} E_R \right] e^{j(-\omega_0 t - kz)} \quad (3)$$

that is, the solution is a coupled set of fields consisting of a longitudinal wave at a base frequency  $\omega_0$ , a right circularly polarized wave at  $\omega_0 - \Omega$  and a left circularly wave at  $\omega_0 + \Omega$ . The dispersion equation for the system (the relation between  $\omega_0$  and  $k$ ) is obtained

by placing the Fourier Transform of Eq. (3) into Eq. (1). It is

$$K_{11}(\omega_0) \left[ \frac{k^2 c^2}{(\omega_0 + \Omega)^2} - K_L(\omega_0 + \Omega) \right] \left[ \frac{k^2 c^2}{(\omega_0 - \Omega)^2} - K_R(\omega_0 - \Omega) \right] = a(\omega_0, k) \quad (4)$$

An unstable solution to this equation due to the anisotropy (i. e., complex  $\omega_0$  for real  $k$ ) has been found for a simple configuration of two beams with the same  $V_T$ , but with initial angles 180 degrees out of phase.

For the case of parallel propagation the complete solution involved only the base frequency and the sum and difference of the base and cyclotron frequencies. In the general case of propagation skew to the applied magnetic field the complete solution requires an infinite number of sum and difference frequencies, implying the spread of energy over a wide band of frequencies.

We wish to study this general case more thoroughly, at least for the Electrostatic modes, and derive the relationship between the propagation constant and base frequency for a truncated band of sum and difference frequencies. We also wish to examine Eq. (4) for more complicated configurations. Since even the simple cases lead to formidable formulas, approximate methods such as coupling of modes will be used.

Joint Services Technical Advisory Committee  
AF 49(638)-1402

F. T. Stone

#### REFERENCES

1. Report No. 32 to the Joint Services Technical Advisory Committee, PIBMRI-452. 32, Polytechnic Institute of Brooklyn, 1967.

#### AN INVESTIGATION OF VLF HISS EMISSION

S. H. Gross and N. LaRocca

Hiss is observed on the ground, in rockets and satellites. More than one band of noise is observed and some are still completely unexplained. The so-called LHR noise band appears to be related to the ions at the observing altitude, but it is far from clear as to its generation and how it reaches mid-latitudes. In very many cases at mid-latitudes it is observed in association with short-hop whistlers, and the connection between these whistlers and the LHR noise band, if any, is not understood. Hiss has also been observed at low altitudes near the geomagnetic equator. Whether such noise is due to an equatorial instability, or propagated from higher latitudes, or whether it is the result of non-ducted whistlers are questions of importance. Hiss has also been detected in the LF and MF bands, and the upper cut-off and connections between all these bands (VLF, LF and MF) are questions of interest. There is some basis for relating the occurrence of hiss to auroral events and magnetospheric phenomena, and it may be that clarification and explanation of hiss will provide some useful insight with regard to the problems of the magnetosphere.

The intent of the study is to provide explanations of observed hiss phenomena in terms of its generation and propagation. The study has been in process for less than a year. The task has been divided into three interrelated areas of research consisting of a phenomenological study, an instability or source study and a propagation study.

Most of the records of observations available to us have been from Alouette I satellite data as received at Ottawa, Canada graciously provided by Dr. R. Barrington of the Canadian Defense Research Telecommunications Establishment (DRTE). Particular emphasis to date has been on the LHR noise band.

Several characteristics of this noise band have been found in the 35 mm film provided by DRTE (October-December, 1964). In all observed cases none appeared clearly stimulated by whistlers, and the occurrences fall into two categories with respect to magnetic latitude and times. It was found that all events occurring below roughly  $60^{\circ}$  N geomagnetic latitude fell around 0800 LMT and those above  $60^{\circ}$  N latitude at about 2000 LMT. Although the number of cases hardly present a good statistical sample, it represents some significance in view of the two periods of peak precipitation, the morning peak for the hard precipitation ( $> 40$  kev) and the evening peak for soft particle precipitation (1-10 kev) as described by Hartz and Brice<sup>1</sup>. The roughly  $60^{\circ}$  latitude separation may also be of some significance in view of the study of McEwen and Barrington<sup>2</sup> on hiss occurrence. In their study they do not clearly distinguish latitudes, lumping occurrences over the range  $50^{\circ}$ - $63^{\circ}$  N, with regard to day or night peaking of occurrences. It is uncertain whether the nighttime peak was due to data for all of this range or for the higher latitudes in this range. This point may be of significance because of the possible effects of changes in the ion distribution between day and night at mid-latitudes on propagation paths from the auroral region. Though the nature of the ionosphere around  $60^{\circ}$  latitude may be expected to change diurnally due to the auroral oval and geomagnetic activity, the hard particle precipitation that peaks in the morning is apparently not much affected by time of day or magnetic activity.

Statistical collection of data for the same time period also included the lower cutoff frequency and its variation over a noise span, the upper cutoff frequency when it was below the maximum of the spectrum analyzer ( $\approx 9$  kc) and quasi-periodic frequency variation data when apparent. The latter variations were noted principally at the higher latitude positions of the satellite passes. It was also noted in a number of cases that the upper cutoff frequency varied in phase with the lower cutoff frequency, a variation not previously noted by experimenters. At this point such variations are judged somewhat subjectively, and it is planned to spectrum analyze the lower and upper envelopes of such noise samples. It is also not known whether such variations are physically significant or characteristic of the AGC system of the Alouette VLF receiver. Data for other time periods will also be examined.

The noise source portion of the study has been concerned with instabilities resulting from electron precipitation. It is known that kilovolt electrons precipitate in the auroral region, and this much energy appears to be necessary to generate VLF waves at large wave normal angles, as is necessary to explain LHR emission. Photoelectrons are also known to be present throughout the sunlit ionosphere and possibly in unlit regions because of diffusion along field lines from sunlit conjugate points. Such electrons have energies in the range of electron volts to 10's of electron volts and could possibly be the source of emission with wave normal angles closer to the magnetic field lines. The analysis of this problem to date has consisted of a model in which monoenergetic electrons are assumed to penetrate a cool plasma. The initial efforts have been for the electron beam along the magnetic field. Beams with components transverse to the magnetic field and with a distribution of energies will also be considered.

A beam in a cool plasma produces both the well-known two-stream and cyclotron instabilities. Consideration was given to the two-stream instability which generates a wide spectrum of frequencies  $\omega$  for a wide range of wave number vectors  $\underline{k}$ . For a beam of monoenergetic electrons with velocity  $V_z$  along the field lines, assumed to be along the z-axis, the dispersion equation is

$$(\omega - k_z V_z)^2 = \frac{\alpha \pi_e^2 \left\{ \frac{k^4 c^4 \cos^2 \theta}{\omega^4} - \frac{k^2 c^2}{\omega^2} S(1 + \cos^2 \theta) + S^2 - D^2 \right\}}{P \left\{ \frac{k^4 c^4}{\omega^4} \cos^2 \theta - \frac{k^2 c^2}{\omega^2} S(1 + \cos^2 \theta) + S^2 - D^2 \right\} + \frac{k^2 c^2}{\omega^2} \sin^2 \theta \left[ \frac{k^2 c^2}{\omega^2} S - (S^2 - D^2) \right]}$$

where  $k_z$  is the z component of  $\underline{k}$ ,  $\theta$  is the angle between  $\underline{k}$  and the magnetic field lines,  $c$  = speed of light in a vacuum,  $\alpha$  is the ratio of the beam electron density  $n_s$  to the background plasma electron density  $n_e$ ,  $\pi_e^2$  is the electron plasma frequency,  $S$ ,  $D$  and  $P$  are given by the following expressions for a single ion plasma:

$$S = 1 - \frac{\pi_i^2}{\omega^2 - \Omega_i^2} - \frac{\pi_e^2}{\omega^2 - \Omega_e^2}$$

$$D = \frac{\pi_i^2 \Omega_i}{\omega(\omega^2 - \Omega_i^2)} - \frac{\pi_e^2 \Omega_e}{\omega(\omega^2 - \Omega_e^2)}$$

$$P = 1 - \frac{\pi_i^2}{\omega^2} - \frac{\pi_e^2}{\omega^2}$$

Here  $\pi_1^2$  is the ion plasma frequency, and  $\Omega_e$  and  $\Omega_i$  are, respectively, the electron and ion cyclotron frequencies.

Instabilities arise in the linear analysis when the right hand side of the equation is negative. The significance of the instability at a given frequency  $\omega$  for a given  $\underline{k}$  vector must be further examined by quasi-linear techniques.

The simpler cases for  $\theta = 0^\circ, 90^\circ$  are readily illustrated. For  $\theta = 0^\circ$  ( $\underline{k}$  along the field lines)

$$(\omega - k_z V_z)^2 = \frac{\alpha \pi_e^2}{P}$$

The condition for instability is  $P < 0$ . Taking  $\omega = \omega_r + i\omega_i$  with  $\omega_i \ll \omega_r$ , one finds that  $\omega_r = k_z V_z$ ,

$$\omega_i = \pm \left( \frac{\alpha \pi_e^2}{\frac{\pi_e^2}{\omega^2} - 1} \right)^{\frac{1}{2}} \approx \pm \sqrt{\alpha k^2 V_z^2}$$

Thus, linear theory predicts instabilities for all frequencies below the plasma frequency for  $\theta = 0^\circ$ , with the greatest growth rate near the plasma frequency. The waves generated are plasma waves for this case.

For  $\theta \approx 90^\circ$

$$(\omega - k_z V_z)^2 = \frac{-\alpha \pi_e^2}{\frac{k_c^2}{\omega^2} - P} = -\alpha \frac{\pi_e^2}{\frac{k_c^2}{\omega^2} + \frac{\pi_e^2}{\omega^2} - 1}$$

$$\text{or } (\omega - k_z V_z) = \pm \left[ -\alpha \frac{\pi_e^2}{\frac{k_c^2}{\omega^2} + \frac{\pi_e^2}{\omega^2} - 1} \right]^{\frac{1}{2}}$$

Instabilities arise when  $k_c^2 + \pi_e^2 > \omega^2$  for which, when  $\omega_i \ll \omega_r$ ,  $\omega_r = k_z V_z$  and

$$\omega_i = \pm \left[ \frac{\alpha \pi_e^2 \omega^2}{k_c^2 + \pi_e^2 - \omega^2} \right]^{\frac{1}{2}} = \pm \left[ \frac{\alpha \pi_e^2 k^2 \cos^2 \theta V_z^2}{k^2 (c^2 - v_z^2 \cos^2 \theta) + \pi_e^2} \right]^{\frac{1}{2}}$$

Since  $\theta \approx 90^\circ$ ,  $\cos \theta$  is small and  $V_z$  must be correspondingly greater than for  $\theta = 0^\circ$



for the same  $\omega_x$  and  $k$ . Thus, electrons with energies in the eV range is sufficient for  $k$  along the field lines, whereas keV energy is needed for  $k$  nearly transverse to the field. The range of frequencies varies with the magnitude of  $k$ , and the growth rate is greatest for large values of  $k$ . The waves generated are not necessarily plasma waves since the  $\underline{E}$  vector may have perpendicular components.

Propagation into the medium depends on the dispersion relation for the surrounding medium. Only those combinations of  $\omega, k$  which are in the pass bands will be seen. It is also possible that plasma waves may be coupled to electromagnetic waves, and that such coupling may be important. Such would appear to be the case if detection were remote from the source for a spinning satellite. Furthermore, Gurnett<sup>3</sup> has detected LHR type of noise with loop antennas on the Injun 3 satellite.

Other waves are also generated when the temperature of the plasma is taken into account, but the conditions for strong generation of these waves are unlikely.

The analysis of the generation of waves as a result of particle beams must be extended to include the cyclotron instabilities, non-monoenergetic beam aspects, transverse beam velocities and quasi-linear growth rate considerations. Propagation out of the region of generation must also be included.

The lower hybrid resonance is an ion-electron effect in the plasma. The particular frequency can be defined for a multi-constituent ion plasma in terms of the electron plasma and cyclotron frequency and the ion masses as follows:

$$\omega_{LHR}^2 = \frac{\pi_e^2 \Omega_e^2}{\pi_e^2 + \Omega_e^2} \sum_{k=1}^S \frac{\alpha_k}{\mu_k}$$

where  $s$  is the number of types of ions,  $\alpha_k = \frac{n_k}{n_e}$ ,  $n_k$  = number density of ions of type  $k$  of mass  $m_k$ ,  $\mu_k = \frac{m_k}{m_e}$  and  $m_e$  and  $n_e$  are the mass and number density of electrons. This relationship is usually put in the form

$$\omega_{LHR}^2 = \frac{\pi_e^2 \Omega_e(\Omega_i)_{eff}}{\pi_e^2 + \Omega_e^2} \text{ where } (\Omega_i)_{eff} \text{ is the ion cyclotron frequency for an effective}$$

$$\text{mass given by } \frac{1}{m_{eff}} = \sum_{k=1}^S \frac{\alpha_k}{m_k} .$$

It has been known that VLF waves at frequencies near or around the lower hybrid resonance can be ducted perpendicular to the magnetic field under proper conditions<sup>4</sup>. More than one ion is necessary for such propagation. In effect, the wave moves up and

down along the field line in the duct, reflecting at lower and upper layers in the ionosphere. Such a possibility arises when a lighter ion is predominant in the upper region and a heavier ion is predominant in the lower region of the ionosphere. A distribution of this sort is always present in the medium, though the condition for ducting may not be present. For ducting it is necessary to fulfill another requirement in terms of the distribution of the ions and the electrons. In its simplest form this condition is that the lower hybrid resonance be a proper multivalued function of altitude. We have found that the condition can be stated more precisely in terms of the index of refraction for  $\theta = 90^\circ$  without specific reference to the lower hybrid resonance.

One can show that ducting is possible over a range of frequencies and that the size of the duct, as determined by the altitude range between reflecting layers, varies with frequency. It can also be shown that the lowest frequency at which ducting will occur for a particular satellite altitude is within the vicinity of the local lower hybrid resonance. Thus, the explanation of the so-called LHR noiseband in terms of the LHR frequency has been accepted on the basis of the effective mass of the ionosphere at the satellite altitude which has usually turned out to be reasonable. That sensible masses are found is not surprising if this duct is indeed the mechanism by which the waves propagate from their source to the satellite.

It is well known now that the distribution of ions varies with latitude, such that hydrogen ions predominate at about 1000 km altitude at lower latitudes. Apparently the changeover from  $O^+$  to  $H^+$  occurs at higher and higher altitudes as latitude increases. It occurred to us that such a latitudinal distribution would create a duct at a given frequency that decreases in altitude over the appropriate latitude range. Furthermore, the significant changes that occur diurnally in the ionosphere would bear on this aspect, and the rapid increases in electron density at about  $60^\circ$  geomagnetic latitude that appear as a regular feature of the quiet nighttime ionosphere at 1000 km (see Refs. 5 and 6), as well as the equatorial anomaly at lower altitudes, might be significant in breaking up this duct. The patchy duct, varying in altitude, would guide energy generated in the duct or propagated into the duct from elsewhere. A satellite, roughly at a fixed altitude, such as Alouette I, would then pick up the noise band over a limited range, the time when it passes through the duct, if noise is in the duct. Furthermore, it would be more probable for noise to be seen at medium latitudes in a satellite such as Alouette I, rather than at low latitudes for two reasons: (1) The height of the duct would be low near the geomagnetic equator and (2) the probability of a breakup in the duct, if the noise source stemmed from precipitation at higher latitudes. Such indeed seems to be the case with Alouette I. Furthermore, the  $60^\circ$  ledge and higher latitude ionospheric trough seen at night would be expected to prevent ducting to lower latitudes. The nighttime occurrence of LHR noise above  $60^\circ$  geomagnetic latitude might indeed result from these barriers.

The sun-lit morning ionosphere with the harder electron precipitation or drizzle might then be understood in terms of occurrence below  $60^{\circ}$  geomagnetic latitude. It is also interesting to note that Gurnett<sup>7</sup> found VLF hiss in the appropriate frequency range in the data from Injun 3 while the satellite was at very low latitudes at altitudes below 350 km. Furthermore, Barrington<sup>8</sup> found intense LHR noise in a simultaneous mid-night rocket flight from Wallops Is., Va. and an Alouette II overpass. The intensity of the noise appeared similar to noise intensities observed in auroral regions, yet the only significant activity observed at the time was an unusually high  $f_oE$  value for a nighttime mid-latitude ionosphere. In this latter case particle precipitation must have occurred at lower latitudes than normal, but not necessarily as low as  $50^{\circ}$  geomagnetic latitude. Confirmation of activity in terms of the  $K_p$  index has not yet been made.

The usual argument made against the duct theory is that frequencies are observed that would be well above the upper cut-off of the duct. Laaspere et al.<sup>9</sup> have observed as high as 16 kHz and Shawhan and Gurnett<sup>10</sup> as high as 30 kHz. However, such frequencies are not necessarily the result of very remote higher energy precipitation and could arise from whistler triggered noise or even photoelectrons.

For the purposes of investigating the significance of the duct theory, its propagation properties are being investigated to establish relationships for (1) determining when one or more ducts may exist, (2) the height of the duct as a function of frequency, (3) the bandwidth of the duct as a function of altitude, and (4) the general nature of the latitudinal characteristics of the duct based on known diurnal and latitudinal variations of ion and electron density distributions.

National Science Foundation  
GU-1557

S. Gross

#### REFERENCES

1. T. R. Hartz and N. M. Brice, "The General Pattern of Auroral Particle Precipitation," *Planet Space Sci.* 15, 301-329 (1967).
2. D. J. McEwen and R. E. Barrington, "Some Characteristics of the Lower Hybrid Resonance Noise Bands Observed by the Alouette I Satellite," *Canad. J. Phys.* 45, 13-19 (1967).
3. D. A. Gurnett, "A Satellite Study of VLF Hiss," *JGR* 71, 5599-5615 (1966).
4. R. L. Smith, I. Kimura, J. Vigneron and J. Katsenfrakis, "Lower Hybrid Resonance Noise and a New Ionospheric Duct," *JGR* 71, 1925-1927 (1966).
5. L. H. Brace and B. M. Reddy, "Early Electrostatic Probe Results from Explorer 22," *JGR* 70, 5783-5792 (1965).
6. L. H. Brace, B. M. Reddy and H. G. Mays, "Global Behavior of the Ionosphere at 1000-Kilometers Altitude," *JGR* 72, 265-283 (1967).
7. D. A. Gurnett, "Observations of VLF Hiss at Very Low L Values," *JGR* 73, 1096-1101 (1968).
8. R. E. Barrington, "Rocket Observations of Antenna Impedance at VLF," paper presented at the Fall URSI Meeting, September 10-12, 1968, Northeastern Univ., Boston, Mass..

9. T. Laaspere, M. G. Morgan and W. C. Johnson, "Observations of Lower Hybrid Resonance Phenomena by Dartmouth's OGO-2 Experiment," Radiophysics Laboratory, Thayer School of Engineering, Dartmouth College, Hanover, New Hampshire, 1968.
10. S. D. Shawhan and D. A. Gurnett, "VLF Electric and Magnetic Fields Observed with the Javelin Sounding Rocket," Dept. of Physics and Astronomy, Univ. of Iowa, Report 68-20, March 1968.

#### DIFFRACTION BY PLANETARY IONOSPHERES

S. H. Gross and J. Pirraglia

The radio occultation experiments performed by Mariners IV and V have provided valuable information concerning the atmospheres and ionospheres of Mars and Venus. Constraints on spacecraft weight and power as well as the past success of these experiments insure the continued utilization of the occultation technique by future planetary missions.

In the experiment, a signal is transmitted to the spacecraft which in turn retransmits the signal back to earth during the time the spacecraft is close to occultation in its orbit. More than one frequency may be utilized. The radio waves pass through the planet's atmosphere and/or ionosphere and the increment in the phase path, as deduced from the doppler, is analyzed to determine the distribution of neutrals in the lower atmosphere and electrons in the ionosphere above. The method of analysis assumes a radial distribution and utilizes ray theory to convert the received data into profiles.

It is well known that such a distribution is unrealistic, both neutrals and ionized particles being distributed in a more complex arrangement that depends on all three coordinates of a spherical system. The neglect of such variations may lead to significant errors, particularly with regard to scale height interpretations, the details about a peak density in the ionosphere, and inferences concerning the distribution about the entire planet and diurnal variations.

The general problem of diffraction of a radio source by a planetary atmosphere or ionosphere is the subject of study of this investigation. The intent is to attack the problem utilizing both full wave and ray theoretical methods with models of increasing complexity approaching realistic distributions. Previously, little work has been accomplished for models with more than one degree of freedom. One of the purposes is to determine the errors resulting from the simpler radial model assumption. It is also of interest to establish the degree of definition attainable by multi-frequency measurements and to provide sufficient data that might lead to suggestions for improved experiments. The results of the analysis may also permit a more systematic basis for comparison of ionospheric measurement techniques for use on future planetary missions.

Work on this problem has been proceeding since about April 1968. The effort has been funded by a NASA grant. To date the studies have emphasized ray theoretical aspects, full wave analysis being postponed to the future.

The first model and the appropriate ray equations were chosen so as to have some physical meaning. An exponential model was chosen with density falling off with altitude and with factors introducing angular variations to present latitudinal and longitudinal changes. More complex models incorporating peak densities and stronger lateral gradients will be introduced at a later date to be more representative of an ionosphere. The exponential model, however, is sufficient for the time being to represent a slowly varying lower atmosphere and the distribution of ionization above a peak density. Isotropy is also assumed.

With regard to angular variation, it is sufficient to take the functional dependence with respect to the sun with symmetry assumed about the direction of the sun. The complications of phase lags in the dependence on zenith angle and non-symmetry can be introduced at a later date, if necessary. Thus, the model initially chosen varies with both altitude and zenith angles, though further complications can be introduced if needed. Further simplification is incorporated by taking the temperature and density variation with zenith angle to be the same, though extension to include different dependence is easily accomplished. To a certain extent these simplifications were made to facilitate the interpretation of results, particularly for use in comparisons with purely radial models. For the purposes of the earlier phases of this study, it is sufficient to make the angular variation as simple as possible, and therefore, a cosinusoidal dependence is assumed.

The index of refraction,  $\mu$ , of the initial model is described by the following equation.

$$\mu = 1 + x \left( 1 + p \cos \theta \right) e^{-\left( \frac{R}{1 + p \cos \theta} \right)}$$

where  $R$  = altitude normalized to a fixed, arbitrary scale height;

$\theta$  = zenith angle of the sun;

$p$  = parameter normalizing the cyclic variation of temperature and density with zenith angle to the steady component of these quantities;

$x$  = a small normalized parameter determining the extent of the refractivity of the medium at some reference level.  $x$  is taken positive for neutral atmospheres and negative for isotropic ionospheres.

A spherical coordinate geometry ( $r, \theta, \phi$ ) is utilized for the ray equations with the origin at the planet's center and the polar axis in the sun's direction. Since the sun is

at a great distance the zenith angle at any point in the atmosphere or ionosphere is, for all intents and purposes, the coordinate  $\theta$  at the point. In the general case  $\mu = \mu(r, \theta, \varphi)$  for  $r \geq r_p$ , the radius of the planet. The ray at some point  $(r, \theta, \varphi)$  has directions specified by two angles  $\psi, \phi$ , where  $\psi$  is the angle between the ray direction along the ray and the radius vector at the point, and  $\phi$  is the angle between the planes formed by the radius vector and the polar axis and the radius vector and the ray. If a vector  $\underline{\mu}$  is defined with direction along the ray and magnitude  $\mu(r, \theta, \varphi)$ , then the three spherical components of this ray are  $p_r = \mu \cos \psi$ ,  $p_\theta = \mu \sin \psi \cos \phi$ ,  $p_\varphi = \mu \sin \psi \sin \phi$ .

The ray equations can be stated in terms of  $r, \theta, \varphi, p_r, p_\theta, p_\varphi$  in Hamiltonian form. Since initial consideration is for a model with  $\varphi$  symmetry ( $\mu = \mu(r, \theta)$ ), and the model is defined in terms of altitude, it is convenient to restate the equations in terms of the altitude variable  $R$  and the zenith angle (or polar angle)  $\theta$ . For  $\varphi$  symmetry it is found that a quantity  $\eta = r \sin \theta p_\varphi$  is a constant of the ray path, since  $\frac{d\eta}{d\tau} = \frac{1}{\mu} \frac{\partial \mu}{\partial \varphi} = 0$ . As a result, the  $\varphi$  derivative can be stated in terms of this quantity and  $r$  and  $\theta$ :  $\frac{\partial}{\partial \varphi} = \frac{\eta}{r \mu^2 \sin^2 \theta}$ , so

that the ray is completely specified once the dependence  $r = r(\theta)$  and  $\eta$  are known. The constant  $\eta$  can be related to the impact parameter of the ray and the ray direction at a far off point, so that  $\eta$  is a constant determined by initial ray launching conditions. The ray equations then reduce to four equations that must be solved to find the ray path. In normalized altitude coordinates these are

$$\frac{dR}{d\tau} = -\frac{\xi_R}{\mu^2 (R_p + R)}$$

$$\frac{d\xi_R}{d\tau} = 1 + \frac{R_p + R}{\mu} \frac{\partial \mu}{\partial R}$$

$$\frac{d\theta}{d\tau} = \frac{\zeta_R}{\mu^2 (R_p + R)}$$

$$\frac{d\xi_\theta}{d\tau} = \frac{1}{\mu} \frac{\partial \mu}{\partial \theta} + \frac{\eta^2 R \cot \theta}{\mu^2 (R_p + R)^2 \sin^2 \theta}$$

where

$$\xi_R = \frac{r p_r}{H}, \quad \zeta_R = \frac{r p_\theta}{H}, \quad \eta = \frac{c t}{H}, \quad R = \frac{r - r_p}{H}, \quad R_p = \frac{r_p}{H}.$$

$H$  is a normalization scale height of the model,  $t$  and  $c$  may be taken to be time and the velocity of light in a vacuum. These equations may be further simplified since  $R_p \gg R$  under usual circumstances.

Unlike the radial model, the ray differential equations cannot be solved analytically for any general function  $\mu = \mu(R, \theta)$ . Only in very special, but entirely unrealistic, cases is the solution tractable. It is necessary to approach the problem either by computation or by approximate techniques. The rays are in general non-planar, whereas a radial

model always produces rays lying in a plane.

A program was written for computation to find the ray trajectories and to study their characteristics for various values of the parameters  $x, p$  and combinations of values of the ray initial conditions. It is assumed that the ray is launched well outside the medium ( $R$  large). The phase path length is also computed, since this quantity is measured by the occultation experiment. Many rays were computed with this program for different conditions.

It is presently intended to compute the phase paths in a simulation of a spacecraft orbiting the planet and receiving radiation from the earth. These phase paths will then be used in a computer program which will invert the problem, assuming a radial model. The results for that model will then be compared with the actual model to determine errors for each set of assumed parameters. Of principal importance for exponential models is the comparison of scale heights for the radial model vs. actual scale heights.

In carrying out these computations, one problem is to find the specific rays that are bent in the direction of the earth. So far, it appears necessary to find these rays by a hunt and trial system. Present efforts involve attempts to find a reasonably efficient method. The determination of caustic surfaces also appears to be analytically intractable and computations are believed necessary. Ray plots will aid in indicating such surfaces.

The analysis utilizing approximation techniques has not been completed as yet. One approach is to find the ray path as a perturbation about the ray paths for a radial model. In this approach, it appears desirable to restate the equations in terms of a parameter with a rate of change proportional to  $\frac{\partial \mu}{\partial \theta}$ . Such a parameter is the quantity  $Q$  defined by

$$Q = (\mu r \sin \psi)^2, \text{ and } \frac{\dot{Q}}{c} = 2 \sqrt{Q - \eta^2 \csc^2 \theta} \frac{1}{\mu} \frac{\partial \mu}{\partial \theta}.$$

When this quantity is used together with the coordinates  $r, \theta$ , only three equations are needed to define the ray. In addition to the equation for  $\dot{Q}$ , the two equations

$$\frac{\dot{r}}{c} = \frac{\sqrt{\mu^2 r^2 - Q}}{r \mu}, \quad \frac{\dot{\theta}}{c} = \frac{\sqrt{Q - \eta^2 \csc^2 \theta}}{r^2 \mu^2} \text{ are necessary.}$$

The approximation procedure would then be based on the assumed smallness of  $\frac{\partial \mu}{\partial \theta}$ , so that  $Q$  is nearly constant along the ray. Some of the problems that have to be treated are the degree of smallness of the partial derivative and the fact that the ray paths for a radial model and  $(r, \theta)$  model are different, though the initiating ray be the same. A bivariate perturbation is involved.

National Aeronautics and Space Administration  
NgR 33-006-047

S. Gross

#### IV. SOLID STATE AND MATERIALS

Augeri, R. C.	D'Aiello, R. V.	Kapash, R.	Schrager, M.
Banks, E.	Das, P.	Kaplan, S.	Schwartz, R. W.
Bergstein, L.	Eschwei, M. A.	Krieger, J. B.	Senitzky, B.
Bharat, R.	Evans, C. R.	Mauro, R.	Silber, L. M.
Boudreaux, D.	Freedman, S. J.	Menes, M.	Stern, R. M.
Cassedy, E. S.	Gervais, A.	Post, B.	Strauss, L.
Chen, L.	Griemsmann, J. W. E.	Rifkin, R. H.	Sucher, M.
Chen, R.	Halperin, A.	Schachter, H.	Tashima, N.
Chiang, C.	Hara, J.	Schleuning, H. W.	Taub, H.
Collins, F. C.	Juratschke, H. J.	Schlosser, H.	Wainfan, M.
			Wang, W. C.

#### CONDUCTIVITY OF SUPERCONDUCTING TIN FILMS AT 20 GHz

R. V. D'Aiello and S. J. Freedman

We have made a careful study of the linear conductivity of thin ( $\sim 150 - 400 \text{ \AA}$ ) superconducting tin films using 20 GHz microwaves in transmission-type experiments. Several studies of the linear microwave properties of superconducting thin films have been published.<sup>1, 2</sup> While the first of these studies indicate that the temperature dependence of the microwave conductivity of thin tin films may be described by the Mattis and Bardeen (MB) conductivity functions<sup>3</sup>, the recent paper by Soderman and Rose<sup>2</sup> shows significant deviation from the MB theory. Our experiments, which were undertaken to examine in detail the microwave conductivity of pure tin films, show excellent agreement with the MB theory.

The films were fabricated by evaporating spectroscopically pure tin (99.999% purity) from tantalum boats onto substrates held at  $80^\circ\text{K}$ . The pressure during evaporation was generally  $6-8 \times 10^{-7}$  Torr; the rate of evaporation was about  $25 \text{ \AA}/\text{sec}$ . The thickness of the films was measured interferometrically by the Tolansky technique.<sup>4</sup> To avoid agglomeration during the anneal to room temperature, the annealing technique described by Caswell<sup>5</sup> was used. Electron micrographs were taken of each film. Only films which showed microscopic continuity and no pin holes were used in the microwave experiments.

The dc resistance of the films was measured at room temperature and at temperatures from  $4.2^\circ\text{K}$  through the transition temperature ( $T_c$ ) which ranged from  $3.9^\circ\text{K}$  to  $4.1^\circ\text{K}$  for these films. The dc transitions were sharp, having a transition width of about  $10 \text{ m}^\circ\text{K}$ . The ratio of resistance at room temperature to that at  $4.2^\circ\text{K}$  was typically 4-5, and the resistance values agreed quite well with the Fuchs<sup>6</sup> theory of conduction in thin films. The room temperature resistance ranged from  $20 \text{ \Omega}/\text{sq}$ . for the thinnest films to about  $10 \text{ \Omega}/\text{sq}$ . for the thicker ones.

The quantities measured in the microwave experiments are  $|T_s/T_n|$  and  $(\theta_s - \theta_n)$ , the amplitude and phase of the transmission through the film in the superconducting state ( $s$ ) relative to that in the normal state ( $n$ ) at  $4.2^\circ\text{K}$ . The quantities are directly



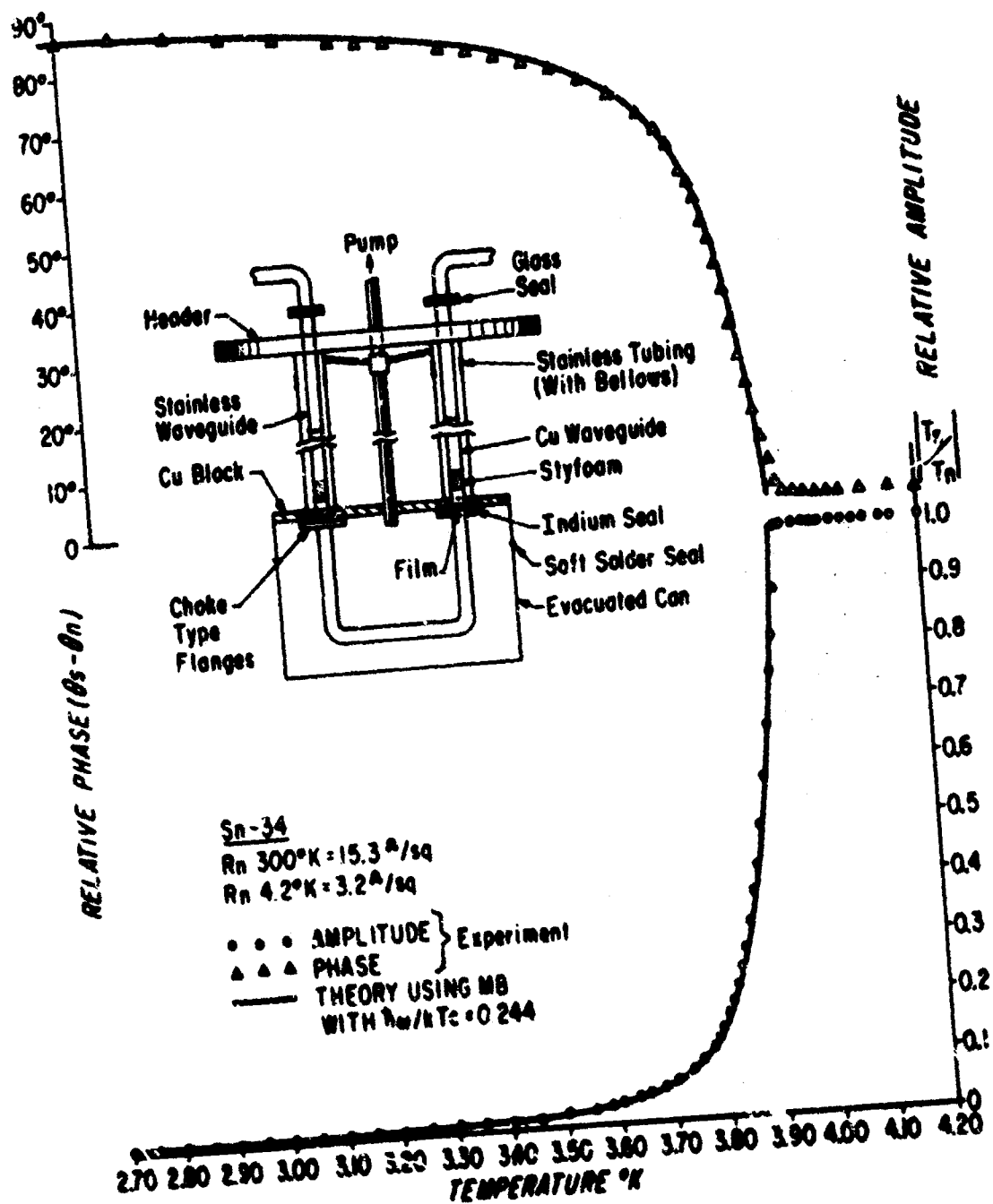


Fig. 1 The temperature dependence of the microwave transmission ratio  $T_s/T_n$  and relative phase  $\theta_s - \theta_n$  for a 200 Å tin film. The solid lines represent the amplitude and phase calculated using the Mattis and Bardeen conductivities. The inset shows the details of the enclosed waveguide and sample mount used in the transmission experiments.

related to the real ( $\sigma_1/\sigma_n$ ) and imaginary ( $\sigma_2/\sigma_n$ ) parts of the normalized film conductivity.<sup>7</sup>

After the films were removed from the vacuum system, they were placed directly across a section of K-band waveguide in a special flange-holder. The flange and holder incorporated an rf choke and indium seals in order to minimize the leakage of microwave energy around the film. (In our early experiments, where the films were simply placed between the waveguide flanges, the transmission at the lower temperatures was higher than the theory predicted, and in some cases nonreproducible bumps in the transmission were seen.)

The amplitude and phase of the transmitted signal relative to the incident signal as a function of temperature were measured using a conventional microwave bridge circuit. In the power range used ( $< 100\mu$  watts), the transmission ratio was independent of power level. The "U" shaped section of waveguide which is immersed in the dewar is enclosed in stainless steel tubing and a brass can as shown in the insert of Fig. 1, and is impervious to liquid helium. A small amount of helium transfer gas is used to provide the thermal coupling to the bath. The exclusion of the liquid helium from the waveguide is important in obtaining reproducible data. We have found in previous experiments that when helium was allowed to enter the guide, erratic data were obtained.

Figure 1 is typical of the transmission data obtained for a variety of tin films. The data are seen to be in excellent agreement with the transmission calculated using the Mattis and Bardeen conductivity functions (with  $\epsilon_0/kTc = 3.52$ ) and the measured dc resistance of the film. No adjustable parameters were used in plotting the theoretical curves. A number of other tin films were measured and displayed similar excellent agreement with the theory.

This work was performed at the RCA Laboratories, Princeton, New Jersey by R. V. D'Aiello as part of a doctoral thesis under the direction of Prof. S. J. Freedman. It was supported in part by the Dept. of the Navy, Office of Naval Research under Contract No. 0014-66-60311 with RCA Laboratories.

This work has been accepted for publication as a Note in the JAP.

Joint Services Technical Advisory Committee  
AF 49(638)-1402

R. V. D'Aiello

#### REFERENCES

1. N. M. Rugheimer, A. Lehoczky and C. V. Briscoe, Phys. Rev. 154, 414 (1967).
2. D. A. Soderman and K. Rose, J. A. P. 39, 2610 (1968).
3. D. C. Mattis and J. Bardeen, Phys. Rev. III, 412 (1958).
4. S. Tolensky, Multiple Beam Interferometry (Oxford Univ. Press, 1948).

5. H. L. Caswell and Y. Budo, J.A.P. 35, 644 (1964).
6. K. Fuchs, Proc. Camb. Phil. Soc. 34, 100 (1938).
7. R. E. Glover III and M. Tinkham, Phys. Rev. 108, 243 (1957).

### FLUCTUATION EFFECTS IN THE MICROWAVE CONDUCTIVITY OF GRANULAR SUPERCONDUCTING ALUMINUM FILMS

R. V. D'Aiello and S. J. Freedman

Schmidt<sup>1</sup> has shown that fluctuations of the Ginzburg-Landau parameter for temperatures above  $T_c$ , the superconducting transition temperature give rise to singularities in the electrical conductivity, indicating the onset of local superconductivity. This behavior manifests itself in an excess conductivity,  $\sigma_{11}^0$ , near  $T_c$  over the normal state value. For sufficiently thin films  $\sigma_{11}^0$  can be written as:

$$\sigma_{11}^0 = \frac{e^2}{16\pi d \epsilon} \left( \frac{\pi}{\omega} - \frac{2}{\omega} \arctan \frac{1}{\omega} - \frac{1}{\omega^2} \ln |1 + \omega^2| \right) \quad (1)$$

where the symbols have the following meanings:  $e$  - the electronic charge;  $\hbar$  - Planck's constant;  $d$  - film thickness;  $\epsilon$  - reduced temperature ( $= \frac{T - T_c}{T_c}$ );  $\omega$  - reduced frequency ( $= \frac{\pi \hbar \omega}{16 k T_c}$ ),  $k$  is Boltzmann's constant.

For small frequencies the expression (1) becomes:

$$\sigma_{11}^0 = \frac{e^2}{16\pi d \epsilon} (1 - \omega^2) \quad (2)$$

It is important to note that the excess conductivity is maximum in D.C. measurements, decreasing thereafter with frequency.

In the course of measurements on the microwave conductivity of granular Al films, we have obtained data on the details of the onset of superconductivity for both D.C. and 20 GHz excitation. The films are made by vacuum evaporation of pure Al in the presence of a controlled  $O_2$  pressure, typically  $10^{-4}$  Torr. We have shown elsewhere<sup>2</sup>, that such films are describable quite closely as BCS superconductors, their microwave impedance below  $T_c$  following the Mattis-Bardeen theory<sup>3</sup> within experimental error in spite of the fact that they consist largely of small ( $\sim 40 \text{ \AA}$ ) grains separated by a thin insulating oxide layer.

Here we wish to present a preliminary comparison of our data with Schmidt's theory. Typical data obtained for the films are shown in Fig. 1. The region of interest for the discussion is that above  $T_c$  so only nearby points are plotted. The circles represent experimental points taken with D.C. excitation; the triangles those with 20 GHz excitation. The solid line is a plot of Eq. 2 for  $\omega = 0$ . It is important to note that in drawing this theoretical curve we have fitted the data at the point indicated by the large

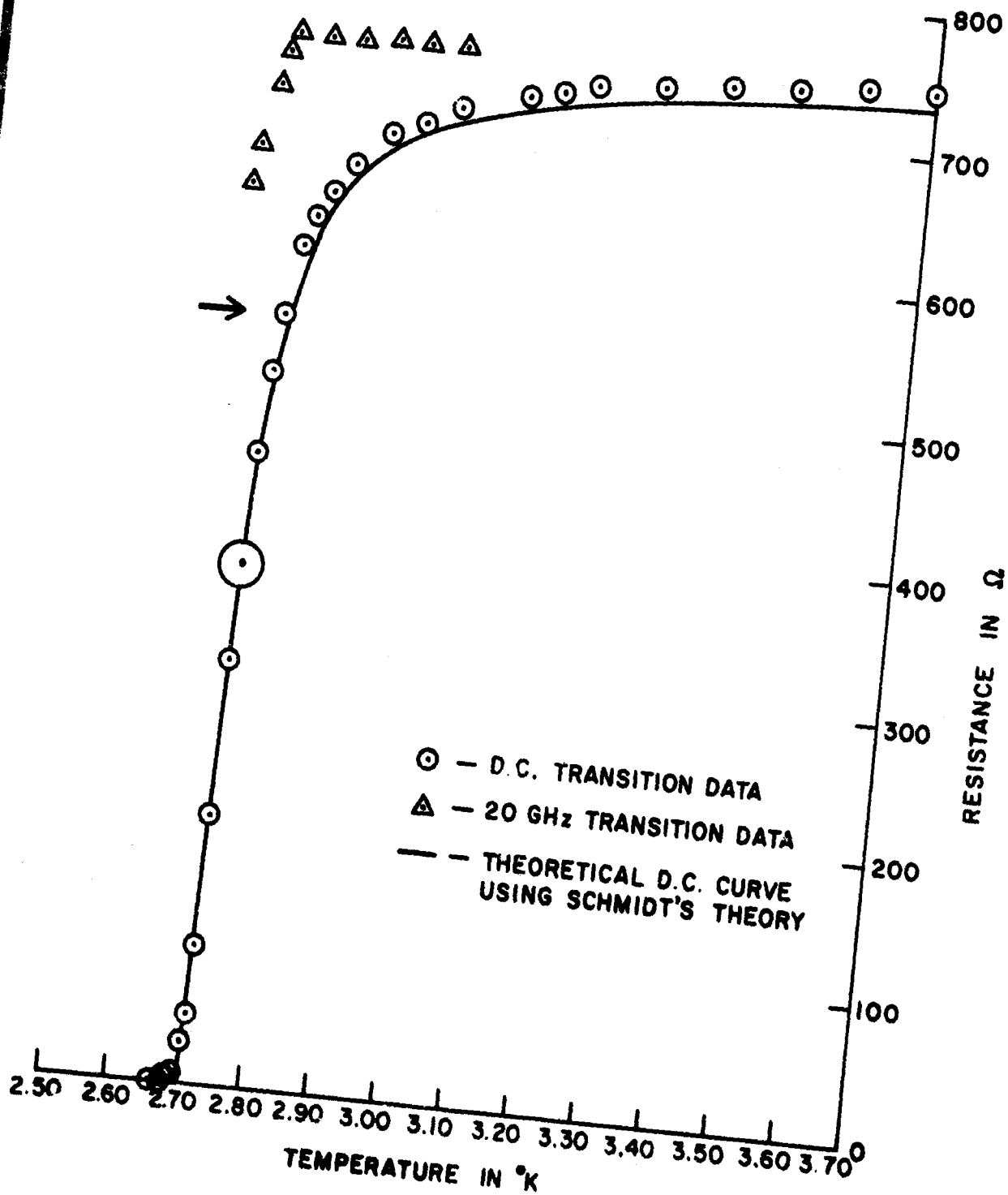


Figure 1

circle. This is somewhat arbitrary, but it can be seen that fitting at any point slightly above  $T_c$  will yield essentially the same result. We remark here that the agreement with the D.C. data seems satisfactory. The same is not true, however, with the 20 GHz data. If one calculates, for the point indicated by the arrow, the ratio of  $\sigma_{11}^0$  (20 GHz) to  $\sigma_{11}^0$  (D.C.) one obtains  $\sim 0.7$ . This means that a departure from the normal state resistivity (which is very nearly constant for a few degrees above  $T_c$ ) of 0.7 of that obtained in the D.C. measurements should appear in the microwave data. Although some rounding close to  $T_c$  is apparent, quantitatively nothing like the predicted conductivity is obtained. The situation gets worse farther above  $T_c$ . A decrease with frequency is obtained.

In obtaining Eqs. (1) and (2), Schmidt used the time dependent Ginzburg-Landau (GL) equation of Abrahams and Tsuneto<sup>4</sup>, which was also derived later by Caroli and Maki<sup>5</sup>. The data presented here are in some sense a test of this equation. Our preliminary conclusion, therefore, is that this equation does not adequately describe relaxation phenomena in a typical BCS superconductor. It should be remarked that other workers have derived time dependent GL equations<sup>6</sup> differing in some detail from that used by Schmidt. We are planning to attempt extensions of Schmidt's theory using other forms for the equations.

The authors are indebted to Dr. R. Cohen for bringing Schmidt's theory to their attention and to Dr. H. Schmidt for making a preprint available to us. This work was supported in part by the RCA Laboratories.

Joint Services Technical Advisory Committee  
AF 49(638)-1402

S. J. Freedman

#### REFERENCES

1. Hartwig Schmidt - To be published
2. R. V. D'Aiello and S. J. Freedman - To be presented at The Conference on Applied Superconductivity, Gatlinburg, Tenn. Oct. 1968; Submitted for publication in J.A.P
3. D. C. Mattis and J. Bardeen, Phys. Rev. 111, 412 (1958).
4. F. Abrahams and T. Tsuneto, Phys. Rev. 152, 416 (1966).
5. C. Caroli and K. Maki, Phys. Rev. 159, 306 (1967).
6. E. R. Pike, Lectures at the NATC Advanced Summer Study Institute on Superconductivity, Montreal, Canada, (1968).

#### THIN FILM DIODES

M. A. Eschwei and J. Hara

In order to study tunneling mechanisms which have so many important applications today, we have been attempting to make a thin film vacuum diode. Such a diode, if it could be made, would have important advantages for basic study over those using

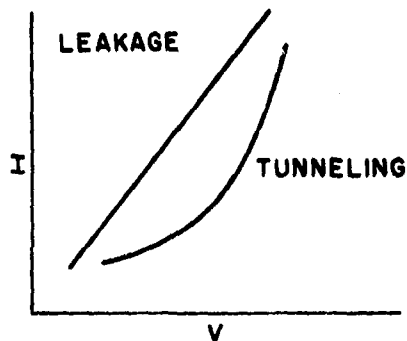


Fig. 1 Current-Voltage Relationships

dielectric or oxide barrier layers. The oxide or dielectric layers introduce variables and unknown quantities such as exact thickness and composition, whereas the vacuum gap can be easily varied and determined.

Two approaches to the vacuum gap diode have been tried. One makes use of a film sandwich of gold, silver and gold. Gold is used as the electrodes because good crystal structure can be obtained and it can withstand etching solutions. The silver film is etched out leaving a space which is accurately determined by measuring the thickness of the silver film by multiple beam interferometry. The diode is tested under vacuum so that the gap is free of absorbed gases.

The other approach consists of two optical flats on which electrodes and chromium spacer films are evaporated. The flats are then clamped together with the variable thickness chromium spacer films providing the vacuum gap separation between the electrode films. In both cases the measured current-voltage relationship should indicate either tunneling or leakage (Fig. 1).

Further work on the gold-silver-gold sandwich diode was done in an attempt to prevent collapse of the top gold film when the separating silver film is etched out, and also to make sure the resulting gap is free of etching and washing residue. The diode consisted of crossed gold films separated by a silver film which was etched out later. Masking during evaporation of the films was such that spots of bottom gold and silver were evaporated under the top gold and contact films so that they would be the same height as the top gold of the cross junction. The mica substrates were fastened to glass backing plates with Rigidax Type W1 Green Wax to prevent flexing, and narrow top glass strips were fastened over the end contacts and across the junction to prevent collapse of the top gold film (Fig. 2). Some film sandwiches were also made on glass substrates, but the gold lifted off the glass during the acid etch. An undercoat of silicon monoxide improved adhesion. Thick silver films of 1100-1300 Å were used to separate the gold films. Etching (1%  $\text{HNO}_3$  as previously reported) again seemed to be complete and the junctions looked good, but testing still indicated a short between the films. The salts or

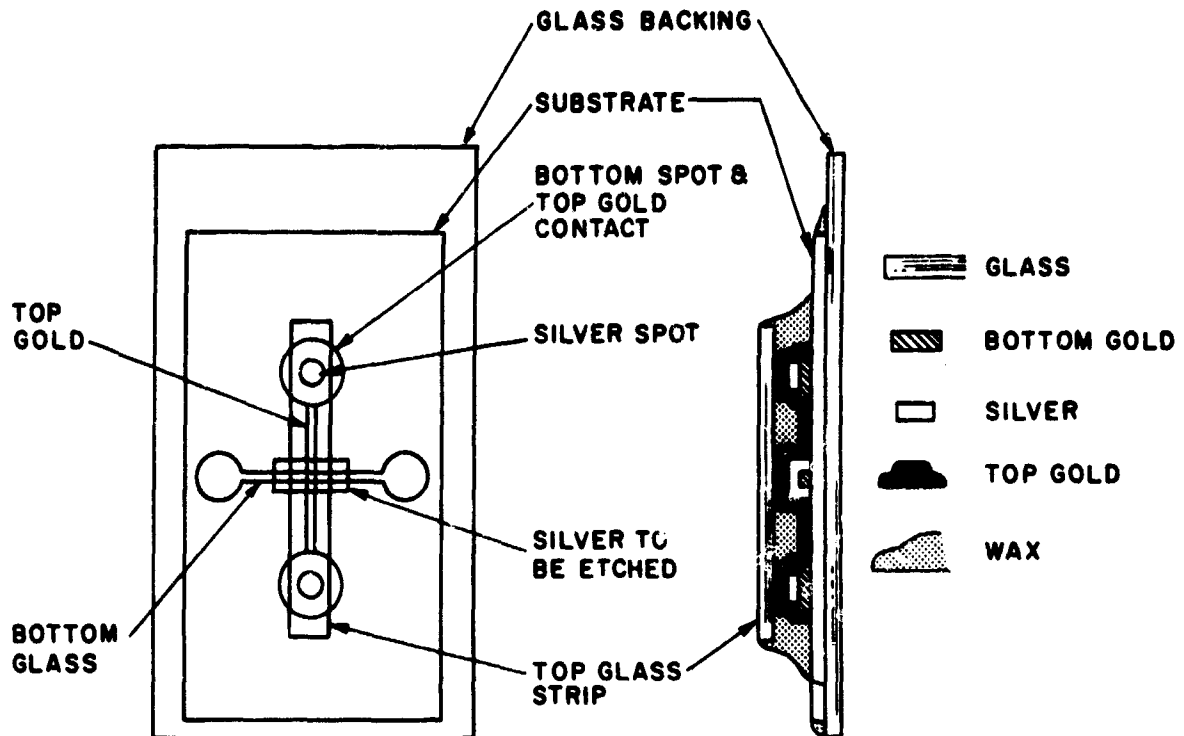


Fig. 2 Cross Film Diode with Backing Glass

possibly acid or water left after washing and drying may well be the cause of the short. Complete cleansing and drying of this very small gap is very difficult. The temperature cannot be raised above  $60^{\circ}\text{C}$  during bake-out to drive out moisture without softening the wax and causing film shift and rupture.

In order to eliminate the wax support system and thus allow a higher bake-out temperature, a different top film support was tried. A narrow piece of glass with a strip of gold film evaporated on it was clamped directly over the top gold film. It was hoped that thermocompression bonding would hold the gold films together and thus prevent collapse of the top gold film after the removal of the silver. The clamping was done before etching and maintained during washing, drying and testing. This method has not been successful so far. Films have been left in .5%  $\text{HNO}_3$  acid solution up to five weeks and the visible silver has not been completely removed. Stronger acid solutions and an addition of a wetting agent are now being tried.

Several film configurations were tried for the optical flat type film diode. Single junction pairs of silver films (Fig. 3) were made and tested, first with silver as a spacer film, then chromium (chromium is harder and less subject to compression or scratching during clamping). Since this method requires no etching of the sandwich, any metal may be used for the electrodes. Silver was chosen because it forms a crystalline film rather easily. The spacer films were  $3600 \text{ \AA}$  for the silver and  $3100 \text{ \AA}$  and  $2230 \text{ \AA}$  for the

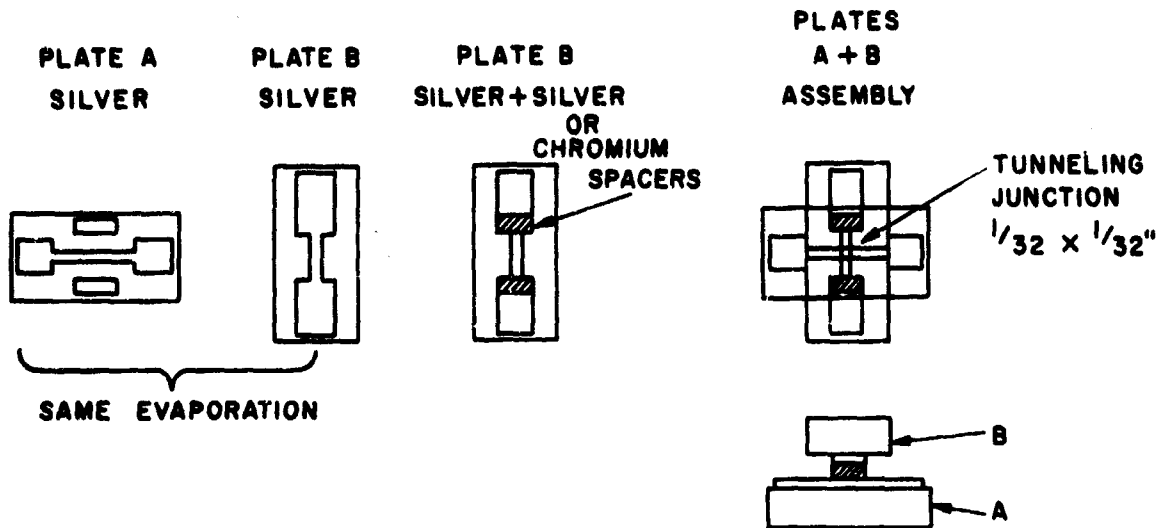


Fig. 3 Single Junction Optical Flat Diode

chromium. Etching off the silver posts on Plate A results in another spacing to be tested, the thickness of the chromium film minus that of the silver film. In this way tests were made of spacings of approximately  $3600 \text{ \AA}$  down to  $380 \text{ \AA}$ . There were no shorts at these spacings but also no tunneling.

Next a series of film arrays with five junctions (Fig. 4) was made. These plates have several advantages. The aligning holes allow the plates to be assembled on a jig so that the films cannot be moved against each other and thus scratch the films. An obvious advantage is the fact that there are five film junctions to check on each substrate pair. Random waviness or deviations from optical flatness across the substrates may make it impossible to obtain correct spacing for tunneling at the junction, while it may be just

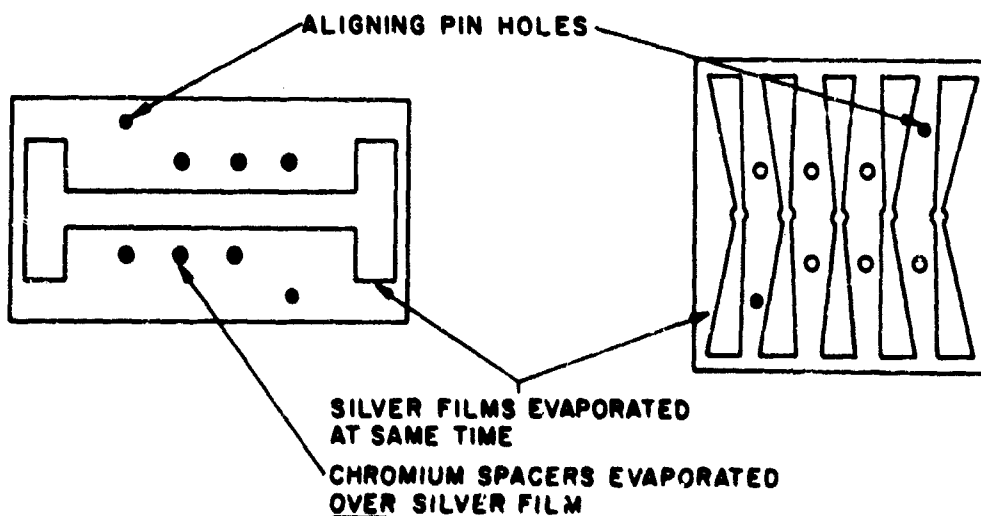


Fig. 4 Five Junction Optical Flat Diodes



right at another. We have been using surplus reflector plate glass for these substrates and have continued with silver films and chromium spacer-posts.

The five junction sandwiches were first tested for shorts and open conditions. It was found upon releasing or tightening the two screws holding the two plates together that one could vary the resistance of the appropriate junction from a few ohms to more than  $100M\Omega$ . Since this test was made at around 20 volts a closer look at the V-I characteristics was imperative.

A series of tests were made applying first ac voltages of about 1kc and a few hundred millivolts. This resulted in nonlinear characteristics resembling those of tunneling. The low and high ranges of voltages and currents were limited in the ac test, and therefore data was taken with an X-Y Recorder with a range of a few microamps to about 20 milliamps. The voltage applied across the junction was a variable dc voltage from a battery supply and the current was measured through a set of precision resistors.

The analysis of these curves tends to indicate very strongly that the observed results are very akin to tunneling. Some numerical calculations allowed us to obtain a few absolute parameters. One of the problems with this configuration was its mechanical instability which rendered duplication of data very difficult. A few questions remain unanswered such as current drift and a sudden shorting or opening of the junctions as voltages are being applied.

The next step will involve improvement in the mechanical clamping to obtain a more stable junction. Control of the environmental conditions will be made through a set of experiments under vacuum. Measurements on first and second derivatives of the current vs. voltages will give us enough information about the potential barrier and its parameters. Further refinements should include the use of very good optical flats and accurate control of the spacing, possibly via the use of piezoelectric devices.

It should be possible to obtain tunneling in this way when the proper spacing is maintained. The major difficulty will probably be the exact measurement of the space between the silver electrodes, since perfect optical flats would be necessary to assume that it is the thickness of the chromium or chromium minus silver film. Capacitance measurements might be a further check. With this design it might also be possible to determine spacing mechanically by incorporating piezoelectric devices for accurately controlled movement of the optical flats. The major advantage of the optical flat diode is that the films are clean, with no acid or salt residue.

Some work has also been started on the more conventional tunnel diode film configuration using a barrier film of anodized tantalum. Tantalum films from 200-450 Å thick were evaporated by use of an electron beam gun on both 7059 glass and mica substrates and also on films of silver and silver-gold. Good quality resistance monitored

films were obtained by placing a tantalum shield over the electron gun source. By cutting down electron or ionized gas bombardment of the test strip with this shield it became possible to read resistance accurately during evaporation. Non-uniformity and cracking of the films which occurred during earlier runs were also eliminated. The shield kept the radiant heat from the source to a minimum so that the substrate temperature could be controlled more easily during evaporation.

The tantalum was anodized in an oxalic acid, ethylene glycol, water solution at room temperature using a simple dc circuit with a 300v power supply controlled by a 1000  $\Omega$  potentiometer connected in parallel. The voltage was gradually increased keeping the current below 2ma per square inch until increased voltage resulted in no current flow. A band of stop-off lacquer painted across the film prevented the more rapid anodization of the film which occurs at the surface of the electrolyte and which causes a circuit break preventing complete anodization of the film in the electrolyte. Some films were completely immersed and held by specially made tantalum clips. Everything in the circuit in the bath must anodize or the film will be by-passed.

The tantalum films on glass and mica anodized completely leaving an almost colorless, adherent film which was non-conducting. The tantalum films evaporated across the silver and gold films presented a problem. The tantalum film evidently did not form a continuous film at the base metal step (films were 1200-1400  $\text{\AA}$ ) and a breakdown occurred along these film edges with the current going to the base film almost immediately and not anodizing the tantalum. Any base film electrode will have to be as thin as possible to minimize the thick step, or it should be under all the tantalum film in the bath thus eliminating the step completely. Possible leakage through the edges of the film can be prevented by application of stop-off lacquer. Work will be continued along these lines.

National Aeronautics and Space Administration  
NsG 589

M. A. Eschwei

#### ELECTRON SHIELDING IN HEAVILY DOPED SEMICONDUCTORS

J. B. Krieger

In the usual calculation of the energy levels of an electron bound to a donor atom in a doped semiconductor,<sup>1</sup> the binding energy relative to the conduction band minima is obtained for a single impurity atom in the crystal. However it is well known, experimentally, that the binding energy of the electron decreases as the number of donors increases until at some critical impurity concentration there is no observed activation energy.<sup>2</sup>

A possible explanation of this phenomena arises from the interaction between electrons bound on different impurity centers.<sup>3</sup> As the average distance between donors

is decreased due to increasing impurity concentration, the wave functions of electrons on different donors will significantly overlap. For small overlap, the impurity levels will be broadened, but for strong overlap this electron-electron repulsion can destroy the bound state. However, it has been observed by Li et al.<sup>4</sup> that this effect cannot explain the fact that the electron binding energy vanishes for impurity concentrations as low as  $10^{14}/\text{cm}^3$  for InSb. In order to account for this, these workers calculated, considering only S wave scattering, the Hartree self-consistent field that an electron experiences due to the singly ionized impurity atom and the screening from conduction band electrons. They calculate the ionization energy over a wide range of conduction band electron concentrations and for several different temperatures. Most significantly, they find that for  $n \approx 6 \times 10^{13}/\text{cm}^3$  donors, the binding energy becomes zero.

In this note we wish to point out that the latter result is a special case of a more general statement given by Mott<sup>5</sup> developed in the course of his investigations on the insulator metal transition. We have generalized Mott's calculation to obtain the ionization energy as a function of  $N$ , the concentration of conduction band electrons and the temperature and find a different  $T$  dependence from that given by Li et al. besides finding a smoother  $N$  dependence near the critical concentration. Finally, we show that it is possible to induce a Mott transition by applying stress to a degenerately doped many-valley semiconductor with a resultant transition from the metal phase to the insulating phase.

National Science Foundation  
GU-1557

J. B. Krieger

#### REFERENCES

1. W. Kohn and J. M. Luttinger, Phys. Rev. 97, 860 (1955).
2. G. L. Pearson and J. Bardeen, Phys. Rev. 75, 865 (1949).
3. C. Hilsum and A. C. Rose-Innes, "Semiconducting III - V Compounds," (Pergamon Press, Inc., New York, 1961) p. 73.
4. S. P. Li, W. F. Love and S. C. Miller, Phys. Rev. 162, 728 (1967).
5. N. F. Mott, Phil. Mag. 6, 287 (1961).

#### ELECTROCHEMICAL BEHAVIOR OF OXIDE FILMS ON SEMICONDUCTORS AND METALS

F. C. Collins, C. Chiang, M. Schragar and L. Chen

##### Introduction:

The studies of the kinetics of thermal growth of oxide films on semiconductors and metals and the properties of these films discussed in earlier reports have been continued. During the current period, these have involved studies of the thermal growth of oxide films on silicon and chromium single crystals and studies of ionic migration in titanium dioxide films.

**Kinetics of the Thermal Growth of Oxide Films on Single Crystalline Chromium:**

An intensive study of the kinetics and mechanisms of the thermal oxidation of chromium has been commenced.

The chromic oxide crystal has a hexagonal crystal structure. Sailors, Liedl, and Grace<sup>1</sup> found that the oxide film thermally grown on chromium is highly oriented which might lead one to predict differing growth rates on different crystal faces of the metal crystal. Gwathmey, Leidheiser, and Smith<sup>2</sup> however reported that the oxidation rate was the same on all crystal planes.

High purity polycrystalline wafers of 3/4" diameter and 1/16" thickness were polished to mirror smoothness as observed under a microscope of 50 x magnification and was subsequently cleaned and rinsed in several solvents. The wafers were oxidized at 600°C in 24 torr of water vapor with added argon to bring the total pressure to 1 atm. The oxidizing ambient was maintained at a flow rate of 5 cm. per minute. A sharply varicolored chromic oxide film was observed after several hours, the interference colors indicating large differences in the growth rates of the oxide on the surfaces of the various oriented crystal grains in the sample.

All subsequent work is being carried out on a single crystal specimen. The orientation of the crystal was determined and the crystal cut and polished to expose the (100) plane.

The oxide film thickness is being determined by a combination of an optical interferometric method and infrared absorption by reflectance measurements. The measurements indicate a single absorption peak centered at 13.7 $\mu$ . This contrasts with the absorption spectrum for solid chromic oxide dispersed in a KBr wafer which yields absorption peaks at 15.5 $\mu$  and 17.5 $\mu$ . The thickness of the films we have studied are all less than 1 $\mu$  so that the interference effects here should be negligible.

The infrared optical density requires calibration against the oxide films thickness as determined by an absolute method. The Tolansky interference method is being used for this purpose. However, it cannot be applied in the usual manner as it is impossible to provide the necessary step boundary of the film by etching as the oxide is extremely inert chemically. Instead, a method has been devised which involves masking part of the oxide with an evaporated silver film. The thickness of the oxide plus the silver film is then determined by interference between the light transmitted through the oxide and reflected by the chromium and the light reflected by the silver surface. The thickness of the silver film is later determined by the conventional Tolansky technique. Monochromatic light of 550 $\mu$  is used which corresponds to a minimum in absorption of the optical absorption spectrum.

**Effect of an Applied Electric Field on the Thermal Growth of Silicon Dioxide Films :**

Previous reports have described the objectives and preliminary results obtained in this study.

The system now being investigated consists of a single crystalline slab with opposite faces mechanically polished. One side is thermally oxidized to an initial thickness of  $600 \text{ \AA}$ . An evaporated platinum electrode provides an ohmic contact to the unoxidized side and a second platinum electrode is evaporated on top of the oxide.

A steady current of the order of  $1 \mu\text{A}$  is passed through the oxide film in the direction corresponding to the anodic oxidation process. The constant electric field thus generated in the film is of the order of  $5 \times 10^5$  volts/cm. The oxide film growth process is carried out at  $580^\circ\text{C}$  in a dry oxygen ambient.

The linear relation between the applied potential and the time which was previously reported has been reconfirmed. As expected, the oxide film growth rate depends upon the thickness of the platinum electrode. Experiments at constant applied potential are in progress. Here we expect to find a parabolic growth rate law.

**Ionic Migration in Titanium Dioxide Films :**

One of the major problems of metal-oxide-semiconductor (MOS) devices has been their lack of long term electrical stability. In the case of silicon-silicon dioxide-metal devices, it has been found that the major cause of this instability is ionic migration in the oxide layer.

The capacitance of the MOS device is voltage dependent because of the carrier density dependence in the surface layer of the oxide upon the applied potential. Large lateral shifts in the C-V curves are produced by a pretreatment which involves biasing the device at elevated temperature and then quenching to room temperature under bias. The shift in the potential at which the characteristic dip in the capacitance occurs (flat band potential) is explained by a drift of cations through the oxide films to the semiconductor surface.

We have extended this technique to study ionic migration in dielectric films other than semiconductor oxides. A study is being made of the MOCS system  $\text{Si-SiO}_2 - \text{TiO}_2 - \text{Au}$ . Both a  $\text{Si-SiO}_2 - \text{Au}$  (MOS) device and the MOCS device are constructed on the same wafer. The elevated temperature bias experiment is performed on both devices. The magnitude of the ionic drift is found by subtracting the flat band potential for the MOS device from that of the MOCS device.

The results indicate that the drift in the  $\text{TiO}_2$  layer is also cationic and is of the same order of magnitude as that usually found in the  $\text{SiO}_2$  layer. However, the temperature at which major ionic migration occurs in  $\text{TiO}_2$  is of the order of  $80^\circ\text{C}$  rather

than 150°C required for the migration in SiO<sub>2</sub>. The thermal activation energy for ionic migration in TiO<sub>2</sub> is 50 kcal/mole.

The C-V shifts observed after biasing the TiO<sub>2</sub> layer at 90°C for the variable time  $t$  can be expressed as

$$V_{FB}(90^\circ\text{C}) = V_{FB}^\infty(90^\circ\text{C}) [1 - e^{-t/\tau}] - 6.0$$

where  $V_{FB}$  is the observed flat band potential after biasing for the time  $t$ ,  $V_{FB}^\infty$  is the extrapolated flat band potential for infinite time, and  $\tau$  is a relaxation time which was found to be 13.7 min. The minimum flat band potential which was observed under any conditions was -6.0 volts.

Joint Services Technical Advisory Committee  
AF 49 (638)-1402

F. C. Collins

#### REFERENCES

1. R. H. Sailors, G. L. Liedl & R. E. Grace; J. Appl. Phys. 38 4928, 1967.
2. A. T. Gwathmey, H. Leidheiser & G. P. Smith; Nat. Advisory Comm. Aeron., Tech. Notes, No. 1460.14, 1948.

#### MICROWAVE CONDUCTIVITY OF POLAR SEMICONDUCTORS IN THE PRESENCE OF HIGH ELECTRIC FIELD

P. Das and R. H. Rifkin

The frequency-dependent small-signal conductivity of polar semiconductors in the presence of high steady electric field is calculated theoretically taking into consideration both the momentum and energy relaxation times. The results obtained are compared with experiments carried out on InSb.

The microwave conductivity of semiconductors in the presence of high steady electric field has been studied experimentally in germanium by Gibson et al.<sup>1</sup> and Gunn<sup>2</sup> and in InSb by Koechner.<sup>3</sup> It is found that the small-signal microwave conductivity is dependent on (a) the orientation of the applied signal with respect to the steady field<sup>4</sup> and (b) the frequency of the applied signal. Theoretically, considering the effects of field-dependent energy and momentum relaxation time, one can calculate the different microwave conductivities. For germanium, the theoretical calculation agrees with experimental results.<sup>1, 4, 5</sup> For InSb, the anisotropy of the microwave conductivity for perpendicular and parallel orientation was explained by the 2-stream instability theory.<sup>3</sup> Recently, Potzl and Richter<sup>6</sup> have done further experiments at different frequencies and suggested that hot-electron theories alone can explain the whole phenomenon. In this letter, the results of the theoretical calculation of hot-electron microwave conductivity for polar semiconductors are reported which question Potzl and Richter's suggestion.

The semiconductor is assumed to have a single valley with isotropic effective mass. The carrier concentration is considered to be greater than the critical value, so that the displaced Maxwellian distribution function with effective hot-electron temperature is valid;<sup>7</sup> so the distribution function of the carriers can be written as

$$f(\vec{K}) = n \left( \frac{\pi}{mkT} \right)^{3/2} \exp \left\{ - \left( \frac{\hbar^2 \gamma}{2mk\theta} \right) |\vec{K} - \vec{d}|^2 \right\}$$

where  $n$  is the carrier concentration,  $m$  is the effective mass,  $T$  is the effective temperature,  $\vec{d}$  is the displacement in the wave-vector ( $\vec{K}$ ) space of the carriers,  $\gamma = \theta/T$ , where  $\theta$  is the characteristic polar optical-phonon temperature of the material,  $k$  and  $h$  are Boltzmann's and Planck's constants, respectively, and  $\hbar = h/2\pi$ .

In the presence of an applied electric field  $\vec{F}$  given by

$$\vec{F} = \vec{F}_0 + \lambda \vec{F}_0 e^{j\omega t}$$

where  $\lambda \ll 1$ , one can assume a small perturbation of the following quantities:

$$d = d_0 + \lambda d_1 e^{j\omega t}$$

$$\gamma = \gamma_0 + \lambda \gamma_1 e^{j\omega t}$$

The subscript '0' refers to the d. c. or unperturbed values and '1' refers to the difference between the perturbed and the d. c. values. Thus there are four unknown quantities, and these are obtained by the energy- and momentum-balance equations which are calculated from the time-dependent Boltzmann transport equation including the effects of energy and momentum relaxation times. The field-dependent d. c. and micro-wave conductivities can be calculated from the following expressions;

$$\sigma_0(\gamma) = \frac{ne\hbar}{m} \frac{d_0}{F_0}$$

$$\sigma_m(\gamma) = \frac{ne\hbar}{m} \frac{d_1}{F_0}$$

Considering polar optical-phonon scattering only, one obtains

$$\sigma_0 = - \frac{n}{M}$$

$$\sigma_m = \sigma_0 \frac{ME' - EM' - j\omega \frac{a}{n} M}{ME' + EM' + \frac{ab}{n} \omega^2 + j\omega (bE' - \frac{a}{n} M)}$$

where

$$E = \alpha \gamma_0^{1/2} (e^{\gamma_L - \gamma_0} - 1) e^{\gamma_0/2} K_0 \left( \frac{\gamma_0}{2} \right)$$

$$M = \beta \gamma_0^{1/2} \left\{ \frac{1}{2} \gamma_0 (e^{\gamma_L - \gamma_0} - 1) e^{\gamma_0/2} K_0 \left( \frac{\gamma_0}{2} \right) + \frac{\gamma_0}{2} e^{\gamma_0/2} K_1 \left( \frac{\gamma_0}{2} \right) X (e^{\gamma_L - \gamma_0} + 1) \right\}$$

$$a = \left( \frac{2k\theta}{\pi m} \right)^{1/2} (e F_\phi N_0)$$

$$\beta = \frac{4}{3} \left( \frac{m}{2\pi k\theta} \right)^{1/2} \left( \frac{F_\phi N_0}{e} \right)$$

$$F_\phi = \left( \frac{mek\theta}{\hbar^2} \right) (\epsilon_{ra}^{-1} - \epsilon_r^{-1})$$

$\epsilon_{ra}$  and  $\epsilon_r$  are the high-frequency and static relative permittivities, respectively;  $\gamma_L = \theta/T_L$ , where  $T_L$  is the lattice temperature,  $N_0 = (\exp \gamma_L - 1)^{-1}$ ,  $e$  is the electronic charge and  $K_0$  and  $K_1$  are modified Bessel functions of zero and first order, respectively.

$$a = \frac{3}{2} \frac{k\theta}{\gamma_0}$$

$$b = m/e^2$$

$a$  and  $b$  are related with energy and momentum relaxation times  $\tau_E$  and  $\tau_m$  by the following relations:

$$\tau_m = b/M$$

$$\tau_E = a n \gamma_0^2 (\gamma_L - \gamma_0) (E(\gamma_0))$$

The above d. c. and microwave conductivities are functions of  $\gamma_0$ , which is related to the electric field by the relation

$$F_0 = \sqrt{(E X M)}$$

It is to be noted that  $\sigma_m$  is a complex quantity and actually can be written as

$$\sigma_m = \sigma(\omega) + j\omega \epsilon'(\omega)$$

where  $\epsilon(\omega)$  represents the change in relative permittivity. From the expression for  $\sigma_m$ , it is easily noted that

$$\lim_{\omega \rightarrow 0} \sigma_m = \sigma_0 \frac{ME' - M'E}{ME' + M'E} = \sigma_{\text{slope}} = \left. \frac{dJ}{dF} \right|_{F_0}$$



where  $\sigma_{\text{slope}}$  is the slope conductivity at the bias point  $F_0$ . For negligible effect of momentum relaxation time, one can easily show that  $\sigma_m$  approaches  $\sigma_0$  as  $\omega$  tends to infinity.

Numerical calculations have been done using a computer and are shown in Figs. 1a and b. The following conclusions can be drawn from the numerical results:

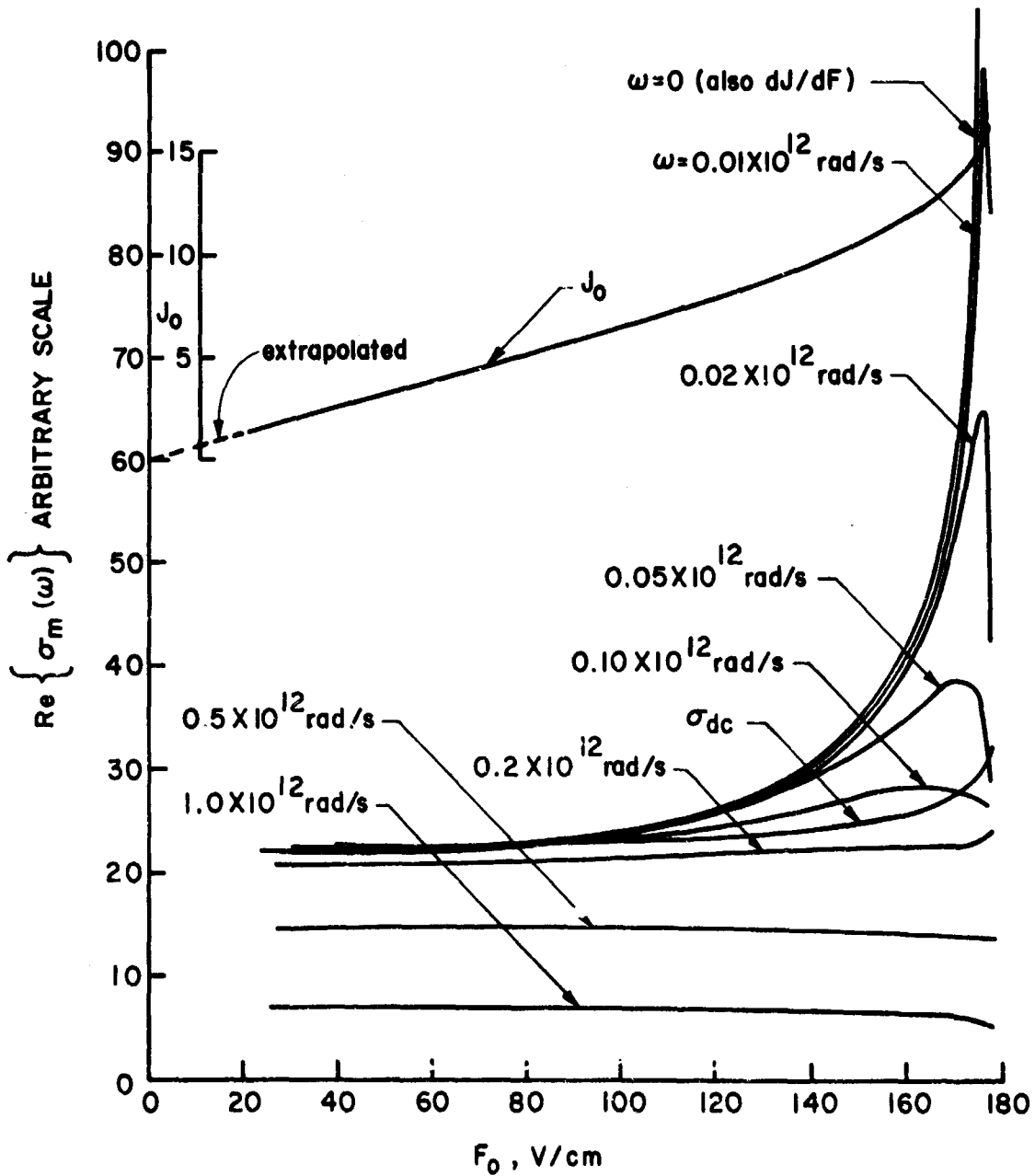


Fig. 1 (a)

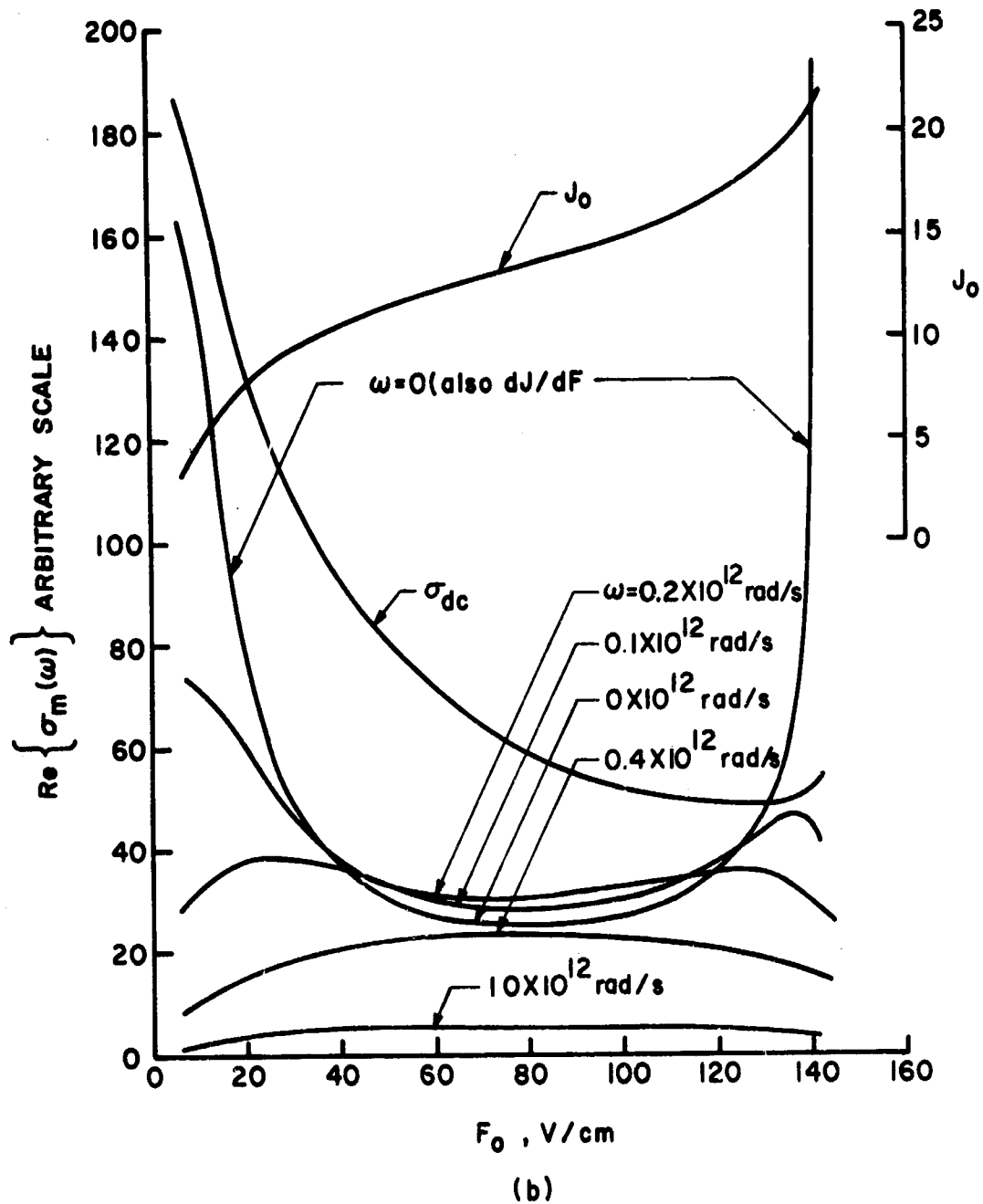


Fig. 1  $\text{Re} \{ \sigma_m(\omega) \}$  against  $F_0$  for n-type InSb. (a)  $T_L = 300^\circ\text{K}$ ; (b)  $T_L = 77^\circ\text{K}$ .

$$m = 0.013 \text{ X electron mass, } F_\phi = 328 \text{ V/cm}$$

(a) At  $300^\circ\text{K}$ ,  $\sigma_{\text{slope}}$  is always larger than  $\sigma_{\text{dc}}$ . As a function of frequency, the real part of  $\sigma_m$  is equal to  $\sigma_{\text{slope}}$  at low frequencies ( $\omega \approx 10^{10}$  rad/s), and as

frequency increases it approaches  $\sigma_{dc}$  ( $\omega \approx 10^{11}$  rad/s). For further increases in frequency it becomes much less than  $\sigma_{dc}$ .

(b) At 77°K,  $\sigma_{slope}$  is always smaller than  $\sigma_{dc}$ , except for fields near the dielectric-breakdown value. For frequencies around  $10^{11}$  rad/s, the real part of  $\sigma_m$  is slightly greater than  $\sigma_{slope}$ , but it is still much less than  $\sigma_{dc}$ . For larger frequencies ( $\omega \approx 10^{12}$  rad/s) it becomes much less than  $\sigma_{slope}$ . These results show that Kochner's experimental results cannot be explained by considering high-frequency relaxation effects as suggested by Potzl and Richter.

(c) The imaginary part of  $\sigma_m$  varies significantly with the applied field and with frequency. Thus measurements of the change in relative permittivity may add to the knowledge of microwave hot-electron conduction in polar semiconductors.

(d) It is to be emphasized that the theory presented is only valid for semiconductors with high carrier concentration. Also the acoustic-phonon scattering has not been taken into account, which may have significant contributions at 77°K. It is to be noted that electric field  $F_0$  is dependent upon  $F_\phi$  which strongly depends upon the parameters used for InSb. Because of this fact, the graphs presented do not agree quantitatively with the experimental results; however, the frequency dependence exhibited is nearly independent of  $F_\phi$ .

Further calculations will include ionized-impurity scattering. It is expected that a better agreement with experiment will result.

Joint Services Technical Advisory Committee  
AF 49(638)-1402

P. Das and R. H. Rifkin

U.S. Army Research Office, Durham  
DA-31-124-ARO(D)-307

#### REFERENCES

1. A. F. Gibson, J. W. Granville and E. G. S. Paige, "A Study of Energy-Loss Processes in Germanium at High Electric Fields using Microwave Technique," *J. Phys. Chem. Solids*, 1961, 19, pp. 198-217.
2. M. W. Gunn, "The Microwave Conductivity of Germanium," *Proc. Inst. Elect. Electronics Engrs.*, 1964, 52, p. 851.
3. W. Kochner, "Investigation of the Two-Stream Instability in InSb.," *ibid.*, 1965, 53, pp. 1234-1235.
4. P. W. Staecker, and P. Das, "Hot Electron Microwave Rotator," *ibid.*, 1965, 53, pp. 1766-1768.
5. B. R. Nag and P. Das, "Microwave Conductivity of Semiconductors in the Presence of High Steady Electric Fields," *Phys. Rev.*, 1963, 132, pp. 2514-2520.
6. H. W. Potzl and K. Richter, "Microwave Conductivity Anisotropy of Hot Electrons in n-InSb at 77°K.," *Proc. Inst. Elect. Electronics Engrs.*, 1967, 55, pp. 1497-1498.
7. R. Stratton, "The Influence of Inter-Electronic Collisions on Conduction and Breakdown in Polar Crystals," *Proc. Roy. Soc.*, 1958 [A], 246, pp. 406-422.

### TRANSPORT PROPERTIES OF COMPOUND SEMICONDUCTORS AT HIGH ELECTRIC FIELDS

R. Bharat and P. Das

In several of the p-type III-V compound semiconductors, the dependence of the energy  $E$  of holes on wave-vector  $k$  is expected to contain a linear term in addition to the usual parabolic term<sup>1, 2</sup>. As a result, in the vicinity of the energy maximum (which is displaced from  $k = 0$ ), the effective mass of holes depends on their energy. Further, as the valence-band constant-energy surfaces are warped, the effective mass

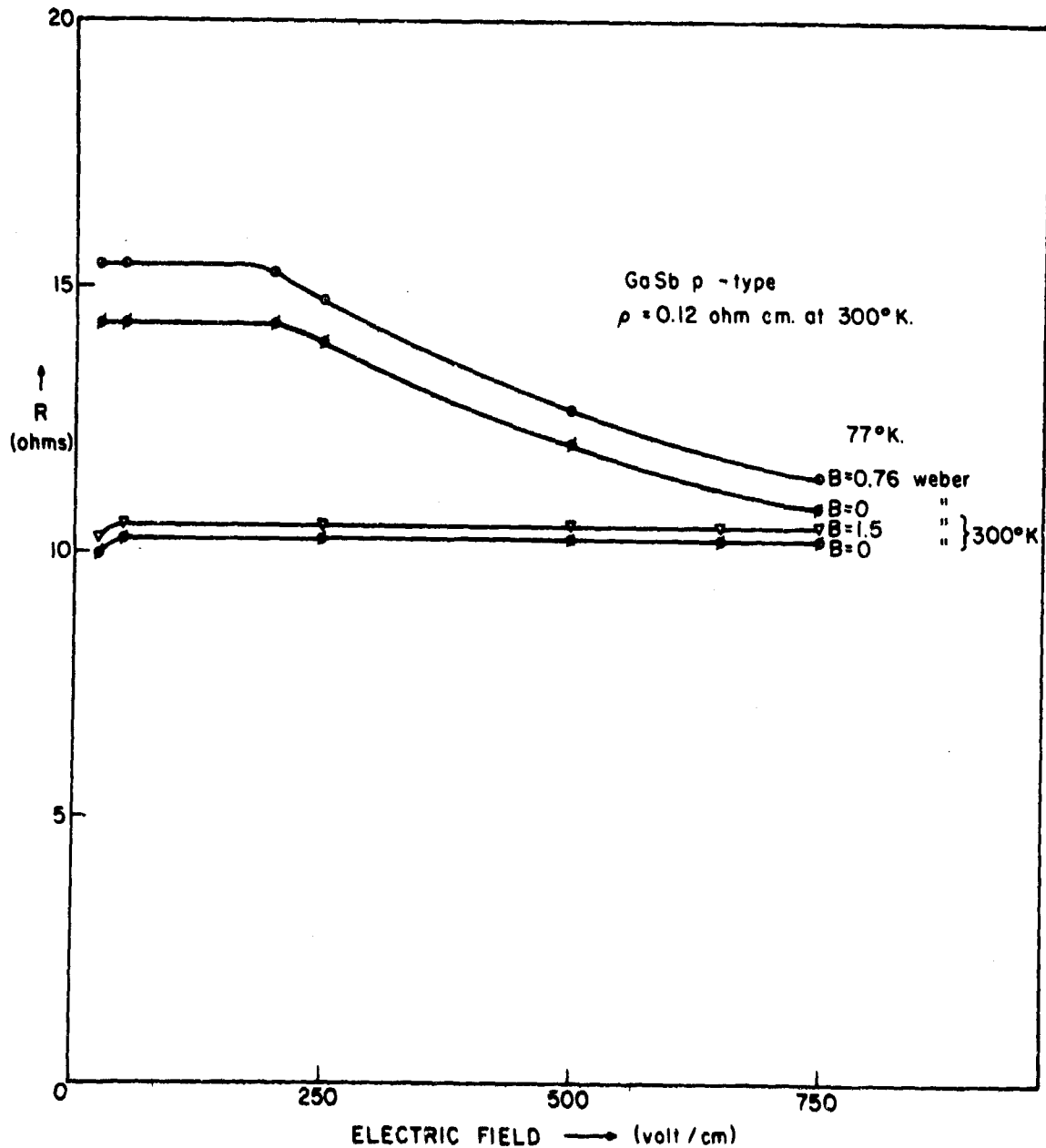


Fig. 1. Resistance of GaSb Sample as a Function of Applied Fields

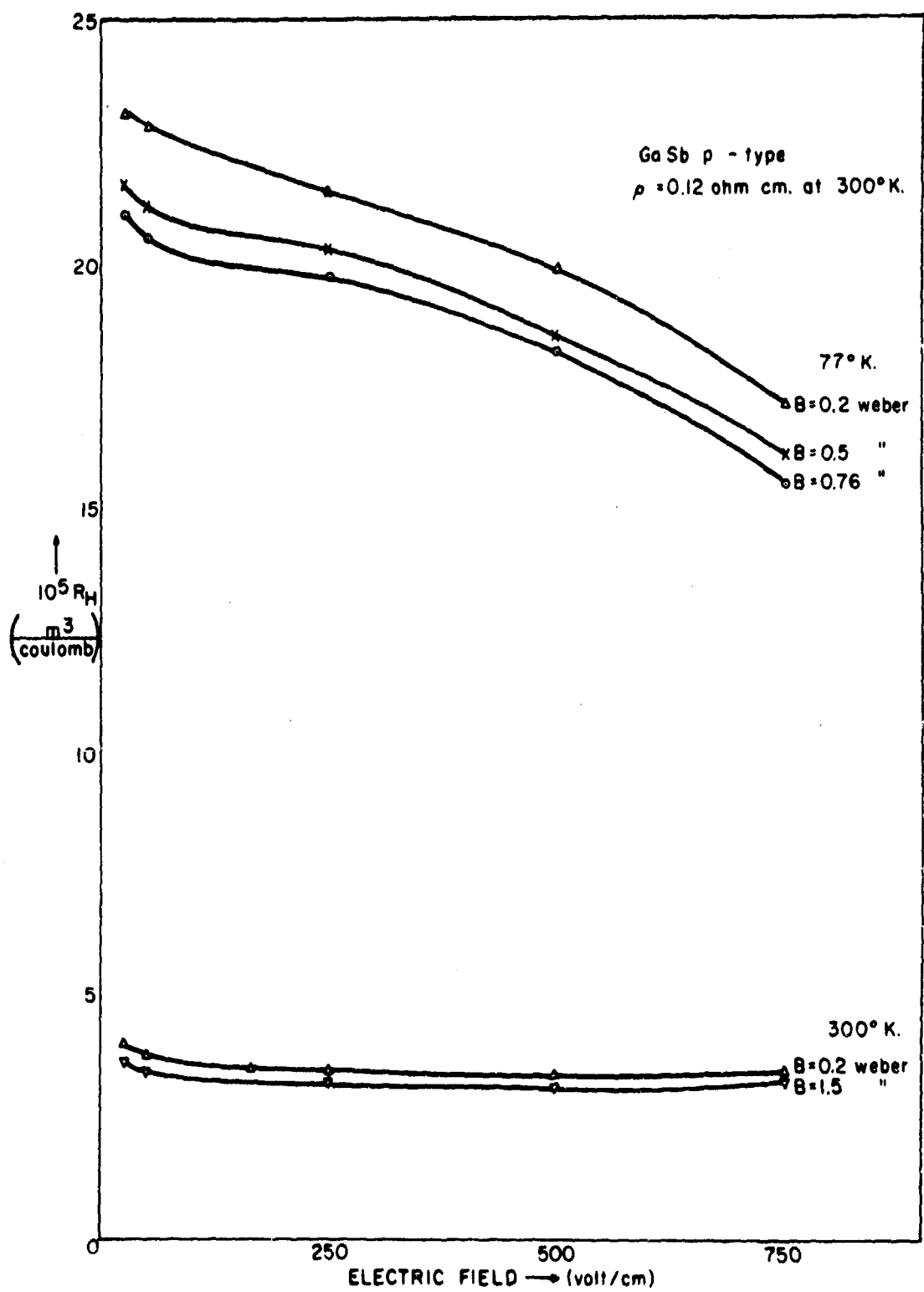


Fig. 2. Hall Coefficient of GaSb as a Function of Applied Fields

is also direction-dependent<sup>1,3</sup>. The effect of these considerations on the conductivity of p-type InSb has been computed though it has not been possible to compare these results with experiments<sup>4</sup>. In the present study, the effect of a high electric field on the transport properties of a p-type semiconductor with the valence-band structure indicated above will be considered at different temperatures.

Hall effect and magnetoresistance measurements were made on p-type GaSb of 0.1 ohm-cm at 300°K and 77°K, up to electric fields of 750 volt/cm and magnetic fields of 15 kilogauss. As the resistivity of the available GaSb is quite low, the sample (4 mm x 0.7 mm x 0.8 mm active region) draws fairly large current at the high electric fields used. In order to reduce dissipation, the electric field was obtained by applying short voltage pulses of about 1  $\mu$ sec duration at a repetition rate of about 10 pulses/sec. This pulse width was found to be large enough to allow steady-state readings. The maximum average power dissipation was about 100 mW.

Figure 1 shows the variation in the resistance of the sample with electric and magnetic fields. The magnetoresistance coefficient  $\Delta\rho/\rho_0 B^2$  computed from this data is seen to be about 1.2%/Weber<sup>2</sup> at 300°K and 9.5%/Weber<sup>2</sup> at 77°K, in reasonable agreement with the low-field data reported in the literature<sup>5</sup>. This coefficient is relatively insensitive to the electric field. At 77°K the resistance is seen to fall rapidly at fields above 200 volts/cm. The Hall coefficient  $R_H$  shown in Fig. 2 also falls in this range at 77°K, and the dependence of  $R_H$  on the magnetic field is also greater than at room temperature. At 300°K the Hall coefficient is independent of the applied electric field. There seems to be a small but definite dependence on the magnetic field, indicating a reduction of about 10% in the hole mobility between 2 and 15 kilogauss.

The experimental results are qualitatively consistent with the behavior to be expected from an E-k dependence having a linear term. At low temperatures, few carriers are present so that the effect of the linear term can be expected to be prominent. The increase in energy due to a high electric field will change the effective mass of the hole significantly, which will contribute to a change in conductivity. At higher temperatures, more carriers are present and have a wider range of energy, and as the band away from the maximum tends to be parabolic, negligible changes can be expected in conductivity with applied electric fields. In order to verify whether quantitative agreement is obtained, theoretical computations have to be carried out in detail, using the appropriate band parameters for p-type GaSb. Future work will be on these theoretical aspects and also on measurements over a wider temperature range.

Joint Services Technical Advisory Committee  
AF 49(638)-1402

R. Bharat  
P. Das

## REFERENCES

1. E. O. Kane, "Band Structure of Indium Antimonide," J. Phys. Chem. Solids, Vol. 1, p. 249 (1957).
2. F. Matossi and F. Stern, "Temperature Dependence of Optical Absorption in p-type Indium Arsenide," Phys. Rev., Vol. 111, p. 472 (1958).
3. D. M. S. Bagguley, M. L. A. Robinson and R. A. Stradling, "Cyclotron Resonance in p-type InSb at Millimeter Wavelengths," Phys. Letters, Vol. 6, p. 143 (1963).
4. R. W. Cunningham, "Statistics for a Semiconductor With an InSb-type Valence Band," Phys. Rev., Vol. 167, p. 761 (1968).
5. W. M. Becker, A. K. Ramdas and H. Y. Fan, "Energy Band Structure of Gallium Antimonide," J. Appl. Phys., Vol. 32, p. 2094 (1961).

## SPACE CHARGE LIMITED CURRENTS

S. Kaplan and H. Schachter

Under investigation in this report is a study of the diffusive and drift components of Space-Charge Limited Currents (SCLC). It is widely accepted that for most cases the diffusion current is negligible. This has been shown to be true for the boundary condition of zero cathode field for all time. The purpose of this work is to bear out these results from a more exact solution of the differential equations governing charge and current flow, with more physically reasonable boundary conditions.

The three problems under consideration are:

1. Steady-state SCLC in an insulator
2. Transient SCLC in an insulator
3. Transient SCLC in a depleted n-type MOS structure.

For the steady state case we find that in a small region near the cathode (point of carrier injection) the current is largely diffusive while in the remainder of the sample the drift process dominates. The distance, beyond which we may neglect diffusion, is given by:

$$d_{\text{Critical}} = (L - X_m) \left[ \frac{V_T}{3(V_o - V_m)} \right] + X_m$$

where

$$X_m = \sqrt{\frac{2\epsilon D}{J}} E_o$$

is the point at which the potential is a minimum

$$V_m = V(X_m)$$

L = sample length

$E_o$  = cathode field (taken to be small but finite)

$V_o$  = applied voltage across sample

J = current density

The transient problem requires a solution to the nonlinear partial differential equation

$$\frac{\partial E(x, t)}{\partial t} + \mu E(x, t) \frac{\partial E(x, t)}{\partial x} = \frac{\partial E(L, t)}{\partial t}$$

Since no exact method exists for solving such equations the approach used here was to assume a solution of the form

$$E(x, t) = f(x, t) + \phi(t)$$

where  $f(x, t)$  is the general solution of the homogeneous equation. The rationale behind this approach is to have the solution satisfy the physics of the problem and the boundary and initial conditions imposed. If this can be done then the solution so obtained is taken to be the correct one.

For the case of an impulse of injected charge the results

$$\begin{cases} x < x_f(t) \\ x > x_f(t) \end{cases} \left\{ \begin{array}{l} E(x, t) = \frac{x - x_f(t)}{\mu(t+m)} + E(L, t) + \frac{m(E_o E_a)}{t+m} u(x - x_f) \\ E(x, t) = E(L, t) \end{array} \right.$$

where

$x_f(t)$  = location of the charge front

$E_o$  =  $E(o, o^+)$

$m$  =  $L^2/NV_a$ ;  $V_a$  = applied voltage

$E_a$  =  $E(L, o)$

Note that for this case the charge front advances as an impulse because we have neglected the diffusion mechanism.

When a step of charge is applied we obtain:

$$\begin{cases} x < x_f(t) \\ x > x_f(t) \end{cases} \left\{ \begin{array}{l} E(x, t) = \frac{x - x_f(t)}{\mu(t+m)} + E(L, t) \\ E(x, t) = E(L, t) \end{array} \right.$$

The transient problem in a depleted MOS structure is considered under the condition that the semiconductor-oxide interface is a perfect blocking contact, admitting no carriers into the oxide.

For this case the diffusion neglected equation for the field is

$$\frac{\partial E(x, t)}{\partial t} + E \left[ \mu \frac{\partial E(x, t)}{\partial x} + a \right] = \frac{\partial E(L, t)}{\partial t}$$



$$\text{where } a = -\frac{q \mu N_a}{\epsilon}$$

$N_a$  = background acceptor concentration

A solution to this equation will be attempted analogous to the preceding case.

National Science Foundation  
GU-1557

S. Kaplan

Joint Services Technical Advisory Committee  
AF 49 (638)-1402

### HOT ELECTRON RELAXATION TIMES IN TWO-VALLEY SEMICONDUCTORS AND THEIR EFFECT ON BULK-MICROWAVE OSCILLATORS

P. Das and R. Bharat

The small-signal microwave conductivity of semi-conductors in the presence of a high electric field is dependent on the (1) energy and momentum relaxation times of the carriers at the effective temperature determined by the bias field<sup>1</sup> and (2) relative orientation of the microwave and bias fields<sup>2</sup>. For negligible momentum relaxation time and parallel orientation, the microwave conductivity at small frequencies is given by slope conductivity whereas, at very high frequencies ( $\omega \tau \gg 1$ , where  $\omega$  is the frequency and  $\tau_E$  is the energy relaxation time) it tends to the dc total conductivity. A necessary criterion in bulk III-V semiconductor materials (Gunn<sup>3</sup> and LSA<sup>4</sup> diodes) is the requirement that the small-signal microwave conductivity exhibit a region of negative value. At high enough frequencies, this conductivity becomes positive, thus restricting this type of devices to an upper frequency limit<sup>5</sup>. Expression for this frequency dependent small-signal microwave conductivity of two-valley semiconductors biased at high electric fields has been derived theoretically. In this report, the energy and momentum relaxation times for a two-valley semiconductor, n-type GaAs, have been calculated numerically as a function of electron temperature from which conclusions about frequency limitation of these devices are drawn.

The time-dependent momentum and energy balance equations for a semiconductor having two valleys with isotropic effective masses,  $m_i$  ( $i = 1, 2$ ) and separated by  $\Delta eV$  can be written as<sup>6, 7</sup>

$$eF_{ni} = \frac{m_i}{e} \frac{J_i}{m_i^2 (V_i)} + \frac{\partial}{\partial t} \left( \frac{m_i}{e} J_i \right) \quad (1)$$

$$J_i F = \frac{n_i k \theta}{V_i \tau_{Ei} (V_i)} + \frac{n_i k \theta}{V_i \tau_{pi} (V_i)} + \frac{\partial}{\partial t} \left( \frac{k \theta n_i}{V_i} \right) \quad (2)$$

$$-n_i / \tau_{ni} (V_i) + n_i / \tau_{nj} (V_i) = \frac{\partial}{\partial t} (n_i) \quad (3)$$

where  $F$  is the applied electric field,  $J_i$  is the current density carried by the carriers

in the  $i$ th valley,  $n_i$  is the carrier concentration in the  $i$ th valley,  $\theta$  is the characteristic polar optical phonon temperature,  $\gamma_i = \theta/T_i$ ,  $T_i$  is the effective electron temperature,  $k$  is the Boltzmann's constant  $\tau_{mi}$  and  $\tau_{Ei}$  are the momentum and energy relaxation times which include both the effects of intravalley and intervalley scattering mechanisms,  $\tau_{ni}$  and  $\tau_{ij}$  correspond to intravalley and intervalley energy relaxation times.

The relaxation times can be evaluated<sup>7</sup> as is noted, in terms of the parameters of the material under consideration - the characteristic intervalley phonon temperature  $\theta_p$ , the static and high-frequency relative dielectric constants  $\epsilon_{10}$ ,  $\epsilon_{\infty}$ , the lattice constant  $a$ , the density  $\rho$  and the deformation potential for internal scattering,  $\Sigma$ . For the parameters of GaAs<sup>6</sup>,  $\tau_{ni}$ ,  $\tau_{mi}$ ,  $\tau_{Ei}$  are plotted in Fig. 1 as functions of electron temperature.

The polar optical phonon scattering is considered to be the only intravalley process and the carrier concentration is considered to be greater than the critical value so that the displaced Maxwellian distribution with effective hot electron tempera-

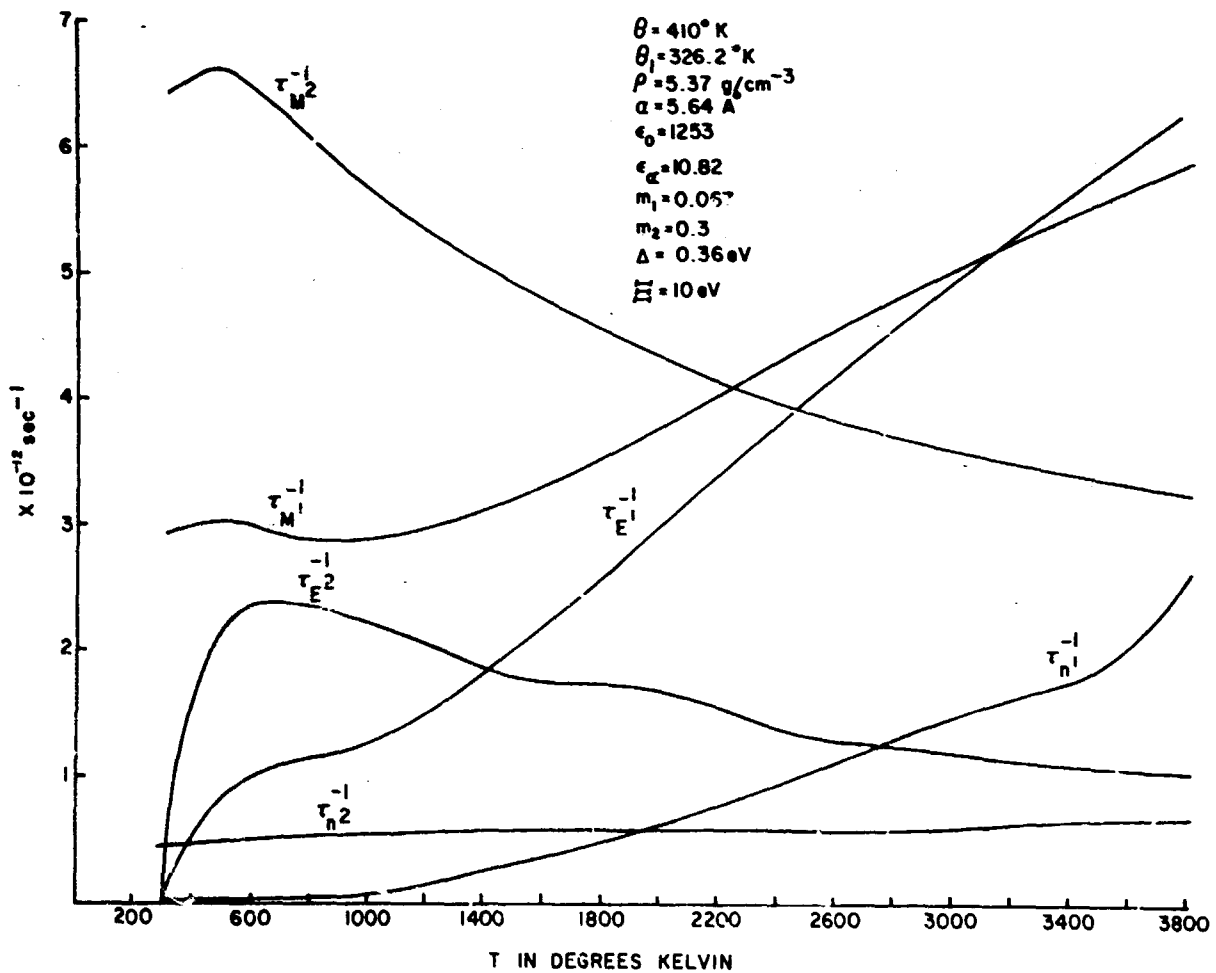


Figure 1.

ture is valid<sup>6</sup>. Also only the first term in the expansion of the distribution function is considered.

In the presence of an applied electric field,  $F$ , given by

$$F = F_0 + \lambda F_0 e^{j\omega t}$$

where  $\lambda \ll 1$ , one can assume a small perturbation of the following quantities:

$$J_i = J_{i0} + \lambda J_{i1} e^{j\omega t}$$

$$Y_i = Y_{i0} + \lambda Y_{i1} e^{j\omega t}$$

$$n_i = n_{i0} + \lambda n_{i1} e^{j\omega t}$$

The subscript "0" refers to the dc or unperturbed values and "1" to the difference between the perturbed and the dc values.

One can obtain

$$\frac{J_{i1}}{J_{i0}} = \frac{1 + (Y_{i1}/Y_{i0}) \left( \frac{\tau'_{mi}}{\tau_{mi}} Y_{i0} + \frac{N_i}{n_{i0}} \right) + \frac{Y_{j1}}{Y_{j0}} \frac{N_j}{n_{i0}}}{(1 + j\omega\tau_{mi})}$$

$$\begin{aligned} \frac{J_{i1}}{J_{i0}} = & \left\{ \frac{Y_{i1}}{Y_{i0}} \left\{ (1 + j\omega\tau_{Ei}) \left( \frac{N_i}{n_{i0}} - 1 \right) - \frac{\tau'_{Ei}}{\tau_{Ei}} Y_{i0} - \frac{N_i}{n_{i0}} \frac{Y_{i0}}{Y_{j0}} \frac{\tau_{Ei}}{\tau_{ij}} \right\} \right. \\ & + \frac{Y_{j1}}{Y_{j0}} \left\{ (1 + j\omega\tau_{Ei}) \frac{N_j}{n_{i0}} + \frac{Y_{i0}}{Y_{j0}} \frac{\tau_{Ei}}{\tau_{ij}} \frac{n_{j0}}{n_{i0}} \left( 1 + \frac{N_j}{n_{j0}} + \frac{\tau'_{ij}}{\tau_{ij}} Y_{j0} \right) \right\} \\ & \left. + \left\{ 1 + \frac{n_{j0}}{n_{i0}} \frac{Y_{i0}}{Y_{j0}} \frac{\tau_{Ei}}{\tau_{ij}} \right\} \right\} \times \left\{ 1 + \frac{n_{j0}}{n_{i0}} \frac{Y_{i0}}{Y_{j0}} \frac{\tau_{Ei}}{\tau_{ij}} \right\}^{-1} \end{aligned}$$

where the prime denotes differentiation with respect to  $Y_i$  and

$$n_{11} = \sum N_i Y_{i1} = -n_{22}; \tau_n^{-1} = \sum \tau_{ni}^{-1}$$

$$N_i = (-1)^i n_{i0} \tau_{ni}' \tau_n / \{ \tau_{ni}^2 (1 + j\omega\tau_n) \}$$

It is clear from the above two expressions that frequency dependence occurs through only the terms  $\omega\tau_n$ ,  $\omega\tau_{mi}$  and  $\omega\tau_{Ei}$ . Also the effect of  $\omega\tau_{mi}$  is to reduce the magnitude of the microwave current. From Fig. 1 it is found that for the negative conductivity region of GaAs as calculated by Butcher and Fawcett (about 500° - 1500°K)

$\omega\tau_n$ ,  $\omega\tau_{mi}$ ,  $\omega\tau_{Ei}$  are of the order of 1 at 200 Gc/sec. So around 200 Gc/sec one should consider the effects of relaxation times in all quantitative calculations. The frequency limit of the devices using bulk negative conductivity of semiconductors also should be of the same order of magnitude. But for actual quantitative determination one should numerically calculate  $\sum J_{ij}$  vs frequency.

Theoretical calculations of the efficiency, negative resistance and conditions for space-charge control relevant to operation of LSA oscillator diode have been done by Copeland<sup>4</sup> without considering the effects of relaxation times. His calculations yield a maximum theoretical low-frequency efficiency of 18%. If, however, the effects of relaxation times are included, then at frequencies of the order of 200 GHz, the calculated efficiency is expected to be much lower.

Joint Services Technical Advisory Committee  
AF 49(638)-1402

P. Das and R. Bharat

#### REFERENCES

1. A. F. Gibson, T. W. Granville and E. A. S. Paige, "A Study of Energy-loss Processes in Germanium at High Electric Fields Using Microwave Techniques," *J. Phys. Chem. Solids*, Vol. 19, p. 198 (1961).
2. P. Das and P. W. Staecker, "Upper Frequency Limit for Gunn Oscillators Imposed by Carrier Energy-relaxation Time," *Electron. Letters*, Vol. 2, p. 258 (1966).
3. "Special Issue on Semiconductor Bulk-effect and Transit-time Devices," *IEEE Trans. on Electron Devices*, ED-13, No. 1 (1966).
4. J. A. Copeland and R. R. Spiwak, "LSA Operation of Bulk n-GaAs Devices," *International Solid State Circuits Conference*, Philadelphia (1967).
5. P. Das and P. W. Staecker, *Proc. of the Sixth Int. Conf. on Micr. Gener. and Ampl.*, Cambridge (1966).
6. P. N. Butcher and W. Fawcett, "The Intervalley Transfer Mechanism of Negative Resistivity in Bulk Semiconductors," *Proc. Phys. Soc.*, Vol. 86, p. 1205 (1965).
7. P. Das and R. Bharat, "Hot Electron Relaxation Times in Two-Valley Semiconductors and Their Effect on Bulk Microwave Oscillators," *Appl. Phys. Letters*, Vol. 11, p. 386, 15 Dec. 1967.

#### CHARGE-TRANSFER AND THERMOLUMINESCENCE IN $\text{CdF}_2:\text{Eu}^{3+}$

E. Banks, A. Halperin and R. W. Schwartz

Single crystals of  $\text{CdF}_2$ , doped with  $\text{Eu}^{3+}$  alone and with  $\text{Eu}^{3+}-\text{Na}^+$  and  $\text{Eu}^{3+}-\text{Y}^{3+}$  were grown in graphite crucibles by the Bridgman technique. Fluorescence spectra were obtained at liquid  $\text{N}_2$  temperature. These were characteristic of  $\text{Eu}^{3+}$ , but the resolution was inadequate for detailed analysis. The thermoluminescence spectrum, after 2537 Å irradiation, at liquid  $\text{N}_2$  temperature was obtained by rapidly warming the sample. This proved identical with the fluorescence spectrum ( $\text{Eu}^{3+}$  species).

A new broad-band absorption at about 3400 Å was observed at 77°K after 2537 Å irradiation, (longer wavelength ultraviolet did not produce thermoluminescence). This

band disappeared after infrared irradiation at 77°K or after the thermoluminescent peak was passed during warming. The band was attributed to the formation of  $\text{Eu}^{2+}$  on irradiation.

A complex ESR spectrum was observed in the irradiated specimens. This was also attributed to  $\text{Eu}^{2+}$ , as its behavior paralleled that of the ultraviolet absorption band when the samples were irradiated with I. R. or warmed up.

The occurrence of bright thermoluminescence at low temperatures, and the effect of infrared, appear to rule out a mechanism previously proposed, involving excitation of an electron from an interstitial  $\text{F}^-$ , trapping at  $\text{Eu}^{3+}$  (forming  $\text{Eu}^{2+}$ ). Subsequently, the phosphorescence or thermoluminescence was alleged to occur by atomic diffusion of the  $\text{F}^0$  atoms to the  $\text{Eu}^{2+}$ , where electron transfer takes place, followed by  $\text{Eu}^{3+}$  emission.

Our proposed mechanism is similar, except that the electron trapped at  $\text{Eu}^{2+}$  is excited to the conduction band, whence it returns to an interstitial  $\text{F}^0$ , forming an excited  $\text{F}^-$  (interstitial). We suggest that this excitation may be resonantly transferred to a nearby  $\text{Eu}^{3+}$  whose emission is responsible for the observed phosphorescence and thermoluminescence.

Army Research Office, Durham  
DA-31-124-ARC(D)-71

E. Banks and R. W. Schwartz

National Science Foundation  
GU-1557

#### MAGNETIC ORDERING IN PEROVSKITES

E. Banks and N. Tashima

We are attempting to investigate the exchange interactions leading to magnetic coupling in perovskites. Currently, we are focusing on interactions between  $d^3$  and  $d^5$  ions in the perovskite structure where there is some hope of obtaining atomic ordering. The system chosen is  $\text{La}_{1-x}\text{M}_x^{2+}\text{Fe}_{1-x}^{3+}\text{Mn}_x^{4+}\text{O}_3$ , where M is Sr, Ba or Pb. Where M is Ba, single phase perovskites were obtained up to  $x = 0.40$ . Above this value, a second phase ( $\text{BaMnO}_3$ ) appears.

Where M is Pb, single phase materials are found up to  $x = 0.70$ , with orthorhombic structure up to 0.30, and rhombohedral from 0.30 to 0.70. In the case of Sr, the single phase region also extends to  $x = 0.70$ .

Magnetization measurements between liquid nitrogen and room temperatures gave very low values ( $\sim 10$  emu) are found over the entire range, suggesting weak ferromagnetism due to canting of a basically antiferromagnetic structure. In the Sr series the magnetization was about 3 emu, even at  $x = 0.70$ .

For Pb-containing compounds, the magnetization at  $x = 0.50$  was around 10 emu, and at  $x = 0.80$  (not single phase) it was about 20 emu. Since chemical analyses are not yet available, no conclusions can yet be drawn, as the valence states are unknown.

Single crystal growth (from  $\text{Bi}_2\text{O}_3$  flux) was attempted for starting compositions of  $x = 0.25$ , 0.50 and 0.75 for the La-Sr and La-Pb series. Crystals of about 1 mm dimensions were obtained. The magnetic data were rather different from those obtained on powders.

For a Pb-containing crystal ( $x = 0.75$ ) a magnetization of 40 emu at liquid nitrogen, falling off sharply was obtained. A Sr-containing crystal of the same initial composition gave a value of 5 emu. Bismuth analysis is now being carried out, and liquid helium data are not complete enough for interpretation.

In addition to complete chemical analysis and magnetic measurements, it will be necessary to determine the extent of ordering of  $\text{Fe}^{3+}$  and  $\text{Mn}^{4+}$ . Mossbauer spectra will also be obtained.

Joint Services Technical Advisory Committee  
AF 49 (638)-1402

E. Banks and N. Tashima

#### DYNAMICAL ORIGIN OF THREE-DIMENSIONAL LOW ENERGY ELECTRON DIFFRACTION INTENSITIES

R. M. Stern, H. Taub and A. Gervais

Low energy electron diffraction has until recently been considered primarily as a tool for the study of surfaces because of the assumed two dimensional character of the diffracting region. Treated as such the observed dependence of diffracted intensities with variation of the incident beam direction must be considered to be anomalous. If treated as an infinite three dimensional problem, the appearance of forbidden fractional order reflections at constant incident direction but varying electron wavelength is likewise anomalous. By introducing the theoretical approach usually applied to high energy electron diffraction, together with the techniques of x-ray structure analysis, it is possible to identify the proper three dimensional nature of the diffracting lattice. In low energy electron diffraction, very strong coupling may exist between diffracted beams. Because the strength of the coupling is extremely sensitive to geometry, it is possible that only one strong reflection is excited at a time. This fact will permit the identification of individual reflections in terms of a two beam model.

The diffraction of electrons from the surface of a periodic solid can be treated as a boundary value problem where the incident wave is expanded at the surface in terms of the appropriate solutions to the wave equation in both the vacuum (Bragg reflections) and the solid (transmitted beam)<sup>1</sup>. Both the vacuum waves outside and the crystal waves inside the solid must satisfy the Schrodinger equation

$$\left( -\frac{\hbar^2}{2m} \nabla^2 + V(\underline{r}) \right) \psi(\underline{r}) = E \psi(\underline{r})$$

In a perfect crystal the potential  $V(\underline{r})$  can be represented by a Fourier series

$$-\frac{2m}{\hbar^2} V(\underline{r}) = v_0 + \sum_{\underline{H}} v_{\underline{H}} e^{2\pi i \underline{H} \cdot \underline{r}}, \quad \underline{H} = h\underline{a} + k\underline{b} + l\underline{c}$$

In the vacuum  $V(\underline{r}) = 0$ . The incident beam sets up a scattered wave field which is a superposition of reflected plane waves and evanescent waves in the vacuum, and a superposition of Bloch waves (both travelling and evanescent) within the solid<sup>2</sup>. In a completely elastic theory as will be discussed here the usual conditions of continuity at the crystal boundary apply. Total energy and momentum parallel to the crystal surface (to within a reciprocal lattice vector) are conserved. The introduction of the crystalline boundary will relax the periodic boundary conditions normal to the surface.<sup>3, 4</sup> This may result in the introduction of selection rules with respect to the allowed electron momenta normal to the crystal surface which are different than those associated with that direction in an infinite crystal (i. e., permitting certain forbidden fractional order reflections) but otherwise the problem can be treated as for the general three dimensional case.

The details of the solutions for internal electrons ( $E < 0$ ) in an infinite solid are well known: this is just the calculated band structure for the solid being considered.<sup>5, 6</sup> The diffraction problem concerns itself with the internal solutions for a given magnitude and direction of the external electron wave vector  $\underline{K}_0$ , which is determined by the energy and direction of the incident, external electron beam. The relation between internal momentum ( $\underline{k}_0$ ) and  $\underline{K}_0$  depends on the orientation of the crystal surface with respect to the reciprocal lattice because of the refraction due to the constant part of the crystal potential.<sup>7, 8, 9</sup>

The concept of the inner potential is introduced in the Bethe approximation<sup>1</sup> of the dynamical theory of electron diffraction to explain the shift of apparent Bragg maxima to lower electron energies than those predicted kinematically. Because of the presence of strong dynamical interactions, the shape and width of the Bragg reflections become distorted from the kinematical predictions. Minima appear on a dynamically broadened reflection which are due to the reduction of the reflection coefficient upon the excitation of strong forward scattered (Laue) beams, giving rise to what can be mistaken for the superposition of reflections of presumably different origin. This introduces difficulty in both the indexing of the Bragg reflection and the determination of the diffraction conditions for its excitation. The inner potential can be associated with the refraction correction providing an expression for the voltage at which a reflection should occur for ar-

bitrary incident directions. This voltage shift as a function of angle behaves as  $1/\sin^2\theta$  leading to large corrections at glancing angles. By taking advantage of this magnification of the inner potential careful measurements far from normal incidence for orientation which do not excite strong multiple diffraction yield a constant value of the inner potential of  $20 \pm 1$  eV for tungsten (110).

In low energy electron diffraction the problem is complicated by the fact that only the back reflected (Bragg) intensities can be directly observed. Thus the object of any low energy electron diffraction theory is to predict the reflection coefficients in terms of a crystalline wave field which cannot be directly measured. In high energy electron or x-ray diffraction the wave field within the crystal can be deduced from the details of the fine structure of the transmitted beam since the finite diffracting crystal has both an entrance and an exit surface.<sup>10, 11, 12</sup>

The understanding of the origin of the intensity variation with diffraction parameters in LEED measurements therefore requires the development of a three dimensional diffraction theory. The Nearly Free Electron Approximation (NFEA) is an appropriate model to use in demonstrating that the mathematical formalism and the underlying physics of the Band Structure approach and Dynamical Diffraction Theory are identical. It can then be shown that the band diagram of band theory and the constant energy dispersion surface of dynamical theory are in fact sections of the same dispersion hypersurface in energy-complex  $K$  space. This dispersion hypersurface defines the totality of allowed electronic states in the crystal. By introducing the crystal surface, the boundary conditions which must be satisfied at the crystal-vacuum interface are defined.

In a particular experiment, the constraints imposed on the magnitudes of the diffraction parameters determine what part of the dispersion hypersurface is excited during the experiment. It is usually possible to construct the dispersion hypersurface in real space (energy, real  $K$ ), and a convenient representation can be made in two dimensions, for those experiments made at constant energy. If this is done, a semiquantitative description of the wave field in the crystal can be made by calculating the position on the dispersion surface where particular waves have extremum values of their amplitude. In particular it can be shown that in the case where three strong beams are excited, there are certain directions along which one of the plane waves in the crystal is always zero: there are also certain conditions under which one of the crystal Bloch waves can be shown to be identically zero. These effects can be readily observed in the LEED intensities. In particular, LEED measurements made at constant energy (rotation diagrams and rocking curves) contain much structure which can be explained on this basis.<sup>13, 14</sup>



The use of low energy electron diffraction for the study of surfaces is therefore subordinate to its use in the determination of the three dimensional band structure. Only after the details of the crystal potential are understood can the effects of the surface on the diffracted intensities be investigated.

The authors wish to acknowledge the contributions of Prof. H. Wagenfeld, Mr. S. Friedman, and Miss J. Perry to the work discussed above. This material will appear in expanded form elsewhere<sup>14, 15, 16</sup>.

Air Force Office of Scientific Research  
AFOSR 1263-67

R. M. Stern

#### REFERENCES

1. H. A. Bethe, *Ann. Phys.* **87** (1928) 55.
2. L. Brillouin, "Wave Propagation in Periodic Structures," McGraw-Hill Book Co., Inc., N. Y., 1946.
3. D. Boudreaux and J. Heine, *Surf. Sci.* **8** (1967) 426.
4. E. G. McRae, *J. Chem. Phys.*, **45** (1966) 1258.
5. P. M. Morse, *Phys. Rev.*, **35** (1930) 1310.
6. A. Sommerfeld and H. A. Bethe, "Handbuch der Physik," Bd. **24**, Berlin (1933).
7. G. P. Thomson and W. Cochran, "Theory and Practice of Electron Diffraction," MacMillan and Co., London (1939).
8. W. E. Laschkarew, *Trans. Far. Soc.*, **31** (1935) 1081.
9. A. Gervais - to be published.
10. G. Lehmpfuhl and A. Reiszland - to be published in *Z. Naturforschg.*
11. P. Hirsch, A. Howie, and M. J. Whelan, *Proc. Roy. Soc.*, **A252** (1960) 499.
12. B. Batterman and H. Cole, *Rev. Mod. Phys.*, **36** (1965) 681.
13. H. Niehrs, *Zeit. f. Physik*, **139** (1954) 88.
14. R. M. Stern, J. J. Perry, D. S. Boudreaux, submitted to *Phys. Rev.*
15. R. M. Stern, H. Taub and A. Gervais, Proceedings of the 4th International Materials Conference, U. of C. Berkeley, June 17-21, 1968, to be published by McGraw-Hill, N. Y.
16. A. Gervais and R. M. Stern, submitted to *Surf. Sci.*

#### CALCULATION OF ACTIVATION ENERGIES BY THE HALF INTENSITY WIDTH OF GLOW CURVES

R. Chen

When the temperature of a suitably prepared phosphor, or any insulator having deep traps for electrons, is raised, the change in occupancy of the traps manifests itself by the emission of light and of currents. The inverse problem is concerned with the determination of the properties of the traps, in particular their activation energy, from the observed glow peaks.

New methods for calculating the activation energy,  $E$ , of first and second order glow peaks have been developed. These methods are based on measurement of two values, the temperature at the maximum,  $T_m$ , and the peak width,  $w =$  difference between the two temperatures  $T_1$  and  $T_2$  in which the glow is half of the maximal intensity. Some previous methods for calculating  $E$  by the use of the low temperature half width,  $\tau = T_m - T_1$  and the high temperature one,  $\delta = T_2 - T_m$  has now been modified. Theoretical considerations as well as numerical calculations show the occurrence of consistent errors in these methods. A way to overcome most of these inaccuracies is given.

Many thermoluminescence (TL)<sup>1</sup>, thermally stimulated current (TSC)<sup>2</sup> and thermally stimulated electron emission (TSE)<sup>3</sup> peaks were found to obey the first order kinetics law:

$$I = -\frac{dn}{dt} = S e^{-E/kT} n \quad (1)$$

Where  $I$  is the emitted light intensity in TL, the conductivity in TSC, or the number of emitted electrons in TSE,  $n$  is the concentration of trapped electrons,  $t =$  time,  $T =$  the absolute temperature,  $S =$  the frequency factor (the pre-exponential factor) having dimensions of  $\text{sec}^{-1}$  and  $k =$  the Boltzmann constant. Some other peaks showed a second order behavior<sup>4</sup> obeying the differential equation

$$I = -\frac{dn}{dt} = S' e^{-E/kT} n^2 \quad (2)$$

where  $S'$  is a constant with dimensions of  $\text{cm}^3 \text{sec}^{-1}$ . If temperature increases linearly, namely,  $T = T_0 + \beta t$ , where  $\beta$  is the heating rate, the solution of (1) is

$$I = S n_0 e^{-E/kT} \exp \left[ -\frac{S}{\beta} \int_{T_0}^T e^{-E/kT'} dT' \right] \quad (3)$$

from which, by differentiation, the condition for the maximum is found to be

$$\frac{\beta E}{kT_m^2} = S e^{-E/kT_m} \quad (4)$$

The solution of Eq. (2) for the linear heating rate is:

$$I = S' e^{-E/kT} \left[ \frac{1}{n_0} + \frac{S'}{\beta} \int_{T_0}^T e^{-E/kT'} dT' \right]^{-2} \quad (5)$$

and the maximum condition for this case is:

$$\frac{S'}{\beta} \int_{T_0}^{T_m} e^{-F/kT} dT + \frac{1}{n_0} = \frac{2kT_m^2 S'}{\beta E} e^{-E/kT_m} \quad (6)$$

By assuming that the area of the glow from the maximum towards higher temperatures equals the area of a triangle having the same height and half width, namely,  $\delta I_m = \beta n_m$  (where  $I_m$  is the intensity and  $n_m$  the concentration of trapped carriers at the glow maximum), Lushchik<sup>5</sup> found the following equation for finding the activation energy for first order peaks:

$$E = \frac{kT_m^2}{\delta}, \quad (7)$$

whereas for second order kinetics his equation is:

$$E = \frac{2kT_m^2}{\delta} \quad (8)$$

By taking a similar assumption about the first half of the peak, the following equations for the activation energies can be found<sup>6</sup>:

$$E = 1.72 \frac{kT_m^2}{\tau} (1 - 1.58 \Delta), \quad (9)$$

for first order peaks, and -

$$E = 2 \frac{kT_m^2}{\tau} (1 - 2 \Delta) \quad (10)$$

for second order ones, where  $\Delta$  is a correction factor,  $\Delta = \frac{2kT_m}{E}$ , usually having values around 0.1.

The assumption of Lushchik  $\frac{\delta I_m}{\beta n_m} = 1$  can be regarded as two separate assumptions: one is  $\frac{\delta I_m}{\beta n_m} = C_\delta$ , where  $C_\delta$  is a constant and the other is  $C_\delta = 1$ . For given

values of  $F$  and  $S$  for first order or  $E$ ,  $S'$ , and  $n_0$  for second order, the values of  $\delta I_m$ , and  $n_m$  can be found in a way to be described here in brief, and thus  $C_\delta$  can be found. By changing the parameters in wide ranges covering the values found in various experiments, the two assumptions about  $C_\delta$  can be checked.

For numerical calculations, the value of the integral is approximated by<sup>7</sup>:

$$\int_{T_0}^T e^{-E/kT'} dT' = T e^{-E/kT} \sum_{n=1}^J \left(\frac{kT}{E}\right)^n (-1)^{n-1} n! \quad (11)$$

Equations (4) and (6) are solved numerically by the Newton-Raphson method to give the value of  $T_m$ , and the equations for finding the half intensity temperatures are being solved in a similar way. The calculations have been done using the IBM 360 computer for values of  $E$  ranging from 0.1 to 2.0 eV and values of  $S$  from  $10^5$  to  $10^{13} \text{ sec}^{-1}$  and  $S'n_0$  (which, in a way, replaces  $S$  when the second order kinetics is investigated) between  $10^6$  and  $10^{15} \text{ sec}^{-1}$ . The values found for  $C_\delta$  were 0.976 to within  $\pm 0.4\%$  for the first order peaks and 0.853 within  $\pm 1.4\%$  for the second order ones. This shows that the assumption that  $C_\delta$  is a constant is quite a good one and that the assumption  $C_\delta = 1$  is reasonable for first order peaks but rather erroneous for the second order ones. It can be easily shown that the formulas for the activation energies (7) and (8) have to be corrected by multiplication by the factor  $C_\delta$  which shows that the results found in this way were quite good for first order kinetics and too big by about 15% for second order peaks. In a similar way, eqs. (9) and (10) should be multiplied by  $C_\tau = \frac{\tau I_m}{\beta(n_0 - n_m)}$  where  $n_0$  is the initial concentration of electrons. For first order kinetics the values of  $C_\tau$  centered around 0.883 ( $\pm 1.4\%$ ) and for second order around 0.707 ( $\pm 1.0\%$ ), showing that the results found by these formulas were usually too high by about 10%.

Equations (8) and (10) and some other ones of a similar nature (corresponding to somewhat different physical conditions) have to be solved iteratively. Such an equation can be written in a general form as:

$$E = A_\alpha \frac{kT_m^2}{\alpha} (1 - b \Delta) \quad (12)$$

where  $\alpha$  stands for  $\tau$  or in other cases for  $\delta$  or  $w$ ,  $A_\alpha$  and  $b$  are constants depending on the order of the kinetics and on the exact nature of the equation. For first order kinetics, for example  $A_\tau = 1.72 C_\tau$ , (corrected Eq. (9)). The first approximation is given by taking  $\Delta = 0$  and the following ones are found each by inserting the previously approximated  $E$  value into  $\Delta = \frac{2kT_m}{E}$ . It has been shown, however, in this work that equally accurate values of  $E$  can be found by:

$$E = A_\alpha \frac{kT_m^2}{\alpha} - 2bkT_m \quad (13)$$

which can be solved noniteratively. By using an approximation similar to the triangle assumption, now for the whole peak,  $C_w = \frac{wI_m}{\beta n_0}$ , it has been found that the activation energy for a first order peak can be written as:

$$E = e C_w \frac{kT_m^2}{w} - 2kT_m \quad (14)$$

and for the second order kinetics:

$$E = 4 C_w \frac{kT_m^2}{w} - 2kT_m \quad (15)$$

$C_w$  was found to be 0.920 ( $\pm 0.8\%$ ) for first order kinetics and 0.878 ( $\pm 0.4\%$ ) for second order. These equations have also the general form of (13) with other parameters. By the equations of the form given by (13) for first order kinetics, the value of  $S$  can be found by using Eq. (4) thus:

$$S = \frac{\beta}{T_m} \left( \frac{A T_m}{\alpha} - 2b \right) \exp \left( \frac{A T_m}{\alpha} - 2b \right) \quad (16)$$

The values of  $S'$  for second order kinetics are harder to find because of the appearance of the integral in Eq. (6).

Equations of similar form are found for cases in which the pre-exponential factors  $S$  or  $S'$  are dependent on temperature in a way given by Keating<sup>8</sup> as  $S = S'' T^a$  where  $S''$  is a constant for a certain peak and  $a$  is another constant,  $-2 \leq a \leq 2$ . The value of " $a$ " can be found by some other measurements<sup>9</sup> and its value influences the calculated values of  $A_\alpha$  and  $b$  in the various cases. The three methods described here are expected to be accurate only for separate peaks having a definite-first or second order-kinetics. In cases where a peak has some satellites or when the process has some intermediate order kinetics, they are expected to give only some approximation to the real value of  $E$ . The first half of the peak is found to be least dependent on the order of the process and thus the values found by the  $\tau$  method are expected to be good even if the order is not defined. The same is true for the case of additional peaks appearing close to the main one. The low temperature peaks can be bleached thermally without affecting the main peak, which is not possible for the high temperature ones. That is why the  $\tau$  method is usually expected to be more reliable than the  $\delta$  one in this respect while the  $w$  method gives intermediate accuracies. The advantage of the  $w$  method is that  $T_1$  and  $T_2$  are more precisely found than  $T_m$  since the derivative of  $I(T)$  at  $T_m$  is zero. The experimental errors in  $w$  are therefore smaller than in  $\tau$  and  $\delta$  and moreover, the relative error  $\frac{\Delta w}{w}$  is much smaller than  $\frac{\Delta \delta}{\delta}$  and  $\frac{\Delta \tau}{\tau}$  as  $w$  is larger than  $\tau$  or  $\delta$ . The only advantage of the  $\delta$  method is in first order cases where the peak is known to be very pure. In this case the calculated variations in  $C_\delta$  are found to be very small so that if the experimental inaccuracies are small, the values are found more precisely than in the other methods.

National Science Foundation  
GU-1557

R. Chen

#### REFERENCES

1. J. J. Randall and M. H. F. Wilkins, Proc. Roy. Soc. (London) A184, 366, 390 (1945).

2. R. R. Haering and E. N. Adams, *Phys. Rev.* **117**, 451 (1960).
3. P. A. Pipins and B. P. Grigas, *Cpt. i. Spekt* (English trans. **18**, 43 (1965)).
4. G. F. J. Garlick and A. F. Gibson, *Proc. Phys. Soc.* **60**, 574 (1948).
5. C. B. Lushchik, *Dok. Akad. Nauk. S. S. R.* **101**, 641 (1955).
6. A. Halperin and A. A. Braner, *Phys. Rev.* **117**, 408 (1960).
7. J. Haake, *J. Opt. Soc. Amer.* **47**, 649 (1957).
8. P. N. Keating, *Proc. Phys. Soc.* **78**, 1408 (1961).
9. M. Lax, *Phys. Rev.* **119**, 1502 (1960).

### ACOUSTOELECTRIC EFFECT IN BISMUTH

R. C. Augeri and S. J. Freedman

Further measurements of the ultrasonic attenuation of longitudinal waves as a function of frequency (30, 50, 70, 90, 110 MHz) and temperature (2°K to 300°K) were made in a single crystal of Bi (doped 30 ppm. Se) along its trigonal axis. The data clearly shows relaxation peaks in the attenuation in the temperature range of 25°K to 40°K. That is, the peak in the attenuation shifts to higher temperature for the higher frequencies. For four successive runs relaxation peaks were seen in the temperature range of 5°K to 6°K which we attribute to phonon assisted electron hole recombination; a mechanism recently proposed by Lopez and Koenig<sup>1</sup> in his work on the acousto-magnetic electric effect (AME) in pure Bismuth. Lopez found that the particular geometry of the Brillouin zone of Bi would allow a 43°K ± 4°K acoustic phonon to couple the electron and hole bands of Bi. Thus Lopez was able to locate for the first time the band edges of Bi within the Brillouin zone. We concluded that if the "modified Weinreich"<sup>2</sup> relation given as

$$\alpha_e = \frac{n_o e}{S} \left( \frac{E_{AME}}{\mu H} \right)^2 \quad (1)$$

was correct, then the peaks in the attenuation between 5°K to 6°K could be explained in a similar fashion. In Eq. (1)  $\alpha_e$ ,  $n_o$ ,  $S$ ,  $E_{AME}$ ,  $\mu$ ,  $H$  and  $e$  are respectively the electronic attenuation in the absence of a magnetic field, carrier density, acoustic intensity, AME field, carrier mobility, the magnetic field and carrier charge. Equation (1) can be related to the sound angular frequency as the difference in deformation potential constants of electrons and holes,  $(\epsilon_n - \epsilon_p)^2$  thru the equation and relaxation time<sup>2</sup>  $\tau_R$ .

$$\alpha_e = \frac{n_o e}{\rho v_s^3} \left( \frac{\epsilon_n - \epsilon_p}{c} \right)^2 \frac{\mu \omega^2 \tau_R}{D (1 + \omega^2 \tau_R^2)} \quad (2)$$

Thus if  $\tau_R$  varies with temperature one can observe peaks in the attenuation at temperatures for which  $\omega \tau_R = 1$ . Using Lopez's<sup>1</sup> equation for recombination time we have been able to describe fairly accurately the location and heights of the peaks between 5°K and

6°K. Recently Lopez<sup>3</sup> working in the frequency range of 6 to 30 MHz and in a magnetic field of 5 to 15 kG, has described observed attenuation peaks and their location in the same fashion for pure Bi. We believe that the doping of the Bi with 30 ppm has had an effect similar to the magnetic field used in Lopez's experiment. Namely, it makes  $l \ll \lambda$  the region for which Eq (2) is valid, where  $l$  is the mean free path. Further theoretical considerations on this matter are currently in progress.

In a previous report<sup>4</sup> we mentioned peaks that were observed around 10°K. Subsequent measurements, while not conclusive, have failed to repeat this data. If these peaks exist they would be also attributable to recombination by a 96°K acoustic phonon (also allowed in the Brillouin zone and in agreement with neutron data of Yarnell) and would indicate 3 other electron ellipsoids within the Brillouin zone or another hole ellipsoid or both. We are currently increasing the accuracy of our measurements to determine the above.

The peaks in the 25°K to 40°K range may in part be dislocation peaks. To check this the crystal will be irradiated to pin the dislocations and the measurements retaken. For the present, however, it appears that the height, shape, and location of these peaks can be accounted for if we assume the validity of Eq. (2) and that the recombination mechanism is due to optical phonons around 120°K. However since Lopez<sup>2</sup> saw the AME effect diminish as the temperature increased, it would mean that this source of electron-hole recombination could not contribute to the AME effect and would indicate a region for which the modified Weinreich relation is violated. It is known that such a violation could occur if there were a strong collision drag effect. This is in agreement with the conclusions of Lopez concerning discrepancies in the magnitudes of  $\tau_e$  and  $\tau_R$  for  $T \leq 50^\circ\text{K}$ .

Joint Services Technical Advisory Committee  
AF 49(638)-1402

R. Augeri

#### REFERENCES

1. A. A. Lopez and S. H. Koenig, Solid State Comm. 4, 513, (1966).
2. T. Tamada, J. Phys. Soc., Japan 20, 1424 (1965).
3. A. A. Lopez, Private Comm. (Article to be published in Phys. Rev.).
4. R. Augeri and S. J. Freedman, Progress Report No. 32 to Joint Services Technical Advisory Committee.

#### MAGNETOELASTIC PARAMETRIC INTERACTIONS

E. S. Cassey and C. R. Evans

A magnetoelastic medium is known to exhibit a great variety of parametric interactions due to the magnetostrictive coupling which characterizes it. For the case of a transverse electromagnetic pump, parametric interactions have been catalogued and

several of them investigated using a coupled mode approach.<sup>1-3</sup> Graphical descriptions of the interactions were given.<sup>2,3</sup>

The Floquet-mode formulation of traveling-wave parametric phenomena developed at this Institute leads to a much more satisfactory graphical representation of these parametric interactions. The basic theory states that if a medium supports waves with dependence  $V_0 e^{j[\omega t - \chi(\omega) z]}$ , and if a pump of frequency  $\omega_p$  and wave number  $\beta_p$  is applied to the medium, the wave-like excitations of the pumped medium will be of the Floquet form:

$$V(z, t) = \sum_{n=-\infty}^{\infty} V_n e^{j[(\omega + n\omega_p)t - (\chi(\omega) + n\beta_p)z]}$$

Further, in the limit of vanishingly-small pump amplitude, the dispersion diagram will be that of the unpumped medium with superimposed dispersion curves with origins at  $(n\beta_p, n\omega_p)$ , where  $n$  takes on all integer values. In the presence of the pump, the dispersion diagram will be modified only in the vicinity of intersections corresponding to different values of  $n$ .<sup>4-6</sup>

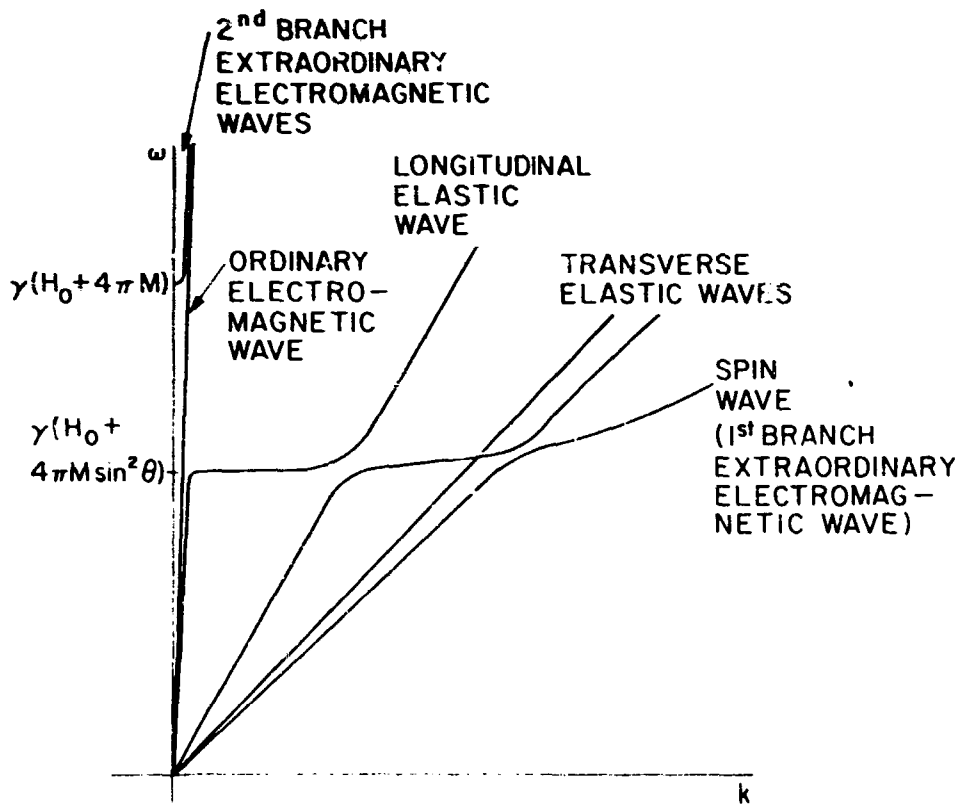


Fig. 1 Dispersion Diagram for Basic Modes of a Magnetoelastic Medium



For the magnetoelastic medium, the basic dispersion diagram is shown in Fig. 1. The waves have been identified by their character in a magnetic but non-magnetostrictive medium. Propagation at some angle  $\theta (\neq 0^\circ)$  to the dc magnetic field is considered. The longitudinal (compressive) elastic wave and the transverse (shear) elastic waves all couple to the spin wave. Electromagnetic propagation effects have been included and both branches of the extraordinary electromagnetic wave are shown. Of course one branch becomes the spin wave at  $\omega = \gamma (H_0 + 4\pi M_S \sin^2 \theta)$ .

Figure 2 is derived following the translation operation specified above for the case of a pump wave which is on the second branch of the electromagnetic wave dispersion curve. This pump is an allowable mode of the infinite magnetoelastic medium and corresponds to the uniform precessional modes which are assumed for the pump

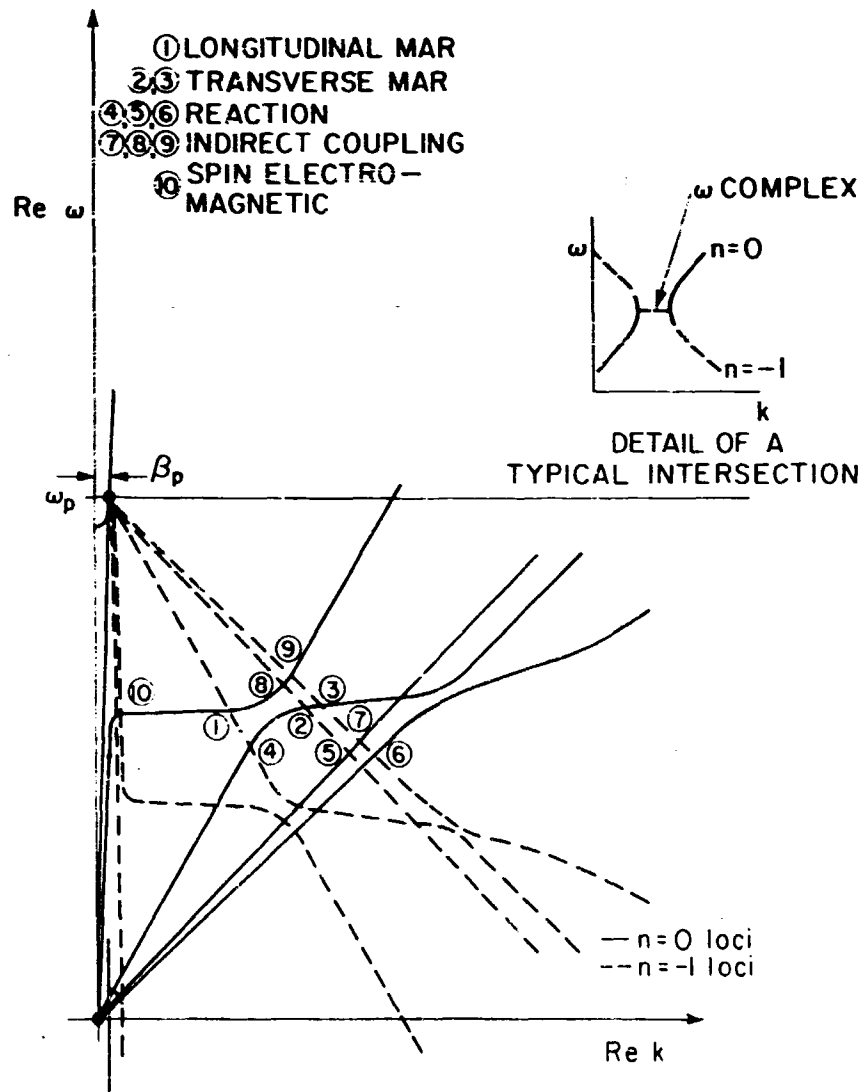


Fig. 2 Dispersion Diagram for Magnetoelastic Medium with an Electromagnetic Pump. Each intersection corresponds to a parametric interaction.

in finite bodies where the finite propagation effects are ignored. The intersections of the curves of the 1st quadrant of the untranslated ( $n=0$ ) diagram with those of the 4th quadrant of the translated diagram ( $n = -1$ ) are shown. Each intersection corresponds to a parametric interaction. Intersections of an acoustic wave branch with a spin wave branch correspond to the parametric process called magneto-acoustic resonance (MAR; Points 1, 2, 3 in Fig. 2). Intersections of an acoustic branch with the other acoustic branch of the same type corresponds to the processes called reaction (Points 4, 5, 6 in Fig. 2). Intersections of acoustic branches with acoustic branches of different type correspond to indirect coupling (Points 7, 8, 9 in Fig. 2). The process corresponding to the intersections of the first branch of the extraordinary electromagnetic wave with the similar translated branch (Point 10 in Fig. 2) might be called spin-electromagnetic resonance; clearly for  $\omega_p > 2\gamma(H_0 + 4\pi M_S \sin^2 \theta)$  this becomes the Suhl or spin-spin process. Since the pump is "Supersonic" (i. e., faster than the acoustic or spin waves), the theory of weakly-dispersive (ideally non-dispersive) media<sup>6</sup> predicts that interactions of the absolute instability type will occur. This result may or may not be applicable to such highly-dispersive media.

Certain interactions occurring in the case of longitudinal elastic pumping are also of interest<sup>7,8</sup>. Figure 3 shows an intersection involving the spin wave and transverse

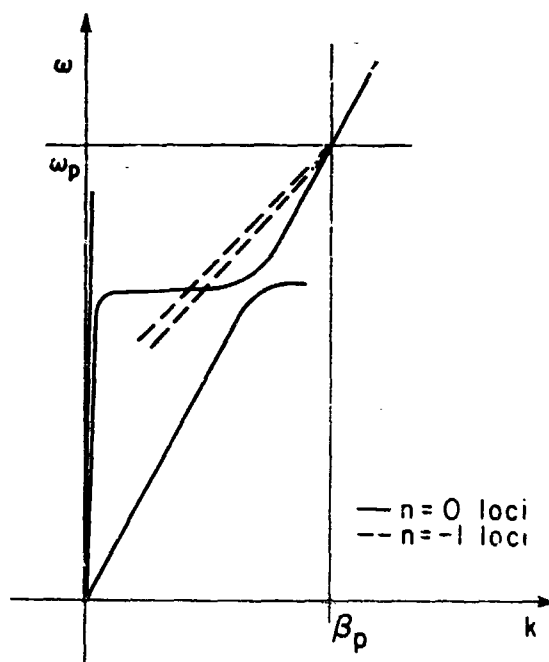


Fig. 3 Portion of Dispersion Diagram for Magnetoelastic Medium with Longitudinal Acoustic Pump. Electromagnetic-shear wave interactions are shown.

elastic waves. The modulation is of the type referred to as intersonic<sup>4</sup>; thus the linear dispersion theory would predict traveling wave amplification for this type of interaction.

Extension of the method to other pumping conditions may be made in a similar manner. The value of this method is especially evident in Fig. 2 where all of the co-linear small signal instabilities occurring under the given pump conditions are identified on a single Brillouin diagram.

Air Force Cambridge Research Laboratories  
Office of Aerospace Research  
F19628-68-C-0075

C. R. Evans

National Aeronautics and Space Administration  
NsG(T)-71

#### REFERENCES

1. R. L. Comstock and B. A. Auld, "Parametric Excitation of Magnetostatic and Elastic Modes," *Jour. Appl. Phys.* Vol. 34, p. 1461-8 (1963).
2. B. A. Auld, Transversely Pumped Magnetoelastic Instabilities, *Jour. Appl. Phys.*, Vol. 36, p. 689-698 (1965).
3. R. W. Damon, et al, "Excitation of Magnetoacoustic Waves at Microwave Frequencies," Final Report Contract AF 19(628) - 4704, Sperry Rand Research Center, Sudbury, Mass. (Nov. 1966).
4. E. S. Cossedy, "The Parametric Coupling of Modes of Propagation in Nonlinear Media," *Proc. of Symposium on Electromagnetic Theory, Delft, 1965.* Pergamon Press, N. Y., pp. 543-568 (1967).
5. E. S. Cossedy and A. A. Oliner, Dispersion Relations in Time-Space Periodic Media: Part I - Stable Interactions, *Proc. IEEE*, Vol. 51, p. 1342 (1963).
6. E. S. Cossedy, Dispersion Relations in Time-Space Periodic Media: Part II Unstable Interactions, *Proc. IEEE*, Vol. 55, p. 1154 (1967).
7. A. G. Gurevich, Parametric Amplification of Magnetic Waves in Ferrites by an Elastic Wave, *Soviet Phys. - Solid State*, Vol. 6, p. 1885 (1965).
8. V. P. Lukomskii, Parametric Amplification of Magnetoelastic Waves, *Soviet Phys. - Solid State*, Vol. 9, p. 467 (1967).

#### THE FOCUSING EFFECT INDUCED BY A D-C DRIVEN CdS PLATE

W. C. Wang and P. Das

A strong lens effect has been observed when a sufficient d-c voltage is applied to a CdS plate.<sup>1</sup> Experimental findings and possible contributing sources will be reported and discussed.

Figure 1 is the experimental configuration. In many instances 5 msec pulses are used in place of the d-c battery and a photodiode detector in place of the screen. Transparent electrodes were put on both the major faces of the CdS plate. They were made by diffusing indium on the surfaces at 500°C for an hour in a closed tube of pressure  $10^{-6}$  mm mercury. The CdS crystal is semi-insulating in the dark and highly photoconductive. The only conductive portion of the crystal is, therefore, where the

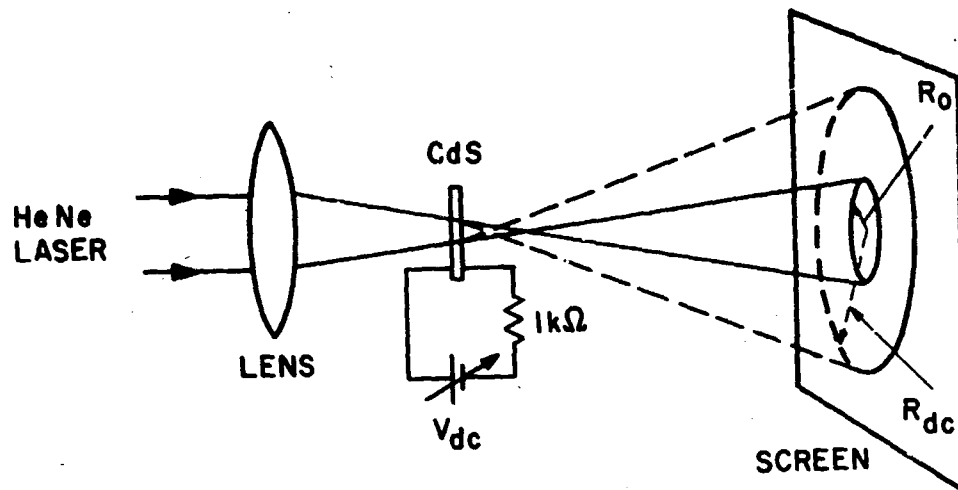


Fig. 1 Experimental Schematic.  $R_0$  and  $R_{dc}$  represent the beam radius without and with d-c voltage applied respectively.

beam passes through. When the d-c voltage is applied, focusing effect results. A list of observations on the effect follows:

1. Beam radius vs. applied voltage: Fig. 2 is a plot of beam radius on the screen versus applied voltage. The sample is of dimensions  $0.3$  (thickness)  $\times 0.2 \times 0.2$  (cm)<sup>3</sup> with its thickness along the C-axis. Curves I and II are measured under pulse condition at two different crystal resistances,  $15\text{k}\Omega$  and  $40\text{k}\Omega$ , respectively. The pulses are of  $\approx 5$  msec long and 15 msec period. Curve III is measured under d-c condition at resistance  $40\text{k}\Omega$ .

2. V-I Characteristics: All the six samples exhibit time-dependent hysteresis in their V-I characteristics. Figure 3a is the d.c. voltage across the CdS plate vs. the current passing through it,  $I_{\text{CdS}}$ . Figure 3b is the same d.c. voltage vs. the current detected by a photo-diode at the screen,  $I_{\text{diode}}$ . The upper portion of the curve, designated by I, is taken as the voltage increases at a rate of  $\approx 30$  volts per sec. II, is the portion where voltage is set approximately constant for 1 minute. And III, the lower portion of the curve is taken as the voltage decreases at a rate of  $\approx 30$  volts per sec. It is noted that a smaller hysteresis is present at Fig. 2b. Four factors are believed to be responsible for the observed V-I characteristics; the acoustoelectric current associated with the sound generation,<sup>2</sup> the decrease in mobility due to thermal heating, the poor ohmic contact, and charge recombination on the plate surfaces. Figure 3c, which is derived from Figs. 3a and 3b, is the plot of power ( $V I_{\text{CdS}}$ ) against  $I_{\text{diode}}$ .

3. Response time: A silicon photodiode of wafer size less than  $1\text{mm}^2$  and frequency response up to 2 GHz was used in place of the screen and the d-c pulses were

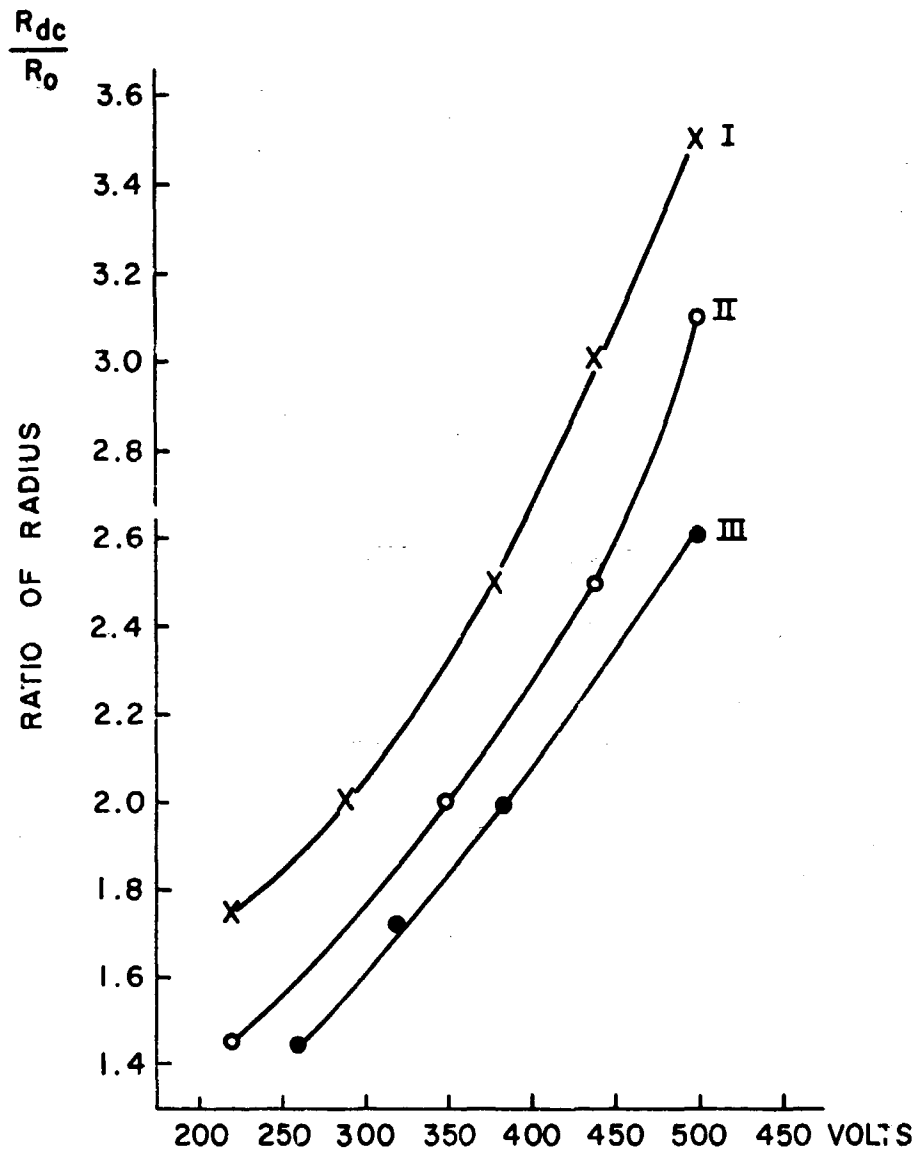


Fig. 2  $\frac{R_{dc}}{R_0}$  as a function of voltage: Curves I and II are measured under pulse condition at crystal resistances  $15k\Omega$  and  $40k\Omega$  respectively. Curve III is measured under d-c condition at  $40k\Omega$ . The beam diameter at crystal position is  $\approx 0.1$  mm.

used. It is found that the typical rise-time detected by the photodiode is  $\approx 0.2$  msec and the decay-time is  $\approx 1.5$  msec. In many instances, the response time is also found to be voltage dependent.

4. d-c polarity: No change is observed as the polarity of the applied d-c voltage is reversed.

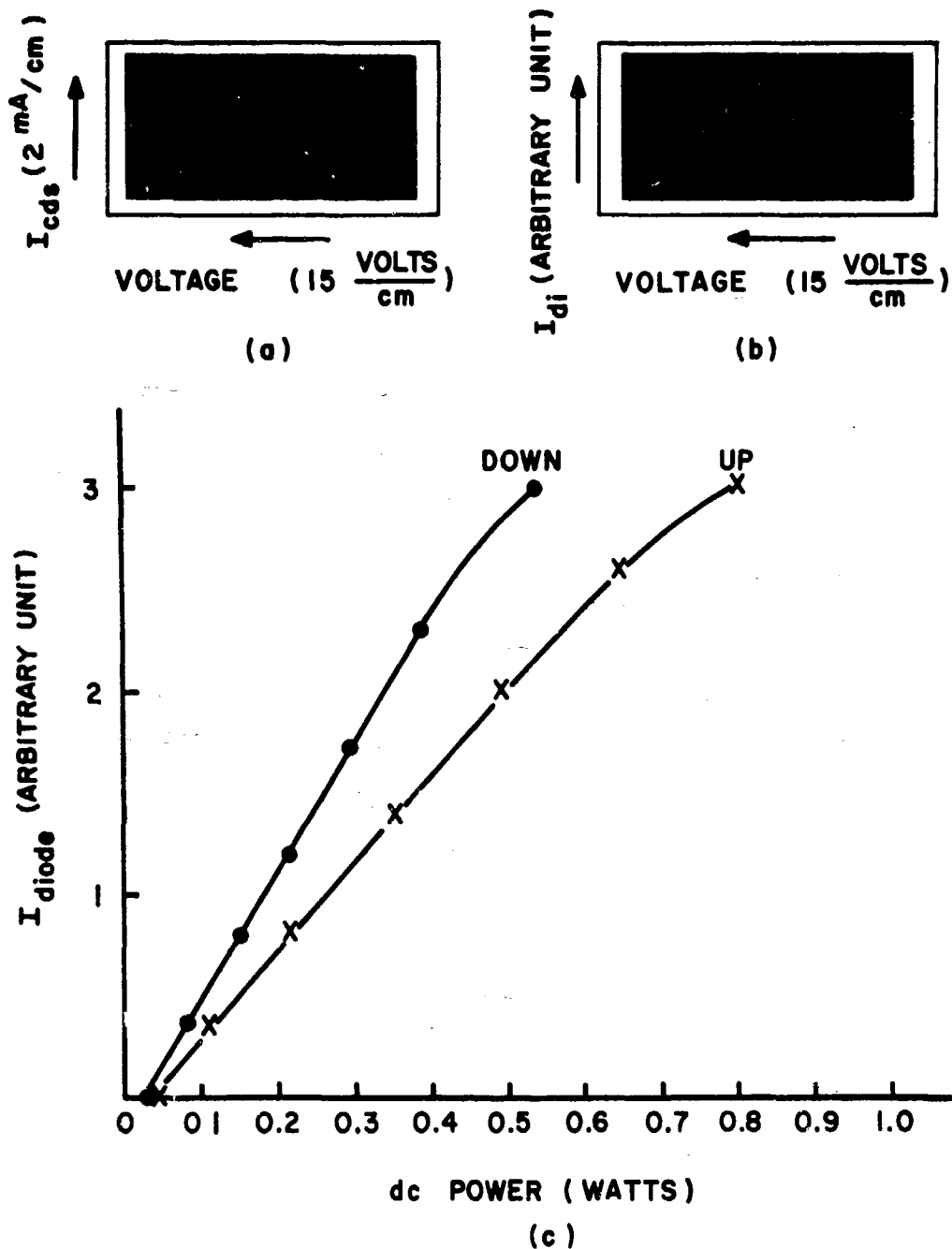


Fig. 3 (a) Current passing through the crystal,  $I_{CdS}$  as a function of d. c. voltage.

I: Voltage increases at a rate of  $30 \frac{\text{volts}}{\text{sec}}$ .

II: Voltage is kept approximately constant for 1 minute.

III: Voltage decreases at a rate of  $30 \frac{\text{volts}}{\text{sec}}$ .

(b) Photodiode current,  $I_{diode}$  as a function of the d. c. voltage.

(c)  $I_{diode}$  as a function of the d. c. power applied to the crystal.

5. Light polarization: No change is observed as the polarization direction of the laser beam is changed.

6. Crystal orientation: The focusing effect seems to be independent of the crystal orientation.

7. Light transmission: The total light transmitted through the CdS plate has been measured before and after the d-c voltage is applied, the change in light transmission is less than 2 percent.

8. Sample thickness, light intensity and field intensity: The effect becomes more pronounced when the sample thickness, the light intensity or the d-c field intensity is increased.

9. Threshold: The threshold field of the focusing effect is found to be quite inconsistent among the samples. Some appear to have a definite threshold, others do not. In general, the threshold appears to be less than the threshold field for sound generation and decreases as the light intensity increases.

10. Ultrasound: As mentioned earlier, in many samples the focusing effect starts before the sound wave is generated in the crystal. However, once a strong ultrasound is generated, its presence is often demonstrated by the unstableness of the focused beam. The unstableness may result from the mode shifting of the ultrasonic wave.

11. Thickness tapered: When the thickness of the CdS plate is tapered to an angle of  $\approx 30$  degrees, the focusing effect is still observed. However, a much longer response time in the photodiode current is also observed. In the case of tapered thickness the center of the laser beam is shifted as the d-c voltage is applied.

12. Pin hole radius: If the lens of Fig. 1 is replaced by a pin hole, it is found that when the applied d-c power is kept constant the focusing effect becomes stronger as the radius of the pin-hole decreases.

The following three sources are thought to be responsible for the observed effect.

i) Ultrasonic generation: The intensity of the laser beam is nonuniform, being greatest along the beam center which will in turn give rise to a similar nonuniform distribution in the free electron density. When the d-c voltage is increased so that the electron drift velocity exceeds the sound velocity, the transverse thermal phonons are amplified through piezoelectric coupling. Since the two major surfaces of the CdS plate are sound reflectors, strong ultrasonic waves are generated inside the crystal. The distribution of the intensity of the ultrasonic wave is expected to be similar to that of the free electron density, i. e., highest along the beam center. Due to the presence of ultrasonic waves, the index of refraction  $n$  of the sample is no longer uniform; the region of highest periodic variation of  $n$  in time and space corresponds to the region of

highest sonic density. Tien, Golden, and Whinnery have theoretically described the focusing effect on a light beam propagating in periodic media.<sup>3</sup> They showed that the whole system of periodic strains can act as a lens with the region of highest sonic density appearing to have an effective refractive index  $n_{\text{eff}}$  greater than the surroundings. In our case, the increase  $\Delta n_{\text{eff}}$  should be proportional to the squares of the variations of  $n$  and would be a maximum at the beam center. Therefore, the beam bends toward the beam center and the focusing effect results.

Attempts have been made to determine if the proposed model would produce the order of magnitude change in the refractive index experimentally observed. However, the results are inconclusive since: (1) no information on the photoelastic constant for the shear waves in CdS can be found in the literature. (2) The strain magnitude ( $S$ ) of the shear wave can only be estimated. According to Isignro, et al., it is in the order of  $6 \times 10^{-5}$ .

ii) Thermal heating: Since the photoconductivity of the CdS plate is controlled by the laser intensity, the crystal conductivity will be highest along the beam center. When the d-c power is applied, heat generated inside the crystal will also be expected to have a radial distribution as that of the conductivity, i. e., more heat generated at the beam center. Since the cross-section of the CdS plate is very much larger than the beam radius, we have a very good heat sink. According to the temperature dependent measurement of the refractive index on CdS<sup>3</sup>,  $dn/dT$  is  $\approx 5 \times 10^{-4}$ . To produce a change of  $10^{-4}$  in the refractive index,<sup>1</sup> from the beam center to the beam edge, it requires a change in temperature of  $0.2^\circ$ . In view of having an efficient heat sink and a large amount of d-c power dissipated it appears possible that such a temperature difference is generated between the beam center and beam edge.

iii) Impurity absorption: The voltage-dependent of response time seems to suggest that a change in the impurity absorption of the laser light may be caused by the application of a d-c field, however, its contribution should be fairly small due to the fact that the total light transmission does not change by more than 2 percent.

National Science Foundation  
GK-1257

W.C. Wang and P. Das

#### REFERENCES

1. W. C. Wang and P. Das, "Focusing of a Laser Beam by an Active CdS Oscillator" *Appl. Phys. Letters* **12**, 204 (1968).
2. W. C. Wang, "Strong Acoustoelectric Effect in CdS," *Phys. Rev. Letters* **9**, 443 (1962).
3. P. K. Tien, J. P. Gordon and J. R. Whinnery, "Focusing of a Light Beam of Gaussian Field Distribution in Continuous and Periodic Lens like Media," *Proc. IEEE* **53**, 129 (1965).
4. D. W. Langer, "Temperature and Pressure Dependence of the Index of Refraction of CdS," *J. Appl. Phys.*, **37**, 3530 (1966).



## A METHOD FOR MEASURING THE TRANSDUCER FREQUENCY RESPONSE OF AN ULTRASONIC AMPLIFIER

R. Mauro

A technique for the measurement of the transducer frequency response in an ultrasonic amplifier, using the acoustoelectric effect, is presented. The validity of this method is experimentally verified by using the measured transducer characteristics to predict the amplifier transmission and comparing this result with the actual transmission data.

In most experiments with cadmium sulphide ultrasonic amplifiers, it is important to determine the frequency response of the input and output transducers. This report demonstrates that such information may be readily obtained from acoustoelectric measurements on the amplifier.

W. C. Wang has previously shown that a simple linear relationship exists in piezoelectric semiconductors between the input acoustic intensity and the detected acoustoelectric voltage.<sup>1</sup> Equation (2) of his paper may be simplified by noting that if the crystal is sufficiently long, then by properly adjusting the illumination, complete attenuation of the acoustic signal within the CdS may be assumed ( $\alpha_e L \gg 1$ ). For this case, the detected acoustoelectric voltage is independent of frequency, and is given by

$$V_{ae} = \left( \frac{R}{R + R_0} \right) \left( \frac{\lambda c}{q n_0} \right) S_0^2 \quad (1)$$

where  $\lambda$  is a numerical constant,  $R$  the external load resistance,  $R_0$  the bulk resistance of the cadmium sulphide,  $c$  the elastic constant,  $n_0$  the density of conduction electrons, and  $S_0$  the input strain to the material. If the amplitude of the applied pulsed RF voltage is held constant, at a particular frequency the amplitude of  $S_0$  will be directly proportional to the transducer response at that frequency. Thus, if all other quantities in (1) are held constant, at any frequency the steady-state transducer response is proportional to the square root of the detected acoustoelectric voltage. By utilizing these voltage measurements the transducer frequency response can therefore be readily computed.

To validate this method, the characteristics of the input and output transducers of a 1-cm-long CdS amplifier were measured using the acoustoelectric technique. This result is shown in Fig. 1. The product of these characteristics was then used to estimate the overall transmission of the amplifier in the insulating state. Figure 2 compared the experimentally measured transmission characteristic for the aforementioned case with that predicted from the acoustoelectric data. The difference between the two curves indicates that complete attenuation of the acoustic signal did not occur, and for this case the detected acoustoelectric voltage is dependent on the

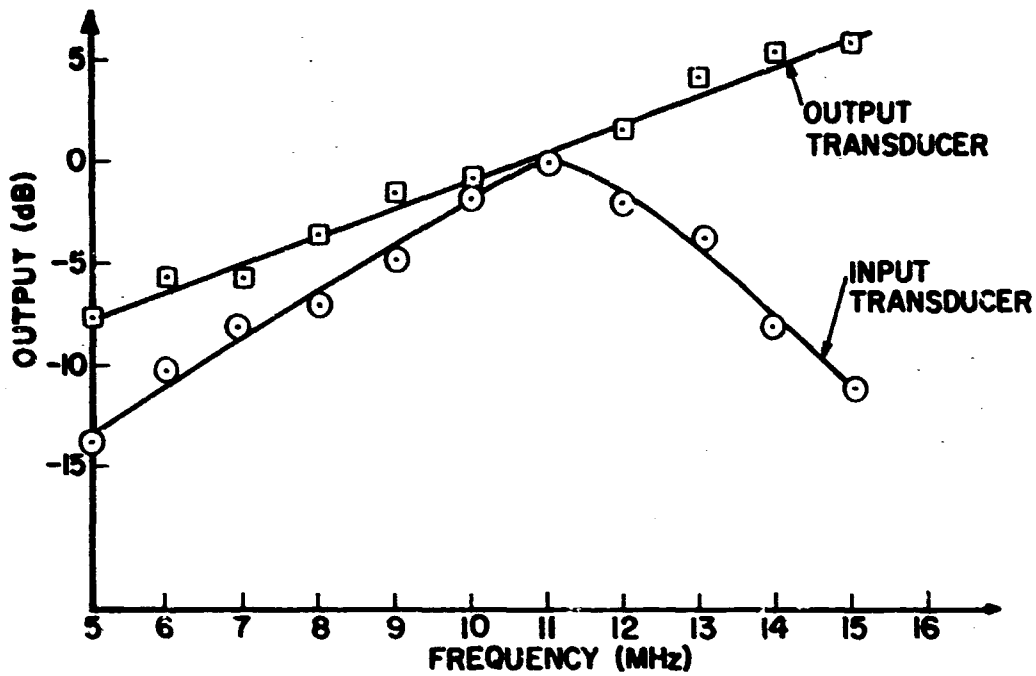


Fig. 1 Input and Output Transducer Response Measured by Acoustoelectric Technique. Transducers are Resonant at 10 and 30 MHz, Respectively.

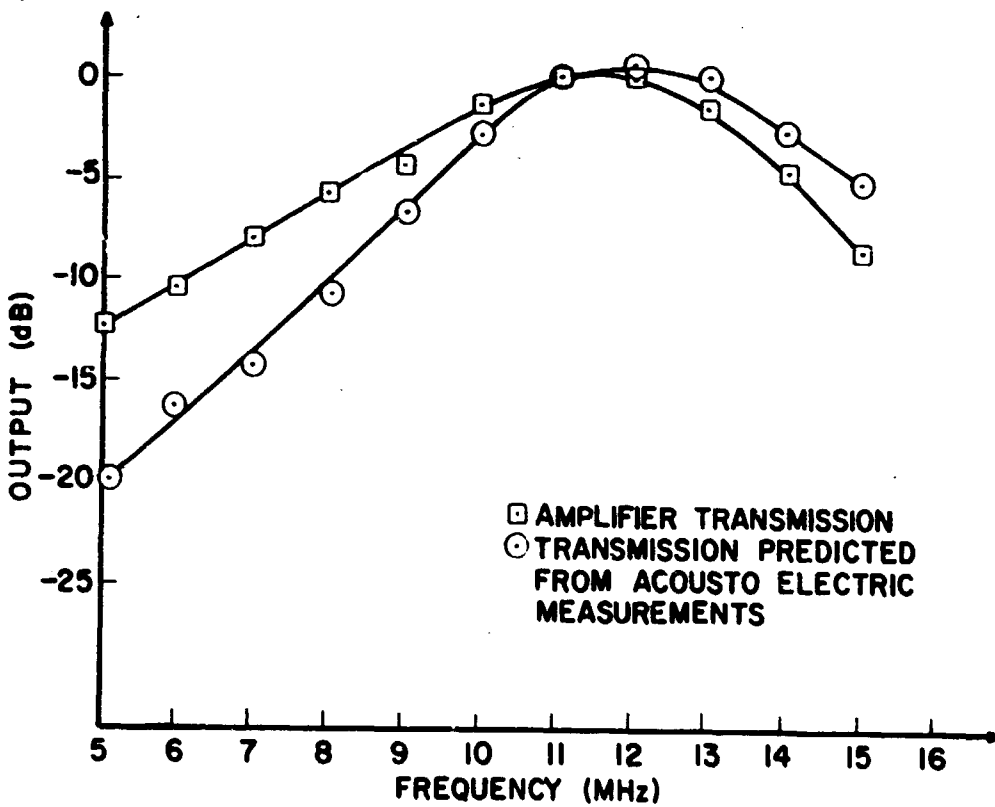


Fig. 2 Comparison of Actual Amplifier Transmission Characteristic With That Predicted From The Product of The Acoustoelectric Input and Output Transducer Measurements.

attenuation coefficient  $\alpha_e$ . In spite of this, however, the reasonable agreement of the two transmission curves demonstrates that acoustoelectric voltage measurements provide a satisfactory estimate of the frequency response of the amplifier transducers. If greater accuracy is required, Wang's complete expression for the acoustoelectric voltage should be used.

National Science Foundation  
GK-1257

R. Mauro

#### REFERENCE

1. W. C. Wang, "Strong Acoustoelectric Effect in CdS," Phys. Rev. Lett., Vol. 9, p. 443, December 1, 1962.

## V. CONTROL THEORY AND COMPUTER SCIENCE

Arkun, M. E.  
 Bharat, R.  
 Bongiorno, J.  
 Braun, L.  
 Coffman, E.  
 Crump, J.  
 Deutsch, S.  
 Dorato, P.  
 Drenick, R. F.

Farmer, D.  
 Gelenbe, S. E.  
 Grobert, K.  
 Habib, S.  
 Haddad, R.  
 Hertzendorf, B. H.  
 Hsieh, C.  
 Kaman, C.

Kantrowitz, A.  
 Kella, J.  
 Kohavi, I.  
 Kozin, F.  
 Krishnan, V.  
 Lawson, H. J., Jr.  
 Nalecz, M.  
 Rijndorp, J. E.

Robinson, P. N.  
 Schultz, R.  
 Schuster, G.  
 Shapiro, S.  
 Shaw, L.  
 Shooman, M. L.  
 Siswosudarmo, M.  
 Smith, E. J.  
 Weiss, G.

### FIXED BASE ALIGNMENT OF A GIMBALLESS GYROLESS INERTIAL NAVIGATOR

V. Krishnan and K. Grobert

Advances in technology of inertial components with the consequent improvement in high speed digital computers have made a totally strap-down navigation system without gyroscopes feasible.<sup>1</sup> The feasibility of such a scheme has been investigated in Ref. 2. In this report a scheme for initially aligning the system is investigated. In conventional gyrostabilized platforms, gyroscopes and accelerometers sense the earth's rotation and the gravitational field and corresponding torquing signals are applied to the gimbal drive mechanism until the platform is aligned to the initial conditions at the starting point. Such a scheme is clearly not possible with the proposed gimballess gyroless navigation system. Even though auxiliary equipment can be used to align such a system, this report presents a scheme whereby initialization is accomplished in the space vehicle without the use of auxiliary equipment. Such an initialization is attempted for the vehicle standing still. Further reports will cover in-flight initialization schemes. The mechanization of navigation equations are accomplished in the local-level coordinate system. The coordinate axes are defined in Fig. 1.

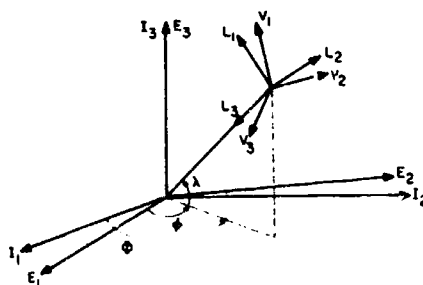


Fig. 1 Coordinate Axes

The accelerometers are aligned along  $V_1$ ,  $V_2$ ,  $V_3$ . The computer updates the direction cosine matrix and converts the measured acceleration along the  $[V]$  axes to acceleration along the local level axes  $[L]$ . If the computer is not initially set to the correct conditions the computed axes  $[L_c]$  will be in error compared to the true axes  $[L]$ . This error, obviously will be small and hence small angle approximations can be applied.

If  $\theta_1$ ,  $\theta_2$  and  $\theta_3$  are the Eulerian angles to obtain the coordinate axes  $[L_c]$  from  $[L]$ , then the following equation holds

$$[L_c] = \begin{bmatrix} 1 & \theta_1 & 0 \\ -\theta_1 & 1 & 0 \\ 0 & 0 & 1 \end{bmatrix} \begin{bmatrix} 1 & 0 & -\theta_2 \\ 0 & 1 & 0 \\ \theta_2 & 0 & 1 \end{bmatrix} \begin{bmatrix} 1 & 0 & 0 \\ 0 & 1 & \theta_3 \\ 0 & -\theta_3 & 1 \end{bmatrix} [\tilde{D}][V] \quad (1)$$

where  $\tilde{D}$  is the direction cosine matrix

$$\begin{bmatrix} d_{11} & d_{21} & d_{31} \\ d_{12} & d_{22} & d_{32} \\ d_{13} & d_{23} & d_{33} \end{bmatrix}$$

If the computer is properly aligned and assuming the vehicle is stationary, the outputs of the computer representing the acceleration along the local level axes will be

$$\begin{bmatrix} A_{L_{1c}} \\ A_{L_{2c}} \\ A_{L_{3c}} \end{bmatrix} = \begin{bmatrix} 0 \\ 0 \\ g \end{bmatrix} \quad (2)$$

Also, if the rotation of the earth is  $\omega_e$  then the output of the perfectly aligned computer will be

$$\begin{bmatrix} \omega_{L_{1c}} \\ \omega_{L_{2c}} \\ \omega_{L_{3c}} \end{bmatrix} = \begin{bmatrix} \omega_e \cos \lambda \\ 0 \\ -\omega_e \sin \lambda \end{bmatrix} \quad (3)$$

where  $\lambda$  is the latitude.

Expanding Eq. (1) the computed accelerations are

$$\begin{bmatrix} A_{L_{1c}} \\ A_{L_{2c}} \\ A_{L_{3c}} \end{bmatrix} = \begin{bmatrix} -\theta_2 d_{13} & -\theta_2 d_{23} & -\theta_2 d_{33} \\ \theta_3 d_{13} & \theta_3 d_{23} & \theta_3 d_{33} \\ d_{13} & d_{23} & d_{33} \end{bmatrix} \begin{bmatrix} A_{v_1} \\ A_{v_2} \\ A_{v_3} \end{bmatrix} \quad (4)$$

The earth's angular velocity expressed as projections along the computed local level system is

$$\begin{bmatrix} \omega_{L_{1c}} \\ \omega_{L_{2c}} \\ \omega_{L_{3c}} \end{bmatrix} = \begin{bmatrix} d_{11} & -\theta_2 d_{13} & d_{21} & -\theta_2 d_{33} & d_{31} & -\theta_2 d_{33} \\ -\theta_1 d_{11} + \theta_3 d_{13} & & -\theta_1 d_{21} + \theta_3 d_{23} & & -\theta_1 d_{31} + \theta_3 d_{33} & \\ d_{12} + \theta_3 d_{12} & & d_{23} + \theta_3 d_{22} & & d_{33} + \theta_3 d_{32} & \end{bmatrix} \begin{bmatrix} \omega_{v_1} \\ \omega_{v_2} \\ \omega_{v_3} \end{bmatrix} \quad (5)$$

The error signals required to correct the direction cosines are derived from  $A_{L_{1c}}$ ,  $A_{L_{2c}}$  in Eq. (4) and  $\omega_{L_{2c}}$  in Eq. (5);  $A_{L_{1c}}$  represents the misalignment about the  $L_2$  axis,  $A_{L_{2c}}$  represents the misalignment about the  $L_1$ -axis and  $\omega_{L_{2c}}$  is used to correct the azimuth and contains misalignments about the  $L_2$  and  $L_3$  axis. The error signals derived are given by

$$\begin{bmatrix} \epsilon_{v_1} \\ \epsilon_{v_2} \\ \epsilon_{v_3} \end{bmatrix} = [D] \begin{bmatrix} 1 & 0 & 0 \\ 0 & 1 & \theta_3 \\ 0 & -\theta_3 & 1 \end{bmatrix} \begin{bmatrix} 1 & 0 & -\theta_2 \\ 0 & 1 & 0 \\ \theta_2 & 0 & 1 \end{bmatrix} \begin{bmatrix} 1 & \theta_1 & 0 \\ -\theta_1 & 1 & 0 \\ \theta_2 & 0 & 1 \end{bmatrix} \left\{ \begin{bmatrix} A_{v_1} \\ A_{v_2} \\ A_{v_3} \end{bmatrix} + [\epsilon'''] \begin{bmatrix} \omega_{v_1} \\ \omega_{v_2} \\ \omega_{v_3} \end{bmatrix} \right\} \quad (6)$$

where,

$$[\theta'] = \begin{bmatrix} \theta_3 d_{13} & \theta_3 d_{23} & \theta_3 d_{33} \\ \theta_2 d_{13} & \theta_2 d_{23} & \theta_2 d_{33} \\ 0 & 0 & 0 \end{bmatrix}$$

and

$$[\theta'''] = \begin{bmatrix} 0 & 0 & 0 \\ 0 & 0 & 0 \\ -\theta_3 d_{13} + \theta_1 d_{11} & -\theta_3 d_{23} + \theta_1 d_{21} & -\theta_3 d_{33} + \theta_1 d_{31} \end{bmatrix}$$

If Eq. (6) is substituted into the differential equations connecting the direction cosines, and neglecting second order terms in  $\theta_1$ ,  $\theta_2$  and  $\theta_3$

$$\begin{aligned} \dot{d}_{11c} &= \theta_2 d_{13} g - \theta_1 d_{12} \omega_{L_1} & \dot{d}_{32c} &= \theta_3 d_{33} g + \theta_1 d_{31} \omega_{L_1} \\ \dot{d}_{21c} &= \theta_2 d_{23} g - \theta_1 d_{22} \omega_{L_1} & \dot{d}_{13c} &= (\theta_3 d_{12} - \theta_2 d_{11}) g \\ \dot{d}_{31c} &= \theta_2 d_{33} g - \theta_1 d_{32} \omega_{L_1} & \dot{d}_{23c} &= (\theta_3 d_{22} - \theta_2 d_{21}) g \\ \dot{d}_{12c} &= \theta_3 d_{13} g + \theta_1 d_{11} \omega_{L_1} & \dot{d}_{33c} &= (\theta_3 d_{32} - \theta_2 d_{31}) g \\ \dot{d}_{22c} &= \theta_3 d_{23} g + \theta_1 d_{21} \omega_{L_1} & & \end{aligned} \quad (7)$$

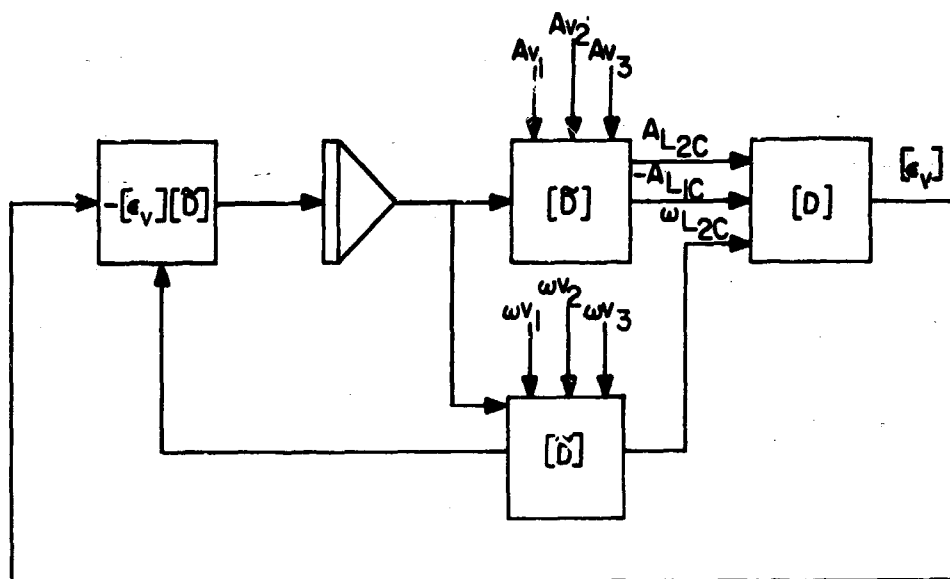


Fig. 2 Fixed-Base Alignment

If Eqs. (7) are integrated, the initial errors will ultimately converge to zero. A block diagram of such a mechanization is given above.

National Science Foundation  
GU-1557

V. Krishnan

Joint Services Technical Advisory Committee  
AF 49 (638)-1402

#### REFERENCES

1. V. Krishnan, "Gimballess Inertial Navigation System," Doctoral Dissertation, Univ. of Penna., 1962.
2. J. Stump, "Feasibility of a Gimballess Inertial Navigator," Master's Thesis, Polytechnic Institute of Brooklyn, 1966.

#### CANONICAL OBSERVERS IN LINEAR CONTROL SYSTEMS

M. Siswosudarmo, P. Dorato

The nonaccessible state variables of a linear, time invariant, completely observable plant can be approximately reconstructed by building a compatible observer. A possible design of a compatible observer is based on the canonical form of the plant and the observer. The first step in the development of canonical forms is the selection of  $n$  linearly independent column vectors from the  $np$  column vectors of the observability matrix. Four canonical transformations are studied in detail. The first and the second canonical systems can be divided into single output canonical subsystems, and the subsystems are coupled to each other through their outputs. If the

orders of the subsystems are almost equal, the third and the fourth canonical transformations can be obtained by interchanging the column vectors of the first and the second canonical transformations.

The canonical observer is constructed by selecting the observer matrices to satisfy the observer condition and the compatibility condition. The plant and the observer are assumed to be in the second or fourth canonical form. The eigenvalues of the observer matrix  $A$  are selected arbitrarily, as long as they have no nonnegative real parts and they are not equal to the eigenvalues of the plant matrix  $F$ . By selecting a special form of the observer transformation matrix  $T$ , the observer matrix  $B$  can be formulated as product and addition of the partitions of  $A$  and  $F$ . It is shown that the canonical observer is compatible.

In the special case of the reconstruction of a single linear functional of the plant state variables, it is shown that a reduction of the order of the observer is possible. The observer and the plant are assumed to be in the second canonical form. The canonical  $A$  is block diagonal, the eigenvalues of each block is a subset of the eigenvalues of the first (largest) block, and the eigenvalues of the first block are distinct. The diagonal blocks are transformed to diagonal matrices. By collecting the state variables corresponding to the same eigenvalues, an observer of the order  $n_o - 1$  is obtained,  $n_o$  is the observability index of the plant.  $n_o - 1 \leq n - p$ . The method can be extended to the design of an observer for multi linear functional of the state variables of the plant, in some cases the design provides a minimum number of integrators.

The use of a compatible observer in feedback control system is investigated. It is shown that the closed loop eigenvalues are the eigenvalues of the observer and the eigenvalues of the closed loop system with an error free compatible observer. When a compatible observer is used in a regulator control system which for error free observer is optimal with respect to a quadratic cost index, for a finite time interval, an increase of cost index is expected. It is shown that for a subclass of initial states, the increase of cost becomes larger when the real parts of the eigenvalues of  $A$  become more negative. The eigenvalues of  $A$  can be selected so as to minimize an upper bound of the increase of cost for all admissible initial states. It is also established that there exists no feedback law better than the optimal regulator, which gives a minimum cost index for all initial states when the overall system is required to be stable.

National Science Foundation  
GU-1557

M. Siswosudarmo

Joint Services Technical Advisory Committee  
AF 49 (638)-1402



## OPTIMAL BANG-BANG CONTROL OF STOCHASTIC SYSTEMS WITH A SMALL NOISE PARAMETER

P. Dorato, C. Hsieh, and P. N. Robinson

The basic problem considered in this study is that of determining a feedback control law which minimizes a performance index of the form

$$S = E \left\{ \int_0^{\tau_R} L(\underline{x}) dt \mid \underline{x}(0) \right\} \quad (1)$$

given a plant with dynamics

$$d\underline{x} = \underline{f}(\underline{x}, u) dt + \underline{g}(\underline{x}) d\xi \quad (2)$$

with a control-input constraint,  $|u(t)| \leq 1$ ; where  $E\{\cdot\}$  denoted the expectation operator,  $\underline{x}$  an  $n$ -dimensional state vector,  $u(t)$  a scalar control input,  $\xi(t)$  a scalar Wiener process with variance parameter  $\sigma^2$ , i. e.  $E\{(\xi(t + \Delta t) - \xi(t))^2\} = \sigma^2 \Delta t$ ,  $\tau_R$  the time required for  $\underline{x}(t)$  to first reach a given terminal region  $R$ , and  $L(\underline{x})$  a positive scalar function of the vector  $\underline{x}$ . The control input  $u$  is assumed to appear linearly in  $\underline{f}(\underline{x}, u)$ , i. e.  $\underline{f}(\underline{x}, u) = \underline{h}(\underline{x}) + \underline{g}u$ .

For a given feedback law the plant dynamics (Eq. (2)) generate a vector Markov process in the state  $\underline{x}(t)$ . It can be shown that a formal application of dynamic programming concepts yields the following optimization equation

$$0 = \min_u \left[ \left( \frac{\partial S^0}{\partial \underline{x}} \right) \underline{f}(\underline{x}, u) + \frac{1}{2} \sigma^2 \left( \frac{\partial}{\partial \underline{x}} \underline{g}(\underline{x}) \underline{g}'(\underline{x}) \frac{\partial'}{\partial \underline{x}} \right) S^0 + L(\underline{x}) \right] \quad (3)$$

where  $\partial/\partial \underline{x}$  denotes the gradient operator (row vector),  $\underline{g}'$  the transpose of  $\underline{g}$ ,  $S^0$  the minimum value of  $S$ , and

$$\left( \frac{\partial}{\partial \underline{x}} \underline{g}(\underline{x}) \underline{g}'(\underline{x}) \frac{\partial'}{\partial \underline{x}} \right) S = \sum_i \sum_j g_i(\underline{x}) g_j(\underline{x}) \frac{\partial^2 S^0}{\partial x_i \partial x_j}$$

The boundary conditions for Eq. (3) are:

1.  $S^0(\underline{x}) = 0$ , for  $\underline{x} \in \partial R$ , where  $\partial R$  denotes the boundary of  $R$ .
2. For large  $\|\underline{x}\|$ , where  $\|\underline{x}\|$  denotes the norm of  $\underline{x}$ , the solution  $S^0(\underline{x})$  approach the deterministic solution; i. e. the solution corresponding to  $\sigma^2 = 0$ .

It should be noted from Eq. (3), the control-input constraints, and the fact that  $u$  is linear in  $\underline{f}(\underline{x}, u)$ , that the optimal control input is given by

$$u^0 = - \operatorname{sgn} \left( \frac{\partial S^0}{\partial u} \right)$$

i. e. the control input is of the bang-bang type.

The following solution is proposed for the case where  $\sigma^2$  is small. Assume that  $S^0(\underline{x})$  may be expanded in a power series in  $\sigma^2$ , i. e.

$$S^0(x) = S_0(x) + \sigma^2 S_1(x) + \sigma^4 S_2(x) + \dots \quad (4)$$

then Eq. (3) becomes

$$\left( \frac{\partial S_1}{\partial x} \right) (h(x) + q^{\pm}) = -\frac{1}{2} \left( \frac{\partial}{\partial x} g g' \frac{\partial}{\partial x} \right) S_{i-1} \quad (5)$$

for  $i = 1, 2, \dots$

and

$$\left( \frac{\partial S_0}{\partial x} \right) (h(x) + q^{\pm}) = -L(x) \quad (6)$$

where

$$q^{\pm} = +q, \quad \text{for } \left( \frac{\partial S_0}{\partial x} q \right) < 0$$

$$q^{\pm} = -q, \quad \text{for } \left( \frac{\partial S_0}{\partial x} q \right) > 0$$

Note that the terms  $S_i$ ,  $i \geq 1$ , represent perturbations on the deterministic solution  $S_0$ . With the above assumption, the nonlinear second order optimization Eq. (3) is reduced to a system of piece-wise linear first order equations. This type of perturbation solution, because it does reduce the order of the equations in question, is referred to as a singular perturbation and in general the simple series solution (Eq. (4)) is not uniformly convergent for all  $x$ . However one can attempt to obtain at least approximate solutions from Eq. (4). In particular the approximation for  $S^0(x)$  is generated for all  $x$ , at least for all  $x$  where  $S^0(x)$  exists, as follows:

1. Assume  $q^{\pm} = -q$ . Solve the system of first order Eqs. (5) and (6) using the method of characteristics, with the boundary conditions

$$S_i(x) = 0, \quad x \in \partial R, \quad i = 0, 1, 2 \quad (7)$$

Denote the set of points where characteristic curves extend and satisfy the boundary conditions (7) by  $\Gamma_0^-$ .

2. With the solution in step one compute a switching segment  $\Gamma_0^+$  from

$$\frac{\partial S_0}{\partial x} q = 0,$$

where  $S^0$  is approximated by a finite number of terms in the expansion (Eq. (4)). Now let  $R_0^-$  denote the set of points bounded by  $\Gamma_0^-$  and  $\partial T_0^-$ . This represents the set of points where the sign of  $\partial S^0 / \partial x q$  is consistent with  $u = -1$ . In a similar way one can compute a positive switching segment  $\Gamma_0^+$ .

3. A cross a switching curve  $S^0(x)$  must be continuous, so that one can now specify the values of  $S^0(x)$  on  $\Gamma_0^+$ . Now repeat step one with a new terminal region made up of

the union of  $R$  and  $\Gamma_0^+$  to obtain the next switching segment  $\Gamma_1^-$ .

4. Repeat the above steps until a complete curve is generated, as the union of individual switching segments.

In the following example the above method yields an exact result.

Example:

For the linear system

$$\dot{\underline{x}} = \begin{bmatrix} 0 & 1 \\ 0 & 0 \end{bmatrix} \underline{x} + \begin{bmatrix} 0 \\ 1 \end{bmatrix} u + \begin{bmatrix} 0 \\ 1 \end{bmatrix} \xi, \quad \underline{x} = \begin{pmatrix} x_1 \\ x_2 \end{pmatrix}$$

with an integral quadratic performance index

$$S = E \left\{ \int_0^T \underline{x}' \begin{bmatrix} 1 & 0 \\ 0 & 0 \end{bmatrix} \underline{x} dt \mid \underline{x}(0) \right\}$$

and the "strip" terminal region  $R$  ( $-0.2 \leq x_1 \leq 0.2, x_2 = 0$ ), the method of characteristics applied to Eq. (5) and (6) yields the exact solution  $S^0 = S_0 + \sigma^2 S_1 + \dots + \sigma^8 S_4$  where

$$S_0 = \frac{2}{15} x_2^5 + \frac{2}{3} x_2^3 x_1 + x_2 x_1^2$$

$$S_1 = \frac{7}{12} x_2^4 + x_1 x_2^2$$

$$S_2 = \frac{3}{2} x_2^3 + x_1 x_2$$

$$S_3 = \frac{9}{4} x_2^2$$

$$S_4 = \frac{9}{4} x_2$$

The switching segment  $\Gamma_0^-$  is determined from

$$\frac{\partial S^0}{\partial \underline{x}} \underline{g} = \frac{\partial S^0}{\partial x_2} = 0.$$

The region  $T_0^-$  in this case is bounded by the switching curve above, the region  $R$ , and the characteristic  $x_1 = -\frac{1}{2} x_2^2 + 0.2$ .

Joint Services Technical Advisory Committee  
AF 49(632)-1402

P. Dorato, C. Hsieh and P. N. Robinson

### MINIMUM SENSITIVITY DESIGN OF ATTITUDE CONTROL SYSTEMS VIA LYAPUNOV FUNCTIONS

P. Dorato

In this study Lyapunov functions are used to design feedback control laws which guarantee asymptotic stability for specified plant-parameter variations. Satellite attitude control dynamics in the nonlinear acquisition phase, when direction cosines are used to specify attitude, are of the general form

$$\dot{\underline{x}}_1 = \underline{x}'_1 A_1 \underline{x}_1 + a_1 N_1$$

where  $\underline{x}$  is an  $n$  dimensional state vector with components  $x_i$ ,  $A_i$  are  $n \times n$  matrices,  $a_i$  are scalar gain factors for the input torques  $N_i$ , and  $\underline{x}'$  denotes the transpose of  $\underline{x}$ . Plant parameter variations include variations in  $A_i$  and  $a_i$ . The basic design approach is then to determine feedback control laws.

$$N_i = \phi_i(\underline{x})$$

such that  $\dot{V}(\underline{x})$  is negative for all anticipated variations in plant parameters. Here  $V(\underline{x})$  is a positive definite "Lyapunov" function. If the design flexibility in the choice of  $N_i$  is parametrized by a constant vector  $\underline{k}$  and the total parameter vector is denoted by  $\underline{a}$ , then the design objective may be characterized by the following problem, determine  $\underline{k}$  such that for all admissible  $\underline{a}$ ,  $\dot{V}(\underline{x})$  is negative.

National Aeronautics and Space Administration  
NgR 33-006-042

P. Dorato

### MODELING AND CONTROL OF A CHEMICAL PROCESS

L. Shaw and A. Kantrowitz

This report is concerned with the development of a feedforward-feedback control system for a distillation column. The process being considered is a multi-input, multi-output nonlinear system. The problem being considered can be broken into four main parts which are: (1) development of an accurate digital simulation based on the physical concepts involved, (2) determination of the most efficient identification technique for the determination of the parameters of the simplified model for use in association with the feedforward controller, (3) development of the feedforward controller, and (4) development of a feedback control scheme which will reduce any errors made by the feedforward controller.

The digital simulation has already been completed. A set of first order nonlinear differential equations was obtained by combining the partial and total mass balance equations taken about each plate, the reboiler, and the condenser. An auxiliary set of equations was also obtained by assuming that the liquid overflow from a tray was linearly re-

lated to the holdup on the tray and the vapor flow rate from the previous tray. These equations were solved with the aid of an IBM subroutine. The simulation allows for five inputs and two outputs. The inputs are the liquid and vapor feed flow rates, the feed concentration, the vapor rate from the reboiler, and the reflux ratio. The outputs are the concentrations at the top and bottom of the column.

The identification problem is now under consideration. Pseudo-random test signals and step input signals are being investigated as possible input test signals. At this time no decision has been made as to which technique is best suited for this system.

As soon as a satisfactory lower order model of the distillation column is determined, it will be used in association with a feedforward controller. The final step in the project will be to add a feedback loop. The purpose of the feedback loop will be to reduce any deviations in the output concentrations which occur because of the use of the lower order model in the feedforward controller.

U. S. Army Research Office  
DA 31-124-ARO(D)-316

A. Kantrowitz

## VARIABLE-LENGTH DISTINGUISHING SEQUENCES AND THEIR APPLICATION TO THE DESIGN OF FAULT DETECTION EXPERIMENTS

I. Kohavi

A variable-length distinguishing sequence (VLDS) is a preset distinguishing sequence  $X_0$  such that, if the machine is started in an unknown state, the output response of the machine to some prefix of  $X_0$  will identify the initial state. The length of the required prefix is a function of the initial state. The properties of such sequences are investigated and a method, which employs a modified version of the diagnosing tree, is developed for generating and displaying all such sequences. The fixed-length distinguishing sequence (FLDS) is shown to be a special case of the more general VLDS. The VLDS is next applied in the design of simple and efficient preset fault detection experiments for sequential machines.

### The Distinguishing Tree,

Machine  $M$  is described by means of its state table (Table I). The response of  $M$  to the sequences 010 and 10 are summarized in Table II.

It is evident that the two input sequences 10 and 010 are distinguishing sequences. Since the DS 10 is the shortest for machine  $M$ , the experimenter might be tempted to use it for the determination of the initial state and in the design of fault detection experiments. However, a closer inspection of the responses of Table II leads to the following observations: (1) Starting from the initial uncertainty (ABCDE), the response

**Table I**  
Machine M

PS	NS, Z	
	x=0	x=1
A	B, 0	B, 1
B	C, 1	D, 1
C	A, 2	A, 1
D	E, 3	A, 2
E	D, 3	B, 2

**Table II**  
Responses of M to input sequences

Initial state	Response to	
	10	010
A	11	013
B	13	110
C	10	211
D	20	321
E	21	320

to an input 1 leads to the uncertainty vector (BDA) (AB) which implies that the initial state was either (ABC) or (DE), depending on whether the response was 1 or 2. No conclusion can be made about the exact initial state unless a second input is applied. (2) starting with the same initial uncertainty, the response to a 0 input leads to the uncertainty vector (B) (C) (A) (ED). Consequently, by observing the response of M to this single input we may conclude that the initial state was A, B or C depending on whether the output was 0, 1 or 2, respectively. If the response to the 0 input was 3, no conclusions can be reached regarding the initial state except for the observation that it was either D or E. Hence, if the experimenter used the first DS which is a FLDS, he is guaranteed to determine the initial state by the application of two input symbols only. However, if he chooses to start with an input of 0 he can determine the initial state by applying a single input symbol or he may have to apply three symbols, depending on the initial state. Consequently the sequence 010 is a VLDS.

The length of a VLDS  $X_0$  is defined as the average length of the shortest distinguishing prefixes (SDP's) of  $X_0$ .

Our first task is to modify the tree procedure so that the various DS's, fixed as well as variable-length, will be generated and displayed. The tree for machine M is given in Fig. 1.

Starting with the initial uncertainty (ABCDE), the application of a 0 input yields the 0-successor uncertainty (B) (C) (A) (ED) which may also be written in a compact form (ED), since the components containing single states only may be omitted. Under the vector (B) (C) (A) (ED) we have written the vector (A) (B) (C) (DE), where the circled states denote those states which have been identified uniquely by the application of the first input, while the component (DE) denotes those states which have not yet been distinguished. Similarly the application of a 1 input leads to the 1-successor (BDA) (AB) which distinguishes the initial states (ABC) from (DE). From the complete tree it is evident that machine M has numerous distinguishing sequences, of which the

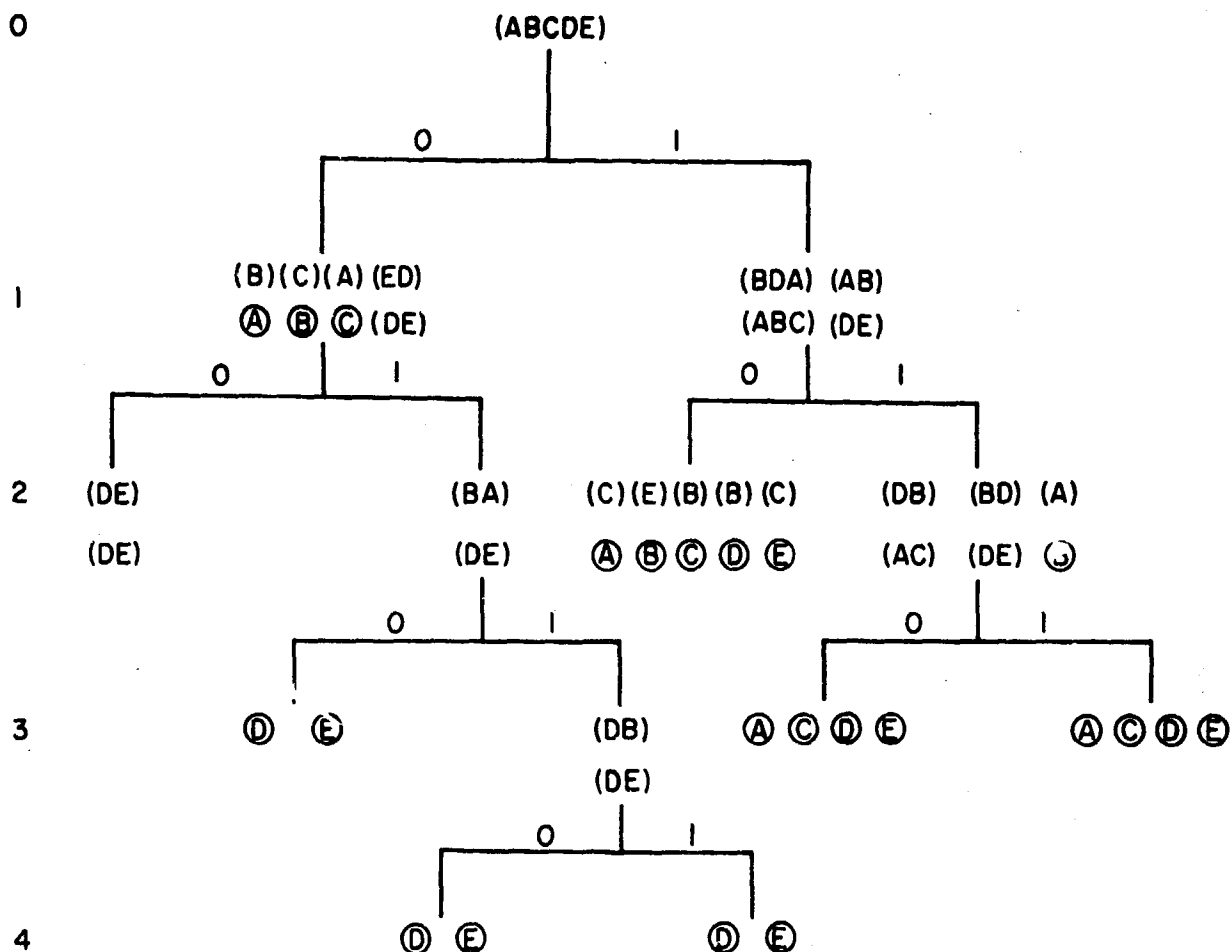


Fig. 1 A Distinguishing Tree for Machine M

sequences 10 and 010 are the shortest fixed and variable length sequences, respectively. (Note that the length of the VLDS 010 is  $9/5$ , while that of 110 or 111 is  $14/5$ ).

There are two major differences between the method outlined above for the construction of the distinguishing tree and the method described in Gill<sup>1</sup>. Since Gill is only concerned with FLDS's he terminates the whole tree in the k-th level, if there exist one or more trivial uncertainties associated with that level. Using that method, the tree of Fig. 1 would have been terminated in the second level and the VLD's 010 would not have been revealed. The second difference is that the tree of Fig. 1 displays the status of the initial uncertainty, i. e., the initial states which have been identified at any point in the experiment, as well as the  $x_1$  - successor uncertainties, while the tree suggested by Gill displays only the latter.

It must be emphasized that an experiment based upon a VLDS is preset and not adaptive since it is predesigned independently of the output. The experiment may,

however, be terminated before its completion if the response is sufficient to uniquely identify the initial state, independently of the remainder of the sequence. It is evident that while not every FLDS may be used as VLDS, every VLDS may be used as FLDS, e. g., the sequence 10 cannot be used as VLDS on M, while the entire sequence 010 can be used as FLDS. In most cases, however, the distinguishing sequences can be used as VLDS's and the above outlined procedure will help to detect such possibilities and evaluate their properties. The applications and advantages of the VLDS will become more evident in the design of fault detection experiments.

#### Design of Fault Detection Experiments with VLDS's.

The design of fault detection experiments has been studied by various authors<sup>2, 3</sup>. The basic tool for these designs has been the FLDS. The length of the fault detection experiment is generally a function of the number of states and the length of the DS. The significance of the length of the DS is further increased by the fact that the DS must be applied repeatedly in order to identify each state and to verify the accuracy of each transition. In a fault detection experiment for a machine having  $n$  states and  $m$  inputs, the DS must be applied at least  $nm$  times and consequently its length is a major factor in the determination of the length of the experiment. As an example we shall design a fault detection experiment for machine M, using the VLDS 010. The response of M, as well as the final states, are summarized in Table III.

Table III

Response of M to the SDP of the VLDS 010

Initial state	Response to SDP of 010	Final state
A	0	B
B	1	C
C	2	A
D	321	C
E	320	B

The sequence 10 is known to be a HS of M, hence its application to the machine together with the appropriate transfer sequence will put M in state A, ready to accept the preset part of the experiment. (A transfer sequence  $T(S_i, S_j)$  is defined as the shortest input sequence which takes M from state  $S_i$  into state  $S_j$ .) If a fault occurred and M did not reset to A, the following experiment, which assumes initial state A, will reveal the existence of such a fault.

The fault detection experiment starts with a 0 input (since 0 is the SDP for A) to check the initial state. If the machine operates correctly it will respond with a 0 out-



put and go to state B. The application of three additional 0 inputs pass the machine through states C and A into state B. At this point another 0 input will not result in any new transition and hence, an input 1 followed by the appropriate SDP is applied. This part of the experiment is as follows:

```
Input:    0 0 0 1 0 1 0
State:   A B C A B D   B C
Output:  0 1 2 0 1 3 2 1
```

If the machine has not produced the above specified output up to this point, we may conclude that it does not operate correctly. If however, the above specified output has been produced, no definite conclusion can be drawn as to whether the machine has operated correctly and is indeed in state C, or whether a fault exists and the actual final state is different from C. We shall therefore assume that the machine is in state C and design the next part of the experiment under this assumption. If the assumption is wrong, it will be revealed by the next parts of the experiment. From the above input-output sequences it is evident that the machine being tested has at least four distinct states since it responded to an input 0 with four different outputs. Furthermore, provided we demonstrate next the existence of a distinct fifth state, this experiment ascertains the transitions, under an input 0 from A to B, B to C and C to A, and under an input 1 from B to D. The only yet unverified transition, in this section of the experiment, is from D under a 0 input.

Starting from state C, we apply an input 1 followed by the SDP 0 in order to check the transition from C to A. This leaves the machine in state B. Since both transitions from this state have already been checked, a transfer sequence  $T(B, D) = 1$  is applied followed by 0010 to cause and check the transition from D to E. At this point all five states of M have been uniquely identified. Also the verification of the transition from D to E under a 0 input, together with the information available from the preceding section of the experiment, is sufficient to ascertain the transition from E to B under an input 1. This section of the experiment is as follows:

```
Input:   1 0 1 0 0 1 0
State:  C A B D E   A B
Output: 1 0 1 3 3 2 0
```

At this point a transfer sequence  $T(B, E) = 10$  is needed followed by a 0010 to check the transition from E into D. This check together with previous information is also sufficient for the verification of the transition from D to A. In a similar manner the experiment is completed as shown below:

```
Input:  000010101010010100010010
Output: 012013211013320133321211
```

This experiment requires 24 input symbols versus 34 symbols which would have been required for an experiment using the FLDS 10. Thus, although the chosen VLDS 010 contained three symbols, versus two symbols required for the FLDS 10, the resulting fault detection experiment is substantially simpler.

A fault detection experiment, constructed in the preceding manner, generally consists of three overlapping parts: a set of transfer sequences; input symbols to cause the desired transitions;  $nm$  applications of the DS. The use of a VLDS affects mainly the latter part of the experiment, which is generally the longest one. The length of this part can be computed as follows.

Let  $Q_{ij}$  be the state to which the machine goes from  $S_i$  when input  $I_j$  is applied, i. e.,  $S_i \times I_j \rightarrow Q_{ij}$ . Let  $L(Q_{ij})$  be the SDP of state  $Q_{ij}$ , then the total length of the DS's in the fault detection experiment is given by

$$l = \sum_{i,j=1}^{n,m} L(Q_{ij})$$

Clearly, if  $L(Q_{ij})$  is a constant ( $=L_0$ ), then  $l = L_0 mn$ . Thus, the usefulness of the VLDS is increased whenever its average length is shorter than that of the FLDS and, in addition, a larger number of the next-state entries  $Q_{ij}$  possess the shorter prefixes of  $X_0$ . Very often it occurs that the maximal length of a VLDS is also the shortest FLDS, in such cases the preceding procedure yields shorter and more efficient experiments.

This work was carried out in collaboration with Z. Kohavi, Department of Electrical Engineering and Project MAC, Massachusetts Institute of Technology, Cambridge, Mass.

National Science Foundation  
GU-1557

I. Kohavi

#### REFERENCES

1. A. Gill, "Introduction to the Theory of Finite-State Machines," (New York: McGraw-Hill 1962).
2. F. C. Hennie "Fault Detection Experiments for Sequential Circuits: Proc. 5th Ann. Symp. on Switching Theory and Logical Design pp 95-110, Nov. 1964,
3. Z. Kohavi, P. Lavallee, "Design of Sequential Machines with Fault-Detection Capabilities," IEEE Trans. Electronic Computers Vol. EC-16 pp. 473-484, (Aug. 1967).

#### DESIGN OF CHECKING EXPERIMENTS FOR SEQUENTIAL MACHINES

D. Farmer and E. J. Smith

The problem of designing a checking experiment for a sequential machine has been studied by F. C. Hennie<sup>1</sup> and C. R. Kime<sup>2</sup>. The problem as formulated by them

consists of finding an input sequence and its associated output sequence which uniquely characterizes the machine being checked. Actually the characterization is unique only if some additional assumptions are made, the most important being that the number of states of the machine has not increased due to the presence of a fault.

The solutions given by Hennie and Kime make use of special input sequences which identify initial states of the machine. The simplest case is the identification of a state by the response of the machine to a single input sequence. The input sequence is called a distinguishing sequence. In order for an  $n$ -state machine to possess a distinguishing sequence, the machine must have  $n$  distinct responses to some input sequence, each response characterizing the initial state of the machine. Not all machines possess this property.

For machines which do not possess distinguishing sequences it is possible to design checking experiments based upon a set of characterizing sequences. A set of characterizing sequences is a set of input sequences for which the set of responses uniquely identifies the initial state. The principal difficulty in the design of experiments using characterizing sequences is that it is necessary to ascertain that the machine is in the same state at several points in the experiment. This type of experiment is usually very lengthy. Table 1 gives an example of a machine which does not possess a distinguishing sequence. Table 2 shows the response of the machine to the set of characterizing sequences 0 and 10. A checking experiment for this machine designed systematically by Hennie's method requires 134 input symbols.

Present State	Next State, Output	
	input = 0	input = 1
A	B, 0	C, 0
B	B, 0	A, 0
C	C, 1	A, 0

Table 1 - Machine which does not possess a distinguishing sequence

Note: The above machine does not possess a distinguishing sequence for the reason that any sequence beginning with a 0 fails to distinguish between states A and B while any sequence beginning with a 1 fails to distinguish between B and C.

Initial State	Output Sequence	
	input = 0	input = 10
A	0	01
B	0	00
C	1	00

Table 2 - Response of the machine of Table 1 to the set of characterizing sequences {0, 10}.

Work is proceeding on alternate approaches to the design of checking experiments. At the moment effort is being concentrated on a more general approach which does not rely on distinguishing or characterizing sequences. Preliminary indications are that lengths of experiments for machines which do not possess distinguishing sequences may be favorable with respect to the existing methods of design.

One approach being investigated is the use of multiple experiments instead of a single long experiment. This is an especially useful technique when the machine can be reset to a reference state whenever desired. Most practical machines fulfill this requirements.

The technique for designing multiple checking experiments is only beginning to take shape and could conceivably move in several directions. Two tools which appear useful are the regular expression formulation of the state diagram and a new state reduction technique due to J. Kella<sup>3</sup>.

Consider the state diagram for the machine of Table 1 as given in Fig. 1. It can easily be shown that the regular expression accepted by this machine for initial state A is the following:

$$R = (00^*1 + 10^*1)^* 10^*0$$

(For details of deriving the regular expression from the state diagram the reader is referred to Ref. 4).

R represents an infinite set of sequences. If all of these sequences were applied to the machine and an output 1 observed at the end of every sequence, this would constitute a checking experiment for the machine. The machine would have to be reset to state A before the application of each sequence. This experiment, however, would not be of practical use since it would be of infinite length. One might, however, extract some of these sequences from R and use these in the design of an experiment. Some finite subset of R will be sufficient to uniquely characterize the machine subject to the upper bound on number of states, but as yet no guidelines have been found for selecting the subset.

To illustrate what may be done suppose that the following subset of R is selected:

$$R' = 10^*0 + 00^*110 + 10^*110$$

Note that  $10^*0$  is included in  $10^*110$ . The sets chosen are still infinite sets but it is now possible to show that a machine under test accepts them by conducting a finite number of experiments if an upper bound for the number of states is assumed. For this machine the upper bound is assumed to be three states. It is apparent that an n-state machine which responds identically to 0, 1, 2, ... n repetitions of a sequence will not respond differently for n + 1 or higher repetitions of this sequence. For the 3-state

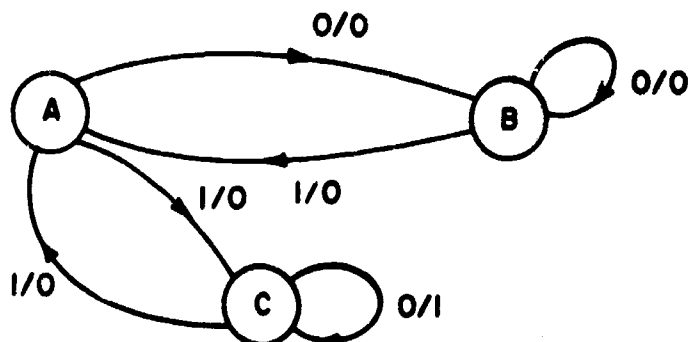


Fig. 1 State Diagram for Machine of Table 1

machine it is sufficient to establish the response to 0, 1, 2, and 3 repetitions of a pattern. It is therefore possible to establish the acceptance of  $R'$  by observing the input-output sequences of Table 3.

Input Sequence	Output Sequence
0110	0001
00110	00001
000110	000001
(This establishes $00^*110$ )	
1110	0001
10110	01001
100110	011001
1000110	0111001
(This establishes $10^*110$ and $10^*0$ )	

Table 3 - Input-output sequences for establishing the acceptance of  $R'$ 

An experiment may be designed to establish the acceptance of  $R'$ , but this is not sufficient to show that the machine under test actually is the machine of Table 1. This is due to the fact that  $R'$  is only a representative subset of  $R$  which was selected arbitrarily. It is possible to augment this subset with other sequences and to establish that the machine under test is in fact the machine of Table 1. In this stage of the experiment design the principal tool is the state reduction technique. Figure 2 represents the state diagram for the most general machine which accepts  $R'$ .

The following questions must be answered:

1) Is a simple self-loop on state 2 established by the proposed experiment? The acceptance of  $00^*110$  establishes that the machine either has a self-loop on state 2 or 2 cycles between states. This latter condition will be referred to as a loop system. If the machine does cycle between state 2 and some other state then the other state must appear somewhere on the diagram if the machine is a reduced machine. It is

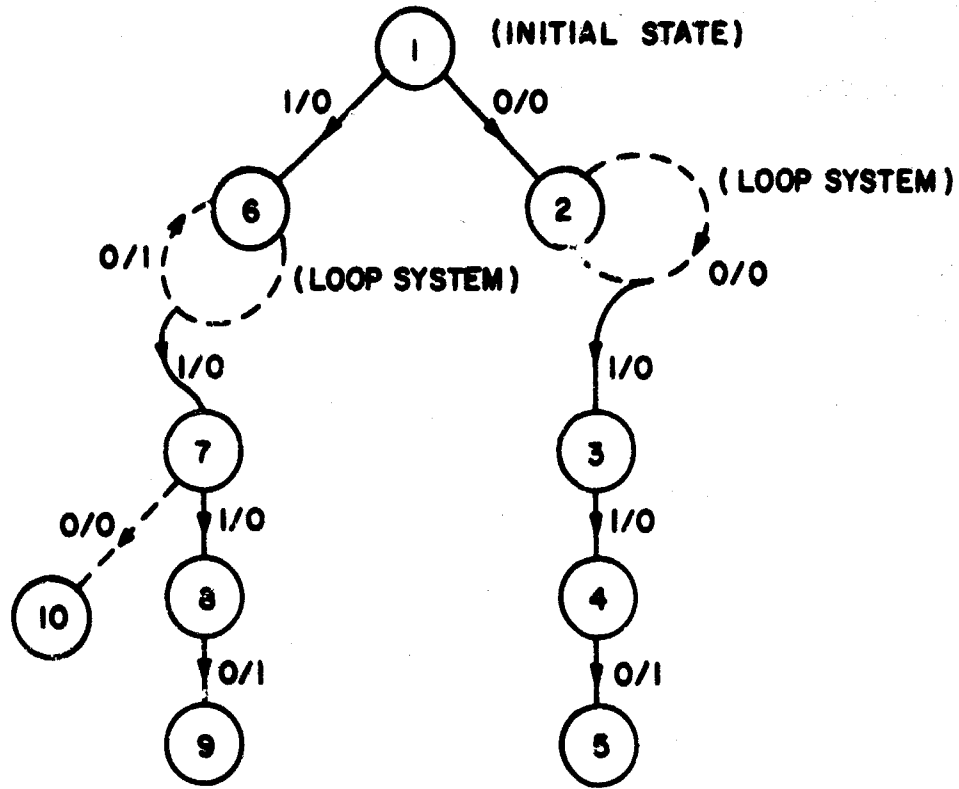


Fig. 2 State Diagram to be Established

Note: The dashed lines represent self-loops to be confirmed and necessary additions to be established.

therefore necessary to establish that state 2 is incompatible with all other states on the diagram. Without the addition of state 10 states 2 and 1 are compatible since the machine when started in either of them could conceivably respond to the input sequence 110 with output sequence 001. It is necessary to augment the proposed experiment to include the sequence 110 so that it can be established that the machine started in states 1 and 2 responds differently to input 110. This results in the addition of state 10 to the diagram. Now it is known that states 1 and 2 are distinct although each has a 0/0 transition out of it. There is also a state (state 6) which has a 0/1 transition out of it. Therefore there is no possible other state for the loop system on state 2. A simple self-loop has been established.

2) Is a simple self-loop on state 6 established by the proposed experiment? Here the answer is clearly yes since there can be only one state which has a 0/1 transition out of it if there are two states which have 0/0 transitions out of them.

3) Is the 10 state machine uniquely reducible to one 3 state machine (that of Table 1)?

The state reduction method of Kella gives only one three state machine for this diagram. Therefore the sequences of Table 3 plus the input sequence 110 (response to which is 000) constitute a checking experiment for the machine of Table 1.

The final experiment consists of a total of 40 symbols and 8 results. This compares with 134 symbols and one initial setting by Hennie's technique.

There are several areas open for investigation. One area is the establishing of criteria to determine a sufficient subset of the regular expression set accepted by the machine. Another area is the formalization and hopefully improvement of the means of determining by state compatibility arguments that the machine is uniquely identified. Results so far have indicated that further study should proceed.

Joint Services Technical Advisory Committee  
AF 49(638)-1402

D. Farmer

#### REFERENCES

1. F. C. Hennie, "Fault Detecting Circuits for Sequential Circuits," Proc. 5th Ann. Symp. Switching Circuit Theory and Logical Design, Princeton, N. J., Nov. 1964.
2. C. R. Kime, "A Failure Detection Method for Sequential Circuits," Technical Report 66-13, Dept. of Elec. Eng., University of Iowa, Jan. 1966.
3. J. Kella, "State Minimization of Incompletely Specified Sequential Machines," to be published.
4. T. L. Booth, "Sequential Machines and Automata Theory," Chap VI, John Wiley and Sons, 1967.

#### SEQUENTIAL MACHINE IDENTIFICATION

J. Kella

This research is directed towards the solution of the problem of sequential machine identification. Given an input signal sequence to an unknown machine and the corresponding output sequence it is required to find the state table or any other complete description of the machine. Generally, the solution is possible only if there is a bound given for the number of states of the machine and the given sequences describe uniquely the given machine i. e., the input output sequences are a checking experiment of the given machine.

We started the above discussion with a somewhat different problem. Given an input output sequence, find all reduced machines which would give this input output sequence. Stated this way, the problem reduces to a state reduction problem. The input output sequence defines an incompletely specified Mealy sequential machine, as described in Fig. 1. This machine has  $n + 1$  states, where  $n$  is the length of the sequence.

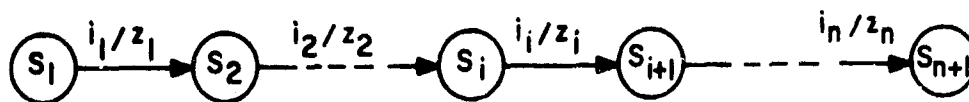


Fig. 1 Input Output Basic Machine

and every state (except  $s_{n+1}$ ) has one and only one specified transition and output, the transitions and outputs may be formulated by:

$$\delta(i_j, s_i) = \begin{cases} s_{i+1} & i_j = i_i \\ (-) & i_j \neq i_i \end{cases}$$

$$\omega(i_j, s_i) = \begin{cases} s_i & i_j = i_i \\ (-) & i_j \neq i_i \end{cases}$$

where  $\delta$  and  $\omega$  are the next state and output mapping and  $(-)$  indicates a non-specified mapping. Based on state reduction theory and on the special mapping of this type of machine it is proved that the reduced machine should be a partition of the states of the original incompletely specified machine. Due to the special characteristics of the machine it is possible to check and mark incompatible pairs of states by a single run through the sequence from the end back to the beginning with no repetition required. An algorithm which makes use of this property is given for the incompatible state listing.

As every state in the basic machine has only one specified transition, and that transition is completely specified, input symbol, output symbol and next state, any two different states specified under two different input symbols are compatible. According to this rule the number of different partitions of all states of the basic machine, while the partitioning is done according to compatibility, is very large. The machine reduction, though, requires preserved partitions, or closed covers, of all states of the basic machine. This requirement is not necessarily fulfilled by all possible partitions. The method presented avoids all non-preserved partitions by generating first all different partitions of the set of states specified under only one input symbol and which includes state  $s_1$ . Starting with any such partition and following the mapping rules leads to a preserved partition of the whole machine.

A detailed practical algorithm was developed for a fast reduction of the original machine into all possible reduced machines. We are now trying to program this algorithm in the PDP-8 language and obtain a completely mechanized identification device.



The method seems to be quite valuable for generation of checking experiments for sequential machines and for the general machine identification problem.

Joint Services Technical Advisory Committee  
AF 49(638)-1402

J. Kella

National Science Foundation  
GU-1557

#### THE ASSOCIATED LEFT COMPLETE EVENT OF A REGULAR EXPRESSION

S. E. Gelenbe, E. J. Smith

For a problem related to the design of sequential machines capable of testing a given sequential machine<sup>1</sup> it is necessary to obtain the set of all prefixes of each sequence in a given regular expression. This note describes an algorithm for this purpose.

Definition 1. Let  $R \subseteq \Sigma^*$ , where  $\Sigma$  is a finite alphabet.  $R$  is said to be left complete if and only if  $xy \in R$  implies  $x \in R$ .

Definition 2. Let  $R \subseteq \Sigma^*$ ,  $\Sigma$  as above.  $R$  is said to be right complete if and only if  $xy \in R$  implies  $y \in R$ .

Definition 3. The left complete event associated with the event  $R$  is defined as

$$R' = \{x \mid xy \in R\}$$

Definition 4. The right complete event associated with the event  $R$  is

$$R'' = \{y \mid xy \in R\}.$$

Theorem 1. Given  $R$  regular,  $R'$  may be obtained from  $R$  by the following algorithm.

Part (i). Obtain the state table for the finite deterministic automaton (FDA),  $M(R)$ , from the regular expression  $R$ . (This can be conveniently done using derivatives<sup>2</sup>).

Part (ii). Let  $M(R) = \{s_0, \Sigma, S, \delta, F\}$  where  $F \subseteq S$  is the set of final states,  $\delta$  is the next state function,  $S$  is the set of states,  $\Sigma$  is the finite (input) alphabet and  $s_0 \in S$  is the initial state.

Step 1. Take  $F_1 = \{s \mid s \in S \ \& \ \exists a \in \Sigma \ \ni \ \delta(s, a) \in F\}$ . This can be easily done by identifying the entries in the present state column of the state table of  $M(R)$  for which the next state entries include a state in  $F$ .

Compare  $F_1$  and  $F$ . If  $F \supseteq F_1$  then  $R = R'$  and  $R$  is a definite regular event.

Otherwise take  $A_1 = F \cup F_1$  and proceed to Step 2.

Step (n + 1). Take  $F_{n+1} = \{s \mid \delta(s, a) \in F_n \text{ \& } a \in \Sigma\}$ . Compare  $A_n$  and  $F_{n+1}$ .  
 $(A_n = A_{n-1} \cup F_n)$ . If  $A_n \supseteq F_{n+1}$ , then stop.

$$M(R') = \{s_0, \Sigma, S, \delta, F'\}$$

where  $F' = A_n$ . Proceed to part (iii).

Otherwise proceed to Step (n + 2).

Part (iii).  $R'$  is obtained from  $M(R')$ . (The approach using the set of equations as described in Ref. 2 may be used.)

Proof: The algorithm given above consists of enlarging  $F$  to  $F'$  so as to include all states  $s \in S'$  such that there exists some  $y \in \Sigma^*$  for which  $\delta(s, y) \in F$ .

$$F' = \{s \mid \exists y \in \Sigma^* \ni \delta(s, y) \in F\}.$$

This implies that  $xy \in R$  if and only if  $x \in R'$ . Hence  $R'$  is indeed the associated left complete event of  $R$ .

Corollary 1. If  $R$  is regular, then so is  $R'$ .

Corollary 2. The F.D.A.  $M$  only accepts definite event if and only if  
 $s \in F \rightarrow F \cap \{q \mid g \in S \text{ \& } \delta(g, x) = s\}$

Theorem 2. If  $M(R)$  is strongly connected, then  $R' = \Sigma^*$ .

Proof: It is clear from Theorem 1 that  $R' = \Sigma^*$ , since if  $M(R)$  is strongly connected then  $F' = S$  and  $M(R')$  accepts any  $x \in \Sigma^*$ .

Theorem 1 also indicates a simple algorithm to determine whether a given regular expression  $R$  is left complete or not. For this purpose it suffices to apply step (1) of part (ii) of the algorithm.

It is intuitively clear that there should exist some relationship between the number of states of  $M(R)$  and the number of steps it will take for the algorithm in part (ii) of the algorithm of Theorem 1 to converge.

Theorem 3. Let  $M(R)$  have  $t + 1$  states  $s_0, s_1, \dots, s_t$ . Then the algorithm of part (ii) of Theorem 1 converges in at most  $t$  steps.

Proof: If  $F$  is empty then  $F_1$  will be empty and the algorithm will terminate in one step since  $F = F_1$ . If  $F$  has  $1 \leq j \leq t + 1$  members, then the slowest conversion process will take place if at the  $i^{\text{th}}$  step  $A_i$  has only one more member than  $A_{i-1}$ . This process will add one more state to  $A_i$  at each step  $i$  so that it will converge in  $t - j + 1$  steps. If  $j = 1$  we shall have the slowest convergence which will take  $t$  steps.

**Example:** Let us use the algorithm of Theorem 1 for the regular expression  $E = (1 + 20^*3)^*$  over the alphabet  $\Sigma = \{0, 1, 2, 3\}$ . The derivatives are obtained as follows:

$$\begin{aligned} \text{(i)} \quad D_0 E &= \phi \\ D_1 E &= E \\ D_2 E &= 0^*3 E \\ D_3 E &= \phi \\ D_{20} E &= D_2 E \\ D_{21} E &= \phi \\ D_{22} E &= \phi \\ D_{23} E &= E \end{aligned}$$

So that the F. D. A.  $M(E)$  is given by

$M(E):$	0	1	2	3	z
1	2	1	3	2	1
2	2	2	2	2	0
3	3	2	2	1	0

(ii) Clearly  $F = 1$ .

We apply the algorithm of part (ii) of Theorem 1:

$$\begin{aligned} \text{Step 1.} \quad F_1 &= \{1, 3\} \\ A_1 &= F \cup F_1 = \{1, 3\} \end{aligned}$$

$$F_1 \supset F$$

$$\begin{aligned} \text{Step 2.} \quad F_2 &= \{1, 3\} \\ A_1 &= F_2 \end{aligned}$$

Hence stop.

$M(E')$ , the F. D. A. obtained from  $E'$ , the definite event associated with  $E$  is

$M(E')$ :	0	1	2	3	z
1	2	1	3	2	1
2	2	2	2	2	0
3	3	2	2	1	1

and  $E'$  may be obtained from  $M(E')$  by standard methods<sup>2</sup>:

$$E' = (1 + 20^*3)^*(\lambda + 20^*)$$

## REFERENCES

1. S. E. Gelenbe, "Monitor Machines," in preparation.
2. J. A. Brzozowski, "Derivatives of Regular Expressions," Journal A. C. M., 1964, pp. 481-494.

## PLAGO/360 A LOAD-AND-GO STUDENT ORIENTED PL/I TRANSLATOR

H. W. Lawson, Jr. and S. Habib

During the spring and summer of 1968, Version I of the PLAGO/360 System was produced. PLAGO/360 is a batch load and go interpretive translator and executor that operates as a program under the Operating System/360 for any IBM System/360 Model 40 or above.

The immediate objectives of PLAGO are as follows:

1. Fast translation and execution for typical introductory student programs (15 to 50 statements).
2. Comprehensive diagnostic facilities to aid the learning student in debugging.
3. To include sufficient language facilities for an introductory programming course.
4. To be highly compatible with the full PL/I programming language so that students may progress easily from the PLAGO subset to full PL/I.
5. To provide facilities in PLAGO which are not necessarily compatible with PL/I, but are of value and easily implemented within the framework of PLAGO.

This project was started to provide an alternative to utilizing the IBM supplied version PL/I compiler which had an average job time of two and one-half minutes using our IBM System/360 Model 50. The Version I of PLAGO reduces this average job time to approximately five seconds. This should result in substantial savings to the Institute. The current version of PLAGO/360 will accept standard key punch cards or Porta-A-Punch\*. The use of the latter cards will enable our students to prepare their source programs and data without the aggravation of waiting for available key punch machines.

The future objectives of PLAGO are as follows:

1. To extend the language facilities of PLAGO to provide more facilities for PLAGO users.
2. To use PLAGO as the basis for future research and development in programming languages and programming language translation techniques.
3. To modify PLAGO to accept its input from remote marked sense card reader stations so that students may submit their jobs without any clerical or operator intervention. The conventions used for encoding marked sense cards will be the same as the conventions for Port-A-Punch cards.

---

\*Port-A-Punch is a registered trademark of the IBM Corporation

4. To create a time sharing version of PLAGO which may be utilized in an interactive terminal environment.
5. To use the language and machine independent characteristics of the PLAGO system to produce language translators and executors for other general purpose and problem-oriented programming systems.
6. To take advantage of the interpretive nature of the PLAGO system by considering the implementation of a programming-language-oriented microprogrammed computer. The language for the microprogrammed version will be based upon PL/I, but will be more consistent, and include operating system commands that will also be implemented through microprogramming.

During the coming academic year we plan to formalize our design plans for the marked sense card version and time sharing version of PLAGO. In addition, in this academic year we plan to investigate the possible hardware configurations to be utilized in performing our microprogramming research activities.

National Science Foundation  
GU-1557

H. W. Lawson

#### RELIABILITY IMPROVEMENT OF DIGITAL SYSTEMS THROUGH THE USE OF MAJORITY VOTERS

R. Bharat and B. H. Hertzendorf

The reliability improvement obtainable through use of redundancy and majority voters is calculated for digital systems consisting of identical stages in tandem, when the failure rate of an individual stage is low. In modern digital systems, the stages are realized with integrated circuits (ICs) which have low failure rates, typically less than  $10^{-6}$  failures/hour<sup>1,2</sup>. If a system consists of  $n$  identical stages in tandem, each with a failure rate of  $\lambda$  per unit time, the probability that the system will fail in time  $t$  is given by

$$q = 1 - (e^{-\lambda t})^n = 1 - e^{-n\lambda t}$$

If  $n\lambda t \ll 1$ ,  $q \approx n\lambda t$ .

As  $n$  increases, the reliability specification that the system unreliability be less than some stated maximum value over a given life will be no longer met.

The use of an odd number of redundant channels with a majority voter deciding among their outputs can improve the system reliability. The inset in Fig. 1 shows a  $1 \times n$  system with 3-input voter, i. e., a system with a 3-input voter at the end of 3 redundant channels, each with  $n$  stages.  $F_{13}$ , the reliability improvement factor of

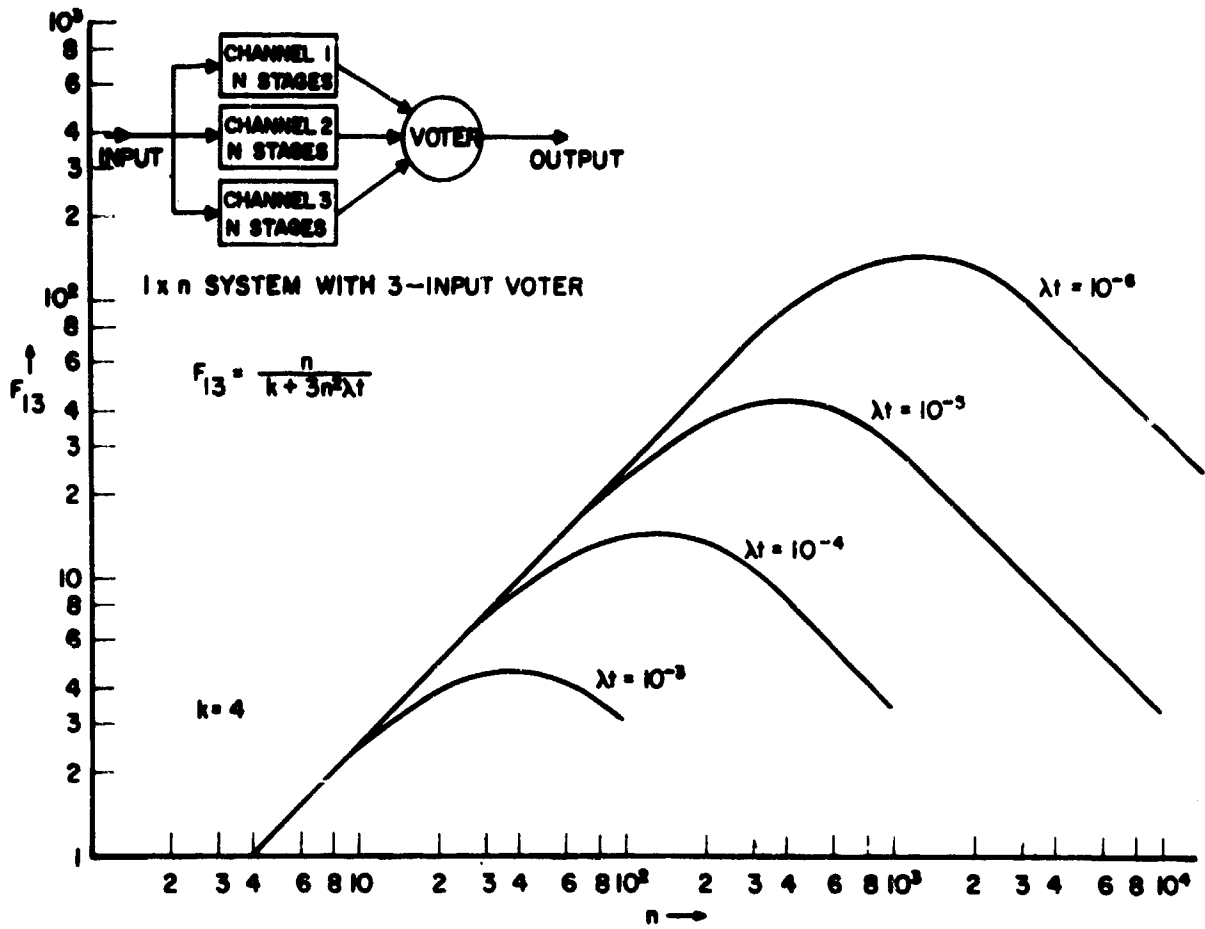


Fig. 1. Reliability Improvement Factor of a 1 x n System with a 3-Input Voter

1 x n system with 3-input voter, can be defined as

$$F_{13} = \frac{\text{probability of failure, using a single channel}}{\text{probability of failure, using a 1 x n, 3-input voter scheme}}$$

Then,

$$F_{13} = \frac{q}{q_v + (1 - q_v)(3q^2 - 2q^3)}$$

where  $q_v$  is the unreliability of the voter. For channels and voters with low failure rates,

$$q, q_v \ll 1.$$

Further, if we assume that

$$q_v = k\lambda t$$

where  $k$  is a constant depending on the particular voter circuit used, we get

$$F_{13} = \frac{n}{k + 3n^2 \lambda t}$$

We note that when there are only a few stages, the improvement depends on the voter reliability; but for large value of  $n$ , channel reliability is the dominant factor.  $F_{13}$  reaches a maximum at

$$n_{13opt} = \left( \frac{k}{3\lambda t} \right)^{1/2}$$

$$F_{13max} = \frac{n_{13opt}}{2k} = \frac{0,288}{(k\lambda t)^{1/2}}$$

In Fig. 1.,  $F_{13}$  is plotted against  $n$  with  $\lambda t$  as a parameter and  $k = 4$ . This value of  $k$  applies, for example, to a system consisting of NAND gates both in the channels and the voter, as a 3-input voter can be realized by interconnecting 4 NAND gates, which are in tandem from the point of view of reliability. With  $\lambda = 10^{-6}$  failures/hour, typical of present day ICs and an operating life of 1000 hours, we get  $\lambda t = 10^{-3}$ . The plot shows  $\lambda t$  values of  $10^{-3}$  to  $10^{-6}$  as reduction in failure rates can be anticipated with improvements in the technology of integrated circuits.

A similar treatment for a  $1 \times n$  system with a 5-input voter (shown in the inset in Fig. 2) leads to a reliability improvement factor

$$F_{15} = \frac{n}{k + 10n^3 (\lambda t)^2}$$

if  $q, q_v \ll 1$ , and  $q_v = k\lambda t$ .

$F_{15}$  reaches a maximum at

$$n_{15opt} = \left[ \frac{k}{20 (\lambda t)^2} \right]^{1/3}$$

$$F_{15max} = \frac{n_{15opt}}{1,5k} = \frac{0,246}{(k\lambda t)^{2/3}}$$

Figure 2 shows the reliability improvement factor  $F_{15}$  for a  $1 \times n$ , 5-input voter system plotted against  $n$  with  $\lambda t$  as parameter and  $k = 11$ . The  $k$  value used is appropriate for a system in which NAND gates make up all the channels and the 5-input voter (which can be realized by using 11 such gates).

Considering that the 5-input voter scheme uses two channels more than the 3-input voter scheme and might thus increase cost and require larger power, the increases in the reliability improvement factor of 5-input voter scheme as compared to the 3-input voter scheme is marginal, unless  $n$  is very large.

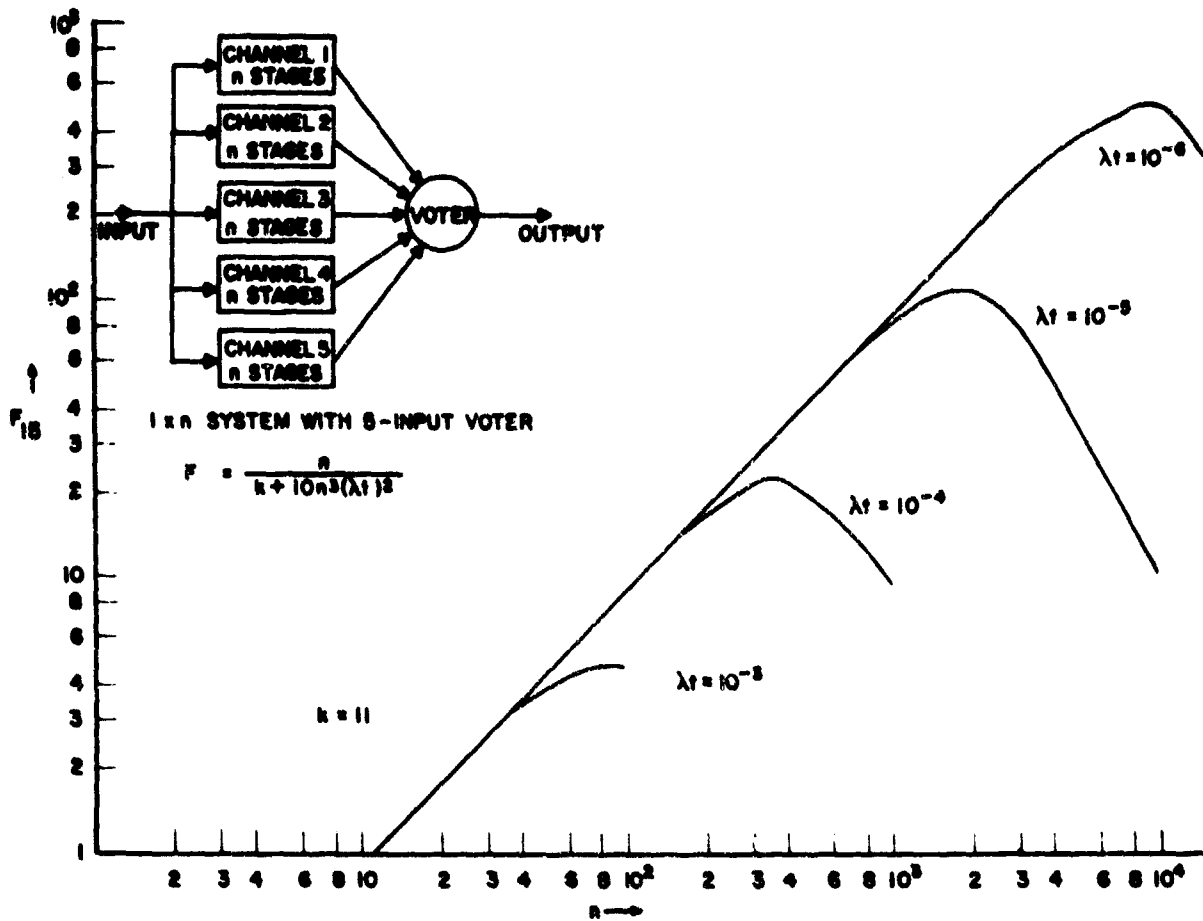


Fig. 2. Reliability Improvement Factor of a 1 x n System with a 5-Input Voter

One method of not increasing the number of channels is to apply redundancy and 3-input majority-voter scheme around sections of the system at a time. The inset in Fig. 3 shows a  $m \times \frac{n}{m}$  system with 3-input voters. Each of the three channels is split into  $m$  identical sections and at the end of each section containing  $\frac{n}{m}$  stages per channel, a 3-input voter is used. Thus one requires  $(m - 1)$  more voters as compared to a  $1 \times n$  system. For this system, the reliability improvement factor is given by

$$F_{m3} = \frac{n}{mk + 3 \frac{n}{m} \lambda t}$$

if  $q_i, q_v \ll 1$ , and  $q_v = k\lambda t$ .

$F_{m3}$  reaches a maximum at

$$n_{m3opt} = m \left( \frac{k}{3\lambda t} \right)^{1/2}$$

$$F_{m3max} = \frac{0.288}{(k\lambda t)^{1/2}}$$



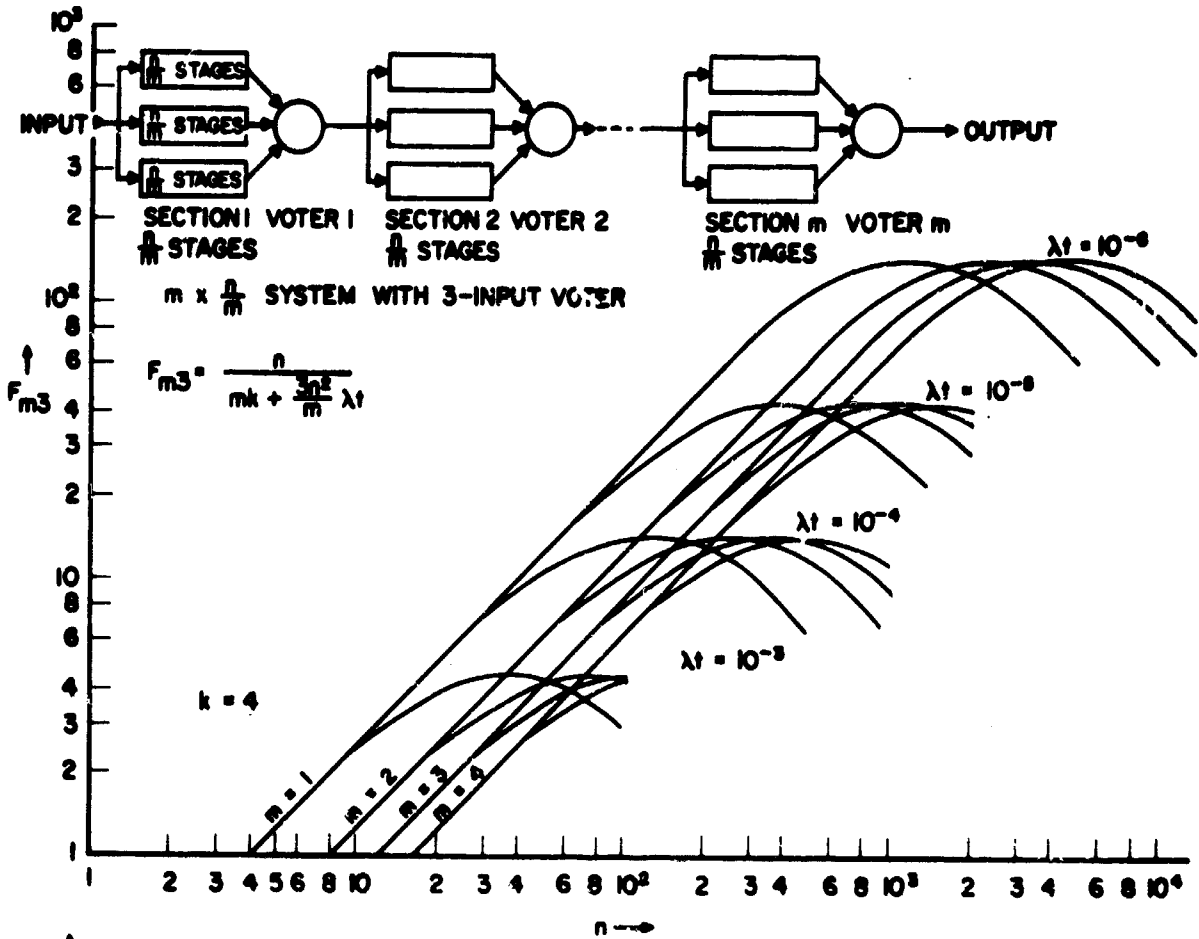


Fig. 3. Reliability Improvement Factor of a  $m \times \frac{n}{m}$  System with a 3-Input Voter

We note that  $F_{m3 \max}$  is independent of  $m$  though the value of  $n$  at which the maximum is reached increases with  $m$ . Fig. 3 shows  $F_{m3}$  plotted against  $n$  with  $k = 4$  and with  $m$  and  $\lambda t$  as parameters. It can be seen that section redundancy is superior to system redundancy only for large values of  $n$  when the voter unreliability becomes negligible.

In large-scale integrated circuits, the successive stages can be expected to have identical failure rates (as assumed in the analysis above) due to the nature of the technology involved in their fabrication. Thus the majority-voter schemes discussed above can be used to improve the reliability of digital systems using large-scale integration.

National Science Foundation  
GU-1557

R. Sharat

REFERENCES

1. C. D. Parker, "Integrated Silicon Device Technology, Vol. XV, Reliability," ASD-TDR-63-316, Wright Patterson Air Force Base, Ohio, May 1967.
2. B. H. Hertzendorf, "Integrated Circuit Reliability and Some Methods of Reliability Improvement," M.S. Report Project, E. F. Department, Polytechnic Institute of Brooklyn, June 1968. On page 20 of the report, there is a summary of failure data from various sources.

## VI. COMMUNICATIONS AND INFORMATION PROCESSING

Boorstyn, R. R.	Hess, D. T.	Oberst, J. F.	Schilling, D. L.
Clarke, K. K.	Hoffman, E.	Pickholtz, R.	Schulman, R. J.
Deutsch, S.	Laemmel, A. E.	Refi, J.	Schwartz, M.
Dosik, P.	Milstein, L. B.	Richman, S.	Stroh, R.
Eddy, T. W.	Muise, R. W.	Rudner, B.	Unkauf, M.
Ergul, F. R.	Muntner, M.	Schiff, L.	Wolf, J. K.
Fawe, A. L.			Yavuz, D.

### DOUBLE ERROR PROBABILITY IN DIFFERENTIAL PSK

J. F. Oberst and D. L. Schilling

A solution for the probability of double errors in differentially coherent phase shift keyed (PSK) communication systems is presented which is simpler than previous analyses and which focuses on the cause of double errors. Results of a digital computer simulation are given which substantiate the theory.

The probability of two consecutive errors in a binary differentially coherent PSK (D-PSK) communication system has been determined by Salz and Saltzberg<sup>1</sup>. The technique employed was to first derive the joint probability density function (pdf) of two successive decision statistics, then integrate this expression over the quadrant corresponding to two errors, and finally manipulate the resulting four-fold integral into the form (see Fig. 1).

DECISION	j	j+1	j+2	
BAUD	j	j+1	j+2	j+3
a.	REF j	DATA j		
		REF j+1	DATA j+1	
			REF j+2	DATA j+2
b.	DATA j	REF j		
		REF j+1	DATA j+1	
			REF j+2	DATA j+2

Fig. 1. Reference and data bauds for D-PSK.

$$P(E_{j+1}, E_j) = \frac{1}{4\pi} e^{-R} \int_0^\pi \operatorname{erfc}^2(\sqrt{R} \cos \theta) (1 + \sqrt{R\pi} \cos \theta e^{R \cos^2 \theta} [1 + \operatorname{erf}(\sqrt{R} \cos \theta)]) d\theta \quad (1)$$

which was evaluated numerically ( $R = E/N_0$  is the effective SNR). A much simpler approach to this problem which makes direct use of the mechanism causing double errors is presented below.

Each decision in D-PSK is based on a phase comparison between adjacent bauds, with the signal of the previous baud serving as the phase reference for the present baud [Fig. 1 a)]. The pdf of the phase error  $\phi$  of any baud due to additive Gaussian noise is<sup>2</sup>

$$f(\phi) = \frac{1}{2\pi} e^{-R} + \frac{1}{2} \sqrt{\frac{R}{\pi}} e^{-R \sin^2 \phi} \cos \phi [1 + \operatorname{erf}(\sqrt{R} \cos \phi)], \quad \phi \in [-\pi, \pi]. \quad (2)$$

The probability of error for the  $j^{\text{th}}$  decision conditioned on the phase error in the  $j^{\text{th}}$  baud is<sup>2</sup>

$$P(E_j | \phi_j) = \frac{1}{2} \operatorname{erfc}(\sqrt{R} \cos \phi_j). \quad (3)$$

Since the transmitted information is carried in the phase transitions between bauds, and the effective SNR is identical for all bauds, the labels "reference baud" and "data baud" may be interchanged for any decision. Relabeling as in Fig. 1(b), it is seen that two consecutive decisions can be considered to result from two independent data bauds and one common reference baud. The double error probability conditioned on the phase error of the reference baud is therefore

$$P(E_{j+1}, E_j | \phi) = \left[ \frac{1}{2} \operatorname{erfc}(\sqrt{R} \cos \phi) \right]^2. \quad (4)$$

Averaging Eq. (4) over the pdf of Eq. (2) yields the following result for double errors:

$$\begin{aligned} P(E_{j+1}, E_j) &= \int P(E_{j+1}, E_j | \phi) f(\phi) d\phi \\ &= \int_{-\pi}^{\pi} \frac{1}{4} \operatorname{erfc}^2(\sqrt{R} \cos \phi) \left\{ \frac{1}{2\pi} e^{-R} + \frac{1}{2} \sqrt{\frac{R}{\pi}} e^{-R \sin^2 \phi} \right. \\ &\quad \left. \cos \phi [1 + \operatorname{erf}(\sqrt{R} \cos \phi)] \right\} d\phi \end{aligned} \quad (5)$$

This result is identical to that of Salz and Saltzberg, but it is obtained more simply, and indicates clearly the cause of frequent double errors in D-PSK.

The same method may be applied to prove that nonadjacent decisions are mutually independent. Consider the  $j^{\text{th}}$  and  $j+2^{\text{nd}}$  decisions of Fig. 1. The  $j^{\text{th}}$  decision is made on the basis of the signals received in bauds  $j$  and  $j+1$ ; the  $j+2^{\text{nd}}$  on signals received in bauds  $j+2$  and  $j+3$ . Since these pairs of bauds are disjoint, the decisions based on them can have no mutual dependence. Then clearly

$$P(E_{j+2} | E_j) = P(E) = \frac{1}{2} e^{-R}. \quad (6)$$

A digital computer simulation of a D-PSK communication system was performed to verify these results. The error counts resulting from 50,000 trials are shown in Figs. 2 and 3. In Fig. 2, the conditional probability of an adjacent error

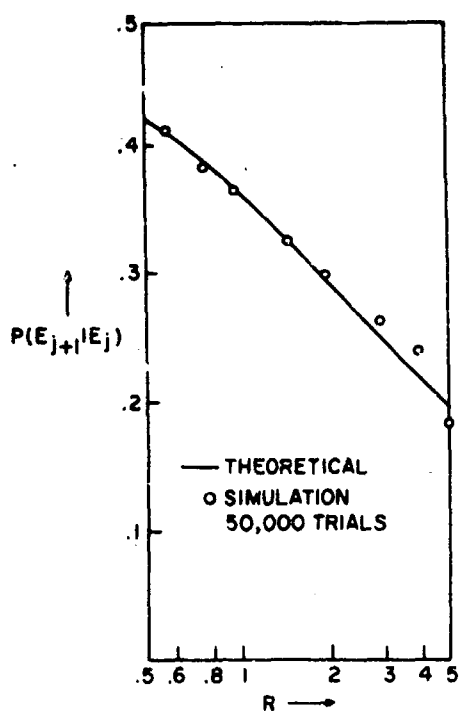


Fig. 2  $P(E_{j+1}|E_j)$  versus  $R$

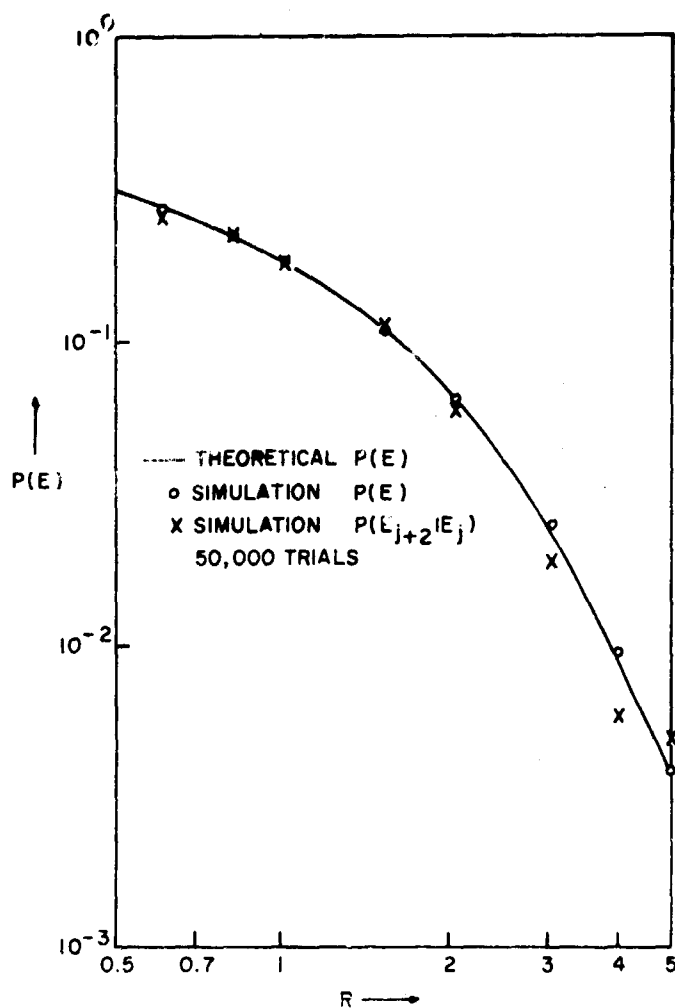


Fig. 3  $P(E)$  and  $P(E_{j+2}|E_j)$  versus  $R$

$$P(E_{j+1}|E_j) = \frac{P(E_{j+1}, E_j)}{P(E)} \quad (7)$$

is plotted versus  $R$ . Fig. 3 shows  $P(E)$  and  $P(E_{j+2}|E_j)$  versus  $R$ . Very close agreement between theoretical and simulation results were obtained.

National Aeronautics and Space Administration  
NgR 33-006-020

J. F. Oberst and D. L. Schilling

#### REFERENCES

1. J. Salz and B. R. Saltzberg, "Double Error Rates in Differentially Coherent Phase Systems," *IEEE Trans. Communications Systems*, vol. CS-12, pp. 202-205, June 1964.
2. J. Oberst, "Binary Phase-Shift Keyed Communication Systems," Ph. D. Dissertation, Dept. of Elec. Engrg., Polytechnic Institute of Brooklyn, June 1969.

## SINGLE CHANNEL PHASE-SHIFT KEYED COMMUNICATIONS

J. F. Oberst and D. L. Schilling

Practical binary phase-shift keyed (PSK) communication systems require a partially coherent reference signal at the receiver. Two major classes of PSK systems may be identified, according to the technique used to obtain the reference signal: transmitted reference (TR) and single channel (SC). Although SC systems are potentially superior, they are difficult to analyze and have an inherent mark-space ambiguity problem.

Four differentially encoded SC PSK systems have been studied, including Decision Feedback (DF), Squaring (SQ), and a variation of SQ called Absolute Value (AB). In addition, a new Maximum Likelihood (ML) SC system, which is optimum under certain restrictions, is derived and studied. Error counts are obtained for these PSK systems using Monte Carlo simulation on an IBM 360/50 digital computer. Analytical bounds on the average probability of error,  $P(E)$ , are derived which indicate that these systems all achieve comparable performance. This is in contrast with results which have been published previously.

Partially Coherent PSK Systems

The degree of radio frequency (RF) coherence which can be established between transmitter and receiver of a communication system greatly influences the performance attainable. Assuming that the signal amplitude and the baud timing, or bit sync, are known at the receiver, we can write the RF signal received in the baud  $[0, T]$  as

$$v(t) = s_i(t, \theta) + n(t), \quad t \in [0, T],$$

where the subscript  $i$  indicates that  $s_i(t, \theta)$  is the signal corresponding to message  $m_i$ ,  $i = 1, 2$ .  $n(t)$  is white Gaussian noise with one-sided power spectral density  $N_0$ .  $\theta$  is the RF phase, assumed to be constant over the baud, which may be known with various degrees of accuracy depending on the particular communication system. The accuracy with which the value of  $\theta$  is known at the receiver determines the degree of RF coherence and thereby the minimum average probability of error  $P(E)$  which can be achieved.

Two important signal parameters are the energies of the two possible received signals,  $E_i$ , and their mutual correlation coefficient,  $\rho$ :

$$E_i = \int_0^T s_i^2(t, \theta) dt$$

$$\rho = (E_1 E_2)^{-1/2} \int_0^T s_1(t, \theta) s_2(t, \theta) dt.$$

If the actual value of  $\theta$  is known accurately at the receiver, the system is termed coherent. It is known that the best signal set for such a system, in the sense of minimum  $P(E)$ , consists of a pair of equal energy anticorrelated ( $\rho = -1$ ) signals. Phase shift keyed sinusoids, defined by

$$s_1(t, \theta) = C \cos(\omega_0 t + \theta)$$

$$s_2(t, \theta) = C \cos(\omega_0 t + \theta + \pi) = -C \cos(\omega_0 t + \theta),$$

form such a set. With the signal energy  $E$  received in each baud and the signal to-noise ratio  $R$  defined as

$$E = \frac{C^2 T}{2}, \quad R = \frac{E}{N_0},$$

it can be shown that the minimum  $P(E)$  attainable is

$$P(E) = \frac{1}{2} \operatorname{erfc} \sqrt{R}. \quad (1)$$

The receiver which attains this  $P(E)$  is the standard correlation detector.

In practical communication systems the received phase is not known with perfect accuracy. Often, however, an estimate  $\hat{\theta}$  of  $\theta$  is available, and systems using such an estimate are called partially coherent. When the estimate is good, and the signals are properly chosen, partially coherent systems may attain a  $P(E)$  close to the lower bound Eq. (1). Unfortunately, the problem of overall system design, including signal specification and receiver design, is quite complex. The difficulty is that the phase estimate is usually derived at the receiver by special processing of the signals received over several bauds. Thus considerations of receiver complexity, signal structure, and channel characteristics all interact. The procedure which has led to many useful partially coherent systems is to postulate a "reasonable" signal set on the basis of the method to be used by the receiver to derive the phase estimate, and then to seek the parameter values which yield the best operation. Since anticorrelated signals are generally superior when a good phase estimate is available, the best choices are usually modifications of the simple coherent PSK system discussed above. These systems usually fall into one of two categories, transmitted reference and signal channel, although combinations of the two are also possible.

#### Single Channel Systems

Transmitted reference (TR) systems transmit a reference signal to the receiver through a channel separate from the data channel. Thus the transmitted signal is a combination of a normal PSK signal and a signal to be used only for RF phase synchronization. The major disadvantage of TR systems is that the available power at

the transmitter must be shared between these two signals. In single channel (SC) systems a normal, fully modulated PSK signal is transmitted. The phase estimation portion of the receiver processes this PSK signal in some nonlinear manner in order to remove the modulation. The various SC systems differ in the nature of this nonlinear processing. The great advantage of SC systems is that the entire transmitter power is used for both data transmission and phase synchronization. Thus SC systems are potentially superior to TR systems.

It is appropriate at this point to introduce the mathematical model used in this study of SC systems and to note the two assumptions involved. First, the carrier frequency  $\omega_0$  is assumed to be known accurately at the receiver. Second, the quality of the phase estimate obtainable in actual system is limited by the rate of change of received phase, caused by channel variations, oscillator phase jitter, etc. This limitation is incorporated into a simple model by postulating a constant received phase, but a limited allowable measurement time. This measurement time is taken as  $qT$ , extending over  $q$  bauds of duration  $T$ . The waveform available at the receiver for the decision on the data transmitted for  $t \in [0, T]$  may therefore be represented as

$$v(t) = m(t) C \cos(\omega_0 t + \theta) + n(t),$$

$$t \in [-qT, T], \quad (2)$$

where  $m(t)$  represents the modulation, and takes on the values  $\pm 1$  in each baud independently and with equal probability. Some receivers also store the last  $q$  decisions.

Although the model Eq. (2) is simple, two major difficulties are encountered in the study of SC systems. The first involves the nonlinear processing of the signal performed by the receiver in order to construct a partially coherent reference waveform. Such processing makes it extremely difficult to obtain results analytically. For this reason, Monte Carlo simulation on a digital computer is useful in studying system performance. The second difficulty encountered in the SC systems is the "mark-space ambiguity" problem. In a simple SC system there is no way of determining the absolute sense of the signal received in each baud. That is, even though in low noise the bauds during which a 1 was transmitted can be distinguished from those during which a 0 was transmitted, it is impossible to determine which of these two groups of bauds actually corresponds to the 1 signal. In most SC PSK receivers, this mark-space ambiguity takes the form of two fairly stable average phase values of the derived reference, separated from each other by  $\pi$  radians. Even if the correct reference sense is established at the beginning of the transmission, noise may cause loss of synchronism and eventual reference reversal during the transmission, inverting the decoded message. Several techniques are available for dealing with this problem, the simplest of which is differential data encoding. In this scheme data of 1 is repre-

sented by no phase change from the signal transmitted in the previous baud, and data of 0 by a phase change of  $\pi$  radians. Since the presence or absence of a phase transition between bauds can be detected equally well using a reference with phase near  $\theta$  or  $\theta + \pi$ , there can be no inversion of the data with this technique. However, in a low error rate system where adjacent decisions are approximately independent, differential encoding almost doubles  $P(E)$  over that given in Eq. (1).

#### Results for Various SC Systems

Since the SC systems studied are difficult to analyze exactly, and also because they are basically discrete, Monte Carlo simulation on an IBM 360/50 digital computer was found to be a useful tool. Differential data encoding was used in all of the simulations. The systems studied include Differential (D) PSK, Decision Feedback (DF) PSK, Squaring (SQ) PSK, and a variation of SQ-PSK called Absolute Value (AB) PSK. In addition, a new Maximum Likelihood (ML) SC system, which is optimum in a restricted sense, is derived and simulated. The results are summarized below; details are contained in reference [1].

We first establish a performance bound for differentially encoded SC PSK systems as follows. A SC system is operating ideally when its derived reference is noiseless. Then the probability  $p$  of incorrectly identifying the sign of the signal received in each baud is given by Eq. (1):

$$p = \frac{1}{2} \operatorname{erfc} \sqrt{R}.$$

Since the reference is perfect, successive decisions are independent, and since differential encoding is used, an error occurs when a wrong detection is followed by a correct detection or vice versa. Therefore, the minimum average error probability is given by

$$P(E) = p(1 - p) + (1 - p)p = \operatorname{erfc} \sqrt{R} \left(1 - \frac{1}{2} \operatorname{erfc} \sqrt{R}\right). \quad (3)$$

We now consider Differential (D) PSK which is the simplest and in certain ways, the basic SC PSK communication system. In D-PSK, the signal received during the previous baud serves as the partially coherent reference for the present decision. Analytical results are available<sup>2</sup> for various error probabilities in D-PSK:

$$\begin{aligned} P(E) &= \frac{1}{2} e^{-R} \\ P(E_{j+1}/E_j) &= \frac{1}{2\pi} \int_0^\pi \operatorname{erfc}^2(\sqrt{R} \cos \tau) \cdot \\ &\quad \left\{1 + \sqrt{R\pi} \cos \tau e^{R \cos^2 \tau} [1 + \operatorname{erf}(\sqrt{R} \cos \tau)]\right\} d\tau \\ P(E_{j+2}/E_j) &= \frac{1}{2} e^{-R} \end{aligned} \quad (4)$$



The D-PSK system was simulated on the digital computer, and the error counts were compared to the analytical results above. The excellent agreement obtained indicated the accuracy of the simulation technique. In addition, it was proven that all of the other SC PSK systems studied reduce to D-PSK for the special case  $q = 1$ . Thus Eq. (4) provides an upper bound on the  $P(E)$  of any of these systems for  $q \geq 1$ . The lower and upper bounds given by Eqs. (3) and (4) differ by approximately 1 dB. in SNR, so we expect all of the SC PSK systems to achieve comparable performance. The simulation results support this conclusion.

In Decision Feedback (DF) PSK, combination with the reference of the signal received during the present baud is delayed until a decision about which signal was transmitted is made. This decision is then used as if it were correct to modify the present signal before it is combined with the reference. Since usually  $P(E)$  is small, the large majority of received signals are combined in the correct way. The error counts from the DF-PSK simulation are shown for three values of  $q$  in Fig. 1, along with the bounds on  $P(E)$  derived above. It is clear that even for medium values of  $q$  the system is operating close to its theoretical limit, Eq. (3).

Another major class of SC PSK systems uses the Phase Doubling (PD) technique. If  $\varphi_i$  is the phase error due to noise in the  $i^{\text{th}}$  baud, the received phase is

$$\psi_i = \theta + \varphi_i \text{ or } \theta + \varphi_i + \pi,$$

depending on the modulation. In either case, the phase doubler output has angle

$$2\psi_i = 2(\theta + \varphi_i),$$

which is independent of the data. These angles from  $q$  bauds are combined to give the phase

$$\theta' = 2(\theta + \varphi'),$$

where  $\varphi'$  represents the total error due to noise.  $\theta'$  is then halved to obtain the final phase estimate  $\hat{\theta}$ :

$$\hat{\theta} = \theta + \varphi'.$$

Two details of this technique demand further attention. First, the  $q$  angles  $2\psi_i$  can be combined in many ways. Two particular methods which were studied are weighting each angle as the square of the signal amplitude in the corresponding baud (SQ-PSK), and weighting proportional to the magnitude, or absolute value, of the signal amplitude (AB-PSK).

The second and most important consideration is that the procedure of halving the phase  $\theta'$  is analogous to taking the square root of a complex number, and therefore, the final phase estimate  $\hat{\theta}$  has two possible values separated by  $\pi$  radians. A

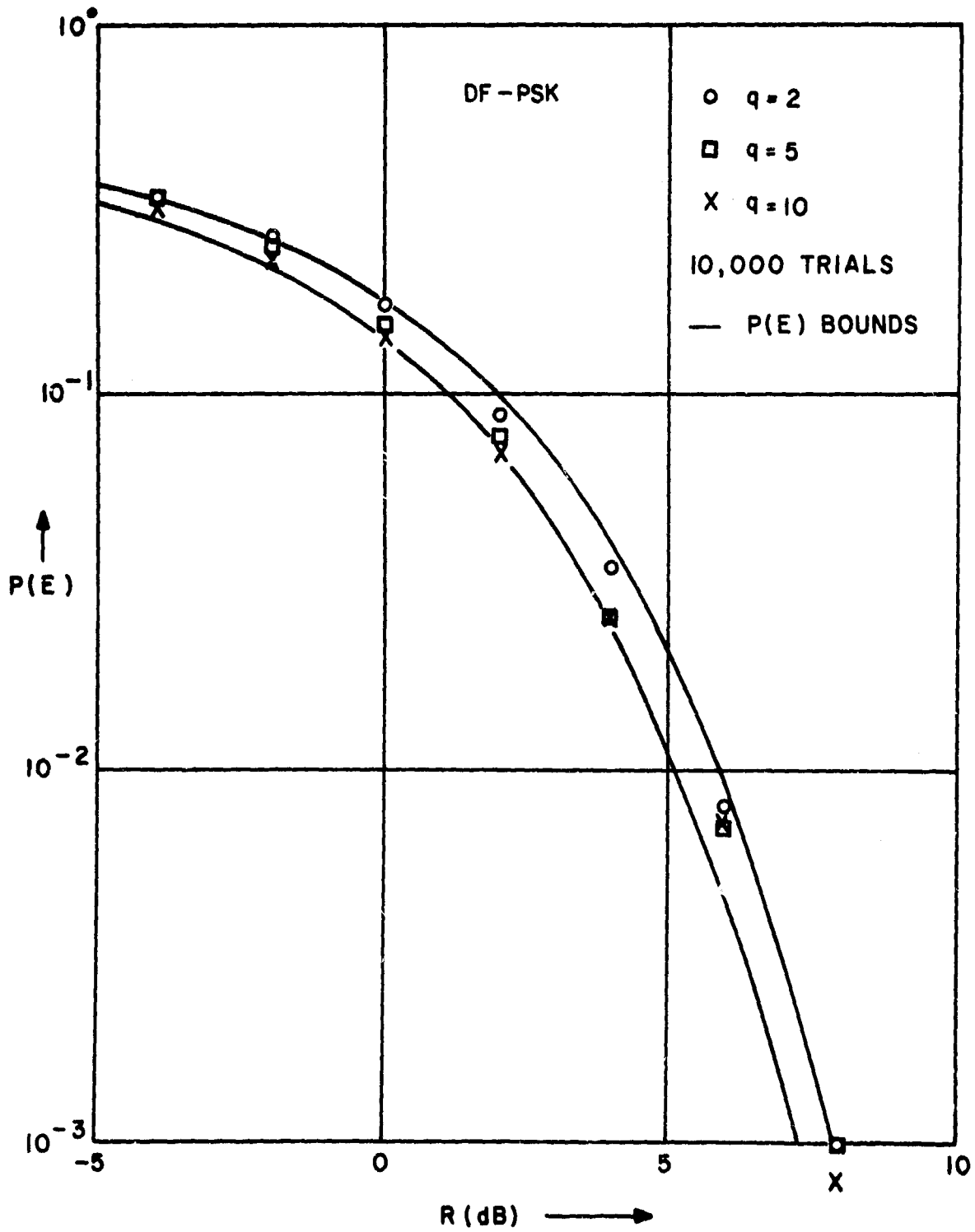


Fig. 1 Simulation Results for DF-PSK

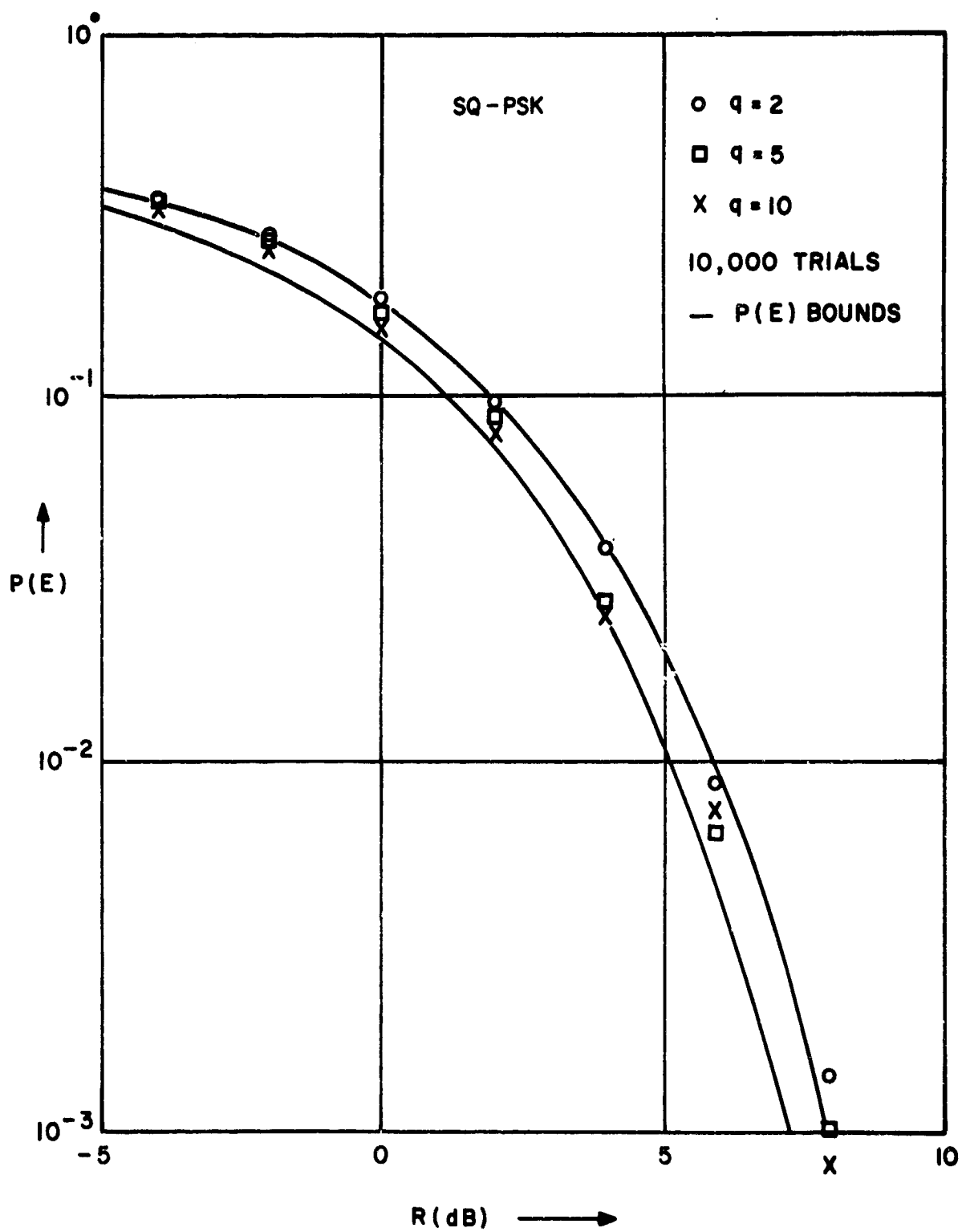


Fig. 2 Simulation Results for SQ-PSK

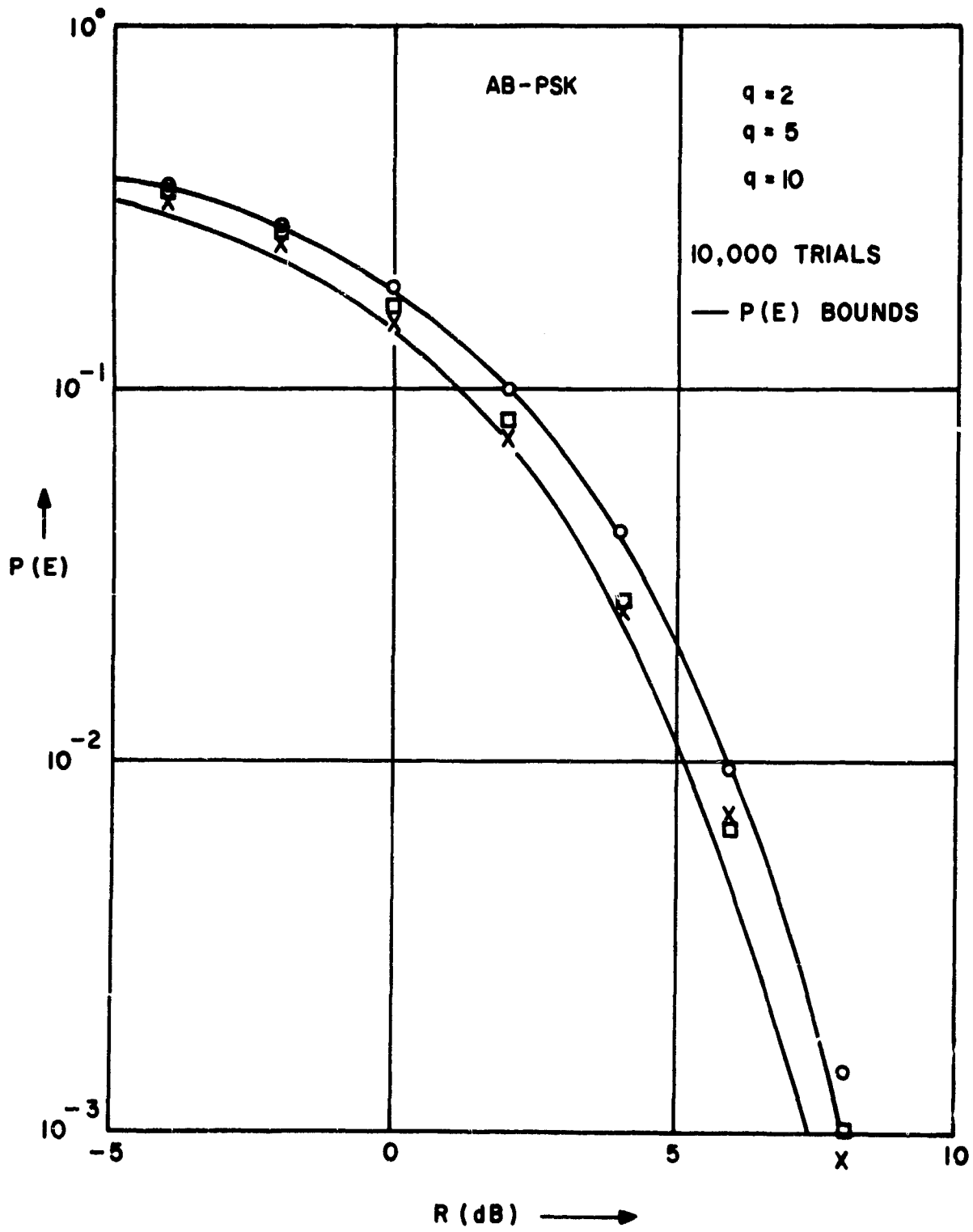


Fig. 3 Simulation Results for AB-PSK

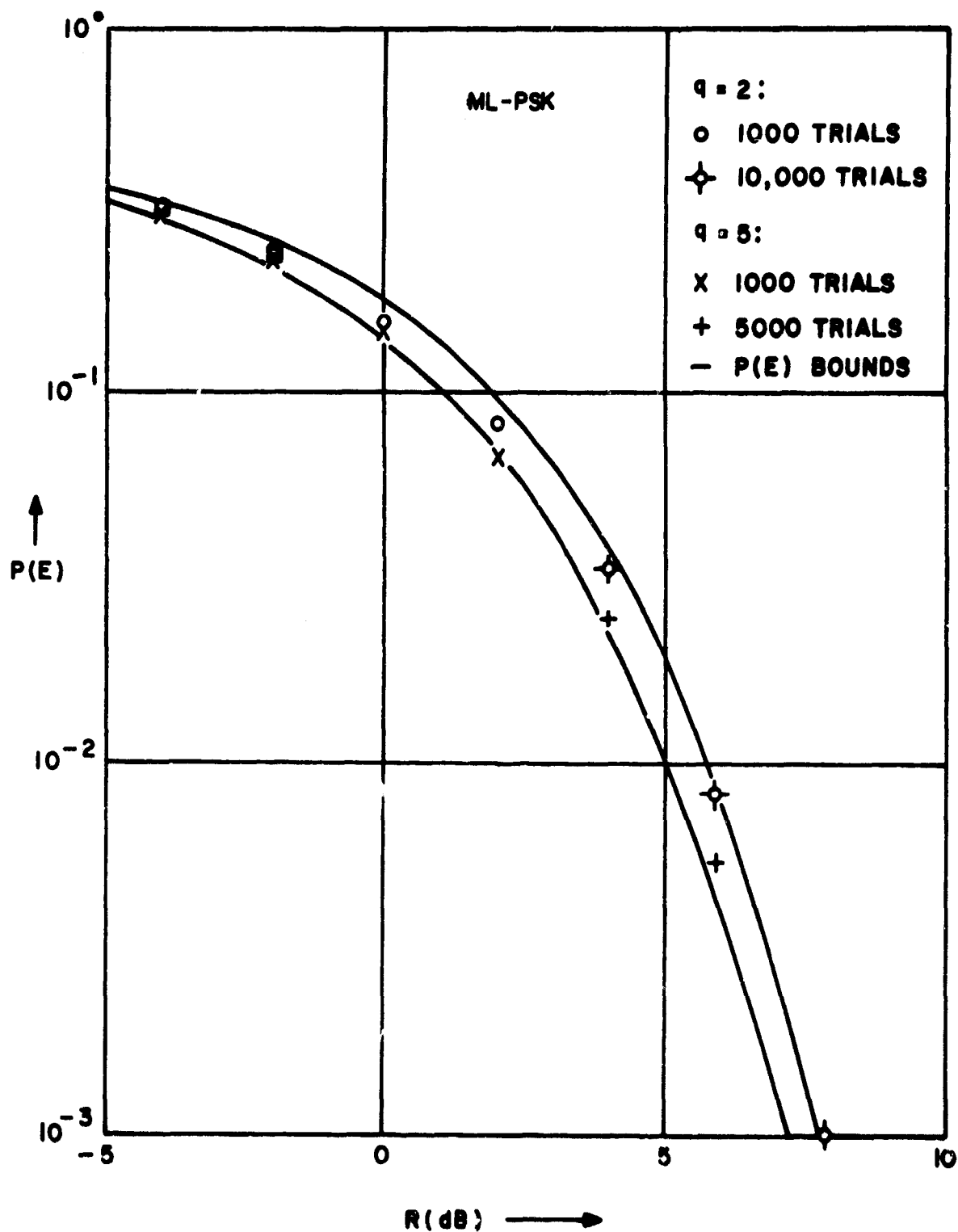


Fig. 4 Simulation Results for ML-PSK

rule must be established for choosing one of these two values. A satisfactory rule is to choose the value of  $\hat{\theta}$  which is closest to the  $\hat{\theta}$  derived for the previous decision. This choice gives good results for all values of  $q$ , and can be shown to be optimum for  $q = 1$ , since PD-PSK is equivalent to D-PSK under these conditions.

The PD-PSK systems described above were simulated on a digital computer. The error counts for SQ-PSK are shown in Fig. 2, and for AB-PSK in Fig. 3. Little difference is discernible between these results and those for DF-PSK in Fig. 1. Proakis et al.<sup>3</sup> on the other hand, have found on the basis of a similar digital computer simulation that DF-PSK is consistently superior to SQ-PSK. Apparently, they simulated a poor SQ system, since their experimental  $P(E)$  for  $q = 1$  is significantly higher than the upper bound, Eq. (4), derived above.

The final system investigated is called Maximum Likelihood (ML) PSK. This system was derived in the following way. Assume that the differentially encoded PSK signal, Eq. (2), is available, but past decisions made by the receiver are not remembered. ML-PSK is the receiver which attains the smallest possible  $P(E)$  for the decision about the latest possible (at  $t = 0$ ) phase transition. This is accomplished by applying a maximum a posteriori decision rule to the received signal. The ML receiver is quite complicated, its complexity growing exponentially with  $q$ , but it can be implemented. This complexity is reflected in the large amount of computer time used in the simulation. For this reason only two values of  $q$  were used, and fewer trials were made for this system than for the others. The error counts are shown in Fig. 4. Even for the relatively small  $q = 5$ , the experimental  $P(E)$  is nearly equal to the theoretical lower bound. Performance is consistently superior to the other SC systems considered, but is not good enough to justify the receiver complexity.

In summary, the simulation results show that the popular SC PSK systems perform similarly. The theoretical lower bound in  $P(E)$  for a differentially encoded SC PSK system is approached quite closely for moderate values of  $q$ . Furthermore, all of the systems studied reduce to Differential PSK for the special case  $q = 1$ .

National Aeronautics and Space Administration  
NgR 33-006-020

J. F. Oberst and D. L. Schilling

#### REFERENCES

1. J. F. Oberst, "Binary Phase-Shift Keyed Communication Systems," Ph. D. (E. E.) Dissertation, Polytechnic Institute of Brooklyn, June 1969.
2. J. F. Oberst and D. L. Schilling, "Double Error Probability in Differential PSK," Proceedings of the IEEE (Corr.), June 1968, pp. 1099, 1100.
3. J. G. Proakis, P. R. Drouilhet and R. Price, "Performance of Coherent Detection Systems Using Decision-Directed Channel Measurement," IEEE Transactions on Communication Systems, March 1964, pp. 54-63.

## ERROR CONTROL ON REAL CHANNELS

M. Muntner and J. K. Wolf

The promise of significant improvement associated with the use of error control techniques on digital communications channels has been based upon the assumption that errors occur independently. Real channels (e. g., telephone circuits, troposcatter radio, etc.), however, do not exhibit this property in that errors occur in bursts. In this research the performance of some of the more complicated coding techniques are examined by using a model that is representative of a real channel.

This model describes the distribution of the errors in time. It relies upon the concept of a renewal channel (i. e., a channel in which the occurrence of an error removes all memory of previous errors). The error model consists of  $M$  renewal channels. At time  $t_0$ , one of the channels is chosen with probability  $\lambda_i$ . This channel generates the error sequences up till time  $t_0+T-1$ . At time  $t_0+T$  another choice of channels is made and this channel is active for the next interval  $T$ . Furthermore, the channel selection points are randomly distributed while being synchronous. That is,  $\text{Prob}(t_0=i) = \frac{1}{T}$  for  $i = 0, \dots, T-1$ .

The properties of this model are such that if  $T$  is large but finite, the error statistics are the weighted average of the statistics of the individual renewal channels. For example, if  $p_i(m, n)$  is the probability of  $m$  errors in  $n$  bits on the  $i^{\text{th}}$  renewal channel, the probability of  $m$  errors in  $n$  bits for the channel model is

$$P(m, n) = \sum_{i=1}^M \lambda_i P_i(m, n)$$

The model has the following properties: stationarity, ergodicity; ability to match error distributions recorded on different types of channels; ease of selection of model parameters; and simplification of code evaluations.

Parameter selection and the matching of recorded statistics are somewhat tied together. Consider the telephone error statistics recorded by Townsend and Watts. If one plots  $\frac{P(m, n_1)}{\binom{n_1}{m}}$ , it is seen in Fig. 1 that the recorded data can be approximated by

the sum of exponentials (i. e., straight lines on semilog paper). Furthermore, as  $n$  is varied, the recorded  $\frac{P(m, n_2)}{\binom{n_2}{m}}$  can be approximated by a parallel set of lines. Renewal

channels with these straight line  $\frac{P_i(m, n)}{\binom{n}{m}}$  can be found and the modeled results are

shown in Fig. 2. The slope and separation between parallel lines uniquely determine the parameters of the respective renewal channel.

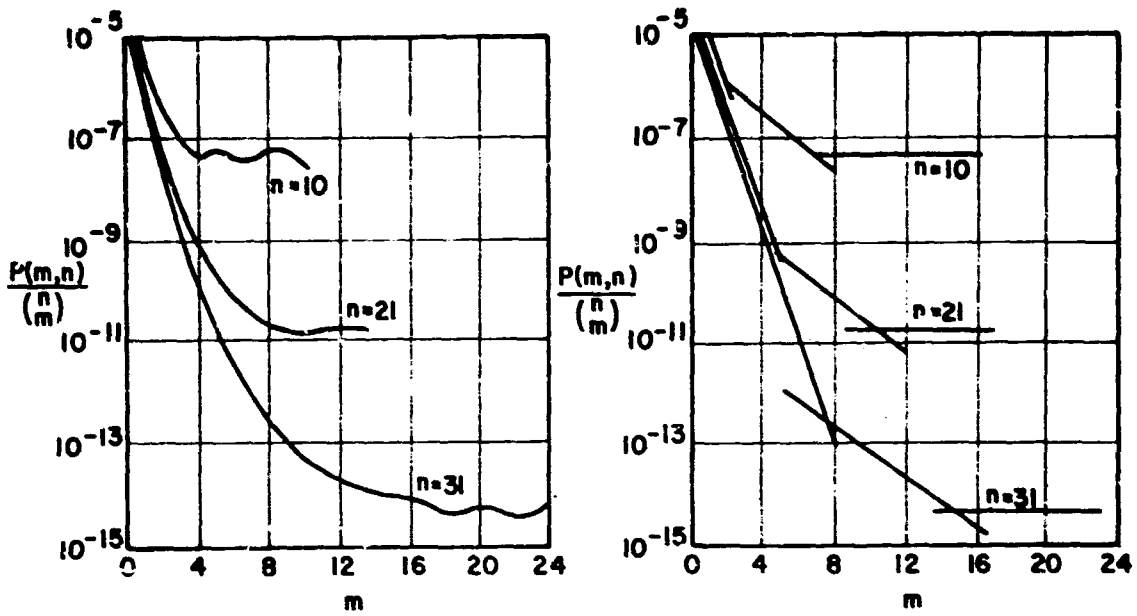


Fig. 1  $P(m,n)/\binom{n}{m}$  vs  $m$

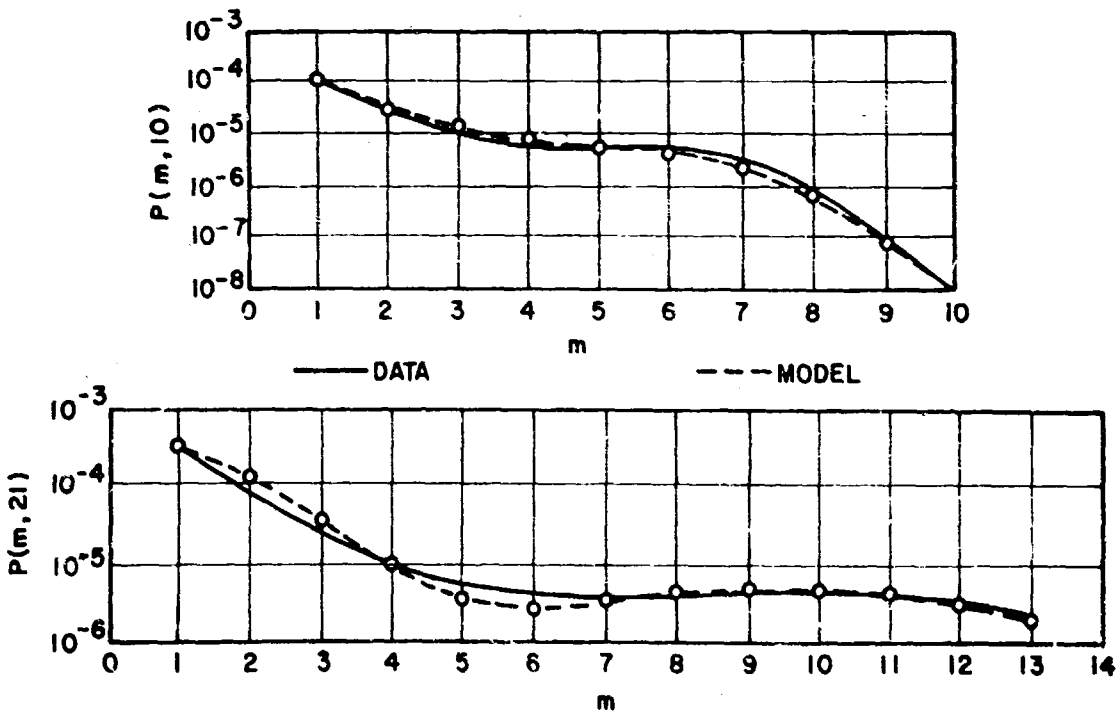


Fig. 2 Equivalent Accuracies for  $P(m, 31)$



Matching recorded data is not an end in itself and any model must be able to predict future experiments. Along this line, the results of Weldon's test of an interleaved burst correction code are examined. In these tests, a code with the capability of correcting a burst of length three or less in a block of 15 bits is interleaved  $t$  times resulting in a word  $15t$  bits long. This code can correct all bursts of length  $3t$  or less and several other error patterns. Using the probability of a burst of length greater than  $3t$  as an upper bound to the probability of a coding failure in the word of length  $15t$ , the following results are obtained:

$t$	Weldon's Data	Upper Bound
73	$4.8 \times 10^{-5}$	$6 \times 10^{-5}$
200	$8.7 \times 10^{-5}$	$2.1 \times 10^{-4}$

Having demonstrated the ability of the model to predict the performance of a tested coding scheme, several techniques are examined using the model parameters (renewal channels) representing the switched telephone network (i. e., Townsend Watts data).

### 1. Interleaving

The blocked bits from the data source are rearranged (by some delay and storage device) and put onto the line so that of two originally adjacent bits in a block, the second is the  $t^{\text{th}}$  bit transmitted following the first. The number  $t$  is called the interleaving constant. When  $t = 1$  there is no real interleaving. By means of the model, it is shown that as  $t$  increases, the probability of  $m$  errors in  $n$  interleaved bits approaches what would have been obtained with a binary symmetric channel of the same average bit error rate.

### 2. Detect and Delayed Retransmit Codes

When return paths are available for error control purposes, an error detection and retransmission scheme can be used. Upon detection of an error in a block of  $n$  bits, the same  $n$  bit block is retransmitted. However, if the retransmission were delayed (i. e., transmit nothing) then perhaps the burst of errors would terminate and the retransmitted block would have a better chance of being error free. This technique is examined on the basis of the probability of an undetected error and the throughput. It is shown that as the delay is increased, up to 200 bits for a Bose-Chaudhuri (31, 21) code, the probability of an undetected error decreased with little loss in throughput and that lengthening the delay decreases the throughput with little improvement in the undetected error rate.

### 3. Concatenated Codes

There has been considerable interest in concatenated codes. A concatenated code is one in which the symbols in a Reed Solomon code of alphabet size  $q = 2^k$ , are

encoded into an  $(n, k)$  binary code. There are several options for the decoding of both types of codes. The three types considered are : 1) the binary code detects errors and the Reed Solomon code considers symbols with detected error as erasures and fills them in; 2) the binary code corrects errors and the Reed Solomon code corrects symbol errors; and 3) the binary code corrects up to  $A$  errors and detects error patterns at a distance greater than  $A$  from any code word and the Reed Solomon code fills in erased symbols. Several binary codes and Reed Solomon codes are considered with the probability of a decoding failure of the Reed Solomon code being used as a criterion. One of the results is that increasing redundancy in the Reed Solomon code beyond some amount often yields no decrease in the probability of a decoding failure.

Air Force Office of Scientific Research  
AF 49(638)-1600

M. Muntner and J. K. Wolf

#### HIGH SPEED BINARY DATA TRANSMISSION OVER THE ADDITIVE, BAND-LIMITED, GAUSSIAN CHANNEL

L. Schiff and J. K. Wolf

The transmission of the linear sum of  $m$  bi-phase modulated signals in a time interval  $T$  was considered for an additive Gaussian white noise channel of bandwidth  $W$ . Previous analyses consider the case where  $m \leq n \equiv 2WT$ . In this study, the probability of error was derived for the case where  $m > n$ . This is a situation which arises when the channel bandwidth is insufficient to support the data rate.

Two distinct problems were considered. In the first, termed uncoded transmission, all  $m$  signals are independently bi-phase modulated. It was shown, for this case, that if the channel signal-to-noise ratio increases linearly with  $n$ , the error probability can be made to go to zero approximately exponentially in  $n$  for any value of  $m/n$ .

In the second problem, termed coded transmission, only  $k < m$  of the signals are independently modulated. (The remaining  $(m - k)$  signals carry redundant information). Using a sub-optimum receiver, it was shown that for a fixed channel signal-to-noise ratio the error probability goes to zero exponentially in  $n$  if  $k/n$  is less than some number  $C^*$ . For high signal to noise ration,  $C^*$  is greater than 1, a situation which could not occur if  $m \leq n$ .

Air Force Office of Scientific Research  
AF 49(638)-1600

L. Schiff and J. K. Wolf

## A FEEDBACK COMMUNICATION SCHEME BASED ON THE KIEFER-WOLFOWITZ PROCEDURE

R. W. Muise, R. R. Boorstyn, and J. K. Wolf

A feedback communication scheme has been studied by Kailath and Schalkwijk<sup>1, 2</sup> which is based on the Robbins-Monro stochastic approximation technique. They assumed that the channel consisted of a noiseless feedback link and an additive white Gaussian noise forward link. The analysis was treated in two parts, first with no bandwidth constraint on the signals and second with a finite bandwidth constraint on the signals. This study considered a feedback communication scheme subject to the same assumptions and constraints but based on the Kiefer-Wolfowitz<sup>3</sup> stochastic approximation technique. It was found that the performance achieved with this scheme is the same as that achieved with the Schalkwijk-Kailath scheme for no bandwidth constraint. However, when a finite bandwidth constraint is imposed on the signals, the Schalkwijk-Kailath scheme was found to perform better, with the difference in performance becoming arbitrarily small as the bandwidth is allowed to increase without limit.

The two feedback schemes were then compared with the best known (simplex signals) one-way scheme and were found to have better performance than the one-way scheme.

Joint Services Technical Advisory Committee  
AF 49(638)-1402

R. R. Boorstyn and J. K. Wolf

## REFERENCES

1. J. P. M. Schalkwijk and T. Kailath, "A Coding Scheme for Additive Noise Channels with Feedback, Part I: No Bandwidth Constraint," IEEE Transactions on Information Theory, Vol. IT-12, No. 2, pp. 172-182, (April, 1966).
2. J. P. M. Schalkwijk, "A Coding Scheme for Additive Noise Channels with Feedback, Part II: Band-Limited Signals," IEEE Transactions on Information Theory, Vol. IT-12, No. 2, pp. 183-189, (April, 1966).
3. J. Sacks, "Asymptotic Distributions of Stochastic Approximation Procedures," Ann. Math. Stat., Vol. 29, pp. 373-405, (June, 1958).

## SOME RESULTS FOR ADDITIVE NOISE CHANNELS WITH NOISELESS INFORMATION FEEDBACK

T. W. Eddy and J. K. Wolf

This study considered some new results for two distinct aspects of the additive noise channel with noiseless information feedback. First, the performance capabilities of channels with additive colored noise in the forward channel were examined. Next, a sequential coding scheme was proposed for the additive white noise channel and its performance analyzed and compared to the performance of the Schalkwijk coding procedures. The coding procedures analyzed in both cases employed the basic ideas of the Schalkwijk<sup>1, 2</sup> coding schemes.

Investigation of the wideband channel with additive colored noise leads to an expression for the channel capacity. In particular, it was proved constructively that the capacity is given by

$$C_{fb} = \frac{P_{avg}}{2 \min_{\omega} S_n(\omega)}$$

where  $P_{avg}$  is the average transmitted power and  $S_n(\omega)$  is the spectral density of the additive noise in the forward channel. With this result it follows that the capacity of the channel with noiseless feedback can, in some situations, be larger than the capacity of the corresponding channel without feedback.

In the case of the bandlimited channel with additive colored noise it was shown that error-free transmission is possible provided the rate  $R$  satisfies

$$R < \frac{P_{avg}}{2 \min_{\omega} S_n(\omega)}$$

and the signal-to-noise ratio is small. On the other hand, when the signal-to-noise ratio is large, it was shown that error-free transmission is possible provided

$$R < W \ln \left( 1 + \frac{P_{avg}}{2WN_0} \right)$$

where

$$N_0 = \frac{1}{2\pi W} \int_0^{2\pi W} S_n(\omega) d\omega$$

and  $W$  is the channel bandwidth in Hz. The capacity of the bandlimited channel with noiseless feedback was found only in the limit as the signal-to-noise ratio goes to zero in which case

$$\lim_{P_{avg} \rightarrow 0} \frac{C_{fb}}{P_{avg}} = \frac{1}{2 \min_{\omega} S_n(\omega)}; \quad 0 \leq \omega \leq 2\pi W.$$

From this result it follows that for small signal-to-noise ratios the capacity of the channel with noiseless feedback can, in some cases, be larger than the capacity of the corresponding channel without feedback.

These results extend the known results for additive white noise channels (for which it is also known that the channel capacity is not increased by noiseless feedback) to channels with additive colored noise.

Finally, a sequential coding procedure using information feedback was proposed

and analyzed. Performance curves for wideband and bandlimited channels were presented and the asymptotic probability of error was determined. For the wideband channel

$$P_e \sim \frac{2e^{-\frac{1}{2} \left( \sqrt{6} e^{\overline{T}(C-\overline{R}) - \frac{1+\nu}{2}} \right)^2}}{\sqrt{2\pi} \left( \sqrt{6} e^{\overline{T}(C-\overline{R}) - \frac{1+\nu}{2}} \right)}$$

where  $\overline{T}$  is the average time per message,  $\overline{R} = \ln M/\overline{T}$ ,  $C$  is the channel capacity and  $\nu = 0.5772156649\dots$  is Euler's constant. Similarly, for the bandlimited channel

$$P_e \sim \frac{2e^{-\frac{1}{2} \left( \sqrt{6} e^{\overline{T}(C-\overline{R}) - \frac{e^{-C/W}}{2}} \right)^2}}{\sqrt{2\pi} \left( \sqrt{6} e^{\overline{T}(C-\overline{R}) - \frac{e^{-C/W}}{2}} \right)}$$

Corresponding results for the Schalkwijk coding procedures are

$$P_e \sim \frac{2e^{-\frac{1}{2} \left( \sqrt{3} e^{\overline{T}(C-R) - \frac{1+\nu}{2}} \right)^2}}{\sqrt{2\pi} \left( \sqrt{3} e^{\overline{T}(C-R) - \frac{1+\nu}{2}} \right)}$$

and

$$P_e \sim \frac{2e^{-\frac{1}{2} \left( \sqrt{3} e^{\overline{T}(C-R) - \frac{e^{-C/W}}{2}} \right)^2}}{\sqrt{2\pi} \left( \sqrt{3} e^{\overline{T}(C-R) - \frac{e^{-C/W}}{2}} \right)}$$

While the error performance is improved by using sequential information feedback, the sequential results are valid only if an infinite buffer is used. The effect of a finite buffer is also examined. It was shown (for a particular algorithm) that the finite buffer introduces an additional probability of error which decreases as  $1/\sqrt{B}$  where  $B$  is the maximum number of messages that can be stored in the buffer. This result illustrates

the significant role played by the buffer in the sequential coding procedure.

Air Force Office of Scientific Research  
AF 49(638)-1600

J. K. Wolf

#### REFERENCES

1. J. P. M. Schalkwijk and T. Kailath, "A Coding Scheme for Additive Noise Channels with Feedback, Part I: No Bandwidth Constraint," IEEE Trans. on Information Theory, Vol. IT-12, No. 2, (April, 1966), pp. 172-182.
2. J. P. M. Schalkwijk, "A Coding Scheme for Additive Noise Channels with Feedback, Part II: Band-Limited Signals," IEEE Trans. on Information Theory, Vol. IT-12, No. 2, (April, 1966), pp. 183-189.

#### EXTENSIONS OF A RECURSIVE APPROACH TO SIGNAL DETECTION

R. R. Boorstyn and R. L. Pickholtz

In a recent paper<sup>1</sup> Pickholtz and Boorstyn described a recursive approach to signal detection. The scheme was based on the following. The received signal was converted into a vector Markov process which was then sampled. The recursive structure of the digital processor followed readily. Of concern here are two aspects of this problem. First, in order to form a vector Markov process derivatives of the incoming signal are usually required. Investigations have been conducted into replacing these differentiation operations with approximating digital operations, such as differences. These studies, including simulation results, indicate that it is possible to replace derivatives with differences without adversely affecting performance. Details will appear in the next report.

Secondly, the previous paper considered a special type of noise - that generated by a linear differential equation driven by white noise. A more general noise description would include numerator dynamics. Work has been initiated extending the recursive approach in this direction.

The essential part of the recursive receiver is to convert the incoming signal plus noise  $[r(t) = s(t) + y(t)]$  into a vector Markov process in such a manner that information is not destroyed. If this is done by a linear processor, then the output of this device is  $\underline{p}(t) = \underline{\sigma}(t) + \underline{\eta}(t)$  where the noise component  $\underline{\eta}(t)$  is to be Markov. Furthermore we insist that  $r(t)$  be recoverable from  $\underline{p}(t)$ . Because of the linearity we need only consider the noise term. In the original work  $\underline{\eta}(t)$  consisted of the derivatives of  $y(t)$  as well as  $y(t)$  itself and satisfied both of the above requirements.

We now consider  $y(t)$  to be generated by the following differential equation

$$\frac{dy^n}{dt^n} + \sum_{k=0}^{n-1} \alpha_k(t) \frac{dy^k}{dt^k} = \sum_{\ell=0}^{n-1} \beta_k(t) \frac{dw^\ell}{dt^\ell}$$

where  $w(t)$  is white Gaussian noise. It is possible to find a state vector  $\underline{x}(t)$  for this system such that the first component  $x_1(t) = y(t)$ . This vector is the solution of

$$\dot{\underline{x}}(t) = A(t) \underline{x}(t) + \underline{b}(t) w(t)$$

$$y(t) = \underline{c}^T \underline{x}(t)$$

where  $\underline{c} = \begin{bmatrix} 1 \\ 0 \\ 0 \\ \vdots \\ 0 \end{bmatrix}$

Although  $\underline{x}(t)$  is Markov it cannot be obtained from  $y(t)$  alone - either  $w(t)$  or  $\underline{x}(t_0)$  is needed in addition (neither are available). We consider next the best mean-square estimate of  $\underline{x}(t)$  given the input  $y(s)$ ,  $s \leq t$ . Thus

$$\hat{\underline{x}}(t) = E[\underline{x}(t) | y(s), s \leq t].$$

Since  $\hat{x}_1(t) = y(t)$ ,  $y(t)$  can be recovered from  $\hat{\underline{x}}(t)$  - it is reversible. Furthermore, because of the Gaussian assumption  $\hat{\underline{x}}(t)$  is obtained by a linear operation on  $y(t)$ . Finally we shall show that  $\hat{\underline{x}}(t)$  is Markov and thus letting  $\underline{z}(t) = \hat{\underline{x}}(t)$  satisfies our requirements.

Proof: For some fixed  $T$  let  $\underline{z}(t) = E[\underline{x}(T) | y(s), s \leq t]$ .  $\underline{z}(t)$  is a Martingale.  $\underline{x}(t)$  can be written in terms of the state transition matrix  $\Phi(t, u)$  as

$$\underline{x}(T) = \Phi(T, t) \underline{x}(t) + \int_t^T \Phi(T, u) \underline{b}(u) w(u) du.$$

$$\text{Then } \underline{z}(t) = \Phi(T, t) \hat{\underline{x}}(t) + \int_t^T \Phi(T, u) \underline{b}(u) E[w(u) | y(s), s \leq t] du.$$

But the last term is zero since  $w(t)$  is white and  $u \geq t$ . Thus  $\underline{z}(t) = \Phi(T, t) \hat{\underline{x}}(t)$  or  $\hat{\underline{x}}(t) = \Phi^{-1}(T, t) \underline{z}(t)$ . To show Markovity, consider

$$\begin{aligned} E[\hat{\underline{x}}(t) | \hat{\underline{x}}(r), r \leq s] &= E[\hat{\underline{x}}(t) | \underline{z}(r), r \leq s] \\ &= \Phi^{-1}(T, t) E[\underline{z}(t) | \underline{z}(r), r \leq s] = \Phi^{-1}(T, t) \underline{z}(s) \end{aligned}$$

because  $\underline{z}(t)$  is a Martingale.

$$\text{Next } E[\hat{\underline{x}}(t) | \hat{\underline{x}}(s)] = E[\hat{\underline{x}}(t) | \underline{z}(s)] = \Phi^{-1}(T, t) E[\underline{z}(t) | \underline{z}(s)] = \Phi^{-1}(T, t) \underline{z}(s).$$

Thus,  $E[\hat{\underline{x}}(t) | \hat{\underline{x}}(r), r \leq s] = E[\hat{\underline{x}}(t) | \hat{\underline{x}}(s)]$ , and  $\hat{\underline{x}}(t)$  since Gaussian is Markov.

The recursive receiver will now consist of a device that estimates  $\underline{x}(t)$  given  $y(t)$  (this will actually operate on  $r(t)$  to yield  $\underline{p}(t)$ ) - some form of a Kalman filter. The remainder of the receiver will parallel the original work. This study is continuing.

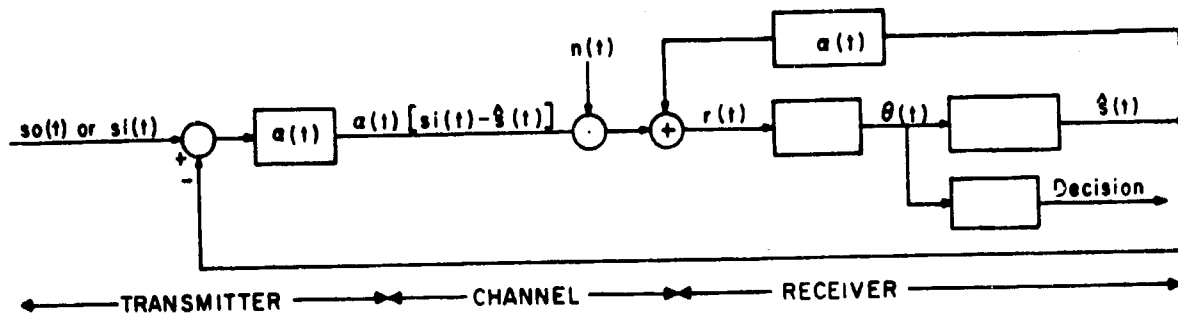


Figure 1

A second extension is to feedback communications. The proposed scheme is shown in Fig. 1.

The received data is  $r(t) = \alpha(t) s_1(t) + n(t)$ . An estimate for the transmitted signal is

$$\hat{s}(t) = \frac{\Lambda(t) s_1(t) + s_0(t)}{\Lambda(t) + 1}$$

where  $\Lambda(t)$  is the likelihood ratio. Letting  $g(t) = \alpha(t) s(t)$  we have

$$\theta(t) = \ln \Lambda(t) = 2 \int_0^t \frac{L[g(u)] L[r(u)]}{n_0(u)} du + \text{initial condition terms}^1.$$

The signal-to-noise ratio  $\gamma(t)$  is similarly given by

$$\gamma(t) = \int_0^t \frac{\{L[g(u)]\}^2}{n_0(u)} du + \text{initial condition terms}.$$

In terms of the latter,  $\theta(t)$  is normal with mean  $2\gamma(t)$  and variance  $4\gamma(t)$ . The problem is to find  $g(t)$  to maximize  $\gamma(t)$  subject to a constraint on the transmitted energy

$$\mathcal{E}_t = 4 \int_0^t \left[ \frac{g(u)}{e^{\theta(u)} + 1} \right]^2 du.$$

A typical constraint might be  $\frac{E(\mathcal{E}_t)}{t} = P$ , a constant. This work is continuing and is in turn easily extendable.

National Aeronautics and Space Administration  
NgR 33-006-020 and NgR 33-006-040

R. R. Boorstyn and R. L. Pickholtz

#### REFERENCE

1. R. L. Pickholtz and R. R. Boorstyn, "A Recursive Approach to Signal Detection," IEEE Trans. on Information Theory, Vol. IT-14, No. 3, May 1968.



## SIGNAL-ZERO-CROSSINGS AS AN INFORMATION CARRIER

A. L. Fawe and R. R. Boorstyn

The purpose of this research was to investigate the representation of bandlimited signals by means of a distribution of points along the time axis and the advantages which arise from such a representation.

The research takes its root in a well-known phenomenon, namely clipped speech intelligibility. Hard limiting of speech retains only the zero-crossings as an information carrier which shows that these are sufficient for a specific receiver: the ear, and a specific type of signal: speech. An interesting observation is the increase of intelligibility when speech is differentiated before clipping; it is easy to see that differentiation increases the zero-crossing density (the number of zero-crossings per second) which tends to prove that the quantity of information is indeed related in some way to the zero-crossing density. From the communication point of view the interest in a representation of bandlimited signals by a zero-crossing distribution follows from the lower signal-to-noise ratio required for a given intelligibility with clipped speech (when compared to normal speech).

For the class of signals which have a bandlimited Fourier transform we find that a subclass is completely defined by the zero-crossings. Moreover any signal in the class can be mapped into a signal in the subclass. Finally the output signal-to-noise ratio of a communication system which uses the subclass for transmission exhibits a very interesting property.

## A. Condition for a Bandlimited Signal to be Uniquely Defined by its Zero-Crossings

Theorem 1. Let  $x(t)$  be a signal whose Fourier transform  $X(\omega)$  exists and vanishes outside the interval  $(-\Omega, +\Omega)$ . If the real and imaginary parts of  $X(\omega)$  are integrable functions the number of zeros,  $n(T)$ , of

$$x_a(\theta) = (2\pi)^{-1} \int_{-\Omega}^{\Omega} X(\omega) \exp(j\omega\theta) d\omega$$

(where  $\theta = t + j\tau$ ) such that  $|\theta_i| \leq T$  ( $\theta_i$  the location of the  $i$ -th zero) tends to  $4WT$  when  $T$  tends to infinity, more precisely

$$\lim_{T \rightarrow \infty} \frac{n(T)}{2T} = 2W$$

and

$$x_a(\theta) = x(0) \prod_{i=1}^{\infty} \left(1 - \frac{\theta}{\theta_i}\right)$$

$x_a(\theta)$  will be called the signal associated with  $x(t)$ <sup>1</sup>.

From this theorem we draw the following conclusions:

i) as  $T \rightarrow \infty$  the number of zeros (complex and real) of the associated signal tends to the same limit as the number of independent parameters required to describe the signal  $x(t)$  truncated to the interval  $(-T, +T)$ ;

ii) a bandlimited signal is completely defined by its zero-crossings if all zeros of the associated signal are real. Then

$$x(t) = x(0) \prod_{i=1}^{\infty} \left(1 - \frac{t}{t_i}\right)$$

Since our purpose is to use a computer to recover the signal from its zero-crossings we require two properties:

i) all zeros of  $x_a(\theta)$  must be real (and therefore the zero-crossing density  $2W$ );

ii) they must be uniformly distributed in the following sense: it is possible to find a division of the time axis in interval  $1/2W$  wide such that there is one and only one zero-crossing in each.

Since a computer can process a finite number of zero-crossings at the same time we are led to the recovery of the signal in an interval from the zeros which belong to it (with a resulting error). Property (ii) insures uniform performance of the recovery scheme in successive intervals. A signal with properties (i) and (ii) will be called optimum.

The scheme for recovery of an optimum signal does not follow from the last equation by dropping the factors corresponding to the zero-crossings outside the interval of interest. Actually such a scheme would lead to very poor results. The scheme we use starts from a representation like a Fourier series:

$$\hat{x}(t) = \sum_{n=-N}^{n=+N} c_n \exp(jn\omega_0 t) \quad |t| \leq T$$

where  $\omega_0 = \frac{\pi}{T}$ . If we let  $z = \exp(j\omega_0 t)$  then the  $2N$ th-order equation

$$0 = \sum_{i=0}^{2N} (c_{N-i}/c_N) z^{2N-i}$$

gives the  $2N$  zero-crossings, and since we can also write the second member as

$\prod_{i=1}^{2N} (z - z_i)$  where  $z_i = \exp(j\omega_0 t_i)$  and  $t_i$  is the location of the  $i$ -th zero we derive a set of relations between the unknown  $c_{N-i}/c_N$  and the known  $z_i$ . Finally we require that

the signal  $\hat{x}(t)$  and its approximation  $x(t)$  have the same energy in  $(-T, +T)$ :

$$\sum_{n=-N}^{+N} |c_n|^2 = (2T)^{-1} \int_{-T}^{+T} x^2(t) dt$$

We have investigated several optimum signals with this technique; the results are given by Figs. 1, 3 and 4. It can be seen that the recovered signal is a close approximation of the original even for a moderate number of zero-crossings. Figure 2 shows that the approximation improves as the length of the interval considered increases which is consistent with theorem 1 (but the transmission delay increases accordingly). Insight into the reasons for the success of the method can be gained by a comparison of the Fourier coefficients for the expansion of  $\sin \Omega t / t$  truncated and the coefficients calculated from the zero-crossings (Table 1): for an interval  $2T$  equal to 6 times the distance between successive zeros the difference is at most 10%. Therefore we are close to the truncated Fourier series which is known as the optimum mean square fitting of a function in a given interval.

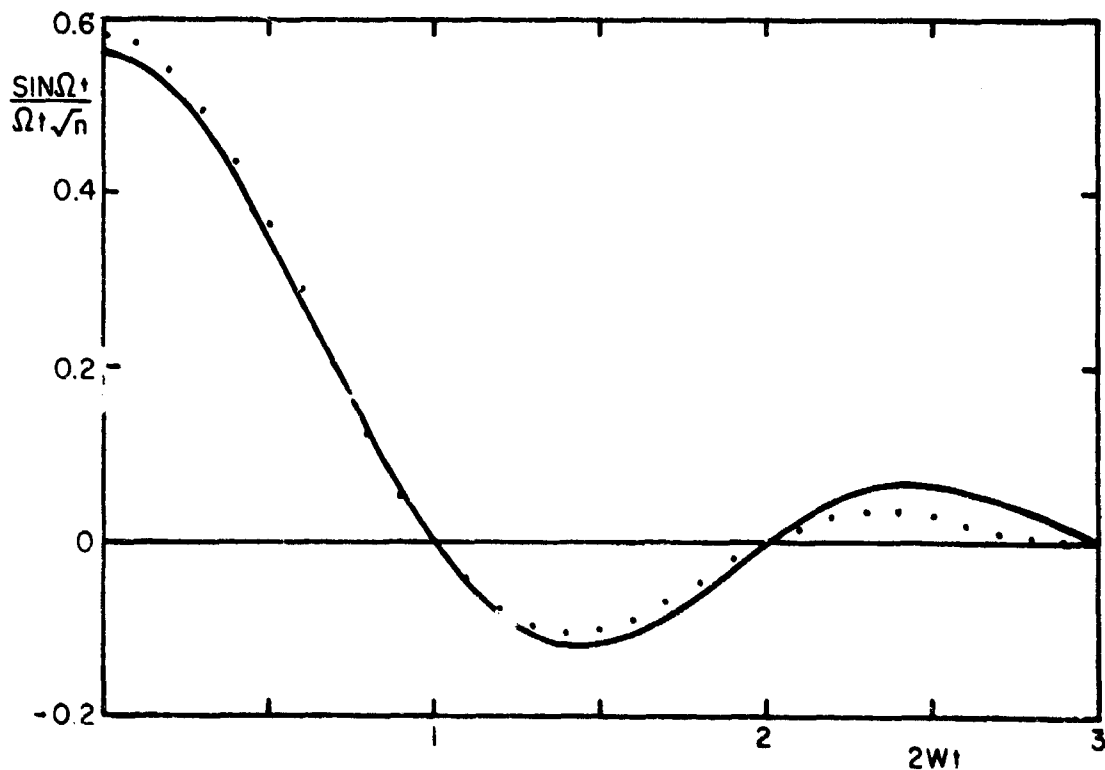


Fig. 1 Recovery of  $\sin \Omega t / \Omega t \sqrt{\pi}$ ;  $T = 3/2W$  ( $N = 3$ )  
 — signal; ... approximation.  
 Signal-to-mean-squared-error ratio: 20.4 dB.

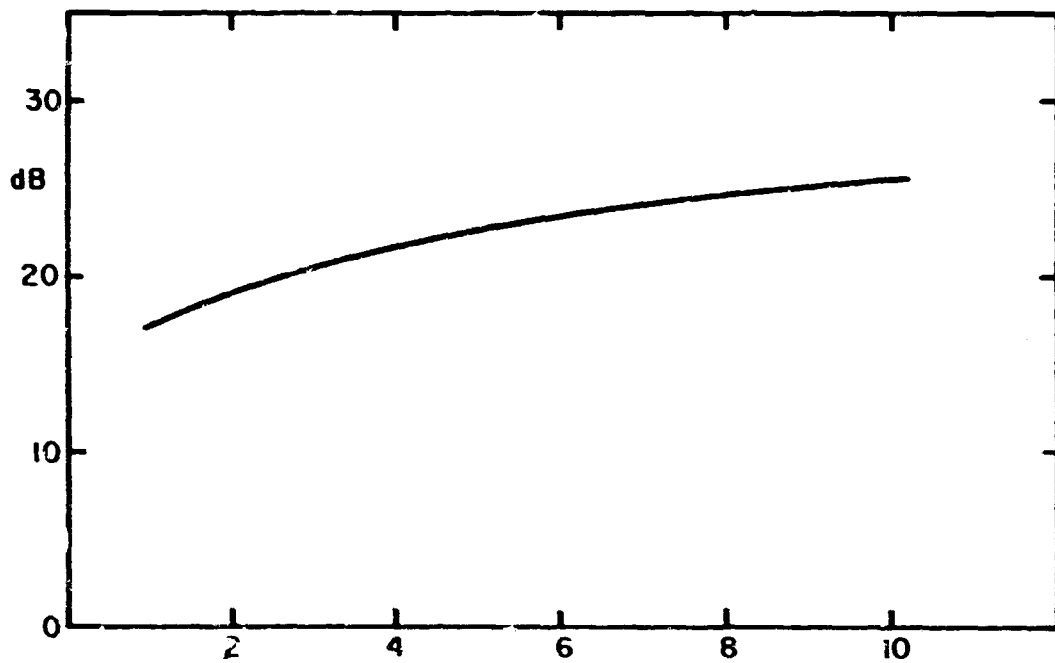


Fig. 2 Recovery of  $\sin \Omega t / \Omega t \sqrt{\pi}$ .  
 signal-to-mean-squared-error ratio vs the  
 number of zeros in half the interval (T).

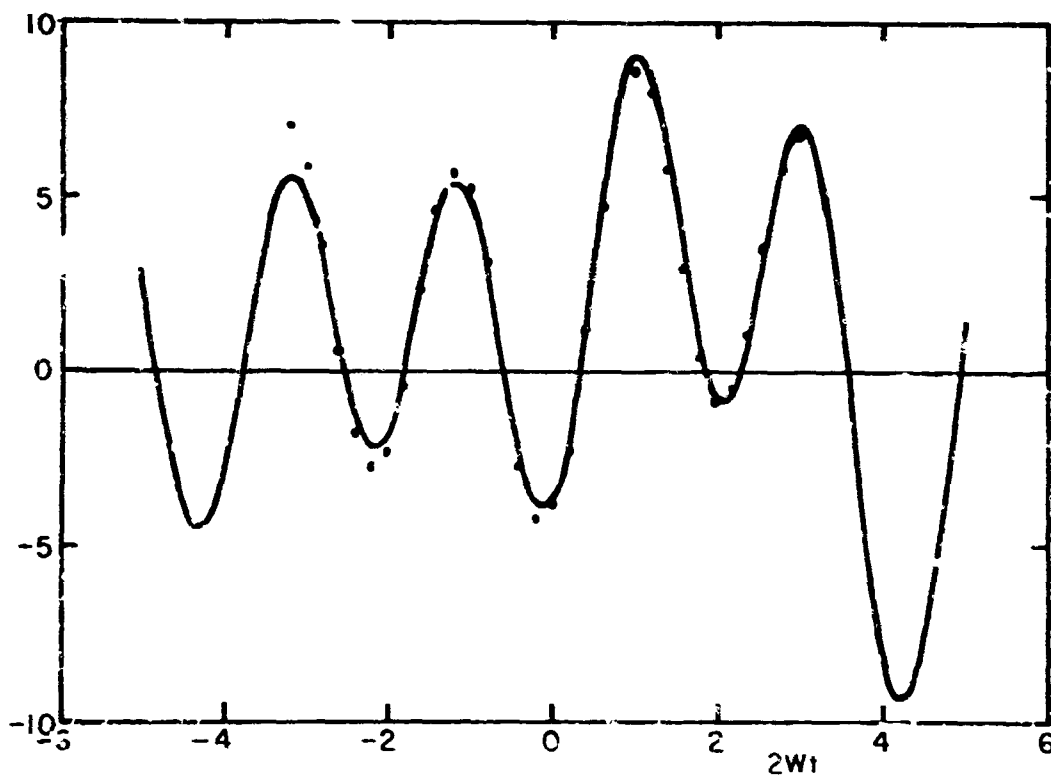


Fig. 3 Recovery of a general optimum signal.  
 — signal; ... approximation.  
 Signal-to-mean-squared-error ratio: 22 dB.

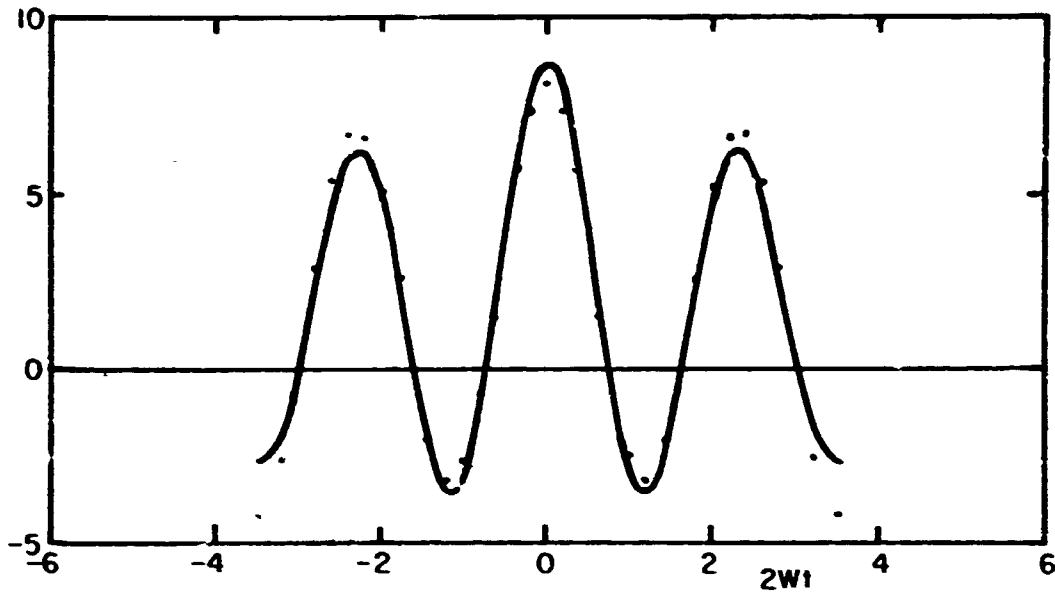


Fig. 4 Recovery of an optimum pulse.  
 — signal; ... approximation.  
 Signal-to-mean-squared-error ratio: 17.8 dB.

	Fourier	Zero-crossings	Difference(%)
$c_0$	.0996	.0966	-3.0
$c_1$	.0879	.0966	+9.9
$c_2$	1.038	.0966	-6.9
$c_3$	.0468	.0483	+3.2

Table 1. Coefficients of the series approximation ( $N = 3$ ) calculated by the classical Fourier formula and from the zero-crossings location.

#### B. Mapping of a Bandlimited Signal on an Optimum Signal

**Theorem 2.** A function  $x(t)$  which has an absolute integrable Fourier transform vanishing outside an interval  $(-\Omega, +\Omega)$  has one zero in each of the intervals

$$\left(\frac{n-1}{2W} + \alpha, \frac{n}{2W} + \alpha\right) \quad (n = \dots -2, -1, 0, 1, 2, \dots)$$

where

$$0 \leq \alpha < (2W)^{-1}$$

if and only if its values at  $\frac{n}{2W} + \alpha$  alternate in sign<sup>2</sup>.

This theorem gives us a necessary and sufficient condition for a bandlimited signal to be optimum and at the same time indicates the system which does the mapping: sample the signal, and reverse the sign of the sample when

$$x(j/2W) x_1((j-1)/2W) > 0$$

where  $x_1(t)$  is the optimum signal associated with  $x(t)$ . It is easily seen that the position of the reversed samples is given by the location of the zero-crossings of a bandlimited signal (with the same bandwidth  $W$ ) obtained by sending a pulse at  $j/2W$  through an ideal low-pass filter. Thus the reversible mapping requires an additional transmission bandwidth equal to  $W$ .

### C. Output Signal-to-Noise Ratio of a Communication System Based on These Principles

We first consider the case of an optimum signal. We shall assume that the interval is wide enough to neglect the error introduced by the recovery itself. Then

$$x(t) = \hat{x}(t) = \sum_{n=-N}^{+N} c_n \exp(jn\omega_0 t)$$

We shall also assume that the zero-crossings are merely transmitted by the clipped version of  $x(t)$  and that the channel does not distort this waveform (note however that in order to compute a channel signal-to-noise ratio we use the assumption that the rectangular wave occupies a bandwidth equal to  $5W$  which actually takes account of the most important frequencies). The output signal-to-noise ratio can be written as

$$(\text{SNR})_o = \frac{\int_{-T}^{+T} \hat{x}(t)^2 dt}{\int_{-T}^{+T} (\hat{x}(t) - \hat{x}_n(t))^2 dt}$$

where  $\hat{x}_n(t)$  is the signal recovered from the zero-crossings displaced by the channel noise. Assuming the received rectangular wave plus noise is first clipped (which eliminates a large amount of noise) the signal-to-noise ratio turns out to be

$$(\text{SNR})_o \cong \pi^{-2} (1 - \rho)^{-2}$$

When the channel noise is stationary, zero-mean, Gaussian, additive and independent of the signal  $o$  is given by

$$\rho = \sqrt{\frac{2}{\pi}} \int_0^{\sqrt{\gamma}} \exp\left(-\frac{u^2}{2}\right) du$$

where  $\gamma$  is the channel signal-to-noise ratio. This result corresponds to curve 1 on Fig. 5. Rice's result<sup>3</sup> for FM (bandwidth equal to  $5W$ ) is given by curve 3.

In the general case the output signal-to-noise ratio can be found in a similar way. The receiver samples the signal whose zero-crossings (in a noise-free situation) gives

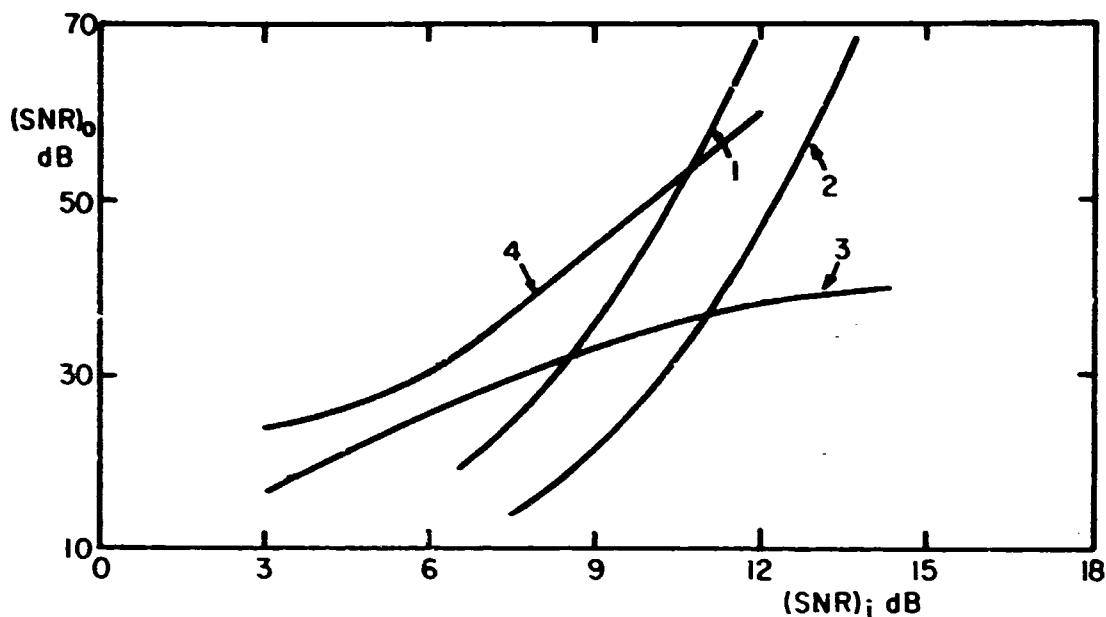


Fig. 5 Signal to noise ratio at the receiver output vs. signal-to-noise ratio at the input.  
 1: zero-crossings technique, optimum signals.  
 2: zero-crossings technique, general bandlimited signals.  
 3: FM without modulation (channel bandwidth: 5W).  
 4: Theoretical limit (channel bandwidth: 5W).  
 In 1 and 2 the rectangular wave carrying the zero-crossings is assumed undistorted by the channel for the calculation of  $(SNR)_o$ .

the location at which the sign of the samples of the recovered optimum signal must be changed to get the original signal; because of the channel noise we are led to a decision problem. The output signal-to-noise ratio due to this type of noise (wrong sample sign at the receiver output due to detection errors) is given by  $4P_e$ , where  $P_e$  is the probability of error in the decision process. The total signal-to-noise ratio is given by

$$(SNR)_o^{-1} \cong 4P_e + \pi^2 (1-\rho)^2$$

since the two noise contributions are independent. This result corresponds to curve 2, Fig. 5.

#### D. Conclusions

In the class of bandlimited signals a subclass exists with the remarkable property that its members are completely defined by the zero-crossings. Among these signals the so-called optimum are well defined at each instant of time by the zero-crossings in the close neighborhood.

A general bandlimited signal can be mapped in a simple way into an optimum signal.

The transmission of a bandlimited signal by the zero-crossings of the associated optimum signal leads to an output signal-to-noise ratio which increases sharply with the carrier signal-to-noise ratio. The curve has an exponential character which is interesting to compare with the theoretical result found by Goblick<sup>4</sup> on the highest signal-to-noise ratio that a communication scheme can achieve (for a bandwidth equal to 5W this result is given by curve 4, Fig. 5).

NATO Scientific Committee, Belgium, and  
National Aeronautics and Space Administration  
NgR 33-006-040

A. L. Fawe and R. R. Boorstyn

#### REFERENCES

1. E. C. Titchmarsh, "The Zeros of Certain Integral Functions," Proc. London Math. Soc., 25, 283-302; 1926.
2. G. Polya, "Ueber die Nullstellen gewisser ganzer Funktionen," Math. Zeitschrift, 2, 352-383; 1918.
3. S. O. Rice, "Noise in FM Receiver," Proceedings Symposium on Time Series Analysis, M. Rosenblatt (ed.), Ch. 25; Wiley, 1963.
4. T. J. Goblick, Jr., "Theoretical Limitations on the Transmission of Data from Analog Sources," IEEE Trans., IT-11; Oct., 1965.
5. A. L. Fawe, "The Use of Zero-Crossings in Signal Processing," Master of Science Report, Electrical Engineering Department, Polytechnic Institute of Brooklyn, 1968.

#### INVESTIGATION OF A CLASS OF NONLINEAR COMMUNICATION SYSTEMS

A. L. Fawe and R. R. Boorstyn

We have started a study of communication systems in which ideal clipping plays a central role. This research is motivated by the results described in our first report.

A convenient representation of the nonlinear part of the system is given by

$$y(t) = \frac{1}{\pi j} \int_{-\infty}^{+\infty} \omega^{-1} e^{j\omega x(t)} d\omega$$

where  $x(t)$  and  $y(t)$  are the clipper input and output respectively. This follows easily from the pair of Fourier transform

$$\text{sgn}(t) \longleftrightarrow \frac{2}{j\omega}$$

Some care is required in the use of this relationship because of the pole of the integrand at the origin. But we are interested in output correlation and input-output crosscorrelation only; we have shown the following relation

$$D \{R_{xy}(t_1, t_2)\} = -\frac{1}{\pi} \int_{-\infty}^{+\infty} \omega_2^{-1} D \left\{ \left[ \frac{\partial \Phi}{\partial \omega_1} \right]_{\omega_1=0} \right\} d\omega_2$$



$$D \{R_{yy}(t_1, t_2)\} = -\frac{1}{2\pi} \int_{-\infty}^{+\infty} \int_{-\infty}^{+\infty} (\omega_1 \omega_2)^{-1} D \{\Phi(\omega_1, \omega_2; t_1, t_2)\} d\omega_1 d\omega_2$$

where  $\Phi(\omega_1, \omega_2; t_1, t_2)$  is the characteristic function of the input process and  $D$  is some differential operator over the time variable  $t_1$  and  $t_2$  chosen in such a way that the poles at  $\omega_i = 0$  disappear. The appropriate operator is in general obvious; an integration over time leads to the function itself. As an example one finds very easily with this technique the well-known arc-sine law for a clipper with a Gaussian stationary input.

#### A. Recovery of a Bandlimited Signal Subject to Clipping

Before undertaking the investigation of any communication system of the kind defined above it is important to show that after filtering of the clipper output we get a good approximation of the signal itself and that by increasing by some means the zero-crossing rate at the clipper input we are able to make the error as small as we wish. We choose the mean-square-error to measure the discrepancy between the output of the filter and the signal; this leads to the choice of a Wiener filter to follow the clipper. We assume the signal  $x(t)$  Gaussian; then among the possible ways to increase the zero-crossing rate two are mathematically tractable because the Gaussian property is conserved: addition of a narrow-band Gaussian process about the frequency  $W$  or multiple-differentiation of the signal. We define the quantity  $a$  as

$$a = \frac{E\{x^2\}}{E\{(x-z)^2\}}$$

where  $x(t)$  is the signal to be transmitted and  $z(t)$  is the output of the Wiener filter.

For the addition of a narrow-band Gaussian process,  $s(t)$ , we found the following result

$$a^{-1} = 1 - \frac{\pi}{2(1+\gamma)} \int_0^1 \left\{ \int_0^\infty \cos(ut) \sin^{-1} \left[ \frac{\frac{\sin(t)}{t} + \frac{\gamma \sin(\alpha t)}{\alpha t} \cos(t)}{1+\gamma} \right] dt \right\}^{-1} du$$

where

$$\gamma = \frac{\sigma_s^2}{\sigma_x^2}; \alpha = \frac{\omega_0}{\Omega}; \Omega = 2\pi W$$

and  $2\omega_0$  is the bandwidth of the narrow-band process. In this result  $x(t)$  and  $s(t)$  are assumed to have a flat power spectrum in the region where it exists. The zero-crossing rate associated with the combined input process is given by

$$\frac{\lambda}{2W} = \sqrt{\frac{1 + \gamma(3 + \alpha^2)}{3(1 + \gamma)}}$$

The quantity  $\lambda_n = \lambda/2W$ , which is at most 1, will be called the normalized zero-crossing rate.

When the signal is differentiated  $n$  times before clipping the quantity  $a$  is given by

$$a^{-1} = 1 - \frac{(2n+1)\pi}{2} \int_0^1 u^{2n} \left[ \int_0^\infty \cos(ut) \sin^{-1} \left[ (2n+1) \int_0^1 v^{2n} \cos(vt) dv \right] dt \right]^{-1} du$$

and the normalized zero-crossing rate at the clipper input is

$$\lambda_n = \sqrt{\frac{2n+1}{2n+3}}$$

When in these two results we let  $\gamma$  and  $n$  respectively go to zero we get the common result

$$a^{-1} = 1 - \frac{\pi}{2} \int_0^1 \left[ \int_0^\infty \cos(ut) \sin^{-1} \left[ \frac{\sin(t)}{t} \right] dt \right]^{-1} du$$

The value of  $10 \log_{10}(a)$  is 7.3 dB in this case. The following table of the zero-crossing rates shows that even with a moderate number of differentiations or amount of narrow-band process power a small mean-squared-error will be achieved. We are now investigating the behavior of the two previous integrals as a function of the parameters  $\gamma$  and  $n$ .

$\gamma$ (dB)	$-\infty$	0	3	6	9	12
$\lambda_n$	.578	.817	.882	.931	.963	.982
$\gamma$ (dB)	$-\infty$	0	3	6		
$\lambda_n$	.578	.885	.975	.994		
$n$	0	1	2	3	4	5
$\lambda_n$	.578	.775	.845	.883	.905	.920

Table 1. Zero-crossing rate as a function of the ratio of the signal power to narrow-band process power (first line: addition of a Gaussian process; second line: addition of a sine wave process), or of the number of differentiations (third line).

The second line of the Table I gives the zero-crossing rate when a sine wave process  $A \sin(2\pi Wt + \theta)$  ( $A$  constant and  $\theta$  random variable with uniform distribution is  $(0, 2\pi)$ ) is added to the signal<sup>1</sup>:

$$\lambda = N_0 \left[ e^{-\alpha} I_0(\beta) + \frac{b^2}{2\alpha} I_e\left(\frac{\beta}{\alpha}, \alpha\right) \right]$$

where  $I_0$  is the modified Bessel function of the first kind,  $N_0$  is the zero-crossing rate of the Gaussian process  $x(t)$  alone

$$N_0 = \frac{1}{\pi} \sqrt{-R''_{xx}(0)/\sigma_x^2}$$

and

$$I_e(k, x) = \int_0^x e^{-u} I_0(ku) du$$

$$\alpha = \frac{A^2}{4\sigma_x^2} \left(1 + \frac{4W^2}{N_0^2}\right); \beta = \frac{A^2}{4\sigma_x^2} \left(1 - \frac{4W^2}{N_0^2}\right)$$

The calculation of  $a$  is more difficult in this case and we were unable to complete it up to now. However the table shows that this technique increases very rapidly the zero-crossing rate and seems to be the most powerful linear one.

In Ref. 2 we have shown that any bandlimited random process can be mapped on a process with a zero-crossing rate equal to  $2W$  (by a nonlinear transformation). This technique is difficult to handle mathematically, and to be reversible would require an additional bandwidth equal to  $W$ .

A last result for this section is the value of  $a$ , for a signal  $x(t)$  with flat power spectrum, when the filter after the clipper is an ideal lowpass filter:

$$a = 7.2 \text{ dB}$$

Although the ideal filter is unrealizable like the Wiener filter (which leads to  $a = 7.3$  dB) this result shows that some simple structure may be worth to be investigated.

#### B. Communication Systems with Clipping

We have just undertaken this part of the work and therefore we cannot quote many results.

We have shown<sup>2</sup> that when a random rectangular wave taking symmetrical values with same probability (as above, such a wave is intended to carry zero-crossings related to the signal to be sent) is contaminated by a zero-mean, additive Gaussian noise independent of the signal, and then clipped the crosscorrelation between the random square wave  $y(t)$  and the clipper output  $\hat{y}(t)$  is

$$R_{y\hat{y}}(\tau) = \frac{R_{yy}(\tau)}{\sigma_y} \sqrt{\frac{2}{\pi}} \int_0^{\sqrt{y}} \exp\left(-\frac{u^2}{2}\right) du$$

where  $\gamma$  is the channel signal-to-noise ratio. This result, which we have already quoted above, leads to

$$a^{-1} = 4Q(\sqrt{\gamma}) [1 - Q(\sqrt{\gamma})]$$

which for high carrier-to-noise ratio becomes

$$a \xrightarrow{\gamma \rightarrow \infty} \frac{\sqrt{2\pi\gamma}}{4} \exp\left(\frac{\gamma}{2}\right)$$

and for small carrier-to-noise ratio

$$a \xrightarrow{\gamma \rightarrow 0} 1 + \frac{2\gamma}{\pi}$$

When the signal  $y(t)$  results from a bandlimited Gaussian process applied to a clipper, then contaminated by the same type of noise, and finally applied to a second clipper we have found that the crosscorrelation function between the Gaussian process,  $x(t)$ , and  $\hat{y}(t)$  is given by the same formula as  $R_{yy}$  except for a factor  $\sqrt{2/\pi}$ .

NATO Scientific Committee, Belgium, and  
National Aeronautics and Space Administration  
NgR 33-006-040

A. L. Fawe and R. R. Boorstyn

#### REFERENCES

1. S. O. Rice, "Statistical Properties of Sine Wave Plus Random Noise," BSTJ, 27, p. 119; 1948.
2. A. L. Fawe, "The Use of Zero-Crossings in Signal Processing," Master of Science Report, Electrical Engineering Department, Polytechnic Institute of Brooklyn, 1968.

#### FM NOISE

D. T. Hess and D. Yavuz

This report generalizes the work done by Rice<sup>1</sup> in approximating the noise output of an FM discriminator, (FMD).

Rice<sup>1</sup> has shown that the output noise of a FMD may be approximated by the sum of two uncorrelated noise components; a parabolic spectrum gaussian noise term and a Poisson shot noise term consisting of impulses of area  $2\pi$ . In this report the noise is considered as a sum of a gaussian term plus a shot noise term that are in general correlated. The shot noise term becomes Poisson for large input carrier to noise ratios (CNR).

It is assumed that the input to the FMD is an unmodulated carrier plus symmetrical bandpass gaussian noise centered on the carrier. Thus the input may be represented as

$$A \cos \omega_0 t + n(t) =$$

$$A \cos \omega_0 t + x(t) \cos \omega_0 t - y(t) \sin \omega_0 t = \sqrt{(A+x)^2 + y^2} \cos [\omega_0 t + \psi(t)] \quad (1)$$

$$\psi(t) = \tan^{-1} \frac{y(t)}{A+x(t)}$$

where  $A$  is the carrier amplitude,  $\omega_0$  the carrier frequency and  $x(t)$  and  $y(t)$  are the low pass equivalents of the noise  $n(t)$ . The output of the FMD is  $\dot{\psi}(t)$ ,

$$\dot{\psi}(t) = \frac{d}{dt} \tan^{-1} \frac{y(t)}{A+x(t)} \quad (2)$$

This output is approximated by  $z(t)$ ,

$$\dot{\psi}(t) \approx z(t) = g(t) + p(t) = \frac{\dot{y}(t)}{A} + p(t) \quad (3)$$

where  $g(t) = \frac{\dot{y}(t)}{A}$  is the familiar output noise for large CNR and  $p(t)$  is the click process. The two terms,  $p(t)$  and  $g(t)$ , are in general correlated.

The click process is formed in the following manner; when  $x(t)$  is less than  $-A$  and  $y(t)$  approaches zero with  $\dot{y}(t)$  negative (positive)  $p(t)$  will have a positive (negative) impulse of area  $2\pi$ . The results may be easily extended to waveshapes other than impulses. The click process may be expressed as,

$$p(t) = -2\pi \dot{y}(t) u[-A - x(t)] \delta[y(t)] \quad (4)$$

where  $u(x)$  is the unit step function and  $\delta(x)$  the unit impulse function.

The autocorrelation of the output noise is given by

$$R_{zz}(\tau) = E\{z(t+\tau)z(t)\} = \frac{1}{A^2} R_{yy}(\tau) + R_{gp}(\tau) + R_{pg}(\tau) + R_{pp}(\tau) \quad (5)$$

The first term is the parabolic spectrum gaussian noise term, the second and third terms are the cross-correlation terms and the last term is the autocorrelation of the spike process. The cross correlation term has the form

$$R_{gp}(\tau) = E\{g(t+\tau)p(t)\} = R_{pg}(-\tau) = E\left\{-\frac{\dot{y}_2}{A} 2\pi \dot{y}_1 u(-A - x_1) \delta(y_1)\right\} \quad (6)$$

where the expectation is over  $t$  and the subscripts 1 and 2 refer to time instants  $t$  and  $(t+\tau)$ . By evaluating the appropriate integrals  $R_{gp}(\tau)$  is found to be,

$$R_{gp}(\tau) = \frac{\sqrt{\pi}}{2\beta} \rho'' \operatorname{erfc} \beta \quad (7)$$

where

$$\rho'' \triangleq \frac{d^2}{d\tau^2} \rho_{xx}(\tau) \quad \rho_{xx}(\tau) = \frac{R_{xx}(\tau)}{N}$$

$$\beta = \sqrt{\frac{A^2}{2N}} \quad N = R_{xx}(0)$$

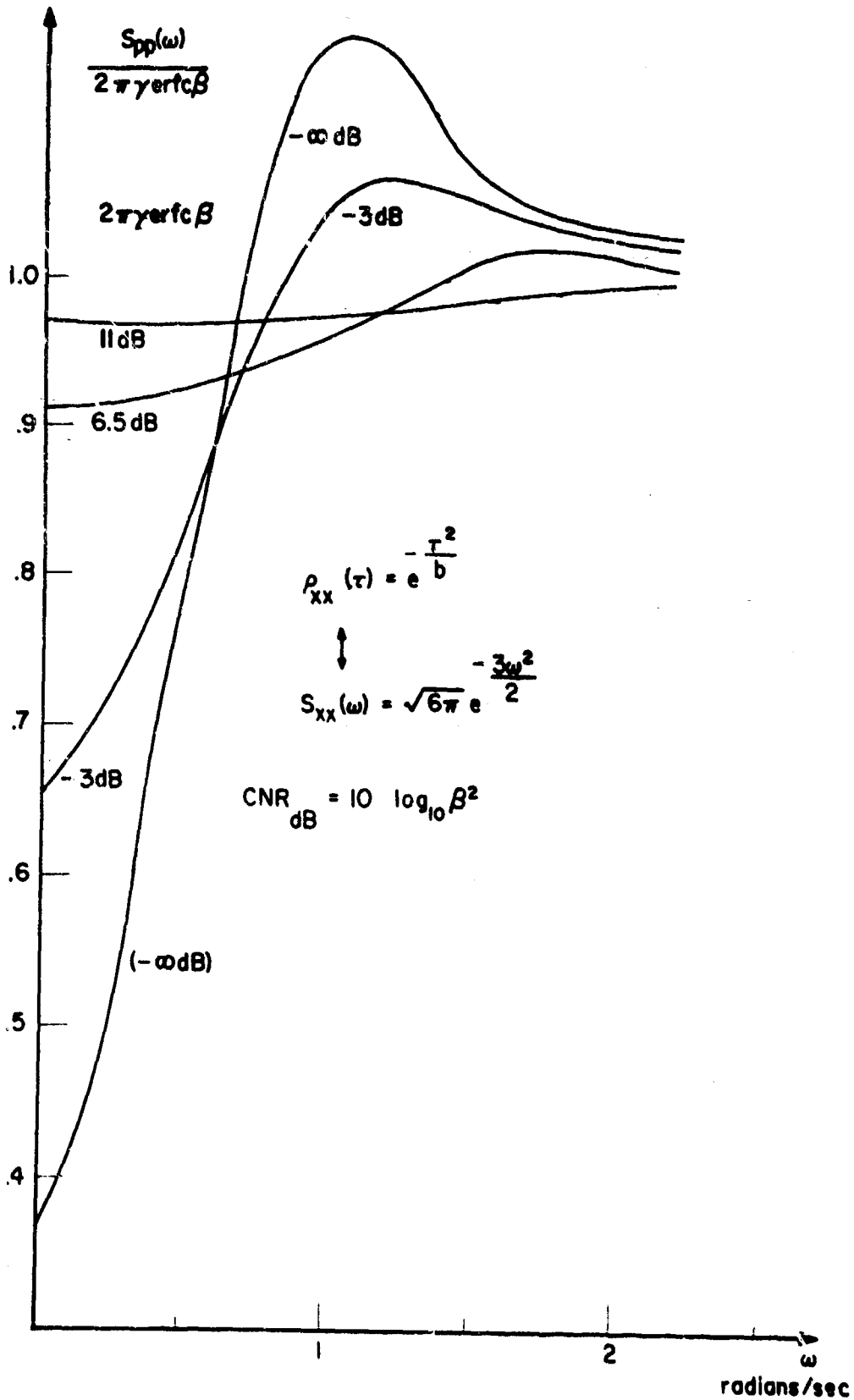


Fig. 1 Normalized Power Spectrum of the Click Process for a Gaussian Shaped Filter

From Eq. (7) is seen that the gaussian noise and the click noise decouple as a complementary error function of  $\beta$ , the decoupling is strongly effected by the input filter shape due to the term  $\rho_{xx}^n(\tau)$ ; however, the two components are indeed uncorrelated for large CNR as is generally assumed.

The autocorrelation of the click process is given by,

$$R_{pp}(\tau) = 4\pi^2 E \left\{ \dot{y}_1 \delta(y_1) u(-x_1 - A) \dot{y}_2 \delta(y_2) u(-x_2 - A) \right\} \quad (8)$$

The corresponding integrals can be evaluated after rather lengthy manipulations and the autocorrelation takes the form

$$R_{pp}(\tau) = 2\pi \gamma \operatorname{erfc} \beta \delta(\tau) - 2\pi \left\{ \frac{1}{4} \operatorname{erfc}^2 \beta + \sum_{n=1}^{\infty} \left[ \frac{\varphi^{(n)}\left(\frac{A}{\sqrt{N}}\right)}{n!} \right]^2 \rho^n \right\} \left\{ \frac{\rho^n}{\sqrt{1-\rho^2}} + \frac{\rho \rho'^2}{(1-\rho^2)^{3/2}} \right\} \quad (9)$$

where

$$\gamma = \sqrt{-\frac{R_{xx}''(0)}{R_{xx}(0)}} \quad \text{radius of gyration of the band pass filter in rps}$$

$$\rho \triangleq \rho_{xx}(\tau) \quad \varphi(x) = \frac{1}{\sqrt{2\pi}} \int_{-\infty}^x \frac{u^2}{e} du \quad \varphi^{(n)}(x) \triangleq \frac{d^n}{d\kappa^n} \varphi(\kappa)$$

For large CNR only the first term in Eq. (9) is significant, and it should be noted that this is the flat spectrum Poisson shot noise term.

The power spectrum of the click process,  $S_{pp}(\omega)$ , may be obtained by taking the Fourier transform of  $R_{pp}(\tau)$  numerically. In Fig. 1 the normalized power spectrum is given for a gaussian shaped filter. The correlation between the clicks produces a dip in the power spectrum around the origin and hence the click power at the output is reduced.

By comparing  $S_{pp}(0)$  with the exact power spectrum of the noise output of the FMD as given by Rice<sup>2</sup> we see that for  $\omega = 0$  they are identical for all CNR (note that for  $\omega = 0$   $S_{zz}(0) = S_{pp}(0)$  since  $S_{pg}(0) = S_{gg}(0) = 0$ ).

The analysis presented is an extension and elaboration of the FM noise problem as studied by Rice<sup>1</sup>. The decomposition of the FM noise into two components provided an understanding of the FM threshold phenomenon. The analysis presented in this report elaborates, extends and justifies the generally used method of FM noise decomposition.

## REFERENCES

1. S. O. Rice, "Noise in FM Receivers," Chap. 25, pp. 375-424, in "Proceedings, Symposium on Time Series Analysis," M. Rosenblatt (ed.), John Wiley and Sons, Inc., N. Y. 1963.
2. S. O. Rice, "Statistical Properties of Sine Wave Plus Random Noise," B. S. T. J., Vol. 27, Jan. 1948.

## AN OUTPUT SIGNAL-TO-NOISE RATIO EQUATION FOR THE FIRST AND SECOND-ORDER PHASE-LOCKED LOOP

D. T. Hess and R. J. Schulman

In this report, an equation is derived which predicts the output signal-to-noise ratio (SNR) with no modulation, for the first-order phase-locked loop (PLL), and with a small modification it also holds for the second-order PLL, when the system IF filter is rectangular and the output low-pass filter frequency characteristic is known. This equation has been experimentally verified for a variety of different system conditions.

## Derivation

The initial approach to this problem is the same as that taken by M. Schwartz<sup>1</sup> in his derivation of a SNR equation for the discriminator. Since a no modulation analysis is being performed, a fictitious output SNR is defined as the ratio of mean-squared signal out, with the noise set equal to zero, to the mean-squared noise with no signal present.

The argument is employed that the spectral density of the total noise at the PLL output is the sum of the spectrum obtained in the high carrier-to-noise case (Gaussian component) plus the spectrum due to noise clicks. Therefore, for a symmetric IF filter the output noise power spectrum of the PLL is given by

$$G_{\text{out}}(\omega) = G_1(\omega) + G_2(\omega) \quad (1)$$

where  $G_1(\omega)$  is the power spectrum of the Gaussian component, and

$G_2(\omega)$  is the power spectrum of the click component. When the input of the PLL is given by

$$e_{\text{in}}(t) = (A+x) \cos \omega_0 t - y \sin \omega_0 t \quad (2)$$

where  $x$  and  $y$  are independent Gaussian random variables, it has been shown<sup>1</sup> that

$$G_1(\omega) = \omega^2 N / 2BA^2 \quad \begin{matrix} -B < \omega < B \\ \Lambda >> \sqrt{N} \end{matrix} \quad (3)$$

where  $N$  is the input noise power, and  $2B$  is the IF filter bandwidth, and that

$$G_2(\omega) \approx 8\pi^2 N_+ \quad (4)$$



where  $N_+$  is the total expected number of positive clicks per second. ( $N_+ = N_-$  for an unmodulated carrier.) Therefore

$$G_{out}(\omega) \approx \omega^2 N/2BA^2 + 8\pi^2 N_+ \quad (5)$$

If there is an ideal low-pass filter (LPF) following the PLL which cuts off at  $f_m$ , the output noise power is given by

$$N_o = 2 \int_0^{f_m} G_{out}(f) df \quad (6)$$

However, the LPF of the typical demodulation system is not ideal. To get around this situation, we define  $f_{m_G}$  and  $f_{m_s}$  as equivalent bandwidths of ideal filters where

$$\int_0^{f_{m_G}} |F(o)|^2 f^2 df = \int_0^{\infty} |F(f)|^2 f^2 df \quad (7)$$

$$\int_0^{f_{m_s}} |F(o)|^2 df = \int_0^{\infty} |F(f)|^2 df \quad (8)$$

and  $F(f)$  is the actual LPF transfer function. The noise power is therefore

$$N_o = 2/3 \frac{\pi^2 f_{m_G}^3}{B\gamma} + 16\pi^2 N_+ f_{m_s} \quad (9)$$

where  $\gamma = A^2/2N$  is the carrier-to-noise ratio.

If the modulating signal is assumed to be of the form

$$\psi = \Delta\omega \cos \omega_m T \quad (10)$$

and it is attenuated by the output LPF by  $G_f$ , the mean-squared output signal is given by

$$S_o = 2\pi^2 (\Delta f)^2 G_f \quad (11)$$

An expression for  $N_+$  for the PLL has been derived by Hess<sup>2</sup> for the first-order PLL. His result for a rectangular IF filter is

$$N_+ = (B/2\sqrt{3}) \operatorname{erfc} \sqrt{\gamma} \left[ 1 + \frac{(0.6)B}{f_L} \right] \quad (12)$$

where  $\operatorname{erfc} \gamma = (2/\sqrt{\pi}) \int_{\gamma}^{\infty} e^{-x^2} dx$ , and  $f_L$  is the closed-loop bandwidth of the PLL.

B. Schwartz has shown<sup>3</sup> that the use of an equivalent first-order PLL bandwidth  $f_{Leq}$  in Hess' equation, allows one to predict  $N_+$  for the second-order loop, where the loop filter for the second-order loop is shown in Fig. 1. The determination of  $f_{Leq}$  is done

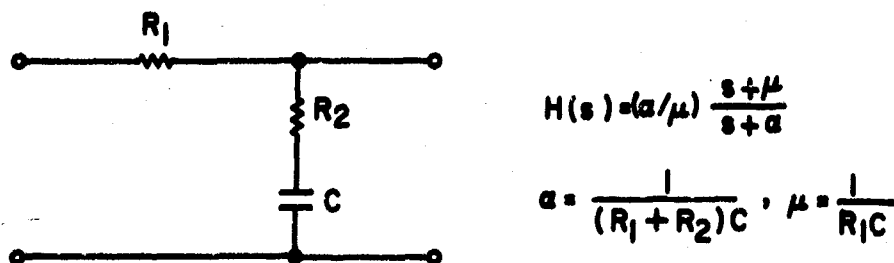


Fig. 1 Loop Filter for Second-Order PLL

by means of a simple graphical construction using the second-order parameters. Therefore, the output SNR for the first and second-order PLL with a rectangular IF filter, using the appropriate value of  $f_L$ , is given by

$$S_o / N_o = \frac{3 (\Delta f / f_{m_G})^2 \gamma (B / f_{m_G}) G_f}{1 + (24/\sqrt{3}) (f_{m_s} / f_{m_G}) (B / f_{m_G})^2 \gamma \operatorname{erfc} \sqrt{\gamma} [1 + \frac{(0.6)B}{f_L}]} \quad (13)$$

where  $\Delta f$  = signal deviation,  $\gamma$  = input CNR,  $B$  = half the IF filter BW,  $f_{m_G}$  = equivalent BW of output LPF for Gaussian noise,  $f_{m_s}$  = equivalent BW of output LPF for click noise,  $G_f$  = output LPF signal attenuation, and  $f_L$  = appropriate closed-loop BW of PLL.

#### Experimental Results

As verification that the output SNR equation holds for the first-order PLL, curves were obtained experimentally and theoretically for various values of closed-loop BW and output LPF bandwidth as shown in Figs. 2 and 3. It can be seen from these curves that agreement between theory and experimental results is good in all cases.

To test the equation for the second-order PLL, an equivalent closed-loop bandwidth had to be determined for each setting of  $f_L$  and for each loop filter, using the rules given by Schwartz<sup>3</sup>. The theoretical and experimental data is shown in Figs. 4 and 5. Again, agreement is good, which indicates the validity of the derived equation.

#### Conclusion

An equation that predicts the output SNR for the first and second-order PLL without modulation, has been derived. Its validity has been examined for various system conditions and it has been shown to hold for all cases tested.

National Aeronautics and Space Administration  
NgR 33-006-020

D. T. Hess and R. J. Schalman

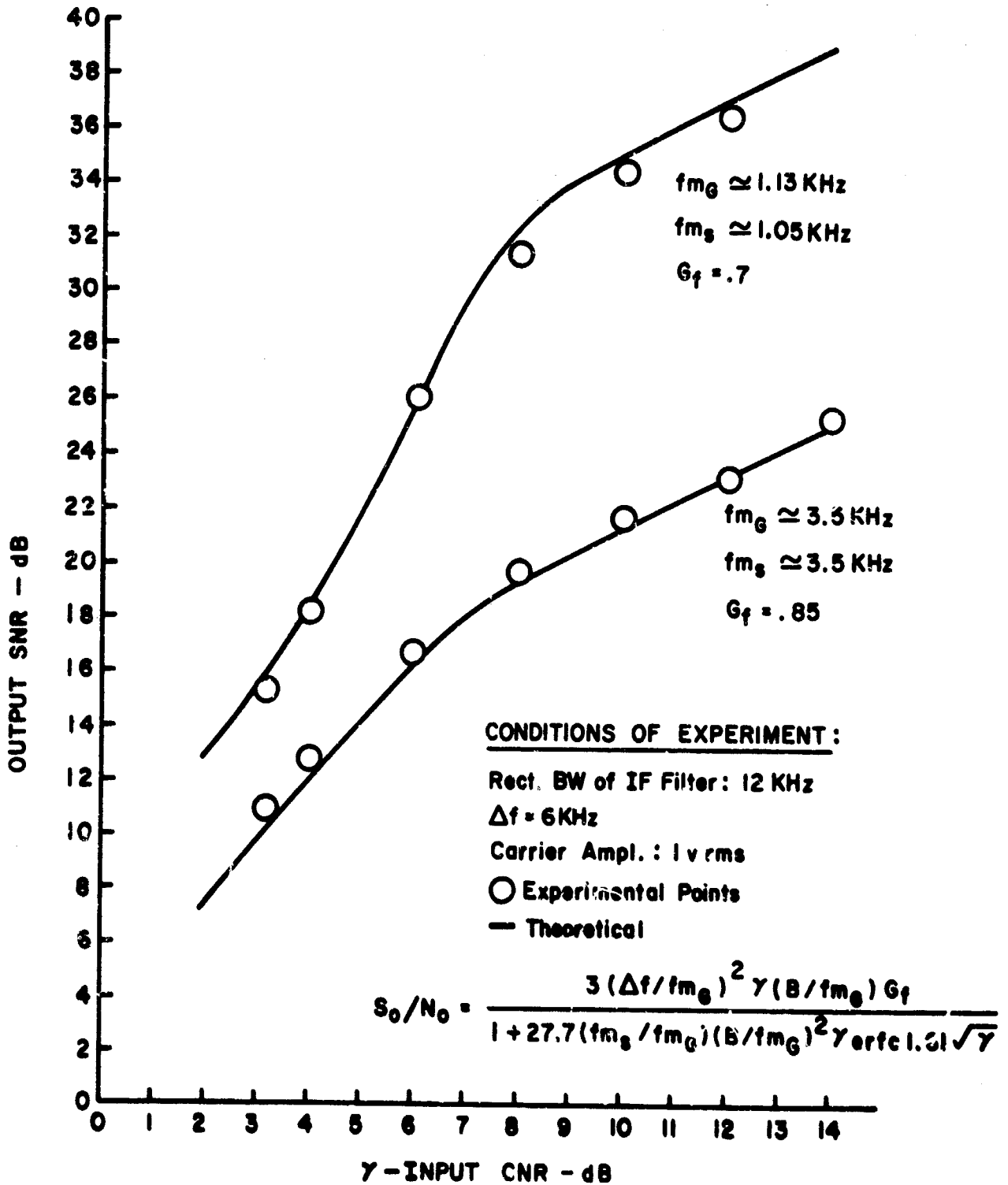


Fig. 2 Output SNR vs Input CNR for a First Order Phase-Locked Loop

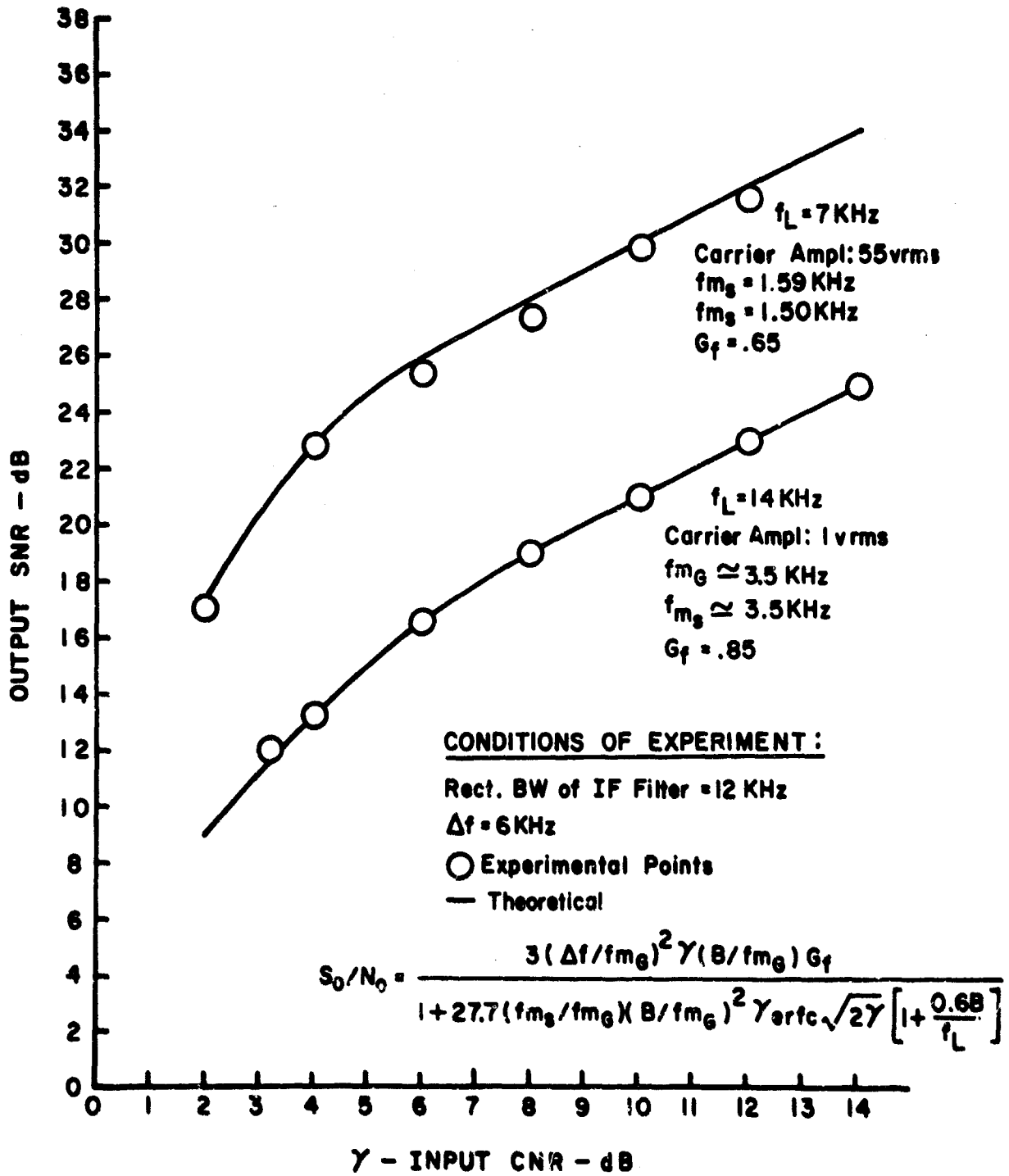


Fig. 3 Output SNR vs Input CNR for a First Order Phase-Locked Loop

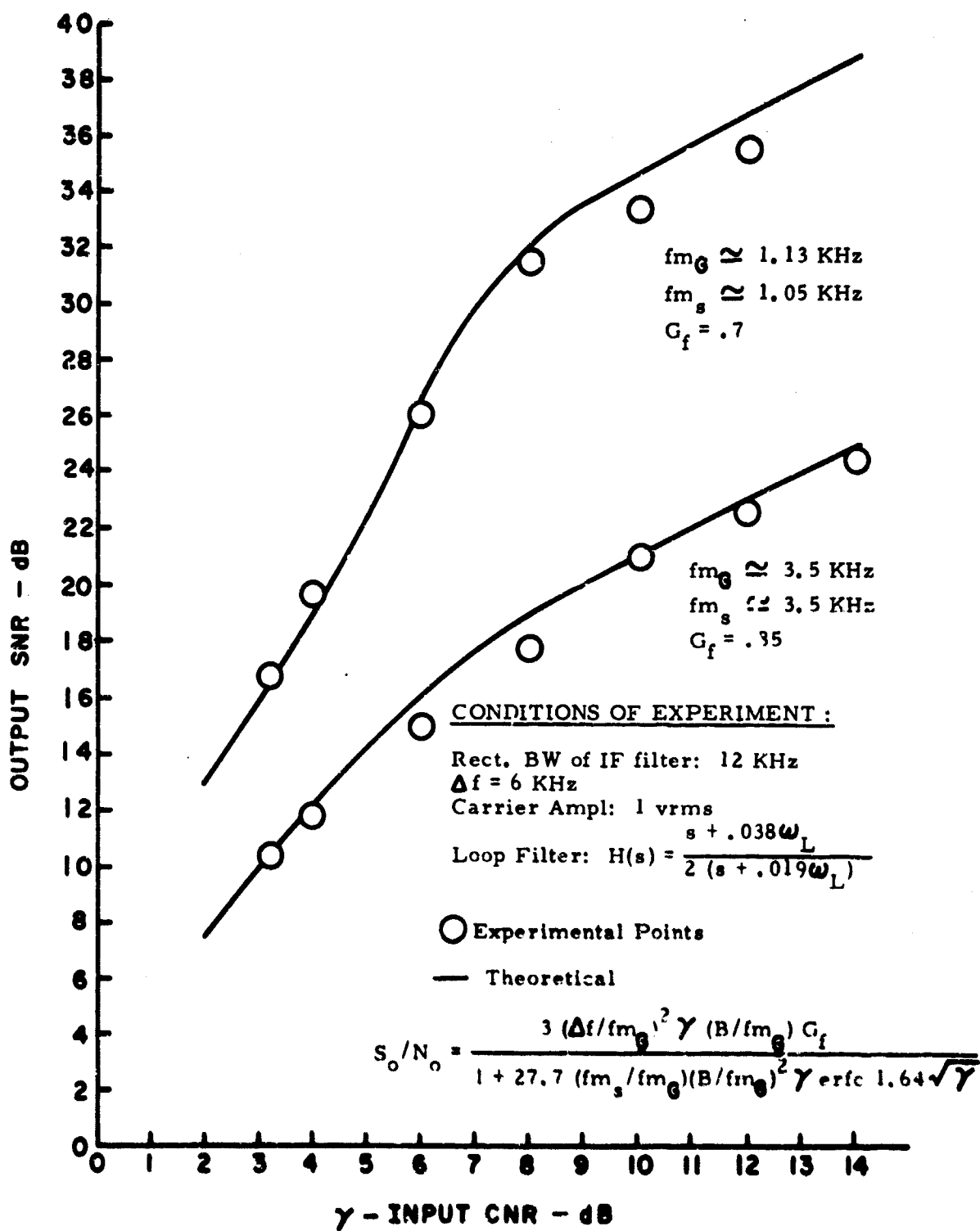


Fig. 4 Output SNR vs Input CNR for a Second-Order Phase-Locked Loop

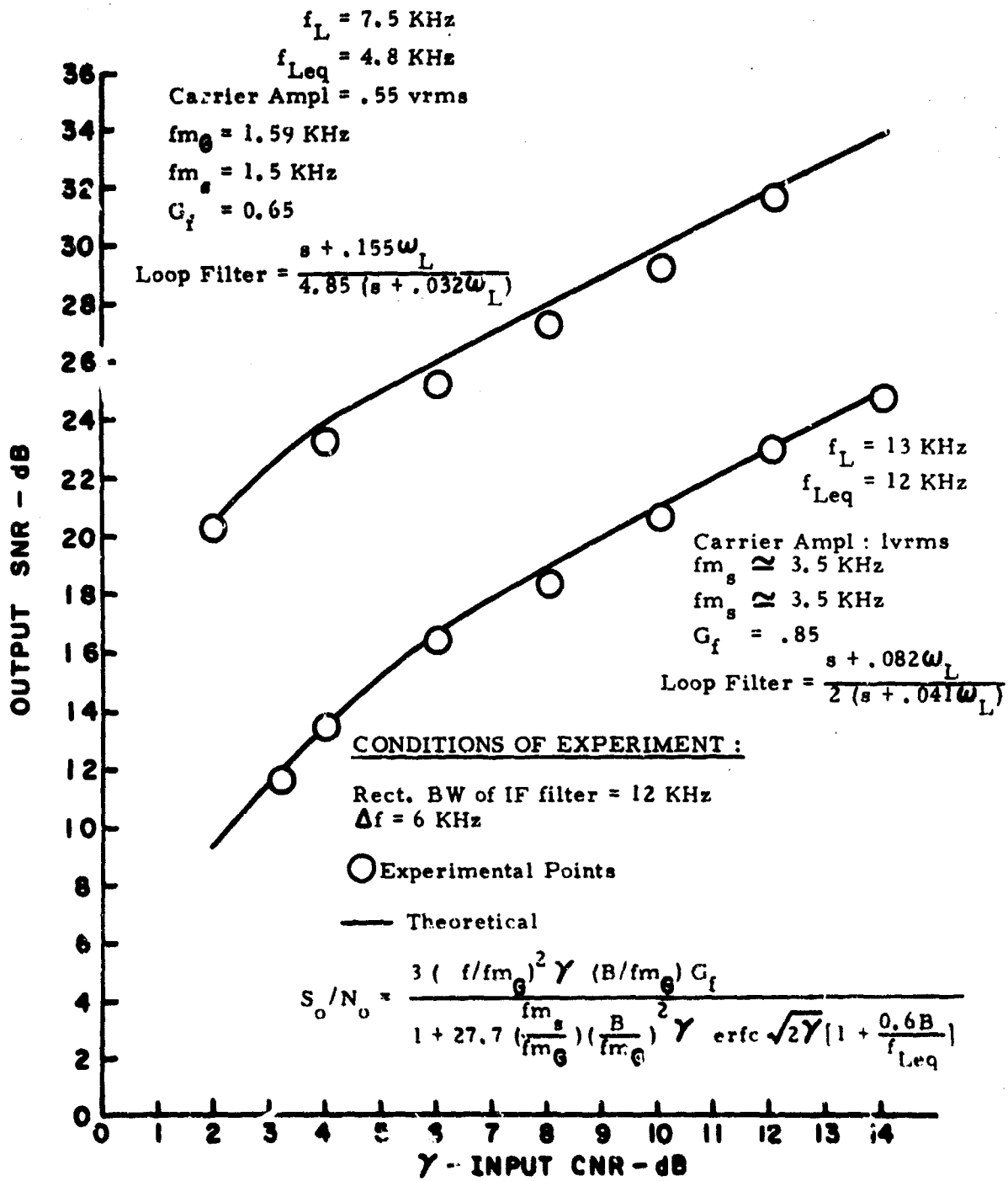


Fig. 5 Output SNR vs Input CNR for a Second-Order Phase-Locked Loop

REFERENCES

1. M. Schwartz, W. R. Bennett, and S. Stein, "Communication Systems and Techniques." (New York, McGraw-Hill, 1966).
2. D. T. Hess, "Cycle Slipping in a First-Order Phase-Locked Loop," IEEE Trans. on Communication Technology, Vol. COM-16, pp. 255-260, April, 1968.
3. B. Schwartz, "Cycle Slipping Events in Second-Order PLL," Master's Project Report, Polytechnic Institute of Brooklyn, June 1968.

## OPTIMIZING SECOND-ORDER PHASE-LOCKED LOOP (PLL) PERFORMANCE WITH MODULATION

D. T. Hess and R. J. Schulman

In this report, a purely experimental investigation into the behavior of the first and second-order PLL with modulation is described: Curves of output signal-to-noise ratio (SNR) vs. input carrier-to-noise ratio (CNR) for the PLL and limiter-discriminator were obtained by varying the numerous parameters of the system. This study culminates in the determination of a "rule of thumb" for choosing an optimum loop filter  $H(s) = \frac{\alpha}{\mu} \left( \frac{s + \mu}{s + \alpha} \right)$  and hold-in range (the maximum static frequency deviation of the input signal from the carrier frequency before the loop loses lock) for the second-order PLL when the modulating signal fills the entire IF filter bandwidth of the system (full-deviation signal).

## General Study

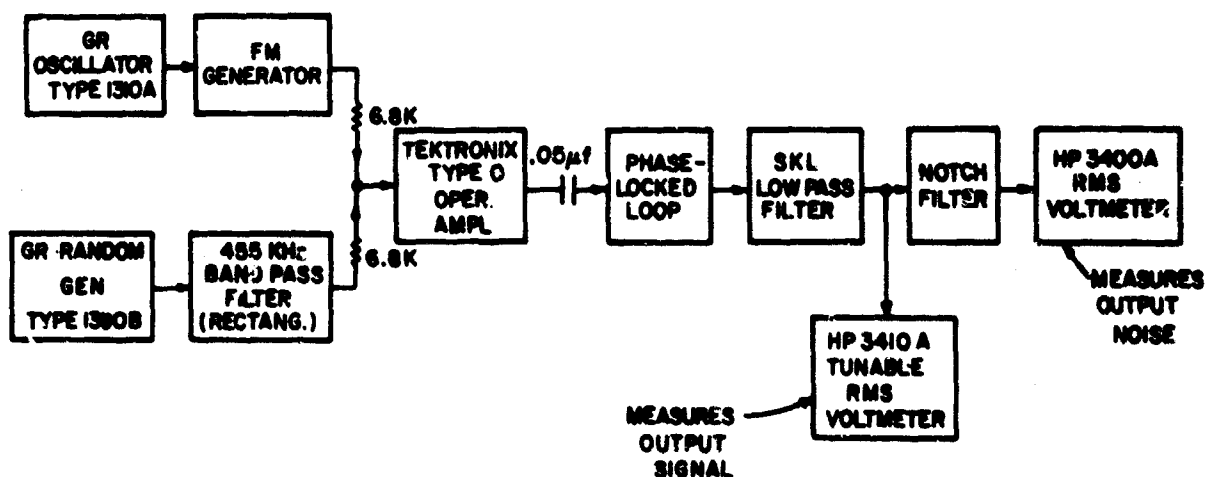


Fig. 1 System For Taking SNR Measurements (with modulation)

To make the SNR measurements with modulation, the system of Fig. 1 was used. The signal and noise were kept on simultaneously, while measuring the output value of either parameter. For the data taken for this report, a full-deviation signal was used, i. e., a signal with deviation  $\Delta f$  given by  $\Delta f = \beta B / (1 + \beta)$  where  $2B$  is the IF bandwidth and  $\beta$  is the modulation index. Besides the many curves obtained for the PLL, some data were taken for the limiter-discriminator to use for comparison. These data were taken by replacing the PLL by a 455kHz limiter and a GR discriminator (model 1142-A) in the system of Fig. 1.

Specifically the output SNR was measured, with the input CNR fixed at 6dB and  $\beta$  fixed at 2, as the hold in range  $f_L$ , the pole of the loop filter  $\alpha$ , and the zero of the loop filter  $\mu$  were independently varied. It was observed empirically that the output SNR

passed through a maximum as each of the parameters,  $f_L$ ,  $\alpha$ , and  $\mu$  were varied. Consequently by sequentially adjusting the parameters the optimum output SNR was obtained for  $\beta = 2$ . With the signal deviation  $\Delta f = 2$  kHz, with the modulating signal frequency  $f_m = 1$  kHz, and with a rectangular IF filter with bandwidth = 6 kHz the empirically determined optimum values were found to be

$$\alpha \approx 1.5 \text{ kHz}$$

$$f_L \approx 12.5 \text{ kHz}$$

$$\mu/\alpha \approx 6$$

$$\text{LOOP FILTER} = \frac{s + 5.6 \times 10^4}{6(s + 9.4 \times 10^3)}$$

$$f_L = 12.5 \text{ kHz}$$

$$\text{OUTPUT SNR} = \frac{\text{SIGNAL AT FULL DEVIATION}}{\text{NOISE AT GIVEN DEVIATION}}$$

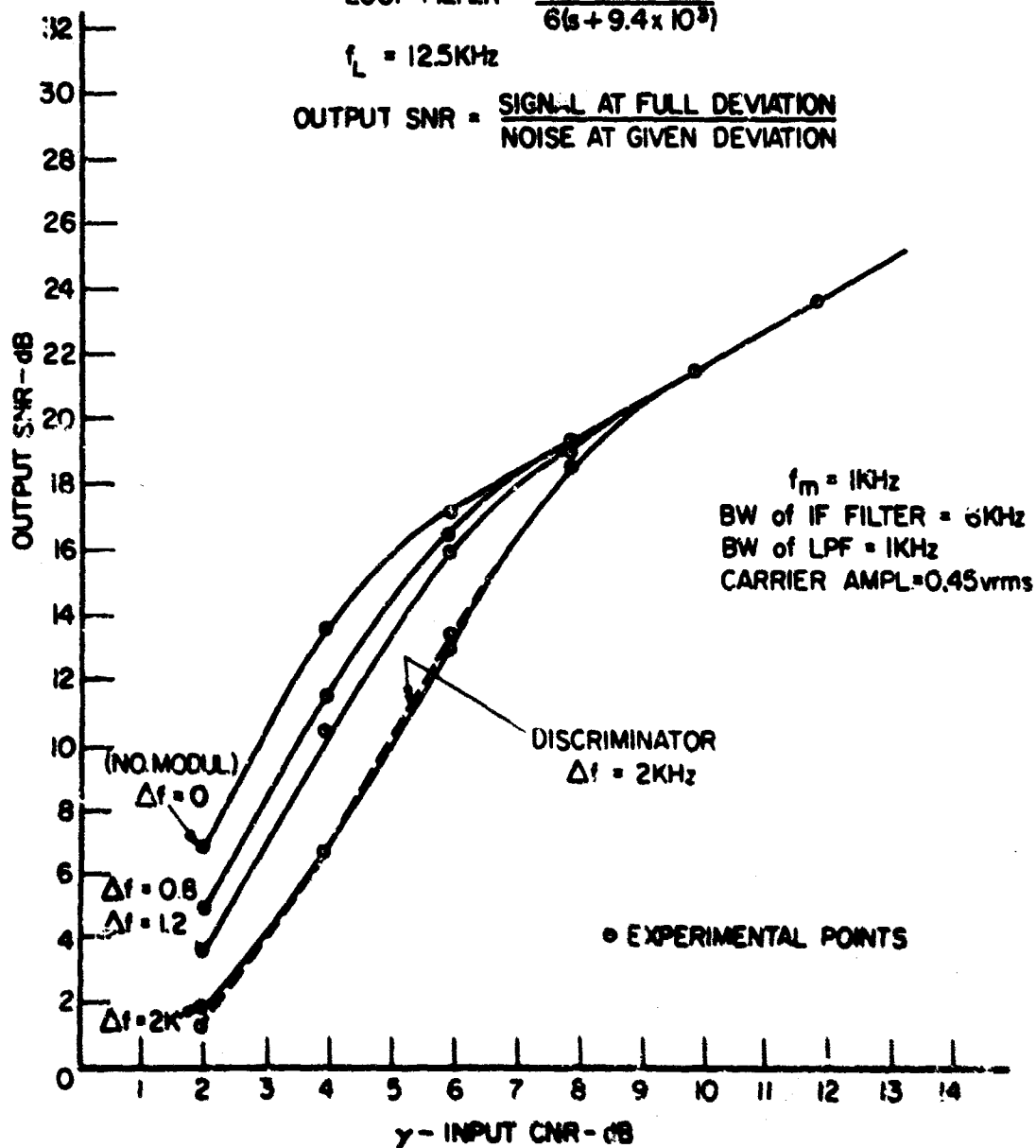


Fig. 2 Output SNR vs. Input CNR for a Second-Order Phase-Locked Loop



Figure 2 compares the optimum second order PLL with the optimum loop filter over the discriminator. It should be noted that with full deviation, little improvement in threshold is obtained with the PLL.

Using the above set of optimum parameters and the knowledge acquired from taking data presented in this report, one may set forth a "rule of thumb" for choosing an optimum hold-in range and second-order PLL for a full-deviation signal. The "rule of thumb" is as follows:

$$f_{L \text{ opt}} \approx 2 \times (\text{IF rectangular filter bandwidth})$$

$$\alpha_{\text{opt}} \approx 1.5 \times f_m$$

$$(\mu/\alpha)_{\text{opt}} \approx 6$$

To test this rule, experimental data were taken for two other cases ( $\beta = 5$  and  $\beta = 6$ ). The systems were set up using the above rule, and then, SNR's were measured for variations of the parameters, to show the PLL was indeed optimally adjusted. In both cases the rule proved to be correct.

#### Conclusion

A study has been made of the first and second-order PLL behavior, with modulation, as a function of various system parameters. A "rule of thumb" has been proposed for choosing the hold-in range, pole position, and zero-to-pole ratio, which would result in optimum performance of the second-order PLL when used with a full-deviation signal. This rule has been tested and shown to give satisfactory results; however even with the PLL optimized little SNR improvement over the discriminator was obtained.

National Aeronautics and Space Administration  
NgR 33-006-020

D. T. Hess and R. J. Schulman

#### OUTPUT SIGNAL-TO-NOISE RATIO OF AN FM DISCRIMINATOR WITH NON-IDEAL LIMITING

D. L. Schilling and J. Rafi

The effect of abrupt-limiting on the output of a frequency discriminator has been treated thoroughly by Middleton. This paper considers the case of smooth bandpass limiting both for the simple differentiator and for the balanced discriminator. The error function is used as a model for the smooth limiter. The ideality of the limiter is related in the quantity " $\mu$ " - the limiting hardness. The analysis reveals that for a balanced discriminator, the output signal-to-noise ratio can be made largely immune to changes in " $\mu$ ". However, for the unbalanced discriminator, the signal-to-noise is not only appreciably " $\mu$ " dependent, but also a function of carrier frequency.

I. The Unbalanced Discriminator

Noise Analysis:

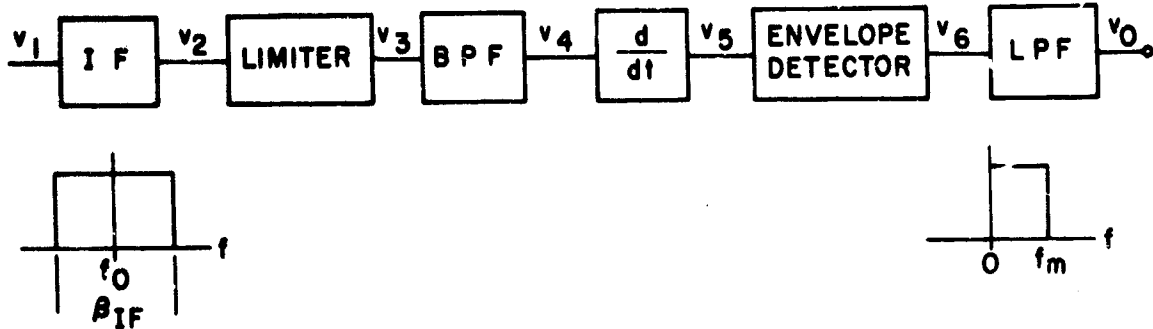


Fig. 1 The Unbalanced Limiter-Discriminator

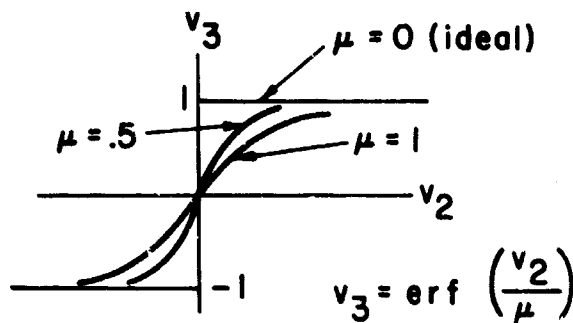


Fig. 2 A Smooth Limiter

An unbalanced discriminator is shown in Fig. 1. It consists of a limiter, differentiator and envelope detector. The smooth limiter is shown in Fig. 2.

The output signal-to-noise ratio of this device is

$$S_o/N_o = \frac{3(\beta + 1) \beta^2 (C/N)_i}{i + \frac{12 f_o^2 (\frac{\mu}{\lambda})^4}{f_m^2 [(\frac{\mu}{\lambda})^2 - 4]} + \frac{12 f_o^2 (\frac{\mu}{\lambda})^4 (4\beta + 3)}{2 f_m^2 (\beta + 1) (C/N)_i [(\frac{\mu}{\lambda})^2 - 4]^2} + \frac{(\frac{\mu}{\lambda})^4 (-2 f_m^3 + 4 B_{IF} f_m^2 - 3 B_{IF}^2 f_m + 2 B_{IF}^3)}{4 f_m^2 B_{IF} (C/N)_i [(\frac{\mu}{\lambda})^2 - 4]^2} \quad (1)$$

where  $\beta$  is the modulation index,  $f_m$  the maximum modulation frequency,  $B_{IF} = 2(\beta + 1)$

$f_m$ ,  $(\frac{C}{N})_i$ ; is the input SNR measured at the IF, and  $\mu/A$  is the relative hardness of the limiter (see Fig. 2).

## II. Balanced Discriminator

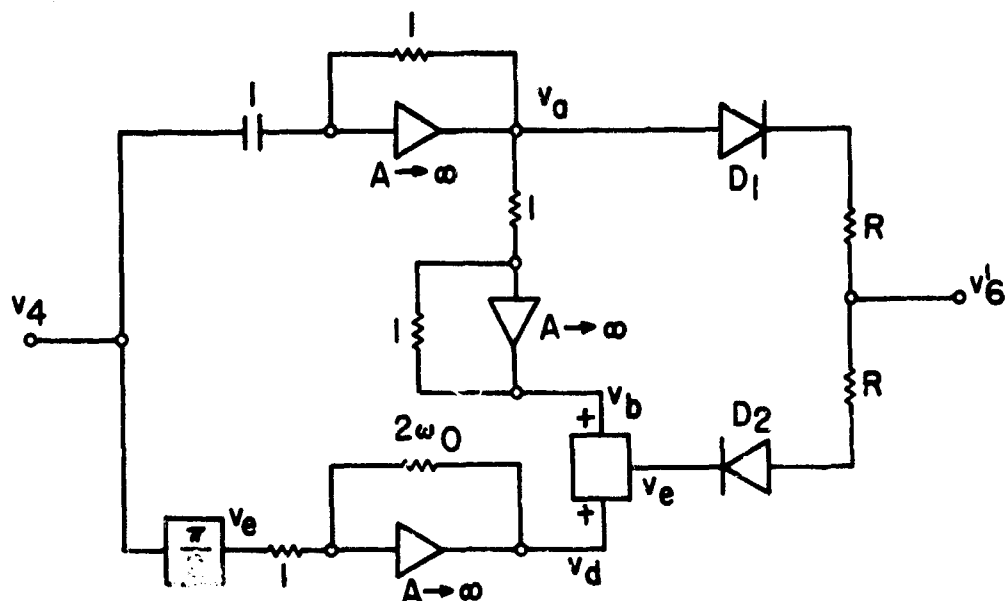


Fig. 3 A Balanced Discriminator

A model for the balanced discriminator is shown in Fig. 3. The output SNR of this device is

$$S'_o/N'_o = \frac{3(\beta + 1) \beta^4 (C/N)_i}{1 + \left(\frac{\mu}{A}\right)^4 \frac{(-2f_m^3 + 4B_{IF} f_m^2 - 3B_{IF}^2 f_m + 2B_{IF}^3)}{4f_m^2 B_{IF} (C/N)_i \left[\left(\frac{\mu}{A}\right)^2 - 4\right]^2}} \quad (2)$$

Conclusion:

Examination of Eqs. (1) and (2) reveals that the output signal-to-noise ratio is frequency dependent for the unbalanced discriminator and is frequency independent for the balanced discriminator.

Equations (1) and (2) were evaluated for some representative numbers

$$f_m = 953 \text{ Hz}$$

$$f_o = 100 \text{ KHz}$$

$$B_{IF} = 21 \text{ KHz}$$

$$(C/N)_i = 20 \text{ db}$$

$$\beta = 10$$

As  $\frac{\mu}{A}$  went from 0 to 1, the SNR for the unbalanced discriminator was degraded by 40db. However, the performance of the balanced discriminator was degraded by only 1db.

From this analysis, the simple differentiator is seen to be largely dependent on the quality of the limiter, whereas the balanced discriminator suppresses this effect.

National Aeronautics and Space Administration  
NgR 33-006-020

D. L. Schilling and J. Refi

### QUANTIZED SECOND ORDER FREQUENCY LOCKED LOOP

D. T. Hess and K. K. Clarke

Several previous papers have presented the basic concepts of the threshold extending FM receiver known as the Frequency Locked Loop (FLL). In this section several significant modifications to the basic FLL are reported. Specifically the modifications entail the optimization of the loop filter and the quantization of the amplitude channel. The paper presents intuitive arguments explaining the improvements expected with these modifications.

Finally, and most important, experimental data are presented. These data indicate that even with full deviation sinusoidal modulation, the FLL extends the FM noise threshold significantly over the discriminator. In addition, when used to demodulate binary signals transmitted by Frequency Shift Keying the FLL yields an output probability of error that is within 1.4dB of that achieved with a matched filter having the same input noise spectral density. The comparison with the matched filter was made with modulation indices in the vicinity of 2 and for error rates between  $10^{-5}$  and  $10^{-2}$ .

#### I. Introduction

In a previous paper the Frequency Locked Loop (FLL) FM Demodulator<sup>1</sup> is introduced and is shown to be capable of extending the FM noise threshold. This extension is achieved by using the envelope information of the incoming noise corrupted FM carrier to directly control the loop gain and in turn the bandwidth of a feedback loop through which the demodulated FM information is passed; thus if the envelope takes on a small value (relative to its average value) the information is passed through a very narrow bandwidth and effectively "held". Since the FM noise threshold is characterized by the occurrence of gross frequency disturbances or clicks<sup>2</sup>, and since, near threshold, these clicks are almost always accompanied by low envelope levels<sup>3</sup> on the incoming noise corrupted FM signal, the holding property of the FLL eliminates the majority of the clicks from its output and thus extends the noise threshold.

The first order analog FLL previously described has several shortcomings. First, the "holding" operation, which occurs far more frequently than the frequency clicks occur, introduces an additional output noise component plus a signal suppres-

sion effect, both of which detract from the possible threshold improvement. Secondly, envelope variations for input carrier to noise ratios above threshold cause the FLL to have an above threshold output signal to noise ratio slightly lower than the discriminator.

In this paper intuitive arguments are presented to show that these shortcomings may be partially overcome by quantizing the envelope information before applying it to the feedback loop and by utilizing a properly designed second order filter within the feedback loop. In addition, experimental data are presented which indicate that the intuitive approach to optimization is indeed valid.

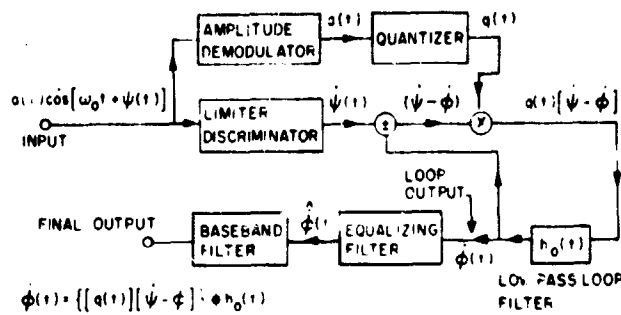


Fig. 1 Block Diagram of the Baseband Frequency Locked Loop

II. Envelope Quantization

The block diagram of the FLL with quantization is shown in Fig. 1. Here the input signal is assumed to be in the completely general form of a carrier centered at  $\omega_0$  modulated by an envelope  $a(t)$  and a phase  $\psi(t)$ . The envelope  $a(t)$  arises when the FM carrier is corrupted by additive narrowband noise centered at  $\omega_0$ , whereas  $\psi(t)$  consists of the desired phase modulation plus perturbations from the narrowband noise. The quantizer consists of a monostable multivibrator which reduces its output  $q(t)$  to zero for a fixed duration  $t_0$  every time the envelope  $a(t)$  drops below the level  $\epsilon A$ , where

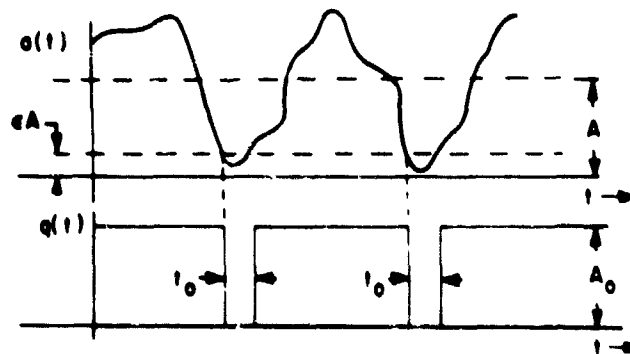


Fig. 2 Relationship Between the Input Amplitude,  $a(t)$  and the Quantizer Output,  $q(t)$

$A$  is the FM carrier amplitude. (With no noise present  $a(t) = A$ .) Figure 2 indicates the relationship between the quantizer output  $q(t)$  and  $a(t)$ .

If the output of the FLL is designated as  $\hat{\phi}(t)$  and the impulse response of the loop filter is given by  $h_o(t)$ , then the defining equation for the loop takes the form

$$\dot{\hat{\phi}}(t) = q(t) [\dot{\psi}(t) - \dot{\hat{\phi}}(t)] * h_o(t) \quad (1)$$

The advantage of quantization in the FLL is now apparent. If the input carrier to noise ratio is high,  $a(t)$  almost always remains above  $\epsilon A$  and  $q(t) = A_o$  (a constant). Thus  $\dot{\hat{\phi}}(t)$  is just a filtered form of  $\dot{\psi}(t)$ . If in addition, an equalizing filter is incorporated after the loop, as shown in Fig. 1, the filtering effect of the loop may be exactly compensated, and thus the equalized loop output  $\hat{\phi}(t)$  and the discriminator output  $\psi(t)$  are identical (within a scale factor) above threshold. Below threshold  $a(t)$  does indeed drop below  $\epsilon A$  during the occurrence of many clicks in  $\psi(t)$ , thereby opening the loop and completely decoupling  $\dot{\psi}(t)$  from the output.

The quantizer depends strongly on two parameters,  $\epsilon$  (the quantization level) and  $t_o$  (the holding time), for its correct operation. Both of these parameters have an optimum value which yields the best threshold improvement. Intuitively we observe that if  $\epsilon$  is very small, very few holds in the loop occur and thus very few clicks are removed at the loop output. On the other hand, if  $\epsilon$  is large the number of holds becomes large which permits almost all of the clicks to be removed; however, since the number of holds far exceeds the number of clicks ( $a(t)$  drops below  $\epsilon A$  many times when a click does not occur) noise induced by holding  $\dot{\psi}(t)$  exceeds the RMS value of the click noise removed. For some intermediate value of  $\epsilon$  a sufficient number of clicks are removed while the noise due to holding still remains sufficiently small such that an optimum is achieved. This optimum is found experimentally to correspond to  $\epsilon \approx 0.2$  and is reasonably broad.

It is interesting to observe the structure of the output noise as  $\epsilon$  is increased empirically from zero. Initially if operation of the FLL is below threshold, the output contains the same impulsive click noise as the discriminator. As  $\epsilon$  is increased a number of the clicks are removed or greatly reduced in area without much additional noise appearing. Finally, as  $\epsilon$  is increased still further, almost all of the clicks disappear and the "Gaussian like" holding noise begins to greatly increase. In effect, varying  $\epsilon$  provides a means of not only reducing the total RMS noise below threshold but also converting a click noise into "Gaussian like" noise. This conversion is highly desirable when video or digital information is transmitted via FM. Figure 3 shows the variation in the noise structure for several different values of  $\epsilon$ .

It is also apparent that if the holding time  $t_o$  is too small, the holding is not accomplished for the entire duration of the click in  $\dot{\psi}(t)$  and only a small portion of the

$\epsilon$	SNR in 1kHz band
0.0	24.5dB
0.1	28.0dB
0.2	31.0dB
0.3	31.8dB
0.4	30.5dB

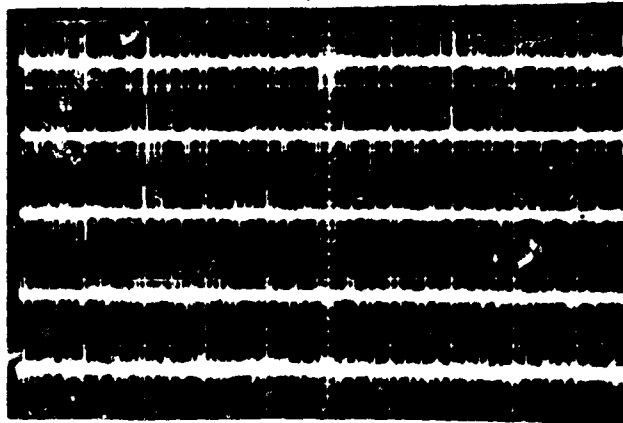


Fig. 3 Variation of Noise Structure with  $\epsilon$  and a Baseband FLL Input Carrier-to-Noise 6dB. Peak-to-Peak "Square" IF Bandwidth 33kHz.  $\Delta f = 15.5\text{kHz}$ ,  $f_c = 1\text{kHz}$ ,  $t_c = 25\mu\text{sec}$ , Modulation Notched Out by More than 50<sup>dB</sup>. Baseband Filter Widened to 3kHz to Show Individual clicks. 100mV/cm Vertical, 50ms/cm Horizontal.

click area is removed from the FLL output. On the other hand, if  $t_o$  is too large, the holding noise again begins to more than compensate for the click noise removed. Experimentally it has been found that the optimum  $t_o$  is approximately  $1/2 (BW_{\text{RMS}})$  where  $BW_{\text{RMS}}$  is the RMS noise bandwidth (in Hertz) of the input narrowband noise. Again this optimum appears experimentally to be rather broad such that a very precise setting of  $t_o$  is not required.

If one observes the FLL output for a fixed value of  $\epsilon$  as  $t_o$  is increased from zero, one notices first that many of the output clicks become reduced in area as a portion of the input click is removed. As  $t_o$  is increased further many of the input clicks disappear completely, and finally as  $t_o$  is increased still further a large amount of "Gaussian like" holding noise appears in the output. Since in general  $\epsilon$  and  $t_o$  are correlated, their optimum values must be obtained simultaneously. This is indeed how they were obtained empirically.

### III. Loop Filter Optimization

The choice of an optimum loop filter is based upon three basic considerations:

- 1) The filter must provide a good estimate of the signal component of  $\dot{\Phi}(t)$  (or  $\dot{\Theta}(t)$ ) during a hold, i. e., when  $q(t) = 0$ .
- 2) The filter must produce a well behaved transient when  $q(t)$  returns from 0 to  $A_o$ .
- 3) The filter must provide an absolutely stable closed loop response.

Clearly requirements 1 and 2 insure that the holding noise is minimized while requirement 3 is essential for any feedback system.

From requirement 1 it is apparent that the loop filter (whose impulse response is given by  $h_o(t)$ ) should have as many poles at the origin as possible. This is the case since each additional pole permits the filter output to estimate the desired output signal with one more degree of precision when the input is reduced to zero by  $q(t)$  dropping to zero. Specifically if  $q(t)$  drops to zero at  $t = t_1$  and  $h_o(t)$  contains  $n$  poles at the origin, for  $t_1 < t < t_1 + t_o$   $\dot{\phi}(t)$  is given by

$$\begin{aligned} \dot{\phi}(t) = & \dot{\phi}(t_1) + \ddot{\phi}(t_1)(t - t_1) + \frac{\dddot{\phi}(t_1)(t - t_1)^2}{2!} \\ & + \dots + \frac{\phi^{(n)}(t_1)(t - t_1)^{n-1}}{(n-1)!} ; t_1 < t < t_1 + t_o \end{aligned} \quad (2)$$

As  $n \rightarrow \infty$ ,  $\dot{\phi}(t)$  would be approximated exactly during a hold (equation 2 would become the Taylor series for  $\dot{\phi}(t)$  and no holding noise would exist. Requirement 3, however, limits the number of poles to 2, since 3 poles at the origin in a feedback loop would produce at best conditional instability. With two poles at the origin for  $h_o(t)$ ,  $\dot{\phi}(t)$  is approximated by its value and slope at  $t = t_o$  during a hold as shown in Fig. 4. Clearly

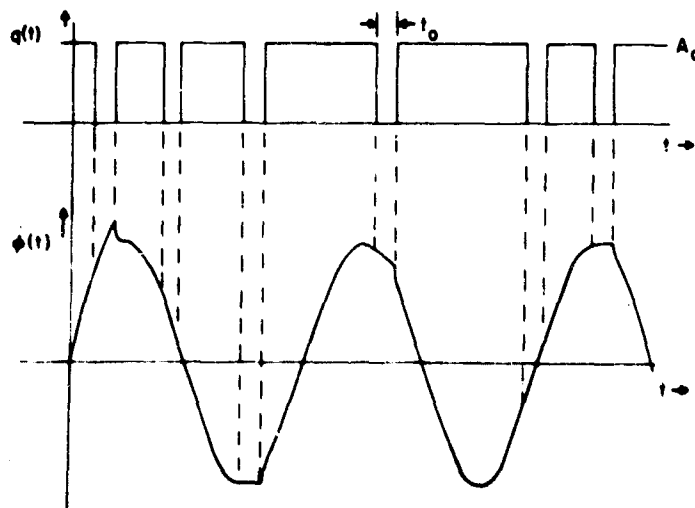


Fig. 4 Second Order Holding

a much poorer approximation to  $\dot{\phi}(t)$  during a hold would result if  $h_o(t)$  contained a single pole at the origin; specifically  $\dot{\phi}(t)$  would remain constant during the hold thereby increasing the holding noise.

Requirement 3 also specifies the zeros of  $h_o(t)$ . In order to keep the closed loop poles from approaching too close to the imaginary axis,  $h_o(t)$  must have a negative real axis zero. Consequently, the pole zero pattern for  $h_o(t)$  must take a form similar to that shown in Fig. 5. The figure also indicates the locus of the poles of the closed loop FLL, with no holding, as the loop gain (or equivalently  $A_o$ ) is increased. In order



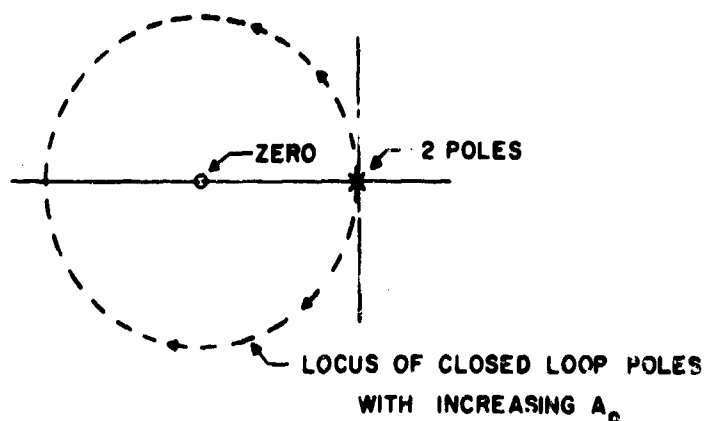


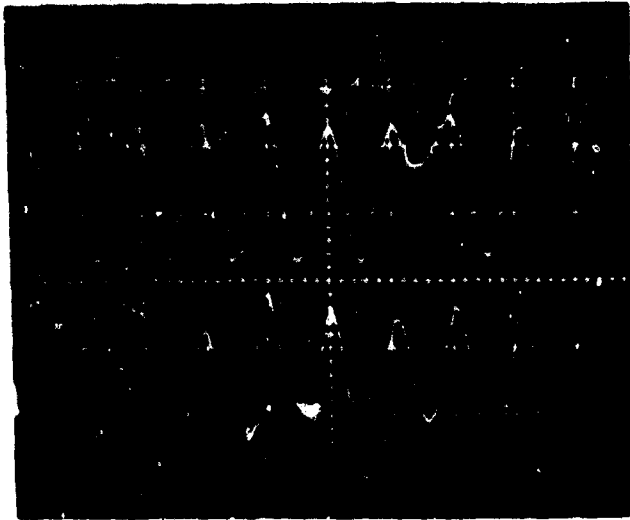
Fig. 5 Pole-Zero Pattern for  $h_0(t)$

to meet requirement 2, a sufficiently large value of  $A_0$  must be chosen to keep the imaginary part of the closed loop poles above the passband of the final baseband filter. At the end of each hold a transient results which has a strong frequency component at a value equal to the distance of the poles from the real axis. If this frequency component is not passed by the baseband filter, the basic holding noise is due to the inexact estimate of  $\dot{\phi}(t)$  during a hold.

On the other hand,  $A_0$  should not be chosen any larger than that value which just keeps the imaginary part of the closed loop poles above the baseband bandwidth. A larger value of  $A_0$  would increase the closed loop bandwidth of the FLL and thereby permit a larger noise component in  $\dot{\phi}(t)$ . Such an additional noise component is highly undesirable since when a hold occurs, the additional noise plus the desired signal component of  $\dot{\phi}(t)$  is estimated, and the output noise is greatly enhanced. This is particularly true of the high frequency noise, which when held generates low frequency noise components which reach the output of the baseband filter. Consequently, the closed loop poles should be placed just slightly above the passband at the baseband filter and the equalization filter should be designed to exactly compensate for the closed loop poles over the entire baseband.

In the FLL which has been constructed, the imaginary part of the closed loop poles is 1.55 kHz, whereas the baseband filter has a -3dB bandwidth of 1 kHz and falls off at 24 dB per octave in the stop band. In addition, the zero of  $h_0(t)$  is at 6.7 kHz. The equalization filter has a pair of complex conjugate zeros which lie at the same position as the closed loop poles.

A subsequent section of this report presents a theoretical derivation of SNR vs. CNR curves with  $\epsilon$  as a parameter. Yet another section presents a comparison of a theoretically derived expression for probability of error in digital FSK transmission with measured results. At this point we present a quick summary of experimental data to provide a framework for these subsequent sections.



ERROR COUNTER OUTPUT

DISCRIMINATOR

FLL



ERROR COUNTER OUTPUT

DISCRIMINATOR

FLL

IF = 6 kHz TOTAL - "SQUARE"

$\Delta f = 2$  kHz PEAK

$f_m = 1$  kHz

BASEBAND LOW PASS FILTER = 1.0 kHz (-3db) 24db/OCTAVE

$T_{HOLD} = 85 \mu\text{SEC.}$   $\epsilon = 0.3$ , RF DELAY =  $10 \mu\text{SEC.}$

Fig. 6 Digital Errors in FSK for a Discriminator and a Frequency Locked Loop

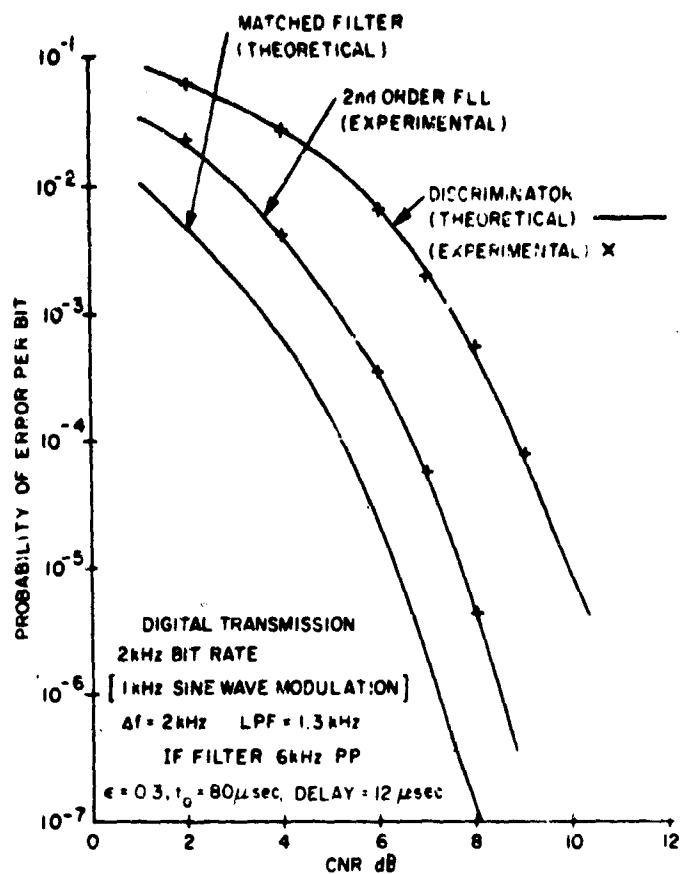


Fig. 7 Probability of Error vs. Carrier to Noise Ratio

#### IV. Experimental Results

Experimental results are shown for both the case of binary frequency shift keying (FSK) and for the case of sinusoidal analog modulation.

Figures 6 and 7 show comparative results for the detection of errors in a  $\beta = 2$ , noisy binary FSK signal detected both by a discriminator and by a discriminator plus a base band frequency locked loop.

Figure 7 plots curves of probability of error vs. the input carrier-to-noise ratio (CNR) in dB. These curves are for a discriminator, for a FLL circuit and for the theoretical matched filter. The theoretical curve for the discriminator was derived by Schilling, et al.<sup>4</sup> At a CNR of 8dB the error rate from the FLL is down by a factor of more than 100 from the discriminator case. From another viewpoint, if the error rate is held constant at  $1/10^5$  bits then the input CNR required by the FLL is 2.2dB less than that required by the discriminator and only 1.4dB more than that required by the matched filter.

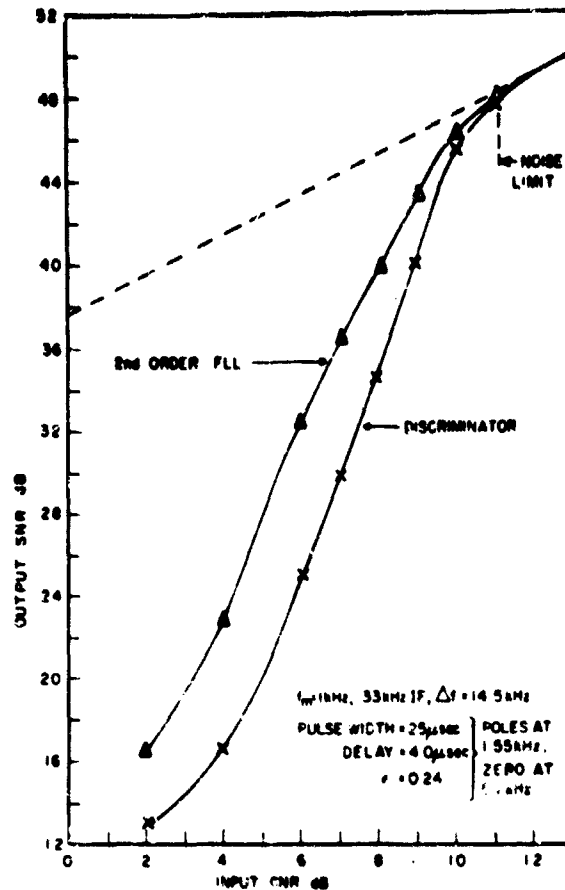


Fig. 8 Output SNR vs. Input CNR for 2nd Order FLL and for a Discriminator with Modulation

Figure 8 plots comparative curves of the output signal-to-noise ratio (SNR) in dB vs. the input CNR for the  $\beta = 14.5$  case. These curves are actual measured curves with full sinusoidal deviation; that is, with a peak deviation of 14.5 kHz in a square IF of peak-to-peak bandwidth of 33 kHz. One should note that for an input CNR of 6dB the FLL has an output SNR that is 7.3dB above the discriminator. Since Fig. 3 is for a CNR of 6dB through the same IF filter ( $\Delta f$  in Fig. 3 is 15.5 kHz while  $\Delta f$  is 14.5 kHz in Fig. 8) one can see from Fig. 3 that not only is the noise 7.3dB less at the FLL output but the noise structure is both somewhat different and, through the control of  $\beta$  is adjustable to best suit a particular system.

#### V. Conclusion

The quantized, second order frequency locked loop has been shown to offer substantial advantages over an ordinary discriminator both in the detection of FSK and in obtaining higher SNR's in the analog modulation case.

National Aeronautics and Space Administration  
NgR 33-006-020

D. T. Hess and K. K. Clarke

## REFERENCES

1. K. K. Clarke and D. T. Hess, "Frequency Locked Loop FM Demodulator," *IEEE Trans. on Comm. Tech.*, Vol. Com-15, (August 1967), pp. 518-524.
2. S. O. Rice, "Noise in FM Receivers," *Time Series Analysis*, M. Rosenblatt, E. (New York: Wiley, 1963), Chapter 25.
3. L. Calandrino and G. Immovilli, "Coincidence of Pulses in Amplitude and Frequency Deviations," *Alta Frequenza, English Issue No. 3*, Vol. 36, (Aug. 1967).
4. D. L. Schilling and E. Hoffman, "Demodulation of Digital Signals Using an FM Discriminator," *Proc. of the National Electronics Conference*, Vol. XXII, (1966), pp. 369-374.

## FM THRESHOLD EXTENSION PERFORMANCE OF THE QUANTIZED FREQUENCY LOCKED LOOP

N. Unkauf, K. K. Clarke, and D. T. Hess

## 1. Introduction

The noise and signal output of the FM discriminator in the threshold region,  $\dot{\psi}(t)$ , may be represented as

$$\dot{\psi}(t) = e_m(t) + n_g(t) + n_c(t) \quad (1)$$

where  $e_m(t)$  is the desired modulation signal;  $n_g(t)$  is the gaussian noise; and  $n_c(t)$  is the noise created by clicks<sup>1</sup>. The noise and signal output of the Quantized Frequency Locked Loop (QFLL) in the threshold region,  $\dot{\phi}(t)$ , is:

$$\dot{\phi}(t) = e_m(t) + n_g(t) + n_c(t, \epsilon) + n_h(t, \epsilon) \quad (2)$$

where  $e_m(t)$  and  $n_g(t)$  are the same as for the FM discriminator;  $n_c(t, \epsilon)$  is the noise due to clicks not recognized and suppressed by the QFLL; and  $n_h(t, \epsilon)$  is due to the signal and Gaussian noise distortion caused by holds (including the "false" holds intended for click suppression)<sup>2</sup>. To the extent that  $n_c(t, \epsilon) + n_h(t, \epsilon)$  for the QFLL are less than  $n_c(t)$  for the FM discriminator, an improvement in output signal to noise ratio will result.

To illustrate the signal to noise ratio improvement obtainable with the second order, baseband version, QFLL, the theoretical and experimental results of Unkauf<sup>3</sup> are presented. In this derivation it is assumed that the loop filter has the response:

$$H(s) = \frac{G(s+a)}{s^2} \quad (3)$$

and that the (pre-equalization) closed loop transfer function,  $T(s)$ , is given by:

$$\frac{G}{a} \frac{(s+a)}{s^2 + c_s + \dots} \quad (4)$$

## 2. Calculation of Signal to Noise Ratio

Consider an FM system with rectangular IF filter of total bandwidth,  $B$ , such that  $B = 2(\beta + 1)f_m$ , where  $f_m$  is the highest modulating frequency,  $\beta = \frac{\Delta\omega}{\omega_m} = \frac{\Delta f}{f_m}$  is the modulation index, and  $\Delta f$  is the peak frequency deviation of the FM carrier. Consider also maximum deviation, maximum frequency modulation of the form:

$$e_m(t) = \Delta\omega \cos \omega_m t \quad (5)$$

For the system parameters given and a rectangular output low-pass filter of cut-off frequency  $f_m$ , the QFLL output noise power has been calculated by Unkauf,

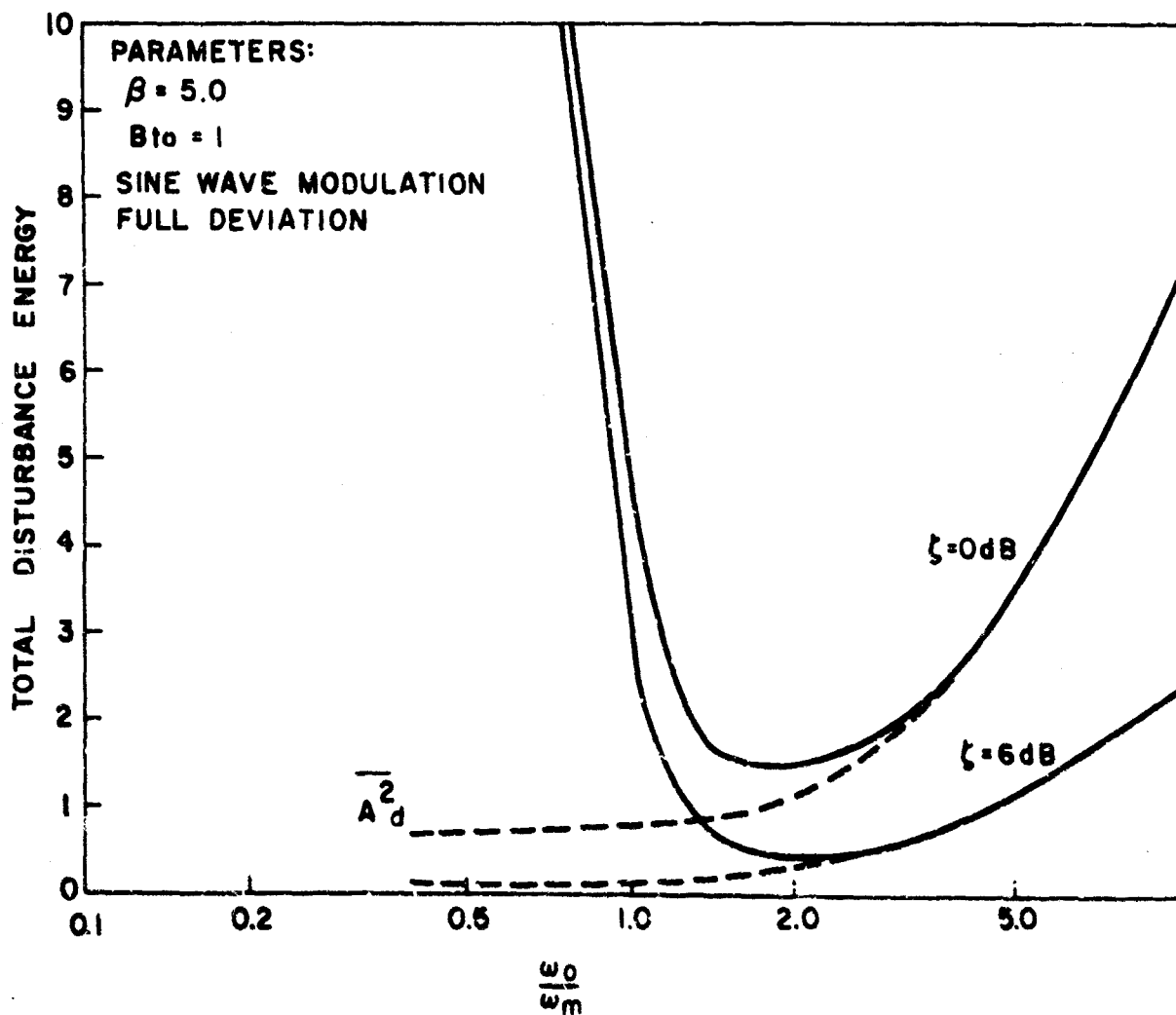


FIG. 1 Second Order FLL Disturbance Energy Versus  $\omega_0 / \omega_m$  with  $\zeta$  as a Parameter

The power corresponding to  $n_g(t)$ ,  $N_g$ , is:

$$N_g = \frac{4\pi^2 f_m^2 \delta}{3\rho} \quad (6)$$

where  $\rho$  is the input carrier to noise ratio and  $\delta$  is the modulation induced, noise reduction factor;  $\delta \approx 1$  for the system considered and large  $\beta$ . The power corresponding to  $n_c(t, \epsilon)$ ,  $N_c$ , is:

$$N_c = 8\pi^2 f_m n_c(\epsilon, \rho) \quad (7)$$

where  $n_c(\epsilon, \rho)$  is the expected number of clicks per second in the FM discriminator output which are not recognized by the QFLL as given in the Appendix. The noise power corresponding to  $n_h(t, \epsilon)$ ,  $N_h$ , is:

$$N_h = \mu^2 8\pi^2 f_m [n_c(o, \rho) - n_c(\epsilon, \rho)] + 2\sigma_D^2 f_m \quad (8)$$

where  $(1 - \mu)$  is the average percentage of click area suppressed by a hold;  $\sigma_D^2$  is the mean-square disturbance created by the holding mechanism on the discriminator gaussian noise and signal components; and  $n_h(\epsilon, \rho)$  is the expected number of holding events per second. These constants are given in the Appendix.

$N_h$  is plotted in Fig. 1 for small  $\mu$ ,  $\beta = 5$ , and  $Ht_o = 1$  (where  $t_o$  is the length of the holding interval).  $N_h$  displays a pronounced minimum in the region  $1.5 < (\frac{\omega_o}{\omega_m}) < 3$  and hence specifies the second order QFLL loop filter design, Eqs. (3) and (4).

Since the other QFLL noise terms are independent of  $\omega_o$ , the QFLL also displays a maximum output signal to noise ratio in the region  $\frac{\omega_o}{\omega_m} \approx 2$ . The position of the loop zero is not critical so long as it is sufficiently large.

The signal power at the QFLL output,  $S_o$ , is:

$$S_o = \frac{\Delta\omega^2}{2} = \frac{\beta^2 \omega_m^2}{2} \quad (9)$$

and the total QFLL output signal to noise ratio  $S_o/N_o$ , is:

$$\frac{S_o}{N_o} = \frac{S_o}{N_g + N_c + N_h} \quad (10)$$

This expression for output signal to noise ratio is plotted in Fig. 2 for a modulation index of 5 with  $r$  (the click detection parameter) as a parameter. Note that the theoretical results are really only valid for  $\rho \geq 4$  dB due to the neglect of discriminator signal suppression and the initial conditions for validity of the noise model. Similar curves for modulation indices of 2 and 15.5 are contained in Ref. 3.

The operation of the second order QFLL is clear from Fig. 2. As  $r$  increases

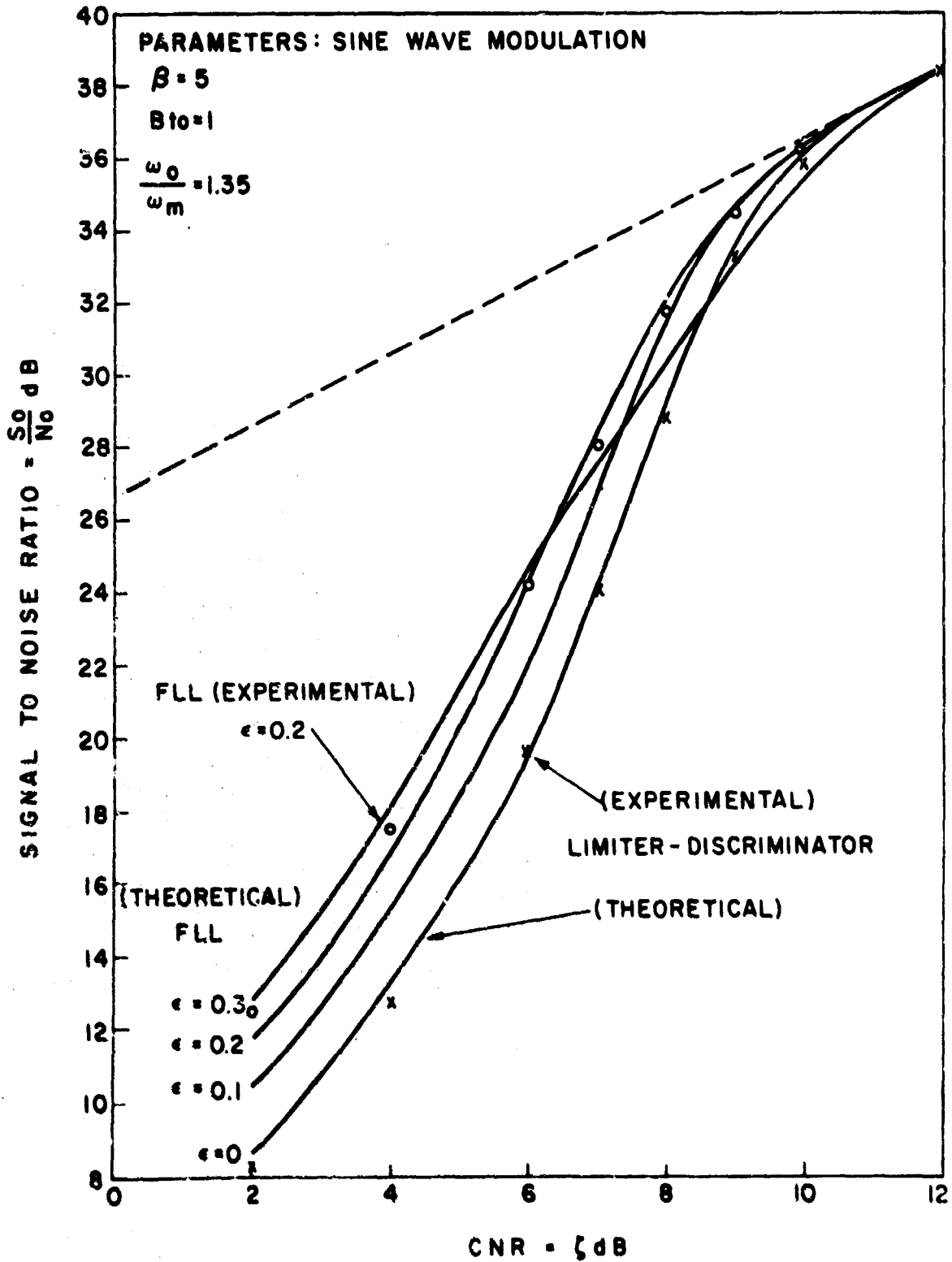


Fig. 2 Threshold Extension Performance of Second Order Frequency Locked Loop



from zero, the average number of clicks suppressed by the QFLL rapidly increases and the QFLL click noise decreases. Also, the number of holding events (attempted click suppression events) increases rapidly with  $\epsilon$  and the noise due to holding increases. Thus, the QFLL output signal to noise ratio first increases with click noise reduction and later decreases again due to holding noise production as  $\epsilon$  is increased. The optimum value of  $\epsilon$  for best overall signal to noise ratio improvement is approximately 0.2 which is experimentally verified. In a future paper, this trade-off in the nature of the QFLL output noise will be shown to be of great value in the demodulation of digital FM signals.

The overall threshold extension obtainable (for all modulating frequencies) with the QFLL is on the order of 1.5 dB as indicated by the results of Fig. 2. This result agrees well with the work of Malone<sup>4</sup> who simulated the case of a linear interpolation during a clock detection and erasure event on the digital computer. It also agrees in the limit with the work of Calandrino and Immovilli<sup>5</sup> who considered the open-loop problem of detecting and processing the discriminator clicks to achieve threshold extension.

Unkauf showed that the threshold extension of the QFLL improves with increased carrier frequency deviation and modulating frequency. Hence, the spectrum of the modulation employed with the QFLL system may be heavily pre-emphasized to yield still further signal to noise ratio improvement on final de-emphasis filtering of the QFLL output.

As a further comparison of the second order QFLL, Fig. 3 compares this circuit with a second order Phase Locked Loop (PLL) that was optimized for the condition of maximum system carrier frequency deviation. This comparison was made for the  $\beta = 5$  case under identical experimental conditions.

The PLL curves are shown dotted. For the no modulation case the PLL shows a maximum improvement of 1.5 dB at an input CNR of 7-8 dB. With the peak allowable sinewave deviation the PLL is not experimentally distinguishable from the ordinary discriminator. From 2-7 dB input CNR the PLL shows an improvement of 4 dB or more over the ordinary discriminator. Similar results have been obtained for betas of 2 and 15, 5.

### 3. Appendix

The following constants and functions have been computed by Unkauf<sup>3</sup> for the conditions indicated in this paper.

The expected number of clicks per second at the QFLL output,  $n_c(\epsilon, \rho)$ , is:

$$n_c(\epsilon, \rho) \cong 2 \frac{\sqrt{2} a}{\pi} e^{-\rho(1+\epsilon)^2} + \frac{2\gamma e^{-\rho(1+\epsilon)^2}}{2\pi(1+\epsilon)\sqrt{4\pi\rho}} e^{-a\rho(1+\epsilon)} I_0(a\rho(1+\epsilon)) \quad (A-1)$$

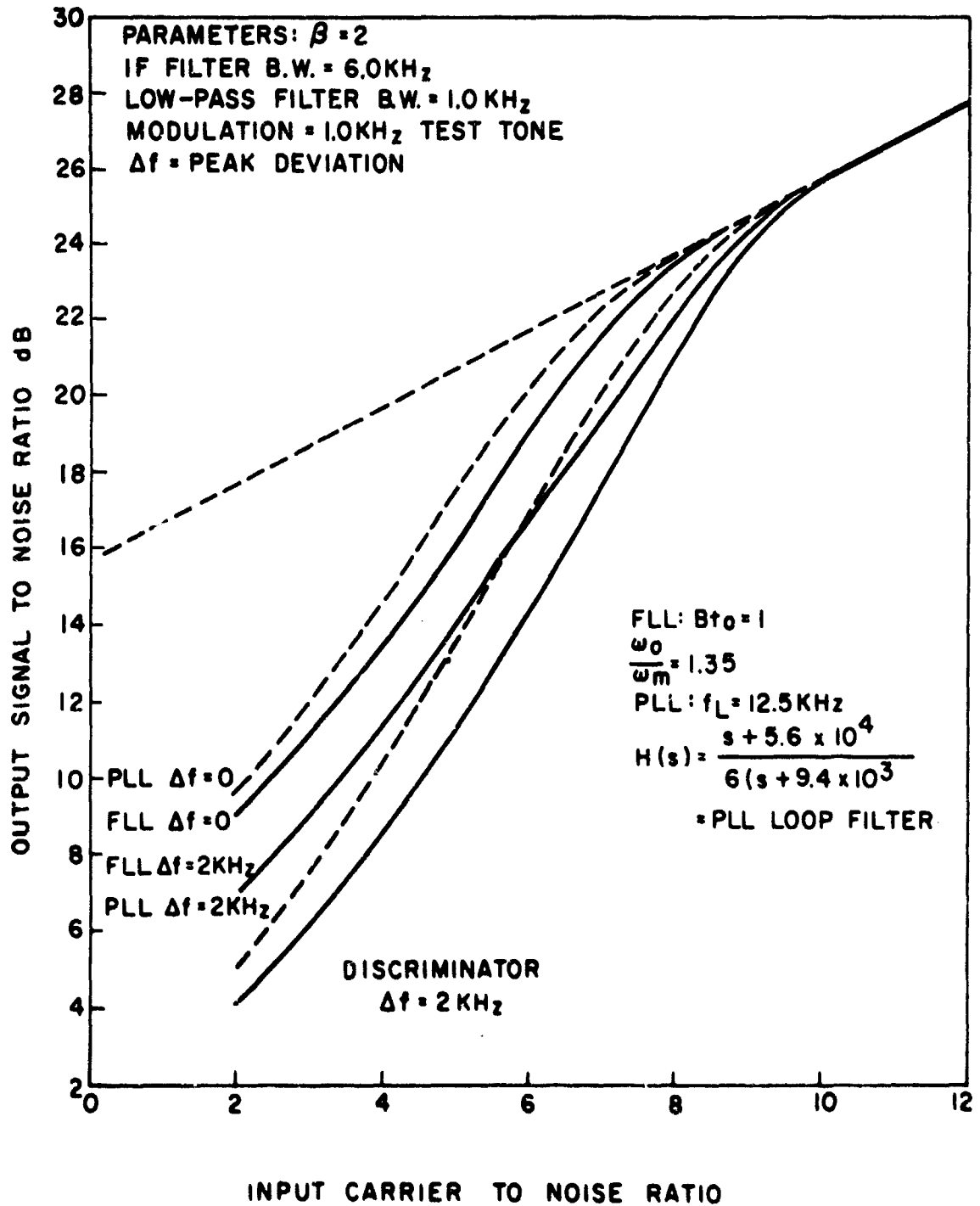


Fig. 3 Signal to Noise Ratio Comparison of Second Order Quantized FLL and Second Order PLL

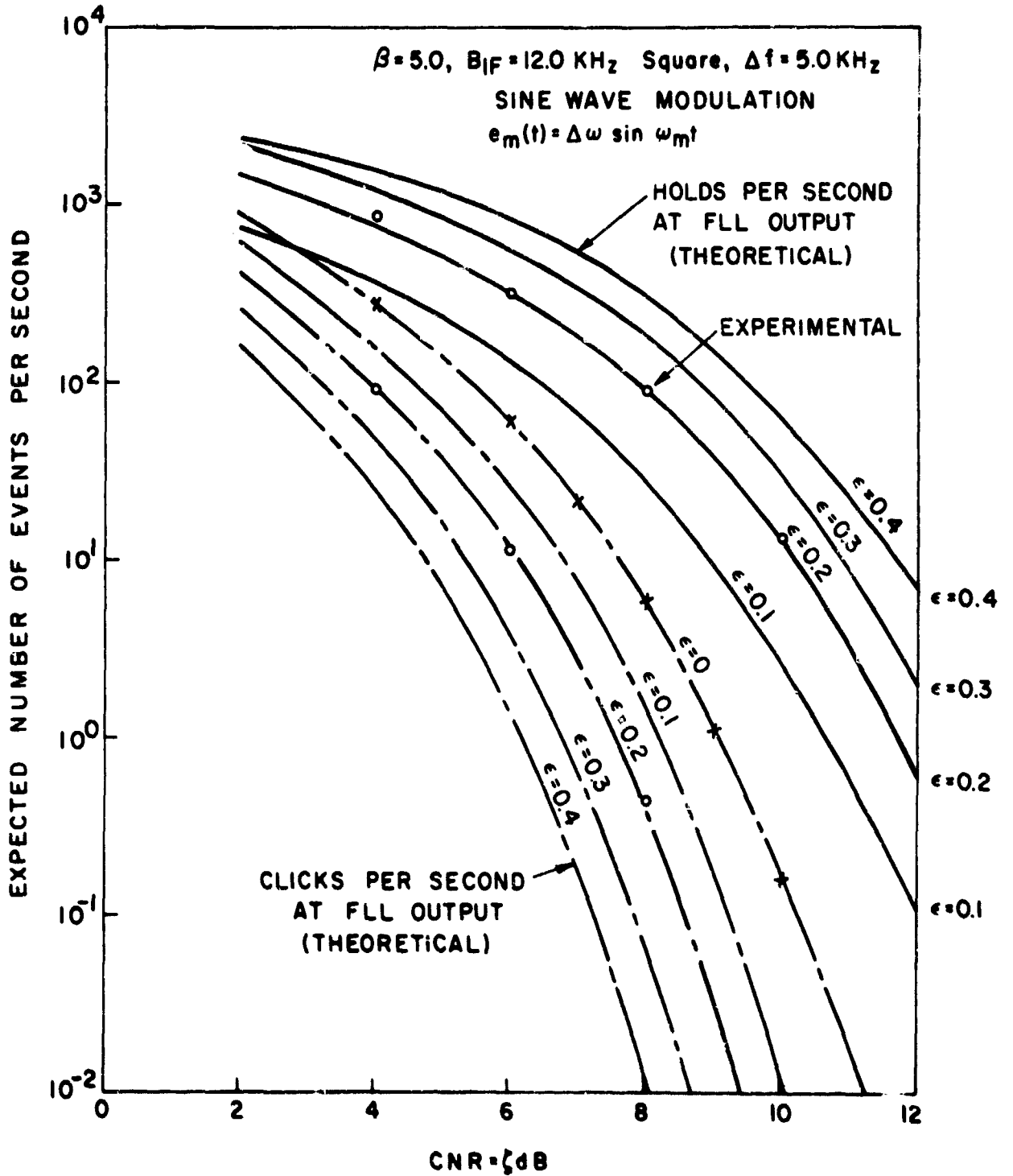


Fig. 4 Expected Number of Clicks and Holds at Quantized FLL Output Versus  $\zeta$  and  $\epsilon$

where  $\gamma$  is the radius of gyration of the IF filter and

$$a = \frac{\overline{e_m^2(t)}}{\gamma^2} = \frac{\Delta\omega^2}{2\gamma^2}$$

The expected number of holds per second,  $n_h(\epsilon, \rho)$ , is:

$$n_h(\epsilon, \rho) = \int_0^{\gamma} H(a^2) p_a^2(a^2) da^2 \quad (A-2)$$

where  $p_a^2(a^2)$  is the probability density of  $a^2$  and

$$H(a^2) = \frac{\epsilon\gamma}{\sqrt{\pi}} e^{-\rho(1-\epsilon^2)} \left[ e^{-x} I_0(x) \right] \left\{ e^{-y} I_0(y) + 2 \sum_{n=1}^{\infty} \frac{I_{2n}(x)}{I_0(x)} I_n(y) e^{-y} \right. \\ \left. + \frac{a^2}{e} \sum_{n=1}^{\infty} \frac{I_{2n-1}(x)}{I_0(x)} \left[ I_n(y) + I_n(y) \right] e^{-y} \right\} \quad (A-3)$$

where

$$a^2 = \frac{e_m^2(t)}{\gamma^2} \text{ and } x = 2\epsilon\rho \text{ and } y = \frac{a^2\rho}{2}$$

These results are plotted in Fig. 4 for the full deviation sine wave modulation assumed.

The expected value of  $\mu$  is determined experimentally:

$$\mu \cong \operatorname{erfc} \left( 0.51 \left[ 1 + \frac{|e_m(t)|}{\sqrt{3} \gamma} \right] \right) \quad (A-4)$$

And the mean-square holding disturbance,  $\sigma_D^2$ , is approximated by:

$$\sigma_D^2 \cong \frac{6}{2\pi} \int_{-\infty}^{\infty} \frac{d\omega s(\omega)}{\omega^2} \left\{ 1 - 4\omega^2/\omega_0^2 + \frac{t_0^4 \omega^4}{4} + \frac{2\omega^4}{\omega_0^4} + \frac{t_0^2 \omega^4}{\omega_0^2} + 2\omega^2 t_0^2 \right. \\ \left. + [\cos \omega t_0] \left( \frac{2\omega^4}{\omega_0^4} - \frac{\omega^4 t_0^2}{\omega_0^2} - \omega^2 t_0^2 + \frac{4\omega^2}{\omega_0^2} - 1 \right) \right. \\ \left. - [\sin \omega t_0] \left( \omega t_0 - \frac{2\omega^3 t_0^2}{\omega_0^2} \right) \right\} \quad (A-5)$$

where

$$s(\omega) \cong \frac{\omega^4}{2rB} \frac{\omega^2}{\omega^4 + (4e^2 - 2\omega_c^2)\omega^2 + \omega_0^4}$$

## REFERENCES

1. S. O. Rice, "Noise in FM Receivers," Time Series Analysis, M. Rosenblatt, Ed. (New York: Wiley, 1963). Chapter 25.
2. K. K. Clarke and D. T. Hess, "Quantized Second Order Frequency Locked Loop," IEEE Prof. Group in Aerospace and Electronic Systems, Eascon 1968 Convention Record, pp. 193-198.
3. M. G. Unkauf, "Quantized Frequency Locked Loop," Ph. D. Dissertation, Polytechnic Institute of Brooklyn, June 1969.
4. M. J. Malone, "FM Threshold Extension without Feedback", IEEE Proceedings, Vol. 56, No. 2, pp. 200-201.
5. L. Calandrino and G. Immovilli, "On the Performance of Amplitude-Phase Correlation FM Demodulators," Alta Frequenza, English Issue No. 2, Vol. 27.
6. R. Schulman, "A Study of the Behavior of the Phase Locked Loop," M. S. Report Project, P. I. B., June 1969.

## PROBABILITY OF ERROR ANALYSIS FOR THE FLL DIGITAL DEMODULATOR

M. Unkauf, K. K. Clarke, and D. T. Hess

Schilling and Hoffman<sup>1</sup> showed that the errors incurred in the discriminator demodulation of binary FM signals corrupted by noise could be treated as errors due to clicks and errors due to Gaussian noise. Thus, the probability of error in demodulation,  $P_e$ , is:

$$P_e = P_{eg} + P_{ec} \quad (1)$$

where  $P_{eg}$  is the probability of error due to the Gaussian noise and  $P_{ec}$  is the probability of error due to click noise. Since the FLL suppresses clicks, it can reduce the errors due to clicks. However, as seen in the previous section, the FLL introduces an extra holding noise which may introduce errors. Thus the probability of error for the FLL is

$$P_e = P_{eg} + P_{ec}(\epsilon) + P_{eh}(\epsilon) \quad (2)$$

where  $P_{ec}(\epsilon)$  is the probability of error caused by clicks which were not recognized by the FLL and  $P_{eh}(\epsilon)$  is the probability of error caused by the holding noise due to "false" holds.

Consider a binary FM system as shown in the block diagram of Fig. 1. The binary information is premodulation filtered such that for a maximum information rate, 1010 test sequence, only the first harmonic of the information is FM modulated and transmitted. The IF filter is rectangular of total bandwidth  $B = 2(\beta + 1)f_m$ , where  $f_m = 1/T$  and  $T$  is the period of a bit. The resultant modulation has the form:

$$C_m(t) = \Delta_m \cos \omega_m t \quad (3)$$

The output low-pass filter is approximately Gaussian with 3 dB cut-off frequency  $f_m$ .

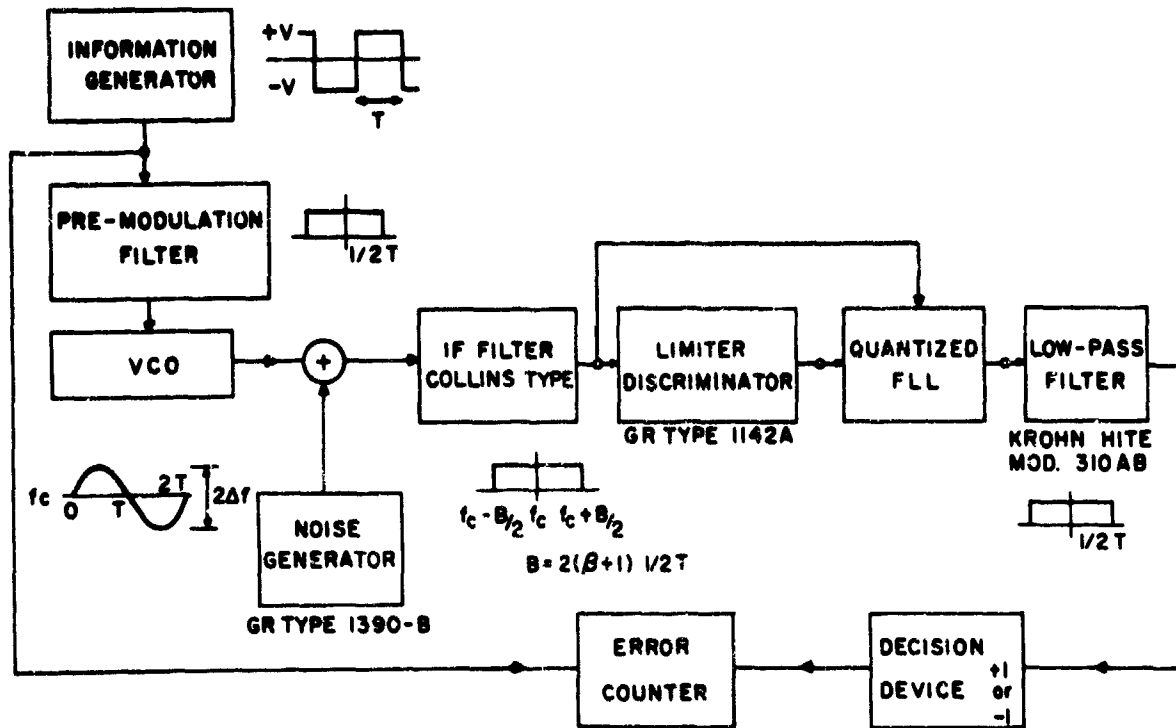


Fig. 1 Digital FM System Block Diagram

For the above system parameters, Schilling and Hoffman showed that the probability of error due to Gaussian noise,  $P_{eg}$ , is:

$$P_{eg} \approx \frac{1}{2} \operatorname{erfc} \sqrt{\frac{\pi^2 \beta^2 (\beta+1) \rho}{14.96 f_o(\beta)}} \tag{4}$$

where

$$f_o(\beta) = \operatorname{erf}(0.937[\beta+1]) - 0.945(\beta+1)e^{-0.7(\beta+1)^2}$$

and

$$f_o(\beta) \approx 1 \text{ for large } \beta.$$

Unkauf<sup>2</sup> showed that the probability of error due to FLL clicks,  $P_{ec}(\epsilon)$ , is:

$$P_{ec}(\epsilon) = \begin{cases} \beta/\pi e^{-\epsilon(1+\epsilon)^2} \sin[\pi/2 \gamma(2\pi)] & 0.734 \leq \beta \leq 4.24 \\ \beta/\pi e^{-\epsilon(1+\epsilon)^2} & \beta \leq 0.734 \end{cases} \tag{5}$$

where

$$\gamma(\eta) = \begin{cases} 0.755 \left[ \ln \frac{3\sqrt{2}\eta}{2\pi\beta} \right]^{1/2} & \beta \leq 4.24 \eta/2\pi \\ 0 & \beta \geq 4.24 \eta/2\pi \end{cases}$$

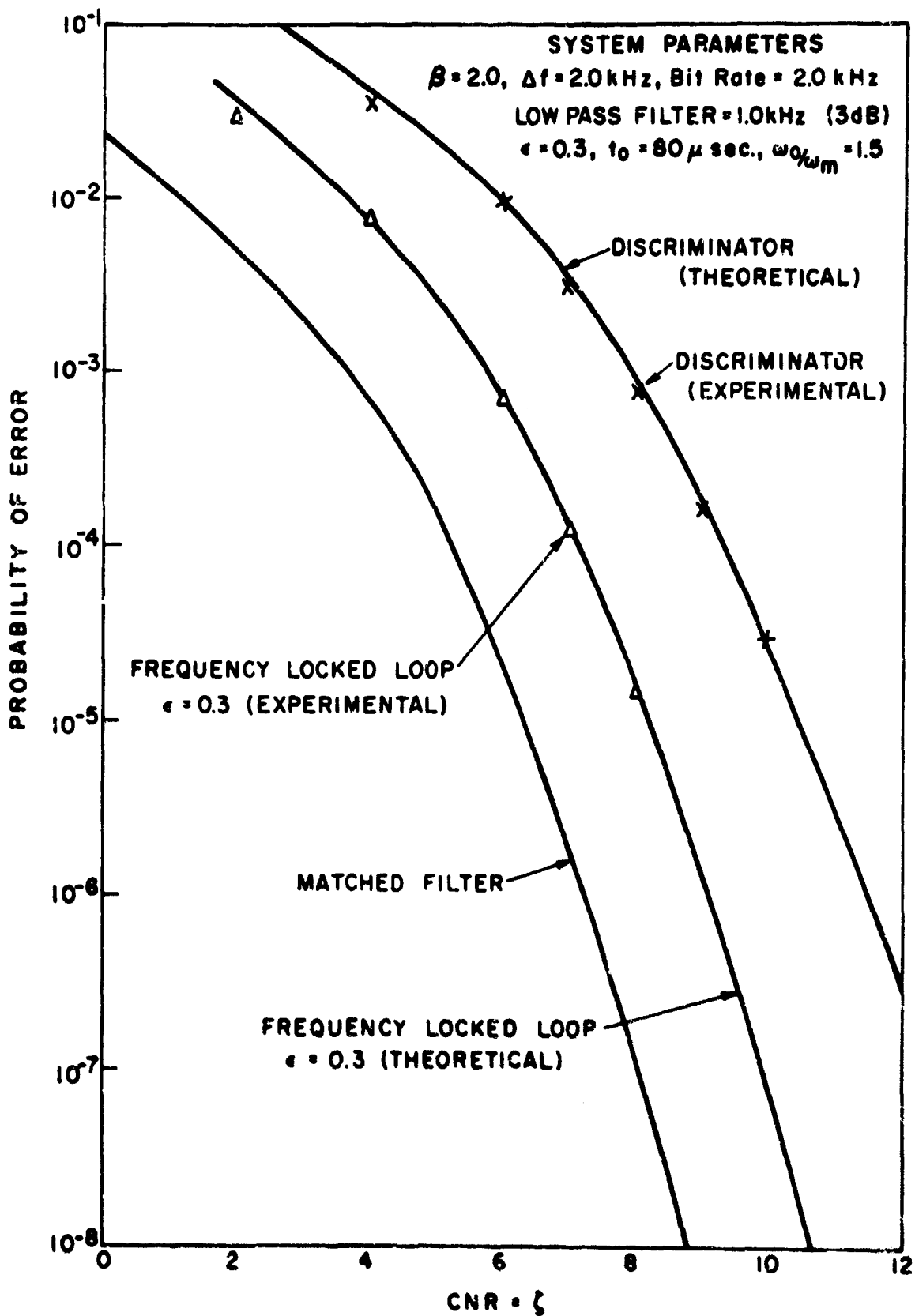


Fig. 2 Digital Error Rates

(It should be noted that clicks can cause errors only in the region  $\beta \leq 4.24$ ). Also, the probability of error due to holds,  $P_{eh}(\epsilon)$ , is:

$$P_{eh}(\epsilon) \approx \frac{\beta}{\pi} e^{-\rho(1-\epsilon)^2} \left\{ \left[ \int_0^{\infty} d\eta \frac{8.37\beta e^{-\eta^2/2\sigma_h^2}}{1.48\beta \sqrt{2\pi\sigma_h^2}} \sin\left(\frac{\pi}{2}\gamma(\eta)\right) \right] + \operatorname{erfc}\left(\frac{6\beta}{\sigma_h}\right) \right\} \quad (6)$$

where  $\sigma_h^2$  is given in the preceding article.

The matched filter detector probability of error for the system described above and for the 1010 sequence is:

$$P_{eMF} = 1/2 \operatorname{erfc}\left\{ \left[ \frac{\beta+1}{2} \left[ 1 - J_0(2\beta) \right] \rho \right\}^{1/2} \right\} \quad (7)$$

$P_{eMF}$  displays a pronounced minimum near  $\beta = 2$  so experimental results were obtained for this condition.

For  $\beta = 2$ , the total probability of error is shown in Fig. 2 for the discriminator, the FLL, and the matched filter. The FLL parameters are  $Bt_0 = 0.6$ ,  $\frac{\omega_0}{\omega_m} = 1.5$ , and  $\epsilon = 0.3$ . It is evident that the FLL represents a 2.2 dB improvement (a decrease in error probability by more than 100 for  $\rho = 9$  dB) over the discriminator and comes to within 1.8 dB of the matched filter result. The experimental results for  $\epsilon = 0.3$  agree well with the theoretical results. It should be noted that a further improvement in system performance can be gained by optimizing the low-pass filter bandwidth. This adjustment results in a further 0.4 dB improvement in the FLL performance.

Caution must be exercised when employing the above theoretical results for  $\epsilon$  greater than 0.3 due to the effect of interference between adjacent holds. The value of  $\epsilon$  employed for the FLL in Fig. 2 was the experimentally determined optimum. The errors due to clicks decrease with increasing  $\epsilon$  while those due to holds increase. When the expected number of clicks and holding errors are equal, the overall error rate is lowest and this occurs for  $\epsilon \approx 0.3$  in the experimental system.

The FLL as indicated in Fig. 2 would require 3.3 dB more signal to noise ratio to perform as well as the matched filter for coherent PSK (assuming constant energy per bit). By way of comparison, a differential detection scheme for binary FM using a product demodulator was shown by Anderson, Bennett, Davey, and Salz<sup>3</sup> to require 4.8 dB more signal to noise ratio for this same performance. Thus, the FLL FM demodulator should prove to be of significant advantage in the demodulation of digital FM signals due to its excellent error rate characteristics and its inherent simplicity of construction.



National Aeronautics and Space Administration  
NgR 33-006-020

M. Unkauf, K. K. Clarke, and D. T. Hess

## REFERENCES

1. D. L. Schilling and E. Hoffman, "Demodulation of Digital Signals Using an FM Discriminator," Proc. of National Electronics Conference, Vol. 22, 1966, pp. 369-374.
2. M. G. Unkauf, "Quantized Second Order Frequency Locked Loop," Ph. D. Dissertation, Polytechnic Institute of Brooklyn, June 1969.
3. R. R. Anderson, W. R. Bennett, J. R. Davey and J. Salz, "Differential Detection of Binary FM," Bell System Technical Journal, Vol. 64, No. 1, January 1965.

## THRESHOLD EXTENSION BY MEANS OF SPIKE DETECTION AND CANCELLATION

D. L. Schilling and E. Hoffman

FM signals, when received in noisy media, are susceptible to a sudden deterioration of receiver output SNR, compared to input CNR, called "threshold". The onset of threshold was determined by Rice to be caused by clicks.

Extension of threshold may be accomplished by three distinct approaches and combinations thereof:

- 1) Reception by means of devices which do not reproduce all input clicks at their output (unlike the ordinary FMD). Examples of such devices are the PLL and FMFB.
- 2) Reception by means of devices which suppress input clicks (such as the FLL).
- 3) Reception through any FM demodulator, and detection of the presence of a spike followed by cancellation.

The present study concerns itself with:

- 1) The theoretical number of spikes which must be detected and cancelled as a function of threshold extension.
- 2) The effect of imperfect cancellation (i. e., the effect of producing doublets).
- 3) Experimental results on the number of spikes which are correctly detected using various circuitry schemes.
- 4) The maximum threshold extension as predicted by information theory, and a comparison to the number of spikes detected.
- 5) The cause and location of threshold when spikes are detected and corrected.

Results to Date:

This interim report covers parts (1) and (3) of the study. The FMD was used as

the basis of the analysis and experimental work.

Threshold of FMD Under Modulation:

The probability of a positive spike is given by Rice:

$$E\left(\frac{\text{negative spikes}}{e_m > 0}\right) = \frac{\alpha}{4\pi} \sqrt{1 + \left(\frac{e_m(t)}{\alpha}\right)^2} \operatorname{erfc} \sqrt{\gamma \left\{1 + \left[\frac{e_m(t)}{\alpha}\right]^2\right\}} - \frac{e^{-\gamma}}{4\pi} \operatorname{erfc} \left\{ \sqrt{\gamma} \frac{e_m(t)}{\alpha} \right\} + \frac{e^{-\gamma}}{2\pi} e_m(t) \quad (1)$$

where

$$\alpha = \frac{E(k^2)}{E(x^2)} = \frac{E(y^2)}{E(y^2)}; \quad \gamma = \frac{\Delta}{2N} \quad (2)$$

and

$$E\left(\frac{\text{positive spikes}}{e_m > 0}\right) = E\left(\frac{\text{negative spikes}}{e_m > 0}\right) - \frac{e^{-\gamma}}{2\pi} e_m(t) \quad (3)$$

Assuming  $\sqrt{\gamma} \frac{e_m(t)}{\alpha} \gg 1$ , Eq. (1) becomes

$$N_+^{\Delta} E(\text{negative spike}) = E\left(\frac{\text{negative spike}}{e_m(t) > 0}\right) = \frac{e^{-\gamma}}{2\pi} e_m(t) \quad (4)$$

Under conditions of Gaussian modulation,

$$e_m(t) = \Delta\omega \sin \omega_m t \quad (5)$$

where  $\Delta\omega$  has a Gaussian probability density distribution given by:

$$p(\Delta\omega) = \frac{1}{\sqrt{2\pi}\sigma_{\omega}} e^{-\frac{\Delta\omega^2}{2\sigma_{\omega}^2}} \quad (6)$$

and where  $\omega_m$ , the modulation frequency, has a probability distribution function which is flat from 0 to  $\omega_c$ :

$$p(\omega_m) = \frac{1}{\omega_c}, 0 < \omega_m < \omega_c \\ = 0 \text{ elsewhere.} \quad (7)$$

The average number of spikes / sec,  $N_+^{\Delta}$ , is given by

$$N_+^{\Delta} = \frac{e^{-\gamma}}{2\pi} E\left(\frac{e_m(t)}{e_m(t) > 0}\right) = \frac{e^{-\gamma}}{2\pi} E\left(\frac{\Delta\omega \sin \omega_m t}{e_m(t) > 0}\right) = \frac{e^{-\gamma}}{2\pi} E\left(\frac{\Delta\omega}{e_m(t) > 0}\right) E(\sin \omega_m t) \quad (8)$$

since the  $\Delta\omega$  and  $\omega_m$  processes are independent.

$$N_+ = \frac{e^{-\gamma}}{2\pi} 2 \left[ \left( \frac{2}{\sqrt{2\pi}} \sigma_\omega \right) \left( \frac{1}{\pi} \right) \right] \quad (9)$$

Since  $e_m(t) > 0$  when  $\Delta\omega > 0$  and  $\sin \omega_m t > 0$   
or  $\Delta\omega < 0$  and  $\sin \omega_m t < 0$

The output signal to noise ratio  $S_o/N_o$  at the low pass filter is expressed in terms of  $N_+$ :

$$\frac{S_o}{N_o} = \frac{3 \beta^2 \gamma B_{IF}/f_c}{1 + 24 B_{IF} \gamma N_+/f_c} \quad (10)$$

Choosing  $B_{IF} = 3\sigma_\omega$  to contain 99.7% of the Gaussian modulation in the IF Bandwidth, and nothing that

$$\beta_{\text{mean}} = E\{\beta\} = \frac{2\sigma_\omega}{\sqrt{2\pi} f_c/2} \quad (11)$$

Equation 10 becomes

$$\frac{S_c}{N_o} = \frac{5.6 \beta_m^3 \gamma}{1 + 58.5 \beta_m^2 \gamma e^{-\gamma}} \quad (12)$$

Threshold in the FMD, therefore, occurs (see Fig. 1) at

$$\beta_m^2 \gamma e^{-\gamma} = 1.7 \times 10^{-3} \quad (13)$$

#### Click Elimination

Combining Eqs. (10) and (11), one obtains (see Fig. 2) an expression for  $N_+$  at threshold

$$28.3 \beta_m^2 \gamma \left( \frac{N_+}{\Delta\omega} \right) = 1 \quad (14)$$

The result of Eq. (14) and the FMD spikes of Eq. (9) are plotted on Fig. 2.

One therefore obtains, combining Figs. 1 and 2, a result showing the percentage of the clicks which must be detected as a function of threshold improvement if all detected clicks are cancelled perfectly. These results are plotted in Fig. 3.

#### Experimental Results

Experimental results for the spikes detected were obtained using the block diagram of Fig. 4. A PLL having a wide bandwidth such that its spike response approaches

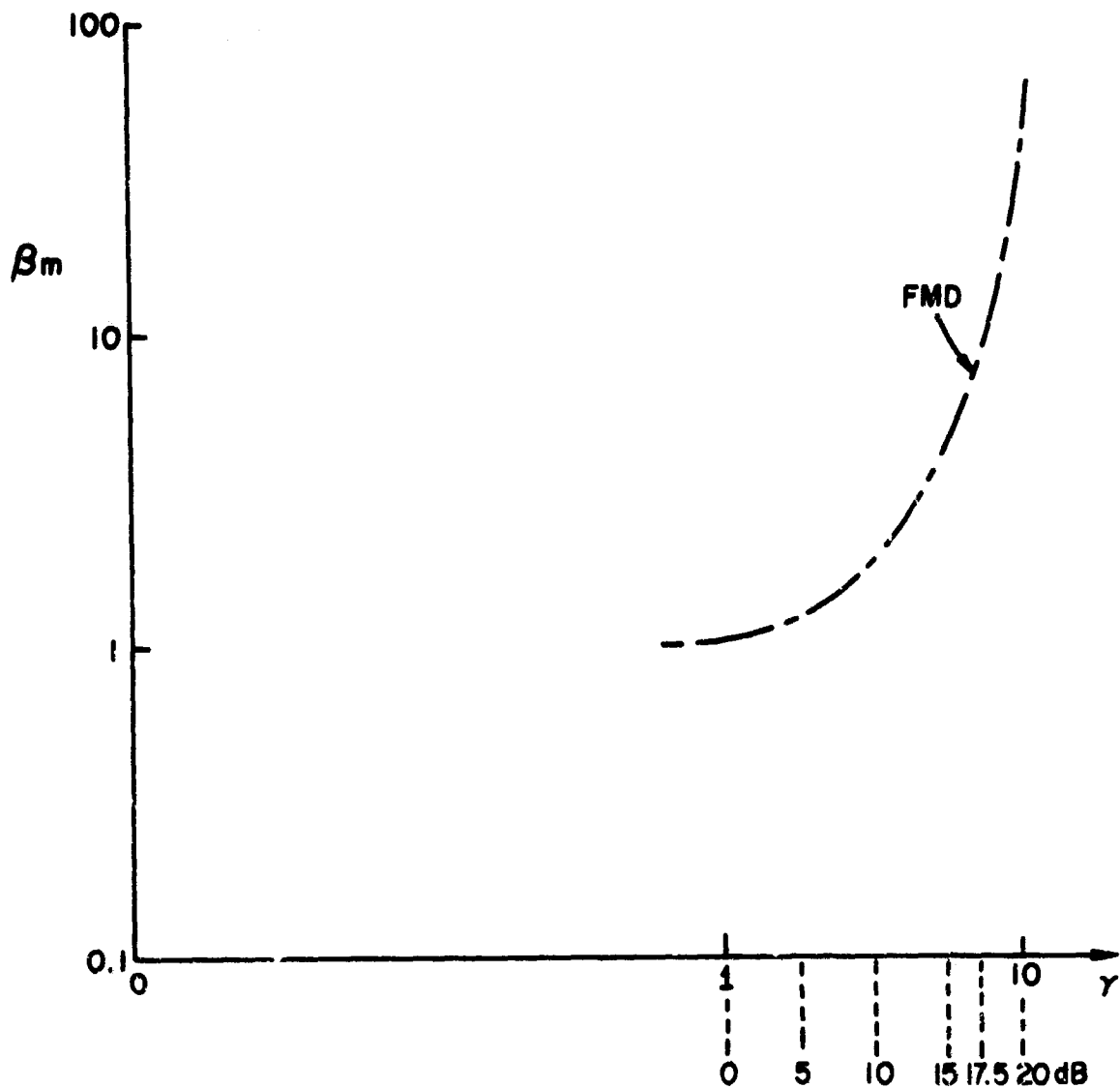


Fig. 1 Gaussian Modulation,  $B_{IF} = 3\sigma_{\omega}$ ;  $\beta_{\text{mean}} = \left(\frac{\Delta f}{f_c}\right)_{\text{mean}}$

that of the FMD was used.

Channel A of the storage scope showed the time of occurrence of all spikes. Its input was the PLL Output less the modulation, leaving the output noise only.

Channel B shows the filtered output of the PLL. Based on the display of Channel B on the storage scope, a prediction was made "by eye" as to where and when a spike occurred. A comparison with Channel A yielded the number of spikes caught correctly, added extraneously, or missed. The  $\%_{\text{detected}}$  spikes detected experimentally were determined by:

$$\%_{\text{detected}} = \frac{\text{spikes caught} - \text{spikes added}}{\text{spikes caught} + \text{spikes missed}}$$

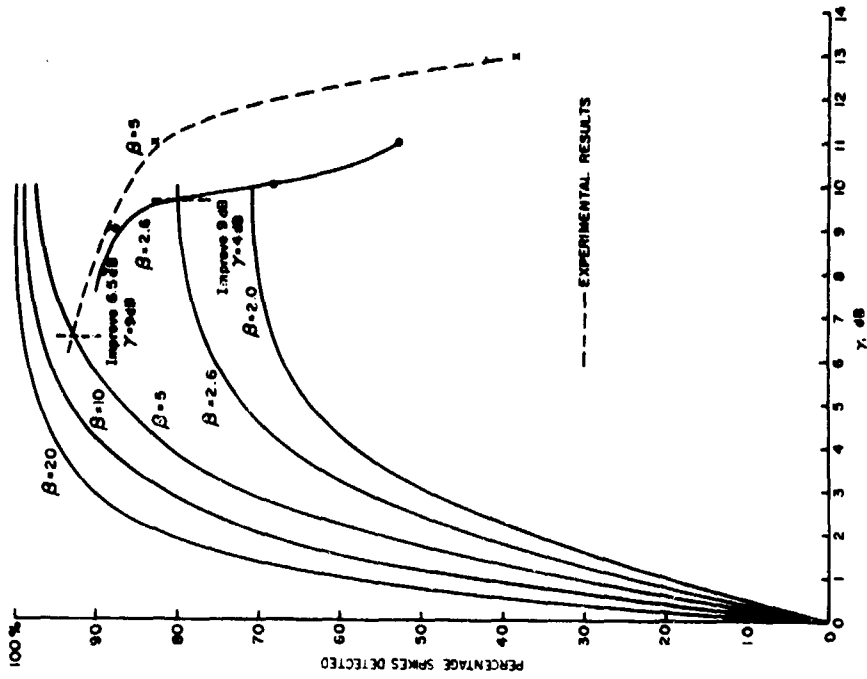


Fig. 3 % Spikes Detected and Cancelled vs. Threshold Improvement (DB)

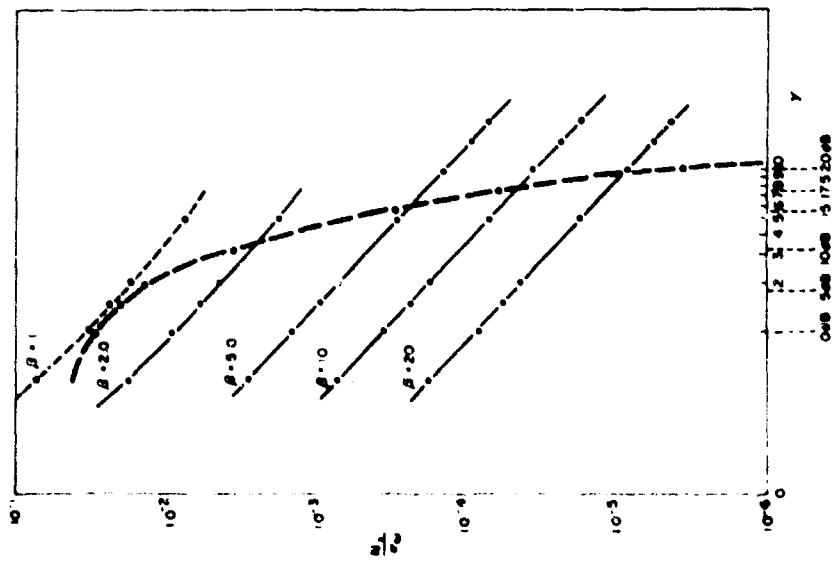


Fig. 2  $(\frac{N_s}{\sigma_s^2})$  vs.  $\gamma$  for FMD and at Threshold with  $\beta$  as Parameter for any FM Detector

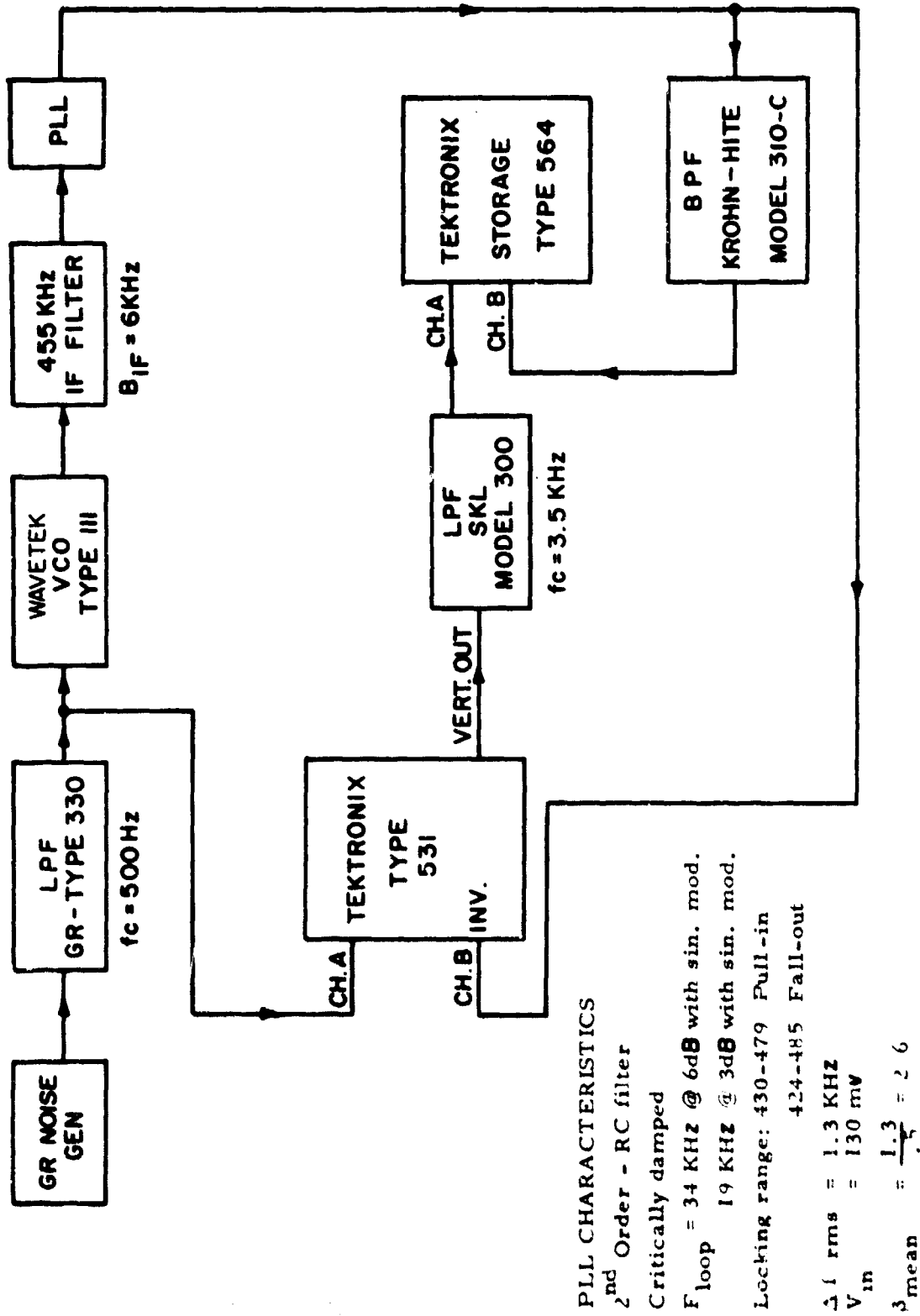


Fig. 4 Spike Detection - "Visual"

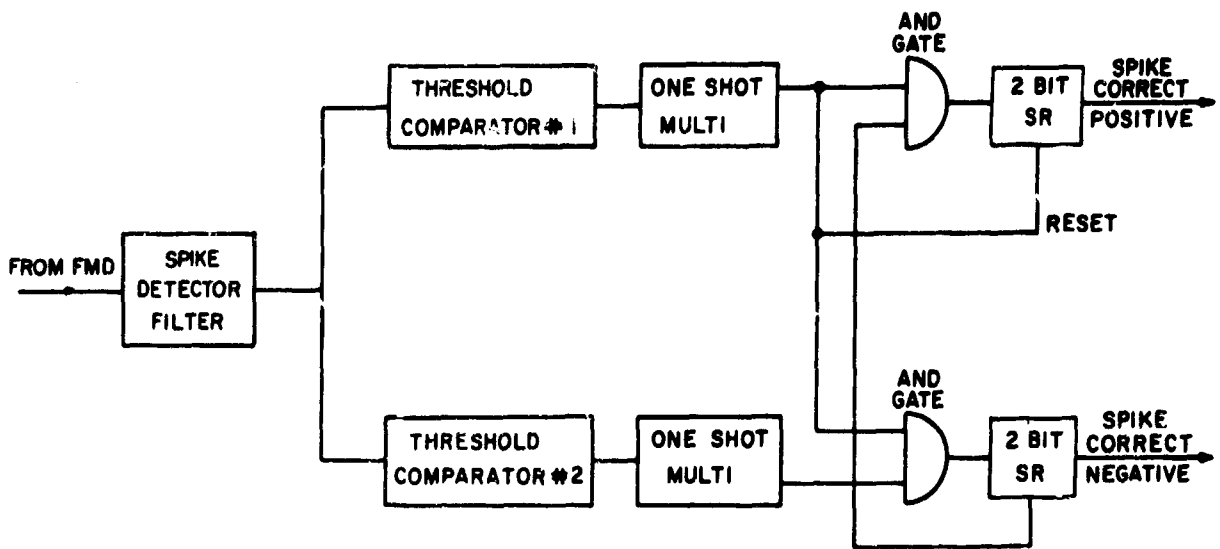


Fig. 5 Elementary, 2-Level Spike Detector Circuit

Results are plotted on Fig. 4. The intersection with the curves showing the % spikes required to extend threshold yields the threshold extension obtainable by cancelling FMD spikes.

A scheme by which the "eye" detection technique is performed electronically was built and is shown in Fig. 5. Results with the two level techniques show that only half of the spikes detected by "eye" are detected automatically using this scheme. With the addition of more levels, the "eye" detection percentage is approachable.

#### Conclusions

The extension of threshold by detection and cancellation of spikes may be accomplished to the extent shown in Fig. 3. The theoretical curves shown actually apply to any device whose output spike percentage is less than that of the FMD. The technique of detection by "eye" yields a possible improvement of 6db at  $\beta = 5$  and 9 db at  $\beta = 2.6$ , assuming that all detected spikes are cancelled perfectly and that threshold occurrence is due to spikes only.

Further studies are presently being performed on automatic detection of spikes, cancellation of spikes, the actual measurement of output SNR, the threshold limit due to information theory and the cause of thresholds other than spikes.

National Aeronautics and Space Administration  
NgR-33-006-020

D. I. Schilling and E. Hoffman

## EQUIVALENCE OF FM THRESHOLD EXTENSION RECEIVERS

D. T. Hess

I. Introduction

It is well known<sup>1, 2, 3, 4</sup> that the FM noise threshold may be extended by employing a properly designed phase locked loop (PLL) or a frequency demodulator with feedback (FMFB) to demodulate the noise corrupted FM signal. It has recently been demonstrated that the frequency locked loop<sup>5</sup> (FLL) is also capable of threshold extension. In this report it shall be demonstrated that the defining equations for the PLL and FLL are limiting forms of the defining equations for the FMFB; hence rather than having three distinct devices capable of threshold extension, we have only one basic device (FMFB) from which the other two devices (PLL and FLL) are derivable. In particular it is shown that as the bandwidth of the internal IF filter of the FMFB is reduced to zero the FMFB and the PLL have the same defining equations. Conversely, as the bandwidth is increased without bound the equations for the FMFB and FLL are identical.

An interesting aspect of this equivalence is that a better physical understanding of the threshold extension mechanism of the FMFB may be obtained. Although some physical insight into the PLL and FLL has been gained, very little exists for the FMFB. In a previous paper<sup>6</sup> it has demonstrated that the PLL improves the FM noise threshold by not tracking (or "losing lock" during) many of the noise "clicks"<sup>7</sup> that would normally appear at the output of the limiter-discriminator. In addition, it has been shown<sup>8</sup> that the FLL improves the FM noise threshold by a "holding" mechanism that reduces the strength of many of the noise "clicks". Consequently, since an FMFB lies somewhere between the FLL and the PLL if its internal IF filter bandwidth is neither zero nor infinity the FMFB should achieve threshold extension by "losing lock" during some noise "clicks" reducing the strength of others.

This phenomenon was indeed observed by Cassara.<sup>9</sup> He compared the outputs of an FMFB and a limiter-discriminator which were excited by the same unmodulated FM carrier plus narrow band noise (both centered about the same frequency  $\omega_0$ ) and noted that some of the noise "clicks" existing at the output of the limiter-discriminator did not exist at all at the output of the FMFB, while other noise "clicks" were reduced in strength or area. With an unmodulated carrier, no noise "click" appeared at the output of the FMFB which did not appear at the output of the limiter-discriminator.

Consequently demonstrating the equivalence of the defining equations of the three devices yields a starting point for the understanding of the FMFB. To begin the analysis the defining equations for the FLL and PLL are developed. The equation for the FMFB is then developed as a function of its internal IF filter, whose bandwidth is first increased without bound and then reduced to zero. Convergence of the FMFB equation to



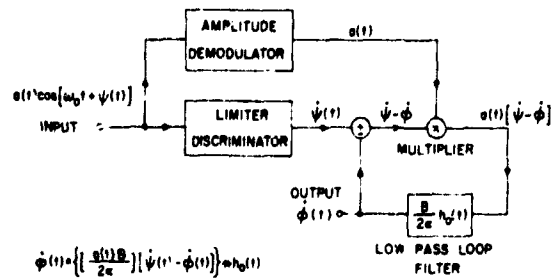


Fig. 1 Block Diagram of Frequency Locked Loop

that of the FLL and PLL is thus demonstrated.

II. Frequency Locked Loop Equation

The block diagram of the baseband version of the FLL is shown in Fig. 1. Here the input is assumed to be in the completely general form of a carrier centered at  $\omega_0$  modulated by an amplitude  $a(t)$  and a phase  $\Psi(t)$ . The amplitude term  $a(t)$  arises when the FM carrier is added to narrowband noise centered about  $\omega_0$ , whereas  $\Psi(t)$  consists of the desired FM modulation plus perturbations from the narrowband noise. Without loss of generality, the constants associated with the limiter-discriminator and amplitude demodulator are taken as unity, and the entire loop constant  $B/2a$  is associated with the loop filter whose impulse response is  $h_0(t)$ . The form of  $B/2a$  for the loop constant is chosen such that the equivalence between the FMFB and the FLL is more evident.

If the output of the loop is defined as  $\dot{\phi}(t)$ , then by proceeding around the loop one quickly obtains the defining equation for the FLL to be

$$\dot{\phi}(t) = \left\{ \left[ \frac{a(t)B}{2a} \right] [\dot{\Psi}(t) - \dot{\phi}(t)] \right\} * h_0(t) \tag{1}$$

where \* denotes convolution.

The block diagram of Fig. 1 provides some insight into the threshold extending mechanism of the FLL. Clearly if  $a(t)$  is small the closed loop bandwidth of the loop decreases and the output  $\dot{\phi}(t)$  is permitted small variations (especially if the low pass loop filter has a pole close to the origin which it should have). However as is known,<sup>10</sup> when a noise "click" occurs in  $\dot{\Psi}(t)$ , which is a step of  $\pm 2\pi$  in  $\Psi(t)$ ,  $a(t)$  has a high probability of lying very close to zero; thus  $\dot{\phi}(t)$  is "held" during the occurrence of a "click" which results in the "click" being suppressed at the output.

III. Phase Locked Loop Equation

The block diagram of the PLL is shown in Fig. 2. Here the same input signal is assumed as for the FLL and the output signal is similarly defined as  $\dot{\phi}(t)$ . In addition

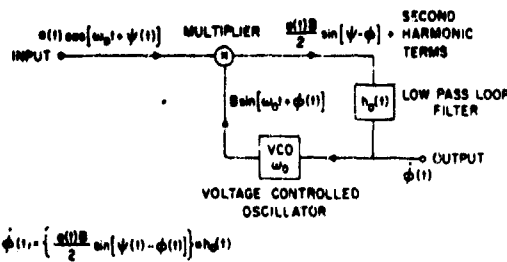


Fig. 2 Block Diagram of Phase Locked Loop

without loss of generality the constant of the voltage controlled oscillator VCO is taken as unity and the entire loop constant B is associated with the output amplitude of the VCO. Here again one proceeds around the loop, recognizes that the loop filter rejects the second harmonic terms (in the vicinity of  $2\omega_c$ ) appearing at the multiplier output, and writes the defining equation for the loop in the form

$$\dot{\phi}(t) = \left\{ \frac{a(t)B}{2} \sin [\Psi(t) - \phi(t)] \right\} * h_o(t) \quad (2)$$

In this loop as in the FLL the closed loop bandwidth is controlled by  $a(t)$ . Here however, during a "click" in  $\Psi(t)$  and a step of  $\pm 2\pi$  in  $\Psi(t)$ , small values of  $a(t)$  prevent  $\dot{\phi}(t)$  or  $\phi(t)$  from changing rapidly. Therefore as  $\Psi(t)$  varies by  $\pm 2\pi$   $\sin[\Psi(t) - \phi(t)]$  passes through an entire cycle and returns to its starting point, thereby leaving the initial conditions of the PLL unchanged from those immediately preceding the "click". Thus the loop "loses lock" for a cycle and no "click" appears at the output. Only those steps in  $\Psi(t)$  during which  $a(t)$  is reasonably large produce output "clicks" since the PLL is then able to track the steps in  $\Psi(t)$ .

IV. Frequency Demodulator with Feedback Equation

The block diagram of the FMFB is shown in Fig. 3. Here again the input signal is identical with the one applied to the FLL and PLL and the output signal is again defined as  $\dot{\phi}(t)$ . Again the constants of the VCO and the discriminator are chosen as unity.

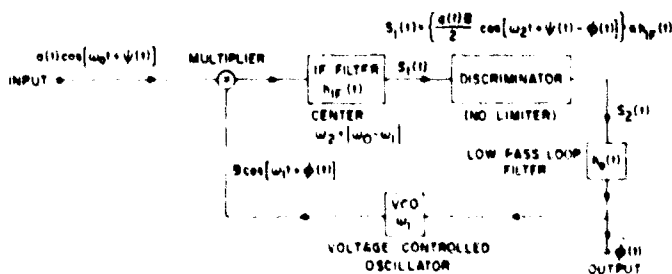


Fig. 3 Block Diagram of Frequency Demodulator with Feedback

The IF filter is assumed to be a single-pole filter (for stability) whose transfer function is given by

$$H_{IF}(s) = \frac{2s}{s^2 + 2as + \omega_2^2} = \mathcal{L}[h_{IF}(t)] \quad (3)$$

where  $\omega_2$  is the difference between the output frequency  $\omega_1$  of the "free running" VCO and the input frequency  $\omega_0$ ,  $a$  is the distance of the poles of  $H_{IF}(s)$  from the imaginary axis in the complex  $s$  plane, and  $\mathcal{L}$  is the Laplace Transform operator.

The discriminator in the loop has no limiter and has the property that if its input  $S_1(t)$  is given by

$$S_1(t) = \delta(t) \cos [\omega_2 t + \lambda(t)] \quad (4)$$

its output  $S_2(t)$  is given by

$$S_2(t) = \delta(t) \dot{\lambda}(t) \quad (5)$$

A little thought readily shows that such a description is valid for any conventional discriminator not preceded by a limiter for which  $\omega_2 - |\dot{\lambda}| \gg \dot{\delta}(t)/\delta(t)$ . In general the complete equation for  $\dot{\varphi}(t)$  for the FMFB may be readily written down from the block diagram of Fig. 3; however its form is so complex that little or no insight can be gained from it. Consequently in the following paragraphs only the two desired limiting forms of the FMFB are considered. First the bandwidth of  $H_{IF}(s)$  is permitted to become large and then it is permitted to approach zero.

#### Large Bandwidth for Loop IF Filter, FMFB Approaches FLL

As the bandwidth of the loop IF filter becomes large compared with the band of frequencies occupied by

$$\frac{a(t)B}{2} \cos [\omega_2 t + \psi(t) - \varphi(t)]$$

the filter output is an attenuated, but undistorted, version of its input which is given by

$$S_1(t) = \left(\frac{1}{a}\right) \left(\frac{a(t)B}{2} \cos [\omega_2 t + \psi(t) - \varphi(t)]\right) \quad (6)$$

where  $(1/a)$  is the transfer function of the IF filter in its pass-band. Consequently the output of the discriminator is given by

$$S_2(t) = \frac{a(t)B}{2a} [\dot{\psi}(t) - \dot{\varphi}(t)] \quad (7)$$

from which the defining equation for the FMFB is readily obtained in the form

$$\dot{\varphi}(t) - S_2(t) * h_0(t) = \left\{ \frac{a(t)B}{2a} [\dot{\psi}(t) - \dot{\varphi}(t)] \right\} * h_0(t) \quad (8)$$

Clearly Eqs. (1) and (8) are identical; hence the equivalence between the defining equations of the FMFB and FLL in this case is demonstrated.

It should be noted that Eq. (8) is strictly valid only if the internal loop bandwidth increases without bound.<sup>†</sup> In practice however, since the input signal to the FMFB has already been band-limited by some external RF filter and since the multiplication of the input signal by the VCO output increases this band of frequencies by at most a factor of 2 or 3 in the vicinity of  $\omega_2$ , the bandwidth of the internal IF filter need be no more than twice as large as the bandwidth of the external RF filter to have the FMFB and the FLL perform in the same fashion.

#### Small Bandwidth for Loop IF Filter, FMFB Approaches PLL

As the bandwidth of the loop IF filter becomes small compared with the band of frequencies occupied by

$$\frac{a(t)B}{2} \cos [\omega_2 t + \Psi(t) - \phi(t)]$$

the filter output is a strongly distorted version of its input. Some idea of the nature of this distortion is obtained by expanding the filter output in the form

$$\begin{aligned} S_1(t) &= \left\{ \left[ \frac{a(t)B}{2} \right] [\cos [\Psi(t) - \phi(t)] \cos \omega_2 t - \sin [\Psi(t) - \phi(t)] \sin \omega_2 t] \right\} * h_{IF}(t) \\ &= \left[ \left\{ \frac{a(t)B}{2} \cos [\Psi(t) - \phi(t)] \right\} * h_L(t) \right] \cos \omega_2 t \\ &\quad - \left[ \left\{ \frac{a(t)B}{2} \sin [\Psi(t) - \phi(t)] \right\} * h_L(t) \right] \sin \omega_2 t \end{aligned} \quad (9)$$

where  $h_L(t)$  is the impulse response of the low-pass equivalent filter of the narrow-band IF filter. In particular if  $H_{IF}(s) = 2s/s^2 + 2as + \omega_2^2$  then

$$H_L(s) = \mathcal{L}\{h_L(t)\} = \frac{1}{s+a} \quad (10)$$

Equation (9) may be rearranged still further to yield

$$S_1(t) = [C + c(t)] \cos \omega_2 t - [D + d(t)] \sin \omega_2 t \quad (11)$$

where  $C$  and  $D$  are the average or dc values of the respective coefficients of the  $\cos \omega_2 t$  and  $\sin \omega_2 t$  terms in Eq. (9), and  $c(t)$  and  $d(t)$  are the respective values of the coefficients less their average values. If the RF filter preceding the loop is symmetric about  $\omega_0$  and if  $\overline{\Psi(t)} = 0$ , it is apparent from symmetry considerations that  $\overline{c(t)} = 0$  and  $\overline{a(t) \sin [\Psi(t) - \phi(t)]} = 0$ ; hence  $D = 0$ . On the other hand,  $C$  is clearly not equal to zero; consequently Eq. (11) may be further rearranged to yield

<sup>†</sup> As the IF bandwidth is increased it is assumed that the out of band signals at the multiplier output, centered at  $\omega_0 + \omega_1$ , are still rejected.

$$S_1(t) = \sqrt{[C + c(t)]^2 + [d(t)]^2} \cos \left[ \omega_2 t + \tan^{-1} \frac{d(t)}{C + c(t)} \right] \quad (12)$$

from which follows

$$S_2(t) = \frac{[C + c(t)] \dot{d}(t) - d(t) \dot{c}(t)}{\sqrt{[C + c(t)]^2 + [d(t)]^2}} \quad (13)$$

It is apparent at this point that as the bandwidth of the IF filter (2a) approaches zero  $c(t)$  and  $d(t)$  become vanishingly small compared with  $C$  (more and more of the ac component is filtered while the dc component remains unchanged) and Eq. (13) reduces to the limiting form

$$S_2(t) = \dot{d}(t) = \frac{d}{dt} \left[ \left\{ \frac{a(t) B}{2} \sin [\Psi(t) - \varphi(t)] \right\} * h_L(t) \right] \quad (14)$$

In addition, as  $\alpha \rightarrow 0$ ,  $H_L(s) \rightarrow 1/s$  which is a pure integrator; hence convolution with  $h_L(t)$  in Eq. (14) corresponds to integration which cancels with the differentiation operation to yield

$$S_2(t) = \frac{a(t) B}{2} \sin [\Psi(t) - \varphi(t)] \quad (15)$$

and finally

$$\dot{\varphi}(t) = S_2(t) * h_0(t) = \left\{ \frac{a(t) B}{2} \sin [\Psi(t) - \varphi(t)] \right\} * h_0(t) \quad (16)$$

Clearly Eqs. (16) and (2) are identical; hence the equivalence between the defining equations of the FMFB and the PLL in this case is demonstrated.

Although the loop IF bandwidth must theoretically reach zero to have the FMFB function as a PLL, it has been found experimentally<sup>9</sup> that for IF bandwidths less than 1/10 of the external RF filter bandwidth the FMFB functions, with respect to a noise-corrupted input carrier, in essentially the same fashion as the PLL.

Several interesting observations may be made at this point. First, the FMFB may have an arbitrarily narrow loop IF filter bandwidth and still successfully demodulate an input FM signal. This is quite obvious since the PLL is capable of performing such a demodulation. Previously it was believed by many writers<sup>1, 3</sup> that the loop IF filter must have a bandwidth at least equal to twice the frequency range occupied by the modulation information.

Secondly, with a sufficiently narrow loop IF filter bandwidth the FMFB has all of the "loss of lock" problems possessed by the PLL. Consequently, large deviations of the input carrier in the presence of noise are capable of throwing the FMFB "out of lock" with the result of a large number of signal induced "clicks". On the other hand, for wide loop IF bandwidths the FMFB can never "lose lock". This is obvious since the PLL (which the FMFB approaches, cf. Fig. 1) has no VCO and therefore no

mechanism by which to lose lock. Perhaps some intermediate value of loop IF bandwidth combines the best features of the PLL and FLL. This might be true since the FMFB is more widely used commercially than the PLL.

#### V. Conclusion

In this report it has been demonstrated that the defining equations of the FMFB degenerate into the equations for the FLL and PLL as the loop IF filter bandwidth of the FMFB approaches infinity or zero respectively. Consequently a possibility of further physical understanding of the FMFB may be obtained by approaching its operation from the limits of FLL operation on one end and PLL operation on the other. More significant, however, is the realization that the three basic threshold extension receivers are equivalent with respect to their defining equations to the single device, the FMFB.

National Aeronautics and Space Administration  
NgR 33-006-020

D. T. Hess

National Science Foundation  
GK-527

#### REFERENCES

1. L. H. Enloe, "Decreasing the Threshold in FM by Frequency Feedback," Proc. IRE, Vol. 50, Jan. 1962.
2. D. L. Schilling and J. Billig, "A comparison of the Threshold Performance of the Frequency Demodulator Using Feedback and the Phase Locked Loop," Rec. 1965 International Space Electronics Symp., p. 3-E1.
3. M. Schwartz, W. R. Bennett, and S. Stein, "Communication Systems and Techniques," Chapter 3, McGraw-Hill, 1966.
4. P. Frutiger, "Noise in FM Receivers with Negative Frequency Feedback," Proc. IEEE, Vol. 54, November 1966.
5. K. K. Clarke and D. T. Hess, "Frequency Locked Loop FM Demodulator" IEEE Trans. on Comm. Tech., Vol. Com-15, August 1967, pp. 518-524.
6. D. T. Hess, "Cycle Slipping in First Order Phase Locked Loops," IEEE Trans. on Comm. Tech., April 1968.
7. S. O. Rice, "Noise in FM Receivers," Time Series Analysis, M. Rosenblatt, Ed. New York: Wiley, 1963, Chapter 25.
8. K. K. Clarke and D. T. Hess. Ibid.
9. F. Cassara, "FM Demodulator with Feedback," MS Project Report, Polytechnic Institute of Brooklyn, June 1968.
10. L. Calandrino and G. Immovilli, "Coincidence of Pulses in Amplitude and Frequency Deviations," Alta Frequenza, English Issue No. 3, Vol. 26, August 1967.

## THE EFFECT OF A FIRST ORDER, OPEN LOOP HOLDING CIRCUIT UPON FM "SPIKES" IN A VIDEO SIGNAL

K. K. Clarke and F. R. Ergul

The PIB experimental TV system was used with a PIB FM system to study single frame video transmission via a noisy FM channel operating at or below threshold. A simple first order, open loop holding circuit was then added to the receiver output in an attempt to improve reception by suppressing some of the below threshold FM "spikes".

The details of basic equipment set-up are reported in Ref. 1. A video signal was used to modulate a wideband, essentially distortionless FM generator. This FM signal at 4 MHz was added to wideband noise centered at 4 MHz and applied to a PIB FM receiver. The receiver selectivity was determined primarily by a single high Q adjustable bandwidth tuned circuit.

The receiver output was then filtered, amplified and reproduced upon a suitable synchronized video receiver. Single frame operation was utilized to show distortion per frame rather than distortion integrated over several frames as is normally observed by the human eye. Figure 1 indicates the effects of below threshold FM transmission upon video material.

Initial distortion is largely of a "spike" or "click" type leading to the characteristic white spots in black material and black spots in white material. An approach to the reduction of this distortion is indicated below. (In the sections of the report dealing with the Frequency Locked Loop, it is demonstrated that feedback loop operators are always superior in theory to open loop operators for distortion reduction of the type studied here. This section illustrates what can be accomplished with open loop systems as well as indicating some of the variables in such systems.)

Assume that the video signal is sampled regularly at times  $t_i$  and represented by the set  $(x_i)$ . If  $N$  past samples are available, then the next sample  $x_{i+1}$  can be predicted using a suitable procedure. Then, using the amplitude data provided by an envelope detector, one can perform a test and determine the probability of spike occurrence during  $(i+1)$  the sampling interval. If the test reveals that a spike may have occurred, then one uses the estimate  $\hat{x}_{i+1}$  instead of the next sample. The procedure has the potentiality of eliminating most of the spikes. Not all spikes will be removed because of the finite uncertainty in spike detection. Actually there will be many "false alarms" between two spike occurrences and therefore an additional distortion will be introduced. However, the video signal is highly correlated and the rms error due to the estimation procedure as well as due to replacing  $x_i$  by  $\hat{x}_i$  may be reasonably small.

A simple sub-optimum system<sup>1</sup> can be obtained if the predictor is replaced by a sample and hold circuit (actually it is a zero-order predictor) and the spike detector



CNR = 8 db



CNR = 3 db



Direct Transmission.



CNR = 6 db

Fig. 1 Video Transmission via a Noisy FM Channel. 70kHz pp Single Tuned IF. 13 volts peak-peak video. 5kHz/V. FM Sensitivity 3.5 frames/sec. rate. Single frame operation.



is replaced by an amplitude comparator that causes the video signal to be held at its sampled value whenever the envelope of the RF signal drops below a certain percentage  $\epsilon A$  of its "normal" amplitude  $A$ . If timing is accurate enough, then spikes that occur during a hold period will be largely eliminated from the video output. The upper bound of the rms error for the described scheme can be expressed as:

$$\epsilon_{\text{rms}}^2 = 2 R_{\text{xx}}(0) [1 - R_{\text{xx}}(a)/R_{\text{xx}}(0)] P\{r < \epsilon\}$$

where  $R_{\text{xx}}(\tau)$  is the autocorrelation function of video signal,  $a$  is a constant delay term and  $P\{r < \epsilon\}$  is the probability of the normalized envelope of carrier being less than the normalized threshold level  $\epsilon$ .

To demonstrate the feasibility of such a system, an amplitude detector feeding an amplitude comparator that fired a monostable multivibrator was added to a PIB FM receiver. The monostable multivibrator fired whenever the envelope of the noisy FM signal fell below  $\epsilon A$  where  $A$  was the normal carrier level. The output pulse of the monostable circuit operated a sample and hold circuit to maintain the FM detector video output at its initial value during the duration of the monostable pulse.

The variables of the system include the level setting  $\epsilon$ , the monostable pulse width,  $t_0$ , the base band filtering in the amplitude and frequency demodulator channels and the distribution of this filtering, and any additional delays introduced between the two channels.

For optimum spike removal, the monostable pulse should be as wide as the majority of the spike and centered upon it. Thus, the optimum pulse width is a function of the IF bandwidth and of the modulation. Widening the pulse width beyond the minimum required value will increase the signal detail suppression caused both during spike removal and during false hold cases.

For  $\epsilon = 0$  no spike removal occurs. As  $\epsilon$  increases then near threshold nearly all spikes should be removed. Below threshold a higher percentage of the spikes are accompanied by larger amplitudes and  $\epsilon$  must be increased. On the other hand, increasing  $\epsilon$  leads to more false holds and to excessive signal suppression.

Figure 2 indicates the effect of varying  $\epsilon$  with  $t_0 = 60$  usec and a pre-sample and hold filter consisting of two poles each at 30 kHz.

While some spike reduction is accomplished, the picture quality reduction is unacceptable.

Following the work reported in the sections on the Frequency Locked Loop it is expected that substantial improvement could be obtained by a combination of:

- (a) Widening and peaking the pre-holding filter to narrow the click width without introducing excessive high frequency noise. (Such noise may introduce new



CNR = 5db  
IF Bandwidth: 70 kHz.  
Deviation: 5 kHz/Volt.  
Video: 3.5 frame/Second.  
No Spike Elimination.  
 $\epsilon = 0$



CNR = 5db  
IF Bandwidth: 70 kHz.  
Deviation: 5 kHz/Volt.  
Video: 3.5 frame/second.  
 $\epsilon = 0.2$



CNR = 5 db  
IF Bandwidth: 70 kHz.  
Deviation: 5 kHz/Volt.  
Hold time: 60 microsec.  
 $\epsilon = 0.4$

Fig. 2 Spike Elimination As A Function of Quantization Level,  $\epsilon$ .

"spikes" when "held".)

- (b.) Narrowing the post holding filter and using it to equalize the overall transmission during non-holding periods.
- (c) Narrowing the monostable pulse width to correspond to (a).
- (d) Introducing proper channel delays so that the pulse and the output spike occur simultaneously.

It remains to be seen whether the post holding transient will allow adequate equalization without excessive ringing. It also remains to be determined whether the results of such a system are sufficiently good to argue for its use instead of a more complicated, but allegedly superior system, such as a second order quantized frequency locked loop<sup>2</sup>.

National Aeronautics and Space Administration  
NgR 33-006-020

K. K. Clarke and F. R. Ergul

#### REFERENCES

1. F. R. Ergul, "Slow Scan TV Systems and the Transmission of Pictures Using FM, MSc Report, PIB, June 1968.
2. D. J. Hess and K. K. Clarke, "Quantized Second Order Frequency Locked Loop," IEEE Trans. on Aerospace and Electronic Systems, EasCon '68 Convention Record pp. 193-197.

#### SLOW-SCAN TV SYSTEM RESULTS

K. K. Clarke and F. R. Ergul

The video portion of the PIB experimental television system consists of a versatile flying spot scanner and receiver. These units are coupled with other laboratory designed RF transmitters and receivers to provide a wide range of video transmission facilities.

The raster generator horizontal sweep operates at 110 times the frequency of the vertical sweep. However, 10% of the time is consumed by retrace periods and hence, the basic raster is 100 lines. The frame rate is easily adjustable from 0.1 to 10 frames per second. Output video bandwidths of approximately 1 kHz to 50 kHz result from these frame rates.

The raster generator contains facilities for single frame or single line operation (line on or line deleted). It also has the capabilities of producing a raster delayed or advanced by any desired portion of a line. This capability allows one to compensate for channel delays of up to 10 milliseconds.

Figure 1 indicates the basic video spectrum produced by the blanking pulses alone

The addition of picture material broadens and blurs the high frequency terms but has little effect upon the first several peaks in the horizontal frequency spectrum.

Figure 2 indicates the changes caused in the spectrum by the slide of Fig. 5. Figure

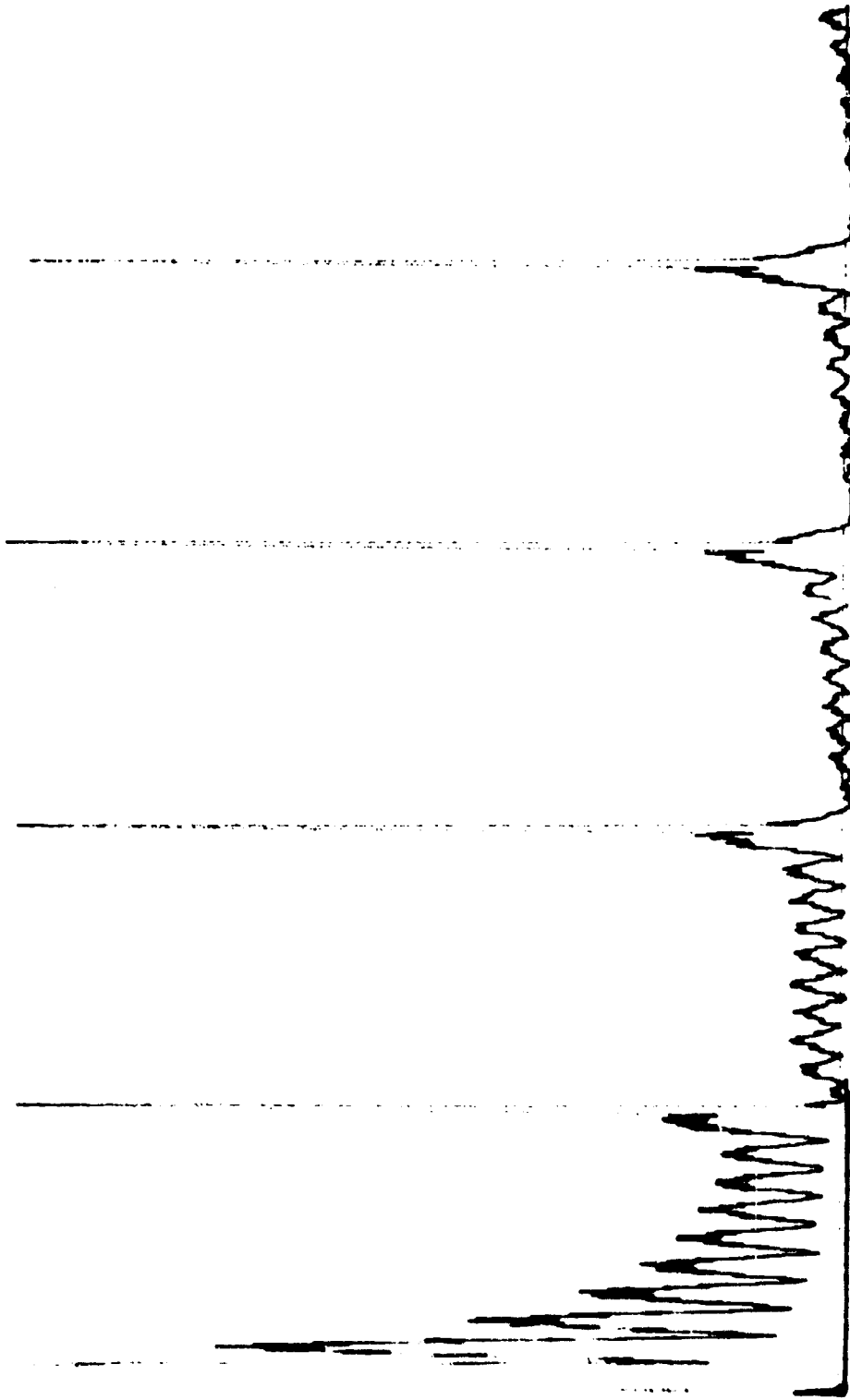


Fig. 1 Spectrum of Blanking Pulses Alone. Frame Rate 7.5 Frames/sec. Measured with Quantech 304 with 0-5 kHz Sweep, 180 Second Sweep Time, 16 Hz Bandwidth, 0.1 sec. time Constant, 360 mV Scale. Video Output 4V Peak-Peak

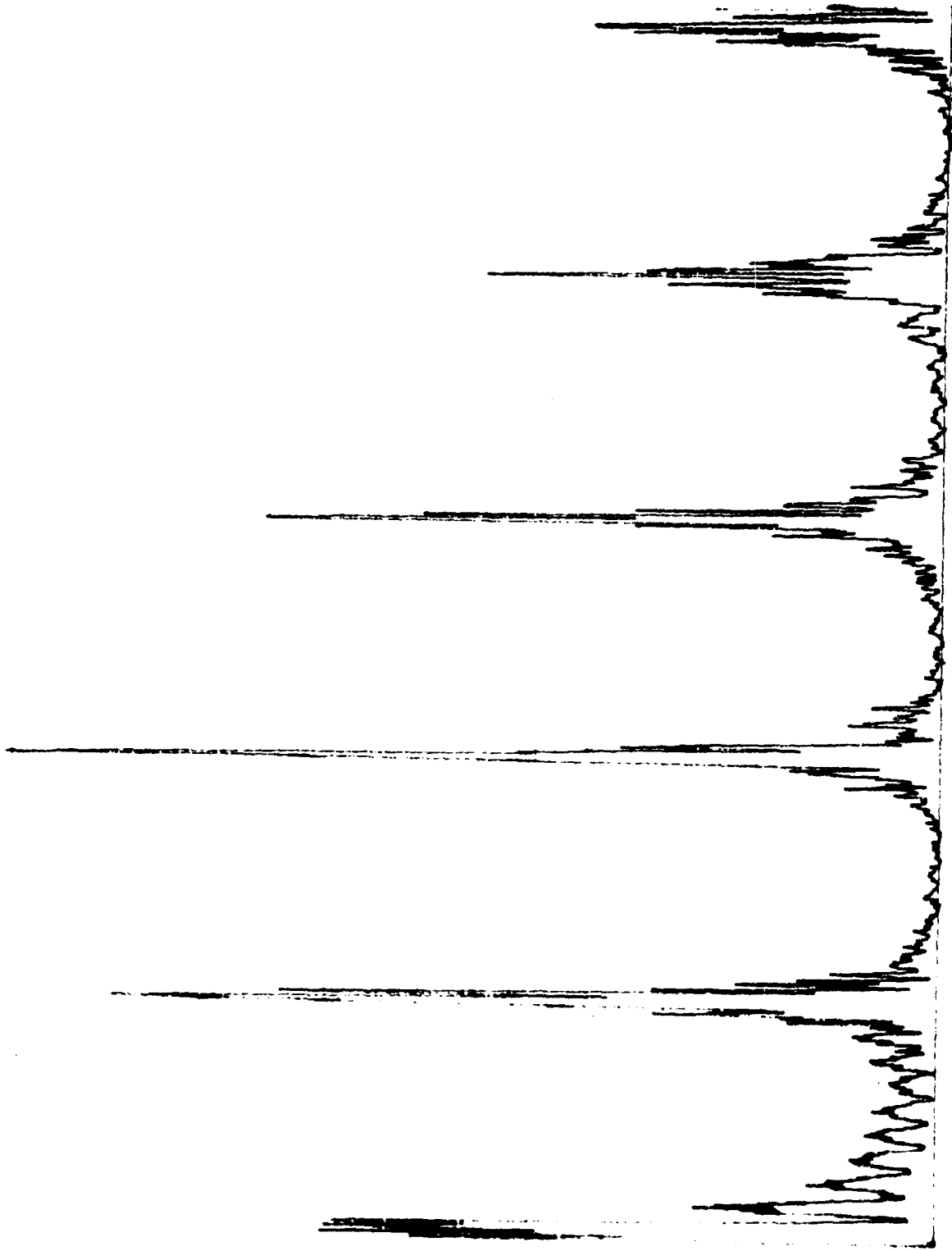
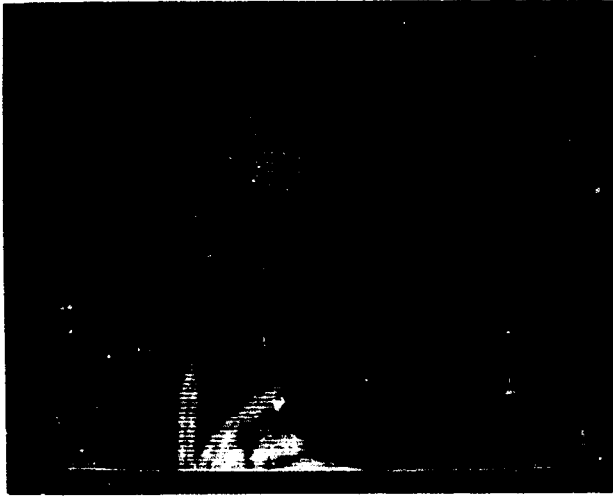
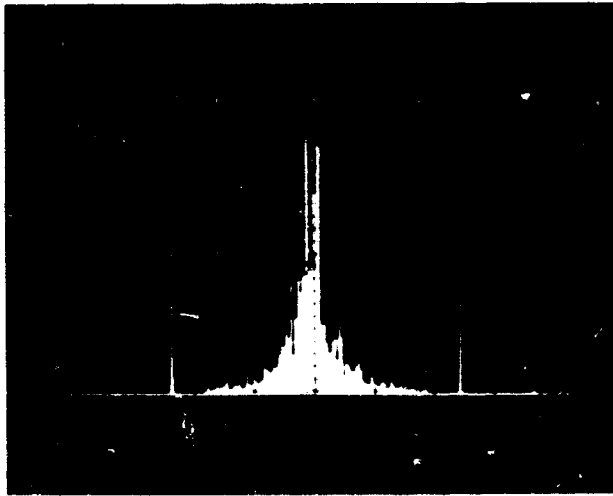


Fig. 2 Spectrum of Blanking Plus Slide of Fig. 3. Frame rate 7.5 Frames/sec. Measured with Quantech 304 with 0-5 kHz Sweep, 180 Second Sweep Time, 16 Hz Bandwidth, 0.1 sec. time Constant, 300 mV Scale, Video Output 4V Peak-Peak



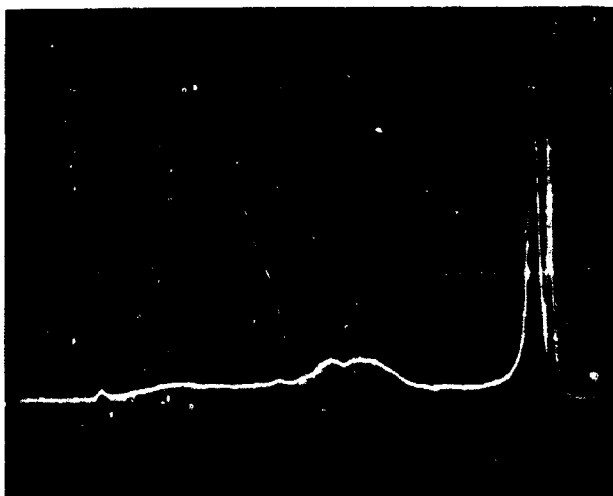
Slide

Video Spectrum

Minimum Frame Rate, 3.5  
frame/sec.

Markers: 25 kHz, 2.5 Vp-p  
Sinewave.

Horizontal Sweep 5 sec/cm.

Probability  
density function

Vertical Scale: 0.1 V/cm.

Markers: 15 and 25 Volts

Horizontal Sweep: 5 sec./cm.

Fig. 3 Three Different Viewpoints of Video Data

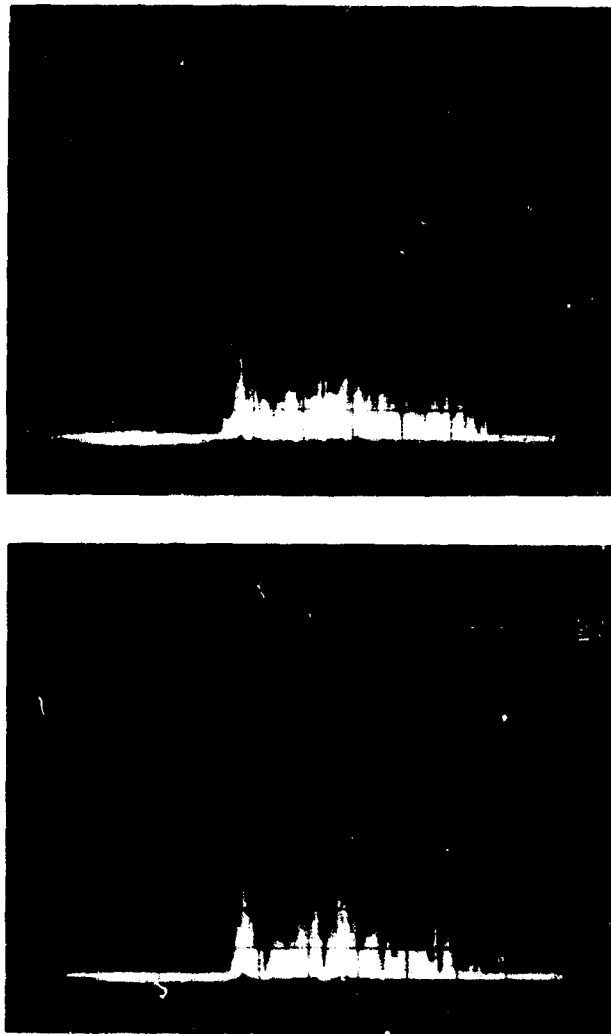


Fig. 4 FM Spectrum from Picture of Slide Shown in Fig. 3. 3.5 Frames/sec. Modulation Sensitivity. 30 kHz/volt. 11 v pp video Signal. Linear Vertical. 50 kHz/cm Horizontal

3 also shows an overall video spectrum as measured with the probability density of the video output as measured with a PIB probability density analyzer. The relatively flat probability density would be expected to lead to a relatively flat FM spectrum if the video is used to frequency modulate an FM generator with a beta of 5 or more. Figure 4 indicates such an FM spectrum using a 4 MHz PIB FM generator with more than 1 MHz deviation and modulation frequency capabilities.

These results are typical of data for a number of different slides as reported in Ref. 1. In all cases, a base band video spectrum and probability density measurement served to allow a reasonable prediction of FM spectrum shape and bandwidth.

Other material reported in Ref. 1 and not reproduced here includes the effects of high and low pass filtering upon picture detail.

National Aeronautics and Space Administration  
NgR 33-006-020

K. K. Clarke and F. R. Ergul

#### REFERENCES

1. F. R. Ergul, "Slow Scan TV Systems and the Transmission of Pictures Using Frequency Modulation," MSc Report - PIB, June 1968.

#### COMPARATIVE TV TRANSMISSIONS: SECOND ORDER QUANTIZED FREQUENCY LOCKED LOOP vs. LIMITER DISCRIMINATOR

D. T. Hess and K. K. Clarke

In order to investigate the effect of the "spike" reduction properties of the second order quantized frequency locked loop (FLL) in video transmission a comparative test was run with a modified version of the PIB TV system as the video source. For the purposes of this test the normal slide input was replaced by a bar pattern synchronized to the raster generator. The composite video output was used to frequency modulate a FM generator. The raster generator was operated in a single frame manner at a 0.2 frame/second rate. The modulating amplitude was adjusted so that the modulated signal occupied 11 kHz centered at 455 kHz. This FM signal was mixed with filtered white noise and applied to the FM receiver under test. The IF noise filter was a 12 kHz pp bandwidth "square" filter [nine pole] centered at 455 kHz.

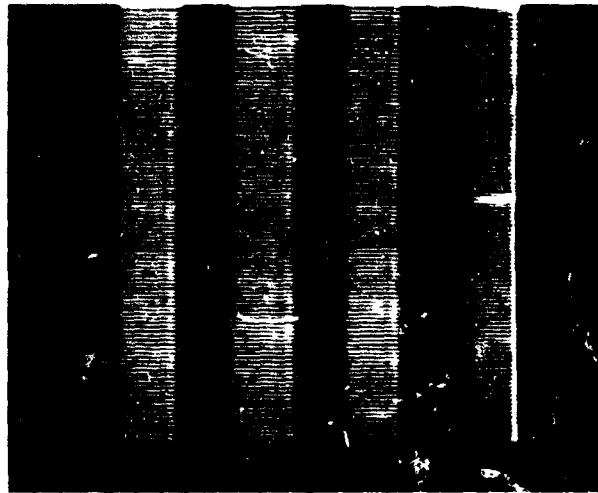
The FM receiver output was passed through a 1 kHz base band filter and presented on a PIB video monitor.

Single frame outputs were recorded on film. Figures 1 and 2 indicate comparative results for the second order, quantized frequency locked loop, and a well adjusted limiter discriminator combination.

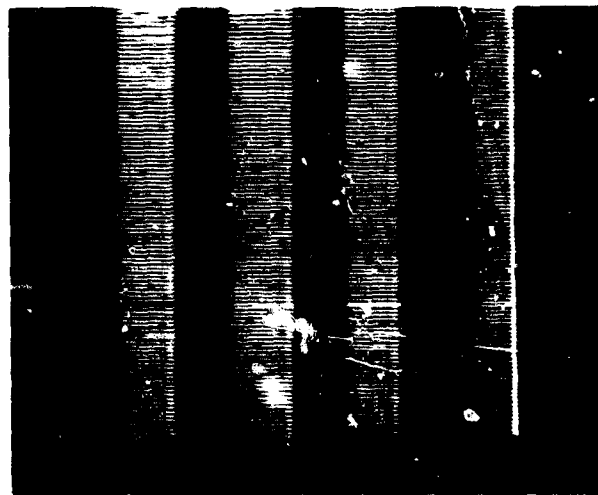
The conditions for the FLL were holding pulse width,  $t_0 = 70 \mu\text{sec}$  and normalized holding level,  $r = 0.28$ . The feedback loop zero was at 6.7 kHz while the closed loop poles were at 1.55 kHz [as a comparison, the optimum conditions for minimizing digital error rates in a  $\beta=2$ , 6 kHz IF system were found in Ref. 2 to be  $r = 0.30$  and  $t_0 = 80 \mu\text{sec}$ ]. Hence, as expected, the "optimum" pulse width for spike "suppression" in video is wider than it would be in the digital error case. (For the present example 70  $\mu\text{sec}$  as compared to the extrapolated value of 40  $\mu\text{sec}$  for the digital case.)

One would expect  $t_0$  to be larger for a given  $r$  since the amount of spike reduction necessary to cause the spike to be unnoticed in a picture is larger than the amount of reduction necessary to prevent an error in the digital situation. For a given  $r$  a wider  $t_0$  gives a better spike suppression when a spike occurs. Of course, the wider pulse also gives more signal suppression on false holds hence the wider  $t_0$  should be





a) Discriminator

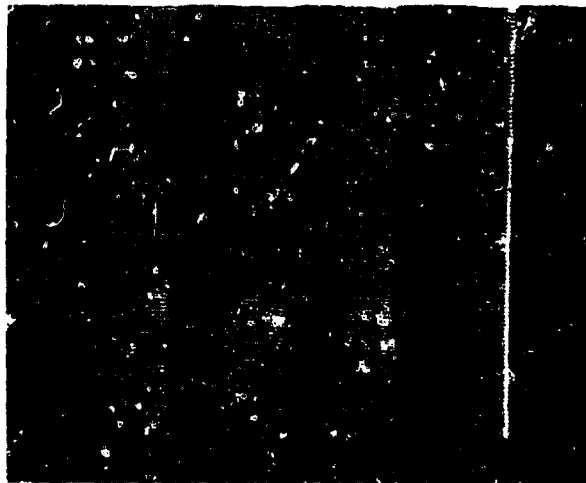


b) Frequency Locked Loop

Fig. 1 Spike Noise in a Video Bar Pattern Transmitted Via a Noisy FM Channel. Comparison of Frequency Locked Loop and Discriminator for 6 dB Carrier to Noise Ratio. 12kHz pp Square IF. 1kHz Baseband Filter.

coupled with a small  $\epsilon$ . The conversion of large spike noise into small spike noise and a gaussian-like term as  $\epsilon$  is increased as illustrated in an accompanying article. With digital transmission the small spikes are unlikely to cause errors, however in video they may be visible. [The visibility of a spike is of course a function of oscilloscope intensity and of the gamma of the film.]

Comparison of the two figures clearly indicates a significant reduction in the number and intensity of "spikes" in the FLL case. Whether the 4 dB FLL picture



a) Discriminator



b) Frequency Locked Loop

Fig. 2 Spike Noise in a Video Bar Pattern Transmitted Via a Noisy FM Channel. Comparison of Frequency Locked Loop and Discriminator for 4 dB Carrier to Noise Ratio. 12kHz pp Square IF. 1kHz Baseband Filter.

would be acceptable in places where the 4 dB discriminator picture would not, is an, as yet, unanswered question.

Further studies to be conducted in this area include comparative transmissions with phase locked loop and FMFB demodulators as well as the study of pre-emphasized signals upon the various circuits. The literature<sup>2</sup> reports that FMFB circuits cannot handle preemphasized material properly. However, the FLL operates in a completely satisfactory manner for relatively high deviation, and relatively high modulating fre-

quency signals. Hence, further overall system gains may be achieved by utilizing pre- and post-filtering circuits of this type.

National Aeronautics and Space Administrator  
NgR 33-006-020

D. T. Hess  
K. K. Clarke

#### REFERENCES

1. D. T. Hess and K. K. Clarke, "Second Order Quantized Frequency Locked Loop" IEEE Professional Group on Aerospace and Electronics Systems, Eascon '68 Convention Record, p 193-197.
2. A. J. Giger and J. G. Chaffee, "The FM Demodulator with Negative Feedback, BSTJ, July 1963, Part I p 1109-1135. Section 4.3.3 on p 1131-1133 concerns television threshold tests.

#### COMPARISON OF DATA COMPRESSION SCHEMES

R. Stroh and R. R. Boorstyn

It is quite apparent that if signals to be transmitted were stationary and perfectly bandlimited, there would be no data compression problem. One would sample at the Nyquist rate and transmit these samples, or coded versions of them. No further data compression would be possible. Real signals do not behave this way, however. They are generally not bandlimited and their statistics are either not known or varying in a non-stationary manner. How does one then perform data compression? One good engineering technique is to first oversample to some extent and then use various types of predictive techniques to reduce the redundancy. Such methods are now well known and have been summarized in the literature<sup>1</sup>.

But these various cut-and-try procedures offer no real insight into the problem of data compression. In an attempt to analyze these various schemes and others that may be developed we have chosen to pick some signal models that deviate from the perfectly bandlimited one, providing some complexity of structure to make them meaningful yet sufficiently simple to enable analysis to be carried out. The two simplest models reported on here are a stationary Gaussian random process, and a discrete Nth order Markov process. For both classes of models and attempt is made to relate the mean-squared reconstruction error to sampling interval for various compressor schemes.

(1) Gaussian process  $x(t)$ . Here we assume a power spectral density

$$S_x(\omega) = \frac{2}{1 + \omega^2}$$

and autocorrelation function

$$R_x(t) = e^{-|t|}$$

Assume samples are taken uniformly every  $T$  sec. Several methods of reconstructing the original signal have been compared. These include various sampling techniques as well as predictive techniques.

(a)  $\sin x/x$  reconstruction. Here the transmitted samples are passed through a lowpass filter with bandwidth  $B = 1/2T$ . It is then found that the mean-squared reconstruction error is given by

$$\overline{e^2} = 2\left(1 - \frac{2}{\pi} \tan^{-1} \frac{\pi}{T}\right)$$

(b) pre-filtering to  $B = \frac{1}{2T}$  prior to sampling, then the same reconstruction method as above. The mean-squared error is then found to be one-half that above.

$$\overline{e^2} = \left(1 - \frac{2}{\pi} \tan^{-1} \frac{\pi}{T}\right), \text{ with pre filtering.}$$

(c) An alternate reconstruction technique, due to Tufts<sup>2</sup>, that minimizes  $\overline{e^2}$  where pre-filtering is not used. For this case

$$\overline{e^2} = \coth T - \frac{1}{T}$$

(d) A finite Karhunen-Loève representation of the random process  $x(t)$ . Here the representation  $\hat{x}(t)$  is given by

$$\hat{x}(t) = \sum_{n=1}^N a_n v_n(t) \quad 0 \leq t \leq \tau$$

where a  $\tau$ -second piece of  $x(t)$  is taken and the  $v_n(t)$ 's are fixed orthonormal functions. The  $N$  discrete numbers  $a_n$  are the numbers to be transmitted and are random variables. The orthogonal functions  $v_n(t)$  are chosen to minimize the mean-squared error power

$$\overline{e^2} = \frac{1}{\tau} E \left\{ \int_0^{\tau} [\hat{x}(t) - x(t)]^2 dt \right\}$$

The resultant expression for  $\overline{e^2}$  vs.  $\tau/N$  (time between samples for this technique) is obtained as the solution of transcendental equations, and is shown plotted in Fig. 1 for  $\tau = 4$  and 10 sec. Also plotted for comparison are the results for the sampling techniques mentioned above.

Note that for this particular power spectrum the pre-filtered,  $\sin x/x$  reconstruction technique is the best of the four shown, but is very closely followed by the Karhunen-Loève technique.

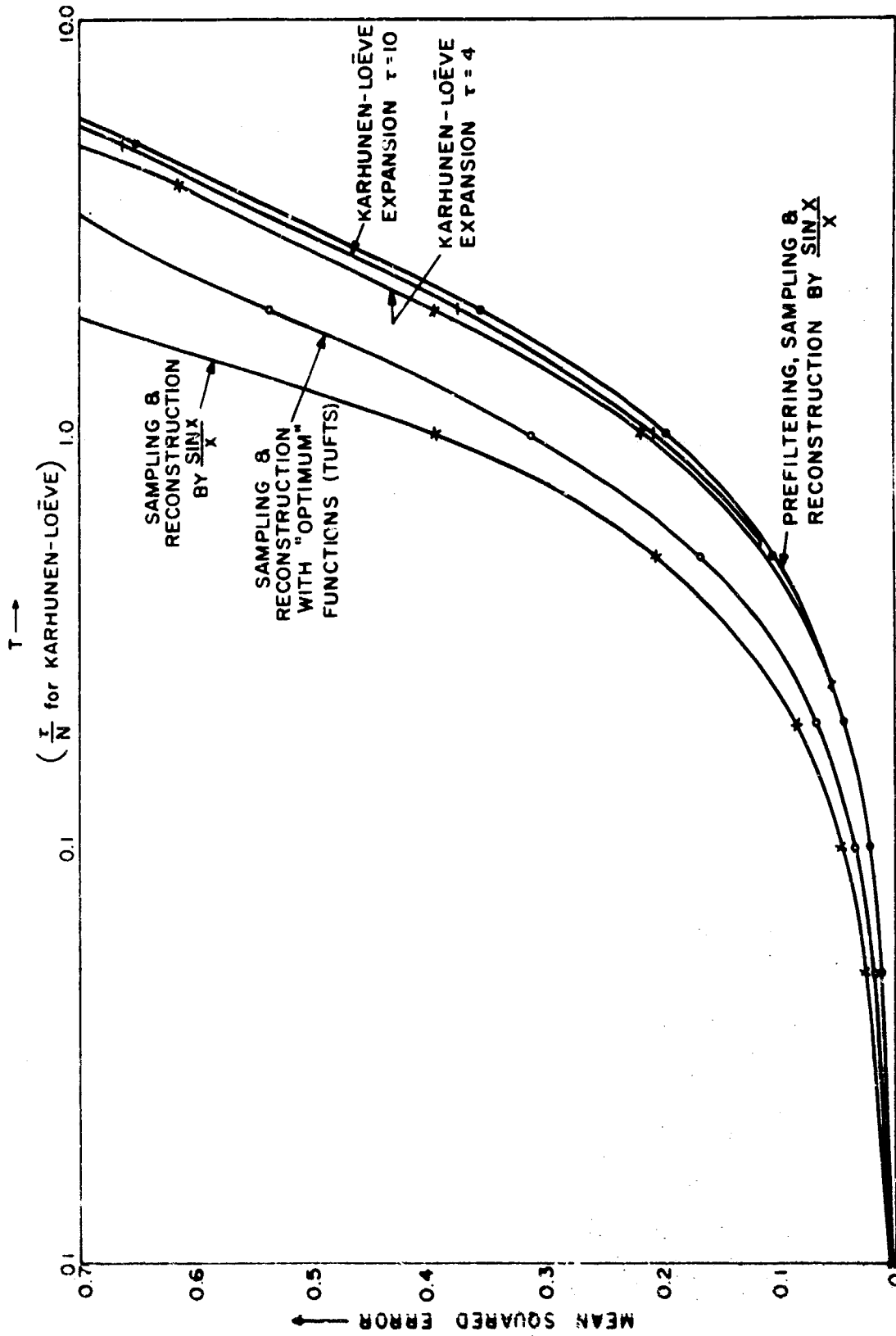


Fig. 1 Digital Error Rates

How do these techniques compare with the ad hoc compressive schemes that are used in practice? As noted earlier these are in general hard to analyze, but Ehrman<sup>3</sup> has obtained the approximate theoretical mean time between transmitted samples for three common techniques<sup>1</sup> - the floating aperture zero-order predictor, the zero-order interpolator, and the fan (first order) interpolator, assuming a Gaussian Markov signal source as done here. His results, valid only for small sampling intervals on the average, and adapted to the example taken here, are

$$\overline{e^2} = 0.6 E(T) \text{ floating aperture predictor}$$

$$\overline{e^2} = 0.33 E(T), \text{ zero-order predictor,}$$

$$\overline{e^2} = 0.23 E(T), \text{ fan interpolator.}$$

In all three cases,  $E(T) \ll 1$ , the half aperture widths  $\Delta x$  are assumed small compared to the standard deviation of the signal process (which is unity here), and the reconstruction error is assumed uniformly distributed between  $\pm \Delta x$ .

As a comparison with the sampling and Karhunen-Loève techniques described above, we may assume  $T$  and  $\tau/N \ll 1$  in the equations given earlier. It is then found that

$$\overline{e^2} = \frac{2}{\pi} T = 0.203 T, \text{ sampling with pre-filtering and } \frac{\sin x}{x} \text{ reconstruction.}$$

$$\overline{e^2} = 0.405 T, \text{ sampling without pre-filtering and with } \frac{\sin x}{x} \text{ reconstruction,}$$

$$\overline{e^2} = 0.33 T, \text{ sampling without pre-filtering and using Tuft's optimum reconstruction.}$$

$$\overline{e^2} = \frac{2}{\pi} \frac{\tau}{N} = 0.203 \frac{\tau}{N}, \text{ Karhunen-Loève expansion.}$$

Note that sampling with pre-filtering and the Karhunen-Loève expansion give almost identical results, and that they are better than the predictor and interpolators. It must also be pointed out that the latter techniques require the transmission of timing information, so that the advantage of sampling is even greater than indicated above. We do not mean to imply, however, that the aperture techniques are inferior: there may be other signals on which they perform better than sampling. The adaptivity and relative simplicity of the aperture techniques are factors in their favor.

(2) Discrete state Markov source. An  $N$ -state Markov chain has been assumed, and both the zero-order predictor and the zero-order interpolator have been considered. Two cases have been analyzed: first, with the aperture width less than the spacing be-

tween adjacent source levels, so that there is no reconstruction error; second, with the aperture greater than the source level spacing, with  $\pm 1$  level reconstruction error allowed.

The compressibility of the source symbols, as measured by the entropy in bits/source symbols, is then found for the zero-order predictor to be given by

$$H_{zop} = \frac{H_x + H_R}{1 + E(n)} \text{ bits/source}$$

where

$H_x$  is the information content of the transmitted sample values,

$H_R$  is the information content of the run length between transmitted samples,

and  $E(n)$  is the average run length.

Average run lengths for a zero-order predictor with no allowable error operating on a discrete state Markov source have previously been computed by Stanley and Liu.<sup>4</sup> Using their results, and assuming as an example, a particular 15 state Markov chain possessing a uniform stationary distribution, and characterized by a relatively large probability of remaining in the same state or going to an adjacent state, the source entropy is calculated to be 2.73 bits/symbol.

For a zero-order predictor, with no reconstruction error, we also find

$$E(n) = 1.05 \text{ symbols}$$

$$H_x = \log_2 15 = 3.9 \text{ bits}$$

$$H_R = 2.04 \text{ bits}$$

$$H_{zop} = 2.91 \text{ bits/source symbol.}$$

Thus, a zero-order predictor used with efficient coding can achieve a transmission rate fairly close to the entropy of this particular source.

This method has been extended to the case where the aperture is greater than the source level spacing. For example, suppose  $\pm 1$  level reconstruction error is allowed. The probability of a run of length  $n$  within the aperture about a level is easily calculated. Once the run length probabilities have been found the entropy may be computed as above. It has also been shown that the run length probabilities for a zero-order interpolator may be written in terms of powers of sub matrices of the Markov transition matrix. For the example considered above, the expected run lengths following one of the "interval" states of the source for the zero-order predictor and interpolator with  $\pm 1$  level error are

$$E(n)_{zop} = 2.10 \text{ symbols,}$$

$$E(n)_{zoi} = 2.62 \text{ symbols.}$$

While the work described above has barely scratched the surface of the problem, it at least provides a little insight into the performance of the simple data compression techniques.

National Aeronautics and Space Administration  
NgR 33-006-040

R. R. Boorstyn and R. Stroh

#### REFERENCES

1. Special Issue on Redundancy Reduction, Proc. IEEE, Vol. 55, No. 3, (March 1967)
2. D. W. Tufts, "A Sampling Theorem for Stationary Random Processes," MIT Research Lab. of Electronics, Cambridge, Mass., Quarterly Progress Report. 53, (1959) pp. 87-93.
3. L. Ehrman, "Analysis of Some Redundancy Removal Bandwidth Compression Techniques," Proc. IEEE, Vol. 55, No. 3, (1967) pp. 278-297.
4. T. P. Stanley and B. Liu, "Data Compression for Discrete Markov Signals," Proc. Nat'l Electronics Conference, Vol. XXIII (1967) pp. 534-539.

#### OPTIMAL ADAPTIVE CONTROL FOR DATA COMPRESSION SYSTEMS

P. Dosik and M. Schwartz

The object here is to determine an optimal controller to minimize the mean squared error between discrete input data,  $x_n$ , and reconstructed compressed discrete output data,  $y_n$ . We plan to evaluate the optimum controller solution and minimum normalized rms error for several data models and compressor algorithms. The present plan is to use a uniformly distributed independent data model and the uniformly distributed first order Markov data model. The compressor algorithms under consideration are both the zero and first order predictors and interpolators. Tables or curves will be obtained from computer runs and will list the compressor aperture,  $K$ , vs. buffer fill or state,  $S$ , and the minimum normalized rms error for several values of the following parameters:  $b$ , the number of input amplitude bits,  $L$ , the buffer length, and  $C$ , the transmission ratio. With these data, the designer will be able to select suitable parameters to satisfy his data compression and rms error requirements.

As a check on the optimal controller solution, the data models and data compression system using the corresponding optimal controller solution will be simulated on a computer to measure the actual normalized rms error. As a test of the sensitivity of the optimal controller solution to the input data statistics, the first order Markov data will be fed into systems optimized for independent data, and independent data will be fed into systems optimized for first order Markov data. Finally, real telemetry data will be obtained, if possible, and fed into these optimized systems to determine the practical use of the chosen data models.



Progress thus far consists of the following: The controller-buffer system has been modeled as a discrete Markov process and a method of solution adopted using an iterative dynamic programming algorithm based on the work of Howard<sup>1</sup>. Once the statistics of the input process  $x_n, n=0, 1, \dots$  and the compressor algorithm have been specified, an optimum controller can be determined using this technique.

For the case of uniformly distributed independent input data and the zero order prediction compressor algorithm, the problem of determining the optimum controller has been solved. The solution is in an iterative form and is best computed on a general purpose digital computer for all possible values of interest of the various parameters noted above. The iterative solution has been programmed in FORTRAN on a digital computer and is presently being debugged. The status of the programming is: writing in FORTRAN completed; program cards punched, verified and listed; diagnostic errors are being eliminated from initial compilations. In order to check the program results, one test case for the specific values of  $b = 1$ ,  $L = 4$ , and  $C = 2$  was computed by hand yielding a mean squared error,  $e^2 = 1/26$ , and the following controller rules:

S(Buffer State)	K(Aperture)	
0	0	$b = 1$
1	0	$L = 4$
2	0	$C = 2$
3	1	$e^2 = 1/26$

For the case of uniformly distributed first order Markov input data and the zero order prediction compression algorithm, the solution of the problem of determining the optimum controller is presently being attempted. The complexity of the mathematics in the Markov case is many times greater than that of the independent case.

National Aeronautics and Space Administration  
NgR 33-006-040

P. Dosik  
M. Schwartz

#### REFERENCE

1. R. A. Howard, "Dynamic Programming of Markov Processes," (Cambridge: MIT Press, 1968).

#### INFORMATION CONTENT OF TIME SERIES AND PICTURES

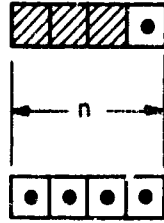
A. E. Laemmel

In his original paper on communication theory<sup>1</sup>, C. E. Shannon defined two sequences of entropy functions,  $F_n$  and  $G_n$ , and showed they approach a common limit  $H$ , which can then be called the information per symbol of the time series.  $F_n$  was defined as the conditional entropy of an element given the previous  $n-1$  elements, and  $G_n$  was defined as the total entropy of a block of  $n$  successive elements. These en-

entropies are related as follows:

$$F_n = n G_n - (n-1) G_{n-1} \tag{1}$$

$$G_n = \frac{1}{n} \sum_{i=1}^n F_i \tag{2}$$



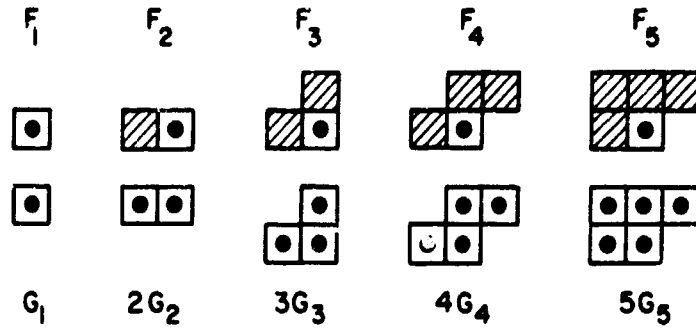
$$H = \lim_{n \rightarrow \infty} F_n = \lim_{n \rightarrow \infty} G_n \tag{3}$$



$$F_{n+1} \leq F_n, G_{n+1} \leq G_n, H \leq F_n \leq G_n \tag{4}$$

In the diagrams above, the dots show the element being guessed and the shaded boxes show the elements assumed known. This work is concerned with possible generalizations of conditional entropies such as  $F_n$  which correspond to various patterns of known elements near the element being guessed. It will be assumed that the reader is acquainted with the basic ideas of communication theory such as the equivalence of the difficulty of guessing or predicting a message and the difficulty of transmitting that message, and how the entropy function measures the corresponding "difficulty of guessing," "uncertainty," or "information content". Note that if the elements of the time series are statistically independent  $F_n = F_1$ , and therefore that  $F_1 - F_n$  measures the statistical dependence or correlation between elements. Certain generalizations of the sequences  $F_n$  and  $G_n$  will be discussed here in one and two dimensions (time series and pictures).

A suitable generalization for  $F_n$  is the conditional entropy of an element  $\square$  given  $(n-1)$  known elements  $\text{shaded box}$  in a certain pattern near the element being guessed, and for  $G_n$  is the average entropy of the total block of  $n$  elements. It is assumed that probabilities, and therefore the entropies, are invariant to translations. A generalization of the sequence of blocks of greater and greater length in one dimension is a sequence of nested blocks, each one including the previous one. Such a sequence is shown in Fig. 1. For this example, relations such as Eq. (1) and Eq. (2) are not true because the element added to the block is not the one being guessed. However, it is obvious that  $F_n$  is monotonic non-increasing because each increase in  $n$  adds another known element to those already known. If the nested blocks are chosen as in Fig. 2 the relations Eq. (1) and Eq. (2) will hold, but it is no longer necessarily true that  $F_n$  is monotonic non-increasing. Returning to the sequence of nested patterns in which known elements are added, many different limits are possible as  $n \rightarrow \infty$ . The meaning



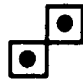
$F_3 \neq 3G_1 - 2G_2$  (but  $F = 3G_3 - 2G'_2$  where  $G'_2$ : )

Fig. 1 Known Elements Added

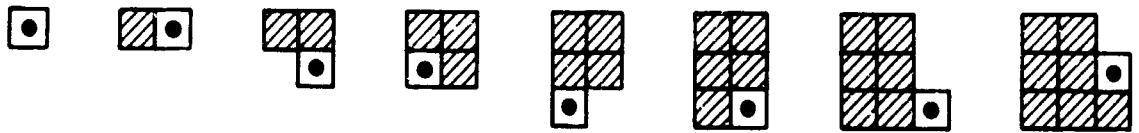


Fig. 2 Guessed Elements Added

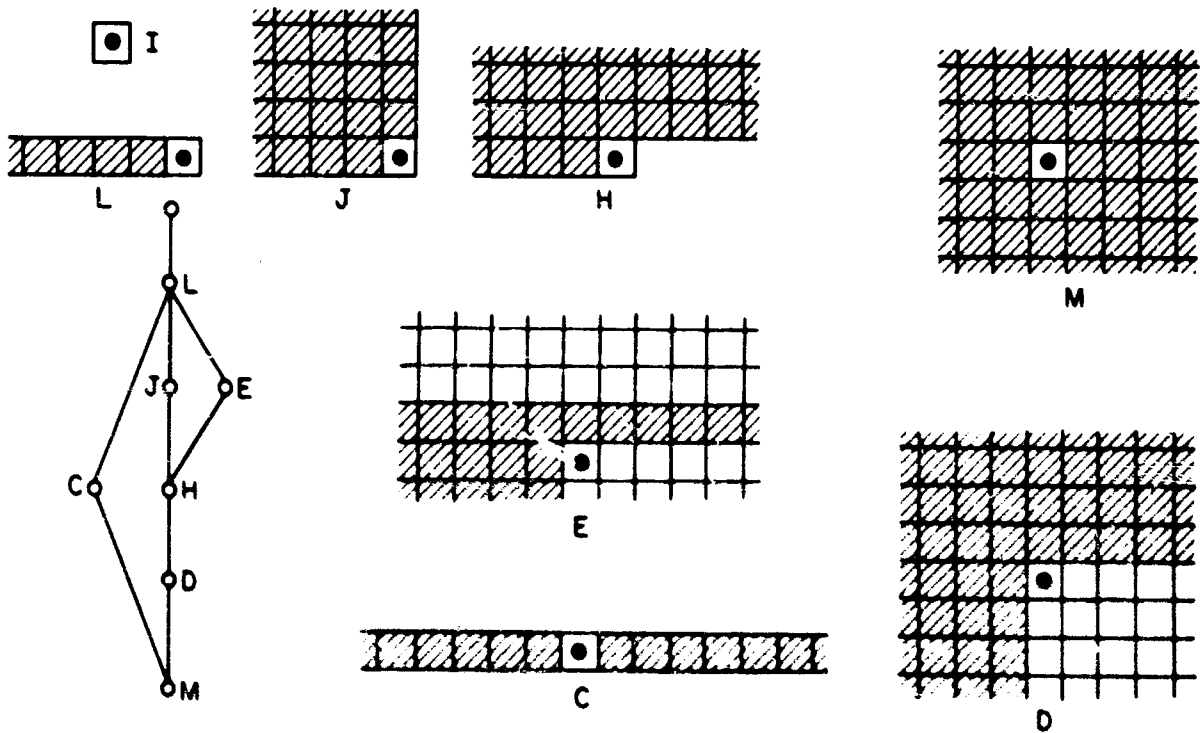


Fig. 3 Various Layouts of Block Sequences

of the limit of the quantity  $\lim_{n \rightarrow \infty} F_n$  can be diagrammed directly as an element  $\square \bullet$  with an infinite block of  $\square \diagup$  as shown in Fig. 3. The various values of  $F_n$  form a partly ordered set, and this could be made into a lattice by adding unions and intersections of known elements. The following questions arise in connection with these generalized  $F_n$  and  $G_n$  sequences:

- (i) What are the necessary and sufficient conditions on a sequence of nested blocks in order that  $F_n$  and  $G_n$  approach limits as  $n$  approaches infinity?
- (ii) If several limits are possible for the same time series or picture, which one gives the information content and what is the significance of the others?
- (iii) How should the block sequence be chosen to make  $F_n$  approach its limiting value as rapidly as possible?

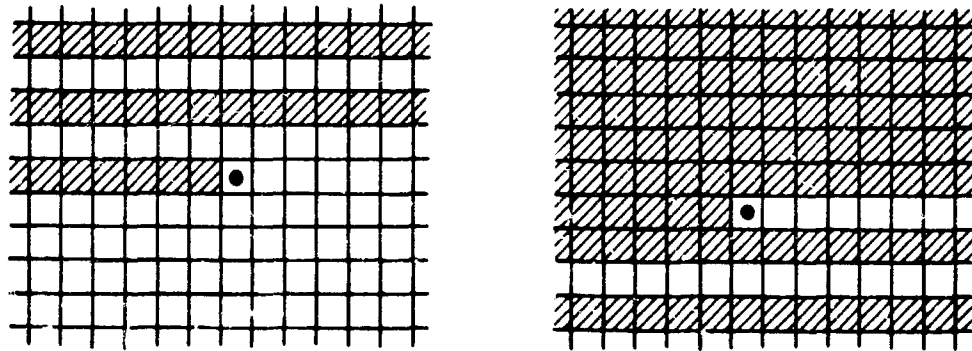
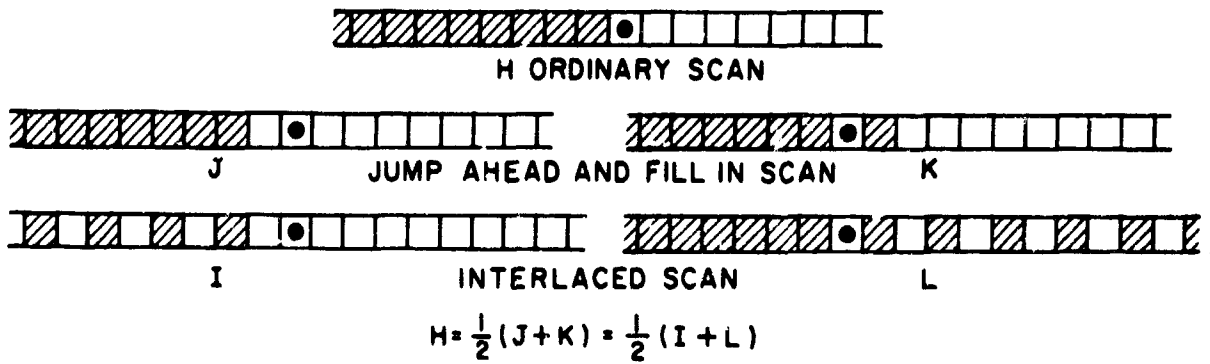
Complete answers to these questions are not available; however, some preliminary results will be sketched here. The first of these results is that  $F_\infty$  (meaning the limit of  $F_n$  as  $n \rightarrow \infty$ ) will be equal to  $H$  (true information content per element) if it corresponds to a block derived from a regular scanning path. The latter will be defined as follows: In one dimension number the elements from left to right ... -3, -2, -1, 0, 1, 2, 3 ... A sequence of numbers can be thought of as the order in which the various elements are transmitted. The above sequence unaltered is the ordinary method of scanning. Another scan corresponds to the sequence ... 1 3 2 5 4 7 ... , the transmitter alternately jumping ahead and filling in. If any number in this sequence is made to correspond to  $\square \bullet$ , then all previous numbers correspond to  $\square \diagup$  since they have already been transmitted and are known to the receiver. This results in two patterns as shown in the second line of Fig. 4. The information content  $H$  is the average of the entropies  $J$  and  $K$  corresponding to these patterns. Still another scan in one dimension corresponds to the sequence ... -3, -1, 1, 3, 5 --- -2, 0, 2, 4 ... diagrammed as the interlaced patterns on the third line in Fig. 4. Again  $H$  is the average of  $I$  and  $L$ . The five entropies mentioned are ordered as follows:

$$L \leq K \leq H \leq J \leq I$$

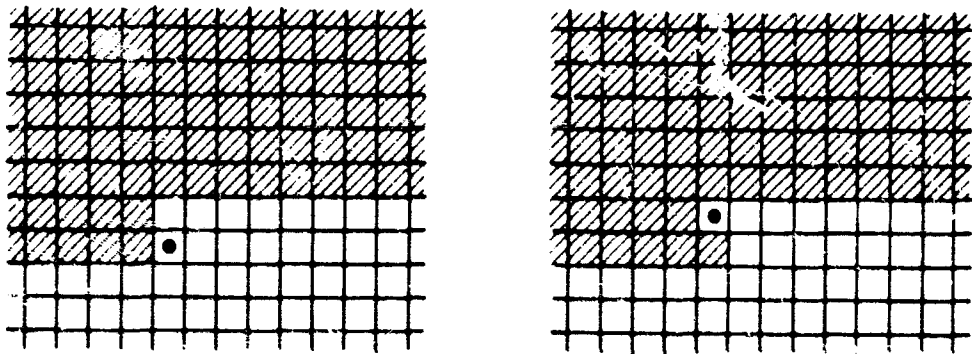
These different entropies have been introduced both to improve practical estimates of the information content and to study the efficiencies of various finite compression codes in reducing redundancy. In connection with the former, consider the word or letter guessing game of Shannon<sup>2</sup>, and note that since  $I \leq F_1$  it follows that

$$H \leq \frac{1}{2} F_1 + \frac{1}{2} L$$

If it turns out that it is easy for a person to guess a word in a sample of text given all previous words, the following word, the third following word ... (pattern  $L$  of Fig. 4),



**INTERLACED SCAN**



**A SIMPLE "SPACE FILLING CURVE"**

Fig. 4 Various Scanning Patterns

then a low upper bound on the information per word of that type of text would be obtained. Two of the many scanning paths in two dimensions are also shown in Fig. 4.

The value and significance of the entropies corresponding to the diagrams C and M of Fig. 3 are of considerable interest. Models can easily be constructed for which these entropies are zero in one and two dimensions, and they are never greater than the

information content  $H$ . Models can also be constructed in which  $C$  or  $M$  measure suitably defined "style" or "dirt" information, while  $H$  measures the total information (style or dirt information plus "meaning" information). Consider the transmission by facsimile of a typewritten page in which the resolution elements are black or white. If the whole page is known except for one resolution element it seems very likely that the whole meaning can be exactly guessed. Therefore, if the entropy  $M$  is not zero, it must be a measure of the uncertainty that the omitted element is black because of dirt or white because of a typewritten imperfection. Whether  $M$  has any such meaning in practice needs to be investigated. Suppose now that all words of a text are known except one. Can the meaning of the text be seen even though there may be some uncertainty as to whether, for example, BIG or LARGE was used by the author? (It is quite possible the context would rule out other adjectives such as SMALL or RED). Models are being sought to test these and other related concepts, and some experimentation is going on to determine the numerical values of the entropies. In particular, D. Fessler has determined some of the entropies of Fig. 1 for typewritten pages.

U. S. Army Research Office, Durham  
DA-31-124-ARO(D)-380

A. E. Laemmel

Joint Services Technical Advisory Committee  
AF 49(638)-1402

#### REFERENCES

1. C. E. Shannon, "The Mathematical Theory of Communication," Bell System Tech. Jour., Vol. 27, July 1948, pp. 379-423. Also in book form: Univ. of Ill. Press 1949.
2. C. E. Shannon, "Prediction and Entropy of Printed English," Bell System Tech. Jour., Vol. 30, Jan. 1951, pp. 50-64.
3. D. Fessler, "Transmission, Compression and Prediction of Black, White Picture Information," Report for MS(EE), P. I. B., June 1968.

#### EXTREMAL STATISTICS IN COMPUTER SIMULATION OF DIGITAL COMMUNICATION SYSTEMS

M. Schwartz and S. Richman

In a previous report<sup>1</sup> the field of extremal statistics was summarized and its extension to the computer simulation of low error digital communication systems indicated.

Briefly, it may be shown that asymptotically many of the most common probability distributions follow a simple exponential law when expanded about an arbitrary point on their tails<sup>2</sup>. This exponential is a function of two parameters which depend on the underlying statistical distributions. If one can determine these two parameters, one is in a position to measure relatively high error rates, using Monte Carlo simulation, then extrapolate to the desired low error rate region using the exponential approximation. In the previous report, details of the computer estimation of the two parameters, and Monte Carlo simulation of known probability density functions, were described and re-

sults presented. It was indicated that the use of extremal statistics resulted in a saving of at least one order of magnitude in computation time.

The previously reported work has now been extended to the simulation of two specific digital feedback communication systems. In both cases low probabilities of error were successfully estimated, with the desired saving of at least a factor of 10 in the processing.

One of the two systems simulated is a binary signalling system, the other an M-ary PAM type system, with the information transmitted as one of M possible amplitude levels. In both cases white gaussian noise is assumed added during forward transmission (this could be thermal noise introduced at the receiving antenna, front end receiver noise, or a combination of the two in general). The feedback path is assumed error free. Errors in signal detection due to the noise may occur and it is desired to estimate the probability of error in both systems.

Both systems may have potential usefulness in space-ground communications. In both cases the information is to be transmitted from space to earth. The forward transmission path is thus limited in power. It is assumed a feedback path from ground to vehicle with much larger power capability is available, so that the effects of noise may be neglected over this path. (Further computer simulation is planned to investigate the effect of noise on the feedback path, as well as other signal disturbances such as fading, for example). Such feedback systems hold great interest in the statistical communications field currently because of their expected high performance (low probability of error) in noise with a minimum of coding effort required.

The binary system investigated represents the application of sequential decision theory of statistics<sup>3</sup> to statistical communications. The operation at the receiver may

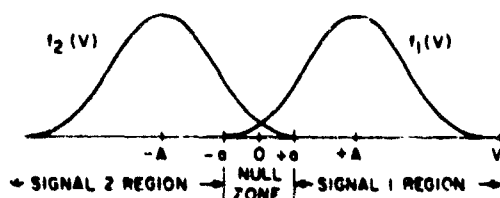


Fig. 1 Received Signal Space, Binary Feedback

be visualized by referring to Fig. 1. Here  $v$  represents a received sample of the composite signal plus noise. As an example, if one binary signal has a received amplitude of  $+A$  volts, while the other is  $-A$  volts (this is the example of bipolar signaling), the resultant probability density functions  $f_1(v)$  and  $f_2(v)$ , respectively, appear in Fig. 1.

In normal binary signalling one would declare signal 1 received if the received signal plus noise sample were to exceed 0, and signal 2 received if the received signal plus noise fell below zero. For small signal-to-noise ratios (SNR), as normally encountered in deep space-ground communications, the resultant probability of error would be intolerably high. To improve the performance, a null zone of width  $\pm a$  about 0 is set up. If the composite received signal falls in this region a decision is deferred and the transmitter asked, via the feedback path, to repeat the signal. The first composite signal sample is then stored and added to the second received sample after transmitter repetition. The two combined received samples are then tested and a decision made only if the sum exceeds  $+a$  or falls below  $-a$ . A third repeat is requested if the sum again falls in the null zone.

This procedure is repeated until the combined received samples fall outside the null zone. (To prevent the system from cycling indefinitely or for too long a time, the number of transmissions may be truncated after a specified interval and a definite decision made.) Such a sequential procedure with a statistically variable number of transmissions may be shown to asymptotically provide a 50% decrease in average transmission time over an equivalent system without feedback with a fixed number of repeats<sup>3</sup> this for the same SNR and probability of error.

Although the scheme outlined is relatively simple to describe, the analysis is quite complex, since the received signals summed are those falling in the null zone only. The statistical behavior of the composite random variable representing the sum of such received signals is difficult to determine and the resultant probability of error not easily found. In fact, asymptotic results only for the probability of error are available; those for small SNR and a large average number of transmissions, or those for high SNR and very small numbers of transmissions. The region in between can only be estimated by extrapolation or by bounding techniques. Computer simulation of such a system is, however, simple to perform. For small probabilities of error, however, the computer time involved can become quite large so that extremal statistics is an obvious answer.

The methods of extremal statistics were therefore used, in a computer simulation of this system, to estimate the probability of error. 10,000 total repeats were used in each simulation, 20 for estimating the two constants for the actual determination of the probabilities. Results are shown in Fig. 2. Note that the experimental (simulation) points follow quite closely an approximate performance line obtained by extrapolating from Wald's asymptotic results, valid for large numbers of transmissions and small probabilities of error<sup>4</sup>. The curves of Fig. 2 are for a SNR of  $\frac{1}{2}$ . A reference curve, that showing the performance of a one-way system with no feedback and a fixed number of repeats, is included. Note that the two curves differ approxi-



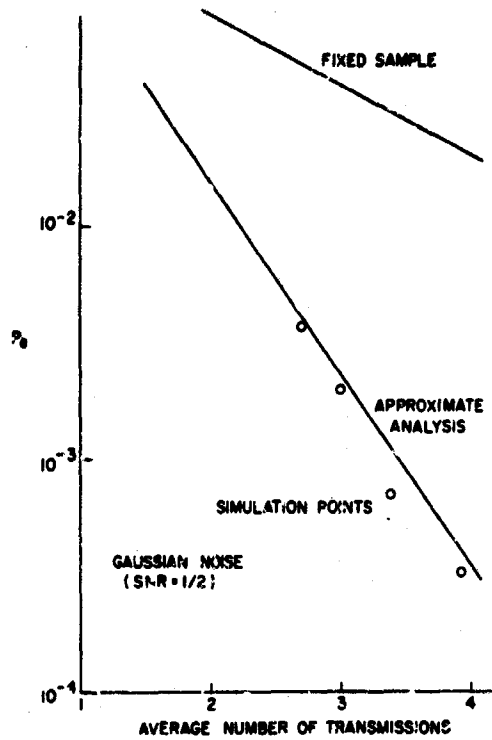


Fig. 2 Computer Simulation of Binary Sequential Decision Feedback System

mately by a factor of two in the transmission time, as would be expected from Wald's asymptotic results.

The second feedback communications system simulated, for which extremal statistics were used in estimating system performance (probability of error), was one first suggested and analyzed by J. P. Schalkwijk<sup>5, 6</sup>. A simplified block diagram appears in Fig. 3. The information to be transmitted consists of one of  $M$  amplitudes,  $\theta = \frac{j}{M}, j = 1, 2, \dots, M$  (the amplitudes are normalized to a range of 0-1 for convenience).  $T$  seconds are available for transmission and it is assumed that  $N$  signal transmissions, each lasting  $\frac{T}{N}$  seconds, are made. (Note that this fixed transmission time scheme contrasts with the sequential binary scheme, requiring a variable transmission time, just discussed.)

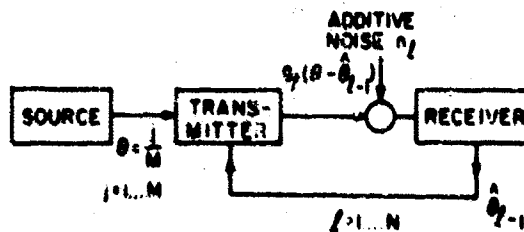


Fig. 3 M-ary Information Feedback System, N Repeats

On the  $k^{\text{th}}$  transmission the signal transmitted is of the form

$$s_k = g_k (\theta - \hat{\theta}_{k-1}) \quad (1)$$

with  $g_k$  a variable but known gain factor, and  $\hat{\theta}_{k-1}$  the receiver's maximum likelihood estimate of  $\theta$ , based on the first  $(k-1)$  transmissions. The receiver transmits  $\hat{\theta}_{k-1}$  to the transmitter via a noiseless feedback path. This system is of the information feedback type, since actual information as to the received signal plus noise is fed back to the transmitter.

On each successive transmission the receiver's estimate of the correct signal,  $\theta$ , improves, so that  $\hat{\theta}_k$  approaches  $\theta$  more closely. After  $N$  repeats the nearest  $\hat{\theta}_N$  is chosen as the correct signal. It may then be shown<sup>5,6</sup> that the probability of error goes essentially as

$$p_e \sim \exp - \left[ \frac{3}{2} e^{2(C-R)T} \right] \quad (2)$$

for large  $T$ , and  $R < C$ . Here the gain  $g_k$  of the  $k^{\text{th}}$  transmission has been optimized to provide minimum probability of error. The parameter  $R$  is the rate, in bits/second, of signal transmission:

$$R = \frac{\log_2 M}{T} \text{ bits/sec.} \quad (3)$$

and  $C$  is the so-called channel capacity in bits/sec. for this gaussian channel:

$$C = W \log_2 \left[ 1 + \frac{P_{av}}{n_o W} \right] \quad (4)$$

Here  $W = \frac{N}{2T}$  is the channel bandwidth,  $P_{av}$  is the average power available from the transmitter, and  $n_o/2$  is the white noise spectral density.

(Equation (4) is exactly the channel capacity of the gaussian channel first obtained, using a random coding argument, by Claude Shannon. It represents the maximum rate of transmission, in bits/sec., available for error-free transmission over such a channel. Schalkwijk's scheme is the first specific signalling scheme known to obey Shannon's previously ideal signalling law, and this accounts for the interest stirred up in it.)

A computer simulation of this system was carried out, with the probability of error found using extremal statistics. Here, because of the relative complexity of the system, only a limited amount of simulation could be carried out. Specifically, for  $N = 25$  repeated signal transmissions and  $R/C = 0.5$ , the probability of error was found to be 0.037, while for 50 signal transmissions, the probability of error was reduced to  $2.3 \times 10^{-3}$ . Both of these numbers compare favorably with results of an exact analysis, possible here, the complexity of the system notwithstanding, because of the additive

white gaussian noise assumed and linear operations at both transmitter and receiver. (Had the noise been non-white or nongaussian, or had some simple nonlinear operations been included, exact analysis would have been out of the question. Yet the simulation complexity would not have been substantially different, pointing out the utility of simulation here.) For the estimation of the probabilities here, 20 extremal values were again used to estimate the two parameters while 50 samples were used in the estimation of probability. The total number of samples per simulation was thus 1,000.

Details of this work were presented at the 1968 Spring Joint Computer Conference<sup>7</sup>.

National Aeronautics and Space Administration  
NgR 33-006-040

National Science Foundation  
CK-527

M. Schwartz  
S. Richman

#### REFERENCES

1. M. Schwartz, S. Richman, Progress Report No. 32, March 15, 1967 - Sept. 14, 1967, JSTAC, Polytechnic Institute of Brooklyn, pp. 176-179.
2. E. J. Gumbel, "Statistics of Extremes," Columbia University Press, New York, 1958.
3. A. Wald, "Sequential Analysis," John Wiley, New York, 1947.
4. M. Hecht, "Non-optimum Sequential Detection Techniques," doctoral dissertation, Department of Electrical Engineering, Polytechnic Institute of Brooklyn, June 1968.
5. J. P. M. Schalkwijk and T. Kailath, "A Coding Scheme for Additive Noise Channels with Feedback - Part I - No Bandwidth Constraint," IEEE Transactions on Information Theory, Vol. IT-12, No. 2, April, 1966, pp. 172-182.
6. J. P. M. Schalkwijk, "A Coding Scheme for Additive Noise Channels with Feedback - Part II - Bandlimited Signals," IEEE Transactions on Information Theory, Vol. IT-12, No. 2, April, 1966, pp. 185-189.
7. M. Schwartz and S. Richman, "Extremal Statistics in Computer Simulation of Digital Communication Systems," Proceedings, 1968, Spring Joint Computer Conference, Atlantic City, N. J.

#### NONPARAMETRIC DETECTION USING EXTREME-VALUE THEORY

L. B. Milstein, D. L. Schilling and J. K. Wolf

##### I. Introduction

In this research, we obtain a nonparametric detector which is based upon Gumbel's extreme-value theory (EVT). This theory is used to estimate the "tails" of the noise and signal-plus-noise probability density functions. These estimates are in turn used to estimate the optimum threshold and error probability of the system.

An example using an on-off signal embedded in unknown noise is presented to demonstrate the detector performance. A fading signal is also considered, and it is shown that the EVT detector is now adaptive. The results obtained are compared with those obtained using a parametric detector, and, in the case of a constant signal, with a non-

parametric detector designed using the rank test. The EVT detector is shown to outperform the rank detector and approach the error rate in the parametric detector.

## II. Nonparametric Detection Using EVT

**1. Extreme-Value Theory.** EVT concerns itself with the distribution of the maximum or minimum of a set of  $n$  independent samples. There are three different asymptotic forms for extreme values, depending upon the probability density functions of the noise and signal-plus-noise, from which the  $n$  samples were taken. The asymptotic form of most interest is called the "exponential" form, which is valid for any density which goes to zero on either "tail" at least as fast as an exponential. Examples include the normal density for both maximum and minimum values, and the Rayleigh and chi-squared densities for maximum values.

The specific forms of the asymptotes are as follows. Defining and density function as  $f(x)$  and the distribution function as  $F(x)$ , we have:

$$\lim_{x \rightarrow \infty} F(x) = 1 - \frac{1}{n} e^{-\alpha_n(x-u_n)} \quad (1)$$

$$\lim_{x \rightarrow -\infty} F(x) = \frac{1}{n} e^{\alpha_1(x-u_1)} \quad (2)$$

where

$$F(u_n) = 1 - \frac{1}{n} \quad \alpha_n = n f(u_n) \quad (3)$$

and

$$F(u_1) = \frac{1}{n} \quad \alpha_1 = n f(u_1) \quad (4)$$

These expressions are only accurate in some reasonably restricted region about either  $u_n$  or  $u_1$ .

**2. Using EVT for Detection.** The four parameters  $\alpha_1$ ,  $\alpha_n$ ,  $u_1$ , and  $u_n$  are estimated from samples taken in an initial learning period (see Section II. 3). Assuming that the estimates are available, they are used as follows: Form the likelihood ratio exactly as if the actual densities were known. However, only use the results in the neighborhood of  $u_n$  and  $u_1$ . This yields

$$\frac{f_N(x_t)}{f_{S+N}(x_t)} = \frac{\alpha_n e^{-\alpha_n(x_t - u_n)}}{\alpha_1 e^{\alpha_1(x_t - u_1)}} \quad (5)$$

for equal a priori probabilities of transmission.  $x_t$  is the threshold.

Solving (5) for  $x_t$  and then computing the false alarm and false dismissal errors, we obtain

$$x_t = \frac{u_1 \alpha_1 + u_n \alpha_n + \ln \frac{\alpha_n}{\alpha_1}}{\alpha_1 + \alpha_n} \quad (6)$$

$$P_{fa} = \frac{1}{n} e^{-\alpha_n (x_t - u_n)} \quad (7)$$

and

$$P_{fd} = \frac{1}{n} e^{\alpha_1 (x_t - u_1)} \quad (8)$$

**3. Estimation of Parameters.** Following Gumbel, the parameters  $\alpha_1$ ,  $\alpha_n$ ,  $u_1$  and  $u_n$  are estimated by obtaining the sample mean and sample standard deviation of  $N$  largest (or smallest) values. Each extreme value is taken from  $n$  independent samples.

This results in the following equations, which can be solved for the four parameters:

$$\bar{x}_n = u_n + \frac{\gamma}{\alpha_n} \quad (9)$$

$$\bar{x}_1 = u_1 - \frac{\gamma}{\alpha_1} \quad (10)$$

$$\text{var}(x_n) = \frac{\pi^2}{6} \frac{1}{\alpha_n^2} \quad (11)$$

$$\text{var}(x_1) = \frac{\pi^2}{6} \frac{1}{\alpha_1^2} \quad (12)$$

In (9) and (10),  $\gamma$  is Euler's constant.

Confidence intervals have been obtained for the  $u$ 's and  $\alpha$ 's, and also for the estimate of the probability of error.

### III. Example: Constant Signal Embedded in Unknown Noise

As a specific example, consider the system shown in Fig. 1.  $A$  is a constant,  $\theta$  a random variable, and  $N_0$  is white gaussian noise. The densities at the output will be Rician when signal is present, and Rayleigh when signal is absent. The tails of interest, are the tail of the Rayleigh at large  $x$ , and the tail of the Rician at small  $x$ . While it might seem, at first, that the tail of the Rician at small  $x$  is not of the exponential characteristic at high SNR.

Using values of  $A = 7.35$ ,  $\sigma = 1$ ,  $n = 100$ , and  $N = 20$ , the results shown in Table I

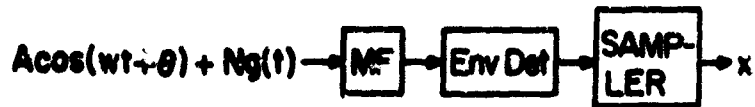


Fig. 1. System Block Diagram

were obtained:

Table I

Variable	Optimum and/or Actual Value	Experimental Result
$u_n$	3.04	3.11
$\sigma_n$	3.04	2.84
$u_1$	5.1	4.95
$\sigma_1$	2.65	3.01
$x_t$	4.03	4.04
$P_{fd}$	$0.404 \times 10^{-3}$	$0.64 \times 10^{-3}$
$P_{fa}$	$0.33 \times 10^{-3}$	$0.71 \times 10^{-3}$

It can be shown that the optimum value of  $n$  is  $1/P_{fa}$  for maximum values and  $1/P_{fd}$  for minimum values. Thus  $n$  should approximately be 1000 rather than 100 to optimise results.

#### IV. Fading

The previous example is now extended to the case where the signal is slowly fading. The fade will be assumed to have a Rician amplitude distribution, and also be slow enough to be considered constant over approximately  $2n$  bits.

The noise is still assumed to be stationary, and the density of signal-plus-noise will be assumed to change only by a shift in its mean as the signal fades. This assumption is only approximately correct, since, even for high SNR, the variance of a Rician density depends upon its DC component. The results will show that the assumption made is not critical, but merely mathematically convenient.

The significant difference in this example and that of Section (III) can be seen from the learning period. Whereas before, all  $nN$  samples were from the distribution, now they are from  $N$  different distributions (in the learning period, it is only necessary to assume the fade is constant over  $n$  bits, not  $2n$ ). Therefore, we cannot use (10) and (12) to estimate  $u_1$  and  $\sigma_1$  as before. Note that we can still use (9) and (11) since the

noise does not fade.

It can easily be shown that if two densities are the same except for their mean values, then the densities of the minima from  $n$  samples of each of them will also be the same, except for a difference in their means (which is equal to the difference in means of the initial variates). Therefore, we can use the minimum of the  $N^{\text{th}}$  set of  $n$  samples as a reference value, add to the remaining  $N-1$  minima the difference in the mean of the  $N^{\text{th}}$  set of samples and their own means (which can be estimated by the sample mean of each set of  $n$  bits), and compare values of  $u_1$  and  $\alpha_1$  as if we had  $Nn$  samples, all of which came from the density corresponding to the  $N^{\text{th}}$  fading amplitude.

Having obtained initial values of  $u_1$  and  $\alpha_1$ , we can estimate a threshold and begin the detection process. After we make  $n$  "signal" decisions (which, for equal a priori probabilities, will come after approximately  $2n$  bits have been received), we now find the new sample mean. New values of  $u_1$  and  $\alpha_1$  and consequently a new threshold are then determined. This procedure is then repeated, and the detector will be adaptive, giving a new threshold for each new fade.

This system was simulated on a computer, and the results are shown in Fig. (2). It can be seen that the EVT detector threshold is similar to the threshold obtained with the optimum detector, even for very deep fades, where Gumbel's theory is less accurate,

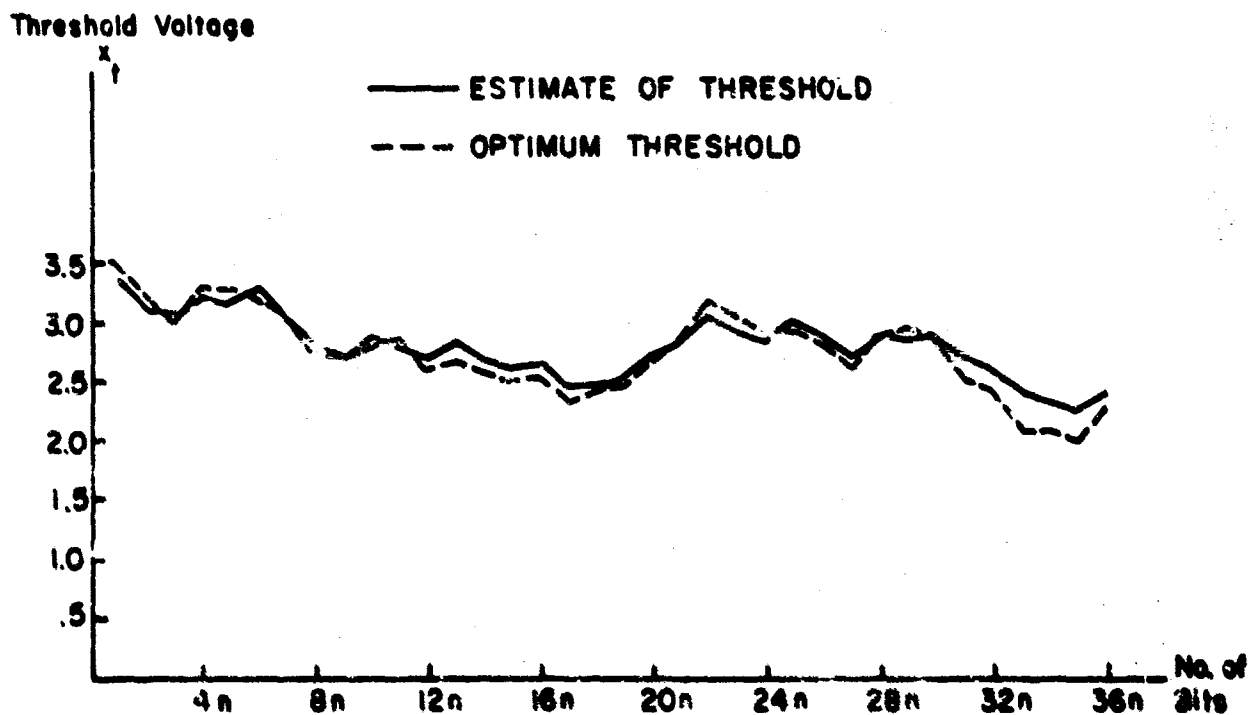


Fig. 4. Comparison of Optimum and Estimated Thresholds

and our assumption that the signal-plus-noise density doesn't undergo any distortion becomes significantly violated. In terms of actual errors made, both systems in Fig. (2) made 180 errors in 3800 bits.

#### V. Comparison with Rank Test

The rank test is a nonparametric test which has been used quite often as the basis for a nonparametric detector. The test consists of having a learning period during which noise samples are taken. A set of unknown samples is then taken and interordered with the control samples according to size (the smallest is first and the largest is last). The ranks (ordering positions) of the unknown set are then added together, and if the sum exceeds a predetermined threshold, it is decided that signal is present.

The comparison was made between the Rank detector and the EVT detector by assigning the same false alarm probabilities to each, and comparing the false dismissal probabilities. Because the rank test uses  $m$  test samples, the bandwidth and hence the noise power in that system was increased by a factor of  $m$ .

The EVT detector was found to give a smaller false dismissal probability, although not much smaller. The significant result was the comparative case in using the EVT detector, which occurred because the rank test must find the sum of the ranks of  $m$  samples, whereas the EVT detector simply compares one sample to a threshold.

Joint Services Technical Advisory Committee  
AF 49(638)-1402

National Aeronautics and Space Administration  
NgR 33-006-020

L. Milstein  
D. Schilling  
J. Wolf



## VII. NETWORKS AND SYSTEMS

Bongiorno, J. J., Jr.	Dorato, P.	Matthews, J. W.	Ruston, H.
Chien, T. M.	Fitz, R.	Ott, G. D.	Shaw, L.
Csurgay, A.	Frankfort, E.	Papoulis, A.	Tissi, P.
Degan, L. J.	Gupta, N. N.	Revkin, S.	Youla, D. C.
Deutsch, S.	Haddad, R. A.	Rubinger, B.	Yuksel, Y. O.

### NOISE-INTENSITY SENSITIVITY IN OPTIMAL STOCHASTIC SYSTEMS

P. Dorato

For stochastic systems which can be modelled by stochastic differential equations of the form

$$d\tilde{x} = \tilde{f}(\tilde{x}, \tilde{u}) dt + \tilde{\sigma}(\tilde{x}) d\tilde{\xi},$$

where

$\tilde{x}$  - n dimensional state vector

$\tilde{u}$  - m dimensional control input vector

$\tilde{\xi}_t$  - scalar Wiener process with variance parameter  $\alpha$ , i. e.,

$$E\left\{\left(\tilde{\xi}_{t+\Delta t} - \tilde{\xi}_t\right)^2\right\} = \alpha \Delta t$$

the only noise parameter is the noise intensity (variance)  $\alpha$ . The problem considered here is the sensitivity problem associated with variations of the cost functional

$$C = E_{\tilde{x}} \left\{ \int_t^T k(\tilde{x}_s, \tilde{u}_s) ds + b(\tilde{x}_T) \right\},$$

where

$E_{\tilde{x}}\{\cdot\}$  - denotes the expectation operation conditioned on  $\tilde{x}_t = \tilde{x}$

$T$  - fixed terminal time

to variations in the parameter  $\alpha$ . In particular, the problem is to evaluate  $\frac{\partial C}{\partial \alpha}$  when an optimal control law,  $u(t) = \Phi(\tilde{x}_t, t)$  designed for a nominal value of  $\alpha$  is used in a system where the noise intensity parameter  $\alpha$  has been perturbed from  $\alpha$  to  $\alpha + \Delta\alpha$ . Since, due to aging or uncertainty, the true value of  $\alpha$  is seldom available, the sensitivity problem is important in any practical design.

The cost sensitivity function  $\frac{\partial C}{\partial \alpha}$  may be evaluated as follows. Let  $V$  denote the minimum (it is assumed here that the optimal system is one which minimizes  $C$ ) value of  $C$ . Then it is well known that  $V$  must satisfy the equation

$$0 = \min_{\tilde{u}} \left[ k(\tilde{x}, \tilde{u}) + \tilde{L}'(\tilde{x}, \tilde{u}) V_{\tilde{x}} + \frac{\alpha}{2} \tilde{\sigma}'(\tilde{x}) V_{\tilde{x}\tilde{x}} \tilde{\sigma}(\tilde{x}) - V_t \right], \quad (1)$$

$$V(\tilde{x}, t) = 0, \quad \text{for all } \tilde{x}$$

where  $\underline{f}'$  denotes the transpose of  $\underline{f}$ ,  $\underline{V}_x$  denotes the gradient (column vector) of  $V$  with respect to  $\underline{x}$ , and  $\underline{V}_{xx}$  denotes the Jacobian matrix with elements  $\left[ \frac{\partial^2 V}{\partial x_i \partial x_j} \right]$ . Let  $u = \Phi(\underline{x}_t, t)$  be the optimal control law determined from (1) at the nominal value for noise intensity,  $\alpha$ . Then the sensitivity function  $v = \frac{\partial C}{\partial \alpha}$  for the control law  $\Phi$  may be computed from the equation

$$0 = \underline{f}'(\underline{x}, \Phi) \underline{v}_x + \frac{1}{2} \underline{\sigma}' \underline{V}_{xx} \underline{\sigma} + v_t + \frac{\alpha}{2} \underline{\sigma}' \underline{v}_{xx} \underline{\sigma} \quad (2)$$

$$v(\underline{x}, t) = 0, \text{ for all } \underline{x}, \text{ where}$$

$\underline{V}_{xx}$  and  $\Phi$  are evaluated at their nominal values.

A paper based on the study of linear systems with both additive and multiplicative noise was presented at the second IFAC Symposium on System Sensitivity and Adaptivity, Dubrovnik, Yugoslavia, August 1968.<sup>1</sup> In particular, for the linear multiplicative noise case where the system dynamics are given by

$$d\underline{x} = A \underline{x} dt + B \underline{u} dt + G \underline{x} d\xi, \quad (3)$$

and cost functional

$$C = E_{\underline{x}} \left\{ \int_t^T [\underline{x}'_s C \underline{x}_s + \underline{u}'_s D \underline{u}_s] ds \right\}, \quad (4)$$

the sensitivity function is given by

$$v(\underline{x}, t) = \underline{x}' S(t) \underline{x}, \quad (5)$$

where  $S(t)$  satisfies the equation

$$S + (A - BD^{-1} B' P) S + S(A - BD^{-1} EP) + G' PG + \alpha G' SG = 0, \quad (6)$$

where  $P$  is the solution of the Riccati equation

$$\dot{P} + A' P + PA + C + \alpha C' PG - P(BD^{-1} B') F = 0,$$

with boundary conditions:  $P(T) = 0$ ,  $S(T) = 0$ .

Work is in progress to extend some of the linear results discussed above to certain classes of nonlinear systems.

National Aeronautics and Space Administration  
NgR 33-006-04c

P. Dorato

National Science Foundation  
GU-1557

#### REFERENCE

1. P. Dorato, "Noise-Intensity Sensitivity in Optimal Stochastic Systems," Preprints, 2 IFAC Symposia on System Sensitivity and Adaptivity, Dubrovnik, Yugoslavia, 1968, pp C52-C57.

SYSTEM IDENTIFICATION

L. Shaw and N. N. Gupta

The problem of system identification consists of finding an approximate simple operator which maps the set of inputs into the corresponding set of outputs, with the minimum possible errors (in a certain sense).

The first step in the process of identification is classification (or model elimination) which consists in using the data and knowledge of how they were generated to suggest a subclass of models worth tentatively entertaining. This is the hardest part of the identification problem and, unfortunately, no general methods of attack are available. The next step in the process of identification is order discrimination.

Specifically, the problem considered here is the determination of the order of a linear differential system, given the input and the corresponding output. The output is observed in the presence of additive stationary noise.

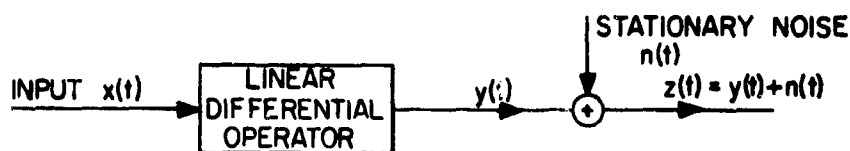


Fig. 1 Model for Identification Problem

Statement of the Problem

Given the input  $u(t)$ , and the output measurements  $z(t) = y(t) + n(t)$ , and assuming that there exists a system satisfying Eq. (1).

$$\sum_{i=0}^n a_i Y^{(i)}(t) = x(t) \text{ and } Y(0) = Y^{(i)}(0) = \dots = Y^{(n-1)}(0) = 0 \quad (1)$$

(The superscript  $i$  refers to the order of the derivative.) Determine the order  $n$  of the system.

The method proposed here for solving this problem uses the following theorem:

Theorem Given the system Eq. (1) then,

- a)  $Y(t), Y^{(1)}(t), \dots, Y^{(n)}(t)$  are linearly independent, and
- b)  $Y(t), Y^{(1)}(t), \dots, Y^{(n)}(t), X(t)$  are linearly dependent.

This theorem suggests the following sequential test procedure for determining the order of a linear differential system.

Test if the order is one by checking whether  $Y(t), Y^{(1)}(t), X(t)$  are linearly dependent or not.

If  $Y(t)$ ,  $Y^{(1)}(t)$ ,  $X(t)$  are linearly dependent, then the order is one.

If  $Y(t)$ ,  $Y^{(1)}(t)$ ,  $X(t)$  are linearly independent, then we proceed to check whether the order is two, and so on.

The test for linear dependence will be based on linear functionals involving the input and output functions.

We shall assume that  $Y^{(n)}(t)$  can be written in the following form over an interval  $I = [0, T]$ ,

$$Y^{(n)}(t) = \sum_{i=1}^m a_{i(n+1)} \psi_i(t) \quad (2)$$

where  $\{\psi_i(t)\}$  is a finite orthonormal set. Also,  $\psi_i(t)$ 's are chosen so that they and their first  $n$  derivatives are zero at the two end points of the interval  $I (= [0, T])$ . In that case the expression for  $a_{i(n+1)}$  becomes

$$a_{i(n+1)} = \int_I Y^{(n)}(t) \psi_i(t) dt = (-1)^n \int_I Y(t) \psi_i^{(n)}(t) dt \quad (3)$$

The linear dependence test is based on the linear functionals involving the input and output functions. These linear functionals are determined by the  $a$ 's which must first be estimated from the available data, i. e., the discrete output measurements  $z(t_1)$ ,  $z(t_2), \dots, z(t_r)$ .

Using Eq. (2) for  $n = 0$ , the output measurements can be expressed as

$$z(t) = \sum_{i=1}^m a_{i1} \psi_i(t) + n(t) \quad (4)$$

where  $\psi_i(t)$  ( $i = 1, 2, \dots, m$ ) are non-random real, orthonormal functions, the numbers  $a_{i1}$  are unknown real numbers, and  $n(t)$  is the stationary random noise.

The problem is to determine the numbers  $\hat{a}_{i1}$ , these being the best unbiased estimates of the values of the linear functionals obtained by the given linear transformation  $L$  of the signal component of the function  $z(t)$  over the interval  $I$ . The transformation  $L$  is given by Eq. (3)

Let

$$\underline{a} = \begin{bmatrix} a_{11} \\ a_{21} \\ \vdots \\ a_{m1} \end{bmatrix}, \quad \psi = \begin{bmatrix} \psi_{1,m} \\ \vdots \\ \psi_{r,m} \end{bmatrix}, \quad r \geq m$$

$$\begin{bmatrix} \psi_1(t_1) \dots \psi_m(t_1) \\ \vdots \\ \psi_1(t_r) \dots \psi_m(t_r) \end{bmatrix}$$

$$L \equiv \begin{bmatrix} L_{11}[\psi_1(t)] & - & - & - & L_{1m}[\psi_1(t)] \\ \vdots & & & & \\ \vdots & & & & \\ \vdots & & & & \\ \vdots & & & & \\ L_{m1}[\psi_m(t)] & - & - & - & L_{mm}[\psi_m(t)] \end{bmatrix}$$

$$z \equiv [z(t_1) \dots z(t_r)]$$

$$L_{ij} \equiv \int_I \psi_i(t) \psi_j(t) dt$$

Let  $E[n(t)] = 0$  for all  $t$ .

Let  $B_{r,r}^{-1}$  be the correlation matrix of  $n(t)$  over the interval  $I$ .

The estimate of  $\underline{a}^1$  is given by Eq. (5)

$$\hat{\underline{a}}^1 = z B \psi (\psi^T B \psi)^{-1} L \tag{5}$$

and dispersion of the estimates by Eq. (6)

$$D_{\hat{\underline{a}}^1} = L^T (\psi^T B \psi)^{-1} L \tag{6}$$

Similarly, we can estimate  $\underline{a}^2, \dots, \underline{a}^{n+1}$ . Further we express the input in terms of

the  $\psi$ 's as  $x(t) = \sum_{i=1}^m a_{i(n+2)} \psi_i(t)$  and  $\underline{a}^{n+2} = \begin{bmatrix} a_{1(n+2)} \\ \vdots \\ a_{m(n+2)} \end{bmatrix}$

Now to test the hypothesis that the system is of order  $(n-1)$  against the null hypothesis that the system is of order  $n$ , we check whether  $\hat{\underline{a}}^1, \hat{\underline{a}}^2, \dots, \hat{\underline{a}}^{n+1}, \hat{\underline{a}}^{n+2}$  are linearly dependent or independent. To do this we proceed as follows. We form the test matrix  $N$ :

$$N \equiv [ \underline{a}^1, \underline{a}^2, \dots, \underline{a}^{n+1}, \underline{a}^{n+2} ]$$

$$\equiv \begin{bmatrix} a_{11} & - & - & - & a_{1(n+2)} \\ \cdot & & & & \cdot \\ \cdot & & & & \cdot \\ \cdot & & & & \cdot \\ a_{m1} & & & & a_{m(n+2)} \end{bmatrix}$$

Then we determine  $N^G$ , the generalized inverse of  $N$  (by the method of LeBude N. Y. U. New York, Private Communication). Our test function is the trace of the

projection transformation  $P(= NN^G)$ . This projects the vectors onto the space spanned by the column vectors of  $N$ . The trace of  $P$  is equal to the rank of  $N$ . (If there were no noise in the observations, this rank would be equal to the order of the system.) Therefore, we test whether the trace of  $P$  is  $n$  or  $(n-1)$ . If the trace of  $P \cong n-1$ , we say the system is of order  $(n-1)$ . If the trace of  $P \cong n$ , then we go ahead to check whether the system is of order  $n$  or of order  $(n+1)$ .

#### Present Status

Programs are being written to test the method in simulated data. The theoretical development is concentrating on the problem of evaluating the errors induced on the trace calculation by the observation noise.

U. S. Army Research Office, Durham  
DA-31-124-ARO-D-316

L. Shaw  
N. Gupta

#### REFERENCE

1. Kovanic, P., "Generalized Discrete Analogue of the Zadeh-Ragazzini Problem," *Automation and Telematics*, 27, 2 (1966).

#### ON STATE ESTIMATORS FOR NONLINEAR SYSTEMS

Y. O. Yuksel and J. J. Bongiorno, Jr.

##### I. A General Description of the State Estimation Problem

Often in control system designs, the state vector of the plant is assumed to be available for measurement. However, in many cases the number of independent outputs is less than the number of states. Hence it is not possible to construct the state vector via a memoryless transformation.

It is shown that <sup>1, 2, 3, 4</sup> if the plant is linear and completely observable, an estimate of the state vector can be constructed using a dynamic system of order less than that of the plant. The estimate of the state vector differs from the actual state vector by an error vector, norm of which decays exponentially to zero.

Methods given in all four papers are essentially the same. Luenberger's work<sup>1, 2</sup> constitutes the original study. Work by Bongiorno and Youla<sup>3</sup> should be noted for its better formulated approach and investigation of effects of the observer in the feedback loop. Finally, the work by Wolowich<sup>4</sup> consists of an algorithm to design the estimator (or observer) and stands alone for its treatment of time varying systems.

The topic of state estimation offers a fruitful area of research. In all of the three methods mentioned there is a certain degree of freedom which can possibly be used to optimize a cost function. For example, observer poles are completely arbitrary.

trary. However, their location affects the rate of decay of the error vector. It is also shown<sup>3</sup> that for some cases, moving these poles to  $(-\infty)$  may result in a very large cost. This final result is obtained using a certain cost index. Investigation of this behavior for other types of cost indices may lead to very interesting and unusual results. Finally, estimators for nonlinear plants are not treated in any publication known to us.

II. Autonomous Systems with Linear State-Output Relationships

In this section we will consider a plant of the form

$$\begin{aligned} \dot{\underline{x}} &= F\underline{x} + \underline{\gamma}(\underline{x}) \\ \underline{y} &= H\underline{x} \end{aligned} \tag{1}$$

where

- $\underline{x}$ : the  $n$  dimensional state vector
- $\underline{\gamma}(\underline{x})$ : an  $n$ -vector valued function of vector  $\underline{x}$
- $F$ : an  $n \times n$  matrix
- $\underline{y}$ : the  $p$  dimensional output vector
- $H$ : a  $p \times n$  matrix

Our aim is to design a dynamical system which gives at its output, an estimate of the state vector  $\underline{x}$  of the plant. For this system which we will call the "state estimator for plant 1" we will assume the form:

$$\begin{aligned} \dot{\underline{z}} &= A\underline{z} + B\underline{y} + \underline{q}(\underline{y}, \underline{z}) \\ \hat{\underline{x}} &= W \begin{bmatrix} \underline{y} \\ \underline{z} \end{bmatrix} \end{aligned} \tag{2}$$

where

- $\underline{z}$ :  $m$  dimensional state vector of the estimator
- $\hat{\underline{x}}$ :  $n$ -vector, the estimate
- $A$ : an  $m \times m$  matrix
- $B$ : an  $m \times p$  matrix
- $\underline{q}$ :  $m$ -vector valued function
- $W$ : an  $n \times m$  matrix
- $m = n - p$

We will also make following assumptions

A-1.  $P = (H' | F' H' | \dots | F'^{n-1} H')'$  has rank  $n$  (3)

A-2.  $Q = (B | AB | \dots | A^{m-1} B)$  has rank  $m$  (4)

A-3. Equation 1 is derived from an  $n$ th order differential equation.

$$n^{(n)} + a_{n-1} n^{(n-1)} + \dots + a_1 n + a_0 + f(n, n, \dots, n^{(n-1)}) = 0$$

i. e.,

$$F = \begin{bmatrix} 1_{n-1} & 0_{n-1} \\ -e' & -a_{n-1} \end{bmatrix} \quad \bar{x} = \begin{bmatrix} a_0 \\ \vdots \\ a_{n-2} \end{bmatrix}$$

and

$$\gamma(\bar{x}) = - \begin{bmatrix} 0 \\ \vdots \\ 0 \\ 1 \end{bmatrix} f(\bar{x}) = -e_n f(\bar{x}) \quad (5)$$

Suppose

$$\bar{z} = T\bar{x} + \bar{e} \quad (6)$$

where  $\bar{e}$  is the  $m$ -dimensional error vector. Substitution of Eq. (6) into Eqs. (1) and (2) together with choice (see Refs. (1), (2), (3))

$$TF - AT = BH \quad (7)$$

yields a differential equation for the error

$$\dot{\bar{e}} = A\bar{e} + \bar{g}(H\bar{x}, \bar{z}) - T\gamma(\bar{x}) \quad (8)$$

It is seen that

$$\begin{array}{l} \bar{x} \rightarrow T\bar{x} \\ t \rightarrow \infty \end{array}$$

when

$$\begin{array}{l} \bar{e} \rightarrow 0 \\ t \rightarrow \infty \end{array}$$

Let

$$T = (T | \bar{t}) \quad (9)$$

then the choice

$$\bar{g}(H\bar{x}, \bar{z}) = 0 \quad (10)$$

reduces Eq. (8) to

$$\dot{\bar{e}} = A\bar{e} \quad (11)$$

stability of which can easily be achieved by choosing eigen values of  $A$  in the left half plane.

Note that the estimator is linear with this choice. One intuitively feels that there must be a better estimator, probably using a nonlinear estimator structure.



We will investigate this possibility for systems with the number of outputs one less than the number of states.

$$\text{i.e. } p = n - 1 \therefore m = 1$$

In this case we can expand  $\alpha$  into a series with respect to the second argument

$$\alpha(Hx, Tx + e) = \alpha(Hx, Tx) + \alpha'(Hx, Tx)e + \dots \quad (12)$$

where  $(')$  denotes the partial derivative with respect to the second argument. Then the choice

$$\alpha(Hx, Tx) = T \gamma(x) = -T e_n f(x) = -t f(x) \quad (13)$$

reduces Eq. (8) to

$$\dot{e} = [A - t f'(Hx, Tx)] e - t f''(Hx, Tx) \frac{e^2}{2} + \dots \quad (14)$$

For some systems second order terms are actually zero (e.g., piecewise linear functions). The remaining problem is the stability of a linear differential equation with time varying coefficients. Note that the estimators obtained by the earlier mentioned choice  $t = 0$  constitute a subclass of the estimators obtained this way.

### III. Non-Autonomous Systems with Additive Input Term

Consider a plant, dynamics of which can be shown as

$$\dot{x} = Fx + \gamma(x) + g(u) \quad (15)$$

where  $g(u)$  is an  $n$ -vector valued function of the input vector  $u$ .

A system

$$\begin{aligned} \dot{z} &= Az + By + \alpha(y, z) + Tg(u) \\ \hat{x} &= W \begin{pmatrix} y \\ z \end{pmatrix} \end{aligned} \quad (16)$$

with  $A$ ,  $B$ ,  $\alpha$  and  $T$  satisfying earlier mentioned conditions will be an estimator for Eq. (15). Proof is trivial.

### IV. Example

Consider

$$\ddot{x} + \frac{1}{3}\dot{x} + f(x) = u$$

where  $f(x)$  is as shown in Fig. 1.

$$F = \begin{pmatrix} 0 & 1 \\ -1/5 & 0 \end{pmatrix} \quad \gamma(x) = -\begin{pmatrix} 0 \\ 1 \end{pmatrix} f(x) \quad G = \begin{pmatrix} 0 \\ 1 \end{pmatrix} \quad \text{E-1}$$

$$\text{Let } H = (-1 \quad 1)$$

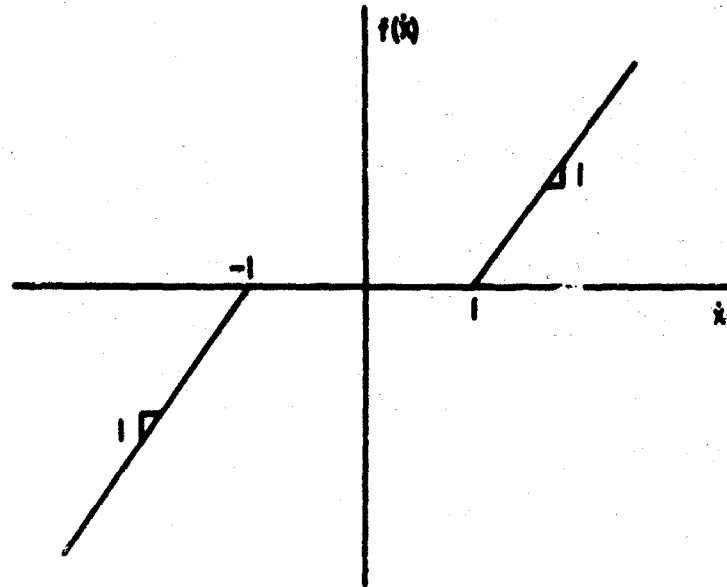


Fig. 1 Nonlinearity for the example

Equation (14) takes the form

$$e = [a - t_2 f'(Hx, Tx)] e \quad \text{E-2}$$

where  $T = (t_1 \ t_2)$  E-3

$f'(Hx, Tx) = u(Tx - 1) - u(-Tx - 1)$  E-4

where  $u$  represents the unit step function. Therefore, a choice satisfying

$$a - t_2 < 0 \quad \text{E-5}$$

satisfies one of the conditions.

Second condition to be satisfied is

$$(t_1 \ t_2) F - a(t_1 \ t_2) = b(-1 \ 1) \quad \text{E-6}$$

Both conditions are satisfied by

$$a = -1, \ t_1 = \frac{2}{5}, \ t_2 = 1, \ b = \frac{3}{5} \quad \text{E-7}$$

which implies

$$W = \left( \frac{H}{T} \right)^{-1} = \begin{pmatrix} -5/3 & 5/3 \\ -2/3 & 5/3 \end{pmatrix} \quad \text{E-8}$$

Hence

$$z = -z + 3/5 y \cdot f(x) + u \quad \text{E-9}$$

$$\hat{z} = 1/3 \begin{pmatrix} -5 & 5 \\ -2 & 5 \end{pmatrix} \begin{pmatrix} y \\ z \end{pmatrix}$$

is an estimator for E-1.

Joint Services Technical Advisory Committee  
AF 49(638)-1402

Y. O. Yrksel  
J. J. Bongiorno, Jr.

REFERENCES

1. D.G. Luenberger, "Observing the State of a Linear System," IEEE Trans. on Military Electronics, April 1964.
2. D.G. Luenberger, "Observers for Multivariable Systems," IEEE Trans. on Automatic Control, April 1966.
3. J. J. Bongiorno and D. C. Youla, "On Observers in Multivariable Control Systems," Polytechnic Institute of Brooklyn, Electrophysics Memo, PIBMRI-1383-67, October 1967.
4. W. A. Wolowich, "On State Estimation of Observable Systems," 1968 Joint Automatic Computer Conference.

STATE ESTIMATION OF A SCALAR LINEAR SYSTEM WITH RANDOM COEFFICIENTS

R. Fitz and R. A. Haddad

The basic problem considered in this study is the state estimation of a scalar linear dynamic system with random coefficients. The model for the message process and observations are given by the It<sub>0</sub><sup>2, 4, 10</sup> equations.

$$dx(t) = [a(t) + d\beta_1 b(t)] x(t) + c(t) d\beta_2(t) \tag{1}$$

$$dz(t) = h(t) x(t) dt + d\eta(t) \tag{2}$$

where  $x(t)$  is the state to be estimated,  $x(t_0)$  is a Gaussian random variable with  $E\{x(t_0)\} = x_0$  and  $E\{(x - x_0)^2\} = u_2$ ,  $a(t)$ ,  $b(t)$ , and  $c(t)$  are continuous time-varying coefficients,  $\beta(t) = [\beta_1(t), \beta_2(t)]^T$  is a two-dimensional Brownian motion process with  $E\{d\beta(t)\} = 0$  and  $E\{d\beta d\beta^T\} = Q dt = \text{diag}\{q_1^2, q_2^2\} dt$ ,  $z(t)$  is the information state,  $h(t)$  is a continuous time-varying gain, and  $\eta(t)$  is a scalar Brownian motion process with  $E\{d\eta(t)\} = 0$  and  $E\{(d\eta(t))^2\} = r^2 dt$  where  $r^2$  is greater than zero. Throughout this note, time indices are omitted in cases where it causes no ambiguity.

The minimum estimate is the mean of the conditional probability density function  $p(t, x|z(t))$  where  $z(t) = \{z(s) : t \geq s \geq t_0\}$ . If  $g(x)$  is a twice continuously differentiable scalar function of the  $x(t)$  process, then Kushner<sup>9</sup> has shown that

$$dE^t g(x(t)) = E^t \mathcal{L}g(x(t)) + \frac{1}{r^2} (E^t g_{xx} - E^t g E^t g)(dz - hE^t x dt) \tag{3}$$

where  $E^t(\cdot)$  denotes expectation of  $(\cdot)$  with respect to  $p(t, x|z(t))$  and  $\mathcal{L}$  is the diffusion operator for the  $x(t)$  process and is given

$$\mathcal{L}(\cdot) = a x(t) \frac{\partial(\cdot)}{\partial x} + \frac{1}{2} [b^2 x^2(t) q_1^2 + c^2 q_2^2] \frac{\partial^2(\cdot)}{\partial x^2}$$

Denoting  $E^t x$  by  $\phi$  and using Eq. (3), the stochastic differential equation for the conditional mean is given by

$$d\phi = a \phi dt + \frac{u_2 h}{r^2} \{ dz - h \phi dt \} \quad (4)$$

$$\phi(t_0) = x_0$$

where  $u_2$  is the covariance of the conditional density function  $p[t, x(t) | z(t)]$ . To derive the stochastic differential equations for the central moments of  $p[t, x(t) | z(t)]$  the product rule for stochastic differentials must be used in addition to Kushner's equations<sup>1, 6, 7, 8, 9</sup>. Denoting  $E^t[(x - \phi)^k]$  by  $u_k$ , the stochastic differential equations for the central moments are given by

$$\begin{aligned} du_k = & (a_{k1} + a_{k2} \frac{u_2}{r^2}) u_k dt + a_{k3} \phi u_{k-1} dt \\ & + (a_{k4} c^2 + a_{k5} \phi^2 + a_{k6} u_2^2) u_{k-2} dt \\ & + \frac{h}{r^2} (u_{k+1} - k u_2 u_{k-1})(dz - h \phi dt) \end{aligned} \quad (5)$$

where the  $a_{ki}$  are dimensionless constants given by

$$a_{k1} = (ka + \frac{k(k-1)}{2} b^2 q_1^2)$$

$$a_{k2} = -k h^2$$

$$a_{k3} = k(k-1) b^2 q_1^2 + (k-1) a(t)$$

$$a_{k4} = k(k-1) q_2^2$$

$$a_{k5} = \frac{k(k-1)}{2} b^2 q_1^2$$

$$a_{k6} = \frac{k(k-1)}{2} h^2$$

Equations (4) and (5) constitute an infinite set of equations which generate the minimum variance estimate of the dynamical system specified by Eqs. (1) and (2).

In practice, Eqs. (4) and (5) represent an infinite set of equations and hence suitable approximations must be found. One approach that has been utilized in finding a finite-order approximation is to introduce an intermediate step of considering truncated Hermite expansions of the conditional probability density function.<sup>3</sup> Under suitable conditions on the conditional density function and for a given  $t_1$  and  $z(t_1)$ , we have the following expansion:

$$p [t_1, x | z(t_1)] = \frac{\exp [\theta^2 / 2]}{\sqrt{2\pi} u_2} \left[ \sum_{n=0}^{\infty} \frac{c_n}{n!} H_n(\theta) \right] \tag{6}$$

where  $\theta = \left[ \frac{x - \phi}{\sqrt{u_2}} \right]$ ,  $\phi$  and  $u_2$

are the mean and covariance respectively of  $p [t_1, x | z(t_1)]$ .  $H_n$ 's are Hermite polynomials, a set of polynomials complete in  $L^2(-\infty, \infty)$  orthogonal with weight  $\exp [-\theta^2 / 2]$ , and  $c_n$  are called the "quasi moments" of  $p [t_1, x | z(t_1)]$ . The Hermite polynomials are given by

$$H_n(x) = (-1)^n \exp [x^2 / 2] \frac{d^n}{dx^n} \exp [-x^2 / 2]$$

and can be expressed explicitly by the following summation

$$H_n(x) = n! \sum_{m=0}^{[n/2]} \frac{(-1)^m x^{n-2m}}{m! 2^m (n-2m)!}$$

where  $[n/2]$  is the largest integer less than or equal to  $n/2$ . In the usual way the coefficients  $c_n$  can be calculated and are seen to have the following dependence on the central moments of  $p(t_1, x | z(t_1))$ :

$$c_n = n! \sum_{m=0}^{[n/2]} \frac{(-1)^m u_{n-2m}}{(U_2)^{\frac{n-2m}{2}} 2^m m! (n-2m)!} \tag{7}$$

Finite dimensional approximations to Eqs. (4) and (5) can be obtained under the following assumption: For all  $t$  and  $z(t)$ ,  $p [t, x | z(t)]$  can be described by a finite Hermite expansion. If  $p [t, x | z(t)]$  is approximated by retaining only the first  $n$  coefficients of (6), then the resulting approximation to Eqs. (4) and (5) is called an  $n^{\text{th}}$  order approximation of the optimal estimator. For an  $n^{\text{th}}$  order approximation,  $c_k = 0$  for all  $k \geq n + 1$ . In particular  $c_{n+1} = 0$ ; which by Eq. (7) implies that

$$u_{n+1} = (n+1)! \sum_{m=1}^{[n/2]} \frac{(-1)^{n-1} u_{n-2m+1}}{(U_2)^{\frac{n-2m+1}{2}} 2^m m! (n-2m+1)!} \tag{8}$$

By Eq. (8) the  $(n+1)^{\text{th}}$  central moment can be expressed in terms of lower order moments, thus the equation for the optimal estimator can be terminated. An  $n^{\text{th}}$  order approximation is specified by: 1) the stochastic differential for the mean, Eq. (4), 2) The stochastic differential equations for the  $n$  central moments, Eq. (5), and 3) the equation for the  $(n+1)^{\text{st}}$  central moment in terms of the lower moments, Eq. (8).

For example, if  $n = 3$ , the 3<sup>rd</sup> order approximation is given by

$$d\phi = a \phi dt + \frac{u_2 h}{r^2} \{ dz - h \phi dt \}$$

$$\phi(t_0) = x_0$$

$$du_2 = [2a + b^2 q_1^2 - \frac{h^2 u_2}{r^2}] u_2 dt + b^2 q_1^2 \phi^2 + c^2 q_1^2 + \frac{h u_3}{r^2} \{ dz - h \phi dt \}$$

$$u_2(t_0) = u_2(0)$$

$$\frac{du_3}{dt} = [3a + 3b^2 q_1^2 - \frac{3h^2 u_2}{r^2}] u_3 + 6b^2 q_1^2 \phi u_2$$

$$u_3(t_0) = 0$$

Work is being completed on the following related topics:

- 1) extension of results to vector models
- 2) stability analysis of the optimal and suboptimal estimators
- 3) engineering realization of the estimator equations.

National Science Foundation  
GU-1557

R. Fitz

#### REFERENCES

1. R. S. Bucy, "Nonlinear Filtering Theory," IEEE Trans. on Automatic Control AC10(2), 198 April 1965.
2. J. L. Doob, Stochastic Processes, New York: Wiley, 1953.
3. J. R. Fisher, "Optimal Nonlinear Filtering," in Advances in Control Theory and Applications, Vol. 5, C. T. Leondes, Ed., New York: Academic Press 1967.
4. K. Ito, "Lectures on Stochastic Processes" (Mimeograph notes) Tata Institute of Fundamental Research, Bombay, India 1961.
5. R. E. Kalman, and R. S. Bucy, "New Results in Linear Filtering and Prediction Problems," J. Basic, Engr. (ASME Trans.) 83D, 95-108, March 1961.
6. H. J. Kushner, "On the Differential Equations Satisfied by Conditional Probability Densities of Markov Processes," S. I. A. M. Jour. on Control 2(1), 106-110, 1968.
7. H. J. Kushner, "On the Dynamical Equations of Conditional Probability Density Functions with Applications to Optimal Control Theory," J. Math. Anal. Appl., 5, 332-344, 1964.
8. H. J. Kushner, "On the Dynamical Equations for Optimum Nonlinear Filtering," Jour. of Diff. Eq., 3(2), April 1967.
9. H. J. Kushner, "Approximations to Optimal Non-Linear Filters," Proceedings of the Joint Automatic Control Conference, 1967.
10. A. V. Skorokhod, Studies in the Theory of Random Processes, (Addison-Wesley, 1965), (Translated from the 1961 Russian Edition).

MINIMUM SENSITIVITY DESIGNS

J. J. Bongiorno, Jr.

The results of an earlier effort<sup>1</sup> have been extended to multivariable control systems of the form shown in Fig. 1. The transfer function matrices  $G_c(s)$  and  $H(s)$  are to be determined and  $G_p(s, g)$  is the transfer function matrix of a stable plant. Without loss in generality, one can assume that all three of the above transfer function matrices are  $n \times n$  and that the normal rank of  $G_p(s, g)$  is  $n$ . (The normal rank of a matrix is  $r$  if there is one minor of order  $r$  which is not identically zero and all minors of order greater than  $r$  are zero.) The symbol  $g$  denotes the nominal value of the plant parameter vector and any deviation from the nominal is denoted by  $\delta g$ . Only small deviations in each component of  $\delta g$  are assumed. It is also assumed that a physically realizable (the elements of the impulse response matrix are causal) nominal transfer function matrix

$$W(s, g) = G_p(s, g) G_c(s) [I_n + H(s) G_p(s, g) G_c(s)]^{-1} \tag{1}$$

has been specified. In Eq. (1),  $I_n$  denotes the  $n \times n$  identity matrix.

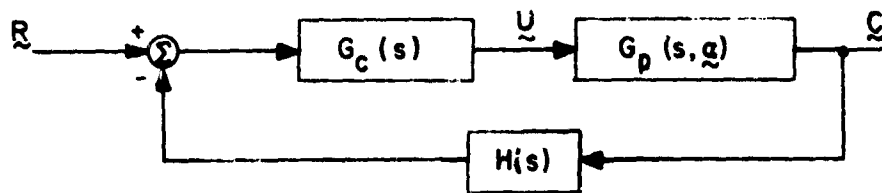


Fig. 1 System Block Diagram

The objective is the determination of physically realizable transfer function matrices  $G_c(s)$  and  $H(s)$  for which the sensitivity measure

$$S = \int_{-\infty}^{\infty} \langle (\xi_a - \xi)^T (\xi_a - \xi) \rangle dt \tag{2}$$

is minimum. In Eq. (2)  $\xi_a$  is the response when instead of  $g$  the parameters take on the value  $g + \delta g$ . The notation  $\langle (\cdot) \rangle$  for the expected value of  $(\cdot)$  is used.

When the elements of  $\delta g$  are all small, are independent of the process generating  $\xi_d(t)$ , and possess zero means it follows to within first-order effects that

$$S = \sum_{i=1}^n \frac{1}{\sigma_i} \int_{-j\omega}^{j\omega} \xi_i^T (I_n - \hat{W} \hat{H})^T (I_n - W H)^T \xi_i ds \tag{3}$$

where  $\xi_i$  is the  $n$ -dimensional vector all of whose elements are zero except for unity

in the  $i$ -row, for an arbitrary matrix function of  $s$  the carat denotes

$$\hat{A}(s) = A(-s), \quad (4)$$

and

$$\Phi = \sum_{l=1}^N \sum_{m=1}^N \sigma_{lm} \begin{pmatrix} \frac{\partial \hat{G}_p}{\partial \alpha_l} & \hat{G}_p^{-1} \\ \hat{G}_p^{-1} & \end{pmatrix} \hat{W} \Phi_{rr} W' \begin{pmatrix} \frac{\partial G_p}{\partial \alpha_m} & G_p^{-1} \\ G_p^{-1} & \end{pmatrix}'. \quad (5)$$

In Eq. (5),  $N$  is the dimension of  $g$ ,

$$\sigma_{lm} = \sigma_{ml} = \langle \delta \alpha_l \delta \alpha_m \rangle, \quad (6)$$

and

$$\Phi_{rr}(s) = \int_{-\infty}^{\infty} \langle \tilde{x}_d(t) \tilde{x}_d'(t+\tau) \rangle d^{-s\tau} d\tau. \quad (7)$$

The solution for the physically realizable  $H(s)$  which minimizes  $s$  is given by

$$H = \Gamma^{-1} \left\{ \Gamma_*^{-1} W_* \Delta' \right\}_+ \left[ \Delta' \right]^{-1} \quad (8)$$

when the spectral factorizations

$$\Phi = \Delta'(-s) \Delta(s) \boxplus \Delta'_*(s) \Delta(s) \quad (9)$$

and

$$\Psi = W'(-s) W(s) = \Gamma'(-s) \Gamma(s) \boxplus \Gamma'_*(s) \Gamma(s) \quad (10)$$

are possible where  $\Delta(s)$  together with  $\Delta^{-1}(s)$  and  $\Gamma(s)$  together with  $\Gamma^{-1}(s)$  are analytic in  $\text{Re } s \geq 0$ . Also,

$$\left\{ \Gamma_*^{-1} W_* \Delta' \right\}_+ = \int_0^{\infty} e^{-st} \left[ \frac{1}{2\pi j} \int_{-j\infty}^{j\infty} \Gamma_*^{-1} W_* \Delta' e^{st} ds \right] dt. \quad (11)$$

The solution for  $G_c$  as obtained from Eq. (1) is then

$$G_c(s) = G_p^{-1}(s, g) [1_n - W(s)H(s)]^{-1} W(s). \quad (12)$$

One can show in certain cases that the specification of  $W(s)$  can be made so as to guarantee the physical realizability of  $G_c(s)$ .

The above solution depends on the spectral factorizations, Eqs. (9) and (10). Conditions for which these factorizations are possible when all matrices are rational have been derived with the aid of Ref. 2. The spectral factorization Eq. (9) is always possible when  $|W(j\omega)| \neq 0$  for all finite  $s = j\omega$  axis. The spectral factorization (Eq. 10)



is always possible when the factorization Eq. (9) is and

1.  $\Phi(s)$  is analytic on the finite  $s = j\omega$  axis
2.  $\Phi_{rr}$  is positive definite for all finite  $\omega$
3.  $\langle \delta g, \delta g' \rangle$  is positive definite
4.  $n \times n$   $N$  matrix

$$\left[ \begin{array}{c|c|c|c} \frac{\partial G}{\partial \alpha_1} & \frac{\partial G}{\partial \alpha_2} & \dots & \frac{\partial G}{\partial \alpha_N} \end{array} \right]$$

has normal rank  $n$ .

National Aeronautics and Space Administration  
NgR 33-006-042

J. J. Bongiorno, Jr.

#### REFERENCES

1. J. J. Bongiorno, Jr., "Minimum Sensitivity Designs," IEEE International Convention Record, Vol. 15, Part 3, pp. 129-135, March, 1967.
2. D. C. Youla, "On the Factorization of Rational Matrices," IRE Trans. on Information Theory, pp. 172-189, July, 1961.

#### AN APPLICATION OF NONLINEAR FILTERING TO THE PROBLEM OF PARAMETER ESTIMATION

L. Shaw and B. Rubinger

There is considerable interest at the present time in the question of nonlinear filtering. This problem pertains to finding the optimum estimate of the state of a system based on the available data; and is of obvious relevance to the problems of satellite tracking and missile interception. The standard approach to nonlinear estimation has been the linearization of the system equations about the present state followed by the application of linear system theory.<sup>1</sup> In problems where the nonlinearity is significant, this technique leads to serious error and subsequently second order approximations have been employed.<sup>2</sup> In lieu of these approximations, the approach of the present study has been to expand the probability density functions in terms of orthogonal polynomials. The effect of the nonlinear system on the terms of such an expansion has been investigated and equations derived for updating the moments of the density function. This method is then applied to a problem of parameter estimation.

This research is concerned with the analysis of a plant which has an unknown parameter. The system under consideration is described by the equations

$$x_{k+1} = a_k x_k + w_k$$

$$z_k = h_k x_k + v_k$$

(1)

where

$x_k$  is the state vector (at time  $t_k$ )

$a_k$  is the plant parameter

$Z_k$  is the measurement at time  $t_k$

$h_k$  is a known parameter of the measurement system

$w_k, v_k$  are white noise sequences with

$$E [w_k] = E [v_k] = 0$$

$$E [w_k^2] = q^2 \quad E [v_k^2] = r^2$$

The initial condition for  $x_0$  is a gaussian random variable:

$$P_{x_0}(x) = \frac{1}{\sqrt{2\pi} \sigma_0} \exp \left[ -1/2 \frac{(x - \hat{x}_0)^2}{\sigma_0^2} \right] \quad (2)$$

and the unknown gain  $a_0$  is assumed to be described by the a priori density

$$P_{a_0}(a) = \frac{1}{\sqrt{2\pi} \sigma_a} \exp \left[ -1/2 \frac{(a - a_0)^2}{\sigma_a^2} \right] \quad (3)$$

If we define  $Z^k$  to be the collection of all data available at time  $t_k$ , the problem is to find the density function  $P(a, x_k | Z^k)$ , which makes use of all currently available information in the estimation of the state. Employing Baye's rule, one obtains an expression for updating the estimate of the state. This relation takes the form

$$P(a, x_{k+1} | Z^{k+1}) =$$

$$\frac{\int P(a, x_k | Z^k) P(x_{k+1} | a, x_k) P(Z_{k+1} | x_{k+1}) dx_k}{\int [\text{numerator}] d(a, x_{k+1})} \quad (4)$$

with the starting relation

$$P(a, x_0 | Z_0) = \frac{P_0(a, x_0) P(Z_0 | x_0)}{\int [\text{numerator}] d(a, x_0)} \quad (5)$$

An examination of Eqs. (4) and (5) reveals that no direct solution to these equations exists and that approximating procedures are necessary. Therefore the density,  $P(a, x_k | Z^k)$  was expressed as a two-dimensional orthogonal series, and expressions were obtained for the corresponding expansion describing  $P(a, x_{k+1} | Z^{k+1})$ . The advantage of this approach over other approximation techniques is that it guarantees mean-square convergence.

National Science Foundation  
GU-1557

B. Rubinger

REFERENCES

1. A. S. Chen, "The Extended Kalman Filter," Stanford Research Institute, SRI Project 5188-103, Dec. 1964.
2. H. W. Sorenson, "A Nonlinear Perturbation Theory for Estimation and Control of Time-Discrete Stochastic Systems," UCLA Report #68-2

COMPUTATIONAL EVALUATION OF EXPECTED PERFORMANCE INDICES

L. Shaw, S. Revkin, E. Frankfort

The work on this subject which was described in the previous semi-annual report was continued.<sup>1</sup> In particular, mean-integral squared performance was evaluated for the following time-delay system.

One axis attitude control of an HUP-1 single rotor helicopter was considered. The vehicle's dynamics are represented by the transfer function

$$T(s) = \frac{12.1}{s(s + 0.96)}$$

Control is applied by a man with transfer function

$$H(s) = \frac{K e^{-.1s}}{1 + sT_n}$$

where  $T_n$  is the random variable neuromuscular time constant. The controller's action is based on an error derived by unity negative feedback, as shown in Fig. 1.

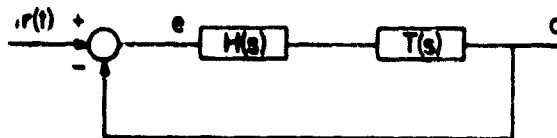


Fig. 1 Feedback System

Considering  $T_n$  to vary from person to person according to a uniform distribution between 0 and 0.7 seconds, the value of

$$E \left\{ \int_0^{\infty} e^2(t) dt \right\} = \sum_{i=0}^{\infty} \int_0^{\infty} e_i^2(t) dt \tag{1}$$

was found for the case of  $r(t) = 0$ , and the non-zero initial state:

$$e(t) = 1; \quad -0.1 < t \leq 0.$$

Truncation of the sum in Eq. (1) at 0, 3, and 9 yielded almost the same results, indicating that such small truncations may well yield good approximations to Eq. (1). When a Monte Carlo method was tried using 5 realizations (comparable in complexity to a truncation at  $i = 4$ ) much poorer stability of the estimate was observed.<sup>2</sup>

A second computational example was based on the system in Fig. 2, in which the reference signal  $r(t)$  was zero,  $\bar{a}$  was a random variable uniformly distributed between zero and one, and the initial conditions are  $e(0) = 1$ ,  $\dot{e}(0) = 0$ . The performance index

$$P = E \left[ \int_0^{\infty} e^2(t; \bar{a}) + \lambda m^2(t; \bar{a}) \right] dt$$

was evaluated directly to be

$$P = (1 + a^2 \lambda k^2) \left[ k + 1.5 + ak \ln \left| \frac{2+k}{1+k} \right| \right] / 2ka + \lambda (0.5 k^3 \ln \left| \frac{2+k}{1+k} \right| - ak). \quad (2)$$

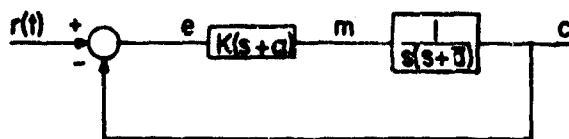


Fig. 2 Computational Example

Numerical values of Eq. (2), for various choices of  $\lambda$ ,  $k$  and  $a$ , were compared to corresponding approximations using 4 and 7 terms of the series expansions.<sup>3</sup> These low order approximations were quite good.

The theoretical basis for this orthonormal function technique is summarized in Ref. 4.

Army Research Office (Durham)  
DA-31-124-ARO-D-316

L. Shaw

#### REFERENCES

1. L. Shaw and P. Chalon, Semi-Annual Report No. 32 to the Joint Services T. A. C. Report R-452, 32-67, pp. 263-4.
2. S. B. Revkin, "Random Variable Techniques applied to Helicopter Control," Project Report for MS in EE, Polytechnic Institute of Brooklyn, June 1968.
3. E. Frankfort, "Evaluation and Optimization of Performance Criteria in Linear Systems Containing an Uncertain Parameter," Project Report for MS in EE, Polytech. Inst. of Brooklyn, June 1968.
4. L. Shaw and P. Chalon, "An Expansion for the Evaluation of Sensitivity with Respect to a Random Variable Parameter," EE Department Memo No. PIBEE 68-0007; and Preprints of IFAC Symposium on Sensitivity and Adaptivity, Dubrovnik Yugoslavia, August 1968.

ERGODICITY FOR NON-STATIONARY PROCESSES

A. Papoulis

In the usual definition of ergodicity it is assumed that a process  $x(t)$  is stationary, and conditions are studied for the time average

$$\bar{x}(\tau) = \lim_{T \rightarrow \infty} \frac{1}{2T} \int_{-T}^T x(t + \tau) x^*(t) dt \tag{1}$$

to equal the ensemble average

$$R(\tau) = E \{ x(t + \tau) x^*(t) \} \tag{2}$$

If  $x(t)$  is not stationary, then its autocorrelation

$$R(t, \tau) = E \{ x(t + \tau) x^*(t) \} \tag{3}$$

is a function of  $t$  and  $\tau$ . It cannot therefore equal the time average  $\bar{x}(\tau)$  which is a function of  $\tau$  only.

However, if we form the time average

$$\bar{R}(\tau) = \lim_{T \rightarrow \infty} \frac{1}{2T} \int_{-T}^T R(t, \tau) dt \tag{4}$$

then in certain cases

$$\bar{R}(\tau) = \bar{x}(\tau) \tag{5}$$

It is of interest to establish conditions for the validity of Eq. (5). We have considered the following special case:

Given a stationary process  $s(t)$  with autocorrelation  $R_s(\tau)$ , we form the periodic process

$$x(t) = s(t), 0 < t < T$$

$$x(t + T) = x(t)$$

This process is non-stationary and its autocorrelation is given by

$$R(t, \tau) = R_s(\tau_1 - \tau_2)$$

$\tau_1 = t + \tau, \tau_2 = t, t = nT + \tau_1, 0 < \tau_1 - \tau_2 < T$  where  $m$  and  $n$  are integers. We show that the time average  $\bar{R}(\tau)$  of  $x(t)$  is given by

$$\bar{R}(\tau) = R_s(\tau) \left(1 - \frac{\tau}{T}\right) + R_s(T - \tau) \frac{\tau}{T}, \quad 0 < \tau < T/2, \bar{R}(\tau + T) = \bar{R}(\tau)$$

and it satisfies Eq. (5)

We note that, with  $g$  a random variable uniformly distributed in the interval  $(0, T)$ , the process

$$\underline{z}(t) = \underline{x}(t - g)$$

is stationary and its autocorrelation is given by

$$R_{\underline{z}}(\tau) = \overline{R}_{\underline{x}}(\tau) = \overline{R}_{\underline{x}}(\tau)$$

Thus, if a random jitter is introduced into the non-stationary process  $\underline{x}(t)$ , the resulting process  $\underline{z}(t)$  is stationary and its autocorrelation equals the time average of the autocorrelation of  $\underline{x}(t)$ .

The validity of Eq. (5) is investigated for more general conditions.

National Science Foundation  
GU-1557

Joint Services Technical Advisory Committee  
AF 49(638)-1402

A. Papoulis

## DUAL OPTICAL SYSTEMS

A. Papoulis

In the following development, all signals are assumed monochromatic with angular frequency  $\omega$  and all lenses thin, illuminated by narrow beams. For simplicity of notation, the analysis is carried out in terms of two-dimensional fields and cylindrical lenses. The extension to three-dimensional fields and spherical lenses is self-evident.

### Diffraction

Suppose that the complex amplitude of an optical field on a plane  $P_1$  equals  $a(x)$ . With the usual approximations,<sup>1</sup> the complex amplitude of the field  $b(x)$  on a plane  $P_2$  distance  $z_1$  from  $P_1$  is given by\*

$$b(x) = \int_{-\infty}^{\infty} a(\xi) e^{jkx} d\xi \quad (1)$$

where [Fig. 1(a)]

$$r = [z_1^2 + (x - \xi)^2], \quad k = \omega/c = 2\pi/\lambda \quad (2)$$

The function  $a(x)$  is such that

$$a(x) = 0 \quad \text{for } |x| > x_0, \quad x_0 \ll z_1.$$

---

\* In all equations, a constant factor (independent of  $x$  or  $u$ ) will be omitted.

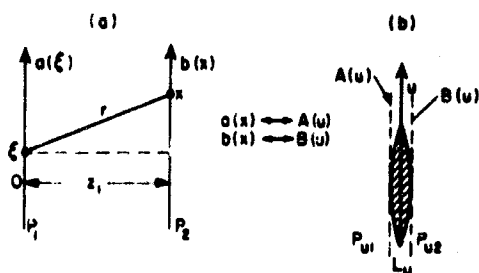


Fig. 1. (a) Diffraction of  $a(x)$ ;  $b(x) = a(x) * \exp(j\alpha x^2)$ ,  $\alpha = k/2z_1$ .  
 (b) Dual of free space;  $B(u) = A(u) \exp(-jku^2/2f_u)$ ,  $f_u = 4\pi^2/\lambda^2 z_1$ .

With the Fresnel approximation

$$r \approx z_1 + (x - \xi)^2 / 2z_1, \tag{3}$$

Eq. (2) yields the convolution integral<sup>2</sup>

$$b(x) = \int_{-\infty}^{\infty} a(\xi) \exp[jk(x - \xi)^2 / 2z_1] d\xi, \tag{4}$$

which is written in the form

$$b(x) = a(x) * e^{j\alpha x^2}, \quad \alpha = k/2z_1. \tag{5}$$

Thus,  $b(x)$  can be considered as the output of a linear system with input  $a(x)$  and point spread

$$h(x) = e^{j\alpha x^2}. \tag{6}$$

The corresponding system function, i. e., the Fourier transform of  $h(x)$ , is given by<sup>4</sup>

$$H(u) = \int_{-\infty}^{\infty} e^{j\alpha x^2} e^{-jux} dx = \left(\frac{\pi}{\alpha}\right) e^{j\pi/4} \exp[-ju^2/4\alpha]. \tag{7}$$

Lenses

Consider a perfect lens  $L$  of focal length  $f$ . If the field on the plane  $P^-$  to its left [Fig. 2(a)] equals  $c(x)$ , then the field  $d(x)$  on the plane  $P^+$  to its right is given by<sup>3</sup>

$$d(x) = c(x) e^{-j\beta x^2}, \tag{8}$$

where  $\beta = k/2f$ . This is a satisfactory approximation provided that the angle of incidence is narrow and  $c(x)$  takes significant values only in a small region (compared to  $f$ ).

With  $A(u)$  and  $B(u)$  the Fourier transforms of  $a(x)$  and  $b(x)$ , respectively, it follows

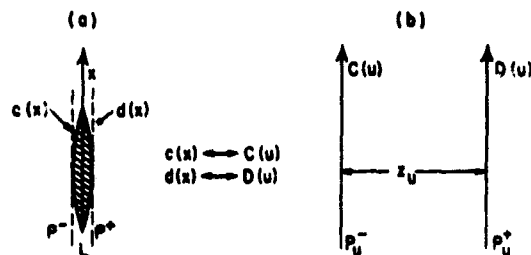


Fig. 2. (a) Perfect lens  $L$ ;  $d(x) = c(x) \exp(-j\beta x^2)$ ,  $\beta = k/2f$ .

(b) Dual of  $L$ ;  $D(u) = C(u) * \exp(jku^2/2z_u)$ ,  $z_u = 4\pi^2/\lambda^2 f$ .

from the convolution theorem and Eqs. (5) and (7) that

$$B(u) = A(u) \exp[-ju^2/4\alpha]. \quad (9)$$

If, in the  $u$ -space,  $A(u)$  is the field on the plane  $P_{u1}$  to the left of a lens  $L_u$  of focal length

$$f_u = 2\alpha k = 4\pi^2/\lambda^2 z_1. \quad (10)$$

[Fig. 1(b)], then [see Eq. (8)] the field on the plane  $P_{u2}$  to its right equals  $B(u)$ .

Thus, the dual of free space between two planes distance  $z_1$  apart, is a lens of focal length  $4\pi^2/\lambda^2 z_1$ , in the sense that if  $A(u)$  is the Fourier transform of  $a(x)$  (Fig. 1), then  $B(u)$  is the Fourier transform of  $b(x)$ .

With  $C(u)$  and  $D(u)$  the Fourier transforms of  $c(x)$  and  $d(x)$ , respectively, it follows from Eq. (8) and the convolution theorem that

$$D(u) = C(u) * \exp[ju^2/4\beta]. \quad (11)$$

If  $C(u)$  is the field on a plane  $P_u^-$ , then the diffracted field on another plane  $P_u^+$  at the distance

$$z_u = 2\beta k = 4\pi^2/\lambda^2 f \quad (12)$$

from  $P_u^-$  [Fig. 2(b)] equals  $D(u)$  [see Eq. (5)].

Thus, the dual of a lens of focal length  $f$  is a portion of free space between two planes (Fig. 2) distance  $4\pi^2/\lambda^2 f$  apart, in the sense that, if  $C(u)$  is the Fourier transform of  $c(x)$ , then  $D(u)$  is the Fourier transform of  $d(x)$ . Repeated application of the preceding conclusions leads to the following duality principle.

Consider a system  $S$  consisting of lenses  $L_i$  of focal length  $f_i$  located on the planes  $P_i$  distance  $z_i$  apart [Fig. 3(a)]. The dual system  $S_u$  is formed by replacing each lens by a portion of space between two planes  $P_{ui}^+$  and  $P_{ui}^-$  distance  $4\pi^2/\lambda^2 f_i$  apart



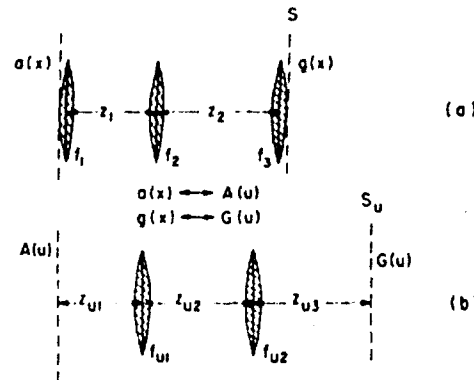


Fig. 3 Optical system  $S$  and its dual  $S_u$ ;  $z_{ui} = 4\pi^2 / \lambda^2 f_i$ ,  $f_{ui} = 4\pi^2 / \lambda^2 z_i$ .

[Fig. 3(b)] and inserting on each plane  $P_{ui}^+$  a lens of focal length  $4\pi^2 / \lambda^2 z_i$ . This system has the property that if the field on its input plane equals the Fourier transform of the field on the input plane of  $S$ , then the field on any other plane will equal the Fourier transform of the field on the corresponding plane of  $S$ .

Example

As an application, the field  $g(x)$  on the right focal plane  $P_r$  of a lens  $L$  [Fig. 4(a)] equals the Fourier transform  $A(u)$  of the field  $a(x)$  on the left focal plane  $P_l$  (properly scaled)

$$g(x) = \Lambda(2\pi x / \lambda f) \tag{13}$$

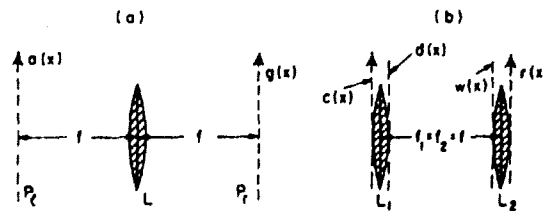


Fig. 4. (a) Fourier transform system;  $a(x) \rightarrow A(u)$ ,  $g(x) = \Lambda(2\pi x / \lambda f)$ .

$$(b) \text{ Dual system } u = k / 2f; r(x) = \{ [c(x) \exp(jax^2)] * \exp(-jax^2) \} \exp * jax^2$$

The dual of the system in Fig. 4(a) is shown in Fig. 4(b). From the duality principle it follows that if  $c(x)$  is the Fourier transform of  $a(x)$ , then  $r(x)$  is the Fourier transform of  $g(x)$ . Therefore, to prove Eq. (13) it suffices to show that  $r(x)$  is the Fourier transform of  $c(x)$ .

The field  $d(x)$  on the right side of lens  $L_1$  is given by

$$d(x) = c(x) e^{-jax^2}, \quad u = k / 2f$$

[see Eq. (8)]. Therefore [Eq. (5)] the field  $w(x)$  on the left side of lens  $L_2$  equals

$$\begin{aligned} w(x) &= d(x) * e^{jax^2} = \int_{-\infty}^{\infty} c(\xi) e^{-ja\xi^2} e^{ja(x-\xi)^2} d\xi \\ &= e^{jax^2} \int_{-\infty}^{\infty} c(\xi) e^{-j2a\xi\xi} d\xi = e^{jax^2} C(2ax), \end{aligned}$$

where  $C(u)$  is the Fourier transform of  $c(x)$ . Finally, the field  $r(x)$  on the right side of lens  $L_2$  is given by

$$r(x) = w(x) e^{-jax^2} = C(2ax) = C(2\pi x / \lambda f).$$

The proof of Eq. (13) is, thus, complete.

National Science Foundation  
GU-1557

A. Papoulis

Joint Services Technical Advisory Committee  
AF 49(638)-1402

#### REFERENCES

1. M. Born and E. Wolf, *Principles of Optics* (New York: Pergamon Press, Inc., 1959).
2. L. Mertz, *Transformations in Optics* (New York: John Wiley and Sons, Inc., 1965).
3. A. Papoulis, *Systems and Transforms with Applications in Optics* (New York: McGraw Hill Book Co., 1968).

#### INTERPOLATION WITH DERIVATIVES

J. W. Matthews

Little is known regarding the question of interpolating with the derivatives of functions beyond the case of polynomials. Utilizing the concepts of reproducing kernel Hilbert spaces, the following general statement can be made:

**Theorem:** Let  $X$  be an  $n$ -dimensional Haar subspace of  $C_1[a, b]$  such that the space spanned by the derivatives of  $X$  is an  $(n-1)$ -dimensional Haar subspace of  $C_0[a, b]$ . Let  $E = [a, b] \subset \mathbb{R}$ , the real line, and take the 2-norm for  $X$ . Then the following statements are true and equivalent:

- (1) for any distinct set  $\{t_1, \dots, t_j\} \subset E$  and any distinct subset  $\{t_{j_1}, \dots, t_{j_l}\} \subset \{t_1, \dots, t_j\}$  such that the total number of points in the set and the subset is  $\leq n$ , and for any  $\{a_1, \dots, a_j, a_{j_1}, \dots, a_{j_l}\} \subset \mathbb{R}$ , there exists an  $x \in X$  such that:

$$x(t_i) = a_i, \quad i = 1, \dots, j$$

$$x'(t_{j_i}) = a_{j_i}, \quad i = 1, \dots, l$$

(2) the set  $\{k_{t_1}, \dots, k_{t_j}, k_{t'_{j_1}}, \dots, k_{t'_{j_l}}\} \subset X$  is linearly independent where the  $k_t$ 's are the reproducing kernels and the  $k_{t'}$ 's are the derived reproducing kernels.

(3) The Gram determinant,  $G(k_{t_1}, \dots, k_{t_j}, k_{t'_{j_1}}, \dots, k_{t'_{j_l}}) > 0$ .

There are many corollaries that result from this theorem. We will list three. The first is a summary of the theorem in terms of interpolation.

**Corollary I:** Given an arbitrary set of distinct points in  $E$ , one may interpolate with a function in these points and may interpolate with the derivative of the function in some or all of these same points provided the total number of times of interpolation, counting as one interpolation the arbitrary specification of the function in one point and counting as one interpolation the arbitrary specification of the derivatives in one point, does not exceed  $n$ .

**Corollary II:** Given an arbitrary set of distinct points in  $E$ , one may interpolate with a function in these points and may also interpolate with the derivative of the function in a different set of distinct points in  $E$  provided the total number of times of interpolation, counting as one interpolation the arbitrary specification of the function in a point and counting as two interpolations the arbitrary specification of the derivative in a point, does not exceed  $n$ .

**Corollary III:** One may interpolate in  $n-1$  distinct points of  $E$  with a function and interpolate the derivative once, anywhere in  $E$ , except at  $n-2$  points, each of these points lying in a distinct open interval  $(t_i, t_{i+1})$ ,  $i = 1, \dots, n-2$ , where  $t_i$ ,  $i = 1, \dots, n-1$  are the points of interpolation with the function.

National Science Foundation  
GU-1557

J. W. Matthews

Joint Services Technical Advisory Committee  
AF 49 (638)-1402

## REALIZATION OF MAXIMUM GAIN RC LADDER NETWORKS

L. J. Degan and H. Ruston

The realization of an RC ladder from two prescribed two-port parameters is a problem well studied in the past. However, all the synthesis methods advanced so far produce a network whose gain is not known until the network is realized. Furthermore,

the mechanism which governs the gain, that is, its control and its tradeoff (for other desirable features of design) was apparently not understood in the past.

It was the object of this study to develop a method for the realization of maximum gain RC ladder with prescribed  $z_{11}$ ,  $z_{12}$ ,  $R_{\max}/R_{\min}$ , and  $C_{\max}/C_{\min}$ . The last two numbers give the permissible spread on the element values.

This study was divided into three cases, namely: (1) Low-pass case; (2) High-pass case; and (3) Band-pass case. The solutions to cases (1) and (2) were found, and were reported in a previous report<sup>1,2</sup>.

Early work on the band-pass case attacked the problem along the traditional lines. Since a ladder is realized by synthesis of a  $z_{11}$  with prescribed transmission zeros (which are the zeros of  $z_{12}$ ), it was believed that it is the order in which the transmission zeros are developed that controls the gain. Thus, early effort was directed on finding the achievable ladder gain prior to synthesis, and on finding the optimal ordering of the transmission zeros. The result of the study was an algorithm utilizing Branch and Bound Theory, which accomplished an ordered search of the many possible networks ( $2^n n!(n+1)!$  networks may exist for  $n$  transmission zeros). However, present investigation showed that even optimum ordering does not lead to maximum gain. To achieve maximum gain, the zero shifting technique must be extended, in that in general, all zeros (rather than a single one) of  $z_{11}$  must simultaneously be shifted. This means that at the beginning, and perhaps also later steps of synthesis, all (or nearly all) poles have to be partially removed (to effect the shifting). Thus, the problem was now re-interpreted into finding the factors (between 0 and 1) that must multiply each residue, for the remainder impedance. With this interpretation the problem can then be attacked by dynamic programming techniques because of the following optimality theorem.

**Theorem A.** If an RC ladder network,  $N$ , has maximum gain and is described by  $z_{11}$  and  $z_{12}$ , then any subnetwork which includes the final stage of  $N$  is also a maximum gain network described by  $z'_{11}$  and  $z'_{12}$ .

Although the method following from the theorem can theoretically be immediately applied, it leads to considering a very large number of stages to find the optimum ones. For a one-stage problem, there are four possible candidates for optimum networks. For a two-stage network, there are about 16 optimum networks, and it goes up exponentially for additional stages. However, theorem A does permit some conclusions to be proven about the last stage of a maximum gain network as given in Theorem B. This theorem and later theorems allow a significant reduction in the number of networks to be considered, thus making the method practical.

Theorem B. If the realization of an RC ladder network has maximum gain  $K$  and is described by  $z_{11}$  and  $z_{12}$ , the network cannot terminate in:

1. a parallel RC impedance across the output terminals,
2. a resistance L-stage network or
3. a capacitance L-stage network.

Additional useful theorems that have been proven are:

Theorem C. For an RC ladder network, described by its series and shunt impedances and assuming that the successive open-circuit input impedances,  $z_{11}^k$ , are ratios of polynomials of the same degree, the gain  $K$  of the voltage transfer function can be found by constructing a reduced RC ladder network. This new network is formed by:

1. shorting all capacitors in the series branches,
2. open-circuiting the shunt resistors and shunt RC impedances if they are paralleled by a capacitor, and
3. opening all shunt impedances across the input after step 1 is performed.

This reduced network has the same  $K$  as the original network.

Theorem D. If an RC ladder network is described by

$$T = \left. \frac{V_2}{V_1} \right|_{I_2 = 0} = \frac{z_{12}}{z_{11}} = \frac{K \prod_{i=1}^m (s+z_i)}{\prod_{i=1}^n (s+p_i)} \quad (1)$$

$$z_i = \frac{\prod_{i=1}^n (s+p_i)}{\prod_{i=1}^n (s+\gamma_i)} \quad (\gamma_i \text{ may be zero}) \quad (2)$$

and a partial pole of  $z_{11}$  is removed as a series impedance, the upper bound for  $K$  is decreased.

Theorem E. If an RC ladder network is described by

$$T = \frac{K \prod_{i=1}^m (s+z_i)}{\prod_{i=1}^n (s+p_i)} \quad (3)$$

$$z_{11} = \frac{\prod_1^n (s+p_i)}{\prod_1^n (s+\gamma_i)} \quad (\gamma_i \text{ may be zero}) \quad (4)$$

the upper bound for  $K$  is not changed when a zero of  $z_{11}$  is partially removed as a shunt impedance.

By using Theorems C, D, and E, an algorithm was developed that will result in an RC ladder network with a very large gain. For the band-pass case, this gain can be made to approach the upper bound on  $T(s)$  (i. e., for any  $z_{11}$ ) given by Paige and Kuh<sup>3</sup>. The gain cannot be made equal to the upper bound without the element spread ratios  $R_{\max}/R_{\min}$  and  $C_{\max}/C_{\min}$  going to infinity. For the low- and high-pass cases, the gain can be made equal to the upper bound. The algorithm is:

- If the degrees of the numerator and denominator of  $z_{11}$  are unequal, remove a shunt capacitor to make them equal.
- Determine the value for  $r$  which is the index of the voltage transfer function pole at the left of the maximum horizontal asymptote on a Bode plot.
- Form the partial fraction expansion:

$$\frac{1}{z_{11}} = k_0 + \sum_1^n \frac{k_i s}{s+p_i} \quad (5)$$

and partially remove the  $n-r$  largest poles of  $1/z_{11}$  by shunt networks given by

$$Y_i = \frac{\alpha_i k_i s}{s+p_i} \quad (6)$$

where  $0 \leq \alpha_i < 1$ . In general,  $\alpha_i$  should be very close to 1 for maximum  $K$ . The actual values of the  $\alpha_i$ 's will be determined on a trial basis by letting  $K$  approach its upper bound but keeping the ratios  $R_{\max}/R_{\min}$  and  $C_{\max}/C_{\min}$  within practical limits.

- Continue to construct the first portion of the ladder network by removing all the zeros of  $T$  which are less than  $z_{r+1}$ . Each step will consist of one of the following:
  - Remove a total conductance.
  - Partially remove a conductance or immittance to shift a pole to a transmission zero.
  - Immediately following step 2, invert and remove the transmission zero.

Caution has to be used to insure that all series impedances have a capacitor across them. Also, a check must be made after each series impedance removal to see that the maximum horizontal asymptote on the Bode plot still passes through the original  $p_r$ . This can be verified numerically if

$$\frac{\prod_{i=1}^r p_i}{\prod_{i=1}^r z_i} > 1 \text{ for all } q < r \quad (7)$$

where  $r$  is the index of the largest pole to the left of the maximum horizontal asymptote and  $q$  is the index of the largest pole to the left of any horizontal asymptote.

The requirements of Eq. (7) can be achieved by trying various pole-zero shiftings on a trial and error basis. An alternate method is to establish barriers on the lower limits of  $p_{q+1}, \dots, p_n$  by partial shunt removal of their residues as given in Eq. (6). If the  $a_i$ 's are made sufficiently large, the transmission zeros can then be removed in increasing order. The best values of the  $a_i$ 's can then be determined later along with the  $a_i$ 's of step (c).

- e. The remaining network after step (d) will be a low-pass network. Synthesis of the low-pass network, with maximum gain, can be accomplished by the procedures given by Paige and Kuh<sup>3</sup> or Johnson<sup>2</sup>.

End of Algorithm

A computer program has been written on a GE625 time-sharing computer to aid in finding a network with a large  $K$  and acceptable limits of  $R_{\max}/R_{\min}$  and  $C_{\max}/C_{\min}$ . The algorithm and computer program have been applied to three band-pass cases with excellent results. The three applications are:

- a simple problem with only two poles in the voltage transfer function,
- the example considered in Ref. 1 which has four poles in the voltage transfer function and
- a complex problem with three peaks in the voltage transfer function. Two of the peaks have equally high horizontal asymptotes on a Bode plot.

National Science Foundation  
GK-236

L. J. Degan  
H. Ruston

#### REFERENCES

1. D. Farmer, D. E. Johnson and H. Ruston, "Synthesis of Maximum Gain RC Ladder Networks with Prescribed Open-Circuit Impedance Parameters," Progress Report No. 30 to the JSTAC, 15 March 1966 through 14 September 1966 of the PIB Microwave Research Institute Programs, pp. 129-134.
2. D. E. Johnson, "Synthesis of Maximum Gain Low-Pass RC Ladder Networks with Prescribed Open-Circuit Impedance Parameters," Master's Report at PIB, June 1967.
3. A. Paige and E. S. Kuh, "Maximum Gain Realization of an RC Ladder Network," I. R. E. Trans. on Circuit Theory, pp. 32-40, March 1960.

## MINIMUM GYRATOR SYNTHESIS

D. C. Youla and G. D. Ott

There are any number of techniques for the synthesis of lumped passive n-ports from prescribed rational bounded real scattering matrices. The realization of a given matrix, however, is by no means unique. Moreover, a given realization may contain superfluous reactive elements, resistors, or ideal gyrators. A realization is said to be minimal with respect to an element type if no other realization can contain fewer elements of the given type.

It is well known<sup>1</sup> that the minimum number of ideal gyrators required for the realization of a rational bounded real matrix,  $S(p)$ , is greater than or equal to one half the normal rank of the skew symmetric part of  $S(p)$ . The problem of proving that  $S(p)$  is realizable with exactly this number of gyrators is now classic. Oono's proof<sup>2</sup> that one needs no more than  $n-1$  gyrators to realize any  $n \times n$  regular para-unitary bounded real matrix is the sharpest result yet obtained for the general case.

In this report it is proven that any skew symmetric regular para-unitary matrix can be realized using simultaneously the minimum number of gyrators and minimum number of reactances. (The phrase "the minimum number of gyrators" will be used synonymously with "one half of the skew symmetric rank of the matrix," throughout this report.) A more general result is also obtained which includes the skew symmetric case. It is proven that any regular para-unitary matrix which has a skew symmetric part that is non-singular along the entire imaginary axis of the  $p$ -plane (including  $p = \infty$ ) is realizable with the minimum number of gyrators. Since the realization of any regular para-unitary matrix can easily be reduced to the realization of one having a skew symmetric part which is not identically singular, the technique encompasses a very large class of matrices.

Minimum Gyrator Synthesis:

Our objective is to realize  $S(p)$ , an  $n \times n$  regular para-unitary matrix, using exactly  $K$  gyrators, where  $K = \frac{1}{2} r [S(p) - S'(p)]$ . We begin by reducing  $S(p)$  to a regular para-unitary matrix having a skew symmetric part which is not identically singular, via the following preamble.

case 1) If  $\det(1_n \pm S(p)) \neq 0$ , there exists a real constant vector,  $\underline{x}$ , satisfying  $S(p)\underline{x} = \epsilon \underline{x}$ , where  $\epsilon = \pm 1$  and  $\underline{x}'\underline{x} = 1$  (Ref. 3). Form a real orthogonal  $n \times n$  matrix which has  $\underline{x}$  as its first column.  $X = [\underline{x} | X_1]$ ;  $X'X = 1_n$ .

$$\text{then } X'S(p)X = \left[ \begin{array}{c|c} \underline{x}'S(p)\underline{x} & \underline{x}'S(p)X_1 \\ \hline X_1'S(p)\underline{x} & X_1'S(p)X_1 \end{array} \right]$$



and using  $S(p)\underline{x} = \underline{\epsilon}_x$  and  $X_1' \underline{x} = \underline{0}_{n-1}$  we obtain

$$X'S(p)X \equiv \hat{S}(p) = \left[ \begin{array}{c|c} \underline{\epsilon} & \underline{0}' \\ \hline \underline{0} & X_1' S(p) X_1 \end{array} \right] \equiv \left[ \begin{array}{c|c} \underline{\epsilon} & \underline{0}' \\ \hline \underline{0} & S_1(p) \end{array} \right].$$

We define the  $2n$ -port frequency independent network,  $N_t$ , by the  $2n \times 2n$  orthogonal scattering matrix

$$S_t = \left[ \begin{array}{c|c} \underline{0}_n & X \\ \hline X' & \underline{0}_n \end{array} \right].$$

$S(p)$  is realized by the  $n$ -port which results by terminating the  $(n+1)$ st port of  $N_t$  in either an open or short circuit, and the last  $n-1$  ports in the realization of  $S_1(p)$ , an  $(n-1) \times (n-1)$  regular para-unitary matrix having the same skew symmetric rank as  $S(p)$ . We may therefore assume, with no loss of generality, that both  $Z(p) = [I_n + S(p)][I_n - S(p)]^{-1}$  and  $Z^{-1}(p)$  exist. Solving for  $S(p)$  and taking its skew symmetric part we obtain

$$S(p) - S'(p) = 2[Z'(p) + I_n]^{-1} [Z(p) - Z'(p)] [Z(p) + I_n]^{-1}.$$

case 2) If  $\det [S(p) - S'(p)] \equiv 0$  then by the last equation  $\det [Z(p) - Z'(p)] \equiv 0$ . Now  $Z(p)$  satisfies the equation  $Z(p) + Z_*(p) \equiv \underline{0}_n$  (where  $Z_*(p) \equiv Z'(-p)$ ). If  $Z(p)$  has a pole at  $p = \infty$  it must have a real symmetric non-negative definite residue matrix and can be extracted reciprocally. The remaining impedance is bounded and skew symmetric at  $p = \infty$ . Since  $Z(p) - Z'(p)$  is identically singular  $Z(\infty)$  is singular and therefore  $Y(p) \equiv Z^{-1}(p)$  possesses a pole at  $p = \infty$ . This pole again has a symmetric non-negative residue which can be extracted reciprocally. The inverse of the remaining admittance may or may not exist. If it does, it is singular at  $p = \infty$  and the process can be repeated. If it does not exist, then case 1 applies and the size of the matrix can be reduced. Eventually, after a finite number of steps, the reduction results in an immittance matrix for which the corresponding scattering matrix possesses a skew symmetric part which is not identically singular.

Therefore, without loss of generality, we may assume that  $\det [S'(p) - S(p)] \neq 0$ . The following case,  $S(p) = -S'(p)$ , is considered in detail since it provided the idea for the approach used in the more general case.

Case of  $S(p) = -S'(p)$

Since  $S(p)$  is skew symmetric, all zeros and poles of its determinant must be of even multiplicities. We shall reduce the degree of  $S(p)$ , which is the same as the degree of  $\det S(p)$  since  $S(p)$  is para-unitary, by extracting reciprocal  $2n$ -port all-pass networks at the singular points of  $S(p)$ .

case 1)  $\det S(\sigma_0) = 0$  ( $\sigma_0$  real, positive)

We define the para-unitary matrix  $W(p)$  by

$$W(p) = B'_*(p) S(p) B_*(p)$$

where  $B(p) = I_n + \frac{2p \underline{x} \underline{x}'}{p + \sigma_0}$ ,  $\underline{x}$  real  $\underline{x}' \underline{x} = 1$ , is a general degree one regular para-unitary matrix normalized to  $I_n$  at  $p = 0$ . We shall attempt to choose  $\underline{x}$  such that  $W(p)$  is regular. Using the fact that  $\underline{x}' S(p) \underline{x} = 0$ , since  $S(p)$  is skew symmetric, we obtain

$$W(p) = S(p) - \frac{2p}{p - \sigma_0} [\underline{x} \underline{x}' S(p) + S(p) \underline{x} \underline{x}']$$

Since  $S(p)$  is regular, the only possible pole of  $W(p)$  in  $\text{Re } p > 0$  occurs at  $p = \sigma_0$ . Choosing  $\underline{x}$  as a real solution of  $S(\sigma_0) \underline{x} = \underline{0}$  yields a zero residue matrix for  $W(p)$  at  $p = \sigma_0$  and  $W(p)$  is regular para-unitary.

$$\therefore S(p) = B'(p) W(p) B(p)$$

case 2)  $\det S(p_0) = 0$  ( $p_0 = \sigma_0 + j\omega_0$ ;  $\sigma_0 > 0$ ,  $\omega_0 \neq 0$ ).

Let  $W(p) = B'_*(p) S(p) B_*(p)$  where

$$B(p) = I_n + \frac{A}{p + p_0} + \frac{\bar{A}}{p + \bar{p}_0}$$

and

$$A = 2 \left[ \frac{[(\bar{u} p_0 - \omega_0^2) \underline{x} - \sigma_0 |p_0|^2 \bar{\underline{x}}]}{|p_0|^2 - \sigma_0^2 |u|^2} \right] \underline{x}'$$

$$\underline{x}' \underline{x} = 1; \bar{\underline{x}}' \underline{x} = u$$

This form of  $B(p)$  is the general form of a degree 2 regular para-unitary matrix normalized to  $I_n$  at  $p = \infty$ .<sup>4</sup> Noting that  $A S(p) A'$  and  $\bar{A} S(p) \bar{A}'$  both vanish identically we have

$$W(p) = S(p) - \frac{\bar{A} S(p) + S(p) \bar{A}'}{p - \bar{p}_0} - \frac{A S(p) + S(p) A'}{p - p_0} + \frac{\bar{A} S(p) A' + A S(p) \bar{A}'}{(p - p_0)(p - \bar{p}_0)}$$

Again  $W(p)$  is para-unitary and regular except possibly at  $p = p_0$  and  $p = \bar{p}_0$ . We choose  $\underline{x}$  such that  $S(p_0) \underline{x} = \underline{0}$  and hence  $S(\bar{p}_0) \bar{\underline{x}} = \underline{0}$ . With this choice of  $\underline{x}$  the residue matrices of  $W(p)$  at  $p = p_0$  and  $p = \bar{p}_0$  both vanish and  $W(p)$  is again regular para-unitary.

We have shown that any skew symmetric regular para-unitary matrix  $S(p)$  may be factored as

$$S(p) = B'(p)W(p)B(p)$$

where  $B(p)$  is regular para-unitary and  $W(p)$  is skew symmetric regular para-unitary of lower degree than  $S(p)$ . We may now apply the same factorization to  $W(p)$ , etc. After a finite number of steps we arrive at the factorization

$$S(p) = \hat{V}'(p)K\hat{V}(p)$$

where  $\hat{V}(p)$  is regular para-unitary and  $K$  is a constant skew symmetric real orthogonal matrix. Now, there exists a real orthogonal matrix,  $T$ , such that

$$K = T'S_\ell T \quad \text{where } T'T = I_n$$

and

$$S_\ell = \begin{bmatrix} 0 & 1 \\ -1 & 0 \end{bmatrix} + \begin{bmatrix} 0 & i \\ -1 & 0 \end{bmatrix} + \dots + \begin{bmatrix} 0 & 1 \\ -1 & 0 \end{bmatrix}$$

Defining  $V(p) = T\hat{V}(p)$ , regular para-unitary, we have

$$S(p) = V'(p)S_\ell V(p)$$

Hence  $S(p)$  is realized by closing the last  $n$ -ports of a reciprocal  $2n$ -port  $N_a$ , possessing for its scattering matrix the  $2n \times 2n$  regular all pass description

$$S_a(p) = \begin{bmatrix} 0_n & V'(p) \\ V(p) & 0_n \end{bmatrix}$$

on  $\frac{n}{2}$  uncoupled ideal gyrators.  $S_\ell$  is the scattering matrix of  $\frac{n}{2}$  uncoupled ideal gyrators. Observe, that  $\delta(S_a) = 2\delta(V) = \delta(S)$  since  $\delta(V) = \frac{1}{2}\delta(S)$ . Thus this realization is also minimal with respect to reactances. The preceding case led to the idea that a judicious factorization of the skew symmetric part of an arbitrary regular para-unitary matrix might prove fruitful in the synthesis procedure. It will be shown that this is indeed true. The minimal realization will be explicitly obtained for the case in which  $\det[S(p)-S'(p)]$  does not vanish along the entire  $p=j\omega$  axis (including  $p=\infty$ ).

Case of  $\det[S(p)-S'(p)] \neq 0$  for  $p=j\omega$  (including  $p=\infty$ ).

We shall attempt to find a reciprocal  $2n$ -port,  $N_a$ , such that when the last  $n$ -ports of  $N_a$  are terminated in  $\frac{n}{2}$  decoupled ideal gyrators, the resulting  $n$ -port realizes  $S(p)$ . If we

Imagine that such a network exists and is described by the symmetric scattering matrix  $S_a(p)$ , then  $S(p)$  is given by

$$S(p) = S_{11}(p) - S_{12}(p) [S_{22}(p) + S_\ell]^{-1} S'_{12}(p)$$

where

$$S_a(p) = S'_a(p) = \begin{bmatrix} S_{11}(p) & S_{12}(p) \\ S'_{12}(p) & S_{22}(p) \end{bmatrix}$$

and  $S_\ell$  is the scattering matrix of  $\frac{n}{2}$  decoupled ideal gyrators. We may rewrite  $S(p)$  identically as

$$S(p) = S_{11}(p) - S_{12}(p) [S_{22}(p) - S_\ell]^{-1} [S_{22}(p) - S_\ell] [S_{22}(p) + S_\ell]^{-1} S'_{12}(p).$$

With the definitions

$$A(p) = S_{22}(p) - S_\ell \quad (1)$$

and

$$V(p) = -S_{12}(p) A^{-1}(p) \quad (2)$$

we obtain the equation

$$S_a(p) = \begin{bmatrix} S(p) + V(p)A(p)V'(p) & -V(p)A(p) \\ -A'(p)V'(p) & S_\ell + A(p) \end{bmatrix} \quad (3)$$

Since  $S_a(p)$  must be symmetric we require

$$A(p) - A'(p) = -(S_\ell - S'_\ell) = -2S_\ell \quad (4)$$

and

$$S(p) - S'(p) = 2V(p)S_\ell V'(p). \quad (5)$$

Now Eq. (5) always possesses a solution  $V(p)$ , the most obvious being obtained using elementary polynomial operations<sup>5</sup>. It is easily shown that since  $S(p)$  is regular,  $V(p)$  may be chosen regular. (This is accomplished via the change of variables  $p = \frac{1-z}{1+z}$ , accompanied by elementary polynomial operations in the variable  $z$ .) Given one solution for  $V(p)$ , any other solution is of the form  $\hat{V}(p) = V(p)K(p)$ , where  $K(p)$  is a symplectic matrix, that is,  $K(p)$  satisfies the equation

$$K(p)S_\ell K'(p) = S_\ell \quad (6)$$

Thus  $S(p)$  possesses a realization using exactly  $\frac{n}{2}$  gyrators if and only if there exists a factorization Eq. (5) of  $S(p)-S'(p)$  and a matrix  $A(p)$  such that  $S_a(p)$  given by Eq. (3) is a symmetric regular para-unitary matrix.

The para-unitary requirement on  $S_a(p)$  yields the three equations

$$SV'_* A_* V_* + VAV'S_* + VAV' V'_* A_* V_* + VAA_* V_* = 0_n \quad (7)$$

$$SV'_* A'_* + VAS'_\ell + VAV' V'_* A'_* + VAA_* = 0_n \quad (8)$$

$$S_\ell A_* + AS'_\ell + A' V' V'_* A'_* + AA_* = 0_n \quad (9)$$

where the  $p$  dependence is understood. It can be shown that

$$A(p) = -2 \left\{ I_n - V_*(p)S'(p)[V'(p)]^{-1}S'_\ell \right\}^{-1} S_\ell \quad (10)$$

satisfies Eqs. (7), (8) and (9) and makes  $S_a(p)$  symmetric. The details are lengthy and are omitted. The problem has been reduced, therefore, to finding that regular solution,  $V(p)$ , of Eq. (5) which results in a regular  $A(p)$  as given by Eq. (10). This would guarantee that  $S_a(p)$  in Eq. (3) is regular and symmetric para-unitary.

We define

$$Z(p) = \frac{1}{2} \left\{ I_n - V_*(p)S'(p)[V'(p)]^{-1}S'_\ell \right\} \quad (11)$$

then

$$A(p) = -Z^{-1}(p)S_\ell \quad (12)$$

Using Eqs. (8) and (9) one arrives at the relation

$$I_n + V_*(p)V(p) = Z(p) + Z_*(p) \quad (13)$$

Now

$$Z(p) = -S_\ell A^{-1}(p) = S_\ell [S_\ell - S_{22}(p)]^{-1}$$

$$Z(p) = [I_n - S_{22}(p)S'_\ell]^{-1}$$

Since  $S_{22}(p)$  is a diagonal block of a regular para-unitary matrix it must be bounded real.

Therefore, from the above equation,  $Z(p)$  must be positive real. Hence it suffices to find a solution,  $V(p)$ , of Eq. (5) which makes  $Z(p)$  in Eq. (11) regular with only simple poles having hermitian non-negative definite residue matrices on  $p = j\omega$ . By Eq. (13)  $Z(p)$  has a positive para-hermitian part on  $p = j\omega$  regardless of the choice of  $V(p)$ . Define

$$T(p) = V_*(p)S'(p)[V'(p)]^{-1}S'_t. \quad (14)$$

By assumption  $\det[S(p) - S'(p)]$  does not vanish for  $p = j\omega$  (including  $p = \infty$ ) and hence  $\det V(p)$  has the same property. By the above equation,  $T(p)$  also has this property. Using Eqs. (11), (13) and (14) it is seen that  $T(p) + T_*(p)$  is negative definite on  $p = j\omega$ . In a forthcoming memorandum, an effective technique is presented for factorizing a rational matrix with the properties of  $T(p)$  into the following form:

$$T(p) = L(p)R(p) \quad (15)$$

where  $L(p)$  and  $L^{-1}(p)$  are both analytic in  $\text{Re } p \leq 0$  ( $p = \infty$  included), while  $R(p)$  and  $R^{-1}(p)$  are both analytic in  $\text{Re } p \geq 0$  ( $\infty$  included). It can be directly verified that  $T(p)$  is a symplectic matrix; i. e.,

$$T(p)S_t T'(p) = S_t. \quad (16)$$

Using Eqs. (15) and (16) we write

$$R(p)S_t R'(p) = L^{-1}(p)S_t [L'(p)]^{-1}. \quad (17)$$

By Eq. (17),  $L^{-1}(p)S_t [L'(p)]^{-1}$  must be analytic in the entire  $p$ -plane and hence must be a non-singular constant skew symmetric matrix,  $K$ .

$$L^{-1}(p)S_t [L'(p)]^{-1} = K = -K' \quad (18)$$

Now there exists a non-singular constant matrix,  $Q$ , such that

$$K = Q^{-1}S_t(Q')^{-1}. \quad (19)$$

Using Eqs. (18) and (19) we get the relation

$$L_*^{-1}(p)Q'S_t Q [L'_*(p)]^{-1} = S_t. \quad (20)$$

Since  $L_*^{-1}(p)Q'$  is a regular symplectic matrix we define a new regular solution,  $\hat{V}(p)$ , of Eq. (5) by

$$\hat{V}(p) = V(p)L_*^{-1}(p)Q' \quad (21)$$

Substituting  $\hat{V}(p)$  for  $V(p)$  in Eq. (14) we obtain  $\hat{T}(p)$

$$\hat{T}(p) = QL^{-1}(p)V_*(p)S'(p)[QL_*^{-1}(p)V'(p)]^{-1}S'_\ell \quad (22)$$

$$\hat{T}(p) = QL^{-1}(p) \left\{ V_*(p)S'(p)[V'(p)]^{-1}S'_\ell \right\} S_\ell L_*(p)Q^{-1}S'_\ell$$

$$\hat{T}(p) = QL^{-1}(p)T(p)S_\ell L_*(p)Q^{-1}S'_\ell$$

and using Eq. (15) we obtain

$$\hat{T}(p) = QR(p)S_\ell L_*(p)Q^{-1}S'_\ell \quad (23)$$

Equation (23) shows that  $\hat{T}(p)$  is regular. Since  $\hat{V}(p)$  is also regular, the resulting matrix  $A(p)$  is regular and hence  $S_a(p)$  is regular symmetric para-unitary. Therefore a realization of  $S(p)$  exists which contains exactly  $\frac{n}{2}$  gyrators and the proof is complete.

In the case when  $S(p)-S'(p)$  is singular on  $p=j\omega$ , it is the conjecture that it is still always possible to choose a factorization Eq. (5) such that  $Z(p)$  in Eq. (11) is positive real. The major difficulty is seen in guaranteeing that  $Z(p)$  has simple poles on  $p=j\omega$ . It is extremely encouraging, however, that the problem has been brought to a stage where the difficulties are clearly defined. The problem has been reduced, essentially, to a problem of factorizing a skew symmetric matrix in a certain manner.

Air Force Systems Command  
 Research and Technology Division  
 Rome Air Development Center  
 AF 30(602)-3951

D. C. Youla and G. D. Ott

REFERENCES

1. R. W. Newcomb, "A Lower Bound on the Minimum Number of Gyrators in a Passive Network," Technical Report No. 6554-8, Stanford Electronics Laboratory, Stanford University.
2. Y. Oono and K. Yasamura, "Synthesis of Finite Passive 2n-Terminal Networks with Prescribed Scattering Matrices," Mem. Kyushu Univ. (Engin.), Vol. 14, 2(1954).
3. D. C. Youla, L. J. Castriota and H. J. Carlin, "Scattering Matrices and the Foundations of Linear, Passive Network Theory," Report R-594-57, PIB-522, September 10, 1957.
4. D. C. Youla, "Cascade Synthesis of Passive n-Ports," RADC-TDR-64-332, August, 1964, p. 56.
5. F. R. Gantmacher, "The Theory of Matrices," Vols. I & II, (New York:Chelsea Publishing Co., 1959).

## THE MAXIMIZATION OF NERVE CONDUCTION VELOCITY

S. Deutsch

The signal that is normally transmitted along an unmyelinated nerve fiber is a 2 msec wide rounded pulse or "action potential".<sup>1</sup> It can be simulated by applying a unit impulse to an RC cable at  $x = 0$ . The impulse response of the RC cable is

$$v = e^{-x\sqrt{RC}} \quad (1)$$

The waveshape corresponding to Eq. (1) is given by inverse Laplace transform tables as

$$v = \frac{x}{2t} \sqrt{\frac{RC}{\pi t}} e^{-x^2 RC/(4t)} \quad (2)$$

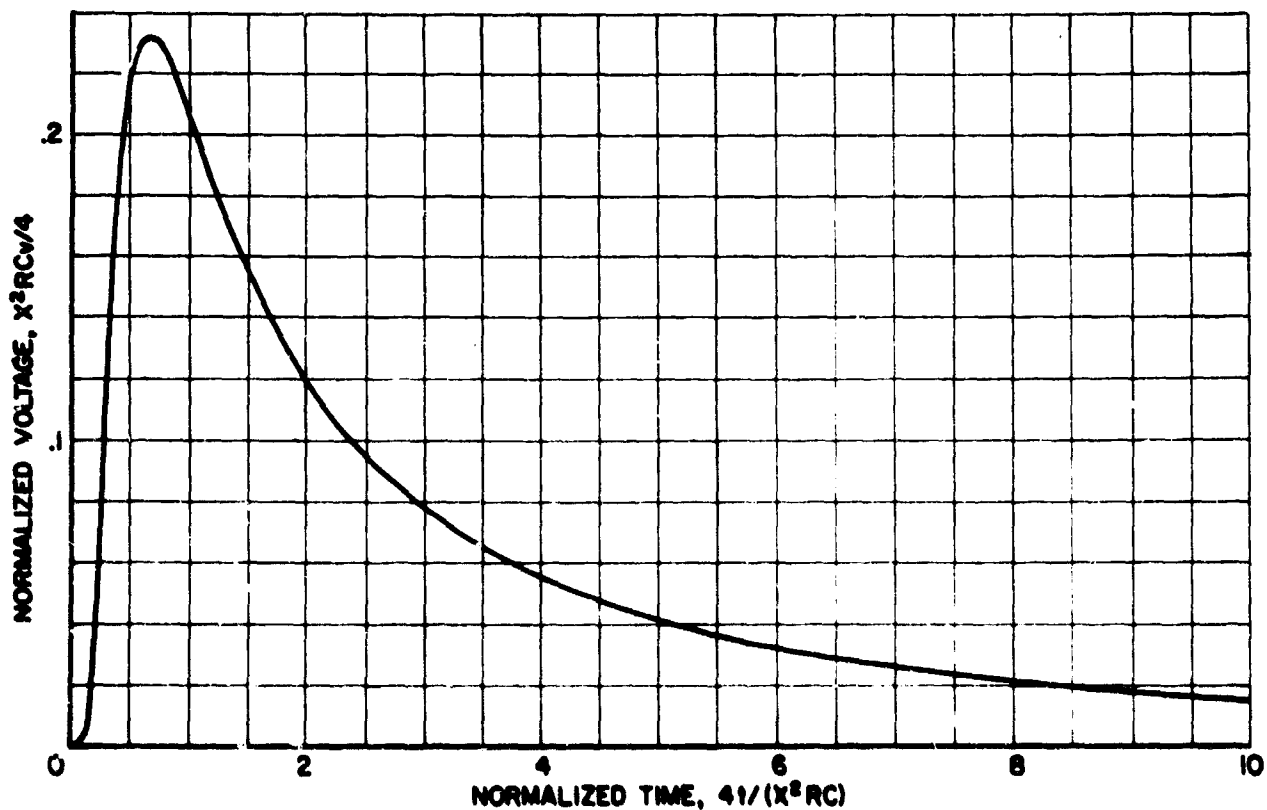


Fig. 1 Normalized Unit-Impulse Response of the RC Cable. The shape is an Excellent Likeness of the Action-Potential Waveshape that is Actually Observed in Vivo. The area Under the Curve is Unity.

Equation (2) is plotted in Fig. 1. The impulse-excited RC cable model is justified because Fig. 1 is an excellent likeness of the action-potential waveshape that is actually observed in vivo.



Differentiation of Eq. (2) with respect to  $1/t$  shows that the peak occurs at time

$$t_p = \frac{x^2 RC}{6} \tag{3}$$

and the corresponding peak value is given by

$$v_p = \frac{6}{x^2 RC} \sqrt{\frac{1.5}{\pi}} e^{-1.5} \tag{4}$$

A reasonable definition for the width ( $T$ ) of the action potential is the width of the curve at  $v_p/2$ . Figure 1 shows that this is approximately  $3t_p$ , so that

$$T = \frac{x^2 RC}{2} \tag{5}$$

Because of the  $x^2$  factor in Eqs. (4) and (5), we come to the conclusion that, in the absence of regeneration, the peak voltage rapidly decreases as the square of the distance while the width correspondingly increases. This situation is depicted in Fig. 2.

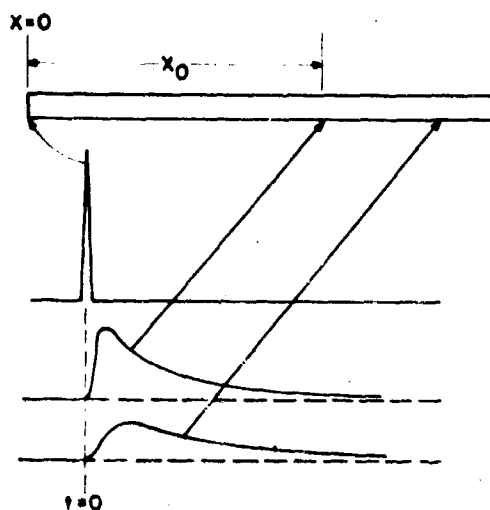


Fig. 2 A Nerve Fiber and the Waveshapes, in the Absence of Regeneration, that are Associated with a Unit Impulse of Excitation at  $x = t = 0$ .

A living fiber continually regenerates the signal so that  $v_p$  and  $T$  remain constant at approximately 100 mv and 2 msec, respectively.

A myelinated fiber is depicted in Fig. 3. Because regeneration requires an access to the interstitial fluid (mainly NaCl), the myelin is periodically interrupted by nodes as shown. The signal is regenerated at the nodes, where the cross section reverts to that of an unmyelinated fiber.

A reasonable value for the node-to-node transit time ( $t_{nn}$ ) is given by the time delay suffered by the  $v_p/2$  point on the leading edge of the action potential. Instead of

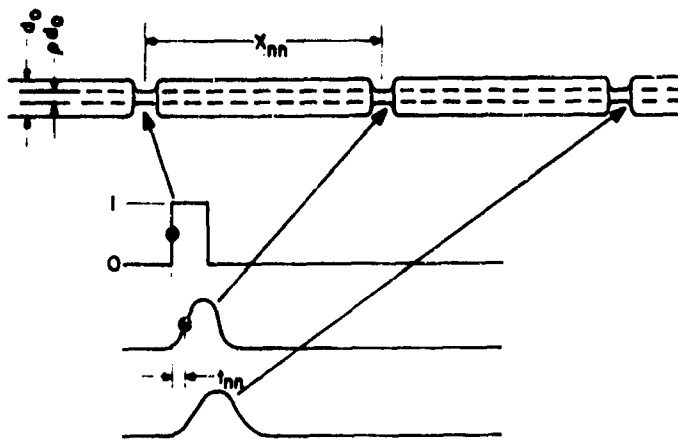


Fig. 3 A Myelinated Fiber and the Waveshapes, in the Absence of Regeneration, that are Associated with a Rectangular Pulse of Excitation at the first node.

dealing with the action potential of Fig. 1, however, which leads to a relatively complicated mathematical exercise, we can assume that the first node is excited by a 1-volt rectangular pulse, as shown in Fig. 3. The leading edge of the pulse at the second node is then described by the unit step response

$$v = \frac{1}{s} e^{-x\sqrt{sRC}} \quad (6)$$

The time function is given by inverse Laplace transform tables as

$$v = \operatorname{erfc} \left( \frac{x}{2} \sqrt{\frac{RC}{t}} \right) \quad (7)$$

Equation (7) is plotted in Fig. 4. The time delay at the 0.5-volt level is approximately given by

$$t_{nn} = x_{nn}^2 RC \quad (8)$$

where  $x_{nn}$  is the node-to-node spacing. The velocity of propagation now appears as

$$\text{velocity} = \frac{x_{nn}}{t_{nn}} = \frac{1}{x_{nn} RC} \quad (9)$$

According to Eq. (9), the velocity of propagation can be maximized by minimizing  $x_{nn}$  and  $RC$ . As  $x_{nn}$  is reduced, however, more and more of the fiber becomes exposed to the high capacitance of the nodes. For example: calculations based on subsequent results show that, for a  $d_0 = 10 \mu$  myelinated fiber, the capacitance is only 5.88 pF/cm in the myelin region compared to 858 pF/cm at the nodes. For this reason, we may conjecture, the fiber evolved so that the actual values of  $x_{nn}$  are relatively large.

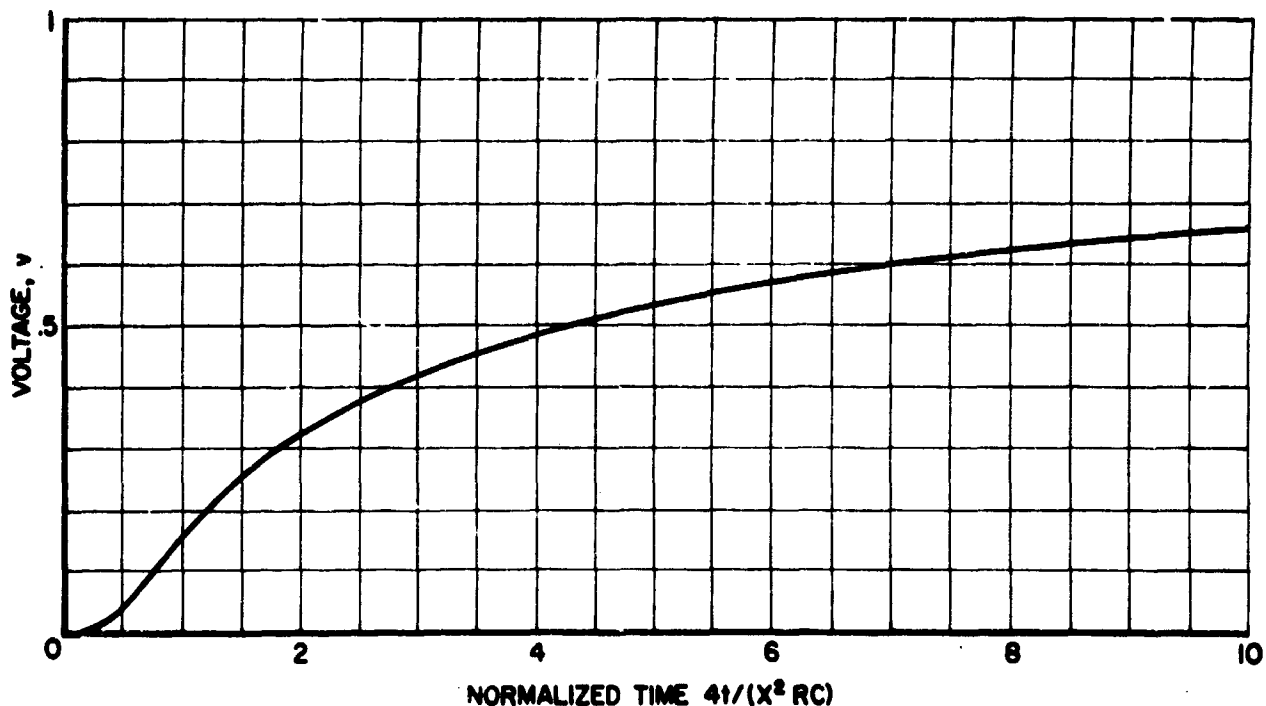


Fig. 4 Normalized Unit-Step Response of the RC Cable. The Curve would Eventually Reach the Full Amplitude of 1 Volt

The minimization of RC, on the other hand, is easily and unambiguously accomplished. For R we have

$$R = \frac{(200)(4)}{\pi \rho^2 d_o^2} \tag{10}$$

ohms per cm of length, where  $\rho$  is the ratio of inside/outside diameter, as defined in Fig. 3. For C we assume that the effective diameter of the cable is the average of inside and outside diameters, or  $d_o(1 + \rho)/2$ . The thickness of the insulation is  $d_o(1 - \rho)/2$ . Then

$$C = \frac{5(1 + \rho)}{36 \times 10^{11}(1 - \rho)} \tag{11}$$

farads per cm of length. Combining Eqs. (10) and (11),

$$RC = \frac{354 \times 10^{-12}(1 + \rho)}{d_o^2 \rho^2 (1 - \rho)} \tag{12}$$

seconds per cm of length.

The factor

$$F = \frac{1 + \rho}{\rho^2(1 - \rho)} \tag{13}$$

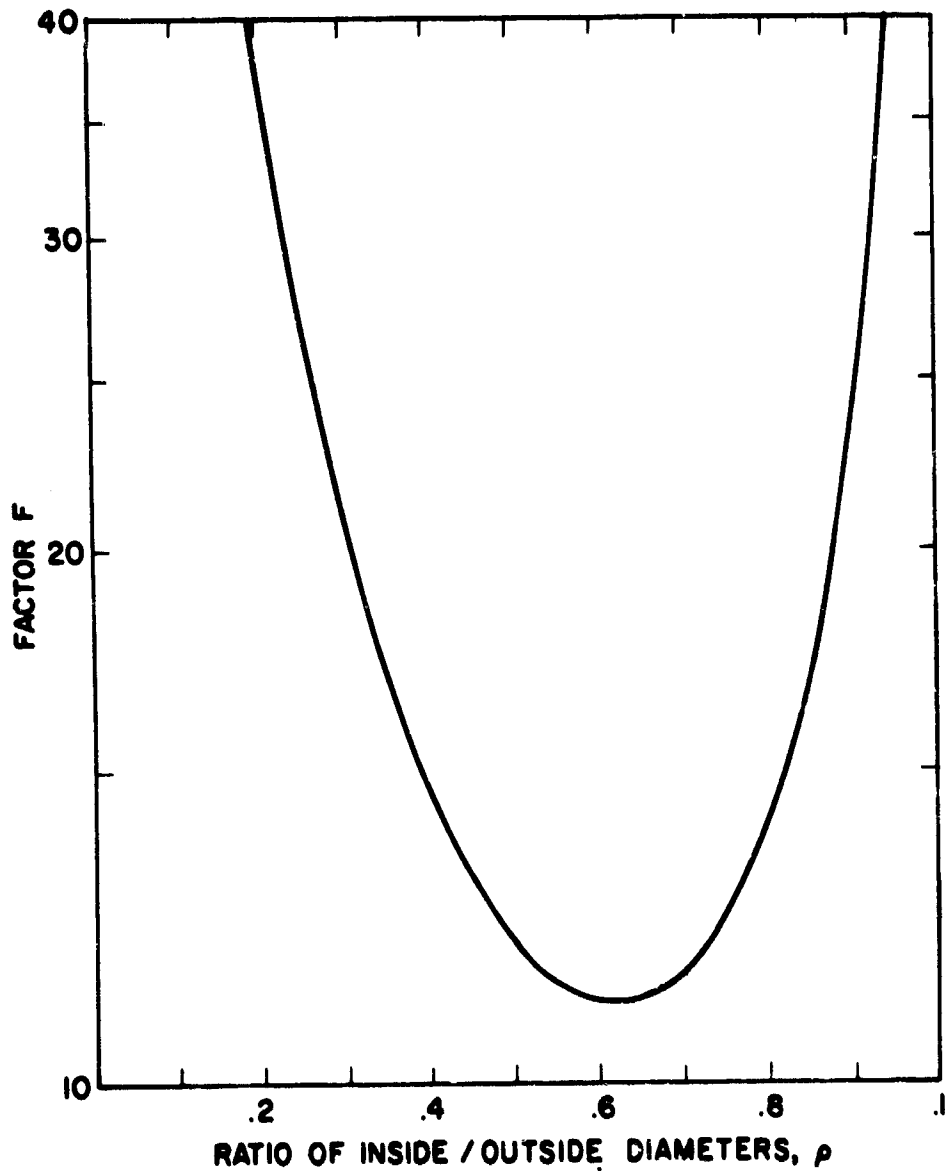


Fig. 5 Factor  $F = (1 + \rho)/(c^2 - \rho^3)$  versus  $\rho$ .

has a minimum at  $\rho_{\text{opt}} = \sqrt{1.25} - 0.5 = 0.618$  corresponding to which  $F_{\text{min}} = 5(\sqrt{1.25} + 1.1) = 11.09$ . As shown in Fig. 5, however, the minimum is broad and any value between  $\rho = 0.4$  and  $\rho = 0.8$  is reasonable. The geometry of actual fibers agrees with the  $0.4 < \rho < 0.8$  prediction (i. e., myelin thickness falls between  $0.1d_0$  and  $0.3d_0$ ).

Substituting  $\rho = 0.618$  in (11), we get  $C = 5.88 \text{ pT/cm}$ , independent of fiber diameter. Equation (12) then yields

$$(RC)_{\text{min}} = \frac{3920 \times 10^{-12}}{d_0^2} \quad (14)$$

seconds per cm of length. For a  $d_o = 10 \mu$  fiber, Eq. (14) yields 0.00392 compared to an unmyelinated value of 0.354 seconds per cm of length.

Measurements show that the velocity of propagation for myelinated axons is  $6 \times 10^6 d_o$ . Substituting this information as well as Eq. (14) into Eq. (9), we get

$$\frac{x_{nn}}{d_o} = 42.5. \quad (15)$$

There are wide variations in node-to node spacing, but the value  $42.5 d_o$  falls in the range that is reported based on histological examination. Substitution into Eq. (8) yields a constant node-to-node transit time,  $t_{nn} = 7.1$  microseconds, independent of fiber diameter.

National Science Foundation  
GU-1557

S. Deutsch

#### REFERENCE

1. S. Deutsch, "Models of the Nervous System," (New York: John Wiley and Sons, 1967).

## PUBLICATIONS AND REPORTS

### MEETING PAPERS

5th International Congress of AICA, Lausanne, Switzerland, August 1967

A. Lewis, M. Athans, W. S. Levine, "A System for the Optimal and Suboptimal Position and Velocity Control of a String of High-Speed Vehicles"

American Crystallographers Association Meeting, Minneapolis, Minn., August 1967

B. Post and R. Feldman, "Simultaneous Borrmann Diffraction"

Gordon Conference on Thin-Films, Tilton School, Tilton, N. H., August 1967

S. Soffer and H. J. Juretschke, "Electron Scattering near Surfaces"

Tokyo Institute of Technology, Tokyo, Japan, Sept. 6, 1967

D. Choudhury, "Intermediate Coupling Theory In The Unified Nuclear Model"

International Conference on Nuclear Structure, Tokyo, Japan, Sept. 7-13, 1967

D. Choudhury, "An Analysis of the Properties of Low-Lying Levels in  $^{131}\text{I}$ "

Department of the Army, Watervliet, New York, September 1967

E. Banks, "New Materials from High-Pressure High-Temperature Processes"

International Symposium on Information Theory, San Remo, Italy, Sept. 1967

R. R. Boorstyn and R. Pikholtz, "A Recursive Approach to Signal Detection"

R. R. Boorstyn and M. Schwartz, "Performance of Analog Demodulators in a Fading Environment"

D. L. Schilling and E. A. Nelson, "The Response of an FM Discriminator to a Digital FM Signal in Randomly Fading Channels"

J. K. Wolf and D. Calabro, "On the Synthesis of Two Dimensional Arrays with Desirable Correlation Properties"

Papers presented during an invited lecture trip of the Soviet Union, September 1967

L. B. Felsen, "Radiation in Anisotropic Plasmas," "Ray Methods in Diffraction Theory"

IEEE International Electron Devices Meeting, Washington, D. C., October 18-20, 1967

P. Rabinowitz, J. T. LaTourrette and G. Gould, "Proposed Ultrastable  $\text{CO}_2$  Oscillator"

1967 Fall URSI Symposium, Ann Arbor, Mich., October 1967

D. Tseng, A. Hessel, A. A. Oliner, "The Brillouin Diagram for Corrugated Structures in the Leaky Wave Region"

A. Hessel, G. H. Knittel and A. A. Oliner, "On the Theory of Resonances in Phased Array Antennas"

University of Southern California, Seminar, October 1967

N. Wainfan, "Time Resolved Studies on the Breakdown of High Current Density Glow Discharges"

The University of Missouri, Rolla, Mo., Seminar, October 28, 1967

B. Post, "Application of X-ray Powder Diffraction Methods to Materials Research"

15th National Symposium of American Vacuum Society, Pittsburgh, Pa., Oct. 29-Nov. 1, 1967

H. Schleuning, "A Brief History of Vacuum Apparatus and Techniques"

International Telemetry Conference, Washington, D. C., October 1967

D. Schilling, "The Detection of PCM/FM"

Conference on MF, LF, and VLF Radio Propagation, London, November 8-19, 1967

S. Maurer, L. B. Felsen, "Ray Methods for Guided Modes"

American Physical Society Meeting, New York, Nov. 16-18, 1967

D. Choudhury (with F. G. Bailey), "Effects of Vibration-Particle Coupling On the Properties of Light Nuclei"

University of Nebraska, Lincoln, Nebr., Seminar, December 1, 1967

H. J. Juretschke, "Metallic Field Effect"

Cooper Union, New York, N. Y., Seminar, December 4, 1967

L. Mendelsohn, "The Independent Particle Approximation in Many Body Theory"

New York Section Soc. Appl. Spectroscopy, Stevens Institute, Hoboken, New Jersey, December 5, 1967

B. Post, "Applications of X-ray Methods to Chemical Problems"

University of Palermo, Italy, Physics Seminars, December 18-20, 1967

L. Silber, "Ferromagnetic Resonance," "Anisotropy in Uniaxial Ferrites," "Galvanomagnetic Interactions in Ferromagnetic Resonance"

American Physical Society Winter Meeting, Pasadena, Calif., Dec. 1967

J. Shmoys and R. Lang, "Lateral Wave on an Epstein Transition"

Hawaii International Conference on System Science, Univ. of Hawaii, Jan. 1968

P. Dorato, "Optimal Bang-Bang Control of Stochastic Systems with a Small Noise Parameter"

I. Kohavi, "New Techniques for the Design of Fault Detection Experiments for Sequential Machines"

A. Papoulis, "New Results in Sampling Theory"

American Physical Society Meeting, N. Y. C., Jan. 1968

D. C. Choudhury (with J. T. Clemens), "The Unified Nuclear Model Description of the Odd-Mass Molybdenum Isotopes"

1968 Annual Symposium on Reliability, Boston, Mass., Jan. 1968

M. L. Shooman and M. Messinger, "Exponential and Weibull Approximations for Chain Structures"

Lowell Technological Institute, Lecture, March 11, 1968

S. H. Holt, "The Electronic Structure of Transition Metal Ions in High Oxidation States"

28th Physical Electronics Conference, Minneapolis, Minn., March 18-20, 1968

R. Stern and H. Taub, "Anisotropic Secondary Emission from Tungsten(110)"

R. Stern and A. Gervais, "Kikuchi Bands of Specular Reflection on Low Energy Electron Diffraction"

1968 Pittsburgh Conference on Analytic Chemistry, Cleveland, Ohio, March 1968

B. R. McGarvey, "Charge Transfer in the Metal Ligand Bond as Determined by ESR"

New York Chapter, Electron Device Group of the IEEE, April 11, 1968

B. Senitsky, "Use of Gases for Mm Wave Components"

PIB Symposium on Turbulence of Fluids and Plasmas, N. Y. C., April 16-18, 1968

K. Chung and D. J. Rose, "Low Frequency Fluctuations in the Weakly Turbulent Hollow Cathode Arc Plasma"

S. Rosenbaum, "On Energy-Conserving Formulations in a Randomly Fluctuating Medium"

ARPA Institutes Meeting at Long Island Graduate Center, PIB, April 19 and 20, 1968

J. W. E. Griensmann, "Non-Uniformity Effects in Resonant Microwave Cavities"

S. Lederman and M. H. Bloom, "Langmuir Probe Behavior"

L. B. Felsen, "Scattering from Fluctuating Media"

G. Gould, "Laser Research at PIB"

A. A. Oliner, "Unexpected Radiation Nulls in Phased Array Performance"

K. Chung, "Plasma Turbulence"

D. Rapp, "Collision Research at PIB"

1968 Spring Meeting of URSI, Washington, D. C., April 1968

D. D. ... and T. Tamir, "The Effect of Antenna Height in Forest Environments"

G. M. ...hitman and L. B. Felsen, "Transient Radiation in Bounded Magnetoplasmas"

Spring Meeting of the American Physical Society, Washington, D. C., April 25-28, 1968

H. J. Juretschke and L. Indyk, "Faraday Effect and Magnetization of Nickel"

H. J. Juretschke and A. Sisting, "H and H<sub>2</sub> in Strong Electric Fields"

F. Levi and H. W. Friedman, "Singularities of the Fluid Equations and Their Relation to Anomalous Diffusion"

R. Stern and H. Taub, "Anisotropic Inelastic Excitation in Low Energy Electron Diffraction"

R. Stern and A. Gervais, "Dynamical Origin of Fine Structure in Low Energy Electron Diffraction"

École Nationale Supérieure d'Électronique, Grenoble, France, Seminar, April 1968

L. Silber, "Hexagonal Ferrites"

National Telemetry Conference, Houston, Texas, April 1968

M. Schwartz and M. Hecht, "Sub-optimal Decision Feedback Communication Systems"



Pennsylvania State University, University, Pa., Seminar, April 1968

H. Juretschke, "Metal Surfaces and Molecules in High Electric Fields"

1968 International Quantum Electronics Conference, Miami, Fla., May 16, 1968

W. T. Walter, "Metal Vapor Lasers"

1968 Spring Joint Computer Conference, Atlantic City, New Jersey, May 1968

M. Schwartz and S. H. Richman, "External Statistics in Computer Simulation of Digital Communication Systems"

4th International Materials Symposium, University of California, Berkeley, June 17-21 1968

D. Boudreaux (with V. Hoffstein), "Some New Results from the Mathing-Band Structure Treatment of LEED Intensities"

R. Stern, H. Taub and A. Gervais, "Dynamical Origin of Three Dimensional Low Energy Diffraction Intensities"

Stevens Institute Society for Applied Spectroscopy, Hoboken, N. J., June 19, 1968

B. Post, "Application of X-ray Methods in Chemistry"

1968 URSI Symposium on Electromagnetic Waves, Stresa, Italy, June 24-29, 1968

L. B. Felsen, "Propagation in Inhomogeneous and Dispersive Media"

D. Tseng, A. Hessel, A. A. Oliner, "Scattering by a Multimode Corrugated Structure with Application to P Type Wood Anomalies"

B. Singer and T. Tamir, "The Field of a Line Source Embedded in a Periodically-Modulated Medium"

Cambridge University, England, June 24-28, 1968

B. Post, "Intensities of Multiple Diffraction Effects". "Accurate Determination of X-ray Intensities and Structure Factors"

American Physical Society Meeting, Los Alamos, New Mexico, June 1968

E. Levi (with H. W. Friedman), "Derivation of Macroscopic Stability Criterion," and "Stability of the Plasma Sheath"

École Nationale Supérieure d'Électronique, Grenoble, France, Seminar, June 1968

L. Silber, "Galvanomagnetic Properties of Ferromagnetic Metals"

International Symposium on Nuclear Structure, Dubna, USSR, July 4-11, 1968

D. C. Choudhury (with J. T. Clemens and F. G. Bailey), "Application of Intermediate-Coupling Unified Nuclear Model to Several Odd-Mass Nuclei"

Second International Federation of Automatic Control Symposium on System Sensitivity and Adaptivity, Dubrovnik, Yugoslavia, August 26-31, 1968

P. Dorato, "Noise Intensity Sensitivity in Optimal Stochastic Systems"

L. Shaw, "An Expansion for Evaluation of Sensitivity with Respect to a Random Variable Parameter"

International Symposium on the "Physics of One and Two Electron Atoms" at the University of Munich, Germany, September 9 - 14, 1968

L. Mendelsohn, "Perturbation Theory to All Orders for a One Electron Ion in a Uniform Electric Field"

L. Mendelsohn (with G. J. Iafrate), "Perturbation Theory to All Orders for an Electron in a Screened Coulomb Potential"

156th National Meeting of the American Chemical Society, Atlantic City, N.J., Sept. 11, 1968

C. A. Kosky and S. L. Holt, "The Electronic Structures of Higher Oxidation States,  $\text{MnO}_4^{2-}$ "

J. Milstein and S. L. Holt, "The Polarized Crystal Spectrum of  $\text{Ca}_2(\text{PO}_4, \text{MnO}_4)\text{Co}$ "

A. Galton, M. Kalafer and F.M. Beringer, "Rearrangements in the Clemmensen Reduction of 1-Indanones and 1, 3-Indandiones"

Laval University, Quebec, Ont., Canada, Seminar, September 20, 1968

B. Senitsky, "Amplification and Noise Properties of Averaged Non-Linearities"

Duke University, Durham, N. C., Seminar, September 20, 1968

S. L. Holt, "The Electronic Structure of Transition Metal Ions in High Oxidation States"

1968 IEEE Ultrasonics Symposium, New York, N. Y., Sept. 25-27, 1968

E. S. Cassedy, "Traveling-wave Photoelastic Amplification of Ultrasonic Waves,"

B. Singer and T. Tamir, "Propagation of a Light Beam Through a Medium Traversed by an Ultrasonic Wave"

URSI Fall Meeting, Boston, Mass., Sept. 1968

J. Shmoys, "Multipath Effects in Topside Sounding in Ionospheric Ducts"

1968 G-AP International Symposium, Boston, Mass., Sept. 1968

W. S. Gregorwich, A. Hessel, G. H. Knittel and A. A. Oliner, "A Waveguide Simulator for the Determination of a Phased-Array Resonance"

University of Florida, Gainesville, Fla., October 3, 1968

S. L. Holt, "The Electronic Structure of Transition Metal Ions in High Oxidation States"

State University of New York at Stony Brook, N. Y., Seminar, October 11, 1968

B. Post, "Structure and Properties of Refractory Binary Borides"

Fall Meeting of the American Vacuum Society, Pittsburgh, Pa., Oct. 30-Nov. 1, 1968

R. Stern and H. Taub, "Origin of the Angular Dependence of Secondary Emission of Electrons"

R. Stern, H. Taub and A. Gervais, "Dynamical Origin of Three Dimensional Electron Diffraction Intensities"

7th Rare-Earth Research Conference, San Diego, Calif., October 1968

G. T. Alfieri, K. Kanematsu and E. Banks, "Effect of High Pressure on the Curie Temperature of Rare-Earth Intermetallic Compounds"

Annual Meeting of the Division of Plasma Physics, Miami Beach, Florida, November 13 - 18, 1968

- G. Dorman, "Theoretical Models for the Resonance Oscillations of Inhomogeneous Plasma"
- G. Dorman, "Landau Damping of Resonance Oscillations in Inhomogeneous Plasmas"
- G. Dorman (with E. M. Barston, N. Y. U.), "Maximal Growth Rates of the Resistive Sheet Pinch"

Canadian Defence Research Board Symposium, Ottawa, Ont., Canada, November 1968

- D. Dence and T. Tamir, "Transmission Losses Associated with the Lateral Wave In Forest Environments"

14th Annual Conference on Magnetism and Magnetic Materials, New York, N. Y., November 1968

- G. T. Alfieri, E. Banks and K. Kanematsu, "The Pressure Dependence of the Curie Temperatures of Ferromagnetic Laves Phase Alloys"
- E. Banks and M. Mizushima, "A Mossbauer Study of Perovskites of Composition  $\text{SrFe}_{1-x}\text{Cr}_x\text{O}_{3-y}$ "

#### JOURNAL ARTICLES AND CORRESPONDENCE

- J. Abbruscato, E. Banks and B. R. McGarvey, "Interpretation of the Optical Spectrum of  $\text{Yb}^{3+}$  in  $\text{CdF}_2$  with the Aid of ESR Spectroscopy", *J. Chem. Phys.*, Vol. 49, No. 2, p. 903 (July 1968).
- N. Alexandropoulos (with H. Brumberger and W. Claffey), "Critical Opalescence of Liquid Sodium-Lithium Mixtures", *Phys. Rev. Letters*, Vol. 19, p. 555 (1967).
- N. Alexandropoulos (with H. Brumberger), "High-Temperature Sample Cell for the Krutky Small-Angle X-ray Camera", *Rev. of Sc. Jour.*, Vol. 38, p. 1579 (1967).
- G. T. Alfieri, E. Banks, K. Kanematsu and T. Ohoyama, "Magnetic Properties of CsCl Type Compounds of Rare Earth Metals with Cadmium", *J. Phys. Soc. Japan*, Vol. 23, pp. 507-510 (1967).
- E. Banks and A. Goldstein, "The Solution of Lithium in Hexagonal Potassium Tungsten Bronze", *Inorg. Chem.*, Vol. 7, pp. 966-969 (1968).
- E. Banks, M. Greenblatt and S. Holt, "The 800K Crystal Spectrum of  $\text{Ca}_2(\text{CrO}_4, \text{PO}_4)\text{Cl}$ ", *J. Chem. Phys.*, Vol. 49 (1968).
- E. Banks, M. Greenblatt and B. R. McGarvey, "ESR and Optical Spectroscopy of  $\text{CrO}_4^{3-}$  in Chlorospodiosite,  $\text{Ca}_2\text{PO}_4\text{Cl}$ ", *J. Chem. Phys.*, Vol. 47, pp. 3772-3780 (1967).
- E. Banks, M. Greenblatt and R. W. Schwartz, "New Analogs of Spodiosite,  $\text{Ca}_2\text{VO}_4\text{Cl}$  and  $\text{Ca}_2\text{AsO}_4\text{Cl}$ ", *Inorg. Chem.*, Vol. 7, pp. 1230-1232 (1968).
- S. Barone, "Optical Resonators in the Unstable Region", *J. Appl. Opt.*, Vol. 6, p. 861 (1967).
- R. Baudouin, R. M. Stern and H. Taub, "Inner Sources in Low Energy Electron Diffraction", *Surf. Sc.*, Vol. 11, p. 255 (1968).
- H. Berger and J. W. E. Griemsmann, "Guided Waves in Moving Dispersive Media. Part I. Nonrelativistic Velocities; Part II. Relativistic Velocities", *IEEE Trans.*, Vol. MTT-16, No. 1, pp. 11-20 (January 1968).

- H. Berger and J. W. E. Griemsmann, "Relativistic Doppler Equations for Attenuated Waves and the Drag Effect", *J. Appl. Phys.*, Vol. 39, No. 8 (July 1968).
- H. Berger and J. W. E. Griemsmann, "Transient Electromagnetic-Guided Wave Propagation in Moving Media", *IEEE Trans.*, Vol. MTT-16, No. 10 (October 1968).
- F. M. Beringer, P. Bodlaender, "Diaryliodosyl Salts", *Jour. Organic Chem.*, Vol. 33, p. 2981 (1968).
- H. L. Bertoni and A. Hessel, "Ray Description for Point Source Excited Surface Waves in Stratified Anisotropic Media", accepted for publication in *Radio Science*.
- L. Birenbaum, G. M. Grosop, S. W. Rosenthal and M. M. Zaret, "Effect of Microwaves on the Eye", to be published in the *IEEE Trans. on Bio-Medical Engineering* (January 1969).
- J. J. Bongiorno and D. C. Youla, "On Observers in Multivariable Control Systems", accepted for publication *Intern J. Control*.
- R. R. Boorstyn and R. L. Pickholtz, "A Recursive Approach to Signal Detection", *IEEE Trans.*, Vol. IT-14, pp. 445-450 (May 1968).
- R. R. Boorstyn and M. Schwartz, "Performance of Analog Demodulators in a Fading Environment", *IEEE Trans.*, Vol. COM-16, pp. 45-51 (February 1968).
- D. S. Boudreaux and V. Heine, "Band Structure Treatment of Low Energy Electron Diffraction Intensities", *Surf. Sc.*, Vol. 8, p. 426 (1967).
- J. Bregman, "SYMMETRY: An Experiment in Film Making", *Commission on College Phys. Newsletter No. 14* (October 1967).
- J. Bregman (with A. Holden), "Structural and Dynamical Symmetry", *The Science Teacher*, Vol. 34, p. 72 (1967).
- E. S. C Cassidy and J. Fainberg, "Scattering Cross Sections of Resistive Antennas", *IEEE Trans.* Vol. AP-16, No. 1, p. 128 (January 1968).
- D. C. Choudhury (with J. T. Clemens and F. G. Bailey), "Application of Intermediate-Coupling Unified Nuclear Model to Several Odd-Mass Nuclei", *Contributed paper to International Symposium on Nuclear Structure, Dubna, USSR* (July 4-11, 1968).
- D. C. Choudhury (with T. F. O'Dwyer), "Intermediate Coupling Approach in the Unified Nuclear Model I. Odd-Mass Pm Nuclei", *Nucl. Phys.* Vol. A93, p. 300 (1967).
- A. Christopher and L. M. Silber, "Ferromagnetic Resonance in Unsaturated Planar Ferrites", *IEEE Trans.*, Vol. MTT-16, No. 5, pp. 315-316 (May 1968).
- K. Chung and D. J. Rose, "Correlation Study of a Drift Wave Instability", *Appl. Phys. Letters*, Vol. 11, No. 8, pp. 247-248 (October 1967).
- K. K. Clarke and D. T. Hess, "Frequency Locked Loop FM Demodulator", *IEEE Trans.*, Vol. COM-15, pp. 518-524 (August 1967).
- K. K. Clarke and D. T. Hess, "Wideband FM Generation", *IEEE Jour.*, Vol. SC-3, No. 1 (March 1968).
- E. G. Coffman, Jr., "Analysis of Two Time-Sharing Algorithms Designed for Limited Swapping", *Jour. of the Association for Comput. Machinery*, Vol. 15, No. 3, pp. 341-353 (July 1968).
- S. Deutsch, "A Probe to Monitor Electroanesthesia Current Density", *IEEE Trans. on Bio-Medical Engineering* (April 1968).
- S. Deutsch, "Narrowband TV Pictures via Oceanographic Sound Waves", *Ocean Engineering* (April 1968).

- S. Deutsch and R. Simpson, "A Continuous-Motion Narrowband TV System", CQ (April 1968).
- R. Dingle and S.L. Holt, "On the Electronic Spectrum of Bis(N-piperidylthiocarbamate) Iron(III) Chloride", Acta Chem. Scand. Vol. 22 (1968).
- P. Dorato, C. Hsieh and P. Robinson, "Optimal Bang-Bang Control of Linear Stochastic Systems with a Small Noise Parameter", IEEE Trans., Vol. AC-13, No. 1 (1968).
- P. Dorato and D.C. Youla, "On the Comparison of the Sensitivity of Open-Loop and Closed-Loop Optimal Control Systems", IEEE Trans., Vol. AC-13, No. 2 (1968).
- F.R. Eirich and E.P. Otocka, "Ionic Bonding in Butadiene Copolymers. I. Network Formation", J. Polymer Science, Part A-2, Vol. 6, pp. 921-932 (1968).
- F.R. Eirich and E.P. Otocka, "Ionic Bonding in Butadiene Copolymers. II. Stress Relaxation", J. Polymer Science, Part A-2, Vol. 6, pp. 933-946 (1968).
- L. B. Felsen, "Propagation in Inhomogeneous and Dispersive Media", accepted for publication in Alta Frequenza.
- L. B. Felsen and S.J. Maurer, "Ray Interpretation of Modes in Curved Nonuniform Waveguides", Electronics Letters, Vol. 4, No. 4 (February 1968).
- L. B. Felsen and H. Y. Yee, "Multiple Interactions by Ray Optics - Some Observations and an Example", IEEE Trans., Vol. AP-16, No. 3, pp. 360-362 (May 1968).
- L. B. Felsen and H. Y. Yee, "Ray Method for Sound-Wave Reflection in an Open-Ended Circular Pipe", J. Acoust. Soc. Am., Vol. 44, No. 4 (October 1968).
- L. B. Felsen and H. Y. Yee, "Ray-Optical Techniques for Waveguide Discontinuities", IEEE Trans., Vol. AP-16, No. 2, pp. 268-269 (March 1968).
- S. J. Freedman (with R. Augeri), "Preparation of Bismuth Surfaces for Ultrasonic Attenuation Measurements", J. Acoust. Soc. Am., Vol. 41, p. 1369 (May 1967).
- J. P. Freidberg, "Nonlinear Plasma Waves. III. Nonlinear Temperature Effects in the Electron-Ion Two-Stream Instability", Phys. Fluids, Vol. 10, No. 11 (November 1967).
- H. W. Friedman, "Nonlinear Asymptotic Analysis of the Positive Column", Phys. Fluids, Vol. 10, No. 9, pp. 2053-2061 (September 1967).
- H. Friedman and E. Levi, "Singularities of the Fluid Equations and Their Relation to Anomalous Diffusion", Phys. Fluids, Vol. 11, No. 3, pp. 678-680 (March 1968).
- G. Gashurov and E. Banks, "The Role of Copper in the Transformation of Hexagonal Zinc Sulfide", J. Electrochem. Soc., Vol. 114, pp. 1143-1148 (1967).
- A. Gervais, R. M. Stern and M. Menes, "Multiple Diffraction Origin of Low Energy Electron Diffraction Intensities", Acta. Cryst., Vol. A24, p. 191 (January 1968).
- G. Gould and K. W. Estridge, "From Whence Tomorrow's Lasers?", Laser Focus, pp. 25-30 (January 1968).
- B. Greenberg and B. Post, "The Crystal Structure of Tetracyanocyclobutane", Acta. Cryst. Vol. B24, p. 918 (July 1968).
- W. S. Gregorwich, A. Hessel, G. H. Knittel and A. A. Oliner, "A Waveguide Simulator for the Determination of a Phased-Array Resonance", IEEE G-AP International Symposium Digest, pp. 134-141 (September 1968).
- A. Halperin (with W. Y. Chu, G. A. Haber and J. J. Dropkin), "The Thermoluminescence and Photoluminescence of ZnS:Er<sup>3+</sup>", International Conference on II-VI Semiconducting Compounds, Brown University (September 1967).

- D. T. Hess, "Cycle Slipping in a First-Order Phase-Locked Loop," IEEE Trans., Vol. COM-16, No. 2 (April 1968).
- A. Hessel and H. Hochstadt, "Plane Wave Scattering from Modulated-Corrugated Structures", Radio Science, Vol. 3, No. 10 (October 1968).
- A. Hessel, G.H. Knittel and A.A. Oliner, "On the Theory of Resonance in Phased-Array Antennas", URSI Fall Meeting Digest, p. 62 (October 1967).
- H. Hochstadt, "Hill's Equations with Half-Periodic Coefficients", Proc. A.M.S., Vol. 19, p. 483 (1968).
- H. Hochstadt, "On Inverse Problems Associated with Second-Order Differential Operators", Acta. Math., Vol. 119, p. 173 (1967).
- H. Hochstadt, "On Some Inverse Problems in Matrix Theory", Archiv der Mathematik, Vol. 18, p. 201 (1967).
- H. Hochstadt, "On the Determination of a Hill's Equation from Its Spectrum II", Arch. Rat. Mech. and Anal. Vol. 23, p. 237 (1967).
- H. Hochstadt, "On the Evaluation of the Wronskian Determinant", Amer. Math. Monthly, Vol. 70, p. 767 (1968).
- H. Hochstadt, "The Mean Convergence of Fourier-Bessel Series", SIAM Review, Vol. 9, p. 211 (1967).
- H. Hochstadt (with B. Stephan), "On the Limit Cycles of  $\ddot{x} + \mu \sin x + x = 0$ ", Arch. Rat. Mech. and Anal. Vol. 23, p. 369 (1967).
- S.L. Holt and C.J. Ballhausen, "The Low Temperature Absorption Spectra of  $\text{KMnO}_4$  in  $\text{KClO}_4$ ", Theoret. Chim. Acta (Berl.) Vol. 7, p. 313 (1967).
- S.L. Holt and R. Dingle, "The Electronic Structure of Trigonal Distorted  $\text{Fe}^{3+}$  Complexes", Acta Chem. Scand. Vol. 22, (1968).
- S.L. Holt and A. Wold, "The 20°K Spectrum of Sodium Thiochromite", Inorg. Chem., Vol. 6, p. 1594 (1967).
- R.G.E. Hutter, "Deflection Defocusing Correction by Means of Rotationally Symmetrical Lenses Only", IEEE Trans., Vol. ED-14, No. 10, pp. 694-699 (October 1967).
- H.J. Juretschke, "Third-Order Elastic Constants of Polycrystalline Media", Appl. Phys. Lett. Vol. 12, p. 213 (1968).
- W.K. Kahn and H. Kurss, "A Note on Reflector Arrays", IEEE Trans., Vol. AP-15, No. 5 (September 1967).
- G.H. Knittel, A. Hessel and A.A. Oliner, "Element Pattern Nulls in Phased Arrays and Their Relation to Coupled Waves", to be published in Proc. IEEE, Special Issue on Electronic Scanning, scheduled for November 1968.
- I. Kohavi, "On Minimal Modulo 2 Sum of Products for Switching Functions", IEEE Trans., Vol. EC-16, No. 5 (October 1967).
- J.B. Krieger (with C. Rosenzweig), "Application of Higher Order WKB Approximation to Radial Problems", Phys. Rev., Vol. 164, p. 171 (1967).
- J.B. Krieger, "Asymptotic Properties of Perturbation Theory", J. Math. Phys., Vol. 9, p. 432 (March 1968).
- J.B. Krieger, "Some Analytic Properties of Finite Band Models in Solids", Phys. Rev., Vol. 156, p. 77 (1967).
- J.B. Krieger (with M.L. Lewis and C. Rosenzweig), "Use of WKB Approximation for Obtaining Energy Eigenvalues", J. Chem. Phys., Vol. 47, p. 2942 (1967).

- J. B. Krieger and S. Strauss, "Singly-Ionized-Impurity Scattering in Degenerate Material", *Phys. Rev.*, Vol. 169, p. 674 (1968).
- R. Lang and J. Shmoys, "Comments on 'Modal Solution of a Point Source in a Strongly Focusing Medium, by E. T. Kornhauser and A. D. Yaghian'", *Radio Science*, Vol. 3, pp. 201-202 (1968).
- R. Lang and J. Shmoys, "Lateral Wave on a Symmetrical Epstein Transition", *J. Appl. Phys.*, Vol. 39, No. 3, pp. 1670-1680 (February 1968).
- H. W. Lawson, Jr., "Programming-Language-Oriented Instruction Streams", *IEEE Trans.*, Vol. EC-17, No. 5 (May 1968).
- L. Levey and L. B. Felsen, "On Transition Functions Occurring in the Theory of Diffraction in Inhomogeneous Media", *J. Inst. Maths. Applics.*, Vol. 3, pp. 76-97 (September 1967).
- M. L. Lewis, "Minimum Size of Proton and Electron in a Non-Relativistic Theory from Hyperfine Structure", *Am. J. of Phys.*, Vol. 35, p. 528 (1967).
- S. J. Maurer and L. B. Felsen, "Ray-Optical Techniques for Guided Waves", *Proc. IEEE*, Vol. 55, No. 10, pp. 1718-1729 (October 1967).
- B. R. McGarvey, "Charge Transfer in the Metal Ligand Bond as Determined by ESR", to be published in a monograph of a symposium held at the Pittsburgh Conference in March 1968 in Cleveland.
- B. R. McGarvey and J. Pearlman, " $N^{14}$  Nuclear Magnetic Resonance of Paramagnetic Complexes", *Jour. of Magnetic Resonance*, In press (1968).
- L. Mendelsohn, "Large-Z Expansion Theory for the Ground State of a One-Electron Ion Perturbed by  $r^N$ ", *Phys. Rev.*, Vol. 160, p. 16 (1967).
- E. A. Mishkin and P. Bertrand, "Anticorrelation Effects in Single Mode Fields", *Phys. Letters* Vol. 25A, No. 3, p. 204 (August 1967).
- E. A. Mishkin and A. Kestenbaum, "Diagonal Coherent Representation in a Model of Interacting Radiation and Matter", *Bull. Am. Phys. Soc.* (January 1968).
- E. A. Mishkin and M. Miller, "Representation of Operators in Quantum Optics", *Phys. Rev.* (December 1967).
- M. C. Newstein, "Spontaneous Emission in the Presence of a Prescribed Classical Field", *Phys. Rev.*, Vol. 167, No. 1, pp. 89-96 (March 1968).
- C. J. Nisteruk and A. Isihara, "Quantum-Statistical Distribution Functions of a Hard-Sphere System", *Phys. Rev.*, Vol. 154, p. 150 (1967).
- G. Oppo (with S. Oneda), "Models of  $z^0 - \pi^0 + 2\gamma$  Decay", *Phys. Rev.*, Vol. 160, p. 1397 (1967).
- E. Ott, "Electromagnetic Pulse Propagation in Lossless, Inhomogeneous, Dispersive, Dielectric Media", *J. Appl. Phys.*, Vol. 38, No. 12, pp. 4632-4640 (November 1967).
- E. Ott and J. Shmoys, "Transient Aspects of Transition Radiation", *Quart. Appl. Math.*, Vol. XXV, No. 4, pp. 377-398 (January 1968).
- E. Ott and J. Shmoys, "Transition Radiation and the Corenkov Effect", *Quart. Appl. Math.*, Vol. XXVI, No. 2, pp. 187-198 (July 1968).

- E. Ott and J. Shmoys, "Transient Radiation in a Plane Stratified Dispersive Medium. I. Half-Space Configuration", *Can. J. Phys.*, Vol. 46, pp. 1059-1071 (1968)
- A. Papoulis, "Dual Optical Systems", *Jour. Optical Society of America* (May 1968)
- A. Papoulis, "Limits on Band-Limited Signals", *Proc. IEEE* (October 1967).
- A. Papoulis, "Truncated Sampling Expansions", *IEEE Trans. on Automatic Control* (October 1967).
- B. Post (with G. Boder and A. L. Bednowitz), "The Crystal Structure of  $\epsilon$ -Aminocaproic Acid", *Acta Cryst.* Vol. 23, p. 482 (1967).
- B. Post (with P. Cherin and W. C. Hamilton), "Positions and Thermal Parameter of Oxygen Atoms in Sodium Nitrite", *Acta. Cryst.* Vol. 23, p. 455 (1967).
- B. Post (with M. Greenblatt and E. Banks), "Crystal Structures of Spodiosite Analogs  $\text{Ca}_2\text{CrO}_4\text{Cl}$   $\text{Ca}_2\text{PO}_4\text{Cl}$ ", *Acta. Cryst.* Vol. 23, p. 166 (1967).
- B. Post (with N. Sklar), "The Crystal Structure of Lithium Aluminium Hydride", *Inorg. Chem.*, Vol. 6, p. 669 (1967).
- S. Rosenbaum, "Edge Diffraction in an Arbitrary Anisotropic Medium. I.", *Can. J. Phys.*, Vol. 45, pp. 3479-3502 (October 1967).
- S. Rosenbaum, "Edge Diffraction in an Arbitrary Anisotropic Medium. II.", *Can. J. Phys.*, Vol. 45, pp. 3503-3519 (October 1967).
- C. Rosenzweig and J. B. Krieger, "Exact Quantization Conditions", *J. Math. Phys.*, Vol. 6, p. 849 (1968).
- R. Rudman and B. Post, "Polymorphism of Crystalline Cyclo-Octanone and Cyclo-nonanone", *Molecular Crystals*, Vol. 3, pp. 325-337 (1968).
- D. L. Schilling, "Error Rates for Digital Signals Demodulated by an FM Discriminator", *IEEE Trans.*, Vol. COM-15, No. 4 (August 1967).
- B. Senitzky, "Noise in the Presence of Strong Coherent Signals", *IEEE Trans.*, Vol. MTT-16, No. 9 (September 1968).
- L. Shaw, "On Mean Square Controllability", *IEEE Trans., Letters*, Vol. AC-13, pp. 106-107 (February 1968).
- J. Shmoys, "Ray Tracing in the Ionosphere", *Electronics Letters*, Vol. 4, pp. 302-304, (1968).
- M. L. Shooman, "Reliability Physics Models", *IEEE Trans.*, Vol. R-17, No. 1, p. 14, (March 1968).
- L. Silber, E. Tsantes and P. Angelo, "Ferromagnetic Resonance in a Uniaxial Anisotropic Ferrite:  $\text{BaFe}_{12}\text{O}_{19}$ ", *J. Appl. Phys.*, Vol. 38, pp. 5315-5318 (December 1967).
- C. Simp, E. Banks and S. Holt, "The 4.2°K Spectrum of  $\text{CoF}_2$  in  $\text{CdF}_2$ ", *Inorg. Chem.*, Vol. 9 (1969).
- C. Simp and S. Holt, "The Polarized Spectrum of  $\text{Co}(\text{Ph}_3\text{P})_2\text{Cl}_2$ ", *Inorg. Chem.*, Vol. 8 (1968).
- E. J. Smith and P. Weiner, "Optimization of Reduced Dependencies for Synchronous Sequential Machines", *IEEE Trans.*, Vol. EC-16, No. 6, pp. 835-847 (December 1967)
- A. Sobel, "Fluorine Nuclear Magnetic Resonance in Dilute Paramagnetic Spinels with Fluorine Charge Compensation", *J. Phys. Chem. Sol.*, Vol. 28, p. 185 (1967).



- S. Soffer, "Statistical Model for the Size Effect in Electrical Conduction", *J. Appl. Phys.*, Vol. 38, p. 1710 (1967).
- G. Stell, "Extension of the Ornstein-Zernike Theory of the Critical Region", *Phys. Rev. Letters*, Vol. 20, pp. 533-536 (1968).
- R.M. Stern, "Three-Dimensional Dynamical Low Energy Electron Diffraction", *Proc. Am. Cryst. Assoc.*, Vol. 4, p. 14 (1968).
- R.M. Stern (with R. Baudoing), "Metastable Surface Structure of the W(110) Face", *Surf. Sc.* Vol. 10, pp. 392-398 (1968).
- R.M. Stern and H. Taub, "Origin of the Angular Dependence of Secondary Emission of Electrons from Tungsten", *Phys. Rev. Letters*, Vol. 20, p. 1340 (1968).
- K. Stuart and E. Levi, "Observation of Resistive Instabilities in a Toroidal Plasma", *J. Appl. Phys.*, Vol. 39, No. 6 (June 1968).
- T. Tamir, "On Radio-Wave Propagation in Forest Environments", *IEEE Trans.*, Vol. AP-15, No. 6, pp. 806-817 (November 1967).
- T. Tamir, "On the Optimization of the Ground Wave Above a Dissipative Half-Space", *IEEE Trans.*, Vol. AP-16, No. 5 (September 1968).
- T. Tamir, "The Field of a Line Source Embedded in a Periodically-Stratified Medium", accepted for publication Special Issue *Alta Frequenza*.
- D. Y. Tseng, A. Hessel and A.A. Oliner, "Scattering by a Multimode Corrugated Structure with Application to P Type Wood Anomalies", accepted for publication Special Issue *Alta Frequenza*.
- H. Wagenfeld, "Ewald's and V. Laue's Dynamical Theories of X-Ray Diffraction", *Acta. Cryst.*, Vol. 24, p. 170 (1968).
- W.T. Walter, "Metal Vapor Lasers", *IEEE Trans.*, Vol. QE-4, No. 5, pp. 355-356 (May 1968).
- W.C. Wang, "Strong Acousto-Electric Effect in CdS", Series of Selected Papers in Physics, Vol. 161, Physical Society of Japan (September 1967). (Originally published in *Phys. Rev. Letters*, 1962).
- W.C. Wang and R. Mauro, "Multiple Wave Interactions in Piezoelectric Semiconductors", *Phys. Rev. Letters*, Vol. 19, p. 593 (1967).
- J.K. Wolf, "Decoding of Bose-Chaudhuri-Hocquenhem Codes and Prony's Method of Curve Fitting", *IEEE Trans.*, Correspondence, Vol. IT-13, No. 4, p. 608 (October 1967).
- J.K. Wolf and B. Nasmick, "On Linear Unequal Protection Codes", *IEEE Trans.*, Vol. IT-13, No. 4, pp. 600-607 (October 1967).
- D.D.H. Yee, "Non-Existence of Self-Conjugate Particles with Half-Integral Spin", *Phys. Rev.*, Vol. 171, p. 2314 (1968).
- D.D.H. Yee, "Wave Equations for Neutral Particles with Arbitrary Spin", *Phys. Rev.*, Vol. 171, p. 2319 (1968).
- H.Y. Yee and L.B. Felsen, "Ray Optics - A Novel Approach to Scattering by Discontinuities in a Waveguide", accepted for publication in *IEEE Trans. on Microwave Theory and Techniques*.
- H.Y. Yee, L.B. Felsen and J.B. Keller, "Ray Theory of Reflection from the Open End of a Waveguide", *SIAM J. Appl. Math.*, Vol. 16, No. 2, pp. 268-300 (March 1968).

## RECENT BOOKS AND FILMS

- C. Belove and D. L. Schilling, "Electronic Circuits, Discrete and Integrated", (New York: McGraw-Hill Book Company, 1968).
- J. Bregman (with A. Holden, R. Davisson and P. Stapp), "SYMMETRY" A ten minute animated film distributed by Contemporary Films, Inc., (267 West 25th St., New York, N. Y.).
- A. Papoulis, "Systems and Transforms with Applications in Optics", (New York: McGraw-Hill Book Company, 1968).
- M. L. Shooman, "Probabilistic Reliability: An Engineering Approach", (New York: McGraw-Hill Book Company, 1968).
- "Proceedings of the Symposium on Tubulence of Fluids and Plasmas", MRI Symp. Ser. Vol. XVIII (Brooklyn, N. Y.: Polytechnic Press, to be published).

## CONTRIBUTIONS TO RECENT BOOKS

- E. Banks and A. Wold, "Oxide Bronzes", (Vol. 4, Preparative Inorganic Reactions) (New York: Interscience Publishers, 1968).
- D. C. Choudhury, "Analysis of the Properties of Low-Lying Levels in  $^{131}\text{I}$ ", Contributions to the International Conference on Nuclear Structure, (Tokyo, Japan, p. 90, 1967).
- J. J. Dropkin (with A. Halpern, W. J. Chu and G. Haber), "The Thermoluminescence and Photoluminescence of  $\text{ZnS:Er}^{3+}$ ", Semiconducting Compounds 1967 International Conference, ed. D. G. Thomas, (New York: W. Benjamin Publishers, Inc., p. 68, book IV-6, 1968).
- L. B. Felsen, "Lateral Waves", Contribution to Electromagnetic Wave Theory, ed. J. Brown, (New York: Pergamon Press, pp. 11-44, 1967).
- A. Gervais, R. M. Stern and M. Menes, "Anisotropy of Low Energy Electron Diffraction Intensities", Proceedings of the 22nd Physical Electronics Conference, (Cambridge, Mass., M. I. T. Press, p. 1, 1967).
- J. W. E. Griemsmann, "Fundamental Properties of Electrical Insulation Materials", Contribution to Plastics for Electrical Insulation, (New York: Interscience Divn. of John Wiley and Sons, 1968).
- A. Hessel, "General Characteristics of Traveling Wave Antennas", Contribution to Antenna Theory, ed. R. E. Collin and F. J. Zucker, (New York: McGraw Hill Book Co., Inc., Chap. 15, to be published in 1969).
- H. Hochstadt, "Inverse Problems Associated with Second-Order Differential Operators", Proc. U.S. -Japan Seminar on Differential and Functional Equations (New York: W. A. Benjamin Publishers, Inc., pp. 535-544, 1967).
- H. J. Juretschke, "Transport Phenomena", Magnetism and Magnetic Materials 1967 Digest, ed. Doyle and Harris (New York: Academic Press, p. 260, 1967).
- T. Tamir, "Leaky Wave Antennas", Contribution to Antenna Theory, ed. R. E. Collin and F. J. Zucker, (New York: McGraw-Hill Book Co., Inc., Chap. 20, to be published in 1969).

## NEW PATENTS

- H. Farber and M. Sucher, Microwave Spark-Gap Switch Having a Trigger Electrode Centered Between and Aligned with the Opposed Electrode, U.S. Patent No. 3,351,806, November 7, 1967.
- H.J. Juretschke and W.G. Egan, Paramagnetic Microwave Power Detector, U.S. Patent No. 3,375,442, March 26, 1968.
- L. Birenbaum, Voltage Standing Wave Indicators for H-Guides, Patent Application Serial No. 488,068. Patent allowed - about to issue.
- K.K. Clarke and D.T. Hess, Frequency Demodulator for Noise Threshold Extension, Patent application filed.
- W.K. Kahn, RF Power Meter, Patent Application Serial No. 390,927. Patent allowed - about to issue.

## TECHNICAL REPORTS

- E. Banks and B. Post, "High Pressure Chemistry and Structure," Final Report, (PIBCM-68-001)
- T. Chien, "Theory of Broadband Matching of Frequency Dependent Generator and Load," (PIBEP-68-010)
- K. Chung, "Plasma Turbulence," (PIBEP-68-012)
- A. Csurgay and D.C. Youla, "On the Postulational Approach to Active Networks," (PIBMRI-1384-67)
- S. Deutsch, "A Four-Sequential-Output-Generator for Research in Electroanesthesia," (PIBEE-68-0002)
- R. F. Drenick, "1967 International Symposium on Information Theory," (PIBEE-68-0004)
- L. B. Felsen, "A Theoretical and Experimental Research Program in Electromagnetic Fields with Emphasis on Temporal and Spatial Networks," Final Report, (PIBEP-68-002)
- G. Gonenc, "An Algorithmic Method for Organizing Checking Experiments," (PIBEE-68-0006, PIBMRI-1387-68)
- T. Kjeldaas, Jr., "Theory of the Interaction of High-Frequency Sound Waves and Electrons," Final Report (PIBPH-68-001)
- A. E. Laemmel, "Detection of Surface Electromagnetic Effects," Final Report, (PIBEP-68-014)
- R. Lang and J. Shmoys, "Lateral Waves on Diffuse Dielectric Interfaces," (PIBEP-68-008)
- G. Louie and H. Farber, "The Characteristics of the Screen Anode Discharge," (PIBEP-68-006)
- F. Maffioli and P. Tissi, "Constrained Variable Metric Optimization of Layered Electromagnetic Absorbers," (PIBEP-68-017)
- H. F. Mark, F.R. Eirich and J. Fock, "New Polymer to Protect Space Vehicles," (PIBMRI-1385-67)
- S. J. Maurer and L. B. Felsen, "Ray Optical Methods for Modes in Guiding and Radiating Structures," (PIBEP-68-004)
- E. Mishkin, "Photon Statistics of the Stimulated Raman Effect," (PIBEE-68-0009)
- J. Oberst, "Binary Phase-Shift Keyed Communications Systems," (PIBEE-68-0010)

- A. A. Oliner, "Application of Electromagnetic Theory to Radiating and Non-Radiating Transmission Lines, " Final Report (PIBEP-68-011)
- A. A. Oliner, "An Equivalent Network for Elastic Waves at a Solid-Liquid Interface, with Applications, " (PIBEP-68-016)
- G. D. Ott, "Two-Variable Synthesis of Cascaded Transmission Lines and Shunt Capacitors, " (PIBMRI-1386-67)
- S. H. Richman, "Extreme Value Statistics in the Simulation of Digital Communication Systems, " (PIBEE-68-0003)
- L. Shaw, "Research in Control Theory, " (PIBEE-68-0001)
- L. Shaw and P. Chalon, "An Expansion for Evaluation of Sensitivity with Respect to a Random Variable Parameter, " (PIBEE-68-0007)
- G. M. Whitman, "Transition Excitation of Bounded Cold Magnetoplasma, " (PIBEP-68-0005)
- R. Yager, "Optimal Time Allocation in Complex Tasks, " (PIBEE-68-0008, PIBMRI-1388-68)
- H. Y. Yee and L. B. Felsen, "Ray-Optical Techniques for Waveguide Discontinuities, " (PIBEP-68-005)

**JOINT SERVICES TECHNICAL ADVISORY COMMITTEE COSPONSORED SYMPOSIUM**  
**1969 INTERNATIONAL SYMPOSIUM ON COMPUTER PROCESSING IN COMMUNICATIONS**

Computer Processing in Communications is the topic of the nineteenth in the series of annual international symposia organized by the Microwave Research Institute of the Polytechnic Institute of Brooklyn. This symposium will be held at the Waldorf-Astoria Hotel in New York City on 8-10 April 1969 with Professor M. Schwartz as Symposium Chairman.

The symposium will stress the role of computer techniques in data transmission and processing and will provide an opportunity for scientists, engineers, and mathematicians to review the latest viewpoints and developments along with specialists in communications and computer processing.

Adaptive communication systems, data compression techniques, antenna array signal processing, adaptive equalization for random channels, feedback communication systems, algorithmic formulation of communication problems, and computer simulation of communication systems will be considered. The range of applications includes space telemetry, seismic signal processing, biomedical processing, underwater communications. The symposium will include a panel discussion focusing on the role that computers are expected to play in signal processing systems of the future. The following outline suggests some of the more prominent features to be explored in a series of consecutive sessions:

Introductory: Overall view and philosophy; role of computer processing techniques in data transmission.

Adaptive Systems: Array processing, equalizers, data compression.

Algorithmic Formulation of Communication Problems: Optimization and search techniques.

Discrete-Time Techniques: Digital filtering, sampling and quantization.

Applications and Implementation: Seismic arrays, radar processing, radar astronomy, biomedical processing, coding and decoding techniques, pattern recognition.

Computer Simulation of Communication Systems

Statistical Estimation: Fast Fourier transform, spectral estimation, computer techniques for channel measurements.

Switching and Routing by Computer.

This symposium is conducted as a portion of the Institute's Joint Services Electronics Program and is organized, as in past years, under the aegis of the Microwave Research Institute of the Polytechnic Institute of Brooklyn with the co-sponsorship of the Air Force Office of Scientific Research, the Office of Naval Research, and the Army Research Office. Once again it will be held in cooperation with the Institute of Electrical and Electronics Engineers. The "Proceedings of the Symposium on Computer Processing in Communications" will be published by the Polytechnic Press as Volume XIX of the MRI Symposia Series.

UNCLASSIFIED

Security Classification

DOCUMENT CONTROL DATA - R & D

(Security classification of title, body of abstract and indexing annotation must be entered when the overall report is classified)

1. ORIGINATING ACTIVITY (Corporate author) Polytechnic Institute of Brooklyn Microwave Research Institute 333 Jay Street, Brooklyn, N. Y. 11201	2a. REPORT SECURITY CLASSIFICATION <b>UNCLASSIFIED</b>
	2b. GROUP

3. REPORT TITLE  
**PROGRESS REPORT NO. 33 TO THE JOINT SERVICES TECHNICAL ADVISORY COMMITTEE**

4. DESCRIPTIVE NOTES (Type of report and inclusive dates)  
**Scientific Interim**

5. AUTHOR(S) (First name, middle initial, last name)  
**Arthur A. Oliner**

6. REPORT DATE <b>November 1968</b>	7a. TOTAL NO. OF PAGES <b>481</b>	7b. NO. OF REFS <b>423</b>
--	--------------------------------------	-------------------------------

8a. CONTRACT OR GRANT NO <b>AF 49(638)-1402</b> b. PROJECT NO. <b>4751</b> c. <b>6144501F</b> d. <b>681305</b>	9a. ORIGINATOR'S REPORT NUMBER(S) <b>PIBMRI R-452. 33-68</b>
	9b. OTHER REPORT NO(S) (Any other numbers that may be assigned this report) <b>AFOSR 68-2163</b>

10. DISTRIBUTION STATEMENT  
1. This document has been approved for public release and sale; its distribution is unlimited.

11. SUPPLEMENTARY NOTES <b>TECH, OTHER</b>	12. SPONSORING MILITARY ACTIVITY <b>Joint Services Electronics Program through AirForce Office of Scientific Research(SREE) 1400 Wilson Boulevard Arlington, Virginia 22209</b>
---	--

13. ABSTRACT  
This report is the thirty-third in a series of progress reports to the Joint Services Technical Advisory Committee since inception of the Joint Services Electronics Program at the Polytechnic Institute of Brooklyn in July 1955. The report, now being issued annually, summarizes research accomplished under the aegis of the Microwave Research Institute and reflects the impact of the Joint Services Electronics Program on the research activities of faculty and students of the participating departments of the Institute. The program covers a broad spectrum ranging from basic theoretical physics, mathematics, and engineering, to experimental investigations involving basic measurements, development of devices, and materials.

Each activity reports in summary fashion on specific results obtained during the report period of 15 September 1967 through 14 September 1968 with individual acknowledgment of the sponsorship which has contributed to the reported work. The report is compiled under seven headings: Electromagnetics and Waveguide Techniques; Quantum Electronics and Optics; Plasma Physics and Electronics; Solid State and Materials; Control Theory and Computer Science; Communications and Information Processing; Networks and Systems.

14. KEY WORDS	LINK A		LINK B		LINK C	
	ROLE	WT	ROLE	WT	ROLE	WT
Electromagnetics						
Waveguide Techniques						
Quantum Electronics						
Optics						
Plasma Physics						
Electronics						
Solid State and Materials						
Control Theory						
Computer Science						
Communications						
Information Processing						
Networks						
Systems						